ANNUAL REPORT

June 1, 1999 – May 31, 2000

CHEMICAL REACTION ENGINEERING LABORATORY (CREL)

Department of Chemical Engineering
Washington University
St. Louis, MO 63130-4899

Dr. M.P. Dudukovic´, Director
and
Dr. M.H. Al-Dahhan, Associate Director

INTRODUCTION

The Chemical Reaction Engineering Laboratory (CREL) is a research and educational center within the Chemical Engineering Department of Washington University in St. Louis. CREL conducts long-term research projects in reaction engineering, with funding from the federal government and industry and performs as well short-term research contracts in the area of multiphase reactors for member companies only.

Reaction Engineering has always played an important role in conversion of renewable and nonrenewable natural resources into fuels, chemicals, food and feed, pharmaceuticals and new materials. By changing the chemical structure or content of a molecule, which is realizable only via chemical transformations performed in suitable reactor configurations, we produce chemical species with new properties. Hence, chemical reactions and reactors are the key to manufacturing materials and chemicals for which market demand is high, and as well in controlling the undesired by-products and in preventing damage to the environment. Proper engineering of chemical reactions and reactors is the key to success of any process. It is well known that reactor performance determines the required number of separation units before and after the reactor and their load, establishes reactor volumetric productivity, selectivity and operability, and dictates the needed pollution abatement effort, if any. Thus, the reactor is the heart of the process and its proper choice and operation affect the whole process and determine the behavior, economics, profitability and environmental acceptability of the whole plant.

We at the Chemical Reaction Engineering Laboratory (CREL) define reaction engineering as a discipline with a powerful and general methodology that quantifies the interactions between **reaction kinetics** (chemical, photochemical, electrochemical, biochemical, biological, etc.) and **transport phenomena** (momentum, mass and heat transfer) at molecular, local and global scale in various reactor types. Such quantification leads to predictive models for reactor design, scale-up/scale-down and operation. Since most industrial processes require the presence of more than one phase, we focus on reaction engineering of multiphase systems.

CREL has been involved in advancing reaction engineering for over 27 years by generating new knowledge. Being an integral part of an educational institution, we strive to provide a unique and stimulating environment for our students. We expect them to gain a broad exposure to, and a good knowledge of, reaction engineering principles so that they can effectively use the state-of-the-art reaction engineering in a variety of applications. We also require them to advance the state-of-the-art in their chosen specialty. CREL is a unique organization that provides rapid transfer of academic research to industrial practice and that has developed and maintained close ties with industry. We serve our industrial sponsors in many ways: (i) by keeping them informed of the latest advances in reaction engineering, (ii) by offering access to truly unique experimental facilities and the best available multiphase flow models, (iii) by providing consulting services and contract work, (iv) by sending qualified students to work on company premises, (v) by offering training opportunities for industrial personnel and short courses, (vi) by doing joint research, (vii) by allowing member companies to provide input for CREL long-term research and for selection of CREL future thesis projects, and (viii) by providing our sponsor with the opportunity to leverage resources.

The current trends in industry on downsizing and increasing the efficiency and company profit margins has had many side effects. For example, even the largest companies cannot

afford any move to have teams of scientists and engineers maintaining their expertise in general areas, they are forced to specialize. Nor can the companies afford to maintain the facilities and equipment for cold flow modeling, pilot plant scale investigations or rigorous kinetic studies. Yet, the diversity of the business that they pursue and the constant pressure to scale-up new production more rapidly, or improve existing plants, require general expertise and tools for modern scale-up. It is for this and other reasons that CREL offers a unique opportunity to our industrial sponsors. We at CREL can be a valuable partner for improved troubleshooting of existing processes and in scale-up of new ones. We also offer breadth and depth in the general methodology of reaction engineering plus some unique facilities. In this new business climate company association with CREL have become more valuable.

In summary, CREL prepares our students to function effectively in an environment dominated by rapid change, and we work continuously on bridging the gap between academic research and its industrial applications, hence, contributing to a positive change. CREL has reached international recognition for its experimental, theoretical and modeling capabilities in the area of multiphase flow systems with the emphasis on reactive three phase flow systems.

The breadth and depth of CREL and its role in establishing fruitful research collaborations between industry, academia and national laboratories have been recognized via prestigious awards and invited lectures. During the last year, Professor Dudukovic won the 1999 Council for Chemical Research (CCR) Malcolm E. Pruitt Award. This award is given annually to recognize "outstanding contributions to research progress in the chemical based sciences and engineering through mutually beneficial interactions among the industrial, academic, and government research sectors". In addition, Professor Dudukovic was honored by being invited to give the keynote address entitled "Opaque Multiphase Reactors: Experimentation and Modeling" at the Institut Francis du Petrol (IFP) International Conference on Chemical Reactors, "From Mock Up to Industrial Reactor: Diagnostic Methods" in Lyon, France.

CREL program currently encompasses: (i) quantification of flow, mixing and reaction in multiphase reactors, (ii) environmentally benign processing of materials and chemicals, and (iii) unsteady state processing. In the area of multiphase reactors we have a unique non-invasive experimental facility that combines **Computer Automated Radioactive Particle Tracking (CARPT)** and **Computer Tomography (CT)** for measurement of instantaneous velocities, turbulence and backmixing parameters, time averaged circulation patterns and complete voidage (holdup) distribution in multiphase gas-liquid-solid, gas-liquid, liquid-solid and gas-solid systems such as bubble columns, fluidized beds, risers and stirred tanks. No other laboratory in the world has this CARPT-CT combination which is the only facility that provides the capabilities for studying systems with large volume fraction of the dispersed phase i.e. systems that we call opaque! In CREL, **Dr. Jay Turner,** a CREL graduate, spearheads the efforts in environmental reaction engineering, while **Dr. P.A. Ramachandran** continues to broaden both the CREL computational base and know-how in multiphase reactors. **Dr. M. Al-Dahhan** spearheads the effort on high pressure bubble/slurry bubble column and has also focused on multiphase reactors and bioreactors such as trickle-beds, packed bubble columns, stirred tank and liquid-solid and gas-solid circulating systems. **Dr. M. Al-Dahhan** is also assisting **Dr. M.P. Dudukovic´** in expanding the CREL base. All research projects in CREL stress advances in fundamentals but applications are always sought in areas of specific interest to our sponsors. We also have close interactions with **Professor B. Joseph** and his group in control and optimization.

CREL has initiated international interactions with a number of national and world renowned university laboratories dealing with various aspects of multiphase systems such as those at the Ohio State University, University of Delft and University of Amsterdam in Holland, University of Norway at Trondheim, University of Stuttgart, University of Hannover and Martin-Luther University in Germany, ENSIC at Nancy in France, Waterloo University, Ecole Polytechnic and Laval University in Canada, Almeria University in Spain and the National Chemical Laboratory in India. We intend to expand this interaction in the forthcoming years.

The continuity of our research in reaction engineering has been made possible by the **Department of Energy (DOE) and our industrial sponsors**. In 1999/2000 they are: **Air Products, ABB Lumus, Bayer, Chevron, Conoco, DuPont, Elf Atochem, Exxon, ICI-Synetix, IFP, Intevep, , MEMC, Mitsubishi, Mobil, Monsanto, Praxair, Shell, Sasol, Solutia, Statoil, Union Carbide and UOP**. To them goes our gratitude for having the foresight to support fundamental research in the areas that are vital to their business.

As is customary we report here only on the **NON-PROPRIETARY WORK** executed under government or general CREL consortium funding. Results of specific industrial contract research work are reported only to the sponsors until released for dissemination and publications.

We would like to alert our sponsors that an effective way of advancing their research objectives is to enter into mini consortia or super membership status with CREL. Both the mini consortium and super membership are described in the next section. We have such an arrangement with Air Products, Conoco, Sasol and Statoil for the high pressure slurry bubble column work. MEMC has also been a super member in supporting the sonification project. We are currently seeking members to form **a mini-consortium for advancing the knowledge and understanding of the gas-solid riser**. Resources in this project are leveraged by CREL participation in the Multiphase Fluid Dynamic Consortium (MFDRC) which is funded by Department of Energy Office of Industrial Technology (DOE-OIT) and industry. We are, as well, looking for partners for our reactive-catalytic distillation initiative. CREL would like to extend our current rate based models and develop an experimental facility for rapid testing and scale-up of the combined catalytic reactor-distillation concept. **Interested CREL sponsors should approach us immediately.** Finally, we are looking for companies interested in supporting research in organic liquid oxidation. In this area we have received three Praxair patents and equipment of which we have notified our sponsors. The donated patens and facility relate to a technology called Liquid Oxidation Reactor (LOR), a reaction process system that can benefit the production of aromatic acids, especially terephthalic acid. The patents improve LOR aromatic acids production by switching from air as the oxidant in the process to oxygen. The equipment and process technology covered by the patents allow safe and efficient use of oxygen in the reactions. We are currently seeking members to form a mini-consortium to advance the understanding, know-how and design of LOR processes using the donated LOR facility and CREL advanced measurement techniques.

CREL INDUSTRIAL PARTICIPATION PLAN

The Chemical Reaction Engineering Laboratory (CREL) at Washington University is a unique academic organization that pools industrial resources for needed long-term fundamental research in reaction engineering, conducts such fundamental research and transfers the results to industrial practice. CREL provides broad and in depth reaction engineering education and training both to students and industrial practitioners. CREL makes it possible for industrial sponsors to take a long term view and participate in the development of new ideas, methods and techniques. **By pooling industrial resources together with governmental funding CREL offers unique and attractive opportunities for leveraging of company resources. Both systematic long term studies via students' theses and contract work for sponsors are pursued.**

CREL's objectives are:

1. To advance the reaction engineering methodology in scale-up, design and trouble shooting of multiphase reactors through basic research of the key phenomena and achieve environmentally acceptable processes. Areas of interest to CREL's industrial sponsors are given special consideration.
2. To educate students and produce new reaction engineers.
3. To develop and verify reliable experimental techniques for measurement of various fluid dynamic parameters in multiphase reactors such as velocity, holdup distribution, turbulence, bubble sizes, heat transfer, etc.
4. To utilize reliable measured data in verification of Computational Fluid Dynamic (CFD) models for multiphase reactor systems.
5. To implement and modify reaction engineering methodology for new emerging technologies in order to speed up the commercialization of bench scale data.
6. To develop and maintain close ties with industry.
7. To utilize state-of-the-art control theory, expert systems and artificial intelligence and advance their applications in reaction engineering.
8. To transfer academic research to industrial practice by bridging the gap between academic research and industrial applications.
9. To provide unique educational and contract services in all of the above areas to our industrial sponsors.
10. To offer access to sponsors to the unique experimental facilities for studies of multiphase systems (e.g. CARPT-CT, optical probe, tracer techniques, etc.) and to provide assistance in utilizing CREL developed models/simulations and with the multiphase flow model simulators (CFDLIB).
11. To offer training to our sponsors.
12. To be of service to industry and community.

In order to accomplish the above objectives CREL relies on industrial partnerships described in Figure 1.

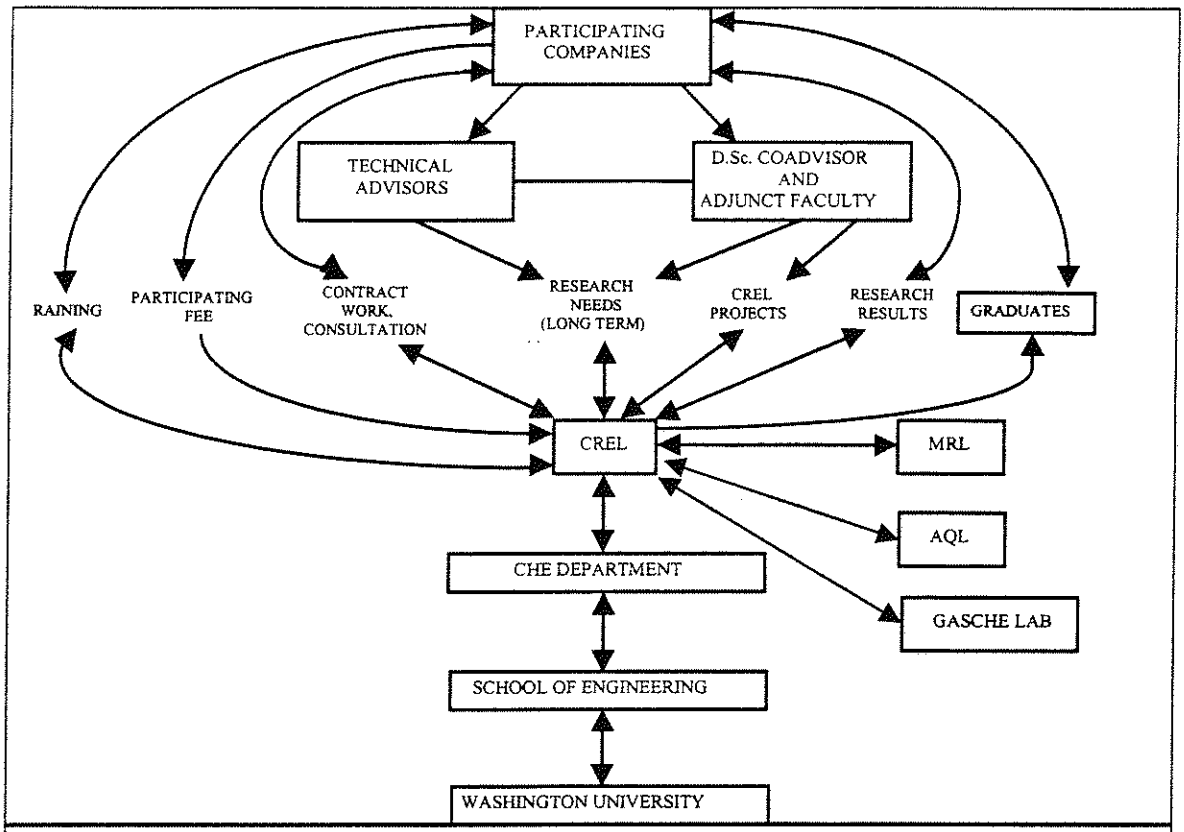

FIGURE 1: CREL Modus Operandi

Industrial organizations can become members of the CREL industrial consortium which we call participating companies by one of the following two means: regular or super membership.

Industrial organizations become regular participants in the CREL consortium by paying the annual participating fee of $20,000/year for which they are invoiced in the December-January time frame. Becoming a regular CREL sponsor entitles the company to appoint one or more technical advisors, as appropriate, for the following interaction avenues with CREL:

i) Technical advisors to CREL review CREL's activities, attend its annual meeting and distribute its annual technical research report to their colleagues. They generate ideas for needed long term research projects and pass this on to the CREL director. CREL doctoral thesis projects are selected from this pool of ideas. The technical advisor from the company, whose idea was selected for thesis work, becomes the student's thesis co-advisor and adjunct faculty member. The CREL projects supported by the fees of regular CREL members and by the federal agencies produce research results which are shared immediately with all the sponsors and then later on via theses and publications with the general public. Participating companies have the option of having students execute part of their research on their premises and

certainly have the best opportunity to hire these individuals upon completion of their degrees.

ii) CREL does provide consulting and contract work only for participating companies. The nature and results of this work are kept proprietary, and the reports are only given to the sponsoring company. It is the task of technical advisors to identify areas in which CREL can contribute to their company via contract work. CREL's unique experimental facilities are accessible only to participating companies.

iii) CREL also provides education and training in various aspects of reaction engineering for industrial sponsors, either at Washington University or on companies' premises.

iv) CREL is always prepared to undertake joint research projects with industrial sponsors with or without federal funding.

Industrial organizations become super members of CREL by paying the annual participating fee of $50,000/year or higher, depending on the scope of work, with three year guaranteed minimum. Super membership, in addition to the interaction avenues described as i) through iv) above, guarantees a D.Sc. (or M.S.) thesis on the topic of direct interest to them with some selected results to be protected by proprietary agreements. The representative of the super member company is appointed as graduate student co-advisor and adjunct faculty member. Research can be conducted at CREL or at company premises.

Both regular and super members have the rights and privileges of joining mini consortia developed for in-depth study of special topics of interest to some companies. The fees for the consortia vary and are determined in consultation with company representatives and depend on the scope and magnitude of the project and work to be done.

Since CREL's major products are research results, technical and scientific consultations, recommendations and graduates, industry is the main customer for these products (Figure 2), **the CREL industrial participation plan provides a unique opportunity for industry to affect the products it is about to receive.**

Benefits to participating companies are many and are not limited to:

- leveraging of industrial resources by having CREL execute needed research with government funding,
- some free consultation on CREL premises,
- providing input to CREL long term research,
- early review of CREL research results and graduates,
- opportunity to gain rights to CREL results, expertise and discoveries,
- having an input for selection for CREL future thesis projects,

- opportunity to co-advise D.Sc. students and serve on D.Sc. thesis committees as adjunct faculty,
- opportunity to subcontract work to proven university personnel,
- having CREL personnel available for short and long term contract work and consultation,
- opportunity to do joint research with CREL,
- having access to unique facilities,
- educational and training courses provided by CREL,
- access and recruitment of high quality graduates.

The regular annual CREL participation fee is **$20,000** which is paid upon an invoice. This entitles the participating company to all the benefits described above. As mentioned above, 'super member' status can be achieved by sponsoring a project for three years at a **$50,000/year** level or higher. In addition to the general benefits described above, the super member status assures a close collaborative effort between the sponsor and CREL. It assures the sponsor of timely research results of direct interest to them and allows some selected results to be protected by proprietary agreements.

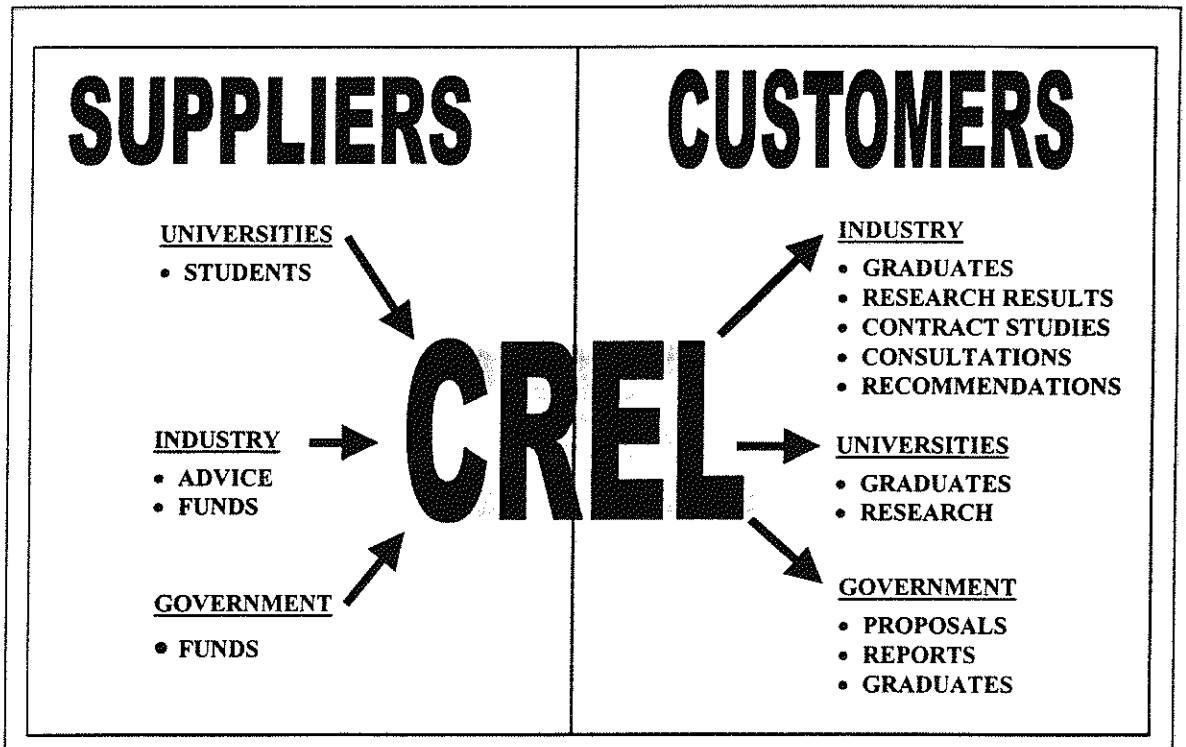

FIGURE 2: Customer-supplier Relationship for a Typical University Laboratory like CREL.

INDUSTRIAL SPONSORS DURING 1999/2000

ABB LUMMUS

AIR PRODUCTS

BAYER

CHEVRON

CONOCO

DUPONT

ELF ATOCHEM

EXXON

ICI - SYNETIX

IFP

INTEVEP

MEMC

MITSUBISHI

MOBIL

MONSANTO

PRAXAIR

SASOL

SHELL

SOLUTIA

STATOIL

UNION CARBIDE

UOP

CURRENT STAFF
1999/2000

During the period covered by this report (June 1, 1999 through May 31, 2000) the following individuals have been associated with the various projects in CREL.

A. Faculty

Dr. M.H. Al-Dahhan, Assistant Professor and Associate Director, CREL
Dr. M. Chang, Adjunct Professor, Exxon
Dr. M. Colakyan, Adjunct Professor, Union Carbide
Dr. M.P. Dudukovic', The Laura and William Jens Professor and Director, CREL
Dr. H. Erk, Adjunct Professor, MEMC Electronic Materials
Dr. B. Joseph, Edward C. Dicke Professor
Dr. W.R. Knox, Adjunct Professor, Consultant
Dr. S. Kumar, Adjunct Professor, UOP
Dr. F. Larachi, Adjunct Professor, Laval University, Canada
Dr. P.L. Mills, Adjunct Professor, DuPont
Dr. R. Mudde, Adjunct Professor, Delft University, The Netherlands
Dr. N. Papayannakos, Adjunct Professor, NTU, Greece
Dr. P.A. Ramachandran, Professor
Dr. V. Ranade, Adjunct Professor, National Chemical Laboratory, India
Dr. B. Toseland, Adjunct Professor, Air Products and Chemicals
Dr. J.R. Turner, Assistant Professor

B. Research Staff

Dr. A. Kemoun, Senior Research Associate
Dr. J. Lee, Research Associate, Chungbuk National University, S. Korea
Dr. Y. Pan, Research Associate
Dr. Y. Wu, Research Associate, Wuhan Institute of Chemical Technology, China
N. Durosier, Visiting Researcher, France

C. Graduate Students

J. Alvare	Y. Jiang	R. Smith
K. Balakrishnan	B. C. Ong	J. Weng
G. Bhatia	N. Rados	J. Xu
P. Cheng	A. Rammohan	Z. Xu
P. Gupta	S. Roy	

A. Undergraduate Students

J. Mettes (undergraduate – Chemical Engineering Dept., Washington University)
D. Magnuski (Undergraduate –Chemical Engineering Dept., Washington University)
D. Cook (Undergraduate – Chemical Engineering Dept., Washington University)
D. Newton (Undergraduate – Chemical Engineering Dept., Washington University)
B.T. Ong (Visiting Undergraduate Student – University of Singapore)

T. Westover, Northwest High School – Solutia-NSF STAR Program (Students and Teachers as Research Scientists Program)

A. Chen (Undergraduate – Chemical Engineering Dept., Washington University)

C. Weigand (Undergraduate – Chemical Engineering Dept., Washington University)

INDUSTRIAL ADVISORY BOARD
1999/2000

NOTE: The full addresses of the members are listed in Appendix A.

B. Toseland	–	Air Products
F. Dautzenberg	–	ABB Lummus
L. Mleczko	–	Bayer
K. Werner	–	Bayer
K. Parimi	–	Chevron
D. Jack	–	Conoco
H. Wright	–	Conoco
P. Mills	–	DuPont
T. Lieb	–	DuPont
R. Bernard	–	Elf Aquitaine
J. Bousquet	–	Elf Atochem
M. Chang	–	Exxon
R. Garton	–	Exxon
H. Stitt	–	ICI – Synetix
C. Boyer	–	IFP
C.G. Dassori	–	Intevep
H. Erk	–	MEMC
T. Ishikawa	–	Mitsubishi
G. H. Ko	–	Mitsubishi
F. Krambeck	–	Mobil
R. Kahney	–	Monsanto
E. Sall	–	Monsanto
J. Sweeney	–	Praxair
W. Williams	–	Praxair
B. Jager	–	Sasol
P.A. Nelson	–	Shell
L. Paul	–	Shell
H. Bhombal	–	Solutia
A. Grislingas	–	Statoil
D. Schanke	–	Statoil
M. Colakyan	–	Union Carbide
A. Oroskar	–	UOP
S. Kumar	–	UOP
W. Knox	–	Consultant

TABLE OF CONTENTS OF THE FULL CREL 1999/2000 REPORT

SUMMARY OF CREL MAIN ACTIVITIES

CREL research activities, achievements and funding during the period from June 1, 1999 through May 31, 2000, are briefly summarized below. Previous CREL research achievements are summarized in Appendix B.

1. CREL RESEARCH ACTIVITIES

Research activities in CREL continued in the following areas:

I. Multiphase reactors and systems.

A. Experimental techniques and models.
B. Computational fluid dynamics (CFD) and computational reaction engineering.
C. Novel reactors and technologies for biochemical and environmentally benign processing.

II. Preparation of new materials.

III. Process monitoring and control.

The broad spectrum of CREL activity is schematically presented in Figure 3. The underlying theme of all our research is the improved understanding and quantification of transport-kinetic interactions in reaction systems using modeling, CFD and experimentation. We are convinced that this knowledge will lead to safer, faster, more economical reactor selection, scale-up and design, environmental benign processes, and improved reactor control. Here we briefly summarize the highlights of each of the above areas leaving it to the individual projects to describe the specific objectives and accomplishments. ***Results of contract research work are not reported here.***

I. MULTIPHASE REACTORS AND SYSTEMS

The main goals of projects in progress are:

i) to further develop our novel experimental techniques (CARPT-CT) and other tools (optical probes, tracer technique via conductivity measurements, pressure fluctuation and pressure drop via differential pressure transducers, CCD camera, etc.) for measurement of flow, mixing and density profiles in multiphase systems;

ii) to use first principles in the development of hydrodynamic and reactor models and verify such models with carefully planned experiments.

Our long-term objective is to establish a unique facility for noninvasive monitoring of multiphase systems and to develop the best possible software for reactor modeling based on firm hydrodynamic principles. At the same time, our students invent and investigate novel reactor types for application to environmental, biochemical and materials processing problems. Our research efforts in the multiphase reactors area can be broadly divided into the three categories which cover: A) experimental techniques and models, B) computational fluid dynamics (CFD) and computational reaction engineering, and C) novel reactors and technologies for environmentally benign processing.

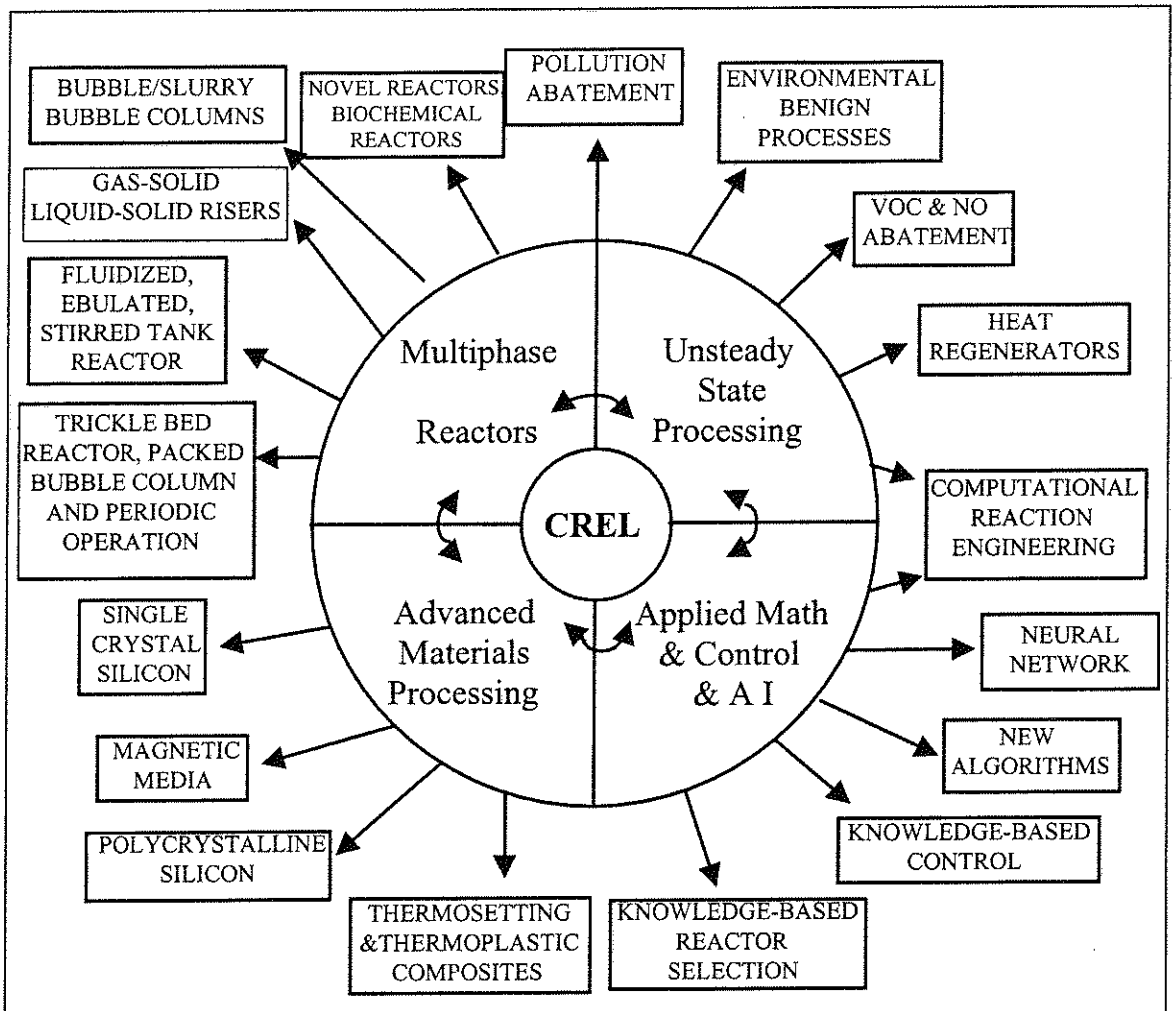

FIGURE 3: Schematic Representation of CREL Activities

A. Experimental Techniques and Models

The main activities of the past twelve months can be summarized as follows:

- Our unique facility for computer assisted radioactive particle tracking (CARPT) has been further improved. The developed Monte Carlo based simulation programs have been verified for accurate and efficient CARPT calibration **(Y. Yang, P. Gupta, A. Kemoun).** Work is in progress to improve the CARPT calibration in stainless steel high pressure bubble column. Wavelet filtering has been applied to CARPT data. Previously, satisfactory comparison was obtained between CARPT and particle image velocimetry (PIV), heat pulse anemometry (HPA), laser doppler anemometry (LDA) and hot wire anemometry (HWA).

- Our unique computed tomography (CT) facility has been utilized to quantify the density profile in various cross sections of our test bubble columns, fluidized beds and liquid-solid risers of various diameters and to investigate the effect of spargers in bubble columns. **(N. Rados, B. Ong, A. Kemoun, Y. Wu)**

- The CARPT/CT facility was also used to complete a number of proprietary contract studies in various opaque multiphase systems. **(A. Kemoun, Y. Wu)**

- The implementation of CARPT/CT in high pressure bubble/slurry bubble column is in progress. This facility will be used to investigate the effect of high pressure and gas velocity on the hydrodynamics of bubble/slurry bubble columns in an attempt to advance the methodology of scale-up and design of these reactors. **(A. Kemoun, N. Rados, B. Ong)**

- A new high-pressure 6" bubble/slurry bubble column facility has been developed which is equipped with ports for probes (e.g., optical and conductivity probes and differential pressure transducers, etc.) and 6 windows along the column. The experimental investigations that will be conducted on this facility and the obtained findings will complement the information obtained by CARPT/CT **(N. Rados, A. Kemoun)**

- For the first time, CARPT has been implemented in a single-phase stirred tank reactor to characterize its mixing and flow pattern. The verification of CARPT results via comparison with the published results has been conducted. These attempts represent the first steps in using CARPT to characterize mixing in multiphase stirred tank reactors with opaque systems where other advanced diagnostics techniques cannot be used. **(A. Rammohan, A. Kemoun)**

- The installation of the 6 inch in diameter and about 30 feet tall gas-solid riser donated to CREL by DuPont has been completed. The project was sponsored by Sandia National Laboratory and Chevron as a part of the Multiphase Fluid

Dynamics Research Consortium Program (MFDRC). Advanced and portable CARPT/CT systems will be developed for gas-solid riser and for other multiphase flow applications. **(S. Roy, F. Larachi, A. Kemoun)**

- The installation of the 18 inch in diameter and 12 feet high ebullated bed has been completed. The facility can be operated as gas-liquid bubble column liquid-solid fluidized bed, gas-liquid-solid ebullated bed and slurry bubble column. **(S. Picker)**

- A phenomenological two-phase cross-flow model with recycle, which accounts for interphase mass transfer and bubble coalescence and breakage, has been extended to describe gas phase mixing. The model will be further improved by accounting for the variation in gas holdup along the reactor due to reaction. **(P. Gupta)**

- Monte Carlo based simulation programs have been developed and verified experimentally in a small tank to accurately and efficiently generate the 3D position-counts calibration maps for CARPT. This results in 3-4 orders of magnitude reduction in time and effort required to calibrate CARPT. The work is in progress to verify the simulation experimentally in high pressure bubble column. **(P. Gupta, A. Kemoun, A. Rammohan)**

- A new algorithm has been developed to filter the conductivity measurements for liquid tracer data obtained by conductivity probe in gas-liquid turbulent flows. The conductivity measurements are used to characterize the mixing in churn turbulent flow regime via tracer experiments. **(P. Gupta)**

- The gas holdup distribution in a counter-current trayed bubble column has been investigated via CT. **(A. Kemoun, N. Rados)**

- The effects of sparger design on the gas-holdup distribution in churn-turbulent bubble column have been investigated using CT technique **(B.C. Ong, N. Rados, A. Kemoun)**

- The developed single and two-bubble class gas-liquid recirculation models have been applied to interpret the gas phase tracer data obtained in the pilot plant scale slurry bubble column at the Alternative Fuels Development Unit (AFDU), LaPorte, Texas. **(P. Gupta, B.C. Ong)**

- Correlations have been developed to predict the time-averaged gas holdup and liquid recirculation profiles in bubble column **(Y. Wu, B.C. Ong)**

- Hydrodynamics study (e.g. overall gas holdup, pressure drop and mixing) on trayed bubble column has been performed. **(J. Alvare)**

- A model based on a series of N stirred tanks has been developed to predict the performance of countercurrent trayed bubble column. **(N. Durosier)**

- A study of particle motion in packed/ebullated beds using CT and CARPT was conducted. **(J. Chen, N. Rados)**

- A method for estimating the solids circulation rate in a closed-loop circulating fluidized bed has been developed and implemented. **(S. Roy, A. Kemoun)**

- Theoretical modeling based on Monte Carlo simulation has been developed to assess the accuracy of CARPT implementation on gas-solid riser. **(S. Roy, F. Larachi)**

- The effect of capillary pressure (wetting) on two-phase flow distribution in trickle beds have been examined via statistical characterization of macroscale flow textures in trickle beds. **(Y. Jiang)**

- A three-phase catalytic partial oxidation reaction has been utilized to implement a parallel approach to catalyst and reactor selection for a fine chemicals process. **(Y. Jiang)**

- The drawbacks of the dissolution method used to measure liquid-solid mass transfer coefficient in packed beds operated under low to high pressure have been evaluated experimentally. **(B.T. Ong)**

B. Computational Fluid Dynamics (CFD) and Computational Reaction Engineering

Computational Fluid Dynamics (CFD) and computational reaction engineering continued to receive considerable attention during the past year.

- Computational Fluid Dynamics (CFD) for bubble columns, slurry bubble columns, liquid-solid riser and trickle-bed reactors using CFDLIB and Fluent codes has received significant attention and work is in progress. The simulation results are compared with CARPT, CT and PIV measurements for verification and for closure improving schemes. **(Y. Pan, S. Roy, Y. Jiang, P. Cheng)**

- The Boundary Element Method is used for different problems related to chemical reaction engineering. **(K. Balakrishnan)**

- The concept of osculatory interpolation and its implementation in the method of fundamental solutions are presented. **(K. Balakrishnan)**

C. Novel Reactors and Technologies for Environmentally Benign Processing

- A theoretical and experimental investigation of wood pyrolysis and combustion in batch charcoal kilns have been performed in the Air Quality Lab. **(G. Bhatia)**

- Our unique findings regarding liquid holdup dependence in rotating packed beds (RPB) on operating conditions have resulted in the only available correlation. **(A. Basic´ and M.P. Dudukovic).** Currently we are exploring the potential of using RPBs in clean processing and pollution abatement.

- A reactive catalytic distillation-fully rate based model has been developed. A test reaction is used to investigate the effects of operating conditions on the column dynamics. **(J. Lee)**

- Work has been initiated to study the hydrodynamics of multiphase bioreactors. **(M. Al-Dahhan)**

II. PREPARATION OF NEW MATERIALS

In preparation of new materials we focus on the problems that could profit the most from implementation of reaction engineering principles in handling transport-kinetic interactions. Our goal is the implementation of reaction engineering in such processes in order to speed up scale-up and technology transfer to manufacturing. CREL has always collaborated with the Material Research Laboratory (MRL) in such efforts. In the materials processing area, CREL has traditionally been involved with:

- semiconductor silicon
- high performance composites
- microcapsules and biomaterials

A project on manufacture of carbon fibers in collaboration with our Materials Research Laboratory (MRL) and a project on developing a new encapsulating material and for time release systems with the model describing such release in collaboration with our Biological Transport Laboratory (BTL) have been completed.

- In the semiconductor silicon area CREL (**M.P. Dudukovic, P.A. Ramachandran** and **associates**) developed the first models for the Siemens decomposer for silicon deposition by hydrogen reduction of chlorosilanes, for the Komatsu decomposer and aerosol reactor for silane pyrolysis, and for the fluidized bed for growth of silicon particles via silane pyrolysis. This was followed up by extensive modeling of the Czochralski crystal puller which resulted in suggestions for improved model based control of the process. Finally, with the insight of **H. Erk** a novel design of an acid

etcher for large silicon wafers was developed and implemented. All of the above know-how is available to sponsors.

- The effect of sonification on the fluid boundary layers at the flat solid surface (wafer) has been quantified and the magnitude of mass transfer intensification to and from the surface has been determined. The results of this work would allow to quantify such effect on the reactivity, effectiveness and specificity of aqueous etching and cleaning chemistries commonly used in the electronics materials industry (**R. Smith**).

III. PROCESS MONITORING AND CONTROL - (Professor B. Joseph)

Our advances in understanding of multiphase systems and the implementation of reaction engineering methodology in preparation of new materials are enhanced by coupling them with various techniques for process monitoring which are also needed for control. We are making sure that CREL students get exposed to advances in artificial intelligence, expert systems and computer technology; and we provide them with the opportunities to utilize and modify these by applying them to reactor design and materials preparation.

Our goal is to investigate the potential of various process monitoring techniques in a number of applications and develop the most promising ones into useful engineering tools such as implementation of wavelets in filtering and dynamic matrix control (DMC), implementing on-line model-based quality control on the autoclave process for curing of composites.

2. CREL ACHIEVEMENTS

Graduation

We are proud that four students completed the work required for their doctoral degrees in CREL during the 1999/2000 academic year.

P. Gupta completed the work for his doctoral degree on the modeling of bubble column reactors. He joined Kohler Company in Wisconsin. He still needs to defend his D.Sc. thesis.

Y. Jiang completed the work for his doctoral degree on the flow distribution in trickle bed reactors. He joined Conoco in Ponca City and is expected to defend his thesis in September 2000.

K. Balakrishnan completed the work for his doctoral degree on boundary element method for reaction engineering problems. He joined GE Plastics and is expected to defend his thesis in Fall 2000.

S. Roy completed the work for his doctoral degree on liquid-solid riser. He joined Corning and is expected to defend his thesis in Fall 2000.

Three students successfully defended their doctoral proposals and became doctoral degree candidates. The students are:

B.C. Ong Hydrodynamics of Bubble Columns.

N. Rados Hydrodynamics of Slurry Bubble Columns.

A. Rammohan Hydrodynamics of Stirred Tank Reactors.

CREL Interactions:

CREL continues to maintain close contact with our industrial sponsors and academia all over the world.

- As part of the interaction between CREL and industrial sponsors that we encourage, some of our students and research associates accepted a summer job on companies' premises.

In addition, we are establishing a Curricular Practical Training (CPT) Program with our sponsors. We encourage all our sponsors to participate in this program where the students register for the CPT course and spend a semester in industry working on a project supervised by both faculty member (the student's advisor) as well as industrial supervisor.

Y. Jiang worked during the summer of 1999 at DuPont Engineering.

K. Balakrishnan worked during the Fall of 1999 at Monsanto.

Yu Pan works closely with the scientists at Exxon Research and Engineering on computational fluid dynamics and during 1999/2000 he frequently visited their premises.

P. Gupta and **P. Cheng** participated during 1999/2000 in the radioactive tracer experiments on the AFDU at LaPorte, Texas.

Previously, we had the following students who took industrial summer jobs:

P. Gupta participated during the week of April 11, 1998 in the radioactive tracer experiments on the AFDU at La Porte, Texas as part of a joint effort among DOE, Air Products, Shell and Washington University.

Sairam Potaraju worked during the summer (May-August 1998) at Solutia, Houston.

S. Kumar, **J. Chen**, and **P. Gupta** spent a week in Summer 1996 at Exxon, Florham Park, NJ.

S. Degaleesan joined Exxon, New Jersey for the Summer of 1994.

P. Gupta joined MEMC Electronic Materials, St. Peters, Missouri, for the Summer of 1995.

S. Karur joined Upjohn, Michigan for the Summer of 1995.

M. Khadilkar joined Union Carbide, Charleston, for the Summer of 1995.

S. Kumar joined Amoco, Chicago for the Summer of 1994.

B. Zou joined Monsanto Enviro-Chem for the Summer and Fall of 1995.

- CREL has also developed strong links with nationally and internationally recognized groups in multiphase flow and reactors and intends to further strengthen such links with
  - **Dr. H. Van Den Akker**, Kramers Laboratorium at Delft University, Holland
  - **Dr. R. Mudde**, Kramers Laboratorium at Delft University, Holland
  - **Dr. R. Krishna**, University of Amsterdam, Holland
  - **Dr. H. Svendsen**, Trondheim Institute of Technology of the University of Norway, Trondheim, Norway
  - **Dr. G. Eigenberger**, University of Dortmund, Germany
  - **Dr. A. Lubbert**, University of Hannover, Germany
  - **Dr. P. Silveston**, Waterloo University, Canada
  - **Dr. R. Lange**, Martin-Luther University, Germany
  - **Dr. F. Larachi**, Laval University, Canada
  - **Dr. J. Chaouki**, Ecole Polytechnic, Canada
  - **Dr. J.C. Charpentier**, CPE-Lyon, France
  - **Dr. Kashiwa**, Los Alamos National Laboratory
  - **Dr. L.-S. Fan**, Ohio State University
  - **Dr. S. Subbiah** and **Dr. Jay Sanyal**, Fluent
  - **Dr. Kim Shollenberg, Dr. Tim O'Hern** and **Dr. John Torczynski,** Sandia National Laboratories
  - **Dr. A. Laurent**, Nancy, France
  - **Dr. J. Grace**, University of British Columbia, Canada

- **Dr. R. Westerterp,** Twente University, Holland
- **Dr. V. Ranade**, National Chemical Laboratory, Pune, India
- **Dr. N. Papayannakos,** National Technical University of Athens, Greece
- **Dr. Fernandez Sevilla**, University of Almeria, Spain
- **Dr. E. Molina Grima**, University of Almeria, Spain

Strengthening of these relationships through work on joint projects and exchange of personnel is being sought.

- CREL has a unique relationship with the Los Alamos group that develops multiphase flow algorithms and codes which are part of the Computational Fluid Dynamics Library (CFDLIB). Our interactions are primarily with **Dr. B. Kashiwa** who is instrumental in getting to us the latest versions of their powerful codes while we test them and try to adopt them for process applications involving multiphase reactors.
- CREL has an excellent cooperation with Fluent which allows us to utilize and test Fluent Computational Fluid Dynamics codes for multiphase flow. An article describing CREL interactions with Fluent entitled "Understanding Multiphase Flows in Bubble Column" was published in FLUENT NEWS – Newsletter, Vol. 7, Issue 2, Fall/Winter 1998. Our interactions are with **Dr. Subbiah** and **Dr. Jay Sanyal.**
- CREL has also instituted collaboration with **Dr. V. Ranade**, from National Chemical Laboratory – India, on the computational fluid dynamics for stirred tank reactors.
- CREL interactions with **Dr. Mudde** of Delft University, Holland have resulted in developing 4 points optical probe to measure bubble size distributions and bubble rise velocity in bubble/slurry bubble columns.
- CREL interactions with **Dr. F. Larachi** have covered several activities which include gas-solid riser, trickle bed reactor modeling and neural network modeling for monitoring the radioactive particle in-situ and for further improvement of CARPT measurements, particularly for the gas-solid riser.
- CREL has initiated since summer 1999 fruitful interactions with **Dr. ~~Niekos~~ Papayanakos** on trickle bed reactors and catalyst development for industrial wastewater treatment.
- CREL is also delighted to have had new visiting scientists and students during the past year. These visitors are trained in various aspects of reaction engineering by participating in different active research projects with our graduate students and research associates.

  Y. Wu, Wuhan Institute of Chemical Technology, China. Yuanxin was involved on high pressure slurry bubble column, trickle bed reactors and rotating packed bed. He was with us between 1992 and 1995 and then visited again in 1999.

  N. Durosier, Elf Atochem, France. Works on modeling of trayed bubble columns.

- **CREL Visitors**

  As part of CREL interactions with industry and academia, we were fortunate to have distinguished visitors during 1999/2000:

  - **Dr. B. Toseland**, Air Products and Chemicals, visited CREL a few times for interactions on the CREL-Air Products-DOE project during the 1999/2000 period.
  - **Dr. In Seon Yoon**, S&K – South Korea, visited CREL on May 11 and 12, 2000.
  - **Dr. Joshua Sweeney**, Praxair, visited CREL several times during the 1999/2000 period.
  - **V. D'Amico** and **Dr. K. Sundaram**, ABB Lummus, visited CREL on April 20-24.
  - **Dr. Dan Driscoll**, DOE, visited CREL on April 26, 2000.
  - **Dr. Bousquet** and **Dr. Bernard**, Elf, visited CREL on March 26, 2000.
  - **Dr. H. Bhombal**, **Managers and High Level Researchers** from Solutia, visited CREL on March 24, 2000.
  - **C. Bizjak**, ABB Lummus, visited CREL on March 16, 2000.
  - **Dr. T. Cartolano**, Air Products and Chemicals, visited CREL on January 11 and 12, 2000.
  - **Dr. Halger T. Glatzer**, Germany, visited CREL on February 12, 2000.
  - **Dr. Ashok Dhingra**, Director of Technology Transfer – DuPont, visited CREL on January 13, 2000.
  - **Suyichi Oguro**, JGC – Japan, visited CREL on December 10, 1999.
  - **Monsanto Managers and Researchers** visited CREL on September 29, 1999.
  - **Dr. F. Dautzenberg**, ABB Lummus, visited CREL on August 31, 1999.
  - **Larry Smith**, CR&L, visited CREL on August 31, 1999.
  - **Dr. R. Ybarra**, University of Missouri – Rolla, visited CREL on September 13, 1999.
  - **B. Hazeltine**, Monsanto-Florida, visited CREL on July 15, 1999.
  - On October 22, 1999 as part of the review meeting, the following attendees have visited CREL:
    - **Dr. B. Toseland**, Air Products and Chemicals, USA
    - **Drs. D. Jack** and **H. Wright**, Conoco, USA
    - **Dr. T. Leib**, DuPont Engineering, USA
    - **Dr. B. Jager**, Sasol, South
    - **D. Sanaes**, Statoil, Norway
  - **Prof. N. Peppas**, Purdue University, visited CREL on September 7, 1999.
  - **Andre Swarts**, Sasol – South Africa, visited CREL during the period of July 5-16, 1999.
  - **Drs. Eric Haupfear, Eric Sall, John Dzenitis**, Monsanto, visited CREL on July 21, 1999.
  - **Dr. C.L. Jenkins** and **N. Courrout**, Elf, visited CREL on June 17, 1999.
  - **Dr. Martin Franke**, **Holger Sequn** and **Shaun Gaus**, Bayer, visited CREL on June 17, 1999.
  - **Dr. N. Papayanakos**, University of Athens, visited CREL during the summer of 1999 on Fullbright Fellowship.
  - **Dr. V. Ranade**, NCL – India, visited CREL during May 2000 for three weeks as a part of the research cooperation between CREL and NCL on stirred tank hydrodynamics.

CREL Research Staff

- CREL is most pleased with our researchers and visiting scientists. They are a group of excellent and dedicated scientists and engineers.

  Dr. Y. Wu, research associate, joined CREL in March 1999. Dr. Wu is Associate Professor at Wuhan Institute of Technology, China. He was a CREL member between 1992 and 1995 and did an outstanding job. Dr. Wu helped to perform the work for the high pressure slurry bubble column and other research activities.

  Dr. Y. Pan joined CREL in April, 1997. He is working on Computational Fluid Dynamics (CFD) in bubble columns related to our DOE contracts.

  Dr. A. Kemoun joined CREL in February 1997. He is instrumental in executing different research contracts. He is also instrumental in implementing CARPT/CT on high pressure bubble/slurry bubble columns and stirred tank reactors.

  Dr. J. Lee from S. Korea, Chungbuk National University, is a key figure in developing reactive catalytic distillation - fully rate based model which will be linked to ASPEN, HYSIS or other data base programs.

  N. Durosier, research assistant, joined CREL in Fall 1999 as visiting engineer from France. She is working on modeling of trayed bubble columns.

- CREL faculty, besides their busy schedules, continue to provide highly qualified services to industry, particularly our sponsors, through consultations and contract work.

- CREL Adjunct Professors, were very helpful in sharing ideas and providing insight regarding various projects and future trends. Their experience and help were invaluable.

CREL Notable Activities

- Professor Dudukovic won the 1999 CCR Malcolm Pruitt award for his outstanding contributions to research progress in the chemical based sciences and engineering through mutually beneficial interactions among the industrial, academic and government research.

- CREL has obtained three patents donated by Praxair on utilizing liquid oxidation reactor (LOR) for terephthalic acid production. CREL is trying to establish a consortium, which is open to all CREL members, to advance the LOR technology and its industrial applications.

- CREL is forming a mini-consortium to advance the understanding and knowledge of gas-solid riser for better design and scale-up. The consortium is currently sponsored by Chevron and DOE and it is open to all CREL members. The consortium is part of the MFRDC consortium sponsored by DOE-OTI and industry which includes a number of universities.

- Professor Dudukovic delivered a keynote address at the IFP International Conference on Chemical Reactors: From Mockup to Industrial Reactors: Diagnostic Methods, December 8-9, 1999, France. The title of the talk was "Opaque Multiphase Reactors: Experimentation and Modeling".

- The fifth year has been successfully completed of the DOE subcontract for a five year period ($1,475,000) which has been officially awarded via Air Products on April 2, 1995 for slurry bubble columns experimental investigations and fundamental hydrodynamics modeling. The results will be in the public domain eventually but CREL sponsors will have an early preview of this work. This represents a significant potential for leveraging of sponsor's resources.
- The DOE subcontract via Air Products on hydrodynamics of slurry bubble columns has been extended for two years (~ $650,000).
- The first year has been successfully completed for the high pressure slurry bubble column consortium sponsored by Air Products and Chemicals (USA), Conoco (USA), Sasol (South Africa) and Statoil (Norway) for the hydrodynamics and modeling studies of high pressure slurry bubble column reactors. CREL is cooperating with Ohio State University (Dr. L.-S. Fan). Consortium membership is $50,000/year for 3 years and is open to additional companies.
- The first year has been successfully completed for the DOE-University Coal Research (UCR) grant for the Advanced Diagnostics Techniques for Three-Phase Slurry Bubble Column Reactors. The total cost of the project is $548,485 for three years (July 1, 1999 – June 30, 2002).
- Dr. M.P. Dudukovic and Dr. M.H. Al-Dahhan received $75,000 from Sandia National Laboratory in addition to $25,000 from Chevron for constructing the gas-solid riser donated by DuPont and for evaluation of CARPT implementation. This work is part of the tasks set for the Multiphase Fluid Dynamics Research Consortium Program (MFDRC).
- CREL in August 1993, has entered in an agreement with Los Alamos and Sandia that provided us with access to excellent CFDLIB multiphase flow codes. Our colleagues at the National laboratories have invested decades of team effort in developing these codes. CREL is entitled to use them to advance both fundamentals and business interests of all American based corporations. As our students and associates get more familiar with these codes we trust that we can put them to good use on problems of interest to our sponsors.
- CREL in January 1998, has entered in an agreement also with Fluent to use and test their Computational Fluid Dynamics Codes. This will advance the fundamentals and the practical use of these codes. Also it provides, along with CFDLIB, great opportunity to our students and researchers to get more familiar with these simulations.
- Y. Jiang won the 1999 Outstanding Chemical Engineering Graduate Student Award.
- M. Muether, NSF Young Scholar, won the 1999 Rueben and Gladys Flora Charitable Trust Award for excellence in research for the work done under the direction of Dr. Al-Dahhan on the hydrodynamics of trayed bubble column.

- No other laboratory in the world has the combination of CARPT/CT facility for measurement of instantaneous velocities, turbulence, and backmixing parameters, time averaged circulation patterns and complete voidage (holdup) distribution in multiphase gas-liquid-solid, gas-liquid, liquid-solid and gas-solid systems. This facility remains only available at CREL! We have further improved its accuracy and are currently taking data for verification of fundamental hydrodynamic models as well as for proprietary use by our sponsors.

  The highlights of our CARPT/CT work include:

  i) Wavelet filtering of CARPT data was developed which dramatically improves the accuracy of fluctuating velocities and parameters derived from these.

  ii) First data was taken on slurry, ebulated bed systems, liquid-solid riser, stirred tanks and multiphase bioreactors.

  iii) First data was taken on single phase stirred tank reactor. The goal is to implement CARPT/CT on multiphase systems (opaque systems) in stirred tank reactors.

  iv) CARPT results have been successfully compared with other techniques such as HPA, HWA, LDA, PIV.

  v) Monte Carlo based simulation programs have been developed and verified to accurately and efficiently generate 3D position-counts calibration maps for CARPT calibration. This results in reduction in time and effort of at least 3-4 order of magnitude.

  Other highlights include:

  - High pressure/high capacity – 6 inch diameter bubble/slurry bubble column facility was installed and utilized with CARPT and CT.

    iii) Another high pressure 6" diameter bubble/slurry bubble column was designed, constructed and tested. The column was equipped with ports and windows along its height (9 ft) to be used for optical probes, dynamic pressure transducers, conductivity probes, etc.

  - Work on trayed bubble column is in progress.
  - Reactive and catalytic distillation – fully rate based model is developed.
  - A novel algorithm was developed for steep moving fronts such as encountered in fixed beds operated in a cyclic mode.
  - High pressure periodic operation of trickle-bed reactor facilities, as well as a phenomenological model to predict the reactor performance under induced pulsing, were developed. The facility is equipped to measure liquid-solid mass transfer coefficients via both electrochemical and dissolution methods.
  - The research activities in pollution abatement and clean processing are progressing well.

Invited Lectures

- A number of invited lectures and presentations have been presented by CREL faculty at several universities and industrial companies.
  - Hydrodynamics of Bubble Column Reactors", Al-Dahhan, M.H., "Praxair, New York, March (2000).
  - "Modeling of Reactive Distillation", M.P. Dudukovic, CCR Meeting on Multifunctional Reactors, Marco's Island, FL, June 13-15 (1999).
  - "Modern Approach to Reaction Engineering", M.P. Dudukovic, General Electric Plastics, Mount Vernon, IN, June 25 (1999.
  - "Slurry Bubble Column Hydrodynamics", M.P. Dudukovic, DOE Fossil Energy Clean Fuels Meeting, Cincinnati, OH, September 22 (1999).
  - "Scale-up in Reaction Engineering", M.P. Dudukovic, Air Products, Allentown, PA, October 6 (1999).
  - "Trickle-Bed Reactors", M.P. Dudukovic, DuPont, Beaumont, TX, November 8 (1999).
  - "Tracer Methods", M.P. Dudukovic, International Atomic Energy Commission, Vienna, Austria, November 22 (1999).
  - "Opaque Multiphase Reactors: Experimentation, Modeling and Troubleshooting", M.P. Dudukovic, Institute Francais du Petrole (IFP) Scientific Meeting, December 8-9 (1999).
  - "CARPT Studies of Bubble Columns", M.P. Dudukovic, 3rd IMUST Conference, Santa Barbara, CA, March 13-15 (2000)
  - "CARPT Studies of Gas-Solid Risers", M.P. Dudukovic, MFDRC Meeting, Sandia, Albuquerque, NM, April 12-14 (2000).
  - "Reaction Engineering, The Environment: Pollution Prevention and Sustainable Development", M.P. Dudukovic, National Science Foundation, Washington, DC, April 17 (2000).
  - "Distributor Effects on Gas Holdup Profiles in Bubble Columns", M.P. Dudukovic, Sandia National Laboratory, Albuquerque, NM, May 9 (2000).
  - "Bubble Column Hydrodynamics", M.P. Dudukovic, Air Products, Allentown, PA, May 24 (2000).
  - "CFD Modeling of Multiphase Flow Distribution in Catalytic Packed Bed Reactors: Scale-Down Issues", M.P. Dudukovic, 3rd International Symposium on Catalysis in Multiphase Reactors (CAMURE 3), Naples, Italy, May 29-31 (2000).
  - "A Parallel Approach to Catalyst and Reactor Selection for a Fine Chemicals Process", M.P. Dudukovic, 3rd International Symposium on Catalysis in Multiphase Reactors (CAMURE 3), Naples, Italy, May 29-31 (2000).

3. CREL PRODUCTIVITY AND FUNDING

Research activities of Professors M.P. Dudukovic´ and M.H. Al-Dahhan are totally channeled through CREL, while Professors J. Turner and P.A. Ramachandran do so partly. CREL cooperates with Professor B. Joseph on some of his activities. Hence, it is fair to say that CREL has the equivalent of 3 full-time faculty. We continue to report on various productivity measures of CREL such as degrees granted per year, number of graduate students and postdoctoral associates involved in research, and journal publications per year.

Table 1: CREL PRODUCTIVITY

DOCTORAL DEGREES GRANTED FOR WORK IN CREL:

1998-99	4	M. Khadilkar	Trickle-Bed Reactor Performance
		Z. Xu	Photocatalytic Distillation
		S. Highfill (M.S.)	Liquid-Solid Mass Transfer in Trickle Beds
		M. Roveda (M.S.)	Ozonation of Water Impurities
1997-98	1	S. Degaleesan	Fluid Dynamics of Bubble Columns
1996-97	5	M. Kulkarni	Simulation of Unsteady State Processes
		K. Kumar (M.S.)	Evaluation of Metal Peroxides for Bioremediation
		K. Ng (M.S.)	Roterfilter for Gas Purification
		B. Sannaes	Slurry Bubble Columns (D.Sc. at University of Trondheim)
		Q. Wang (M.S.)	Bubble Columns
1995-96	5	S. Karur	Computation Chemical Reaction Engineering
		S. Limtrakul	Gas/Liquid/Solid Fluidized Beds
		R. Shepard	Long Carbon Fiber Manufacture (Jointly with MRL)
		P. Mathias	Material and Model for Release from a Brittle Matrix Due to Osmotically-Induced Surface Erosion (Jointly with BTL)
		M. Thomas	On-Line Model Based Quality Control for Curing of Composites
1994-95	3	S. Kumar	Bubble Columns
		S. Palavajjhala	Wavelet in Process Control
		H. Vedam (M.S.)	Controller Design
1993-94	3	M. Al-Dahhan	Trickle Beds
		J. Turner	Pollution Abatement
		J. Vasat	Composites (Jointly With MRL)
1992-93	2	A. Basic	Rotating Packed Bed
		H. Erk	Phase Change Regenerators
1991-92	6	P. Hanratty	Expert Systems-Reactors
		V. Kalthod	Bio-Reactors
		S. Pirooz	Plasma Reactors
		D. Shieh	Data Acquisition/Control
		J. Zhou	Microencapsulation
		B.S. Zou	Transient Micro Reactor

NUMBER OF CREL GRADUATE STUDENTS (RESEARCH ASSOCIATES):

YEAR	91/92	92/93	93/94	94/95	95/96	96/97	97/98	98/99	99/00
Number	13(2)	12(6)	13(5)	15(5)	19(6)	16(10)	14(9)	16(7)	14(5)

CONTRIBUTIONS TO LITERATURE (1990-99):

YEAR	90	91	92	93	94	95	96	97	98	99
CREL Journal Publications	19	5	14	6	12	11	22	19	13	13
CREL Presentations in Conferences	6	5	13	7	13	31	20	22	25	15

The last five years of CREL funding of graduate students is summarized in Table 2. ***(Contract work funded by individual sponsors is not shown).*** We hope to sustain this funding since fundamental work should continue and, in addition, CREL can provide needed high quality services at low cost. Hence, we expect continued industrial support. We hope that our funding from federal agencies will remain steady as we capitalize on the fully operational CARPT-CT facility.

TABLE 2: CREL FUNDING (EXCLUDING CONTRACTS)

YEAR	91/92	92/93	93/94	94/95	95/96	96/97	97/98	98/99	99/00
Industrial Fees	227,500	227,500	213,000	192,000	180,000	230,000	230,000	260,000	~300,000
Industrial Foundations					20,000	35,000	20,000	5,000	-
Industrial Grants - MEMC						50,000	50,000	50,000	-
Exxon - for high pressure slurry bubble column facility							98,000		
Air Products, Conoco, Sasol and Statoil, High Pressure Slurry Bubble Column Consortium grant								200,000	200,000
NSF	96,358	158,800	160,000	80,000		40,000	40,000	40,000	-
DOE-Air Products			40,000	353,000	518,000	365,000	385,000	283,000	~300,000
DOE-UCR and Air Products Cost Sharing									87,667
TOTALS	323,858	386,300	413,000	625,000	718,000	720,000	823,000	838,000	887,667

The 1999 CREL Annual Industrial Meeting

CREL has successfully organized the annual meeting on October 21, 1999 for industrial participants jointly with the Gasche laboratory. More than 41 industrial participants from 29 companies (ABB Lummus, Air Products & Chemicals, AVL North America, Bayer Corporation, Chevron, Conoco, CR&L, DuPont, Eastman Chemical, Exxon, Exxon Chemical, Fluent, ICI – Synetix, IFP, MEMC, Mobil Technology, Monsanto, Ohio State University, Praxair, Reaction Design, Rubicon, Sandia National Laboratories, Sasol, Science Applications International Corp., Solutia, Statoil, UOP, US Department of Energy, Union Carbide) attended the meeting. The agenda included plenary lectures, poster session, industrial perspective, lab tours and Ad-Hoc discussions – all of which were very well received. Table 3 lists the presentations and posters that were presented during this extraordinary occasion.

Announcement: This year (2000), the CREL annual industrial meeting will be held on October 19 (Thursday). The meeting for the high pressure slurry bubble column consortium will be held on October 20 (Friday). Please, mark your calendars.

1999 CREL ANNUAL MEETING GATHERING

The CREL Annual Meeting '2000' will be held on October 12th instead of October 19th.
The meeting for the high pressure slurry bubble column consortium will be held on October 13th instead of the 20th.

1998 CREL ANNUAL MEETING POSTER SESSION

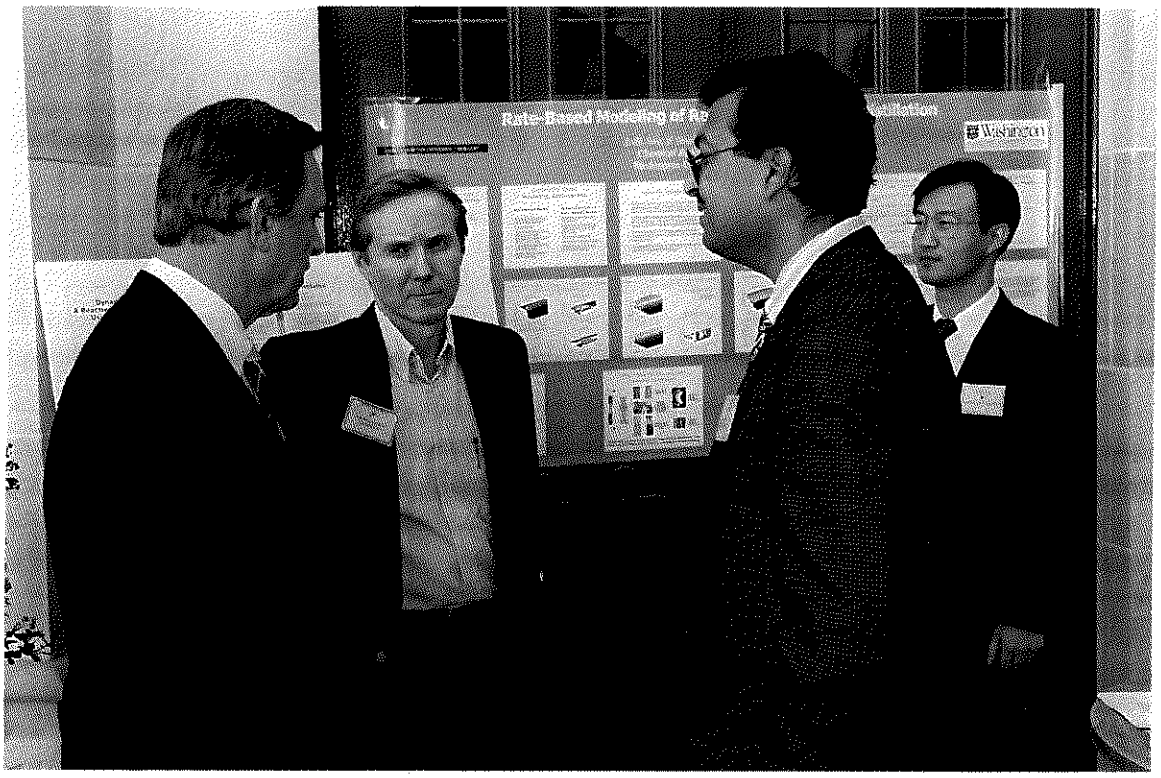

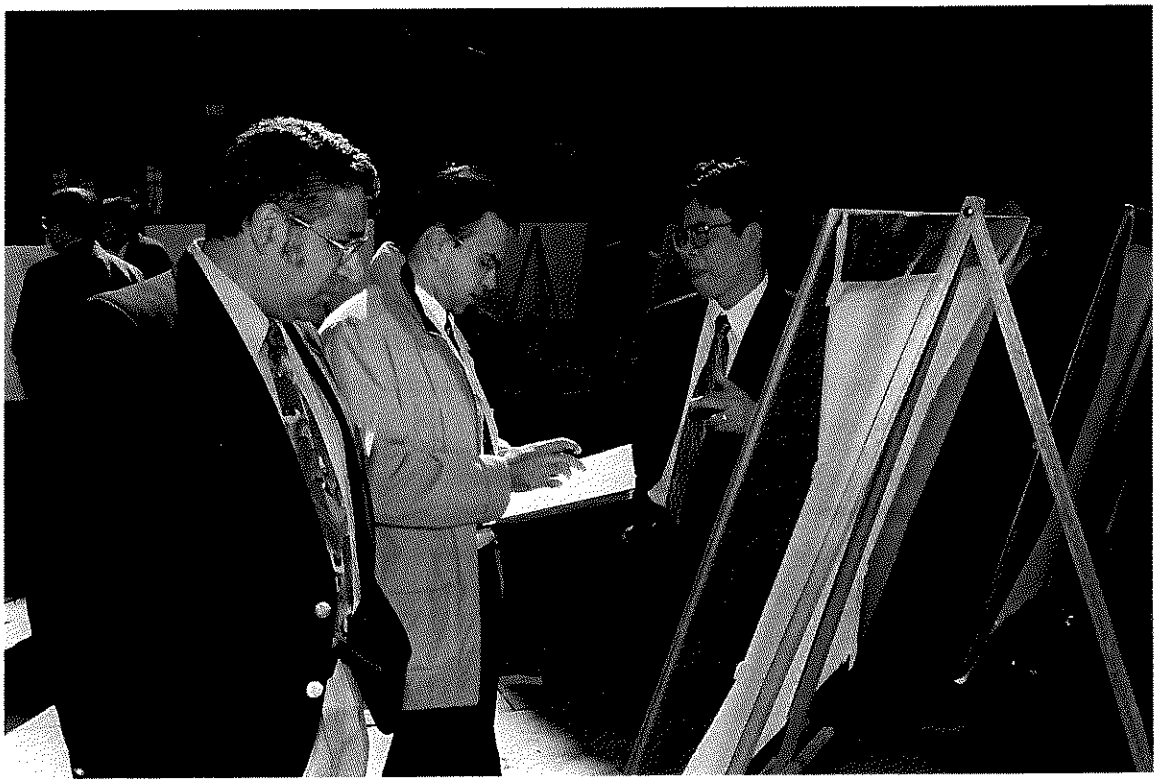

TABLE 3: 1999 CREL ANNUAL MEETING PRESENTATIONS LIST

PRESENTATIONS

1. CREL Overview - **M.P. Dudukovic**
2. Reactor Modeling of Churn-Turbulent Bubble Column - **Puneet Gupta**
3. Flow Mapping and Modeling of Liquid-Solid Risers - **Shantanu Roy**

POSTERS

1. High Pressure Bubble Column - **Abdenour Kemoun**
2. Distributor Effects on Gas Holdup - **B. Ong**
3. Prediction of Gas Holdup Profiles in Bubble Columns – **Y. Wu**
4. Prediction of Axial Liquid Velocity Profiles in Bubble Columns – **Y. Wu**
5. Hydrodynamic Measurements in a Slurry Bubble Column - **Novica Rados**
6. Gas Holdup in Trayed Bubble Columns – **T. Alvare**
7. Numerical Simulation of the Flow in 2D Bubble Columns Using Fluent – **P. Cheng**
8. Dynamic Simulation of Bubble Column – **Y. Pan**
9. Monte Carlo Simulation of Radiation Emissions – Radioactive Particle Tracking in Multiphase Flow - **P. Gupta**
10. Study of Particle Motion in Packed/Ebullated Beds by CT and CARPT – **Novica Rados**
11. Flow Mapping in a Gas-Solid Riser via CARPT – **R. Dodson**
12. Characterization of Single Phase Flow in a Stirred Tank Reactor (STR) Using CARPT - **A. Rammohan**
13. Statistical Characterization of Two Phase Flow Distribution in Trickle Beds - **Y. Jiang**
14. Mixing-Cell Network Model Development – **Y. Jiang**
15. Current Status and Future Direction of Packed-Beds Research at CREL – **Y. Jiang**

16. Dynamics of Catalyst Pellets Under Periodic Operation – **B. Balakrishnan**

17. Dynamic Simulation of a Reactive Distillation Tray Column Using a Rate-Based Model – **J.H. Lee**

18. A New Method for Determining Gas Diffusivities in Complex Porous Media Using TAP Pulse Response Experiment – **S. Shekhtman**

19. A New Method for Determining the Number of Active Sites on Complex Catalysts Using TAP Pulse Response Experiment – **G. Yablonsky**

20. Wood Pyrolosis: Modeling and Experiments – **G. Bhatia**

21. Advanced Design of Photobioreactors: Integration of Fluid Dynamics and Cell Illumination History – **M. Al-Dahhan**

22. Modeling and Control of Composite Materials Manufacturing Processes – **S. Potaraju**

23. Simulation of the Thermo-oxidative Stabilization Process During the Continuous Manufacture of PAN-Based Carbon Fibers - **R.-M. Liao**

4. CREL FUTURE DIRECTIONS

We will continue to work on developing a scientific base for an improved multiphase reactor methodology and understanding for scale-up/scale-down and design and on providing service to our sponsors.

Our goal for the next few years is to maintain a balanced experimental and computational approach to studies of multiphase reactors.

On the experimental side we want to:

i) extend our unique CARPT/CT data base to high pressure systems and for this purpose we have developed a high pressure facility in CREL.

ii) extend CARPT-CT data base to new reactor types such as gas-solid riser stirred tanks, ebullated beds, moving beds, slurry systems and multiphase bioreactors and bioprocessing.

iii) augment the experimental base with techniques for bubble size distribution and other measurements.

On the computational side we are determined to develop the best closure schemes utilization of the two fluid model based codes for multiphase systems.

Our research on improved unsteady state processing, environmentally friendly processes, novel reactors and multiphase bioreactors will continue.

In addition, we actively seek to participate with industrial partners in new process development efforts.

CREL EXPERIMENTAL FACILITIES

We enclose here only a brief description of the available unique experimental facilities at CREL in order to encourage our sponsors to use them on joint projects or for contract work. The main facilities consist of:

- **Computer Automated Radioactive Particle Tracking (CARPT)**

  This is a unique facility for monitoring velocity profiles and backmixing parameters of solids and/or liquids in gas-liquid, gas-solid, liquid-solid and gas-liquid-solid systems. CARPT is used for model verification, cold modeling, scale-up, evaluation of distributors and column internals on flow profiles.

- **Computed Tomographic Scanner (CT)**

  This is a unique facility for evaluation of three dimensional density profiles in composites and in three phase reactors. CT is used in cold modeling, scale-up, examination of the effect of internals, etc.

  Highlight: CARPT/CT facilities are unique for studying the hydrodynamics of opaque multiphase systems which is not accessible by other means. No other laboratory in the world has such a combination. These experimental systems are versatile in the sense that they are capable of providing experimental data over a wide range of operating conditions, and they provide data not only on the local scale but also over the entire domain of the flow. Together the two techniques are capable of acquiring information for the complete description of the flow in a time average sense, with CARPT providing instantaneous velocities as well. In addition, these systems can be extended for measurements at high pressure and temperatures. **Only CARPT/CT have the capabilities of providing data in multiphase systems at very high holdups of the dispersed phase i.e. systems that are opaque.**

- **Optical Probes and Dynamic Pressure Transducers**

  Four points optical probe and its data acquisition system have been acquired from Delft University to measure bubble size distribution and bubble rise velocity in bubble/slurry bubble columns. Low to high pressure differential pressure and absolute pressure transducers (Validyne) and data acquisition systems have been acquired and used for pressure fluctuations measurements and for obtaining overall gas holdup via pressure difference measurements in bubble/slurry columns. The range of the pressure measurements of these transducers can be adjusted over a wide range.

- **Bubble/ Slurry Bubble Columns Laboratories**

* **Low Pressure Bubble /Slurry Bubble Columns Laboratories**

  Different acrylic column sizes (1 inch to 18 inch diameters) and distributors are available for various hydrodynamics studies using CARPT/CT, tracer methods, pressure transducers, etc. The 18 inch diameter column can be equipped with internals (16 tubes of 1 inch diameter) which simulate the heat exchangers.

* **High Pressure Bubble /Slurry Bubble Column Laboratory**

  A high pressure 6 inch diameter bubble/slurry bubble column facility has been developed. The high pressure setup can be operated at pressure up to 175 psig at air superficial velocity of up to 50 cm/s. Two columns of 6 inch diameter and 9 ft height have been developed to characterize the hydrodynamics of high pressure bubble/slurry bubble columns. One is for conducting CARPT/CT experiments and the other is equipped with ports and windows along its height (9 ft) for probes (e.g., optical probes, conductivity probes, heat transfer probes, etc.) and pressure transducer measurements.

* **Pilot Plant Scale Set-Up for Bubble/Slurry Bubble Columns and Ebullated Beds Studies**

  A pilot plant scale set-up consisting of an 18 inch diameter 12 foot high column has been developed to characterize the hydrodynamics of bubble/slurry bubble columns. The set-up can be operated for upflow of gas and liquid as well as for liquid as a batch and gas in continuous upflow. The facility can be operated at high capacity of liquid (up to 160 GPM) and of gas. The reactor can be utilized to study the hydrodynamics of bubble column/slurry bubble column, ebullated bed and liquid-solid fluidized bed (gas holdup, pressure drops and fluctuation, liquid mixing, bubble size distribution and bubble rise velocity, etc. measurements can be performed).

- **2D Bubble Column**

  2D bubble column is available to investigate its hydrodynamics using CCD imaging camera.

- **Liquid-Solid Riser Facility**

  Six inch 9 ft high liquid-solid riser facility is available for hydrodynamics studies. CARPT/CT and other measurements techniques are utilized for such investigations.

- **Gas-Solid Riser**

  A six inch diameter, 30 foot tall gas-solid riser has been installed. This is the newest addition to CREL facilities. CARPT-CT studies are being performed. Figure 1 shows a schematic diagram of the riser.

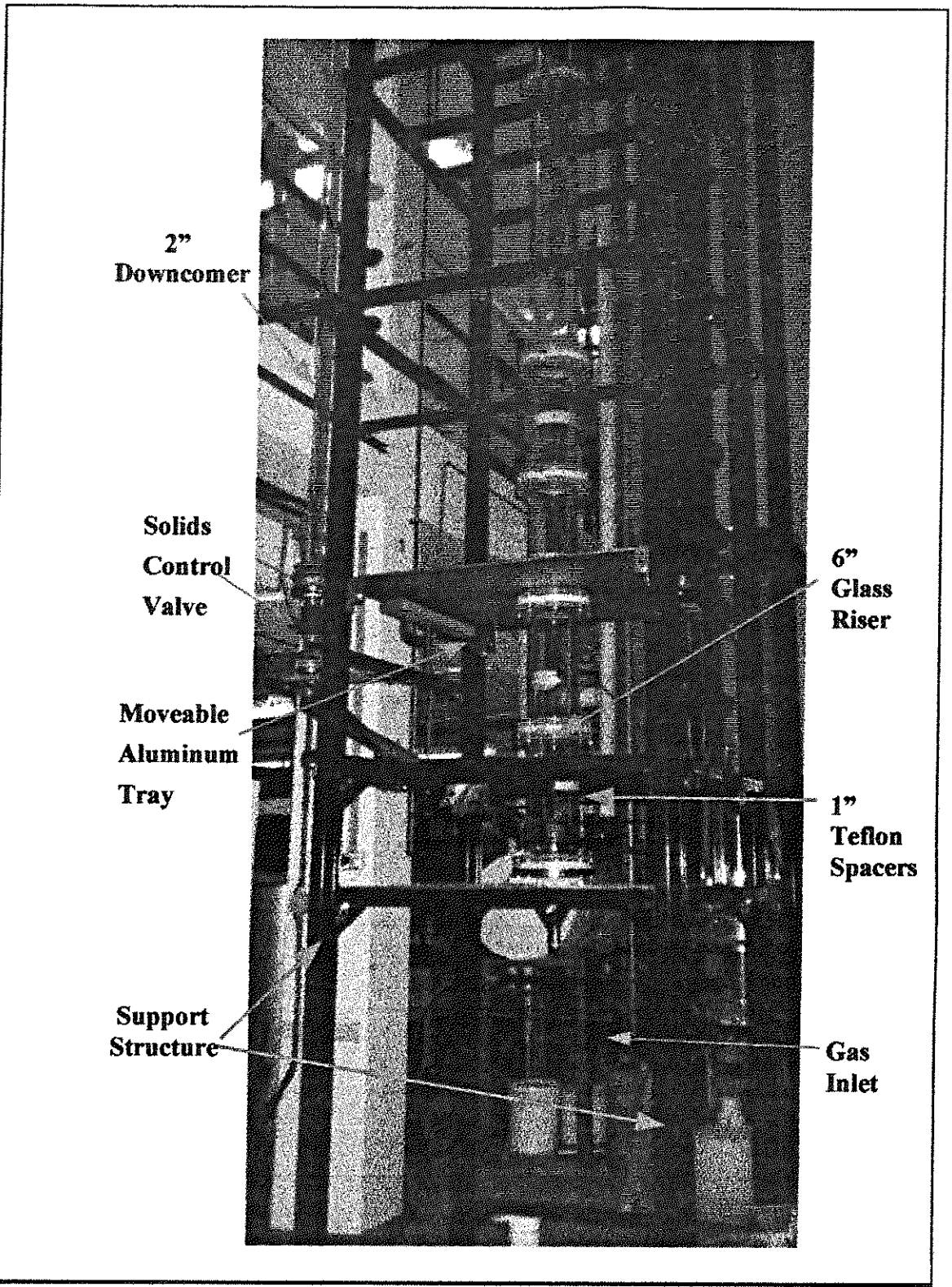

FIGURE 1: CREL gas-solids riser

- **Trickle-Bed Reactor (TBR) Laboratory**

  This laboratory consists of high pressure, atmospheric and high temperature facilities for studies of reactions, hydrodynamic parameters and catalyst wetting efficiency. The high pressure trickle-bed reactor facility can be operated up to 1000 psig and can accommodate different reactor sizes. Currently it consists of 1/2", 3/4", 1", and 2" I.D. 0.57m and 1m long high pressure trickle-bed reactors (where one of them has an optically clear section-12 inches in length), gas and liquid delivery systems, and an on-line tracer analytical unit (differential refractometer) for tracer experiments. This facility is flexible enough to perform widely different investigations from low (atmospheric) to high pressure (70 atm). High temperature operation is possible in the stainless steel reactor without the optically clear section. Liquid holdup and pressure drop are measured in situ. The facility is also equipped with the periodic operation set-up option.

  The atmospheric pressure trickle-bed reactors facility consist of 1 inch, 3 inch and 5-5/8 inch diameter reactors, gas and liquid delivery systems. These reactors have several pressure transducers along the bed to detect flow regime transition. Pressure drop via pressure transducer, and holdup via load cells, are measured. The unit is currently equipped with periodic operation set-up.

  Electrochemical and dissolution techniques are developed to measure liquid-solid mass transfer coefficient in high pressure trickle bed reactors.

  An additional high temperature packed-bed facility consists of 1 inch stainless steel reactor mounted in a high temperature cabinet, and temperature controller. This unit is currently used to support tracer and reaction experiments by purifying the solvents and activate the catalyst. All trickle-bed facilities are interfaced with a portable and user friendly data acquisition system.

- **CREL-XYTEL Unit (XYCREL)**

  This unit is a laboratory-scale reactor system which can be used for a variety of multiphase reaction studies. It consists of two separate systems which can be operated in parallel or combined into a single system. Each system can deliver up to five gases to the reactor zone. One system is designed for atmospheric pressure studies; the second system can handle pressures up to 60 atm. Three heated saturators are also integrated into the gas delivery lines. Virtually any reactor of choice can be inserted into the reactor zone; available equipment include two furnaces (maximum temperature 2000° F) and a liquid feed pump. Analytical equipment includes two dual-column gas chromatographs equipped with TCD detectors (both GCs) and FID detectors (one GC). Samples are injected on-line using gas sampling valves; the configuration can be easily rearranged to permit multidimensional GC analysis. Data acquisition and control hardware is interfaced using a dedicated 386 PC running a Visual Basic Program developed specifically for the CREL-XYTEL unit.

- **Rotating Packed Bed (RPB)**

  Rotating gas-liquid contactor is a device in which centrifugal force is employed as an adjustable drive for flow of liquid through a porous medium countercurrently to gas which is driven by pressure difference. The rotating porous medium, or the rotating packed bed (RPB), can be viewed as centrifugal analog of conventional packed beds with, however, much higher mass transfer rates.

  The device is equipped with transducers to measure pressure drop across the rotor and with electrodes spaced in radial and axial direction to measure liquid holdup.

- **Slurry and Basket Reactors**

  Autoclave (1 liter) and atmospheric/high temperature (2 liters) slurry and basket reactors systems for kinetics studies and catalyst evaluation are available.

- **Ozonation Reactor Set-Up**

  A flexible ozonation reactor set-up equipped with ozone generator for studies of waste water oxidation is available.

- **Hydrodynamic Measurement Techniques**

  Besides CARPT/CT, CREL is equipped with various hydrodynamics measurement techniques such as, heat pulse anemometry (HPA), optical probes (reflectance and transmittance), CCD camera , heat transfer probe, tracer techniques, dynamic pressure transducers, etc.

- **Analytical Equipment**

  Gas Chromatographs (TCD, FID, PID and ELCD detectors) with auto sampling, Differential Refractometer, Mass Spectrometer, Atomic Absorption Spectrophotometry, UV/VIS Spectrometer, FI-IR Infrared Spectrometer, Ph meter, Dissolved Oxygen meter, Ozonator, Fume Hoods, Shaking Table, Magnetic Stirrers, High Accuracy Electronic Scale, Ovens, Refrigerator.

  A brief description of some of the above experimental facilities follows. More detailed information is available upon request.

Brief Description of CARPT/CT Facility

- **COMPUTER AUTOMATED RADIOACTIVE PARTICLE TRACKING (CARPT)**

In the CARPT facility a single radioactive particle of size and density designed to match the properties of the phase to be traced (solids in gas or liquid fluidized beds, liquid in gas-liquid bubble columns) is introduced into the flow. Instantaneous particle position is identified by the simultaneous monitoring of the radiation intensities received at a set of NaI detectors located strategically around the column. The technique therefore is somewhat analogous to emission tomography. For a given operating condition of the flow, the particle motion is continuously tracked for long periods of time. Pre-established calibration curves for radiation intensity versus distance for each detector are then used in a linear regression scheme to determine the position of the particle at each sampling instant. Time differentiation of this position data yields instantaneous velocities and accelerations of the particle. To infer the flow field from this, the flow domain is divided into a set of compartments and the calculated instantaneous velocities are assigned to the compartment in which the particle resides at that instant of time. Each compartment ultimately has a large number of such assignments corresponding to the data collected over the period of investigations during which the system is operated at steady state. Invoking the ergodic hypothesis an ensemble average of all such velocities in a compartment yields the average velocity for each of the compartments in the flow. The instantaneous and time averaged velocities can then be used to determine various turbulence parameters of interest. Existence of stationary state has been shown by obtaining the same ensemble average when all or part of the collected data is utilized. In addition, from the number of particle occurrence in various regions of the flow one can obtain information concerning the flow stagnancies. It is the only technique that maps the flow field over the entire domain and provides particle Lagrangian velocities. The schematic of the CARPT facility is shown in Figure. 2a. Scandium 46 at 250 μ Ci activity and a half life of 84 days is used as the source of radiation. The system incorporates 32 NaI scintillation detectors and the signals from these detectors can be sampled and processed simultaneously at frequencies up to 500 Hz.

- **COMPUTED TOMOGRAPHIC SCANNER (CT)**

The tomographic scanner at CREL (Figure 2b) uses the third generation scanning configuration, in which an array of collimated detectors are arranged in an arc at the center of which is the source of radiation. The whole assembly of the detectors and the source are mounted on a gantry that is capable of being rotated about the axis of the test section through a stepper motor interfaced to a host computer. The source used is an encapsulated 100 mCi Cesium-137 isotope. The encapsulation is such that it provides a fan beam subtending an angle of 40° in the horizontal plane. The source has been further collimated using a 20 x 10 x 10 cm lead brick with a central slit such

that the emerging beam has a thickness of 6.5 mm at a distance of 28 cm from the source. It was necessary to use the same 2" x 2" NaI detectors that are used in the CARPT facility due to economic considerations. The arc in which the detectors were set, has a radius of 92.33 cm. This radius was necessary to accommodate test sections as large as 45 cm in diameter. Given this radius and the size of the detectors only eleven of them could be accommodated in the fan beam arc of 40°. If one were to use the system in this configuration there would be only eleven chordal transmittance measurements (with the number going down as the size of the test section reduces) leading not only to a coarse spatial resolution, but also to severe aliasing according to signal sampling considerations. Using a novel approach the number of detectors in the arc was effectively increased by making use of a collimator, which for a given view moves across the detector arc, so that each detector samples multiple rays, each of which is unique. However, the price that is paid is in the form of increased scan time (the scan time increases in proportion to the number of additional rays sampled by a detector). The movement of the collimator is effected by another independent stepper motor, also interfaced with the host computer. The collimator made of lead is 6.35 cm deep and has a height of 7.62 cm so that the detectors are completely shielded by the collimator. It also has rectangular holes 5 x 10 mm at locations appropriate to each of the detectors for sampling the beams. The whole assembly weighs about 90 kgs and consequently the maximum rotational speed that can be achieved is about 1 rpm. Therefore the voidage distribution that can be obtained can only be a time averaged one. The entire scanning assembly has a central opening large enough for it to translate up and down with respect to the test section. This latter motion is effected by means of four precision square threaded screws supporting the scanning assembly at the corners. They can be driven synchronously to accomplish the axial positioning required for scanning different horizontal sections of the column. The data acquisition system for CT is the same as that for CARPT. However, the acquisition program differs in that it additionally accommodates the software for stepper motor control required for the scanning motions.

The algorithm that is adopted for image reconstruction constitutes a truly unique feature of the scanner. It is conventional for scanners to use for image reconstruction either a Fourier based algorithm such as the Filtered-Back projection, or an algorithm based on the Algebraic Reconstruction Technique. However, we have demonstrated that the Estimation-Maximization algorithm based on maximum likelihood principles, results in better reconstructions than any of the others.

Various sizes of bubble /slurry bubble column are used with CARPT/CT facility.

- **THE SIGNAL PROCESSING AND DATA ACQUISITION SYSTEM FOR CARPT AND CT**

γ photons randomly emitted from the source get attenuated in number proportional to the void distribution that the beam encounters as it traverses the test section. Each photon entering the crystal produces a light pulse, which is sensed and amplified by a ten stage photo multiplier tube integrated with the detector. The biasing of the cathodes of the detectors (1000 Volts) is provided by two high voltage power supplies (Canberra, Model 3002D). The voltage pulses are amplified using timing filter amplifiers (Canberra 2111). The amplifiers accept positive or negative current pulses from the detectors and deliver output pulses in the range of $\pm$ 5V range. They have independent adjustments for the differential and integral time constants in their RC-CR circuits. These controls enable one to shorten the tail of the signal pulse and to choose a suitable amplitude, respectively. The power to the amplifiers is fed by NIM/BIN power supplies (Canberra 2000). The signals from the amplifiers are fed to discriminators to eliminate undesired secondary emissions. The threshold for the discriminators is continuously adjustable from 15 mV to 1 V either by a potentiometer on the front panel or by software control. A threshold voltage of 45 mV was found to be adequate for removing most of the secondary emissions. Thus, the discriminator produces a logic pulse corresponding only to those photons depositing their full energy in the detector. The logic pulses are counted directly using a multichannel 24 bit scaler (binary counter). The scaler also carries a temporary buffer corresponding to each channel for storing the accumulated counts. A function generator inputs a sine wave at a known frequency to one of the channels of the scaler as a reference input for error control. A list sequencing crate controller with 8K FIFO (first in - first out) memory serves as a buffer when the contents of the scaler are emptied at user specified sampling rates. When the FIFO memory is half full a CAMAC (Computer Automated Measurement and Control) crate controller transfers its contents to the host computer hard disk via a GPIB (General Purpose Interface Bus (IEEE 488). The transfer from the scalar buffer to the FIFO memory, as well as the transfer from the FIFO memory to the computer memory and later to the hard disk, proceed in parallel with no data loss. The advantage of using CAMAC instead of A/D converters is that it allows a wide range of modular instruments to be interfaced to a standardized crate. The crate has a dataway that provides a pathway between the modules and a host computer. The crate has a number of stations in which different modules (such as scalers, discriminators, etc.) can be inserted. The last two stations of the crate are meant for crate controllers whose purpose is to issue commands to the modules and also transfer information between the modules and the host computer.

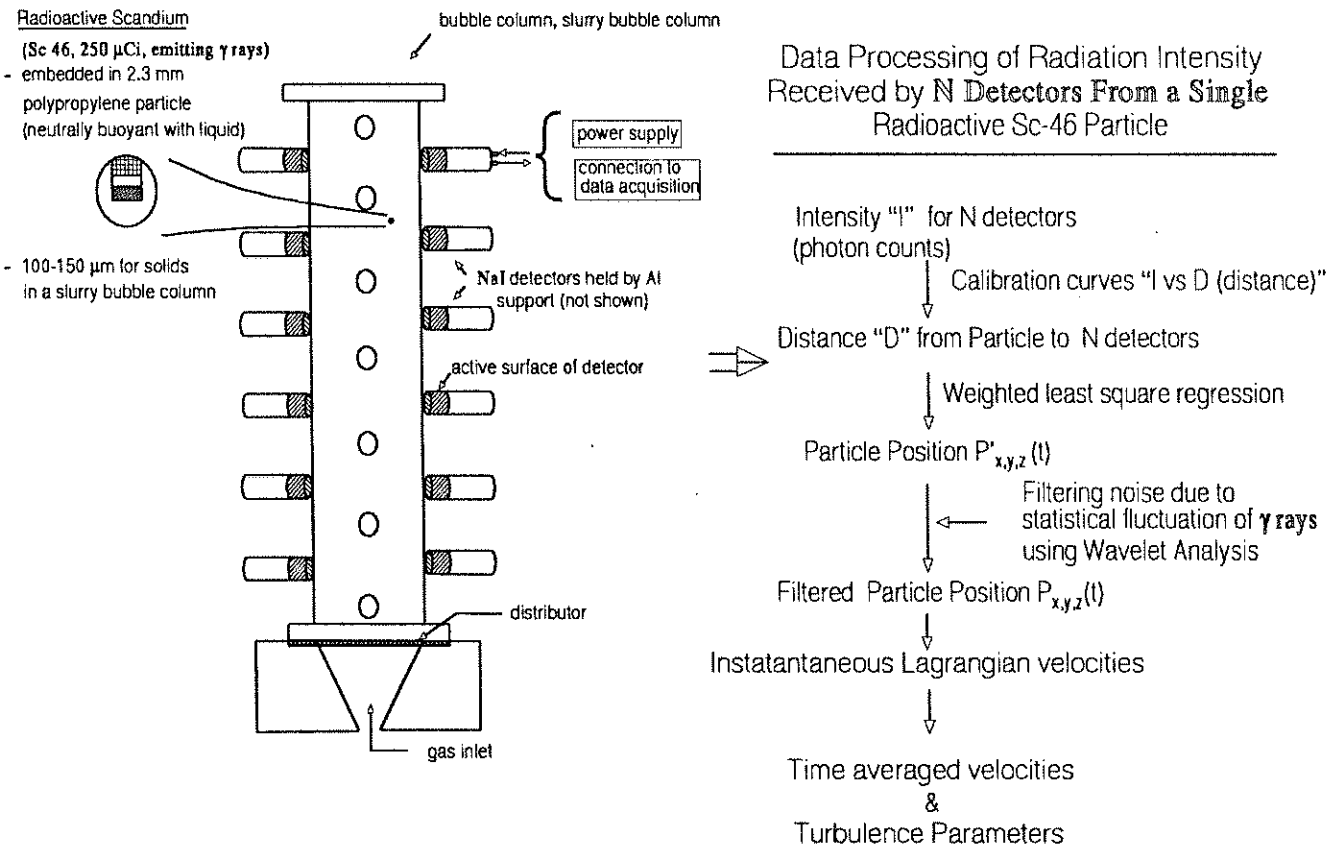

Figure 2(a). Schematic of the Computer Automated Radioactive Particle Tracking (CARPT) Facility

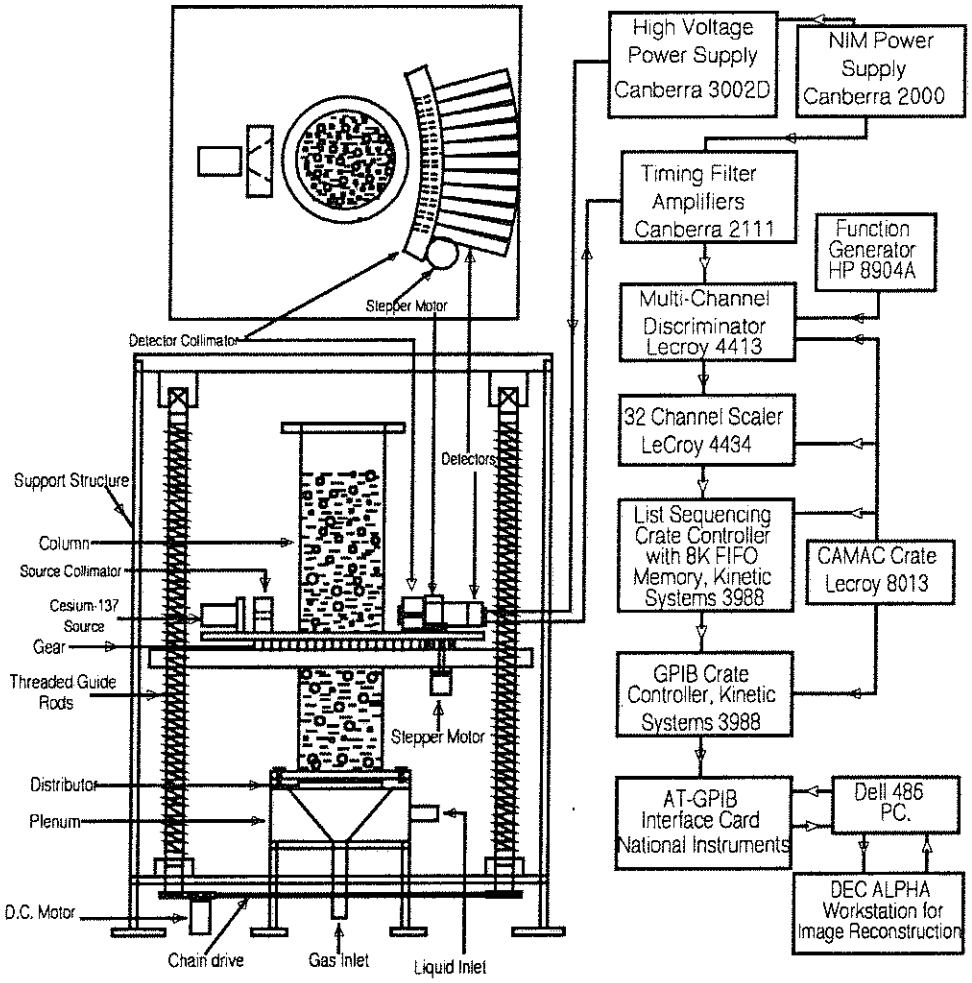

Figure 2(b). Schematic of the CT Scanner

LISTING OF ACTIVE PROJECTS (1999/2000)

Projects active during the period June 1, 1999 through May 31, 2000 are classified into categories of multiphase reactors, preparation of new materials, and process monitoring and control. The working titles of all active projects and graduate students or researchers involved are listed below:

Name **Title: key words**

AREA I. MULTIPHASE REACTORS AND SYSTEMS

A. EXPERIMENTAL TECHNIQUES AND MODELS

A1. Bubble Columns, Slurries, Fluidized Beds, Stirred Tanks

B.C. Ong, N. Rados
(graduate students)

A. Kemoun, Y. Wu
(research associates)

A1-1. Gas Holdup in Bubble Columns at Elevated Pressure via Computed Tomography: The effect of high pressure operation on gas holdup distribution in bubble column has been studied by implementing CT on a 6" diameter stainless steel high pressure bubble column.

S. Degaleesan
(graduate student)

Y. Pan
(research associate)

A1-2. Application of Wavelet Filtering to the Radioactive Particle Tracking Technique (CARPT): A filtering technique based on the wavelet theory has been applied to CARPT to remove the white noise from the acquired data. This reduces the level of noise in the data by 80 to 90%. The suitability and necessity of wavelet filtering are discussed.

B. Ong, N. Rados
(graduate students)

A. Kemoun
(senior research Associate)

A1-3. Analysis of Distributor Effects on Gas Holdup Profiles in Churn-Turbulent Bubble Columns: The effects of sparger design on gas holdup distribution in churn-turbulent bubble columns have been investigated via CT. The results are discussed and presented.

P. Gupta
(graduate student)

A1-4. Comparison of Single and Two-Bubble Class Gas-Liquid Recirculation Models – Application to Pilot Plant Radioactive Tracer Studies During Methanol Synthesis: Single and two-bubble class gas-liquid recirculation models have been developed. These models are applied to interpret the radioactive gas tracer measurements conducted during liquid phase methanol synthesis in a pilot scale slurry bubble column at the Alternative Fuels Development Unit (AFDU), LaPorte, Texas.

P. Gupta, B.C. Ong
(graduate students)

A1.5. Hydrodynamics of Churn Turbulent Bubble Columns: Gas-Liquid Recirculation and Mechanistic Modeling: A phenomenological (mechanistic) model has been developed for describing the gas and liquid/slurry mixing in churn-turbulent bubble columns. Sub-models are developed to estimate the gas and liquid phase recirculation based on the two-fluid approach, using estimated effective bubble diameter and volumetric mass transfer coefficients.

M.H. Al-Dahhan,

M.P. Dudukovic
(faculty)

A1.6. High Pressure Slurry Bubble Column Consortium: A consortium has been formed in 1999 jointly with Ohio State University to advance the knowledge and understanding of the high pressure slurry bubble columns for FT-synthesis and other chemical processes. The consortium is sponsored by Air Products and Chemicals (US), Conoco (US), Sasol (South Africa) and Statoil (Norway) and is open to additional companies.

N. Rados
(graduate student)

A. Kemoun
(senior research associates)

A1-7. Hydrodynamic Measurements in a Slurry Bubble Column: An outline of hydrodynamic measurements in air-water-glass beads slurry bubble column is presented. This represents one of the tasks set for the high pressure slurry bubble column consortium. The results will be reported first to the consortium members and hence only the outline is reported here.

Y. Wu
(research associate)
B.C. Ong
(graduate student)

A1-8. Prediction of Radial Gas Holdup Profiles in Bubble Column Reactors: A correlation has been developed to predict the radial time-averaged gas holdup profiles in bubble columns.

Y. Wu
(research assistant)

A1-9. Prediction of Axial Liquid Velocity Profile in Bubble Columns: A correlation has been developed to predict the time averaged liquid recirculation profile in bubble columns.

A. Kemoun
(senior research assistant)

N. Rados, F. Li
(graduate students)

A1-10. Gas Holdup in Trayed Bubble Columns: The effects of sieve trays on the time-averaged gas holdup profiles and the overall gas holdup have been investigated via CT in a countercurrent trayed cold-flow bubble column scaled-down from a commercial unit.

P. Gupta
(graduate student)

A1-11. A Novel Signal Filtering Methodology for Obtaining Liquid Phase Tracer Responses from Conductivity Probes: A special purpose software filtering techniques has been developed to cleanly extract the actual liquid phase conductance from response signals representing the instantaneous point conductance of a bubbling two-phase gas-liquid mixture.

J. Alvare
(graduate student)

A1-12. Hydrodynamics of Trayed Bubble Columns: The effect of trays and gas sparger design on the overall gas holdup and axial gas holdup profile in a trayed bubble column has been investigated at a range of superficial gas and liquid velocities.

N. Durosier
(visiting researcher)

A1-13. Hydrodynamic Model of a Trayed Bubble Column: A model based on a series of N stirred tanks has been developed to predict the performance of a countercurrent trayed bubble column.

J. Chen
(research associate)

N. Rados
(graduate student)

A1-14. Study of Particle Motion in Packed/Ebullated Beds by CT and CARPT: Computer Tomography (CT) and Computer Automated Radioactive Particle Tracking (CARPT) were used to study the gas phase distribution and the incipient particle motion in a packed/ebullated bed in which gas and liquid are in co-current upflow.

S. Roy
(graduate student)

A. Kemoun
(senior research associate)

A1-15. A Method for Estimating the Solids Circulation Rate in a Closed-Loop Circulating Fluidized Bed: A method for accurately estimating the solids circulation rate in a closed-loop liquid-solid circulating fluidized bed has been developed based on the use of radioactive isotopes for estimating the solids velocity and volume fraction distribution in a chosen section of the circulating fluidized bed.

S. Roy
(graduate student)

A1-16. Optimal Design of Radioactive Particle Tracking Experiments for Flow Mapping in Opaque Multiphase Reactors: Theoretical modeling based on Monte Carlo simulation has been used to describe how the accuracy of radioactive particle tracking set-up may be assessed a priori. A gas-solid riser has been used as an example for such development.

A. Rammohan
(graduate student)

B. Kemoun
(senior research associate)

A1-17. A Lagrangian Description of Flows in Stirred Tanks via Computer Automated Radioactive Particle Tracking (CARPT): CARPT technique has been successfully implemented in single phase stirred tank to investigate its hydrodynamic and to characterize its flow structure. The aim is to apply CARPT in stirred tank reactors (opaque, multiphase systems).

A2. Trickle Beds and Packed Beds

Y. Jiang (graduate student)

A2-1. Statistical Characterization of Macroscale Flow Textures Distribution in Trickle Beds: The effects of capillary pressure (wetting) on two-phase flow distribution in trickle beds have been examined. A relationship between bed structure, particle wetting and flow distribution has been developed.

Y. Jiang (graduate student)

A2-2. A Parallel Approach to Catalyst and Reactor Selection for a Fine Chemicals Process: A three-phase partial oxidation reaction has been utilized to implement the parallel approach of catalyst and reactor selection in the development of a fine chemicals process.

W. Highfill (graduate student)

B.T. Ong (visiting undergraduate student)

A2-3. Drawbacks of the Dissolution Method for the Measurement of Liquid-Solid Mass Transfer Coefficient in Two-Phase Flow Packed Bed Reactors Operated at Low and High Pressures: The drawbacks in utilizing the dissolution method for measuring liquid-solid mass transfer coefficient in packed beds have been characterized and demonstrated experimentally.

N. Papayannakos (visiting faculty)

A2-4. The Effect of Particle Dilution on the Wetting Efficiency and Liquid Film Thickness in Small Trickle Beds: A method is presented to relate the wetting efficiency obtained at different operating conditions and at different laboratories for diluted and non-diluted beds.

B. *COMPUTATIONAL FLUID DYNAMICS AND COMPUTATIONAL REACTION ENGINEERING*

B1. Computational Fluid Dynamics (CFD)

CREL has the access to the multiphase computational fluid dynamics library (CFDLIB) codes developed by the Los Alamos group and to the multiphase computational fluid dynamics codes developed by Fluent. CREL's advanced noninvasive CARPT/CT measurement techniques, as well as other techniques, are used for measuring the important hydrodynamic parameters to verify various closure schemes in CFD modeling. Thus, this part is closely interlinked with section A "Experimental Techniques and Models".

P. Chen
(graduate student)

B1-1. Two-Dimensional Axisymmetric Simulation of Gas-Liquid Flow in Cylindrical Bubble Column Reactor by Fluent and Comparison with CARPT/CT Measurements: Fluent codes have been used to simulate the hydrodynamics of bubble columns. The predictions are compared with CARPT/CT data..

Y. Jiang, M. Khadilkar
(graduate students)

B1-2. CFD Modeling of Multiphase Flow Distribution in Catalytic Packed-Bed Reactors: Scale Down Issues: K-fluid model has been applied to simulate the gas and liquid holdup distribution and their velocity field in the bench-scale trickle-bed reactors. The effect of periodic liquid-feed model on the liquid holdup distribution has been examined.

B2. Computational Reaction Engineering

P.A. Ramachandran
(faculty)

B2-1. Computational Reaction Engineering: Suitable mathematical methods are investigated for a number of problems in reactor modeling and materials preparation.

K. Balakrishnan
(graduate student)

B2-2. Osculatory Interpolation in the Method of Fundamental Solutions for Non-Linear Poisson Problems: The concept of osculatory interpolation and its implementation in the method of fundamental solution for nonlinear poisson problems with uniform and mixed boundary conditions are presented.

C. *NOVEL REACTORS AND TECHNOLOGIES FOR ENVIRONMENTALLY BENIGN PROCESSING*

J. Turner
(faculty)

C1. Air Quality Engineering: A new research area which addresses the interface between reaction engineering, air quality, and public policy is introduced.

G. Bhatia
(graduate student)

C2. Kinetic Parameter Estimation for a Refined Scheme for Biomass Pyrolysis Differentiating Organic and Inorganic Gases: An improved reaction scheme for biomass pyrolysis has been proposed. The proposed kinetic scheme lumps the products of wood pyrolysis into char (solid residue), tar (liquid residue), organic gases and inorganic gases.

M.P. Dudukovic
(faculty)

C3. **Rotating Packed Beds:** The potential of using rotating packed beds in industrial processes and waste treatment is outlined.

J. Lee
(research associate)

C4. **Dynamic Simulation of a Tray Column for Multicomponent Reactive Distillation Using a Rate-Based Model:** A reactive catalytic distillation-fully rate based model is developed. A test reaction is used to investigate the effects of operating conditions on the column dynamics.

A. Kemoun
(senior research associate)

J. Fernandez
(visiting faculty)

C5. **CARPT Applied to the Analysis of Photobioreactors:** CARPT technique has been applied to describe the cells movement in photobioreactors used for microalgal culture.

AREA II. PREPARATION OF NEW MATERIALS

M.P. Dudukovic,

P.A. Ramachandran
(faculty)

II-1. **Semiconductor Grade Silicon:** CREL know-how reviewed.

AREA III. PROCESS MONITORING AND CONTROL

B. Joseph
(faculty)

III-1. **Process Monitoring and Control:** The activities in process monitoring and control continue in Professor Joseph's control group that is only loosely associated with CREL. At the moment no joint project is being pursued. However, fruitful cooperation existed in the past and can readily be revised if an appropriate topic for investigation is initiated.

REVIEW OF ACTIVE RESEARCH PROJECTS

AREA I: MULTIPHASE REACTORS AND SYSTEMS

Faculty:	M. Al-Dahhan M.P. Dudukovic P.A. Ramachandran J.R. Turner
Adjunct Faculty:	M. Chang, Exxon M. Colakyan, Union Carbide S. Kumar, UOP F. Larachi, Laval University P.L. Mills, DuPont R. Mudde, Delft University N. Papayannakos, NTU V. Ranade, NCL B. Toseland, Air Products Y. Yang, Abbot Labs
Research Associates and Assistants:	A. Kemoun J. Lee Y. Pan Y. Wu N. Durosier
Graduate Students:	K. Balakrishnan G. Bhatia P. Cheng P. Gupta Y. Jiang B. Ong N. Rados A. Rammohan S. Roy J. Weng J. Xu

Professors Dudukovic´, Al-Dahhan, Ramachandran, Turner and their research associates, visitors and graduate students are focusing on improving our basic understanding of multiphase systems and on transferring these improvements into industrial practice.

Our research in multiphase reactor systems covers three broad areas:

A) Experimental techniques and models.
B) Computational fluid dynamics (CFD) and computation reaction engineering.
C) Novel reactors and techniques for environmentally benign processing and for biochemical technology.

We have developed an advanced and unique experimental facility based on Computer Automated Radioactive Particle Tracking (CARPT) for monitoring velocities and fluid dynamics measurement in multiphase systems (gas-liquid-solid, gas-liquid, liquid-solid, gas-solid). We have also developed and implemented, using the same facility, a complete and automated computed tomography (CT) for monitoring density profiles in various cross sections of multiphase systems. CREL is the only laboratory that can perform both density profile and velocity measurement in the whole column! We continue to improve this unique CARPT-CT experimental facility and to utilize it in generating a data bank for verification of two- and three-phase flow models. For this purpose, a new wavelet based filtration algorithm has been introduced which improves the accuracy of turbulent measurements. Monte Carlo simulation based calibration algorithm to calibrate the CARPT facility has been developed and tested. This will enhance the accuracy and minimize the effort needed during CARPT calibration. At the same time we pursue improved models for bubble column, trickle-bed, ebulated bed and fluidized bed reactors.

The work summarized in this report is complemented by additional contract studies with specific applications for individual sponsors. We strive whenever possible to utilize our improved understanding of multiphase systems in facilitating scale-up and introduction of new technologies and processes.

Computational fluid dynamics (CFD) of multiphase reactors and computational reaction engineering continued to receive considerable attention. More detailed simulation of reactors requires improved and efficient mathematical techniques. We lead in adopting boundary element methods for solution of diffusion and reaction problems. A novel algorithm has been developed for steep moving fronts such as encountered in fixed beds operated in a cyclic mode. Improved algorithms for two-phase flow and modeling of periodic operation of trickle-bed reactors have been accomplished.

AREA I: MULTIPHASE REACTORS AND SYSTEMS

A. *EXPERIMENTAL TECHNIQUES AND MODELS*

Our work here focused on the following areas:

i) Development of a unique noninvasive facility for monitoring of phase velocities and density profiles in fluidized beds, bubble columns, slurries, three phase fluidized beds, liquid-solid risers, gas-solid risers and stirred tanks. This facility is invaluable in generating data needed for verification of two and three phase flow models and in cold model studies of new reactor configurations and distributor designs.

ii) Development of the following techniques:

1. Work is in progress to further validate experimentally the developed Monte Carlo simulation programs to generate the 3D positions-counts calibration maps for CARPT calibration.
2. Work is in progress to implement CARPT/CT on multiphase stirred tank reactors.
3. Development of a new algorithm to measure phase distribution in slurry bubble column via CT, CARPT, and pressure drop measurements.
4. 4-points optical probe for measurement of bubble size distribution and bubble rise velocity in bubble/slurry bubble columns.
5. Development of new algorithms for filtering the conductivity probe signals used in the presence of bubbles for tracer method and for measurement of bubble sizes and rise velocities in bubble/slurry bubble columns.
6. Dynamic and absolute pressure drop measurements for holdup measurements and flow regime identification in bubble/slurry bubble column ebulated beds, trayed bubble column.
7. Development of electrochemical method for measurement of liquid-solid mass transfer coefficient and identifying the liquid flow maldistribution in high pressure trickle-bed reactors.

iii) Development of improved models for bubble columns, slurry bubble columns, fluidized beds needed in synfuels production, biotechnology and Fischer Tropsch.

iv) Establishing scale-up and scale-down rules for bubble/slurry bubble columns and trickle-bed reactors. This is aimed at speeding up trouble-shooting and process changes in petroleum, chemicals, and synfuels processing. High pressure periodic operation and a phenomenological model to predict trickle bed performance are developed.

Project summaries are included for:

A1. Bubble Columns, Slurries, Fluidized Beds, Stirred Tanks

A1-1. Gas Holdup in Bubble Columns at Elevated Pressure via Computed Tomography. **(B.C. Ong, N. Rados, A. Kemoun, Y. Wu)**

A1-2. Application of Wavelet Filtering to the Radioactive Particle Tracking Technique (CARPT). **(S. Degaleesan, Y. Pan)**

A1-3. Analysis of Distributor Effects on Gas Holdup Profiles in Churn-Turbulent Bubble Columns. **(B. Ong, N. Rados, A. Kemoun)**

A1-4. Comparison of Single and Two-Bubble Class Gas-Liquid Recirculation Models – Application to Pilot Plant Radioactive Tracer Studies During Methanol Synthesis. **(P. Gupta)**

A1.5. Hydrodynamics of Churn Turbulent Bubble Columns: Gas-Liquid Recirculation and Mechanistic Modeling. **(P. Gupta, B.C. Ong)**

A1.6. High Pressure Slurry Bubble Column Consortium. **(M.H. Al-Dahhan, M.P. Dudukovic)**

A1-7. Hydrodynamic Measurements in a Slurry Bubble Column. **(N. Rados, A. Kemoun)**

A1-8. Prediction of Radial Gas Holdup Profiles in Bubble Column Reactors. **(Y. Wu, B.C. Ong)**

A1-9. Prediction of Axial Liquid Velocity Profile in Bubble Columns. **(Y. Wu)**

A1-10. Gas Holdup in Trayed Bubble Columns. **(A. Kemoun, N. Rados, F. Li)**

A1-11. A Novel Signal Filtering Methodology for Obtaining Liquid Phase Tracer Responses from Conductivity Probes. **(P. Gupta)**

A1-12. Hydrodynamics of Trayed Bubble Columns. **(J. Alvare)**

A1-13. Hydrodynamic Model of a Trayed Bubble Column. **(N. Durosier)**

A1-14. Study of Particle Motion in Packed/Ebullated Beds by CT and CARPT. **(J. Chen, N. Rados)**

A1-15. A Method for Estimating the Solids Circulation Rate in a Closed-Loop Circulating Fluidized Bed. **(S. Roy, A. Kemoun)**

A1-16. Optimal Design of Radioactive Particle Tracking Experiments for Flow Mapping in Opaque Multiphase Reactors. **(S. Roy)**

A1-17. A Lagrangian Description of Flows in Stirred Tanks via Computer Automated Radioactive Particle Tracking (CARPT). **(A. Rammohan, A. Kemoun)**

A2. Trickle Beds and Packed Beds

A2-1. Statistical Characterization of Macroscale Flow Textures Distribution in Trickle Beds. **(Y. Jiang)**

A2-2. A Parallel Approach to Catalyst and Reactor Selection for a Fine Chemical Process. **(Y. Jiang)**

A2-3. Drawbacks of the Dissolution Method for the Measurement of Liquid-Solid Mass Transfer Coefficient in Two-Phase Flow Packed Bed Reactors Operated at Low and High Pressures. **(W. Highfill, B.T. Ong)**

A2-4. The Effect of Particle Dilution on the Wetting Efficiency and Liquid Film Thickness in Small Trickle Beds. **(N. Papayannakos)**

GAS HOLDUP IN BUBBLE COLUMNS AT ELEVATED PRESSURE VIA COMPUTED TOMOGRAPHY

See the attached report for:

A. Problem Definition
B. Research Objectives
C. Research Accomplishments

Gas Holdup in Bubble Columns at Elevated Pressure via Computed Tomography

Abdenour Kemoun, Boon Cheng Ong, Puneet Gupta, Muthanna H. Al-Dahhan† and Milorad P. Dudukovic'

Chemical Reaction Engineering Laboratory
Department of Chemical Engineering, Campus Box 1198
1 Brookings Drive, Washington University St. Louis, MO 63130-4899

Abstract: Gas holdup in a pressurized bubble column (pressures from 0.1 to 0.7 MPa) was studied in a laboratory scale vessel (diameter 0.162 m) with air-water system over a range of superficial gas velocities (0.02 to 0.18 m/s) using non-invasive γ-ray based Computed Tomography (CT). It was found that the cross-sectional average gas holdup increases with pressure, as well as with superficial gas velocity. At all operating conditions, the azimuthally averaged radial gas holdup profiles exhibit a characteristic shape with greater gas holdup in the column center than by the walls. It is also observed that with an increase in pressure, the transition to churn-turbulent regime characterized by the change of the radial gas holdup profile from relatively flat to almost parabolic, is delayed to higher superficial gas velocities. The average cross-sectional gas holdup at each operating condition was compared with predictions of existing correlations and large discrepancies in predictions (as high as 300%) were found.

Keywords: Gas-liquid flow, bubble column, computed tomography, high pressure, high superficial gas velocity.

† Corresponding Author Tel: (314) 935-7187
Fax: (314) 935-7211
E-mail: muthanna@wuche.wustl.edu

1. Introduction

Bubble column reactors are vertical cylindrical columns, with or without internal heat exchanger tubes, where a gas is contacted with a liquid or slurry for production of chemicals and other products. Two-phase bubble columns as well as three phase slurry bubble columns of various configurations have gained considerable attention in the chemical process industry due to their use in a number of processes, such as, Fischer-Tropsch synthesis, liquid phase methanol synthesis, wet oxidation of heavily polluted effluent, hydrogenation of heavy oils, etc. For commercially important applications, bubble column reactors are usually operated at conditions of elevated pressures (Deckwer, 1992; Joshi *et al.*, 1998). However, research on details of bubble column hydrodynamics has primarily been limited to studies performed at atmospheric conditions. For lack of anything better, design and scale-up of such bubble column reactors for commercial applications invariably utilize information from studies performed at atmospheric conditions, which has often been reported to result in either over-design or poor estimates of bubble column performance. This raises a question as to whether one can rely solely on the database established at atmospheric pressure.

Bubble columns have been extensively studied for the last several decades, with almost all the studies on bubble column hydrodynamics discussing the importance of gas holdup, defined as the volume fraction of the gas phase in the reactor, and how it affects liquid recirculation and backmixing. Kölbel *et al.* (1961) reported that gas holdup in a bubble column with a porous plate distributor was not affected by pressure in the range 0.1 MPa to 1.6 MPa when the superficial gas velocity, evaluated at the pressure in the column, was less than 0.03 m/s. Deckwer *et al.* (1980) measured gas holdup in a slurry bubble column with a porous plate distributor containing fine particles at pressures up to 1.1 MPa and with superficial gas velocity below 0.04 m/s. They also found no significant effect of pressure on gas holdup in that range of operating variables. Idogawa *et al.* (1986) observed that the behavior of bubbles depends closely on the type of gas distributor, and this dependence weakens as the pressure is increased. The effect vanished above 10 MPa. In a later study, Idogawa *et al.* (1987) reported that pressure had no effect on bubble diameter in bubble columns with gas superficial velocity in the range of 0.005 to

0.05 m/s. Jiang *et al.* (1995), studying a column of 0.0508 m in diameter at superficial gas velocities of up to 1 m/s and in the pressure range from 0.1 to 21 MPa, observed that as pressure increases, the bubble size decreases, and the bubble size distribution becomes narrower. Many other studies have been reported in the literature which discuss the effect of pressure and superficial gas velocity (Hammer *et al.*, 1984; Oyevaar *et al.*, 1989; Kojima *et al.*, 1991; Shollenberger *et al.*, 1995; Adkins *et al.*, 1996; Shollenberger *et al.*, 1997; Kojima *et al.*, 1997, Lin *et al.*, 1998, and Luo *et al.* 1999).

The main aim of this study is to investigate the effect of pressure on gas holdup and its distribution over a range of superficial gas velocities using a non-intrusive technique, Computed Tomography (CT). A γ-ray based CT has been developed (Kumar *et al.*, 1995) for imaging phase holdup distribution in two-phase flow systems such as bubble columns and other multiphase reactors. The CT measurements were performed using an encapsulated γ-ray radiation source (Cs^{137}) and a fan beam arrangement of detectors. The details of the hardware and software have been described elsewhere (Kumar, 1994; Kumar *et al.*, 1995, 1997) and will not be repeated here. Instead, the obtained experimental measurements are discussed. The average cross-sectional holdup is compared to values obtained from various correlations reported in the literature.

2. Experimental Setup

Figure 1 displays the flowsheet for the high-pressure system used in this study. The system is designed to handle a high flow rate of air at a pressure of up to 1.5 MPa. The bubble column is made of a stainless steel tube with inner diameter 0.162-m (6.359") and height 2.5-m (8.2'). A transparent glass window is situated at the top of the column and is named "blue eye". This window allows viewing the system before starting the CT scan. The gas was dispersed into the column through a perforated plate distributor. The distributor used in this study has 61 holes each of 0.0004-m diameter, providing an open area of 0.04%. The holes are arranged in 3 concentric circles with 20 holes on each circle and one at the center of the distributor plate. The increment in radius between the circles on which holes are centered is 0.015-m. This particular distributor was used because a significant amount of data for gas holdup distribution and liquid velocity is available for

this distributor from our previous studies conducted at atmospheric pressure conditions. In this study, tomographic scans were conducted at three pressures (P = 0.1, 0.3, 0.7 MPa) and four superficial gas velocities (U_G = 0.02, 0.05, 0.12, 0.18 m/s).

Air was used as the gas phase and was filtered before being continuously introduced into the system at ambient temperature (T = 20 °C), while tap water served as the liquid medium with no net flow of the liquid (operation was batchwise with respect to the liquid). The gas flow rate was maintained at the desired values with the aid of a set of needle valves and rotameters. After exiting the bubble column, the gas passes through a backpressure regulator, which is used to control the pressure in the column. It is then discharged into the atmosphere through a vent. Two pressure safety valves are mounted both at the top and bottom of the column to prevent accidental over-pressurization. The height of the two-phase gas-liquid mixture in all experiments was maintained between 1.8 to 2.0 m from the distributor and therefore, the initial height of the liquid varied depending on the operating condition.

As already mentioned, in this study time-averaged cross-sectional gas holdup distribution was measured using the γ-ray scanner and associated tomography reconstruction algorithms developed in Chemical Reaction Engineering Laboratory (CREL) and discussed by Kumar *et al.* (1995; 1997). The CREL scanner is a versatile instrument that enables the quantification of the time-averaged holdup distribution for two-phase flows under a wide range of operating conditions. The fan beam configuration of the scanner consists of an array of NaI detectors of 0.05 m in diameter (5 detectors were used in this study), and an encapsulated 100 mCi Cs^{137} source located opposite to the center of the array of detectors. During each scan, the source-detectors assembly is rotated 360° around the test section to obtain multiple projection measurements. The total time of a complete 360° scan is approximately two hours. The tomographic scans can be acquired at different axial positions, which allows for the quantification of the effects of operating conditions on the axial variation of gas holdup distribution. In this study however, the axial variation of gas holdup was not considered, and measurements were conducted at only one axial location about 0.92 m from the distributor, which is in the fully developed flow region of the column.

3. Results and Discussions

3.1 Cross-sectional Gas Holdup Distribution

Figure 2 shows the time-averaged cross-sectional distribution of the gas holdup in the bubble column at different pressures and at different superficial gas velocities studied (results for only a few conditions are shown). For example, Figure 2 (a) shows the pixel map for P = 0.3 MPa, and U_G = 0.05, 0.12 and 0.18 m/s. A gradual variation in the color shades for the gas holdup from the column center to the wall indicates a change in gas holdup value. The plots confirm that gas holdup increases with pressure and superficial gas velocities. Visual observations of the column in the vicinity of the wall via the "blue eye" revealed much smaller bubbles when the pressure was increased. This could be explained in terms of a decrease in the rate of coalescence and a corresponding increase in bubble breakup rates at pressurized conditions. Hence, gas holdup increases as pressure increases, and the transition to churn-turbulent regime gets delayed to higher superficial gas velocities, which is characterized by the relatively flatter azimuthally averaged radial gas holdup profiles.

3.2 Radial Gas Holdup Distribution

From Figure 2, one can see that in the long time-averaged sense, the cross-sectional gas holdup distributions in bubble columns are close to being axisymmetric. Therefore, one is justified in representing the cross-sectional distribution by azimuthal averaging of the two-dimensional data as represented by Equation 1.

$$\varepsilon_G(r) = \frac{1}{2\pi}\int_0^{2\pi} \varepsilon_G(r,\theta)\, d\theta \qquad (1)$$

where $\varepsilon_G(r)$ represents the radial gas holdup profile.

Figures 3 to 6 display respectively the azimuthally averaged radial gas holdup distributions at different superficial gas velocity as a function of operating pressure.

These plots were obtained from the CT measured holdup distribution in a cross-section of the column 0.92-m above the distributor. This axial location was chosen for this study as it was far away from the distributor and the gas-liquid interface in the freeboard region. Our past experience indicates that at *L/D* ratio of 6 or above (where *L* is the total height of the dispersed two-phase mixture; and *D* is the diameter of the column), the holdup profiles in the well-developed region (region excluding the entrance and exit zones) are relatively invariant to axial position (Kumar, 1994). The profiles at atmospheric conditions indeed conform to the results previously obtained by Kumar (1994). From these figures it is apparent that the differences in the radial gas holdup profiles, as a result of increase in pressure, become more pronounced with an increase in the superficial gas velocity.

Figure 7 displays the results obtained by Shollenberger *et al.* (1995) at atmospheric conditions. The trend in gas holdup profiles at atmospheric pressure with increasing superficial gas velocities observed in our laboratory (Figures 3-6) agrees well with their results. However, the gas holdup obtained in this study is slightly higher than that observed by Shollenberger *et al* (1995). For example, at a velocity of 0.1176 m/s, the gas holdup value at the center of the column observed by Shollenberger *et al.* (1995) is about 0.22 (Figure 7), whereas in our case, a gas holdup value of about 0.28 is obtained (Figure 5) at the column center. Such discrepancies might be due to the differences in the type of distributor and the column diameter used in these two studies. Shollenberger *et al.* (1995) used a bubble cap distributor, whereas in this study a non-uniform perforated plate was used as the gas distributor. It is also possible that the observed differences were a result of the different tap water used in the two laboratories.

From Figures 3 to 6, it is evident that gas holdup increases both with pressure, and with superficial gas velocity in agreement with the experimental data reported in the literature (Idogawa *et al.*, 1986, Jiang *et al.*, 1995, Kojima *et al.*, 1991, Kojima *et al.*, 1997, Lin *et al.*, 1998, Oyevaar *et al.*, 1989 and Luo *et al.* 1999). At a velocity of 0.12 m/s (Figure 5), the radial gas holdup profile at atmospheric pressure is parabolic in nature, indicating churn turbulent flow, whereas at higher pressure, the profile is flatter. This can

be seen more clearly from Table 1, which shows the three parameters of the power law expression (Equation 2) used to fit the radial gas holdup profiles.

$$\varepsilon_G(r) = \tilde{\varepsilon}_G\left(\frac{m+2}{m}\right)\left[1 - c\left(\frac{r}{R}\right)^m\right] \tag{2}$$

where m is the exponent; c allows the possibility of nonzero gas holdup close to the wall; R is the column radius; and $\tilde{\varepsilon}_G$ is related to the cross-sectional average gas holdup, $\bar{\varepsilon}_G$, by Equation (3).

$$\bar{\varepsilon}_G = \tilde{\varepsilon}_G\left(\frac{m+2-2c}{m}\right) \tag{3}$$

This expression has been frequently used to represent the radial gas holdup distribution. Parameter m is indicative of the magnitude of the gradient of the radial gas holdup profile. If m is approximately equal to 2, then the profile is parabolic. As m increases the profile becomes flatter. One can see from Table 1 that as the pressure increases, for a given superficial gas velocity, the value of m goes up indicating that the radial gas holdup profile gets flatter except for U_G = 0.05 m/s which is in the transition regime at atmospheric pressure. The radial gas holdup profiles fitted to the expression in Equation 2 for each operating condition have also been plotted in Figures 3 to 6, respectively.

Adkins *et al.* (1996), who used a different gamma-ray tomography system, report slightly different observations as can be seen in Figure 8, which displays their radial gas holdup distribution at U_G = 0.1 m/s. In a 0.48-m ID and 3 m tall column, they found that the gas holdup profile is parabolic at a pressure of 0.394 MPa and gas superficial velocity of 0.1 m/s. In their study, the sparger was a 0.15-m diameter ring formed from 0.011-m ID stainless steel tubing. There were 12 holes equidistantly distributed on the ring, each of 0.00318 m in diameter. Hence, the discrepancies might be due to the type of distributor and size of column used or difference in water quality.

3.3 Cross-sectional Average Gas Holdup

The cross-sectional average gas holdup is calculated via Equation 3 by averaging the radial gas holdup profiles obtained from Equation 1.

$$\bar{\varepsilon}_g = \frac{2}{R^2}\int_0^R r\,\varepsilon_g(r)\,dr \tag{3}$$

The cross-sectional average gas holdup can be taken as a good estimate of the overall gas holdup (Kumar, 1994). Figure 9 displays the cross-sectional average gas holdup as a function of pressure at different superficial gas velocities.

Figure 9 further confirms that gas holdup increases with pressure, except at low superficial gas velocities (below and up to 0.05 m/s) where it is rather insensitive to pressure. At atmospheric pressure, the cross-sectional average gas holdup seems almost constant after certain superficial gas velocity is reached as indicated by Figure 9. This leveling off effect seems to occur at higher gas velocities at higher pressures. These observations have also been reported in the literature (Kölbel *et al.*, 1961; Deckwer *et al.*, 1980). Wilkinson and van Dierendonck (1990) explained the effect of pressure on gas holdup in terms of the Kelvin-Helmholtz stability analysis. They concluded from their analysis that pressure mainly affects the stability of large bubbles, which tend to break due to growth of surface instabilities. Since at low superficial gas velocities the large bubble holdup is negligible, pressure does not significantly influence gas holdup.

Table 2 compares the average gas holdup measurements obtained by Adkins *et al.* (1996) and Shollenberger *et al.* (1997) with gas holdup values obtained from this study. One can see that there is significant deviation in the values of cross-sectional average gas holdup obtained in these studies. The cause of the discrepancies is unknown. Neither the fluid (tap water) nor the distributor or column diameter was matched. Moreover, the data at U_G = 0.05 m/s superficial gas velocity is probably in the transition regime at atmospheric pressure conditions, which could possibly explain the observed differences. However, it is known that gas holdup increases with increasing column diameter (Akita and Yoshida, 1973), and one should expect a higher holdup in the studies of Adkins *et al.*

(1996) and Shollenberger *et al.* (1997) as compared to our experimental data, which is acquired in a smaller diameter vessel. The only other possible reason for this observed trend could be the effect of the water quality, or more significantly, the effect of the rigidity of the column support structure, which could explain the higher holdups observed in our studies due to stabilized bubbly flow even at significantly high superficial gas velocities.

3.4 Comparison with Various Correlations in the Literature

Numerous correlations for overall gas holdup in bubble columns have been reported and those that seem applicable to the conditions investigated in this study (based on the pressure range, gas flow rates, and column diameter) are summarized in Table 3. Since Kumar (1994) has shown that the cross-sectional average holdup measured at heights above the distributor larger than 4 to 5 column diameters is in close agreement with the overall gas holdup in the column, the cross sectional average holdup determined in this study was compared to the prediction for overall gas holdup obtained from the reported correlations. Figure 10 shows the predictions for the overall gas holdup as a function of superficial gas velocity based on various correlations at $P = 0.1$ MPa. It can be concluded that the correlation of Idogawa *et al.* (1985) agrees closely with our experimental data followed by correlations of Hikita *et al.* (1980), Luo *et al.* (1999), Wilkinson *et al.* (1992) and Akita and Yoshida (1973). At $U_G = 0.05$ m/s, the above mentioned predictions deviate from the observed holdup (refer to Table 4 which gives an error analysis of the various correlations against experimental data obtained in this study).

Since the superficial gas velocity of 0.05 m/s is close to the transition velocity at P=0.1 MPa that changes bubbly flow into churn turbulent flow, and the precise value of the transition velocity is a function of the non-measurable water quality, it is possible that the deviation between data and correlation predictions at $U_G = 0.05$ m/s is caused by the fact that the correlations predict the holdup in one flow regime while the data reflect the other flow regime. It is evident from Figure 10 that the experimental holdup value at $U_G =$ 0.05 m/s at $P = 0.1$ MPa is considerably higher than the value predicted by any of the

correlations indicating perhaps a different flow regime during our experiment than observed in the data used to develop the correlations.

In the same manner, Figures 11 and 12 display the plots for the cross-sectional average gas holdup as a function of superficial gas velocity at P = 0.3 MPa, and P = 0.7 MPa, respectively. Among the correlations reported in Table 3 those of Idogawa *et al.* (1985), Idogawa *et al.* (1987), Wilkinson *et al.* (1992) and Luo *et al.* (1999) were developed by considering high-pressure data also. As evident from Figures 11 and 12, the gas holdup predictions based on the correlation of Hammer *et al.* (1984) are in good agreement with the observed cross-sectional gas holdup, which yields an average deviation of about 12% (for 0.3 MPa) to 17% (for 0.7 MPa), except for low superficial gas velocities where the correlation is in error of 21%. The correlations of Wilkinson *et al.* (1992) and Idogawa *et al.* (1987) also predict holdup values in reasonable agreement with experimental observations, and have average deviation of about 18% for all conditions, except at low superficial gas velocities where these correlations are in error of about 40%. The correlation of Kojima *et al.* (1997) gives reasonable estimate of holdup at all pressures investigated in this study. However, it has limited applicability to superficial gas velocities less than 0.1 m/s (Kojima, 1999).

4. Conclusions

The gas holdup and its cross-sectional distribution were measured at elevated pressures up to 0.7 MPa using γ-ray Computed Tomography (CT). These measurements indicate that gas holdup increases very slightly with pressure at low superficial gas velocities of less than 0.05 m/s and then increases significantly with system pressure at higher superficial gas velocities owing to a decrease in the stable bubble size, which results in an increase in the number of small bubbles. As mentioned earlier, this reduction in bubble size with increasing pressure is usually attributed to a decreased rate of coalescence of bubbles and an enhanced breakup of large (unstable) bubbles, which gets promoted under pressurized conditions. It was also shown that the radial gas holdup distribution tends to become relatively flatter at a higher pressure as compared to that at atmospheric pressure. For example, at atmospheric pressure and U_G = 0.12 m/s, the

gradient of the radial gas holdup distribution is steeper, indicating churn-turbulent flow conditions; whereas at higher pressures of 0.3 and 0.7 MPa, the gradient is not so steep which indicates a stabilized bubble regime.

The cross-sectional average gas holdup was calculated using the collected data and compared with various correlations found in the literature. The main findings are:

- At atmospheric pressure, the correlation of Idogawa *et al.* (1985) was in the best agreement with our experimental data except for U_G = 0.05 m/s. This operating condition is near the transition point, and the correlation and data may not belong to the same flow regime.
- At higher pressures and over the entire superficial gas velocity range investigated in this study, the correlation of Hammer *et al.* (1984) gives the best prediction of our gas holdup data (average error of 12-17%) followed by Wilkinson *et al.* (1992; average error of 14-18%) and Idogawa *et al.* (1987; average error of 18-20%).
- At higher pressures and high superficial gas velocity ($U_G > 0.1$ m/s), in addition to the correlations of Idogawa *et al.* (1987), and Hammer *et al.* (1984), the correlation of Krishna *et al.* (1996) and Luo *et al.* (1999) also seem to provide reasonable predictions of the measured gas holdup.

In spite of several correlations giving reasonable predictions, we did not find any correlation that consistently predicted our experimental data, which indicates the need for better characterization of the levels of liquid recirculation and turbulence which are needed for development of a more fundamentally based model for prediction of gas holdups. Such work is currently underway.

5. Acknowledgements

Department of Energy grant (DE-FG2295PC-95212) through the University Coal Research Program (UCR), Exxon Research and Engineering support, and Department of Energy grant (DE-FC-22-95 PC 95051) through Air Products and Chemicals, Inc. are gratefully acknowledged.

References

Adkins, D. R., Shollenberger, K. A., O'Hern, T. J., and Torczynski, J. R., "Pressure Effects on Bubble Column Flow Characteristics," ANS Proceedings, 1996 National Heat Transfer Conference, Technical Sessions sponsored by Thermal Hydraulics Division American Nuclear Society, **9**, 318-325, Aug 3-6, 1996.

Akita, K., and Yoshida, F., 'Gas Holdup and Volumetric Mass Transfer Coefficient in Bubble Columns,' *Ind. Eng. Chem. Process Des. Dev.*, **12**, 76-80, 1973.

Deckwer, W.-D., 'Bubble Column Reactors', John Wiley & Sons, New York, 1992.

Deckwer, W. D., Louisi, Y., Zaidi, A., and Ralek, M., 'Hydrodynamic Properties of the Fischer-Tropsch Slurry Process, ' *Ind. Eng. Chem. Process Des. Dev.*, **19**, 699-708, 1980.

Hammer, H., Schrog, H., Hektor, K., Schönau, K., Küsters, W., Soemarno, A., Sahabi, U., and Napp, W., 'New Subfunctions in Hydrodynamics, Heat & Mass Transfer for Gas/Liquid and Gas/Liquid/Solid Chemical and Biochemical Reactors,' *Front. Chem. Reac. Eng.*, 464, 1984.

Hikita, H., Asai, S., Tanigawa, K., Segawa, K., and Kitao, M., 'Gas Holdup in Bubble Columns,' *Chem. Eng. J.*, **20**, 59-67, 1980.

Idogawa, K., Ikeda, K., Fukuda, T., and Morooka, S., 'Effect of Gas and Liquid Properties on the Behavior of Bubbles in a Bubble Column under High Pressure,' *Kag. Kog. Ronb.*, **11**, 432, 1985.

Idogawa, K., Ikeda, K., Fukuda, T., and Morooka, S., 'Behavior of Bubbles of the Air-Water System in a Column under High Pressure,' *International Chem. Engng.*, **26**, 3, 468-474, 1986.

Idogawa, K., Ikeda, K., Fukuda, T., and Morooka, S., 'Effect of Gas and Liquid Properties on the Behavior of Bubbles in a Column under High Pressure,' *Int. Chem. Eng.*, **27**, 93-99, 1987.

Jiang, P., Lin, T.-J., Luo, X., and Fan, L.-S., 'Flow Visualization of High Pressure (21 MPa) Bubble Column: Bubble Characteristics,' *Trans IChemE*, **73**, Part A, 269-274, April 1995.

Joshi, J. B., Parasu Veera, U., Prasad, Ch. V., Phanikumar, D. V., Deshphande, N. S., Thakre, S. S., and Thorat, B. N., 'Gas Holdup Structure in Bubble Column Reactors,' *PINSA*, **64A**, 4, 441-567, 1998.

Kojima, H., Personal Communication, 1999.

Kojima, H., Jun, S., and Hideyuki, S., 'Effect of Pressure on Volumetric Mass Transfer Coefficient and Gas Holdup in Bubble Column,' *Chem. Eng. Sci.*, **52**, 21/22, 4111-4116, 1997.

Kojima, H., Okumura, B., and Nakamura, A., 'Effect of Pressure on Gas Holdup in a Bubble Column and a Slurry Bubble Column,' *J. Chem. Eng. Japan*, **24**, 1, 115-117, 1991.

Kölbel, H., Borchers, E., and Langemann, H., *Chemie -Ing. -Techn.*, **33**. 668. 1961.

Krishna, R., and Ellenberger, J., 'Gas Holdup in Bubble Column Reactors Operating in the Churn-Turbulent Flow Regime,' *AIChE J.*, **42**, 9, 2627-2634, 1996.

Kumar, S. B., 'Computed Tomography Measurements of Void Fraction and Modeling of the Flow in Bubble Columns', PhD Thesis, Florida Atlantic University, Boca Raton, FL, 1994.

Kumar, S. B., Moslemian, D., and Dudukovic, M. P., 'A Gamma Ray Tomographic Scanner for Imaging Void Fraction Distribution in Bubble Columns,' *Flow Meas. Instr.*, **6**, 1, 61, 1995.

Kumar, S. B., Moslemian, D., and Dudukovic, M. P., 'Gas Holdup Measurements in Bubble Columns Using Computed Tomography,' *AIChE J.*, **43**, 6, 1414-1425, 1997.

Lin, T.-J., Tsuchiya, K., and Fan, L.-S., 'Bubble Flow Characteristics in Bubble Columns at Elevated Pressure and Temperature,' *AIChE J.*, **44**, 3, 545-560, March 1998.

Luo, X., Lee, D. J., Lau, R., Yang, G., and Fan, L. S., 'Maximum Stable Bubble Size and Gas Holdup in High-Pressure Slurry Bubble Columns, ' *AIChE J.*, **42**, 4, 665-680, 1999.

Oyevaar, M. H., De La Rie T., Van Der Sluijs, and Westerterp, K. R., 'Interfacial Areas and Gas Holdups in Bubble Columns and Packed Bubble Columns at Elevated Pressures,' *Chem. Eng. Process.*, **26**, 1-14, 1989.

Oyevaar, M. H., and Westerterp, K. R., 'Mass Transfer Phenomena and Hydrodynamics in Agitated Gas-Liquid Reactors and Bubble Columns at Elevated Pressures: State of the Art,' *Chem. Eng. Process.*, **25**, 85-98, 1989.

Reilly, J. G., Scott, D. S., de Bruijn, T., Jain, A., and Diskorz, J., 'Correlation for Gas Holdup in Turbulent Coalescing Bubble Columns,' *Can. J. Chem. Eng.*, **64**, 705, 1986.

Shollenberger, K. A., Torczynski, J. R., Adkins, D. R., and O'Hern, T. J., 'Bubble Column Measurements Using Gamma Tomography,' ASME FED, Fluid Measurement and Instrumentation, **211**, 25-30, 1995.

Shollenberger, K. A., Torczynski, J. R., Adkins, D. R., O'Hern, T. J., and Jackson, N. B., 'Gamma-densitometry Tomography of Gas Holdup Spatial Distribution in Industrial-Scale Bubble Columns,' *Chem. Eng. Sci.*, **52**, 13, 2037-2048, 1997.

Sotelo, J. L., Benitez, F. J., Beltran-Heredia, J., and Rodriguez, C., 'Gas Holdup and Mass Transfer Coefficients in Bubble Columns. 1. Porous Glass-Plate Diffusers,' *International Chem. Eng.*, **34**, 1, 82-91, 1994.

Wilkinson, P. M., Spek, A. P., and van Dierendonck, Laurant L., 'Design Parameters Estimation for Scale-Up of High-Pressure Bubble Columns,' *AIChE J.*, **38**, 4, 544-554, 1992.

Wilkinson, P. M., and van Dierendonck, Laurent L., 'Pressure and Gas Density Effects on Bubble Break-Up and Gas Hold-Up in Bubble Columns,' *Chem. Engng. Sci.*, **45**, 8, 2309-2315, 1990.

List of Tables

List of Figures

Table 1: Parameters of the Fitted Radial Holdup Profile

P, MPa	U_G, m/s	$\bar{\varepsilon}_G$	m	c
0.1	0.02	0.053	3.633	0.422
	0.05	0.151	4.372	0.368
	0.12	0.145	2.228	0.605
	0.18	0.165	2.068	0.622
0.3	0.02	0.059	5.133	0.283
	0.05	0.168	4.792	0.345
	0.12	0.272	3.765	0.466
	0.18	0.270	2.955	0.487
0.7	0.02	0.062	5.424	0.307
	0.05	0.170	3.557	0.346
	0.12	0.315	3.937	0.356
	0.18	0.326	2.997	0.396

Table 2: Comparison of results from this study with literature data

Study	Column ID, m	U_G, m/s	Pressure, MPa	$\bar{\varepsilon}_G$
Shollenberger *et al.* (1997)	0.19	0.0147	0.1	0.024
Present	0.162	0.02	0.1	0.069
Shollenberger *et al.* (1997)	0.19	0.0588	0.1	0.082
Present	0.162	0.05	0.1	0.191
Shollenberger *et al.* (1997)	0.19	0.1176	0.1	0.126
Present	0.162	0.12	0.1	0.193
Adkins *et al.* (1996)	0.48	0.125	0.141	0.211
Present	0.162	0.12	0.3	0.342
Adkins *et al.* (1996)	0.48	0.066	0.299	0.185
Present	0.162	0.05	0.3	0.210

Table 3: Correlations for Gas Holdup

References	Gas-Liquid System	Apparatus	Conditions	Correlations
[a] Akita & Yoshida (1973)	He/CO_2/O_2/air-H_2O/ Glycol/Methanol/CCl_4/ Na_2SO_3/NaCl	D = 0.152, 0.301, 0.6 m Sparger (5.0 mm)	P = 0.1 MPa T = 283 - 313 K U_G = 0.5 - 40 cm/s	$\frac{\bar{\varepsilon}_G}{(1-\bar{\varepsilon}_G)^4} = 0.2\left(\frac{gD^2\rho_L}{\gamma_L}\right)^{0.125}\left(\frac{gD^3}{\nu_L}\right)^{0.083}\frac{U_G}{(gD)^{0.5}}$
[a] Hikita *et al.* (1981)	H_2/CO_2/CH_4/C_3H_8/H_2+N_2/ air-H_2O/Sucrose/ Methanol/n-Butanol/ Aniline/i-Butanol/NaCl/ Na_2SO_4/$CaCl_2$/$MgCl_2$/ $AlCl_3$/KCl/K_2SO_4/K_3PO_4/ KNO_3	D = 0.10 m Nozzle (1.1 cm)	P = 0.1 MPa H/D = 15 U_G = 4.2 - 38 cm/s	$\bar{\varepsilon}_G = 0.672 f\left(\frac{U_G\mu_L}{\gamma_L}\right)^{0.578}\left(\frac{\mu_L^4 g}{\rho_L\gamma_L^3}\right)^{-0.131}\left(\frac{\rho_G}{\rho_L}\right)^{0.062}\left(\frac{\mu_G}{\mu_L}\right)^{0.107}$ where $f = \begin{cases} 1.0 & \text{for non-electrolyte solution} \\ 10^{0.0414I} & \text{for } 0 < I < 1.0 \text{ kg ion/m}^3 \\ 1.1 & \text{for } I > 1.0 \text{ kg ion/m}^3 \end{cases}$
[a] Hammar *et al.* (1984)	N_2/He/Ar/CO_2/Air-H_2O/Organic liquids-glas ballotini	D = 0.106, 0.2 m Annuli or stars spargers (17 to 40 holes of 0.5, 1 or 2 mm ID)	P = 0.1 MPa T = 293 - 363 K U_G = 0.5 - 13 cm/s	$\frac{\bar{\varepsilon}_G}{1-\bar{\varepsilon}_G} = 0.4\left(\frac{U_G\mu_L}{\gamma_L}\right)^{0.87}\left(\frac{\mu_L^4 g}{\rho_L\gamma_L^3}\right)^{-0.27}\left(\frac{\rho_G}{\rho_L}\right)^{0.17}$
[a, b] Idogawa *et al.* (1985)	Air-H_2O	D = 0.05 m Porous plate (2, 100 μm) Capillary tubes (1, 3, 5 mm) Perforated plate (19 holes of 1 mm)	P = 0.1 - 15 MPa T = 288 - 293 K, H/D = 16.6 U_G = 0.5 - 5 cm/s	$\frac{\bar{\varepsilon}_G}{1-\bar{\varepsilon}_G} = 1.44 U_G^{0.58}\rho_G^{0.12}\sigma_L^{-0.16\exp(-P)}$
[a] Reilly *et al.* (1986)	He/Ar/air-H_2O/solvent/ trichloroethylene-glass beads	D = 0.3 m Perforated plate (293 holes,1.5 mm) Single sparger Multiorifice sparger (13.4 mm)	P = 0.1 MPa T = 283 - 323 K U_G = 0.4 - 40 cm/s	$\bar{\varepsilon}_G = 296 U_G^{0.44}\rho_L^{-0.98}\rho_G^{0.19}\gamma_L^{-0.16} + 0.009$
[a, b] Idogawa *et al.* (1987)	H_2/He/Air-H_2O/Methanol/ Ethanol/Acetone/Aqueous alcohol solution	D = 0.05 m Perforated plate (19 holes of 1 mm)	P = 0.1 - 5 MPa T = 284 - 293 K, H/D = 16.6 U_G = 0.5 - 5 cm/s	$\frac{\bar{\varepsilon}_G}{1-\bar{\varepsilon}_G} = 0.059 U_G^{0.8}\rho_G^{0.17}\left(\frac{\sigma_L}{72}\right)^{-0.22\exp(-P)}$

Table 3: Correlations for Gas Holdup - Continued

References	Gas-Liquid System	Apparatus	Conditions	Correlations
[a] Wilkinson *et al.* (1992)	N_2-H_2O/n-Heptane/Mono-ethylene glycol	D = 0.158, 0.23 m Sparger ring (4 holes of 7 mm)	P = 0.1 - 2.0 MPa H = 1.2 m U_G = 0 - 60 cm/s	$U_G < U_{TRANS}$ $\quad \bar{\varepsilon}_G = \frac{U_G}{U_{S.B.}}$ $U_G > U_{TRANS}$ $\quad \bar{\varepsilon}_G = \frac{U_{TRANS}}{U_{S.B.}} + \frac{U_G - U_{TRANS}}{U_{L.B.}}$ where $\frac{U_{TRANS}}{U_{S.B.}} = 0.5\,exp(-193\,\rho_G^{-0.61}\mu_L^{0.5}\gamma_L^{0.11})$ $\frac{\mu_L U_{S.B.}}{\gamma_L} = 2.25\left(\frac{\gamma_L^3\rho_L}{g\mu_L^4}\right)^{-0.273}\left(\frac{\rho_L}{\rho_G}\right)^{0.03}$ $\frac{\mu_L U_{L.B.}}{\gamma_L} = \frac{\mu_L U_{S.B.}}{\gamma_L} + 2.4\left[\frac{\mu_L(U_G - U_{TRANS})}{\gamma_L}\right]^{0.757}\left(\frac{\gamma_L^3\rho_L}{g\mu_L^4}\right)^{-0.077}\left(\frac{\rho_L}{\rho_G}\right)^{0.077}$
[a, c] Sotelo *et al.* (1994)	Air/CO_2-H_2O/ ethanol/ saccharose/glycerin	D = 0.04, 0.08 m Porous gas diffusers (30,65,150μm)	P = 0.1 MPa H = 1.5-2.0 m U_G = 0 - 20 cm/s	$\bar{\varepsilon}_G = \left\{ 129\left(\frac{U_G\mu_L}{\gamma_L}\right)^{0.99}\left(\frac{\mu_L^4 g}{\rho_L\gamma_L^3}\right)^{-0.123}\left(\frac{\rho_G}{\rho_L}\right)^{0.187}\left(\frac{\mu_G}{\mu_L}\right)^{0.343}\left(\frac{d}{D}\right)^{-0.089} \right\}$

Table 3: Correlations for Gas Holdup - Continued

References	Gas-Liquid System	Apparatus	Conditions	Correlations
[a] Krishna & Ellenberger (1996)	Air/He/Ar/SF_6-H_2O/ paraffin oil/ Separan/ tetradecane	D = 0.1,0.174,0.19,0.38,and 0.63m Spider sparger Sintered glass plate (mean pore size of 150-200 μm) Polyacrylate sieve plate (2.5mm ID) Sintered bronze plate (mean pore size of 50 μm)	P = 0.1 MPa U_G = 0.1 - 85 cm/s	$U_G < U_{trans}$ $\quad \bar{\varepsilon}_G = \varepsilon_b$ $U_G > U_{TRANS}$ $\quad \bar{\varepsilon}_G = \varepsilon_B + \varepsilon_{TRANS}(1-\varepsilon_B)$ where $\varepsilon_B = 0.268\frac{(U_G - U_{TRANS})^{0.58}}{D^{0.18}}$ $U_{TRANS} = V_{SMALL}\varepsilon_{TRANS}(1-\varepsilon_{TRANS})$ $V_{SMALL} = \frac{\gamma_L^{0.12}}{2.84\rho_G^{0.04}}$ $\varepsilon_{TRANS} = 0.59(3.85)^{1.5}\sqrt{\frac{\rho_G^{0.96}\gamma_L^{0.12}}{\rho_L}}$
[a, d] Kojima *et al.* (1997)	Air-H_2O/Aqueous buffered solution/Aqueous enzyme solution	D = 0.045 m Nozzle (1.38, 2.1, 2.9, 4.03 mm)	P = 0.1 - 1.1 MPa T = 290 - 300 K, H/D = 20 - 26.7 U_G = 0.005 - 0.15 cm/s	$\bar{\varepsilon}_G = 1.18U_G^{0.679}\left(\frac{\gamma_L}{\gamma_{L,0}}\right)^{-0.546} exp\left[1.27\times10^{-4}\left(\frac{\rho_L Q^2}{d_o^3\gamma_L}\right)\left(\frac{P}{P_0}\right)\right]$
[a] Luo *et al.* (1999)	N_2-Paratherm NF- alumina particles	D = 0.102 m Perforated plate (120 squared-pitched holes of 1.5 mm ID)	P = 0.1 - 5.6 MPa T = 298 - 351 K, U_G = up to 45 cm/s	$\frac{\bar{\varepsilon}_G}{1-\bar{\varepsilon}_G} = \frac{2.9\left(\frac{U_G^4\rho_G}{\gamma_L g}\right)^{\alpha}\left(\frac{\rho_G}{\rho_{SL}}\right)^{\beta}}{\left[cosh\left(Mo_{SL}^{0.054}\right)\right]^{0.41}}$ where $Mo_{SL} = \frac{(\xi\mu_L)^4 g}{\rho_{SL}\gamma_L^3}$; $\alpha = 0.21Mo_{SL}^{0.0079}; \beta = 0.096Mo_{SL}^{-0.011}; \rho_{SL} = \rho_L; \xi = 1$

a: γ_L is the liquid surface tension in N/m; $\gamma_{L,0}$ is the surface tension of water at 20 °C in N/m; ν_L is the liquid kinematic viscosity in m^2/s; ρ_G is the gas density in kg/m^3; and ρ_L is the liquid density in kg/m^3

b: σ_L is the liquid surface tension in mN/m; *c*: d is the inner diameter of single nozzle in m

d: d_o is the orifice ID in mm; P_0 is the standard atmospheric pressure; and Q is the volumetric flow rate of gas under the condition in the bubble column in m^3/s

Table 4: Error Analysis for Different Correlations (Percent error is reported).

$$\text{Absolute Error} = \left|\frac{\text{Measured Value} - \text{Predicted Value}}{\text{Measured Value}}\right| \text{x}100\%$$

P = 0.1 MPa

U_G, m/s	Akita (1973)	Hikita (1980)	Hammer (1984)	Idogawa (1985)	Reilly (1986)	Idogawa (1987)	Wilkinson (1992)	Sotelo (1994)	Krishna (1996)	Kojima (1997)	Luo (1999)
0.02	22.1	10.6	0.7	9.5	51.5	38.3	11.9	71.6	88.7	23.5	5.0
0.05	44.1	45.1	26.4	36.0	20.3	5.7	37.6	74.5	13.7	16.8	32.7
0.12	6.2	9.9	34.4	2.7	13.7	59.0	5.6	40.0	9.3	-	10.3
0.18	0.05	0.8	50.1	2.1	17.6	71.4	13.8	22.0	7.6	-	19.0
Avg.	18.1	16.6	27.9	12.6	25.8	43.6	17.2	52.0	29.8	20.2	16.8

P = 0.3 MPa

U_G, m/s	Hikita (1980)	Hammer (1984)	Idogawa (1985)	Reilly (1986)	Idogawa (1987)	Wilkinson (1992)	Sotelo (1994)	Krishna (1996)	Kojima (1997)	Luo (1999)
0.02	10.4	10.6	28.4	72.1	53.2	6.6	67.3	199.62	17.2	32.8
0.05	46.5	21.5	28.0	11.6	0.1	26.6	71.5	13.7	17.7	19.0
0.12	45.6	13.3	33.3	21.6	1.7	25.4	58.5	16.2	-	20.2
0.18	34.2	4.9	23.9	10.8	18.8	12.9	40.6	12.5	-	7.1
Avg.	34.2	12.6	28.4	29.0	18.5	17.9	59.5	60.5	17.5	19.8

P = 0.7 MPa

U_G, m/s	Hikita (1980)	Hammer (1984)	Idogawa (1985)	Reilly (1986)	Idogawa (1987)	Wilkinson (1992)	Sotelo (1994)	Krishna (1996)	Kojima (1997)	Luo (1999)
0.02	9.6	20.7	56.3	91.3	66.3	7.3	63.3	330.3	18.9	59.1
0.05	48.0	18.5	16.9	4.9	3.0	15.0	69.2	45.9	9.5	8.2
0.12	52.1	20.0	31.8	23.4	6.9	21.3	59.3	6.25	-	20.4
0.18	44.6	8.6	26.6	16.7	2.7	13.3	44.5	9.1	-	12.8
Avg.	38.6	17.0	32.9	34.1	19.7	14.2	59.1	97.9	14.2	25.1

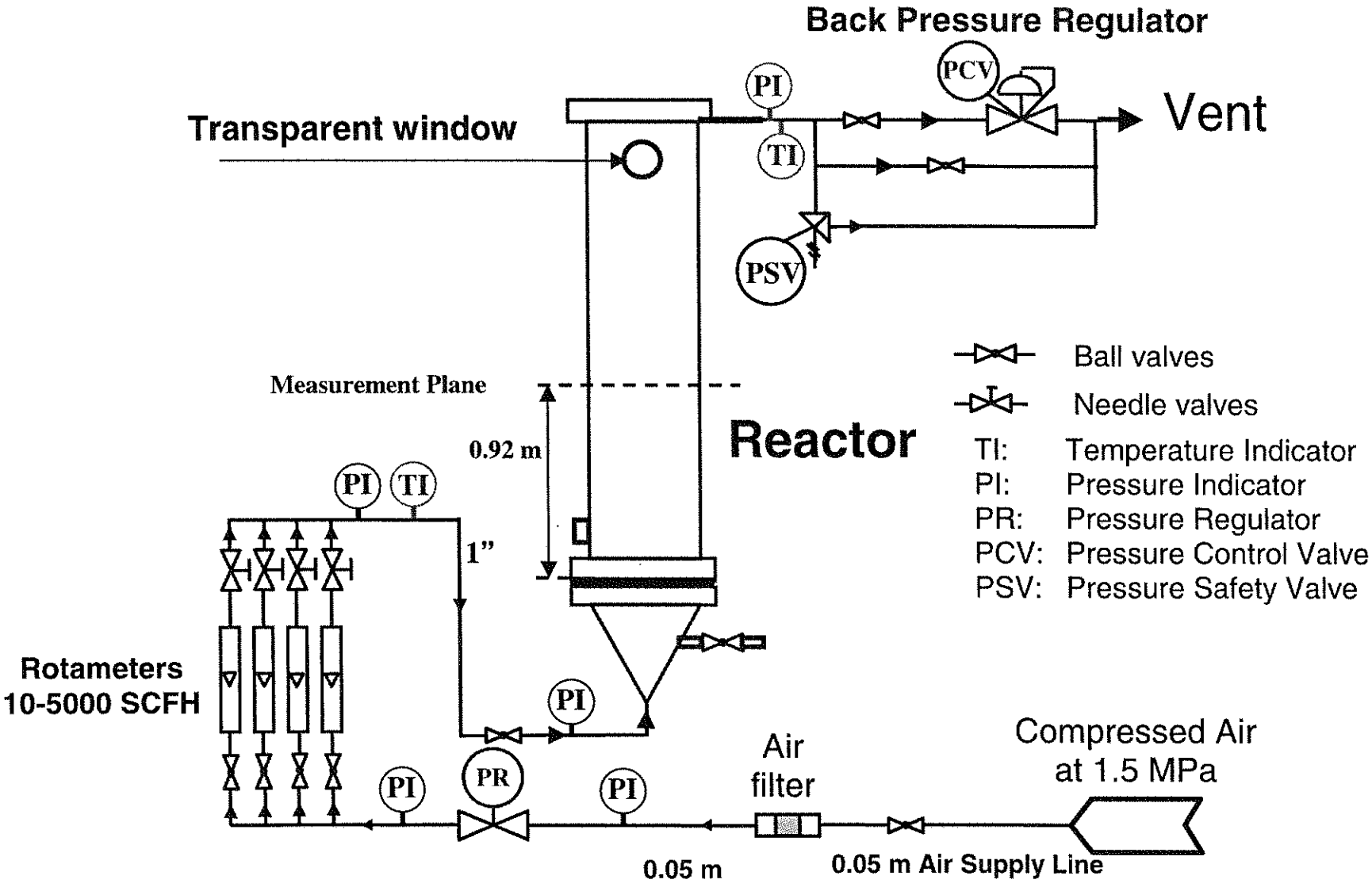

Figure 1: Flowsheet for High Pressure Bubble Column facility.

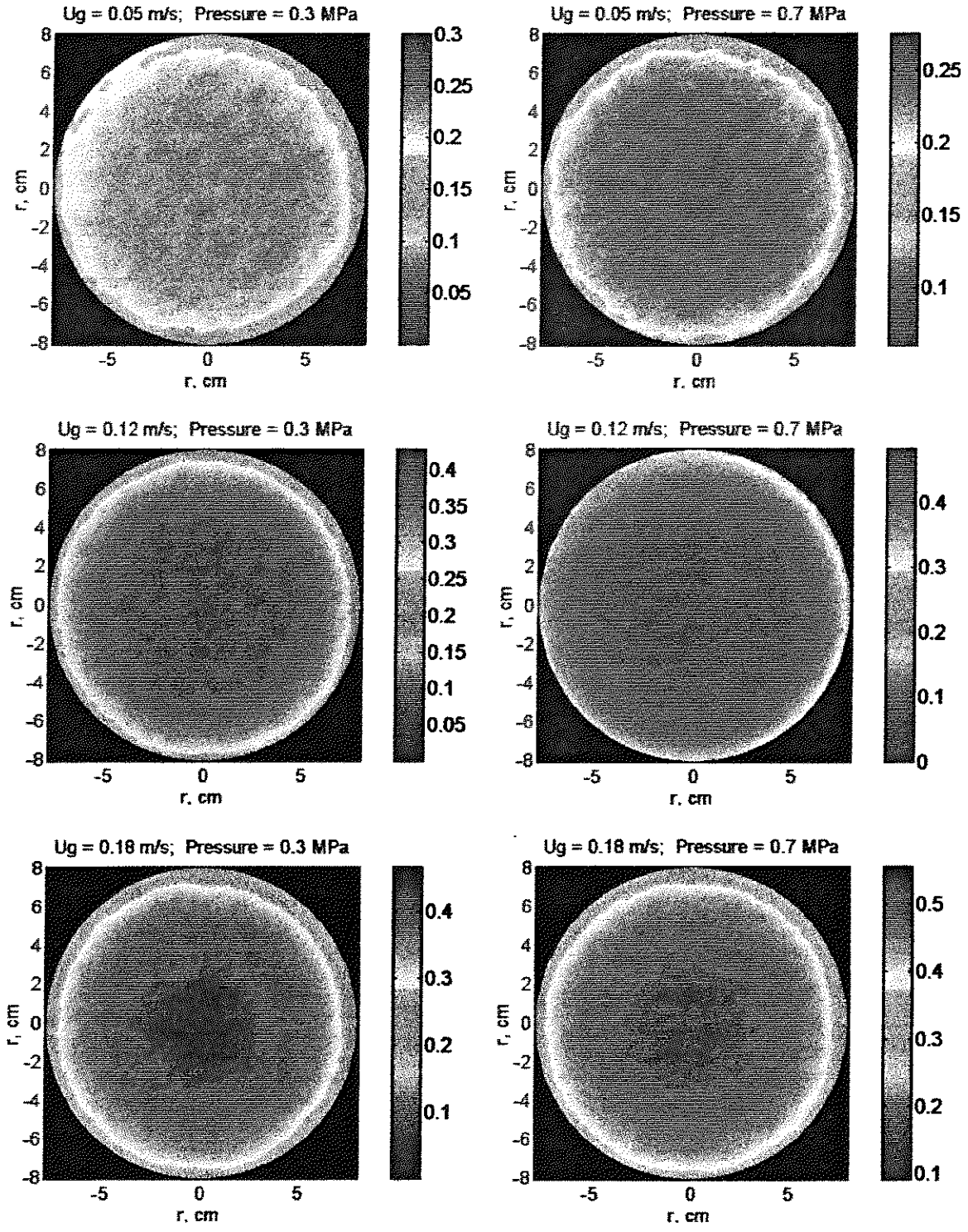

Figure 2: Cross sectional Gas Holdup Distribution at (a) $P = 0.3$ MPa, and (b) $P = 0.7$ MPa for $U_G = 0.05$, 0.12 and 0.18 m/s.

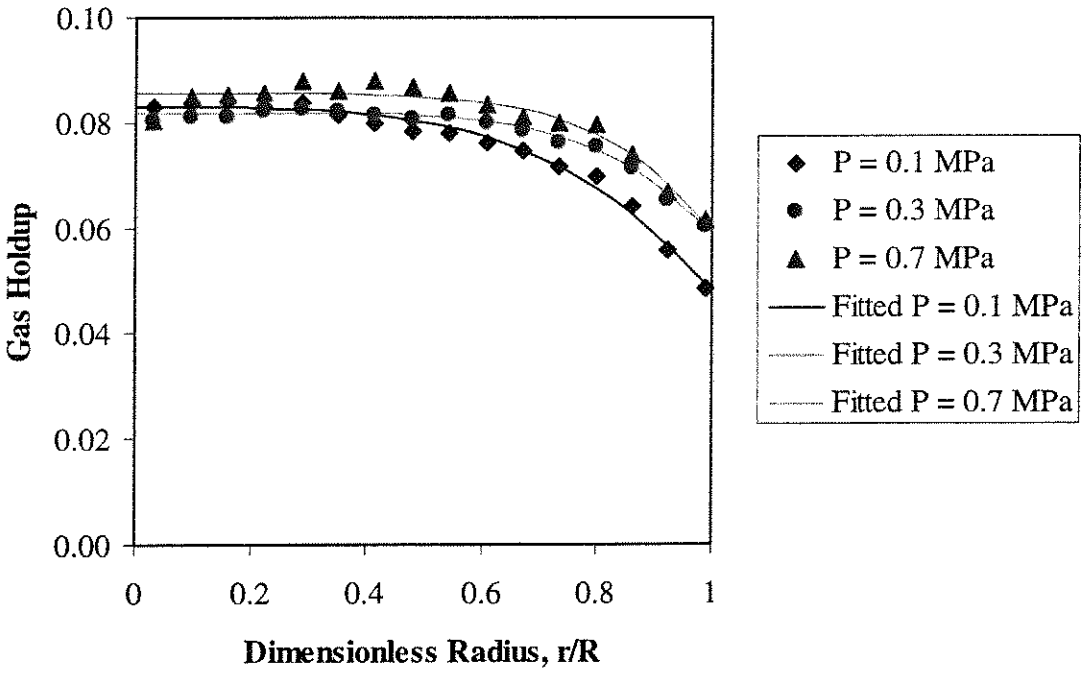

Figure 3: Radial Gas Holdup Distribution as a Function of Pressure for U_G = 0.02 m/s.

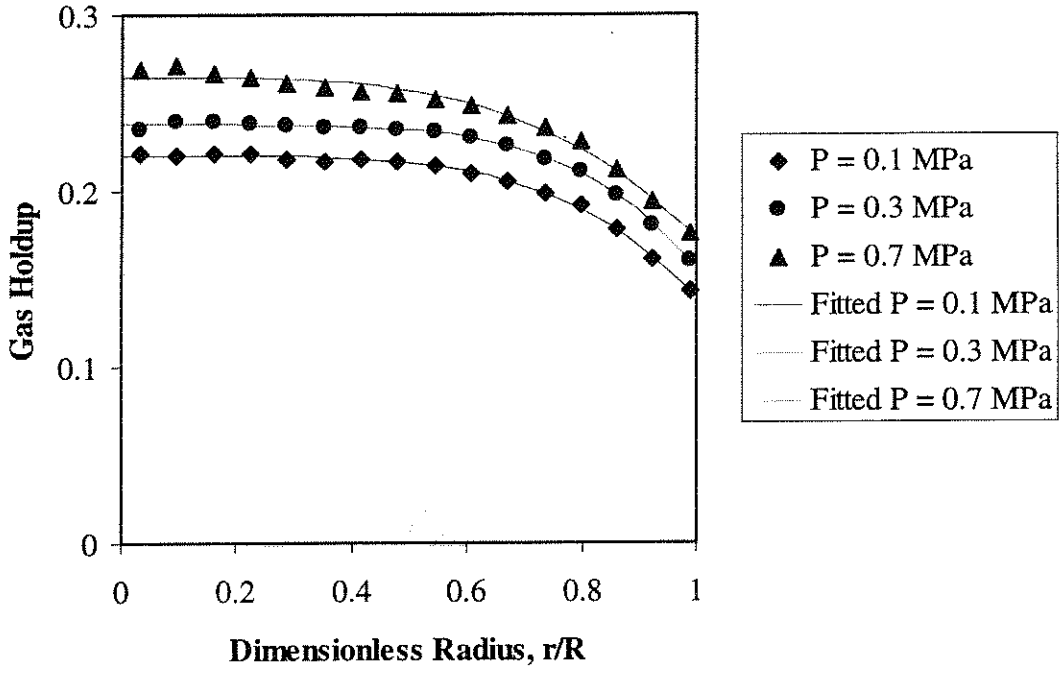

Figure 4: Radial Gas Holdup Distribution as a Function of Pressure for U_G = 0.05 m/s.

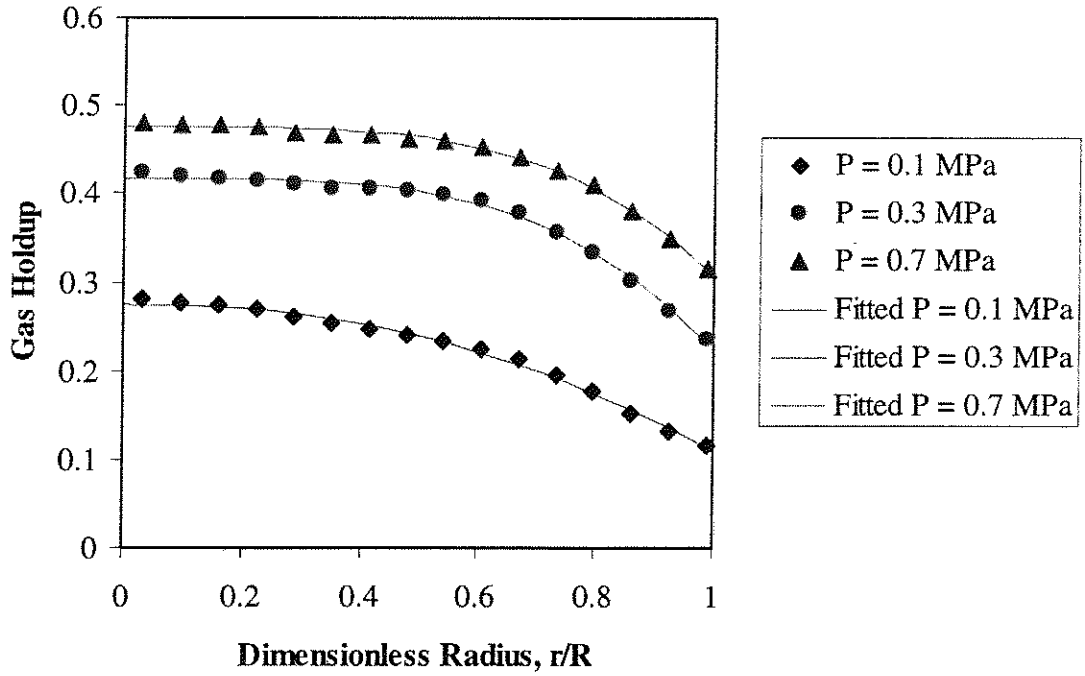

Figure 5: Radial Gas Holdup Distribution as a Function of Pressure for $U_G = 0.12$ m/s.

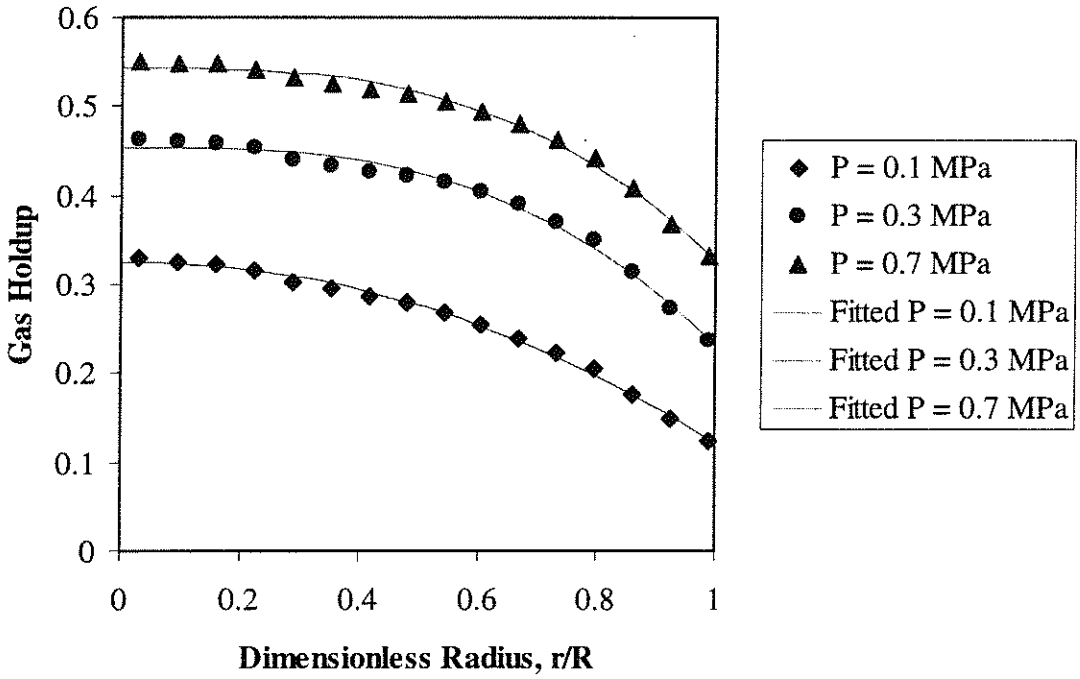

Figure 6: Radial Gas Holdup Distribution as a Function of Pressure for $U_G = 0.18$ m/s.

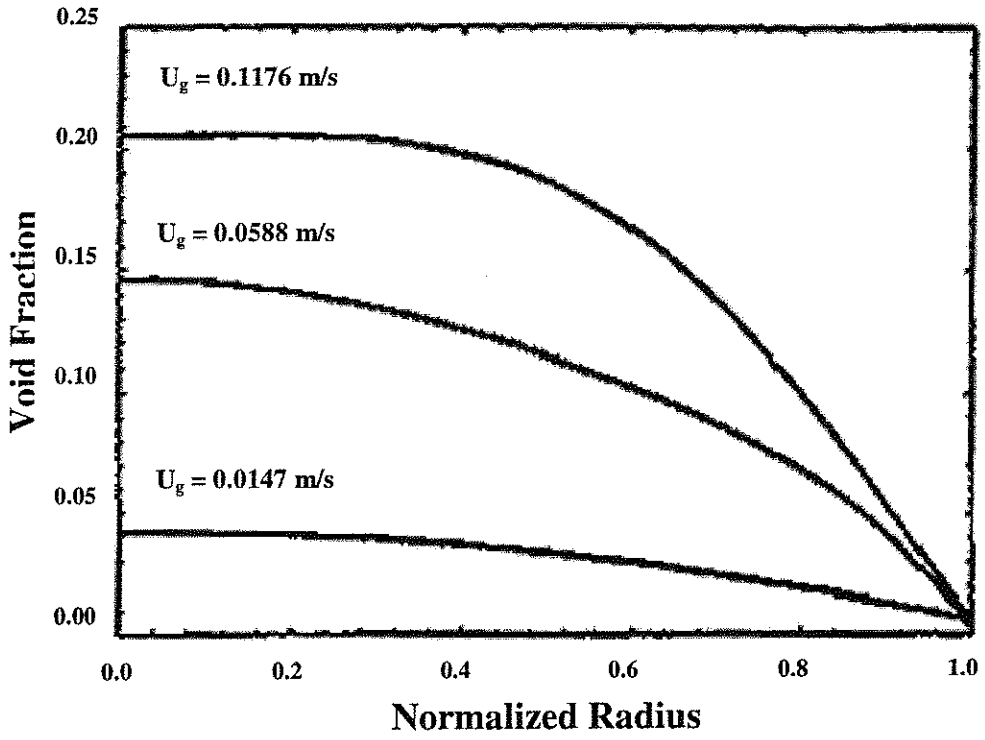

Figure 7: Radial distribution of gas holdup at atmospheric pressure as a function of superficial gas velocity for 0.19-m air-water column with bubble cap distributor (Shollenberger *et al.*, 1995).

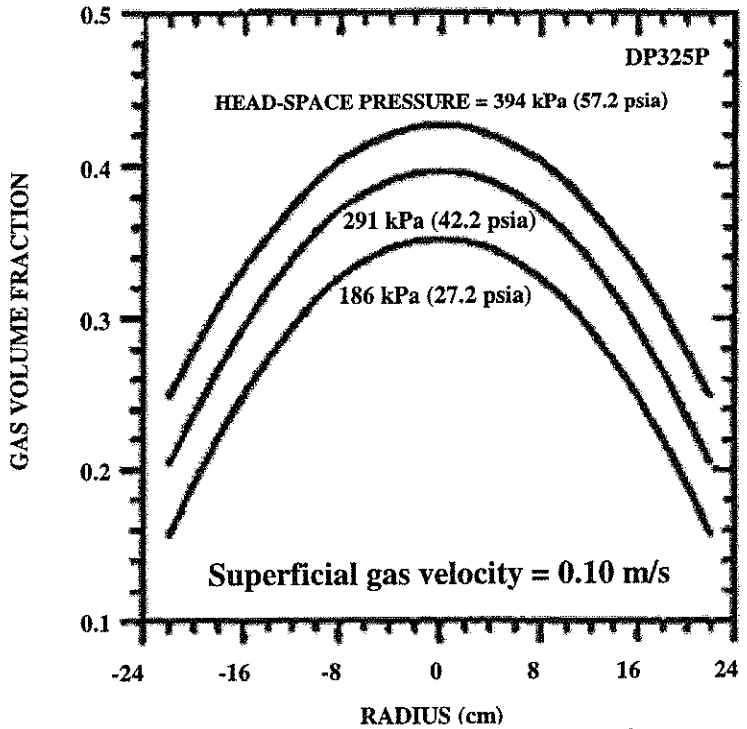

Figure 8: Radial distribution of gas holdup as a function of pressure for U_G = 0.1 m/s (Taken from Adkins *et al.*, 1996).

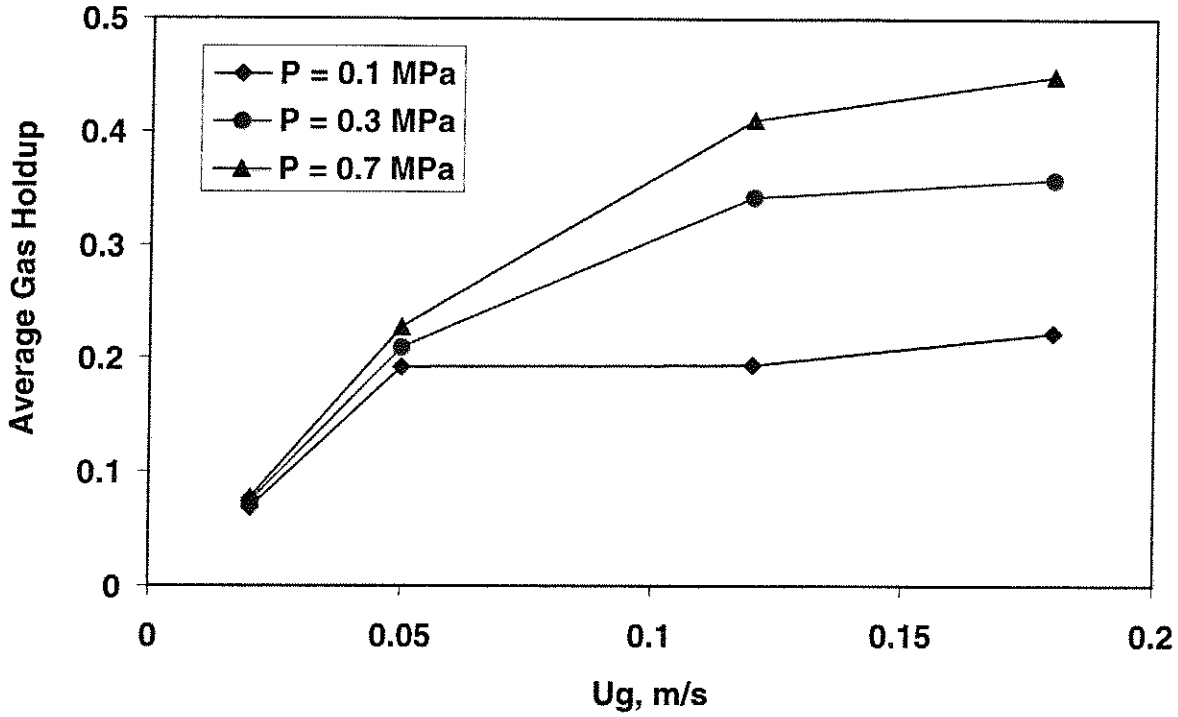

Figure 9: Cross-sectional Average Gas Holdup as a Function of Superficial Gas Velocity at Different Pressures.

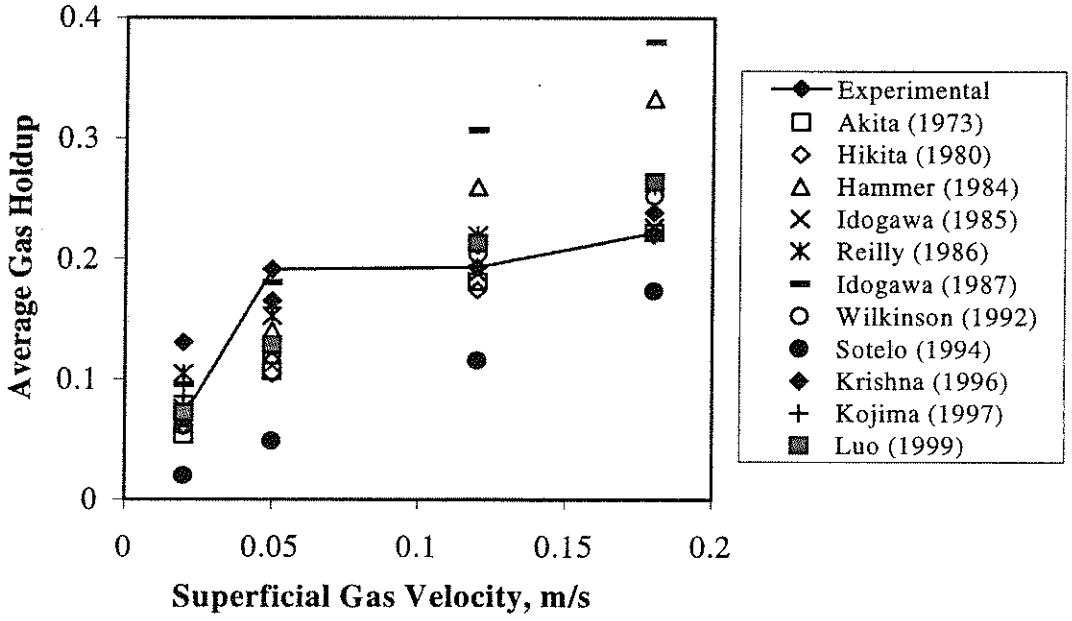

Figure 10: Cross-sectional Average Gas Holdup as a Function of Superficial Gas Velocity at Atmospheric Pressure.

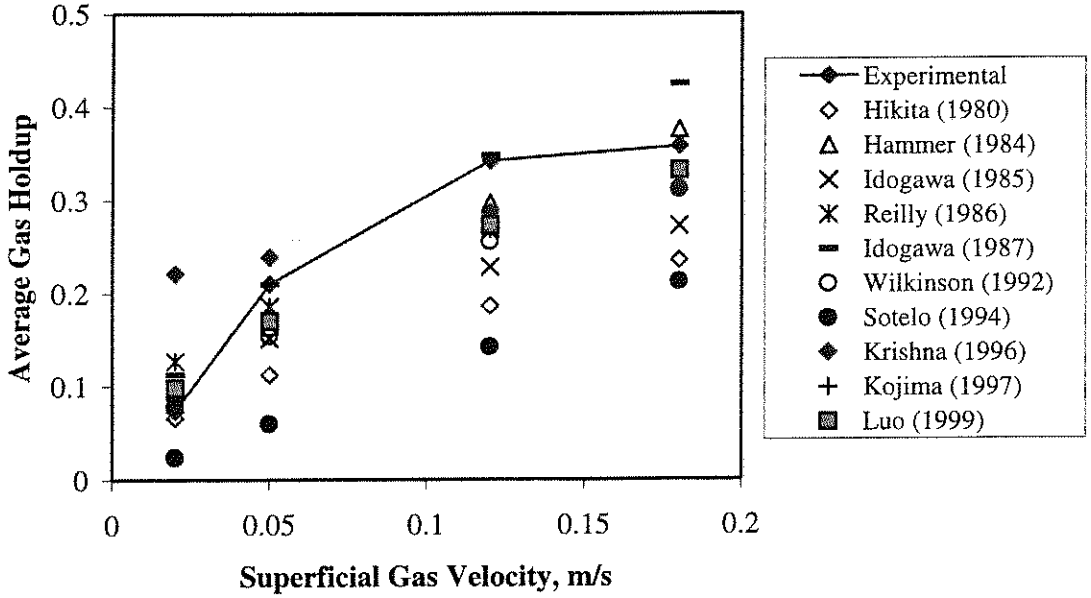

Figure 11: Cross-sectional Average Gas Holdup as a Function of Superficial Gas Velocity at $P = 0.3$ MPa.

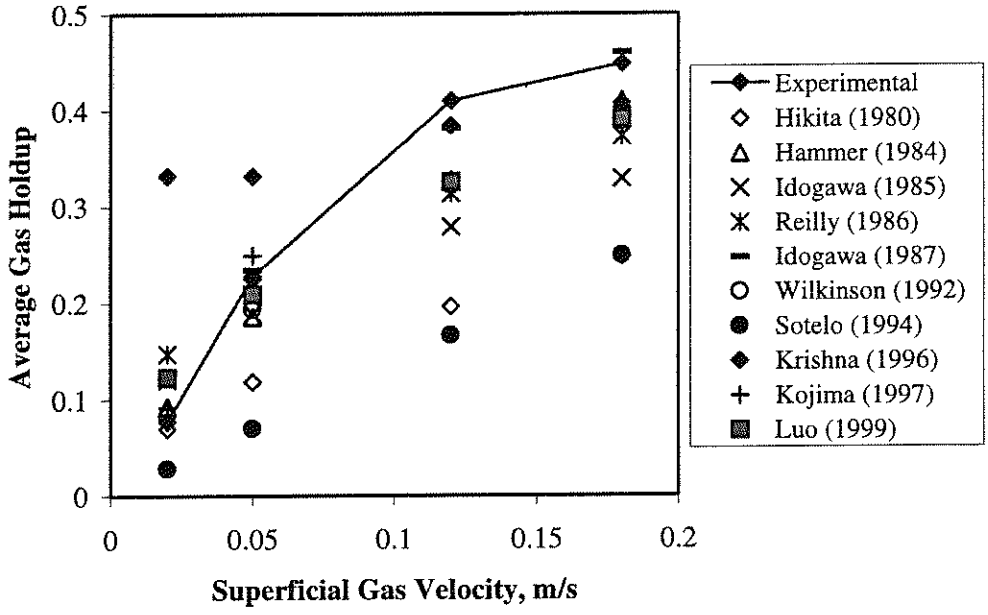

Figure 12: Cross-sectional Average Gas Holdup as a Function of Superficial Gas Velocity at $P = 0.7$ MPa.

APPLICATION OF WAVELET FILTERING TO THE RADIOACTIVE PARTICLE TRACKING TECHNIQUE (CARPT)

See the attached report for:

A. Problem Definition
B. Research Objectives
C. Research Accomplishments

Application of Wavelet Filtering to the Radioactive Particle Tracking Technique

S. Degaleesan[#], M. Dudukovic and Y. Pan
Chemical Reaction Engineering Laboratory
Department of Chemical Engineering
Washington University, St. Louis, MO 63130

Abstract

The Computer Automated Radioactive Particle Tracking (CARPT) technique has been used for the investigation of fluid dynamics, material dispersion and mixing in various multiphase rectors. The accuracy of the CARPT measurement depends on the properties of the tracer particle, the algorithm and the technique for calibration and signal processing. In this paper, a filtering technique based on the wavelet theory for the removal of white noise from the data is presented. It is shown, experimentally, that the adopted wavelet-based filtering algorithm reduces the level of noise in the data by 80 to 90%. The suitability and necessity of wavelet filtering are further demonstrated by performing a group of typical CARPT experiments in an air-water bubble column operated at different superficial gas velocities. It is demonstrated that use of the unfiltered data results in significant over-estimation of turbulent parameters while the influences on the mean velocities are minor.

Introduction

The study of the hydrodynamics of multiphase flow systems requires non-invasive techniques for the measurement of the flow fields. The opaqueness of most multiphase systems limits the applicability of the optically based techniques, such as Laser Doppler Anemometry (LDA) and Particles Image Velocimetry (PIV), in quantifying the velocity filed. The recently developed non-invasive technique –

[#] Present address: Shell Oil Company, Houston, TX.

Computer Automated Radioactive Particle Tracking, has been successfully applied in various multiphase systems, that are widely used in chemical and petroleum industries, such as bubble columns (Devanathan *et al.* 1990; Yang *et al.* 1992, 1993), fluidized beds (Moslemian *et al.* 1987) and gas-solid risers (Roy *et al.* 1999). Originally the technique was employed by Kondukov *et al.* (1964) in fluidized beds. The lack of a proper data acquisition system, at that time, prevented obtaining quantitative results. Meek (1972) developed a radioactive particle tracking with six detectors to track solids in a turbulent liquid. The detectors were mounted on an axially moving carriage, in order to maintain the particle within the control volume of the detectors. Since the carriage cannot always keep pace with the tracer particle, the particle often went out of the control volume leading to the loss of data. In addition, the use of only a few detectors and analog processing resulted in low resolution. Lin *et al.* (1985) were the first to develop a modern computer aided radioactive particle tracking facility to study solids motion in a fluidized bed. An array of 12 detectors was used. They showed the existence of multiple circulation cells at low gas velocities, and a change in the direction of solids motion with an increase in gas velocity. Moslemian (1987) improved the data acquisition system of Lin *et al.* (1985) by introducing digital pulse counters, resulting in faster sampling rates. Devanathan (1991) applied radioactive particle tracking, using a neutrally buoyant particle, to study the liquid phase motion in bubble columns. Larachi *et al.* (1994) also built a radioactive particle tracking facility and studied the motion of solids in three-phase fluidized beds, using a Monte Carlo method to model the detected radiation.

In a CARPT experiment, the position of the particle is determined by an array of scintillation detectors that monitor the radiation emitted by the particle. A set of instantaneous position data is therefore obtained for the particle at successive sampling instants. Time differentiation of the successive particle positions yields the instantaneous Lagrangian velocities of the particle, i.e., velocities as a function of time and position of the particle. From the Lagrangian particle velocities, ensemble averaging is performed to calculate the average velocities and various velocity-related quantities of the phase whose motion is being tracked. As introduced by Devanathan (1991) we use a neutrally buoyant tracer particle to map out the liquid velocity field in bubble columns.

The reliability and accuracy of the CARPT measurement largely depends on several key factors which include the tracer particle, calibration and signal processing. The issues regarding to the calibration and tracer particle have been discussed in detail by Degaleesan (1997), Kumar *et al.* (1997) and Larachi *et al.* (1997). The present paper is focussed on the topic of removing the noise inherently contained in the CARPT raw data. Owing to the quantized nature of the γ photons, the intensity of the radiation emitted by the radioactive tracer particle exhibits continuous fluctuations in time. The instantaneous particle position evaluated from the radiation signal carries such fluctuations. In turn, the Lagrangian velocity of the tracer particle, which is directly calculated from the instantaneous position of the tracer particle via time-differencing, contains spurious velocities. Usually, the noise of this type would result in inaccuracies in the estimation of turbulence-related quantities, such as turbulence intensity, eddy diffusivity etc., although the mean quantities may not be affected. Since most of the systems where the CARPT technique is applied exhibit highly turbulent nature, such consequence is obviously undesired. How to remove the noise in the position data of the particle, which causes spurious velocities, therefore, becomes an important issue in implementation of CARPT technique. Apparently, the calibration cannot eliminate the noise. In the present paper, we propose a filtering algorithm, based on wavelet analysis, for the removal of intrinsic noise in the instantaneous position data generated by the CARPT measurement. The suitability of such filtering for the CARPT data and its advantage over the conventional filtering technique based on the Fourier transform is proven and discussed. The efficiency of the wavelet filtering and its ability to improve the accuracy of measurement are experimentally validated by processing the CARPT data for a particle of controlled motion. It is shown, via processing the numerically generated 'chirp' signal, that the method works well for the multi-frequency data. Finally, the CARPT data for bubble columns of different size and superficial gas velocity are filtered by the technique. We show that the unfiltered the data results in a significant over estimation of turbulence related quantities and the wavelet filtering largely reduce such bias.

CARPT Equipmental Setup

A schematic of the bubble column and the CARPT setup is shown in Figure 1. The detectors are strategically positioned around the column, spanning its entire length. Each detector unit is a cylinder 2.125" in diameter and 10.25" long, and contains an active cylindrical NaI scintillation crystal (2" by 2"). The total number of detectors used varies depending on the size of the column. Typically 16 (140-cm diameter column) to 26 detectors (44-cm diameter column) were used. Each detector is held on the aluminium support structure such that the axis of the detector is perpendicular to that of the column and the circular face of the detector is tangential to the wall of the column at a given location. The positions of the detectors are recorded in cylindrical coordinates. For each detector, it is thus assumed that the axis of the detector is along the radial coordinate of the column. Hence, accurate alignment of the detectors to conform to the cylindrical geometry is necessary, for any misalignment would lead to error in location of the particle position.

The CARPT facility developed by Devanathan (1991) is of the third generation. Since then some aspects of the data acquisition have been improved in order to achieve faster data transfer rates and, hence, increase the sampling frequency capacities of the technique. This has lead to the fourth generation CARPT that we show here. The details of this CARPT facility have been given by Degaleesan (1997).

Wavelet-Based Filtering of CARPT Data

Owing to the quantized nature of the γ photons, the intensity of the radiation emitted by the radioactive tracer particle exhibits continuous fluctuations in time. The emission of γ photons from a radioactive source is a statistical process which follows a Gaussian distribution, with the mean n_c and standard deviation $\sqrt{n_c}$, where n_c is the number of counts emitted per unit time. The standard error which is defined as the standard deviation/mean counts, is found to vary inversely with the intensity of counts (Tsoulfanidis 1983), as expected in a Gaussian distribution. Ideally three detectors with precise signals are sufficient to locate the particle. However, since the radiation intensity

measured at a given sampling instant is not exact and exhibits variations due to the statistical fluctuations, a redundancy of detectors is employed and a weighted least square algorithm is used as a first step in determining the approximate particle position followed by position refinement (Degaleesan 1997). The detector that is the closest to the particle measures the maximum radiation and, therefore, exhibits the least standard error ($1/\sqrt{n_c}$), and is, hence, weighted the most, and vice-versa. The weighted regression algorithm helps reduce the error in position estimation and results in reasonable estimates of particle positions. However, the fluctuations in the radiation intensity data are still ``transmitted" to the instantaneous position data. Figure 2(a) shows a time series of the instantaneous position of a stationary particle estimated over 512 sampling instants. The power spectral density of the instantaneous position data in Figure 2(b), has the characteristics of white noise, indicating that the statistical fluctuations in the gamma radiation gets transmitted as white noise to the instantaneous position data. The apparent continuous movement of the actually stagnant particle results in the generation of ``spurious velocities", i.e., non-zero velocities for a physically stationary particle. Figure 3 shows the spurious velocities calculated for a stationary particle in a 14-cm diameter column operated at a superficial gas velocity of 9.6 cm/s. Consequently, the instantaneous velocities obtained during an actual CARPT experiment contain a partial contribution from the statistical fluctuations in the source particle emission. Ensemble averaging of the instantaneous velocities assigned to each column compartment eliminates these source fluctuations since the fluctuations have a Gaussian distribution with zero mean. This is reflected in the negligible mean spurious velocity calculated, which is for a stagnant particle, as one can see in Fig. 3, is of the order of 0.1 cm/sec or less, which is very small when compared with the actual liquid velocities monitored (10 cm/sec to 60 cm/sec). Hence, the radiation caused noise in the data does not affect the time-averaged velocities. However, the fluctuations (spurious velocities) do contribute to the instantaneous velocities of the particle as it follows the liquid during an experiment, and in turn to the calculated turbulence quantities that involve correlations of instantaneous velocities. This causes an over-estimation of the turbulence-related quantities.

In order to obtain an accurate estimate of the turbulence it is therefore necessary to filter the instantaneous position data and thereby eliminate, or reduce to the best possible extent, the contribution of the spurious velocities to the measured instantaneous velocities. Traditional Fourier transform filtering (FFT) was first attempted using a third order low-pass Butterworth filter. The cut-off frequency for the low-pass filter was chosen as 20Hz. An estimate of the cut-off frequency is based on the size of the tracer particle used (2.36 mm). It was shown (Degaleesan 1997) that the tracer particle, due to it finite size, can follow the liquid only, up to a frequency of about 30 Hz. Results of FFT filtering using a low-pass filter are shown in Figure 4(a). It can be observed from the middle part of Figure 4(a), which is the blowup of the region enclosed in the dash-lined box within the upper part of Figure 4(a), that the resulting filtered signal is unable to capture the sharp peaks of the original signal. As a result, these sharp changes that characterize the flow are removed as noise (refer to the lower part of Figure 4(a)). Increasing the cut-off frequency does not improve the situation as it results in preserving the residual high frequency components of the white noise in the signal. Another factor to be considered is that the actual cut-off frequency required may vary with position in the column. This suggests that a traditional Fourier transform low pass filter is not quite suitable for the purpose of filtering CARPT data, considering the non-stationary nature of the data with its sharp inflections and peaks, which are characteristic of the dynamics of the liquid in the system.

Wavelet transformation, which is a time-frequency based method, is a suitable alternative and has the distinct advantage over the Fourier transform technique as it can be used to analyze non-stationary and localized data, which exhibit varying frequency characteristics with time. This is illustrated in Figure 4(b). By comparing the middle parts of Figure 4(b) with 4(a), one can see that the sharp peaks are much better preserved after wavelet-based filtering. The lower part of the figure shows the noise that is filtered using the wavelet transformation method. This resembles white noise that is present in CARPT data (compare to Figure 2(a)). On the other hand the noise filtered using Fourier transform based filtering contains some characteristic features of the original signal and does not represent white noise, as one can recognize in the Fig. 4(a) (lower part).

Due to its advantages, wavelet analysis has been applied in our laboratory to filter the white noise from CARPT data. To demonstrate the suitability of the method for filtering CARPT data and thereby obtaining a more reliable estimate of the fluid dynamic parameters, an experiment has been conducted with a controlled motion of the radioactive tracer particle. This enables a priori knowledge of the trajectory of the particle and provides a reference against which the results from CARPT experiments subject to wavelet packet filtering can be compared. A quantitative estimate of the errors involved in the estimation of the particle position is obtained and the extent to which the intrinsic noise in the data is removed is demonstrated. Thereafter, a few typical bubble column results after wavelet filtering are presented and compared with the results obtained prior to filtering.

Wavelet Packet Filtering

The noise present in the radiation intensity data, gets transmitted to the estimated particle position data in Cartesian coordinates, $\mathbf{x}^{\mathrm{p}}(x, y, z)$. It is found that the noise in each coordinate is white noise, uncorrelated with each other. Filtering can be applied either to the radiation intensity data, measured by each detector following which the particle position is estimated, or to the instantaneous position data. Since the results from the two methods are equivalent, the latter approach of filtering the position data is chosen as it is more efficient in computing resources.

Wavelet packet decomposition using Daubechies' (1988) orthonormal, nearly symmetric wavelets is employed for this analysis. In Appendix A, a brief introduction to wavelet transform and wavelet packet decomposition is given followed by a description of the algorithm used for filtering CARPT data. The original signal data, i.e. the instantaneous position of the tracer particle measured by CARPT, is divided into data sets of length $N=2^L$; $L=10$, $N=1024$. For each data set of length N sampled at a constant frequency, the wavelet packet decomposition is performed and subsequently the best basis representation, based on minimizing the entropy of the coefficients, i.e. Eq. (A-11), is obtained. The wavelet packet coefficients (wpc) in the chosen best basis are arranged

in descending order of amplitude (*wpc*). The fraction of the coefficients corresponding to those with the largest magnitude, i.e., the first few significant coefficients, represent the coherent part of the signal while the remaining weak coefficients, of low magnitude depict the noise. The energy level of the noise in the data is very low and constitutes typically less than 5% of the total signal energy. This information is obtained by analysis of the CARPT calibration data, as described below.

The objective of the wavelet filtering is to extract only the coherent part of the signal leaving out the noise. This is achieved by selecting a signal threshold for the wavelet packet coefficients, ` *st* '. All the coefficients below this threshold are set to zero. Only the fraction of coefficients with magnitudes larger than the set threshold are retained, re-ordered and reconstructed to yield the filtered signal. The filtering algorithm hence requires a predetermined value for the signal threshold, ` *st* '. The choice of ` *st* ' depends on the extent of noise in the data for the particle position coordinates, $x(t)$, $y(t)$ and $z(t)$. An initial estimate of *st* is obtained using the experimental data for a stationary particle measured during the calibration. Fine tuning of ` *st* ' is then done, to ensure that the noise filtered from the data has the characteristics of white noise. The power spectral density is used as the basis for verification. White noise has a uniform distribution of energy over all the frequencies (maximum is the Nyquist frequency) sampled. The value of ` *st* ' is adjusted such that the filtered noise shows a uniform power spectrum, with no peaks (the presence of peaks is an indication that a part of the actual signal is removed). The process of tuning is done with several randomly chosen data sets to arrive at the final value of *st* for the data, which is then used for filtering the instantaneous position data. The initial estimates of ` *st* ', from the calibration data, are usually slightly higher than the final tuned value. The values of the threshold, *st*, can vary for x, y and z. Typically *st* is anywhere between 0.7 to 2.0, increasing with column diameter, and is found to be dependent on the operating conditions as well. At very high gas velocities, the effect of the fluctuations from the bubbles seems to increase the noise in the data. The filtered results are, however, insensitive to minor variations in the threshold value (±0.05 to 0.15).

Filtering using the above described algorithm ensures maximum extent of reduction of the noise in the data, resulting in a smoother version of the signal and simultaneously helps in retaining the sharp features arising from the nature of the flow in the system. In order to verify the applicability and effectiveness of the algorithm for filtering the noise from the experimental data, the algorithm is tested with data produced from experiments with a controlled motion of the tracer particle.

Experiments with Controlled Movement of Tracer Particle

The experimental setup principally consists of two motors, a screw conveyor and a plate as shown in Figure 5. Motor-I is secured at the bottom of the structure and is geared to a screw conveyor that is positioned vertically. The screw conveyor supports a vertical frame on top of which the plate is mounted. The shaft of motor-II, which is fixed to the top of the plate, is connected to a smooth, circular disc. The radioactive particle to be tracked is fixed to the tip of a thin Plexiglas rod attached to the disc. The operation of motor-II causes the particle to move in a circular motion. The maximum frequency of motion is 3 Hz. The distance of the particle from the axis varies from 7 to 8 cm. Simultaneously motor I causes the plate held to the frame to move vertically in ``up and down" motion (with frequencies of the order of 0.1 Hz). The maximum vertical distance traversed by the particle is 6.4 cm. By this arrangement the particle is made to move in a spiraling 3D motion, with high (3 Hz) and low (0.2 Hz) frequencies. The two motors are driven by microprocessors, which are interfaced with a personal computer. This arrangement ensures the precision with which the particle moves. A trolley system with guiding wheels provided for guiding the frame helps in minimizing the vibration of the setup. The entire structure is supported on the plenum centered between the detector supports (not shown in figure). Sixteen strategically positioned detectors are used for detecting the γ radiation from the source particle. Calibration is first performed using various particle positions that cover the entire range of experimental runs. Subsequently the experimental runs are performed. In each run, the speed of the two motors is varied, thereby varying the velocity of the particle.

The details of the experiments carried out are shown in Table 1. The experiments are conducted in air. Motor-I moves the particle in a linear vertical motion, i.e. along the z axis in Cartesian coordinates. Motor-II moves the particle in a horizontal 2-D circular trajectory, i.e. in a $x-y$ plane. A parametric representation of particle trajectory, **x**, in Cartesian coordinates, is given as;

$$x(t) = x_c + r_p \cos\left(\theta_0 \frac{\pi}{180}\right) + r_p \cos(2\pi\omega_2 t) \tag{1}$$

$$y(t) = y_c + r_p \sin\left(\theta_0 \frac{\pi}{180}\right) + r_p \sin(2\pi\omega_2 t) \tag{2}$$

$$z(t) = z_0 + \omega_1 t \tag{3}$$

where x_c and y_c are biases in position due to experimental constraints, r_p is the radius of curvature which the particle traverses, θ_0 is the initial angular position of the particle, ω_2 is the frequency of rotation of motor I, ω_1 gives the displacement of the particle per unit time and is related to the rpm of motor-I. Motor-I is programmed to move 800 steps, first in the clockwise direction, followed by the counter clockwise direction. This periodic motion is repeated several times. 125 steps in the clockwise direction is equivalent to 1 cm. This induces a frequency of about 0.1 Hz in the z direction of motion. Based on the above known trajectories, the actual Lagrangian velocities, v_i, are calculated.

The instantaneous position data $\mathbf{x}^{\mathrm{p}}$ resulting from the CARPT measurements for the controlled motion of the particle are subject to wavelet packet filtering (st_x = 0.9 to 1.1, st_y = 0.9 to 1.1, st_z = 1.0 to 1.3) yielding filtered results $\mathbf{x}^{\mathrm{f}}$. Thereby, the particle velocities from CARPT measurements (sampling frequency=50 Hz) before filtering, $\mathbf{v}^{\mathrm{p}}$, and after filtering, $\mathbf{v}^{\mathrm{f}}$, are obtained. The results are analyzed by comparing the magnitude of the error in position and velocity. For this purpose the root mean square (*rms*) error is defined as

$$Q_i^{\alpha} = \left[\frac{1}{N}\sum_{n=1}^{N}\left(x_i^{\alpha} - x_i\right)^2\right]^{1/2}; \qquad P_i^{\alpha} = \left[\frac{1}{N}\sum_{n=1}^{N}\left(\mathrm{v}_i^{\alpha} - \mathrm{v}_i\right)^2\right]^{1/2}; \quad i = x, y, z;\ \alpha = p, f \tag{4}$$

where N is the number of samples considered.

Figure 6(a) shows the actual trajectory $y(t)$ for a period of 10 seconds, for Run 5 listed in Table 1. Figure 6(b) is a comparison of the error in estimating the successive y positions of the particle. Figures 7, 8 and 9 show all the three components of particle velocity along with the errors before and after filtering. The particle trajectory projected on the horizontal x - y plane is essentially a circle. Such a trajectory for two cycle periods is shown in Figure 10 for Run 3, before and after filtering, along with the actual trajectory. One can clearly see the spurious velocity induced by the error in particle position. A summary of the results for the entire set of runs is presented in Table 1 which reports the errors in position x, y and z, and spurious *rms* velocities, before and after filtering.

It is evident by examining the results, that there is significant improvement due to filtering in the accuracy of estimation of both the positions and velocities of the moving particle. The residual error (spurious rms velocities) after filtering the data is 2-5 cm/sec. This represents an average of 75% (maximum of 95%) reduction in the level of noise in the data. With regard to the magnitude of the *rms* fluctuating velocities of the liquid in bubble columns, which are an order of magnitude higher, the reduction in error is considered substantial.

The experiment for the controlled motion of the tracer particle thus provides a basis for the validation of the CARPT technique in estimating the trajectory and velocities of the moving particle, using the wavelet analysis technique for filtering the intrinsic noise in the instantaneous position data.

Due to experimental constraints, it has been possible to perform experiments with the controlled motion of the particle only at fixed frequencies. It is also of interest to illustrate the capability of the present filtering algorithm for the case of time series data containing varying frequencies, which are characteristic of the instantaneous position data measured in bubble column experiments. This is done by numerically generating a

time series with varying frequency components, and superimposing on this signal white noise that is characteristic of the fluctuations present in the instantaneous position data from CARPT. The signal considered for this purpose is defined by the following equation:

$$f_{ch}(t) = A_n\left(\sin\left(\frac{\pi t^2}{6}\right)+\sin\left(\frac{\pi t^3}{200}\right)\right) \tag{6}$$

The two terms on the right hand side of the above equation are referred to as 'chirp' signals, (the first is a linear 'chirp' and the second is a quadratic 'chirp'). The square and cubic variation of time in the first and second term, respectively, induces a frequency variation in the time series $f(t)$. White noise, $n(t)$, that is typical of the noise present in CARPT data is superimposed on $f(t)$ resulting in a noisy signal, $f_n(t)$.

$$f_n(t) = f_{ch}(t)+n(t); \qquad \sigma_n^2 = 0.1 \tag{7}$$

The wavelet filtering algorithm is applied to $f_n(t)$, using a threshold of st=1.0, which is arrived at by studying the wavelet packet decomposition of the noise, $n(t)$, as described earlier. The noisy signal and the filtered signal are shown in Figure 11.

The root mean square error in the signal is reduced from 0.44 cm to 0.109 cm after filtering. Effects of filtering are apparent in Figure 12 that shows the velocity computed by time differencing the signal. The root mean square error in the velocity is reduced from 19.9 cm/s, before filtering, to 3.19 cm/s after filtering. This demonstrates the suitability of the proposed wavelet-based filtering algorithm for filtering signals similar to CARPT data, with multi components varying from low to high frequency.

Wavelet Filtering of CARPT Data in Bubble Columns

The wavelet filtering algorithm is applied to all the bubble column experimental data obtained by Degaleesan (1997). The thresholds required for performing the filtering are obtained using the procedure described in the earlier section (`st' varies from 0.7 to 1.0 for a 14 cm diameter column; 0.8 to 1.2 for a 19-cm diameter column; 1.4 to 1.8 for a 44-cm diameter column).

A few typical results are presented comparing the effects of filtering on the various fluid dynamic parameters. Figure 13 shows the comparison of the time averaged axial liquid velocity in a 14-cm diameter column, at two superficial gas velocities. The results before and after filtering are nearly identical. This is expected, as it is known that the spurious velocities get averaged out in the process of time averaging, and therefore do not affect the mean velocities. On the other hand there is a significant reduction in the magnitude of the turbulent normal stresses as seen in Figures 14 and 15 for superficial gas velocities of 2.4 cm/s and 9.6 cm/s, respectively, in a 14-cm diameter column. Figure 15 for the lower gas velocity shows a lower level of noise, as discussed earlier.

Figure 16 shows the effects of filtering on the turbulent shear stress in a 14-cm column at superficial gas velocities of 2.4 cm/s and 9.6 cm/s. As opposed to the normal stresses and turbulent kinetic energy, the effect of filtering cannot be judged based on the reduction in the magnitude of the shear stress. The reason for this is because the shear stress measurement involves the cross-correlation of the radial and axial turbulent velocities. Unlike the results for the normal stresses, the presence of noise in the data causes the shear stress calculated to oscillate between positive and negative values (due to the cross-correlation) and does not necessarily result in an increase in the magnitude of the quantity. This is clearly illustrated in the positive and negative values of the shear stress calculated from the unfiltered data, while for the filtered data the results show expected trends. Various components of the turbulent stress tensor (e.g. axial normal, azimuthal normal and axial-azimuthal shear, etc.), computed from filtered CARPT data, were compared to LDA determined values (Mudde *et al.* 1997) and were found to be of the right order of magnitude at gas superficial velocities of about 2.5 cm/s and at 9.6 cm/s (Degaleesan, 1997). Unfiltered CARPT data yield values of normal stresses that far exceed those determined by LDA. This provides additional evidence that the adopted filtering procedure removes noise without impairing the real signal.

Summary

An algorithm for noise filtering based on the wavelet analysis has been applied to the Computer Automated Radioactive Particle Tracking (CARPT) system developed in our laboratory for the measurement of the liquid velocity field in bubble column reactors. We have demonstrated, via the experiments with controlled movement of the particle and the numerically generated multi-frequency signal, that filtering the white noise is a necessary step in a CARPT experiment and that the wavelet based filtering is more suitable for the removal of this type of noise than the traditional Fourier transform filtering. Filtering of CARPT data using the wavelet-based algorithm thus helps in reducing the level of noise in the data by 80 to 90%, and therefore enables a better and more accurate estimation of the fluid dynamic parameters in bubble columns.

Acknowledgements

The authors would like to thank the Department of Energy for the financial support (DE FC2295PC95051). Our gratitude also goes to ExxonMobile Research and Engineering Company (EMRE) for providing the CARPT hardware and to Air Products & Chemicals (APCI) for providing the motivation for this work. One of the authors (S.D.) would like to especially thank Dr. B. A. Toseland from APCI and Dr. M. Chang from EMRE for their valuable discussion and comments.

Notation

U_g = superficial gas velocity; cm/s.

D = column diameter; cm.

$\boldsymbol{u}$ = liquid phase velocity vector; cm/sec.

Literature Cited

Chaouki, J., F. Larachi and M. P. Duduković, `Noninvasive Tomographic and Velocimetric Monitoring of Multiphase Flows`, *Ind. Eng. Chem. Res.*, **36**, 4476-4503 (1997)

Chui, C. K., *Wavelet Analysis and its Applications: Volume I, An Introduction to Wavelets*, Academic Press (1992).

Coifman, R. and M. V. Wickerhauser, "Entropy-based algorithms for best basis selections', *IEEE trans. On Inf. Theory*, **38**, 713-718 (1992).

Coifman, R., F. Majid and M. V. Wickerhauser, "Denoise', Preprint, Yale University (1993).

Daubechies, I., `Orthonormal bases of compactly supported wavelets`, *Comm. Pure Appl. Math.*, **41**, 909-996 (1988).

Degaleesan, S., *Fluid Dynamic Measurements and Modeling of Liquid Mixing in Bubble Columns*, D.Sc. Thesis, Washington University, St. Louis, MO (1997).

Devanathan, N., D. Moslemian and M. P. Dudukovič, `Flow Mapping in Bubble Columns Using CARPT', *Chem. Engng. Sci.*, **45**, 2285-2291(1990).

Devanathan, N., *Investigation of Liquid Hydrodynamics in Bubble Columns via Computer Automated Radioactive Particle Tracking (CARPT)*, D.Sc. Thesis, Washington University, St. Louis, MO (1991).

Joseph, B. and R. L. Motard, ``*Wavelet Applications in Chemical Engineering*'', Kluwer Academic Publishers (1994).

Kondukov, N. B., A. N. Kornilaev, I. M. Skachko, A. A. Akhromenkov and A. S. Kurglov, `An Investigation of the Parameters of Moving Particles in a Fluidized Bed by a Radioisotopic Method', *Int. Chem. Eng.*, **4,** 43-47 (1964).

Kumar, S. B., M. P. Dudukovič and B. A. Toseland, `Measurement Techniques for Local and Global Fluid Dynamic Quantities in Two and Three Phase Systems', *Non-Invasive Monitoring of Multiphase Flows*', Edited by J. Chaouki, F. Larachi and M. P. Dudukovič, Elsevier, Chapter 1, 1-46 (1997).

Larachi, F., G. Kennedy and J. Chaouki, `A ϒ-Ray Detection System for 3-D Particle Tracking in Multiphase Reactors', *Nucl. Instr. Meth.*, **A338**, 568-576 (1994).

Larachi, F., J. Chaouki, G. Kennedy and M. P. Dudukovič, `Radioactive Particle Tracking in Multiphase Reactors: Principles and Applications`, *Non-Invasive Monitoring of Multiphase Flows*, Elsevier, (Chaouki, J., F. Larachi and M. P. Dudukovič eds.) Chapt. 11, 335-406 (1997).

Lin, J. S., M. M. Chen and B. T. Chao, `A Novel Radioactive Particle Tracking Facility for Measurement of Solids Motion in Gas Fluidized Beds', *AIChE Journal*, **31,** 465-473 (1985).

Mallat, S. and Z. Zhong, 'Matching pursuits with time-frequency dictionaries,' Preprint, New York University (1992).

Meek, C. C., *Statistical Characteristics of dilute particulate suspensions in turbulent fluid field*, Ph.D. Thesis, University of Illinois, Urbanana, IL (1972).

Moslemian, D., *Study of solids motion, mixing and heat transfer in gas-solid fluidized beds*, Ph.D. Thesis, University of Illinois, Urbanana, IL (1987).

Moslemian, D., N. Devanathan and M. P. Duduković, `Radioactive Particle Tracking technique for Investigation of Phase Re-circulation and Turbulence in Multiphase Systems', *Rev. Sci. Instrum.*, **63**, 4361-4372 (1992).

Mudde, R. F., J. S. Groen and H. E. A. Van den Akker, `Liquid Velocity Field in a Bubble Column: LDA Experiments,` Chemical Engineering Science 52, 4217-4224 (1997).

Palavajjahala, S., R. L. Motard and B. Joseph, `Computational Aspects of Wavelets and Wavelet Transforms', ``Wavelet Applications in Chemical Engineering'', Edited by R. L. Motard and B. Joseph, Kluwer Academic, Chapter II, 33-85 (1994).

Tsoulfanidis, N., *Measurement and detection of radiation*, McGraw Hill, New York (1983).

Wielopolski, L., 'The Monte Carlo calculation of the average solid angle subtended by right circular cylinder from distributed sources,' *Nucl. Instr. Meth.*, **143**, 577-581 (1977).

Yang, Y. B., N. Devanathan and M. P. Duduković, `Liquid Backmixing in Bubble Columns', *Chem. Engng. Sci.*, **47**, 2859-2864 (1992).

Yang, Y. B., N. Devanathan and M. P. Duduković, `Liquid Backmixing in Bubble Columns via computer-automated Radioactive Particle Tracking (CARPT)', *Experiments in Fluids*, **16**, 1-9 (1993).

Appendix A Some Basic Concepts of Wavelet Analysis

Wavelet transform maps a time domain signal onto a time-scale plane. The transformation is performed using a family of wavelets, $\psi_{a,b}(t)$, generated by the dilation and translation of a function $\psi(t)$, called the basis or mother wavelet, i.e.,

$$\psi_{a,b}(t) = |a|^{-1/2}\psi\left(\frac{t-b}{a}\right), \qquad a,b \in R \tag{A1}$$

is a family of wavelets, where a and b are the dilation and translation parameters, respectively. These functions have prescribed smoothness, are well-localized in time and

frequency and form a well behaved basis (Daubechies 1988). Each wavelet has a specific time-frequency localization. Parameters a and b determine the compromise between time and frequency. For instance, wavelets of high frequency, i.e., large a, are narrow in time, while wavelets of low frequency are broad in time. As a result wavelets are able to ``zoom-in'' on short-lived high frequency phenomena, and ``zoom-out'' on long lived low frequency phenomena. Wavelet transformations, thus work well for cases of filtering non-stationary signals clouded with white noise, and are still able to capture the sudden changes in the signal. There are a number of wavelets with different properties available in the literature, for example, Chui-Wang wavelets, Coiflets, Daubechies wavelets, etc. (for example, see Chui 1992; Palavajjhala *et al.* 1994). In this investigation Daubechies orthonormal wavelets (Daubechies 1988) are used.

Wavelets are broadly classified as continuous wavelets and discrete wavelets. The term wavelet transform is very generic and can be categorized as continuous wavelet transforms and discrete wavelet transforms which use continuous wavelets and discrete wavelets, respectively. The theory regarding wavelet transforms and various aspects of wavelet analysis and their applications can be found in Chui (1992), Daubechies (1992) and Joseph and Motard (1995). In what follows the aspects of wavelet analysis that are used in this work is described. A brief introduction along with the underlying basic concepts to discrete wavelet transforms (DWT) and wavelet packet decomposition (WPD) is first presented.

Discrete wavelet transforms involve the projection of a data set onto discrete wavelets to give discrete wavelet coefficients. This is represented as:

$$\left\langle f, \psi_{m,n} \right\rangle = 2^{-m/2} \int_{-\infty}^{+\infty} f(t) \psi\left(2^{-m} t - n\right) dt \qquad \text{(A2)}$$

Where the dilation and translation parameters, a and b, in Equation (B1) are discretized respectively as $a = a_0^m$, $b = n b_0 a_0^m$ ($a_0 = 2$ and $b_0 = 2$ are constants). The inner product defined in Equation (B2) for various values of m,n are called the discrete wavelet coefficients. The reconstruction of $f(t)$ from these coefficients for orthogonal wavelets is given by

$$f(t)=\sum_{m,n\in Z}\psi_{m,n}(t)\langle f(t),\psi_{m,n}(t)\rangle \tag{A3}$$

DWT is a special case of Wavelet Packet Decomposition (WPD). In WPD, a library of wavelet packets are generated, from which a variety of bases can be extracted to represent the signal. The construction of wavelet packets can be represented in a hierarchy as shown in Figure??. Using two filters, *H*, a low-pass filter and *G*, a band-pass filter, the entire library of wavelet packets is generated using a recursive scheme (Wickerhauser 1991) as follows:

$$\psi_0 \equiv H\psi_0; \qquad \int\psi(t)dt=1 \tag{A4}$$

$$\psi_{2f} \equiv H\psi_f; \qquad \psi_{2f}=\sqrt{2}\sum_j h(j)\psi_f(2t-j) \tag{A5}$$

$$\psi_{2f+1} \equiv G\psi_f; \qquad \psi_{2f+1}=\sqrt{2}\sum_j g(j)\psi_f(2t-j) \tag{A6}$$

$$\psi_{s,f,p}=\psi_f\left(p-2^{-s}t\right) \tag{A7}$$

where *s, f, p* denote the scale, frequency and position indices, respectively. *h* and *g* are the filter coefficients associated with the low-pass and band-pass filters *H* and *G*, which are characteristic of the wavelet function used. The nature of the wavelet packets generated depend on *h* and *g*. There are a variety of wavelets available, of which Daubechies' (1988) orthonormal, compactly supported wavelets are most popular.

The decomposition of the signal onto these wavelet packets constitutes WPD. As in the case of DWT, the wavelet packet coefficients are given by:

$$\lambda_{s,f,p}=\left\langle f,\psi_{.f,ps}\right\rangle=2^{-s/2}\int f(t)\psi_f\left(p-2^{-s}t\right)dt \tag{A8}$$

where λ is the wavelet packet coefficient. Alternatively,

$$\lambda_{s+1,2f,p}=H\lambda_{s,f,p} \tag{A9}$$

$$\lambda_{s+1,2f+1,p}=G\lambda_{s,f,p} \tag{A10}$$

The resulting library of wavelet packet coefficients contains redundant information from which a variety of bases can be chosen. The best representation is the one that has the least number of significant coefficients. There are several ways of identifying a best basis representation using some type of information cost. The most appealing is the one that

has the least information entropy. An additive measure of entropy (Coifman and Wickerhauser 1992) is defined as

$$e = -\sum_i |\lambda_i|^2 \ln|\lambda_i|^2 \tag{A11}$$

where λ_i are the wavelet packet coefficients. The more randomness in the signal, the greater its entropy, and therefore the greater the number of coefficients required to represent the signal accurately which means larger information cost. This concept has found applications in denoising a noisy signal, data compression and speech scrambling, among others. This can be illustrated by the following example

Consider a signal such as a sinusoidal wave, $f_s = \sin(10\pi t)$, at a frequency of 10 Hz, with an amplitude of 1, such that the signal energy $\sum_i^N f_s(i)^2$ = 500 units, where $N = 1024$ is the length of the signal. This periodic signal represents a coherent structure. Using the wavelet packet decomposition and the best basis representation, this signal can be well represented with a minimum of 90 wavelet packet coefficients. On the other hand, if one considers a signal characterizing white noise, f_n, with the same energy level of 500, a best basis representation of this white noise requires at least 750 coefficients (largest coefficient is 1.8 in magnitude, as opposed to 28 for the sinusoidal wave). This illustrates the difference between a coherent signal, which can be represented by a few large wavelet packet coefficients, and white noise which is an incoherent signal and can only be represented by a large number of small wavelet packet coefficients.

It is of interest to apply the wavelet packet decomposition and the best basis algorithm in denoising or filtering of noisy signals. The idea is to extract coherent parts present in the signal, i.e. the signal features with good time-frequency localization, by adopting the method of adapted waveform denoising proposed by Coifman *et al.* (1993). The signal is first transformed to wavelet packet coefficients from which the best basis coefficients are selected. A part of the signal represented by a few largest coefficients is used to extract a coherent part of the signal. The remaining incoherent part is decomposed several times to extract all the coherent parts remaining in it. All the

individual coherent parts, thus extracted, are superimposed to give the filtered signal. The incoherent part remaining at the end is rejected as noise. The advantage of the algorithm is that exact characterization of the process is not required. This method is similar to the Matching Pursuit Algorithm discussed by Mallat and Zhong (1992).

In the present work, the waveform denoising algorithm (Coifman *et al.* 1993) described above is adopted with some modifications. Since the signal to noise ratio of the data is high, 95:5, i.e., the energy level of the noise in the signal is low, a suitable threshold for the magnitude of the wavelet packet coefficients is chosen, by which a large number of coefficients with magnitudes below the threshold are set to zero. These coefficients, having low energy, are considered to represent the noise in the signal and are thereby removed.

Table 1. Details of experiments for controlled motion of particle

Run No.	r_p cm	θ_0 degree	ω_1 1/sec	z_0 cm	z_f cm	ω_2 1/sec
1	6.964	315	2	112.21	118.61	2.75
2	7.989	270	2	112.81	119.41	0.00
3	7.180	315	2	112.21	118.61	1.00
4	7.180	315	2	112.21	118.61	2.00
5	7.180	315	2	112.21	118.61	2.75
6	7.989	315	2	112.21	118.61	1.50

Table 2. Errors in the estimation of particle position and velocity.

Run No.	Direction	Error in position (cm)				Error in velocity (cm/sec)	
		Before filtering		After filtering		Before filtering	After filtering
		Q_i^p	*min/max*	Q_i^f	*min/max*	P_i^p	P_i^f
1	X	0.32	-1.17, 1.12	0.19	-0.70, 0.60	20.50	4.16
	Y	0.36	-0.15, 1.20	0.26	-0.75, 0.80	20.01	4.66
	Z	0.49	-1.70, 1.40	0.25	-0.70, 0.74	30.36	1.68
2	X	0.31	-0.97, 1.03	0.03	-0.04, 0.03	16.99	0.07
	Y	0.28	-1.10, 1.15	0.01	-0.01, 0.02	17.94	0.04
	Z	0.40	-1.30, 1.03	0.25	-0.79, 0.50	24.29	1.05
3	X	0.32	-1.16, 1.13	0.21	-0.70, 0.90	19.3	3.20
	Y	0.31	-1.20, 1.20	0.21	-0.85, 0.80	18.0	3.60
	Z	0.47	-1.50, 1.75	0.17	-0.90, 0.60	28.9	1.34
4	X	0.32	-1.08, 1.12	0.22	-0.75, 0.86	19.5	4.80
	Y	0.32	-1.50, 1.25	0.23	-0.70, 0.75	19.0	4.50
	Z	0.46	-1.40, 1.40	0.21	-0.65, 0.60	29.0	1.38
5	X	0.30	-1.11, 1.32	0.19	-0.90, 0.66	20.2	5.40
	Y	0.29	-0.89, 0.90	0.16	-0.61, 0.65	18.7	3.80
	Z	0.47	-1.60, 1.40	0.22	-0.87, 0.72	29.2	1.56
6	X	0.31	-1.16, 1.08	0.21	-0.80, 1.00	19.78	4.18
	Y	0.28	-1.14, 1.11	0.14	-0.84, 0.82	18.69	3.51
	Z	0.37	-1.09, 1.21	0.20	-0.86, 0.72	25.73	1.48

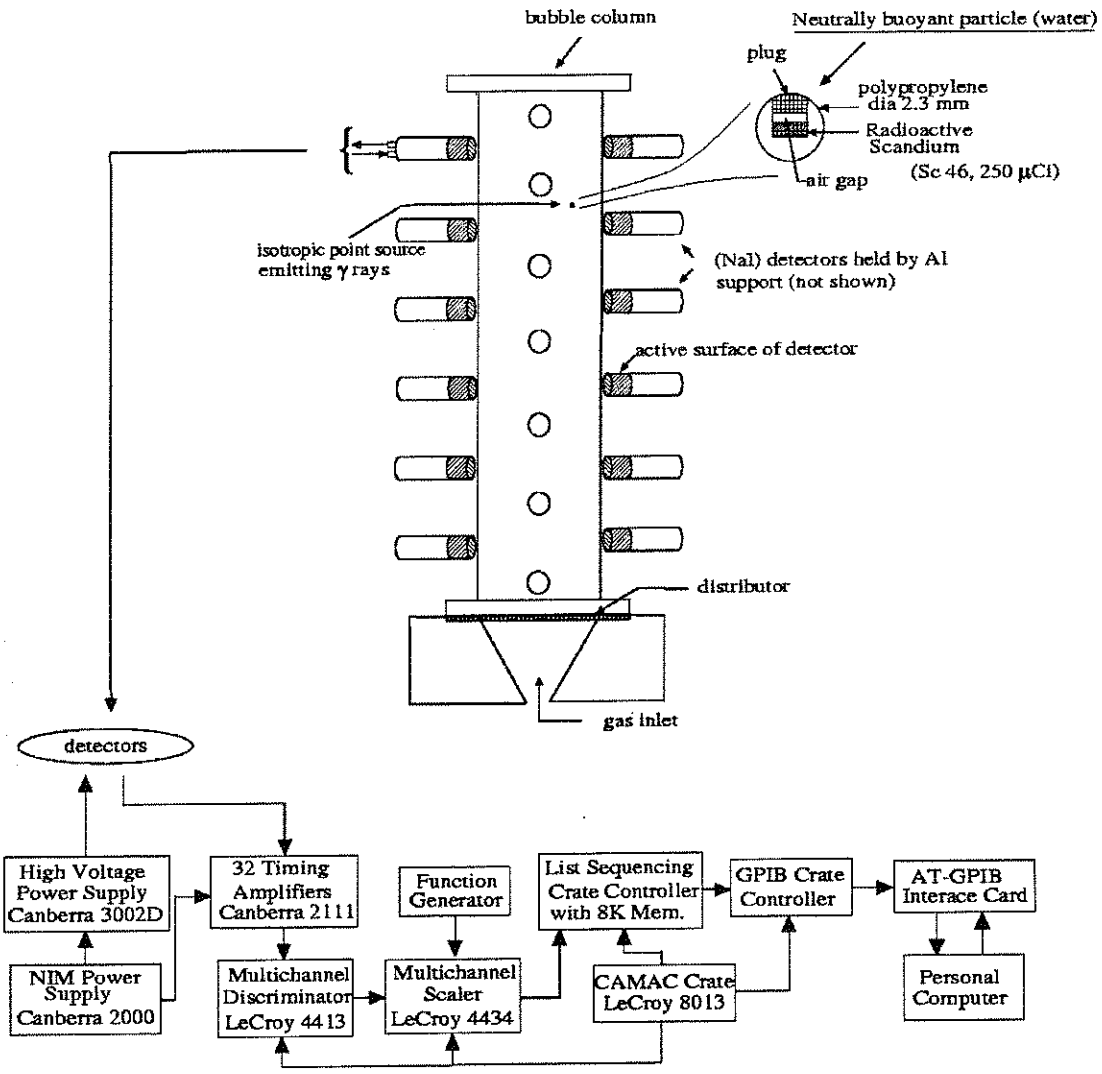

Figure 1. Schematic of the CARPT facility.

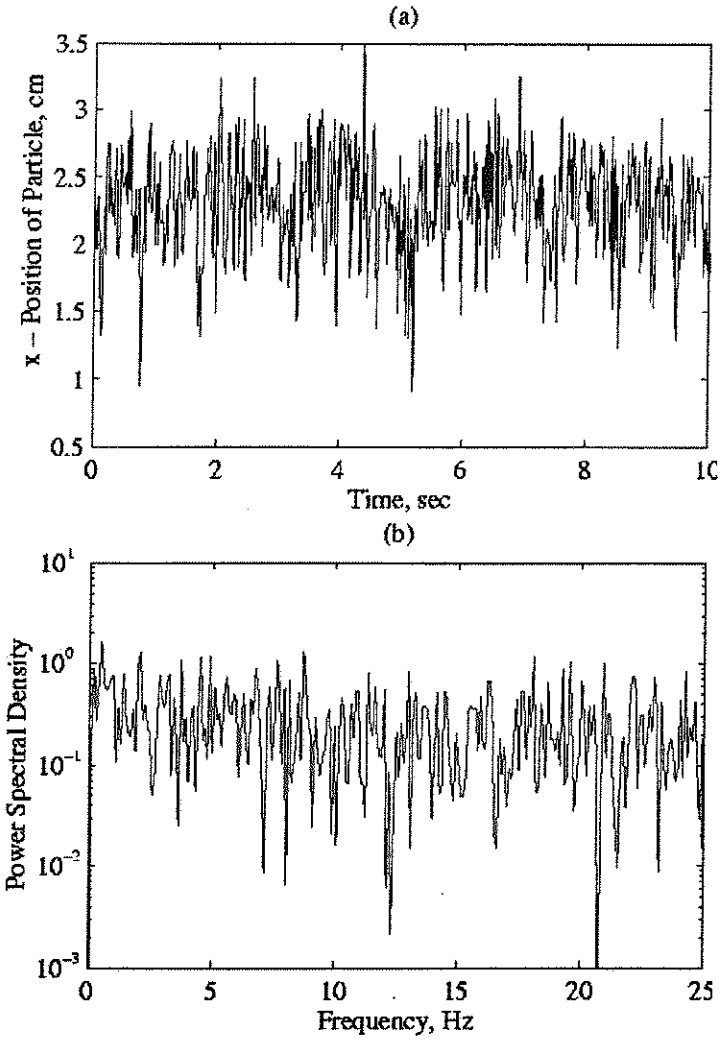

Figure 2. Fluctuations in the position of a stationary particle in a 14-cm diameter column operated at superficial gas velocity of 9.6 cm/s.

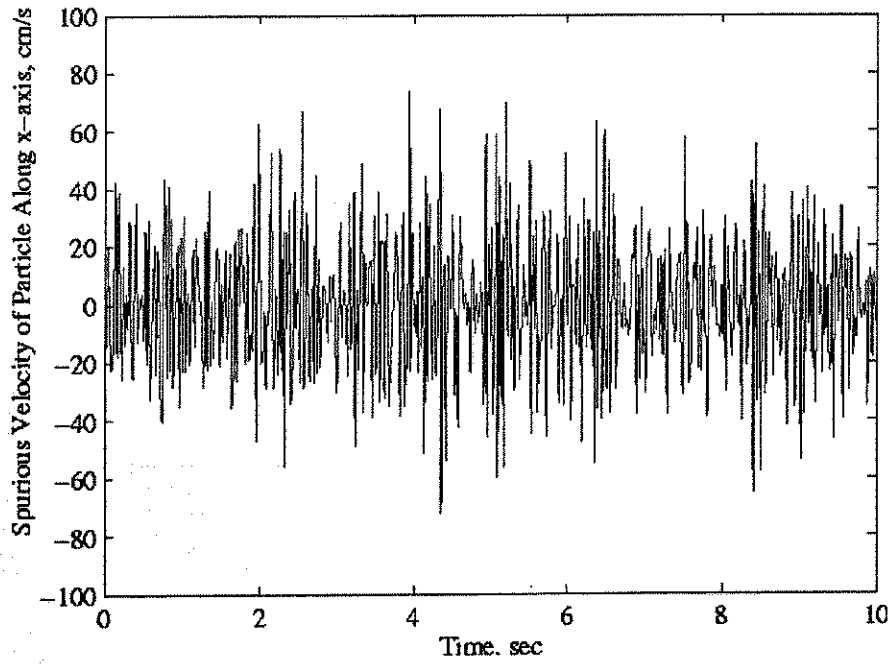

Figure 3. Spurious velocity. $\overline{u_x} = 5\times10^{-2}$ cm/s, $\sqrt{\overline{u_x' u_x'}} = 26.4$ cm/s.

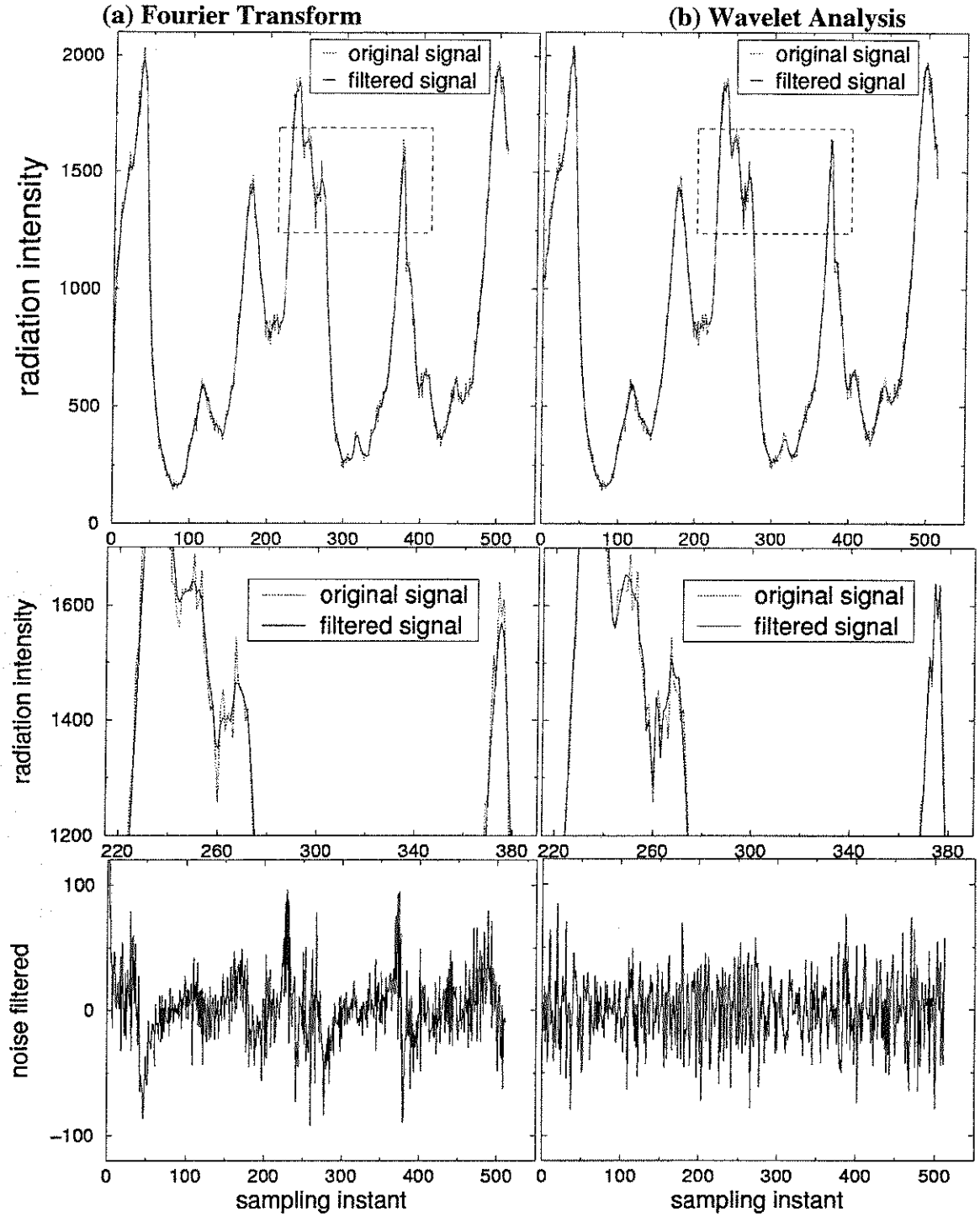

Figure 4. Comparison of Fourier transform and wavelet analysis techniques for filtering CARPT data.

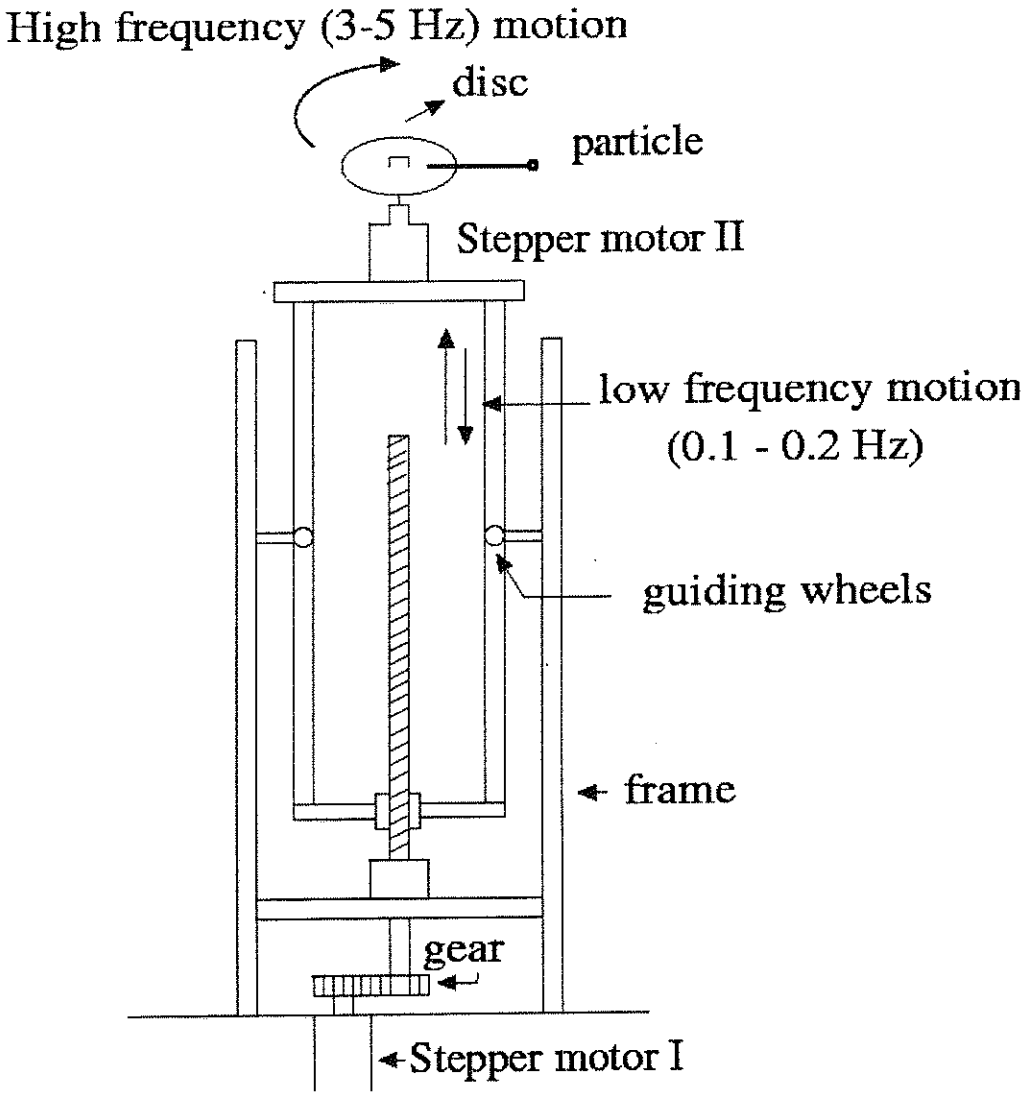

Figure 5. Experimental setup for controlled motion of particle.

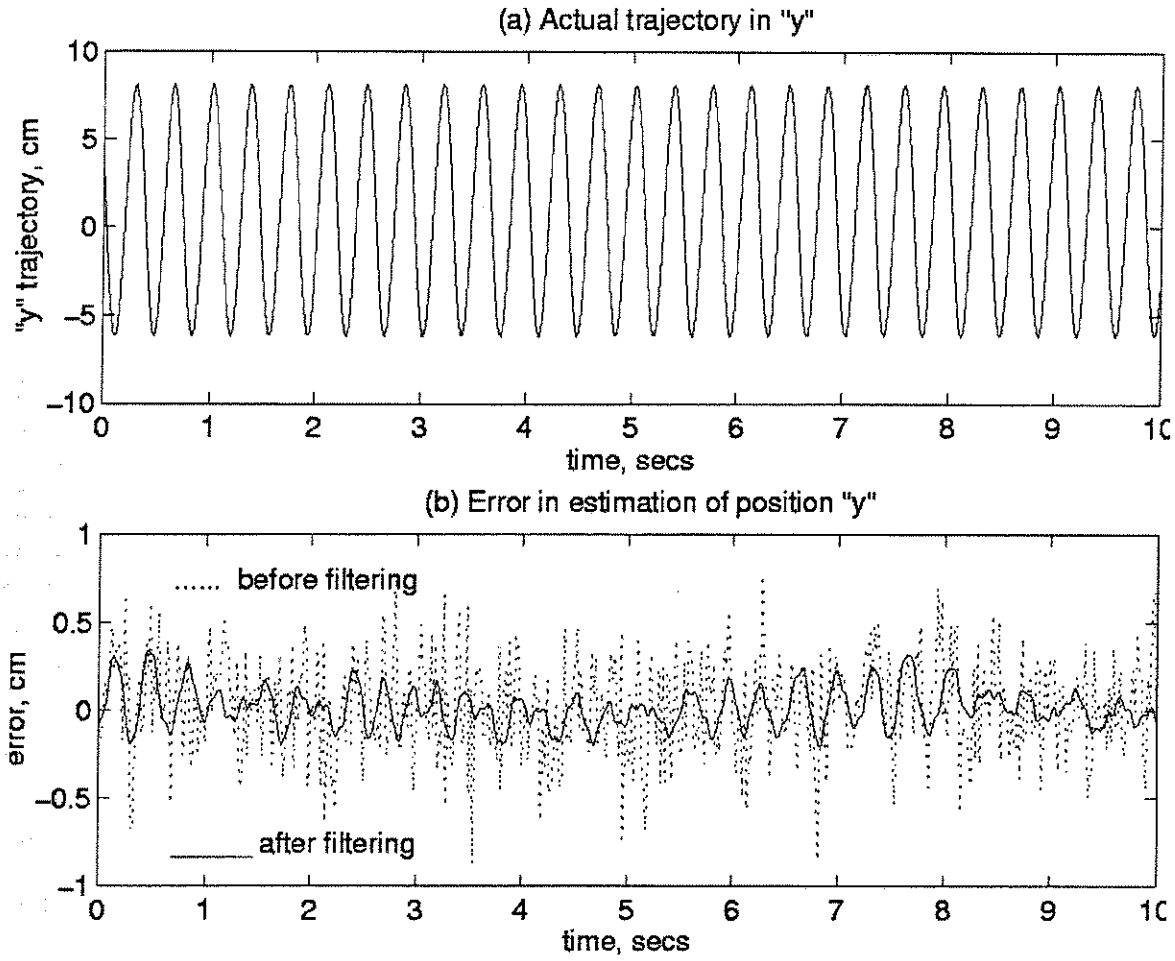

Figure 6. Results for Run 5: trajectory y of particle.

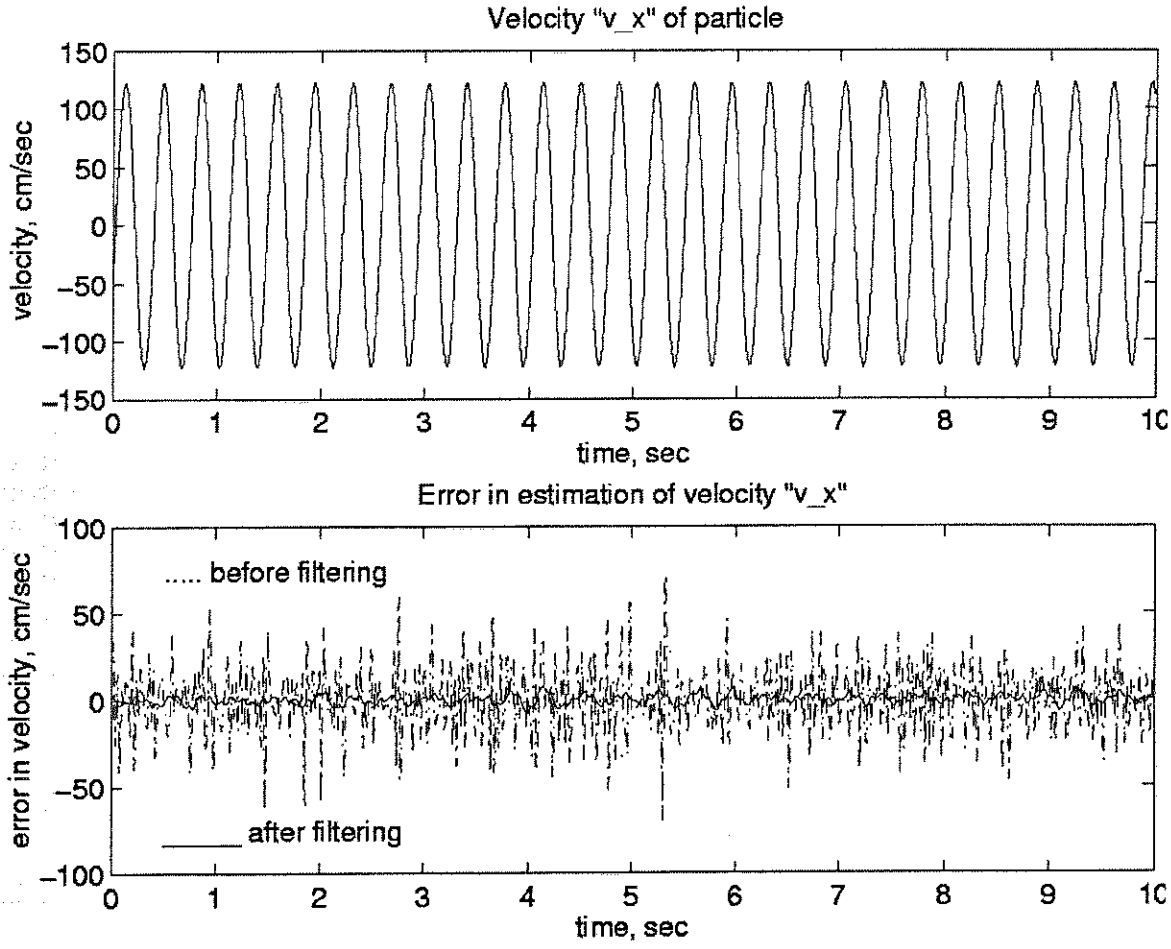

Figure 7. Results for Run5: Velocity v_x and error in estimation of velocity of particle.

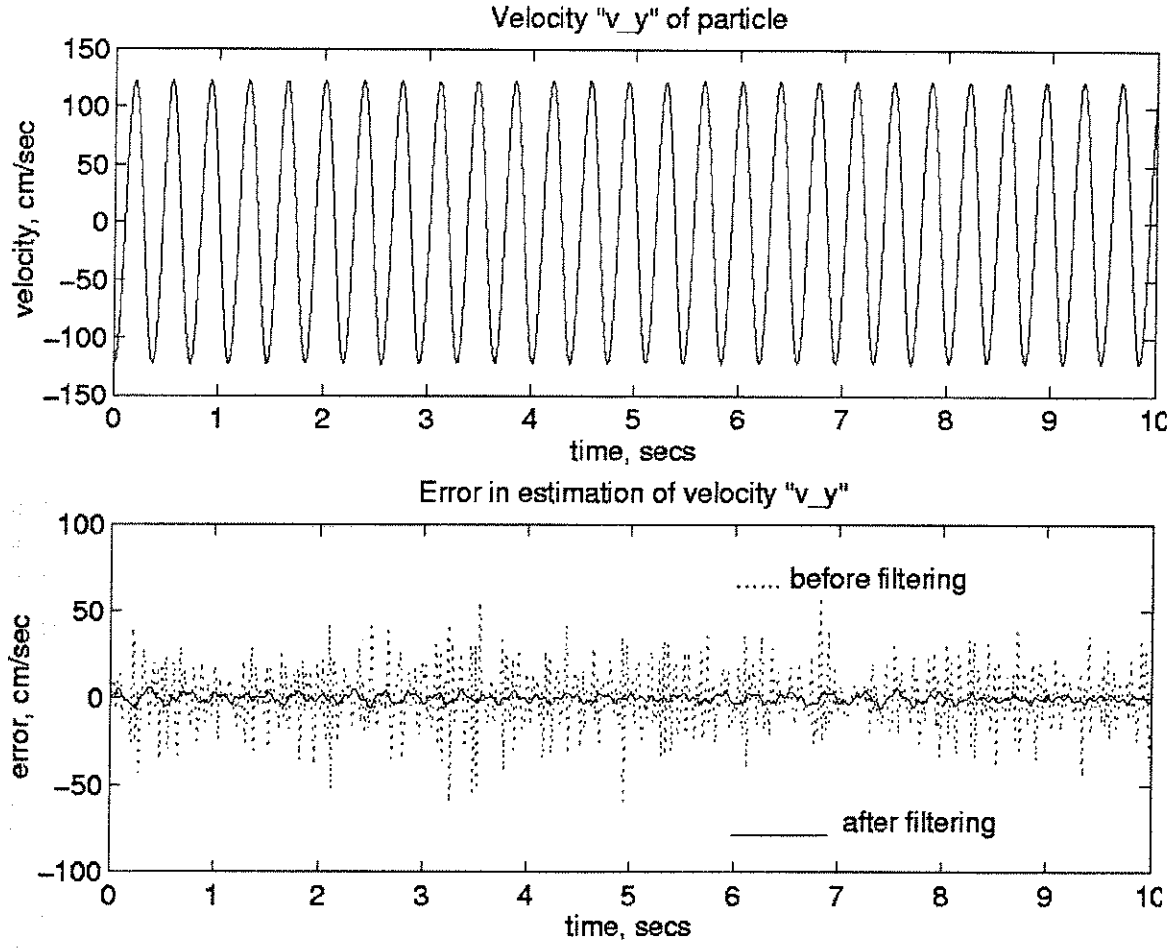

Figure 8. Results for Run5: Velocity v_y and error in estimation of velocity of particle.

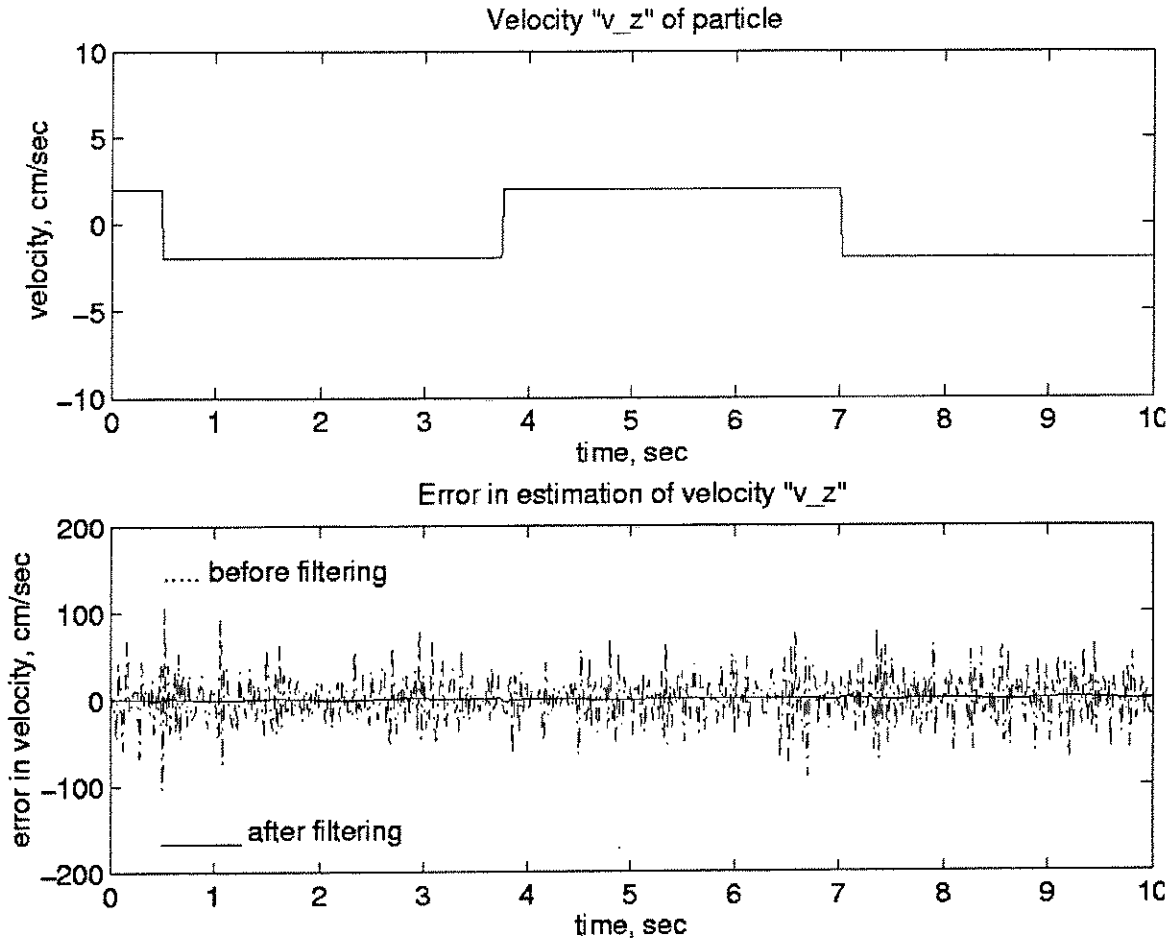

Figure 9. Results for Run5: Velocity v_z and error in estimation of velocity of particle.

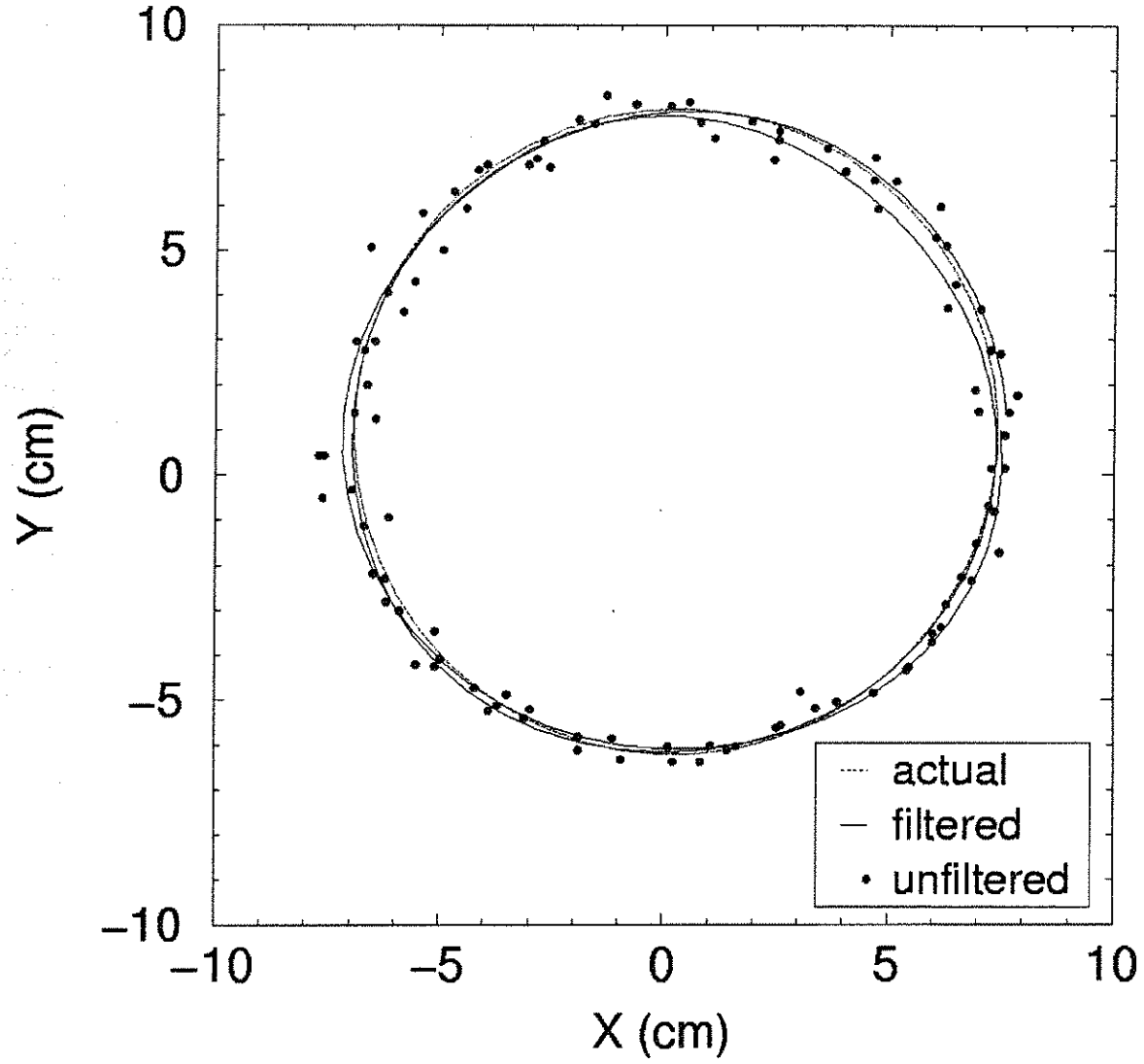

Figure 10. Circular trajectory of particle for Run 3.

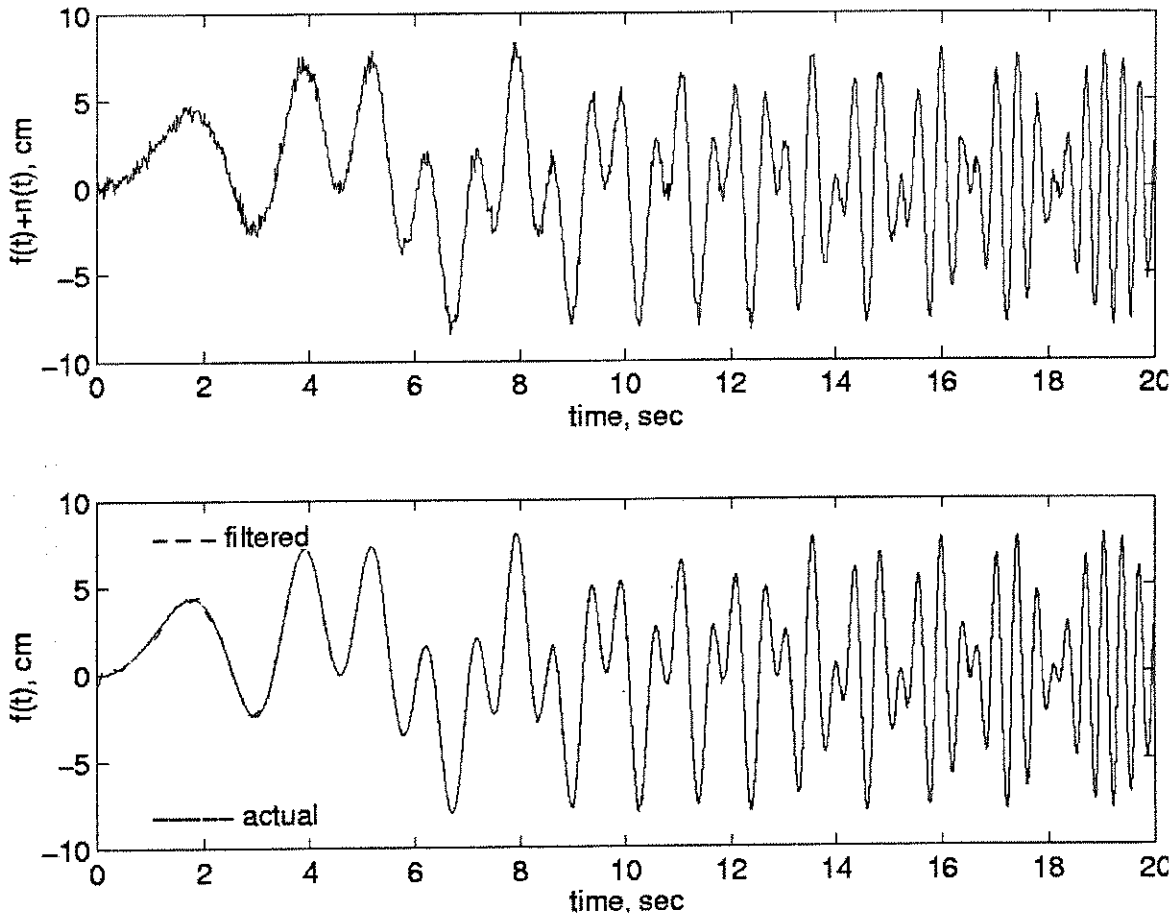

Figure 11. Filtering of the numerically generated noisy 'chirp' signal.

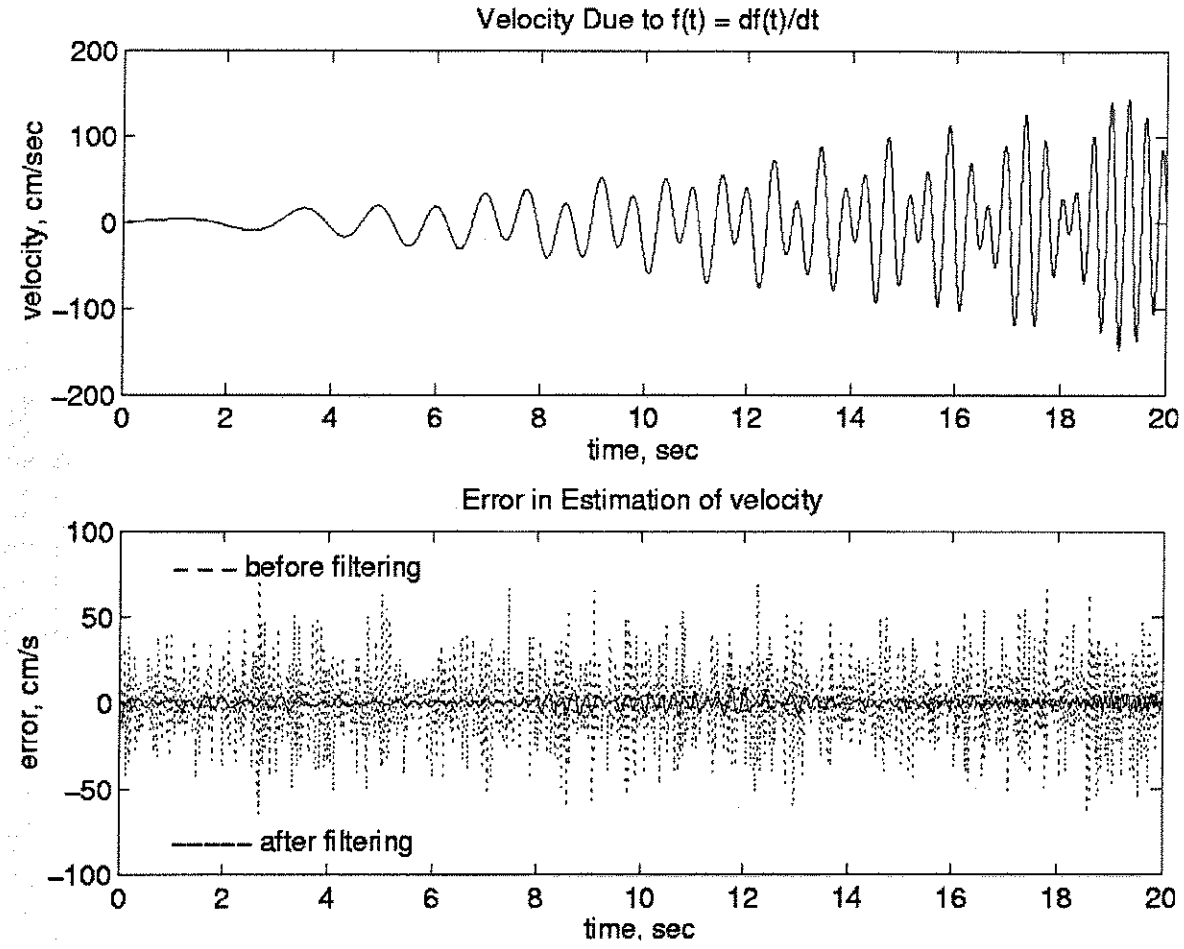

Figure 12. Error in the velocities computed by differentiation of the chirp.

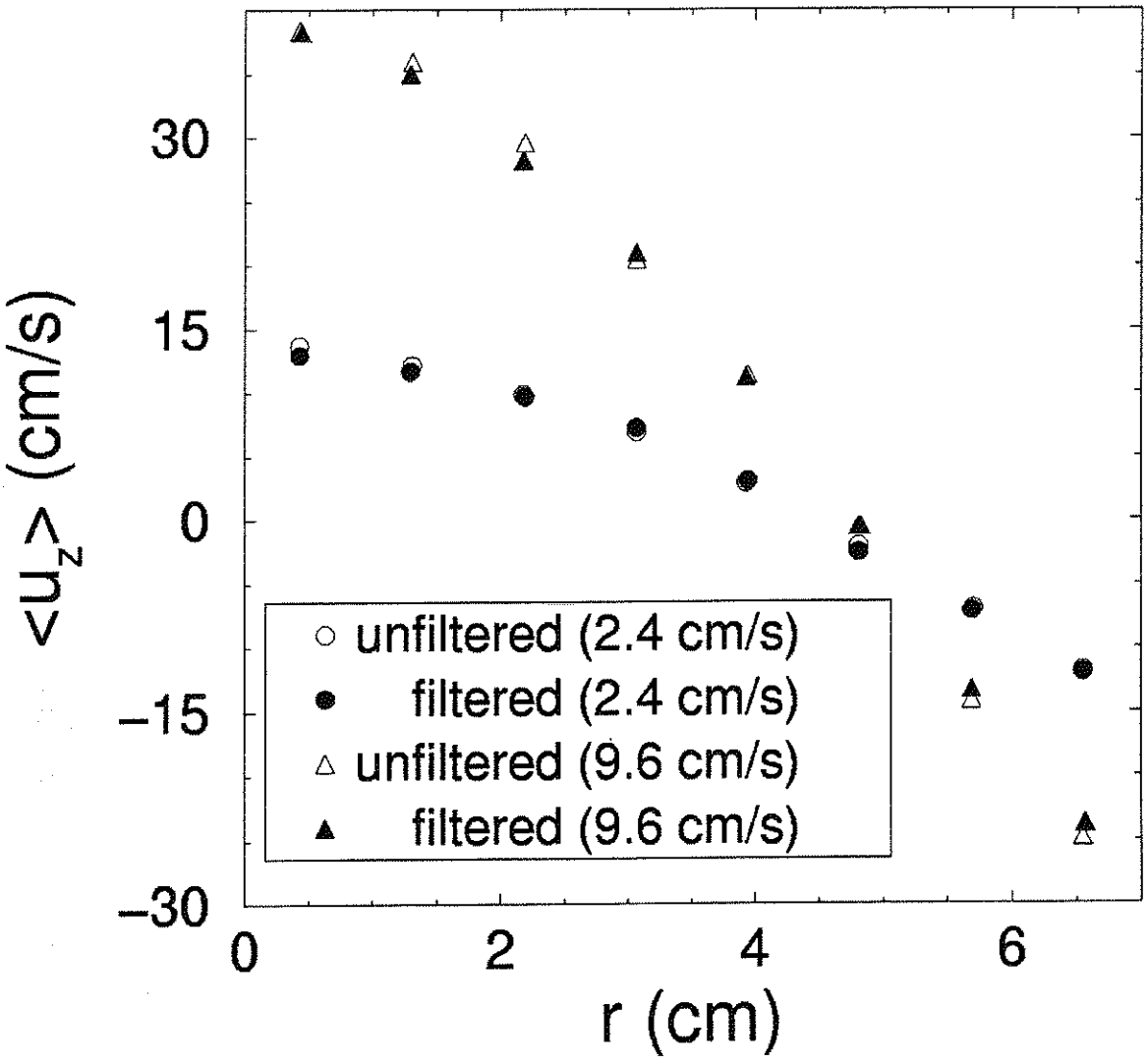

Figure 13. Comparison of time-averaged liquid axial velocity before and after filtering for a 14-cm diameter column.

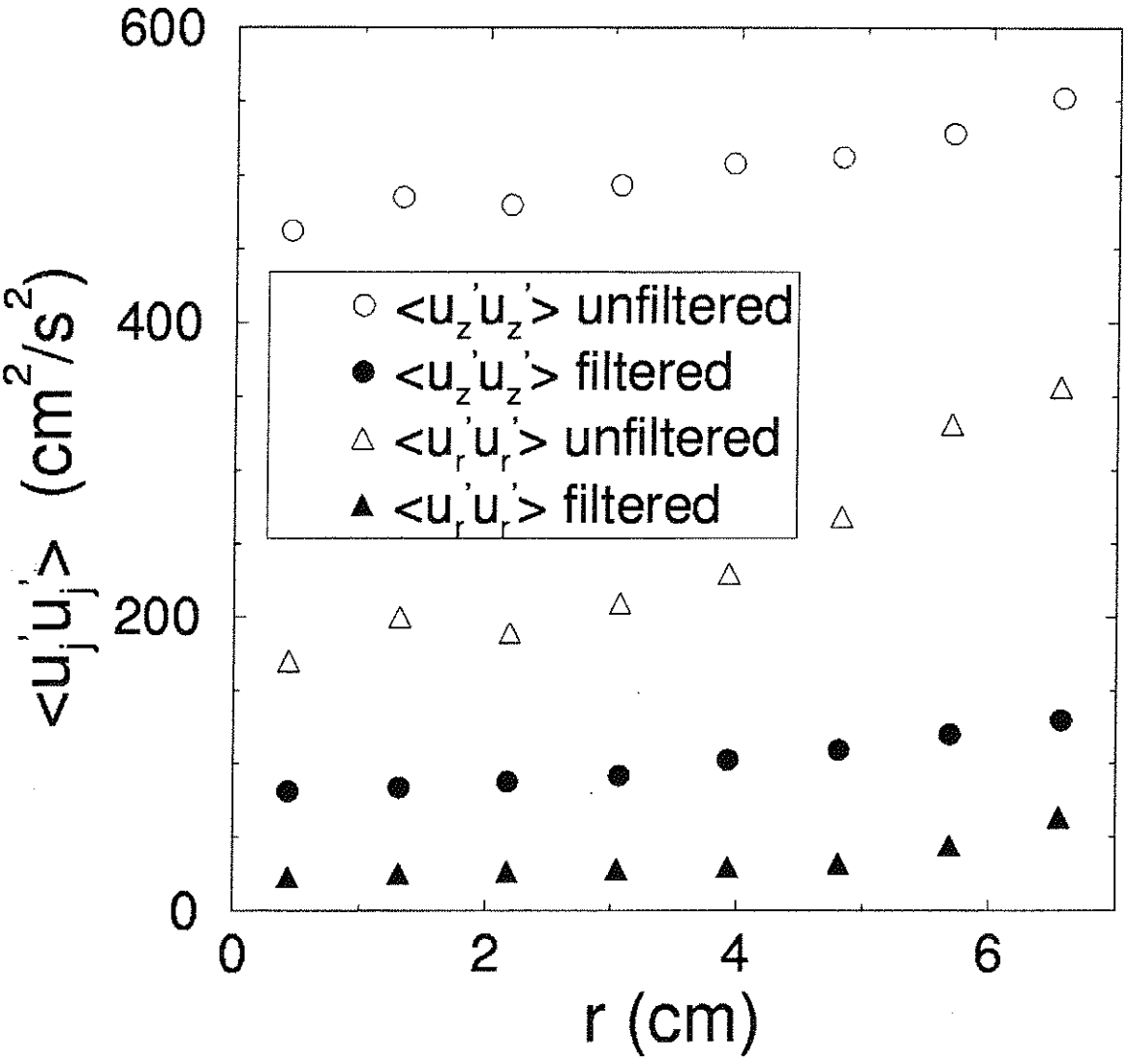

Figure 14. Comparison of turbulent normal stresses, $\overline{u_r' u_r'}$ and $\overline{u_z' u_z'}$, before and after filtering for a 14-cm diameter column at U_g=2.4 cm/s.

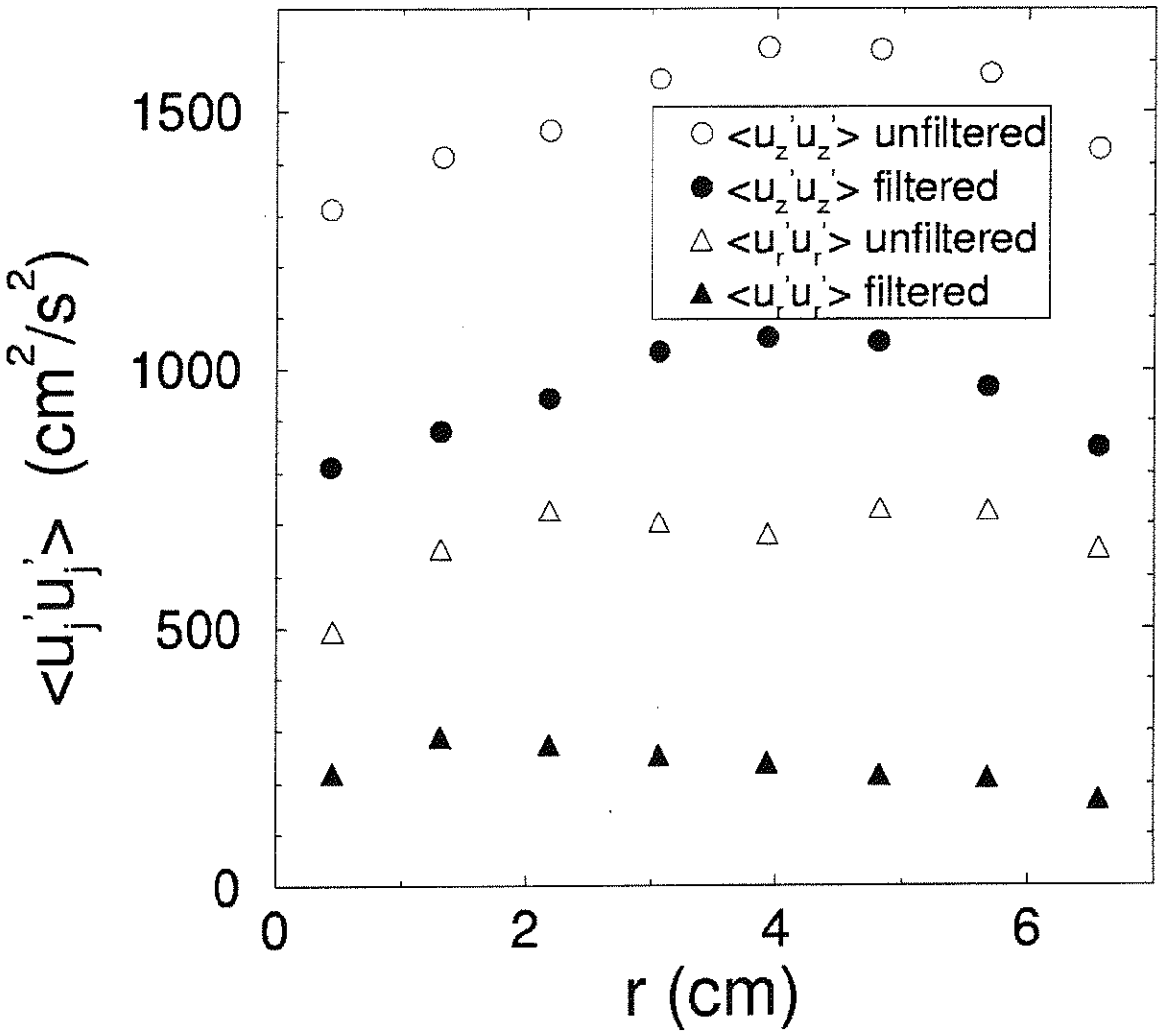

Figure 15. Comparison of turbulent normal stresses, $\overline{u_r'u_r'}$ and $\overline{u_z'u_z'}$, before and after filtering for a 14-cm diameter column at U_g=9.6 cm/s.

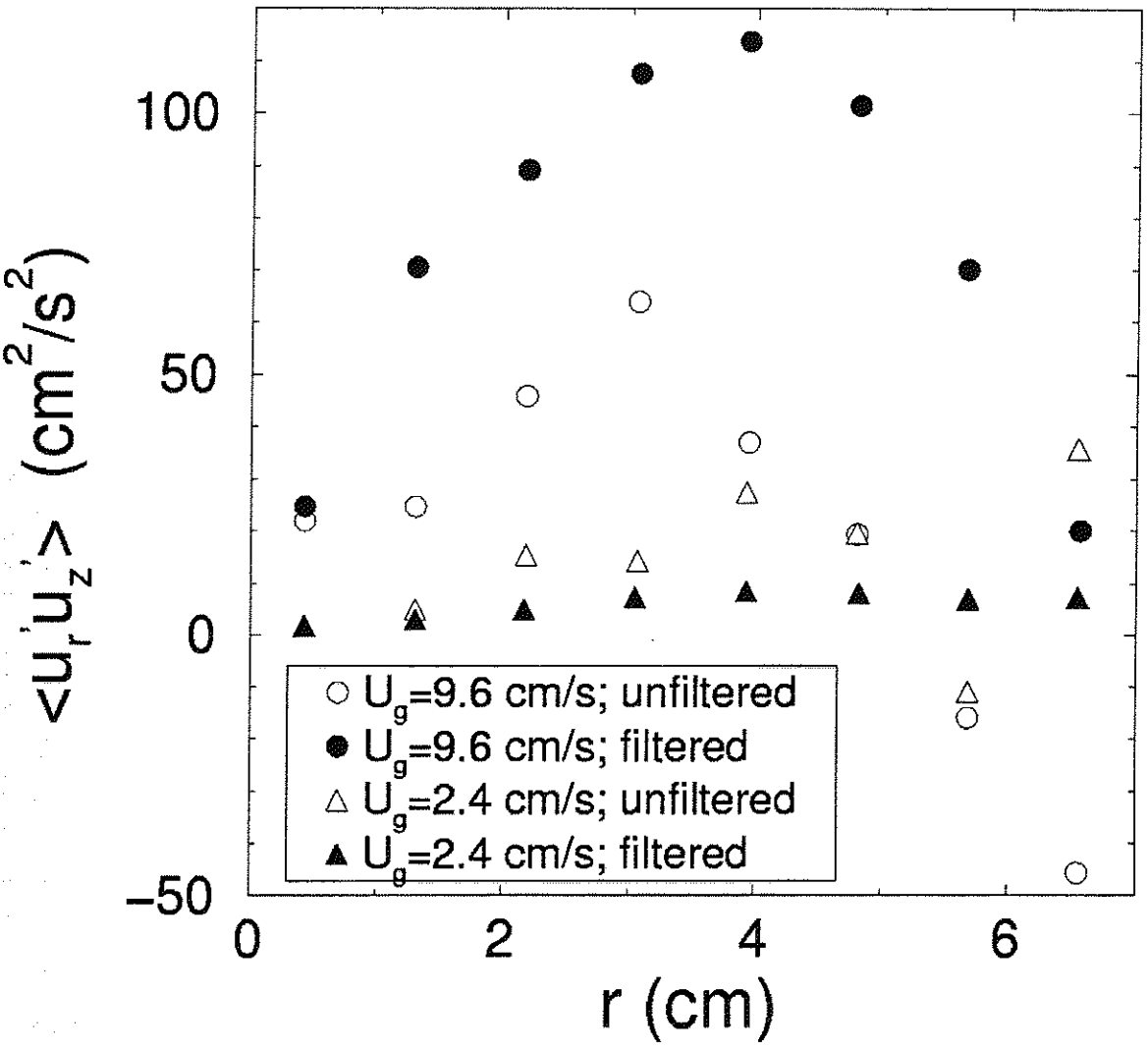

Figure 16. Comparison of turbulent shear stresses, $\overline{u_r' u_z'}$, before and after filtering for a 14-cm diameter column.

ANALYSIS OF DISTRIBUTOR EFFECTS ON GAS HOLDUP PROFILES IN CHURN-TURBULENT BUBBLE COLUMNS

A. Introduction

Bubble column reactors are widely used in various areas such as chemical processing, biotechnology, and production of pharmaceuticals. One typical example is Fischer-Tropsch (FT) synthesis of liquid fuels from synthesis gas derived from coal. The commercial viability of such processes is dependent on high product throughput that can only be achieved at high superficial gas velocities. Overall gas holdup and its cross-sectional distribution are important parameters which govern the prevalent hydrodynamics in the column under particular operating conditions. The parameters that determine the gas holdup in a bubble column reactor are the operating conditions of the system, the reactor geometry, as well as the coalescing nature of the liquid phase.

B. Objectives

In bubble column design and operation, another frequently asked question is whether sparger (gas distributor) design and configuration affect column performance. Knowing the answer to this question is important since simpler sparger designs could represent significant cost savings in column construction. Towards this effect, a collaborative study has been initiated among Air Products and Chemicals, Sandia National Laboratories and Washington University to characterize sparger effects on column hydrodynamics in terms of gas and solid holdups and their distribution using non-intrusive tomographic techniques. It is known that gas holdup radial profiles are the primary factor in driving liquid recirculation (due to radial buoyancy force differences), which in turn affects the extent of backmixing and reaction progress in the column. For this reason at the Chemical Reaction Engineering Laboratory (CREL) at Washington University in Saint Louis, Computed Tomographic measurements of cross-sectional distribution of gas holdup were acquired using five different spargers in a 6.4" diameter stainless steel column using a number of gas distributors at various axial locations and at different superficial gas velocities. In addition, overall gas holdup was obtained by comparison of the height of the two-phase mixture to the static liquid height.

Since operation of bubble column at high superficial gas velocity is of utmost interest, the issue of whether sparger design affects bubble column hydrodynamics in a major way under such operating conditions is addressed by conducting a set of experiments at superficial gas velocity of 30 cm/s. To understand better the role of sparger design on bubble column hydrodynamics, it was also necessary to investigate sparger effects at lower gas superficial velocity of 14 cm/s. Traditional understanding of bubble column flow leads one to expect churn turbulent flow at a superficial gas velocity of 14 cm/s at atmospheric pressure in an air-water system. Hence, it is often assumed that at such conditions the sparger effects are minimal. In this study we show how large such effects could be.

C. Research Accomplishments

C1. Experimental setup

Figure 1 shows the flowsheet for the system used in this study. The system is designed to handle a high flow rate of air up to 5000 SCFH at a pressure of up to 150 psig. All the equipment is designed to support operation at a maximum pressure of 200 psig. The bubble column is made of a stainless steel tube with inner diameter 0.162 m (6.4") and height 2.5-m (8.2-ft).

As shown in Figure 1, a transparent glass window is situated at the top of the column and is named "blue eye". This window allows viewing the system before starting the CT scan. The gas was dispersed into the column through different distributors. Figure 2 shows the various distributors used in this study. The first three distributors (D1-D3) were chosen in a collaborative effort with SNL to characterize the effect of sparger design on bubble column hydrodynamics. The following configurations of the spargers were employed.

A) Three distributors with 0.1 % open area
- D1: Uniform perforated plate (163 holes of 0.4 mm ID, triangular pitch of 1 cm)
- D2: Cross sparger (4 holes of 2.6 mm ID)
- D3: Single nozzle (1 hole of 5.1 mm ID)

B) One distributor with 0.15 % open area
- D4: Uniform perforated plate (163 holes of 0.5 mm ID, triangular pitch of 1 cm)

C) One distributor with 0.04 % open area
- D5: Non-uniform perforated plate (61 holes of 0.4 mm ID located on 3 concentric circles 1.5 cm apart)

Compressed air was used as the gas phase after appropriate filtering and for the liquid phase tap water (σ_L = 72 mN/m, μ_L = 993 μPa.s) was used. The experiments were conducted batchwise with respect to the liquid but with a continuous flow of gas at ambient temperature (T = 20 °C). The static water height was in the range 120-150 cm. Table 1 lists the operating conditions employed in this work. The gas mixture was filtered before being introduced into the system. The gas flow rate was controlled by the rotameters. After exiting the bubble column, the gas passes through a backpressure regulator, which can be used to control the pressure in the column. It is then discharged into the atmosphere through the vent. Two pressure safety valves are mounted both at the top and bottom of the column to prevent accidental over-pressurization.

The gas holdup cross-sectional distribution was measured using the gamma ray scanner and associated tomography reconstruction algorithms developed in CREL and discussed by Kumar (1994). The CREL scanner is a versatile instrument that enables the quantification of the time-averaged holdup distribution for two-phase flows under a wide range of operating conditions. The fan beam configuration of the scanner consists of an array of NaI detectors of 5 cm in diameter (5 detectors were used in this study), and an encapsulated 100 mCi Cs^{137} source located opposite to the center of the array of detectors.

The measurements can be made at different axial locations. This allows the quantification of the effects of operating conditions on the gas holdup distribution.

Measurements Performed

Overall gas holdup was determined by comparing the height of the two-phase mixture for the column in operation to the static liquid height. Radial gas holdup profiles, presented below, at various axial locations were obtained by azimuthal averaging of the CT scans performed at those elevations. The gamma ray scanner developed in CREL and discussed by Kumar (1994) was used. The spatial resolution of the scanner was about 4 mm and the density resolution is better than 0.05 g/cm^3.

C2. Results and Discussion

C2.1 Radial Holdup Profiles

First, the excellent reproducibility of the radial gas holdup profiles generated from the CT scans for a superficial gas velocity of 30 cm/s is established. Figure 3 exhibits the gas holdup radial profile obtained with distributor 4 at the elevation of z/D = 5.5 on three different days. The bounds for the 95% confidence interval, consisting of two standard deviations on each side of the mean, are at every radial location well within ± 2%, except at the points close to the wall which are within ± 5%. It is not reasonable to expect that various distributors could produce gas holdup profiles within the range of reproducibility of a single distributor. We are not looking for identical behavior among distributors, but for insignificant differences in the hydrodynamics due to different distributors. For this reason, it was decided to plot the radial holdup profiles, $\varepsilon_{gi}(r)$, for all distributors taken at the same elevation. We then calculate the mean at each radial location $\varepsilon_g(r) = \sum_{i=1}^{N} \varepsilon_{gi}(r) \Big/ N$ and call the distributor effect to be insignificant if $\varepsilon_{gi}(r)$ lies within the range from 0.95 $\varepsilon_g(r)$ to 1.05 $\varepsilon_g(r)$. This represents a narrow (less than ± 5%) band around the mean.

C2.1.1 Ug = 30 cm/s

Figures 4, 5 and 6 display the radial gas holdup profiles at Ug = 30 cm/s for distributors D1, D2, D3, and D4 scanned at three different elevations of z/D = 2.1, 5.5 and 9.0, respectively. Also, displayed in the figures is the lower bound of the allowable band at 0.95 $\varepsilon_g(r)$ and the upper bound at 1.05 $\varepsilon_g(r)$. All the data falls within this band except for some points for distributor D4, which has a different percent open area, and for two points near the wall for distributor D1 at z/D = 9.0. Nevertheless, including data for D4, the maximum difference between the highest and the lowest holdup value observed at any radial location did not exceed 25%, and that maximum difference occurred in the wall region where holdup values are low so that the actual absolute differences in holdup were not large. For the holdup data for dimensionless radius r/R < 0.9, the maximum difference in recorded local

holdup values did not exceed 10%. Based on this, and upon examination of Figures 4 to 6, we can conclude that for practical engineering purposes the distributor effects is insignificant at superficial gas velocity of 30 cm/s. This insignificant effect on gas holdup profile was maintained even when the open area of the distributors was changed from 0.1 % (D1, D2, D3) to 0.15 % (D4). The only slight difference was observed with slightly higher holdups at r/R greater than 0.9 for D4 with 0.15 % open area than for D1, D2, and D3 with 0.1 % open area.

C2.1.2 Ug = 14 cm/s

The same plots as for Ug =30 cm/s are shown for all distributors at Ug = 14 cm/ in Figures 7, 8 and 9. As can be seen from these figures, not all the distributors generate gas holdup profiles in the ± 5% band around the mean and some differences are very significant not only near the distributor zone, but also throughout the column. Noteworthy are the significant differences in the gas holdup at dimensionless radius location of $r/R < 0.8$ in the core of the column.

In spite of the differences in the performance of the various distributors at Ug = 14 cm/s, distributors D2 and D3, which are the cross and the single nozzle spargers, respectively, generate almost identical gas holdup profiles for all elevations except at z/D = 9.0. The differences observed at z/D = 9.0 are most likely an artifact due to the loss of liquid in the experiment with the cross sparger and drop of the gas-liquid interface in the proximity of that elevation. This gave erratic holdup readings. The behavior of D2 and D3 is significantly different even from distributor D1, which has the same percent open area, but is a uniform perforated plate. Since perforated plates are rarely employed for industrial systems, with spargers similar to D2 and D3 getting the preference, it can be said that for industrially important spargers, the effect of sparger design is negligible even at a superficial gas velocity of 14 cm/s. Nevertheless, considering all the spargers evaluated in this study, sparger design does has a significant influence on gas holdup even under operating conditions which are normally taken to be in the churn-turbulent regime.

In addition, when one compares the radial gas holdup distribution trends for three perforated plate distributors (D1 - uniform, 0.1 POA; D4 - uniform, 0.15 POA; D5 - non-uniform, 0.04 POA), one sees that the holdup obtained using D4 is systematically higher than that from D1 at all radial locations. This is probably due to the same distribution of orifices on the perforated plates in the two cases, one with larger size (0.5 mm for D4) and with smaller size for the other (0.4 mm for D1). The holdup obtained with D5 is lower than that obtained with D1 probably due to a lower percent open area (POA), however, there is no clear trend in the differences at various radial locations.

In conclusion, since radial holdup profiles drive liquid recirculation, the same holdup profiles should cause the same recirculation pattern provided the turbulence structure, represented in the simplest fashion by a mixing length or turbulent kinematic viscosity, is the same. Computer Automated Radioactive Particle Tracking (CARPT) studies are planned for the future to determine whether the same radial holdup profiles resulted in the same liquid recirculation and turbulent kinetic energy patterns.

C2.2 Axial Holdup Variation

The axial variation in the radial gas holdup profiles was examined and reported next. For the four distributors (D1-D4) investigated at Ug=30 cm/s, the axial variation is shown in Figures 10, 11, 12 and 13, respectively. These figures indicate that the radial gas holdup profile is not a function of axial position (except for points at r/R > 0.85 for some distributors at z/D = 2.1). This implies that the entry region at this superficial gas velocity is confined to about two column diameters.

Figures 14 to 18 show gas holdup radial profiles at different elevations for all distributors at Ug = 14 cm/s. From Figures 14, 17 and 18, which are for uniform and non-uniform perforated plate spargers, one can clearly see a significant axial variation. One also observes a consistent trend for all these three perforated plate distributors, where the gas holdup uniformly decreases with height. This implies that at this superficial gas velocity the primary bubble size at the distributor is smaller than the secondary (stable) bubble size (Joshi *et al.*, 1998). Barring the discrepancy observed at z/D = 9.0 for the cross sparger (D2) as mentioned earlier, Figures 15 and 16 indicate that there is relatively insignificant variation of axial gas holdup for spargers D2 and D3. This observation can be explained in terms of the stable bubble size, which is attained relatively close to the sparger, implying that the sparger zone for these two distributors is confined to less than two column diameters.

C2.3 Overall Holdup

Overall holdup is obtained in two ways. Radial holdup profiles obtained by the CT scan are averaged in a cross-section to obtain a cross-sectionally averaged holdup, $\bar{\varepsilon}_{gi}(z)$ at the desired elevation z for each distributor (i = 1, 2, 3, 4, 5).

$$\bar{\varepsilon}_{gi}(z) = \frac{2}{R^2}\int_0^R r\varepsilon_{gi}(r)\,dr \tag{1}$$

These cross sectional average values are interpolated between z/D = 2.1 to z/D = 9.0 using cubic splines and are axially averaged to obtain average total holdup.

$$\varepsilon_{gi,CT} = \frac{1}{(9.0-2.1)}\int_{z/D=2.1}^{z/D=9.0}\bar{\varepsilon}_{gi}(z/D)\,d(z/D) \tag{2}$$

Cross-sectional averaged holdups at three elevations and axially averaged holdups determined from CT scans at Ug = 30 cm/s and 14 cm/s, as described above, are listed in Tables 2 and 3, respectively. Also shown in the tables is the overall column holdup ε_{gi} for each distributor (i = 1 to 5). Overall holdup was obtained by dividing the difference in dynamic height of the two-phase mixture and static liquid height by the static liquid height (Eq. 3).

$$\varepsilon_{gi} = \frac{H_{di} - H_s}{H_s} \tag{3}$$

Due to the inherent inaccuracies in firmly establishing the dynamic liquid height for the column in operation, these holdup values can be subject to errors of ± 10 %. Table 2 reveals that the difference between CT determined average holdup and average column holdup is always well within 10 %. It is also clear from comparison of columns 5 and 6 in the table that column holdup is always higher than the CT estimate average. This is to be expected, as the holdup in the sparger region, which is not measured by CT, is higher than the holdup in the fully developed flow region. CT captures the holdup only in the fully developed zone, while the overall column holdup captures the contribution of all the zones.

However, at Ug = 14 cm/s, by the similar analysis of columns 5 and 6 in Table 3, one can see that the CT determined average is higher than the column average for the cross and single nozzle spargers (D2 and D3). This is to be expected since the bubble size at the distributor should be much larger for these spargers than the stable bubble size resulting in a lower holdup near the distributor. Therefore, the column average holdup is expected to be lower as compared to the CT determined average, which is based on holdup values outside the distributor region. In addition, the column average holdup for all the perforated plate distributors is higher than the CT determined average, indicating a higher gas holdup in the distributor zone with the primary bubble size being much smaller than the stable bubble size.

C2.4 Comparison of sparger effects for Ug = 14 cm/s with Ug = 30 cm/s

Figures 19 and 20 show the comparison of variation in gas holdup profiles due to different spargers at the two superficial gas velocities investigated in this study. From these two figures, it can be clearly seen that sparger effects are minimal for Ug = 30 cm/s. This is indicated by the narrow band of ± two standard deviations; whereas this is not the case for Ug = 14 cm/s. Also, Figure 19 indicates that the normalized deviations are the largest near the wall.

C2.5 Cross-sectional gas holdup distribution

Figures 21 and 22 show the representative cross-sectional gas holdup distribution for cross sparger (D2) at Ug = 14 cm/s and 30 cm/s scanned at z/D = 5.5, respectively. A gradual variation in the color shades for the gas holdup from the column center to the wall indicates a change in gas holdup values. As can be seen from these two figures, the time-averaged gas holdup distribution is nearly axisymmetric and indicates more gas in the column center with gradual decay towards the wall.

C2.6 Comparison with earlier work

It is interesting to compare the results obtained in this study with the work performed earlier by Kumar (1994) and Degaleesan (1997). Using CT scanner at CREL, Kumar (1994) studied the effect of distributor types on gas holdup distribution in an air-water system using

a column with a slightly larger diameter of 19-cm. In his study, he used the following spargers.

- Perforated plate (166 holes of 0.33 mm ID, square pitch, 0.05 % open area)
- Bubble cap distributor
- Cone distributor

However, only two relatively low superficial gas velocities (5 cm/s and 8 cm/s) were investigated. The conclusions from that study were that the gas holdup obtained with perforated plate distributor was higher than that obtained from the bubble cap and cone distributors. This observation is similar to the observations at Ug=14 cm/s in the current study even though the employed superficial gas velocity is significantly higher.

Degaleesan (1997) investigated the effect of gas distributors on liquid recirculation using the same experimental set-up as that of Kumar (1994). The Computer Automated Radioactive Particle Tracking (CARPT) technique was used to assess the level of liquid recirculation and turbulence at a superficial gas velocity of 12 cm/s. It was found that the time-averaged axial liquid velocity, for both bubble cap and cone distributors, was lower as compared to that for the perforated plate. This was explained in terms of relatively larger bubbles that are formed when one uses a bubble cap or a cone distributor as opposed to a perforated plate distributor. The presence of large bubbles was reported to result in lower overall gas holdup and higher turbulent kinetic energy which in turn generates larger scale turbulence. More details on that study can be found in the 14th and 15th Quarterly Reports. This indirectly implies that the gas holdup using the perforated plate distributor was significantly higher than that from bubble cap and cone distributors even at a superficial gas velocity of 12 cm/s. This observation is in agreement with the measurements reported in this study at a comparable Ug of 14 cm/s.

C3. Conclusions

The study at a high superficial gas velocity of 30 cm/s under atmospheric condition confirms the findings of Shollenberger *et al.* (1999) that in churn-turbulent flow the gas distributor does not affect the gas holdup on radial gas holdup profile. Moreover, the entry length is confined to $z/D \leq 2$. However, at a superficial gas velocity of 14 cm/s, where the regime of bubble column operation is usually reported to be churn-turbulent, significant radial gradients in the gas holdup profile are observed with a greater concentration of gas in the column center. Therefore, it was anticipated that sparger design would have a minimal effect under such operating conditions. On the contrary, the findings from this study indicate that there is a significant variation in gas holdup from perforated plate type distributors to nozzle type distributors. Such differences were not observed at superficial gas velocity of 30 cm/s where the turbulent intensities are much higher. Whether the sameness of the radial gas holdup profile at Ug = 30 cm/s implies the same or similar liquid recirculation and mixing patterns is the subject of future research

At a superficial gas velocity of 14 cm/s, the perforated plate spargers exhibit a similar behavior of axially decreasing gas holdup, whereas the cross and single nozzle spargers show

insignificant variation of gas holdup with height at heights above two column diameter. In addition, it is interesting to note that Kumar (1994) and Degaleesan (1997) also observed similar trends when using perforated plate distributors compared to nozzle type distributors in a different column geometry.

Since the transition to the churn-turbulent regime is delayed at elevated pressures, it needs to be investigated (future studies) whether a superficial gas velocity of 14 cm/s still represents the churn-turbulent regime (indicated by steeper radial gas holdup profiles) and what effect spargers have at such conditions.We believe that our findings at superficial gas velocity of 30 cm/s will be confirmed also at elevated pressure (future studies) as long as the churn-turbulent regime is maintained.

D. Future Work

To address the question of sparger design on liquid recirculation, turbulence and bubble sizes at high superficial gas velocity; as well as to complement the computer tomographic measurements completed as part of this work, CARPT measurements will be executed on the same column under atmospheric conditions at a gas superficial velocity of 30 cm/s. This work is still in the process.

E. Bibliography

Degaleesan, S., 1997, Turbulence and liquid mixing in bubble columns, *Ph.D. Thesis*, Washington University, St. Louis

Joshi, J. B., Parasu Veera, U., Prasad, Ch. V., Phanikumar, D. V., Deshphande, N. S., Thakre, S. S., and Thorat, B. N., 1998, Gas Holdup Structure in Bubble Column Reactors, *PINSA*, **64**, A, 4, 441-567

Kumar, S. B., 1994, Computed tomographic measurements of void fraction and modeling of the flow in bubble columns, *Ph.D. Thesis*, Florida Atlantic University

Shollenberger, K. A., Torczynski, J. R., and George, D. L., June 2, 1999, Monthly Progress Report for Collaborative Sparger Study, submitted to Air-Products.

F. Acknowledgments

This study is being supported in part by the Department of Energy under contract to Air-Products, DOE FC 22 95 PC 95051.

Table 1. Experimental Conditions used.

Column ID, cm (in.)	16.2 (6.4)
Ug (Air), cm/s	14, 30
Liquid (Water)	Batch
Pressure, MPa (atm)	0.1 (1)
Temperature, °C	25
CT scan levels from the distributor, cm	34, 89, 145
z/D	2.1, 5.5, 9.0

Table 2. Cross-sectional averaged gas holdup and overall gas holdup at Ug = 30 cm/s and atmospheric pressure.

Sparger	Cross-sectional averaged gas holdup			$\varepsilon_{g,CT}$	ε_g	% difference between $\varepsilon_{g,CT}$ & ε_g
	z/D = 2.1	z/D = 5.5	z/D = 9.0			
1	0.277	0.263	0.285	0.269	0.293	9.0
2	0.268	0.263	0.272	0.265	0.281	5.9
3	0.289	0.259	0.270	0.266	0.284	7.0
4	0.300	0.2817	0.2924	0.287	0.300	4.7
Avg. ± 2SD	0.283 ± 0.028	0.267 ± 0.021	0.280 ± 0.022	0.272 ± 0.020	0.290 ± 0.017	6.7 ± 3.6

Table 3. Cross-sectional averaged gas holdup and overall gas holdup at Ug = 14 cm/s and atmospheric pressure.

Sparger	Cross-sectional averaged gas holdup			$\varepsilon_{g,CT}$	ε_g	% difference between $\varepsilon_{g,CT}$ & ε_g
	z/D = 2.1	z/D = 5.5	z/D = 9.0			
1	0.249	0.211	0.196	0.215	0.225	4.7
2	0.183	0.180	0.184	0.181	0.179	1.1
3	0.170	0.187	0.189	0.188	0.180	4.1
4	0.288	0.264	0.229	0.262	0.277	5.7
5	0.236	0.205	0.193	0.208	0.224	7.8
Avg. ± 2SD	0.229 ± 0.086	0.209 ± 0.067	0.198 ± 0.036	0.211 ± 0.074	0.207 ± 0.049	4.7 ± 4.9

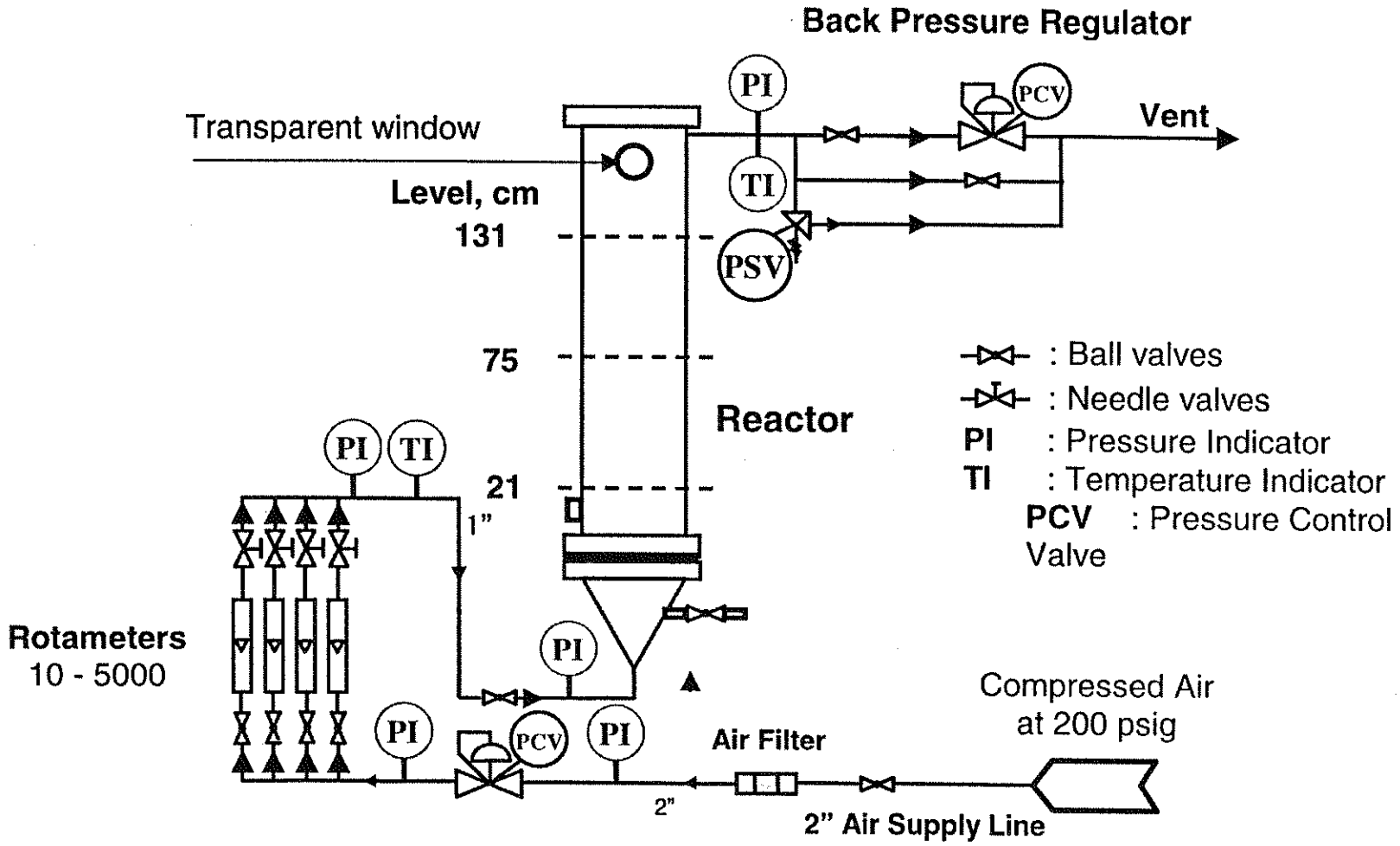

Figure 1. Schematic diagram of the experimental setup.

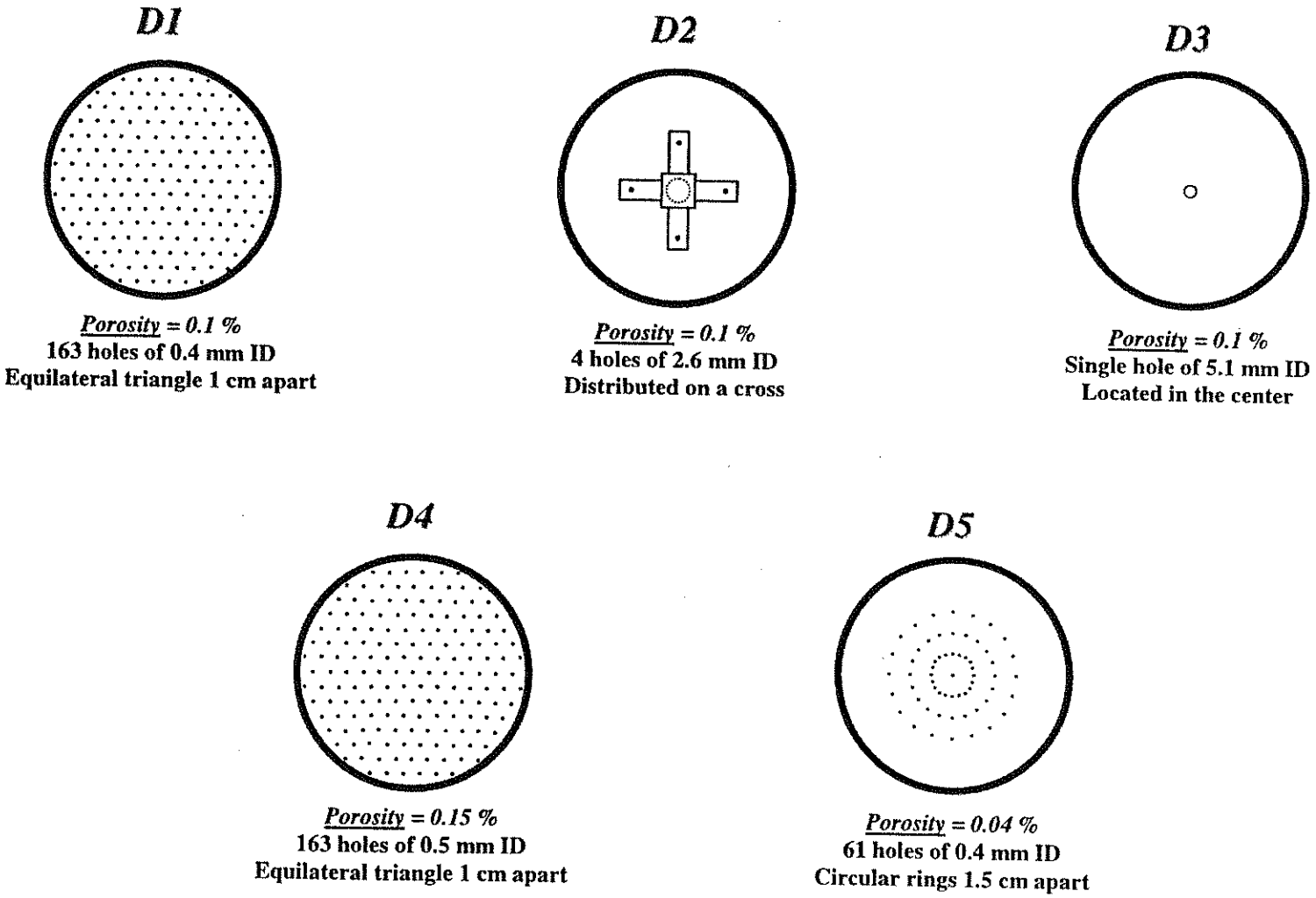

Figure 2. Sparger design and configurations.

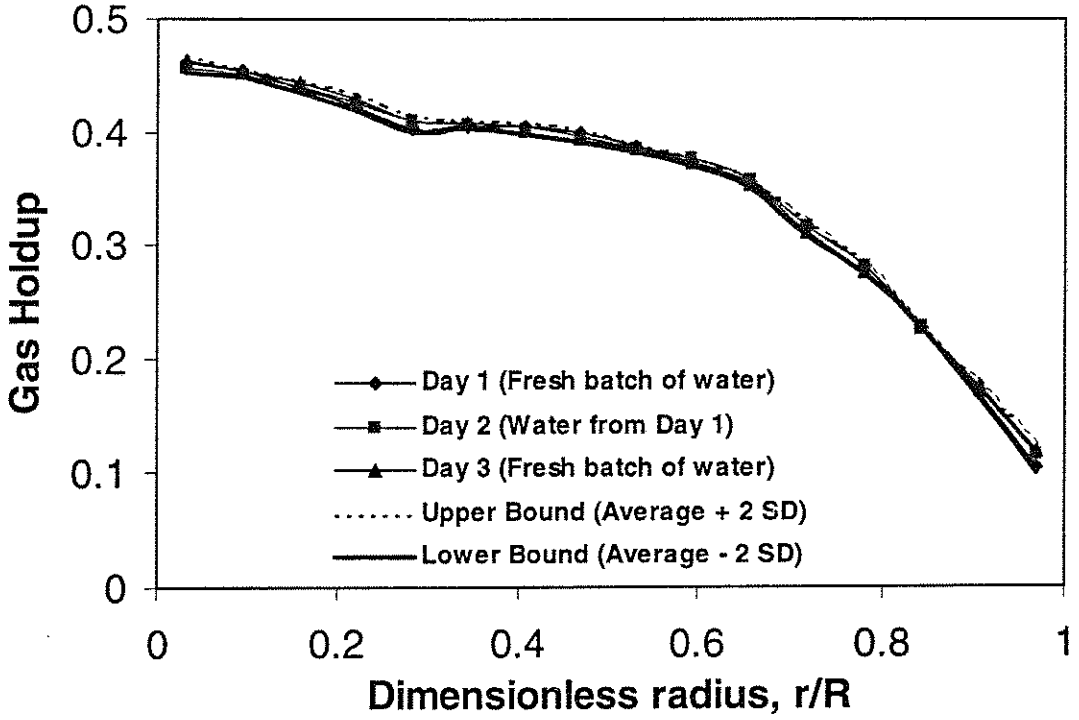

Figure 3. Reproducibility plots using D4, different batches of water on three different days.

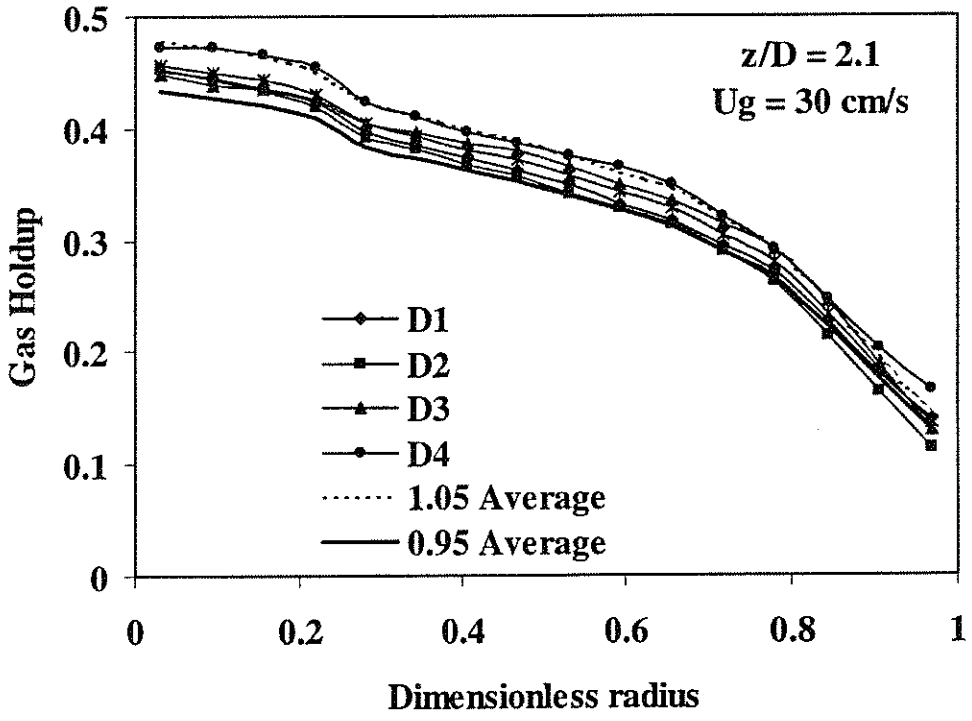

Figure 4. Effect of spargers at Ug = 30 cm/s at scan level z/D = 2.1.

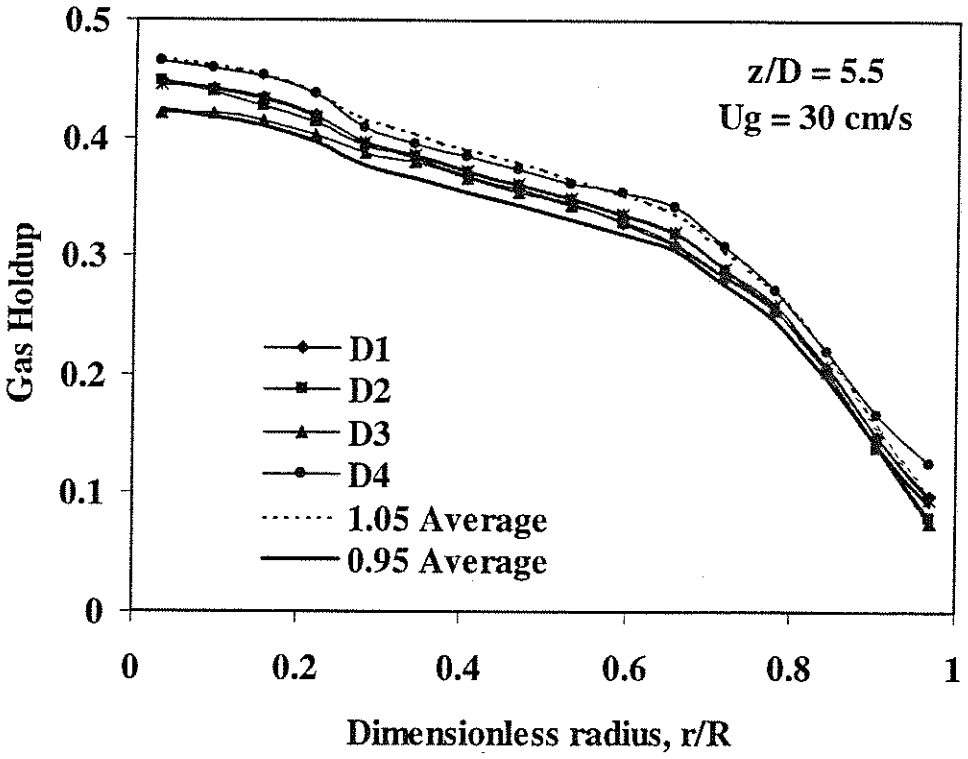

Figure 5. Effect of spargers at Ug = 30 cm/s at scan level z/D = 5.5.

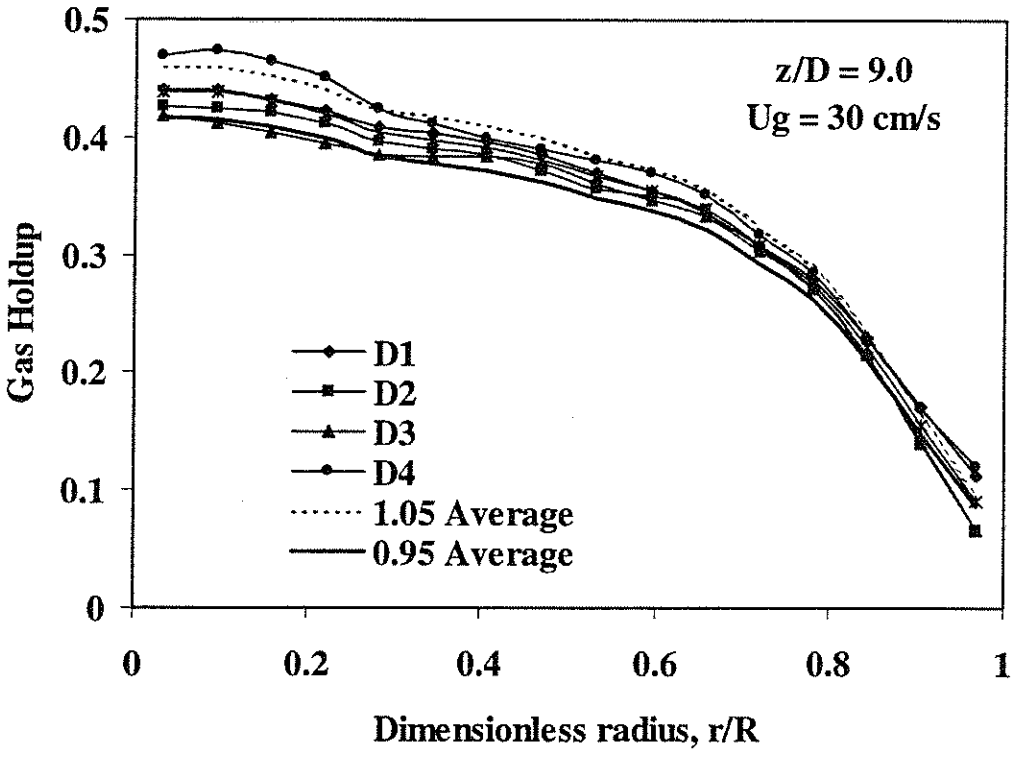

Figure 6. Effect of spargers at Ug = 30 cm/s at scan level z/D = 9.0.

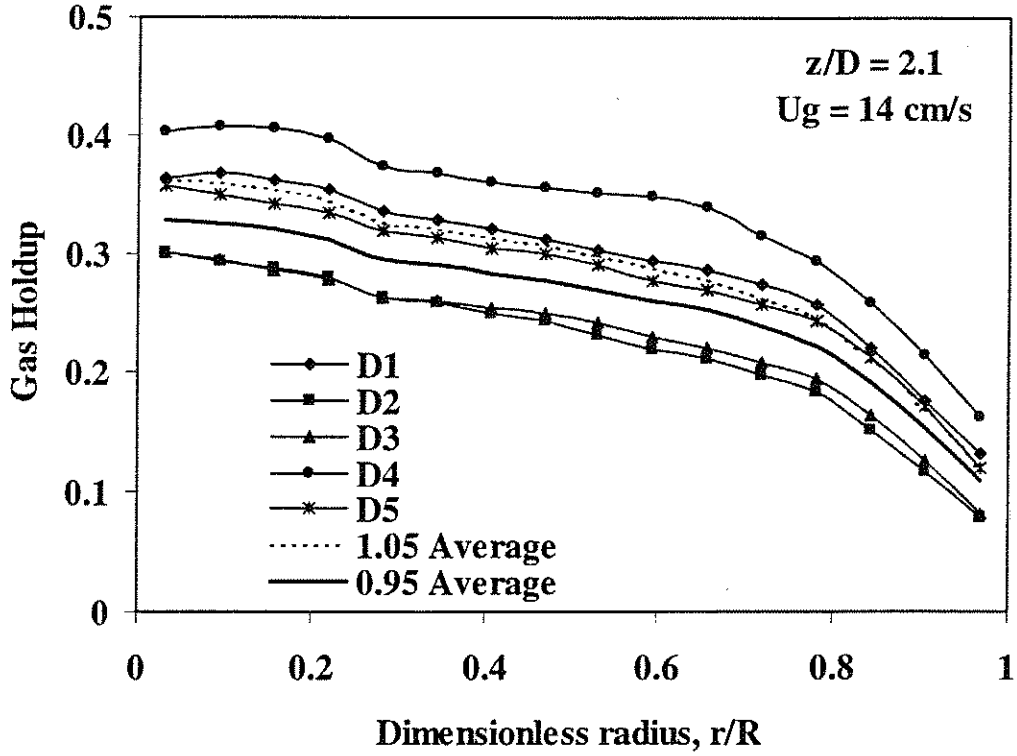

Figure 7. Effect of spargers at Ug = 14 cm/s at scan level z/D = 2.1.

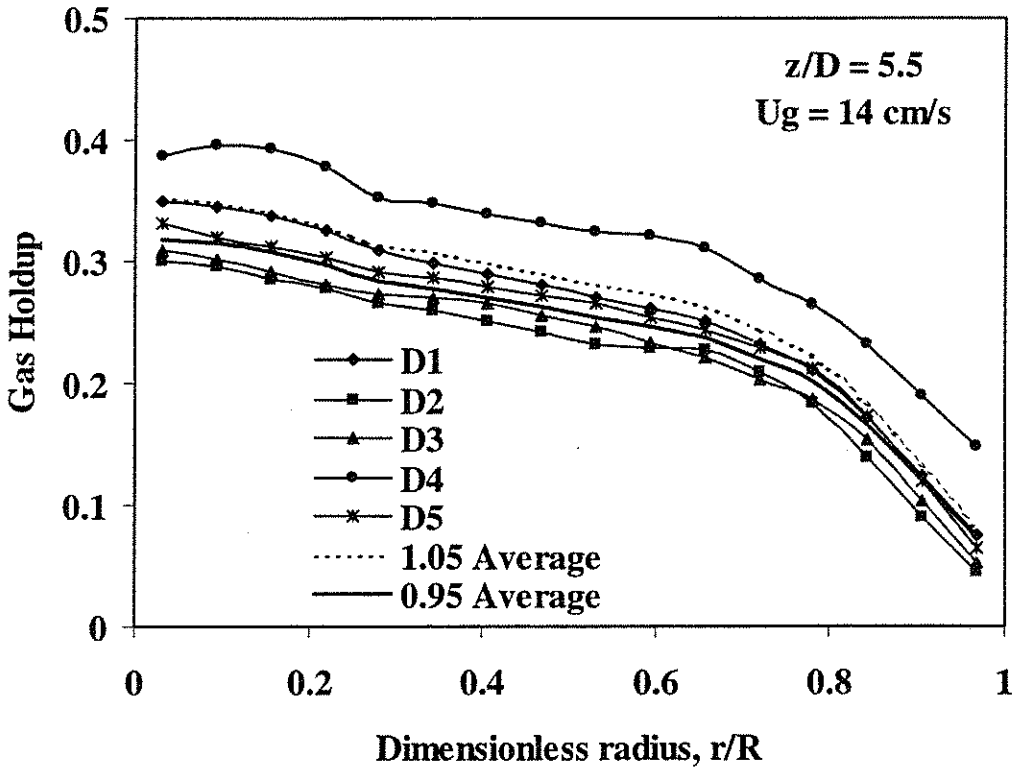

Figure 8. Effect of spargers at Ug = 14 cm/s at scan level z/D = 5.5.

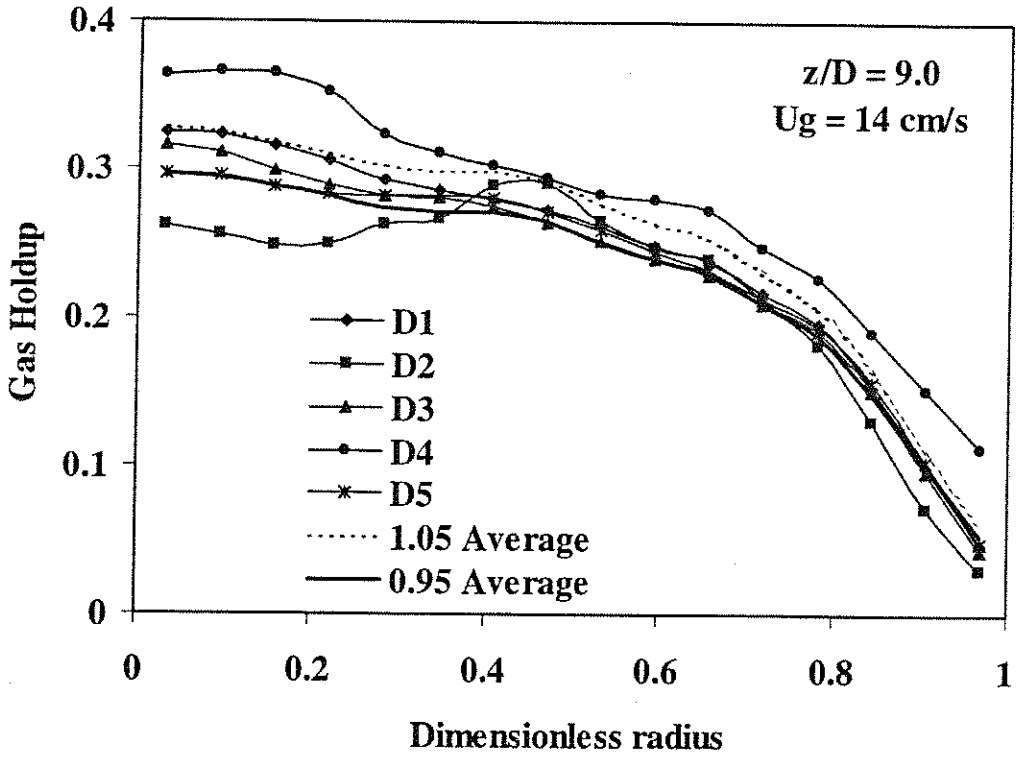

Figure 9. Effect of spargers at Ug = 14 cm/s at scan level z/D = 9.0.

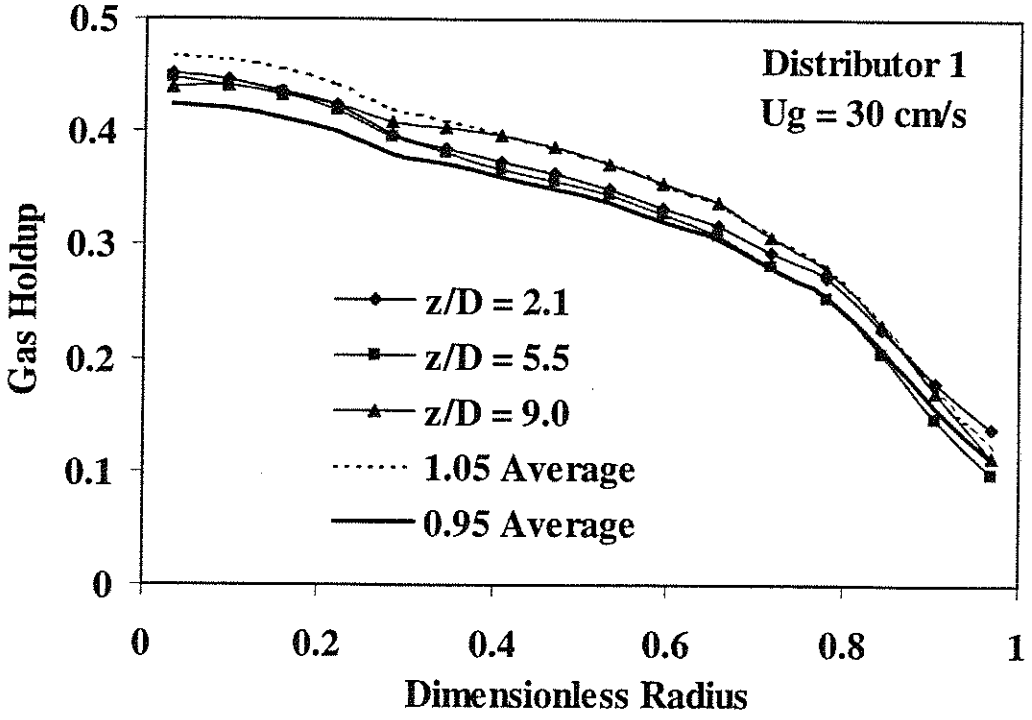

Figure 10. Axial variation of gas holdup for distributor 1 at Ug = 30 cm/s.

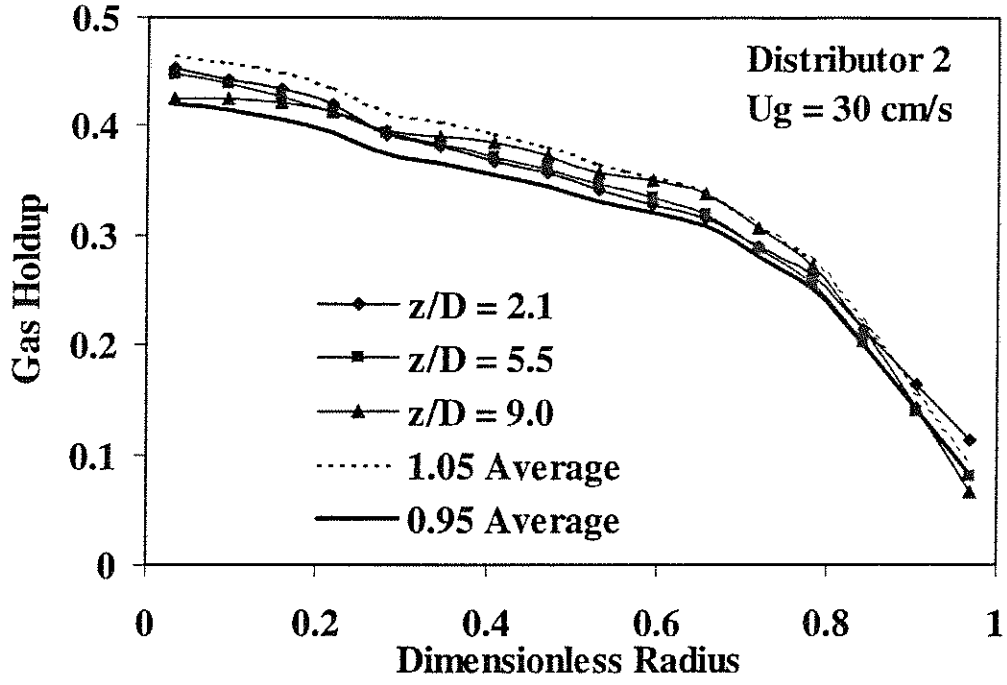

Figure 11. Axial variation of gas holdup for distributor 2 at Ug = 30 cm/s.

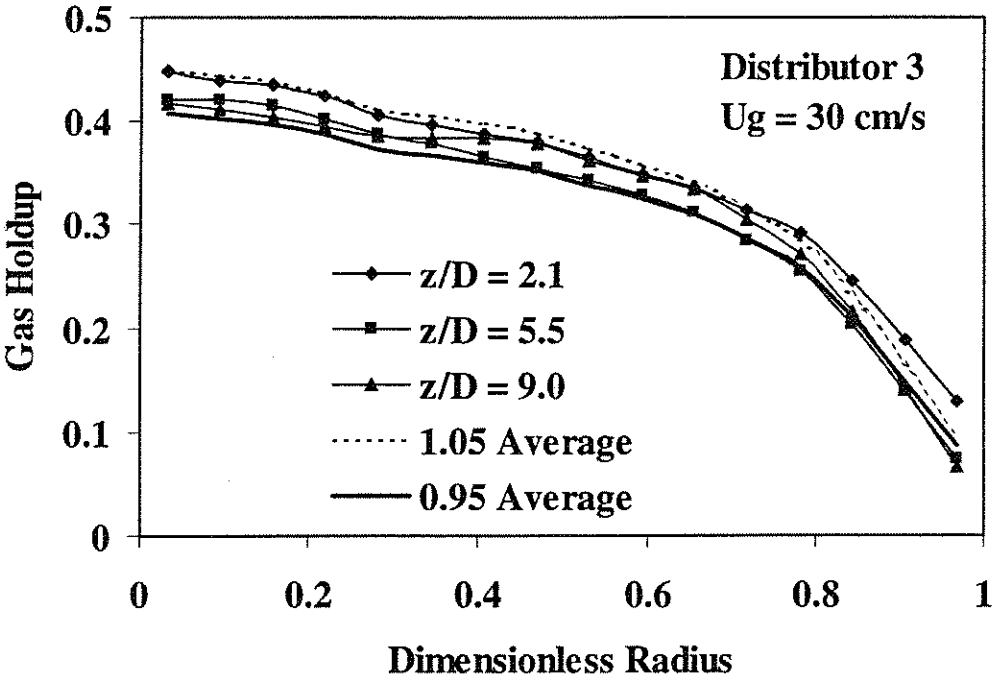

Figure 12. Axial variation of gas holdup for distributor 3 at Ug = 30 cm/s.

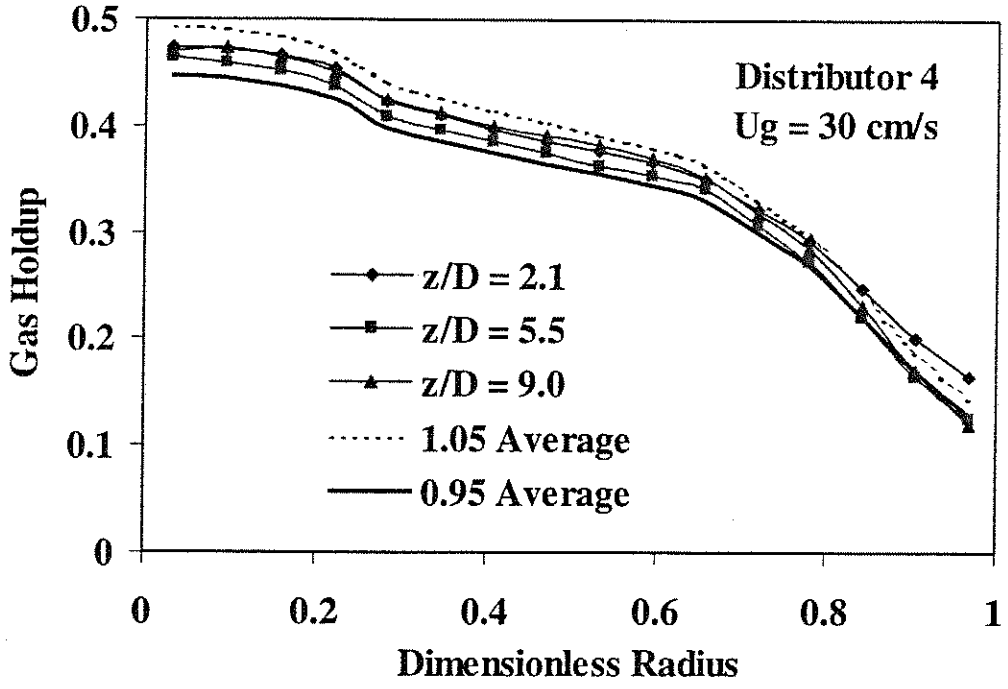

Figure 13. Axial variation of gas holdup for distributor 4 at Ug = 30 cm/s.

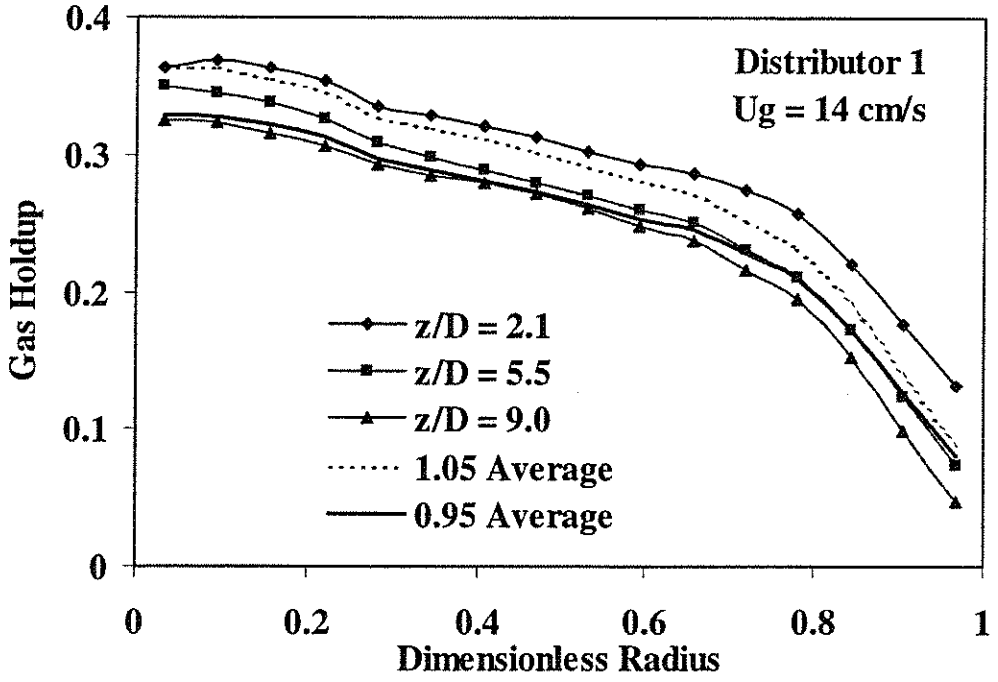

Figure 14. Axial variation of gas holdup for distributor 1 at Ug = 14 cm/s.

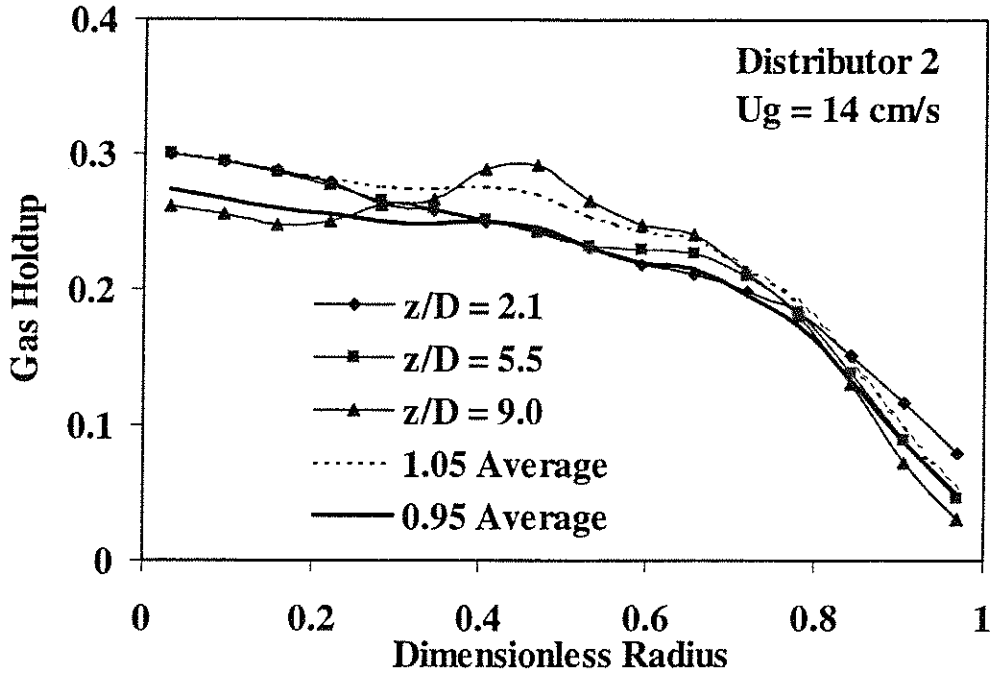

Figure 15. Axial variation of gas holdup for distributor 2 at Ug = 14 cm/s.

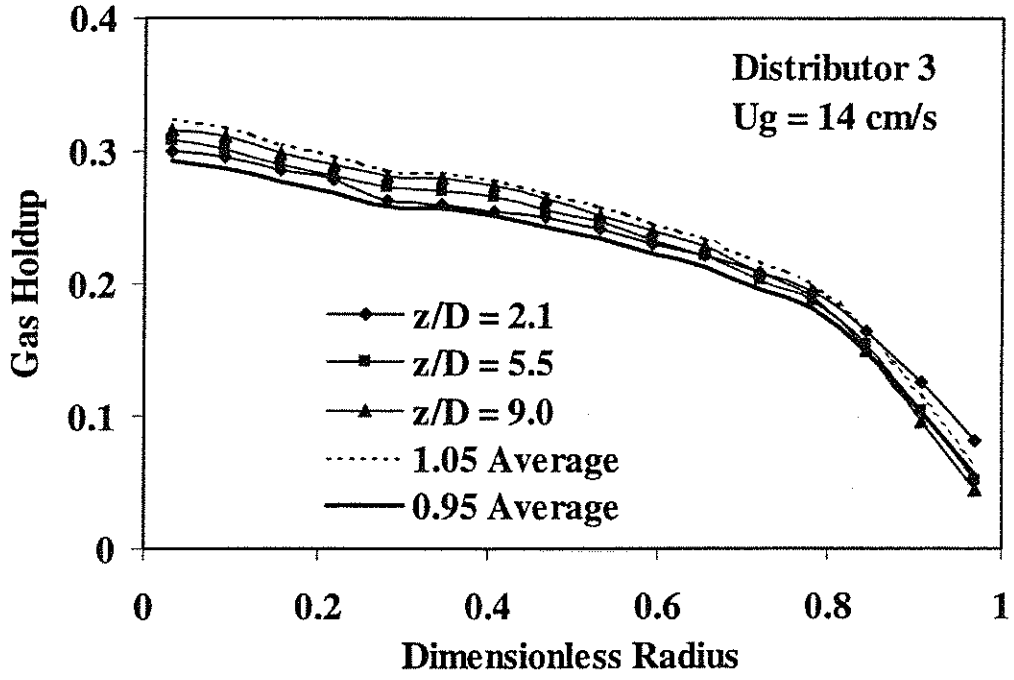

Figure 16. Axial variation of gas holdup for distributor 3 at Ug = 14 cm/s.

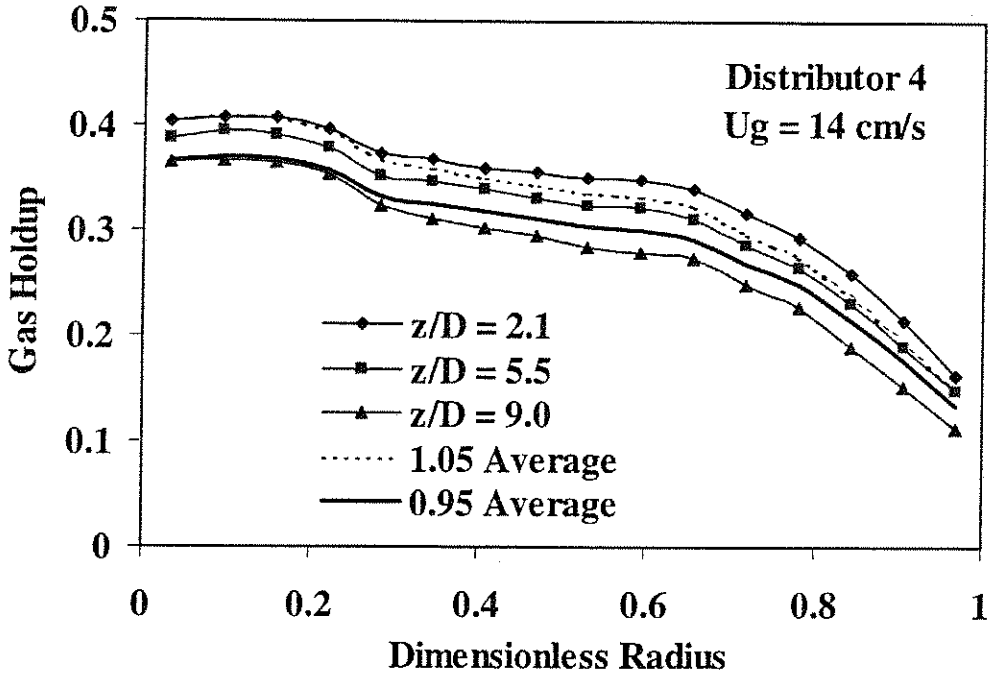

Figure 17. Axial variation of gas holdup for distributor 4 at Ug = 14 cm/s.

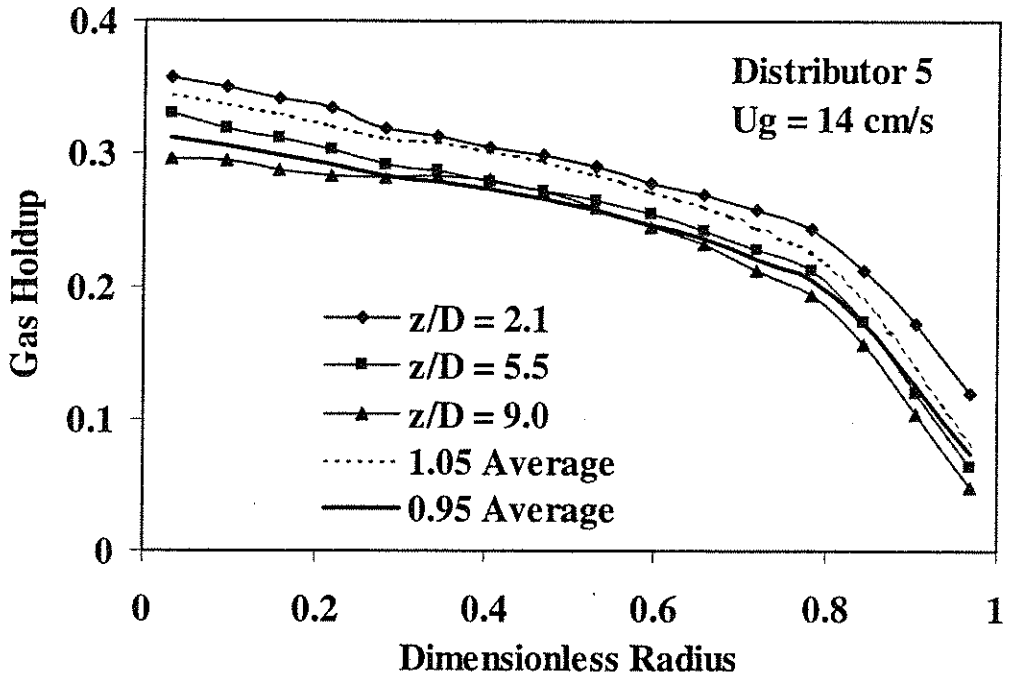

Figure 18. Axial variation of gas holdup for distributor 5 at Ug = 14 cm/s.

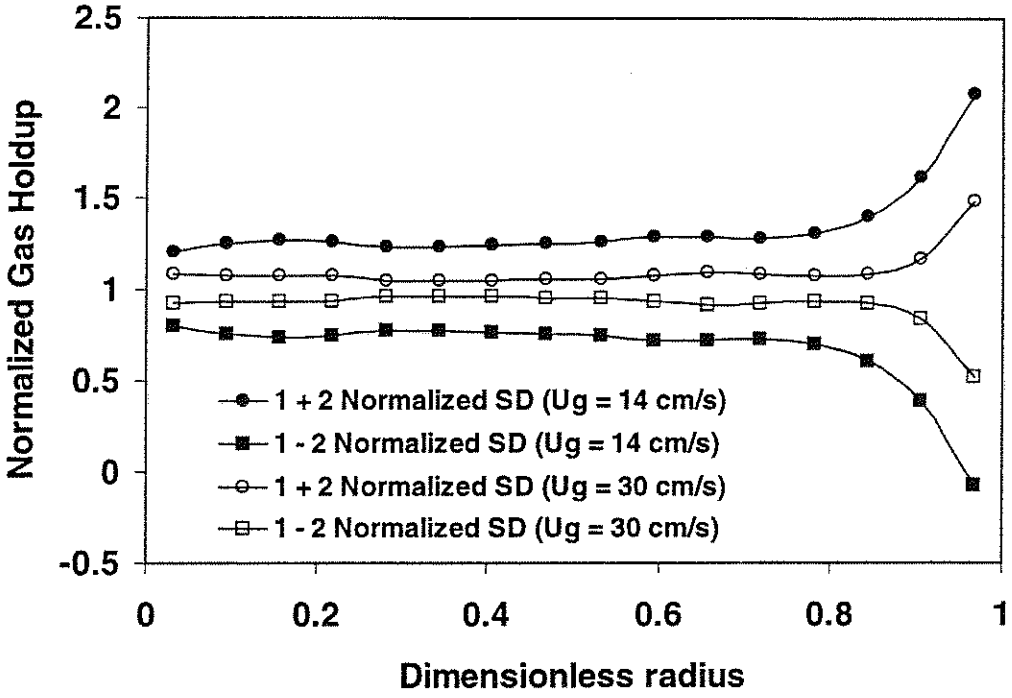

Figure 19. Comparison of normalized gas holdup variation due to different spargers at Ug = 14 cm/s and 30 cm/s.

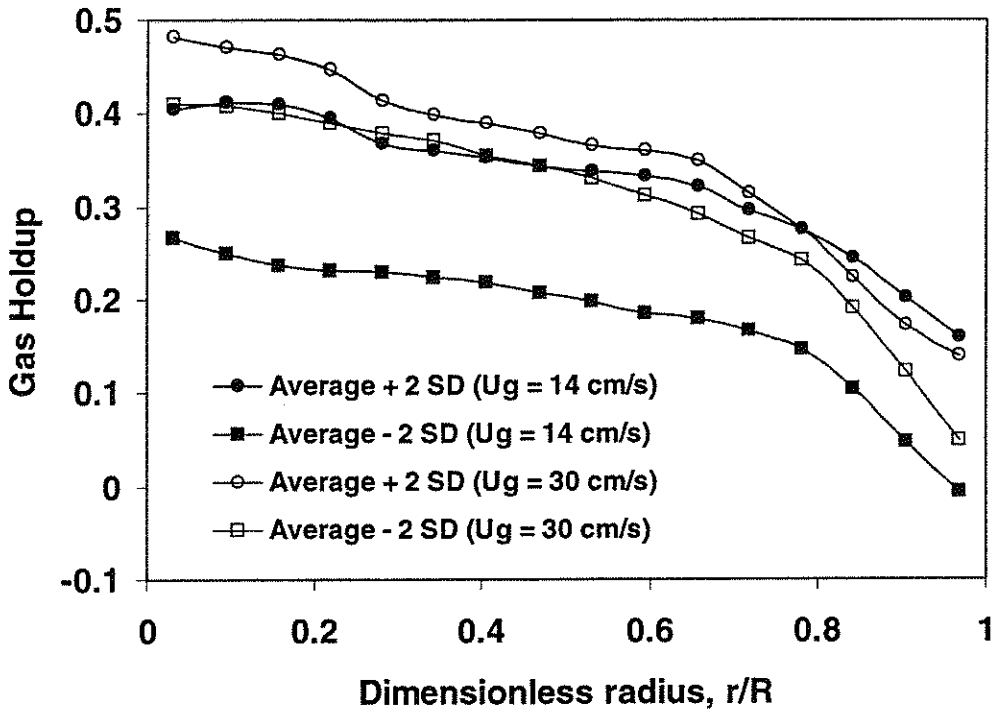

Figure 20. Comparison of gas holdup variation due to different spargers at Ug = 14 cm/s and 30 cm/s.

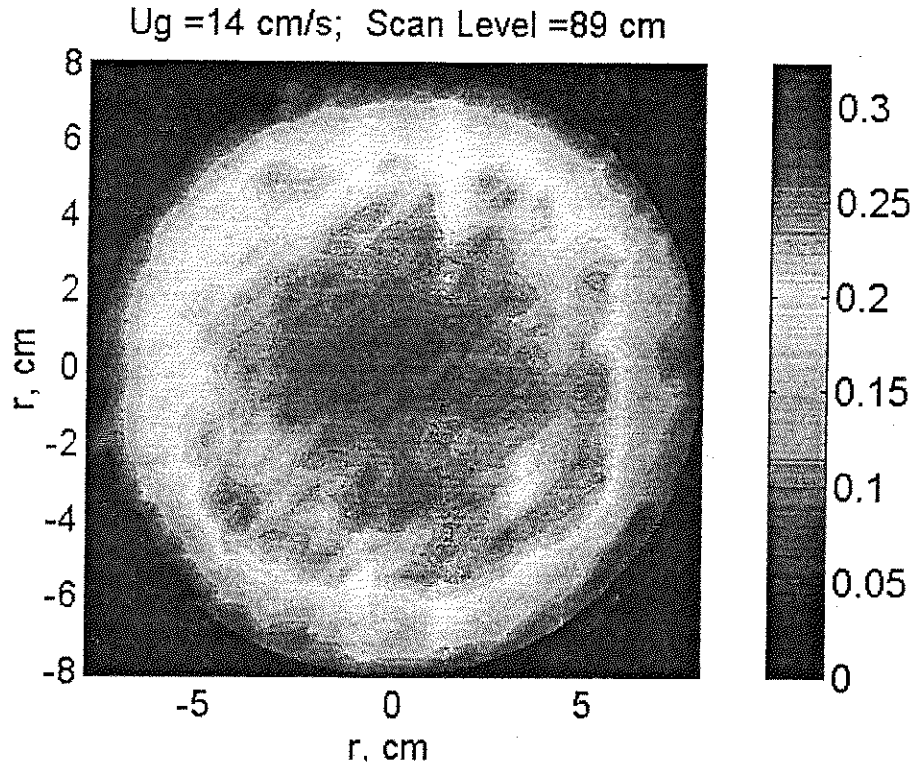

Figure 21. Cross-sectional time-average gas holdup distribution for the cross sparger (D2) at Ug = 14 cm/s at z/D = 5.5.

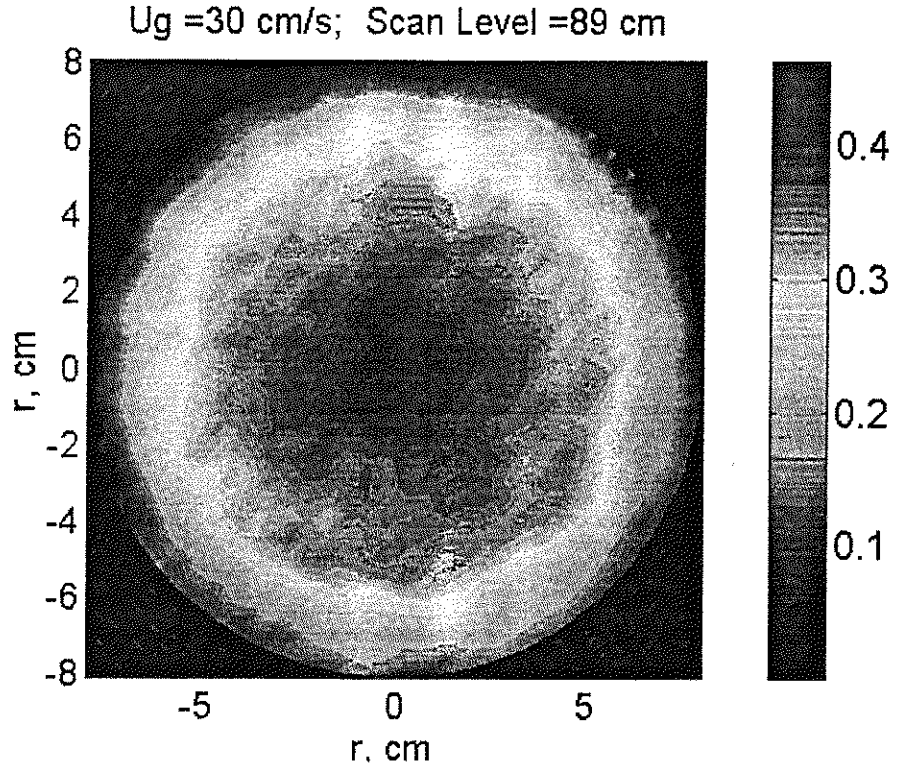

Figure 22. Cross-sectional time-average gas holdup distribution for the cross sparger (D2) at Ug = 30 cm/s at z/D = 5.5.

COMPARISON OF SINGLE AND TWO-BUBBLE CLASS GAS-LIQUID RECIRCULATION MODELS – APPLICATION TO PILOT PLANT RADIOACTIVE TRACER STUDIES DURING METHANOL SYNTHESIS

See the attached report for:

A. Problem Definition
B. Research Objectives
C. Research Accomplishments

Comparison of Single and Two-Bubble Class Gas Liquid Recirculation Models - Application to Pilot Plant Radioactive Tracer Studies During Methanol Synthesis

Puneet Gupta, Muthanna H. Al-Dahhan and Milorad P. Dudukovic'
Chemical Reaction Engineering Laboratory (CREL), Department of Chemical Engineering
Campus Box 1198, Washington University St. Louis, MO 63130-4899, USA

Bernard A. Toseland
Air Products & Chemicals, Inc., PO Box 25780, Lehigh Valley, PA 18007, USA

Abstract—Radioactive gas tracer measurements conducted during liquid phase methanol synthesis from syngas in a pilot scale slurry bubble column at the Alternate Fuels Development Unit (AFDU), La Porte have been compared with simulations from two mechanistic reactor models - Single Bubble Class Model (SBCM) and Two-Bubble Class Model (TBCM). The model parameters are estimated from an independent sub-model based on gas-liquid recirculation, which indicates that the longtime-averaged slip velocity between the gas and liquid/slurry in the column center could be as high as 50-60 cm/s depending on the operating conditions. Comparison of experimental data with simulation results from the two models indicates that accurate description of interphase gas-liquid mass transfer is crucial to the reliable prediction of tracer responses. Coupled with a correct description of gas-liquid recirculation, the models provide a simple and fundamentally based methodology for design and scale-up of bubble column reactors.

Keywords: Gas-liquid recirculation, slurry bubble column, mechanistic reactor modeling, radioactive tracer studies.

1. Introduction

The chemical industry places demands on operating bubble column reactors at high superficial gas velocities under high pressures and as large diameter vessels, especially in processes like the Fischer-Tropsch synthesis of liquid hydrocarbons or liquid phase methanol production that are viewed as alternate sources of fuels/chemicals from synthesis gas. Under these conditions, bubble columns operate in the *churn-turbulent* regime characterized by frequent bubble coalescence and breakage and a nearly chaotic two-phase system. The characterization of the extent of gas and liquid/slurry phase mixing in these reactors is very critical to their proper design and scale-up.

Traditionally, the Axial Dispersion Model (ADM) with interface mass transport has been used to describe the degree of backmixing in both phases and has been the basis for design of bubble and slurry bubble column reactors. Kastanek *et al.* (1993) have presented a detailed review of the correlations available for estimating the gas as well as liquid phase effective dispersion coefficients pertinent to the Axial Dispersion Model. However, these correlations are mostly empirical and do not provide reliable estimates for design and scale-up purposes. One of the reasons for the poor predictive capabilities of these correlations is that the ADM is suitable only for modeling of mixing processes in which the flow is not far away from ideal plug flow conditions. Therefore, for recirculation dominated convective flows such as those occurring during bubble column operation, the application of Axial Dispersion Model to describe the state of mixing is without a physical basis and has had limited success only in fitting the experimental data. Degaleesan *et al.* (1996[a]) presented in detail the shortcomings of the ADM applied to gas tracer data from a pilot-scale slurry-bubble column during liquid phase methanol synthesis at the La Porte Alternate Fuels Development Unit (AFDU). It was shown that the gas and liquid phase dispersion coefficients fitted to the tracer responses measured at various elevations did not exhibit a consistent trend and the values were widely scattered around the estimated means. Moreover, attempts to extract other parameters from the tracer data such as volumetric mass transfer coefficients did not seem to produce consistent results. It was subsequently shown in a separate study that the liquid phase mixing was predicted in excellent agreement with experimental data using a two-compartment mechanistic model (Degaleesan *et al.*, 1996[b]; Degaleesan, 1997), which accounted for mixing dominated by convective recirculation. Degaleesan and Dudukovic' (1998) also derived the relationship between the axial dispersion coefficient and the parameters of the phenomenological recirculation and eddy diffusion model and explained the difficulties involved in obtaining a predictive axial dispersion coefficient.

The study of mixing in the gas phase, however, has still not received much attention, with the ADM being used for lack of better alternatives. Some models describe the gas phase dynamics in terms of "small" and "large" bubble classes resulting from a bimodal distribution of bubble sizes caused by the non-uniformity of the gas flow through the column (Vermeer and Krishna, 1981; Shah *et al.*, 1985). These two classes of bubbles were shown to coalesce and interact frequently with each other resulting in higher mass transfer rates (de Swart, 1996). However, in spite of a better basis resulting from the consideration of a possible bimodal distribution of bubble sizes, these models do not account for the effect of gas and liquid recirculation and the

accompanying turbulence responsible for majority of the ensuing mixing. Given the inherent inadequacies of the ADM in describing gas backmixing in bubble column flows, phenomenological gas-liquid recirculation models have been developed as part of this study. The basis for these models is the liquid and gas recirculation resulting from the radial gas holdup distribution supported by extensive experimental database from the non-invasive measurement techniques consisting of Computed Tomography-CT and Computer Automated Radioactive Particle Tracking-CARPT (Devanathan *et al.*, 1990; Kumar *et al*, 1997; Degaleesan, 1997; Chen *et al.*, 1998).

The first of the models is the Two-Bubble Class Model (TBCM), which is based on the assumption that the gas phase dynamics and recirculation are described by the presence of two bubble classes - a "small" bubble class and a "large" bubble class, with the interaction between the two being modeled using an exchange coefficient. However, the assumption of a bi-modal bubble size distribution needs to be tested, and therefore, a second model has been developed where the gas phase dynamics is based just on a single bubble size (SBCM). Both models take into account the recirculation in the gas and liquid phases. For the estimation of the levels of gas and liquid recirculation, a sub-model was developed to estimate the radial profiles of the axial time-averaged liquid and gas velocities. This sub-model is based on a simplification of the two-fluid equations for Eulerian multiphase flows; and the liquid phase turbulence is closed by the modified mixing length closure from Kumar *et al.* (1994). Details of the sub-model equations, method of solution and model parameter estimation from the solution of the sub-model equations have been discussed elsewhere (Gupta *et al.*, 2000).

2. Experiments

The experimental data for this study was obtained in a pilot-scale slurry-bubble column reactor at the Department of Energy (DOE) facility at La Porte, Texas (Alternate Fuels Development Unit-AFDU). Radioactive gas tracer measurements were conducted using Ar^{41} in a 46-cm diameter slurry bubble column. The dispersed gas-slurry height was maintained at approximately 13.25-m with the chemical process being the liquid phase synthesis of methanol from Syngas ($CO+H_2$). Figure 1 shows the schematic of the experimental setup with the gas tracer injected below the sparger in the inlet Syngas stream. The temporal evolution of the tracer inside the reactor at three different operating conditions was measured using scintillation counters at seven different axial locations with four detectors at each level (see Figure 1). To estimate the gas holdup distribution in the column, pressure-drop and Nuclear Density Gauge (NDG) measurements were made along the column length. The measurements indicated that the gas holdup in the column was fairly constant except in the distributor and the free board regions. Table 1 shows the parameters in the estimated radial gas holdup profile under the three different operating conditions. Details of estimation of these parameters, detector calibration and experimental procedure can be found elsewhere (Degaleesan *et al.*, 1996; Degaleesan, 1997).

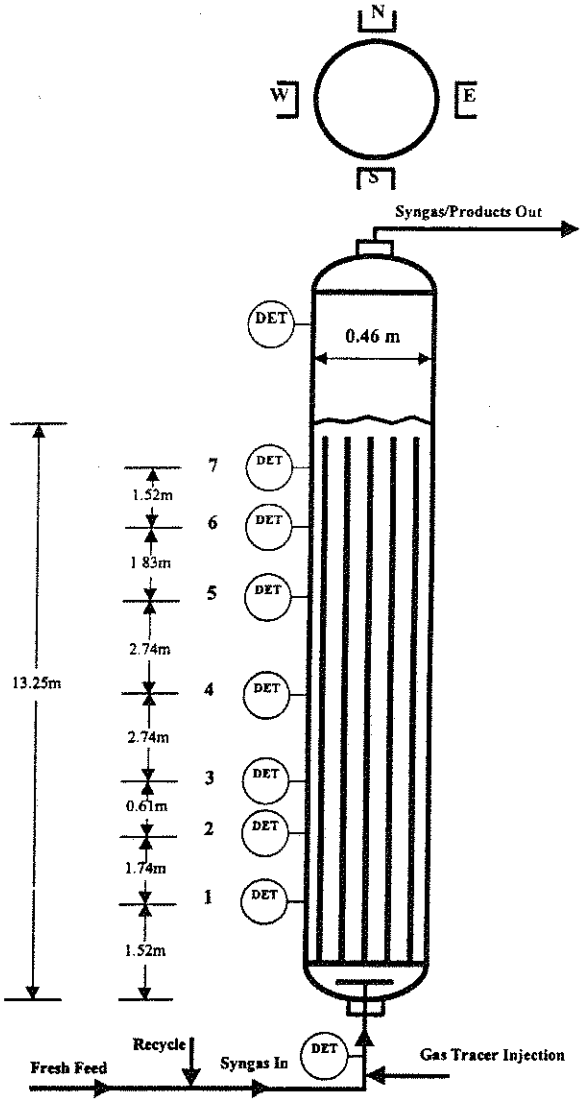

Figure 1. Schematic of pilot scale slurry bubble column reactor at the AFDU, La Porte.

3. Mechanistic Reactor Models

The reactor compartmentalization for the Single Bubble Class Model is shown in Figure 2a, whereas Figure 2b shows the same for the Two-Bubble Class Model. In both models, the gas phase is assumed to be recirculating along with the liquid/slurry phase, which has been assumed to be pseudo-homogeneous for the purposes of this study. For the SBCM, the gas phase is assumed to consist only of a single mean bubble size both in the core up-flow as well as the wall down-flow regions. For the TBCM on the other hand, the up-flowing gas in the core of the reactor is assumed to be made up of a lean "large" and a dense "small" bubble phases (de Swart, 1996), while the down-flowing gas in the annular region consists only of small bubbles, which do not possess sufficient momentum and get recirculated with the down-flowing slurry. The model equations resulting from the two reactor models are presented in Table 2 and are the classical transient-convection-diffusion-reaction PDEs, one for each

compartment in the well-developed regions; while the end-zones are modeled as Continuous Stirred Tanks (CSTs) the dynamics of which are well-represented by ODEs. The estimation of the model parameters from a hydrodynamic sub-model based on gas-liquid recirculation (equations presented at the bottom of Table 2 and discussed in detail by Gupta *et al.*, 2000) requires the knowledge of the radial gas holdup profile, which is frequently represented in terms of the following exponential function and is known to fit the experimental data well (Kumar *et al.*, 1994).

$$\varepsilon_g(\xi) = \bar{\varepsilon}_g \left(\frac{m+2}{m+2-2c} \right) \left(1 - c\xi^m\right) \qquad (1)$$

The radial distribution of the effective mean bubble-size (Equation 2) is obtained as part of the solution of the sub-model equations by satisfying the gas phase continuity in the computation of the radial gas velocity profile.

$$d(\xi) = \begin{cases} \bar{d} & \textit{for use in SBCM} \\ \bar{d}_{G_{1,LB}} \left(1 - c\xi^m\right) & \textit{for use in TBCM} \end{cases} \qquad (2)$$

Thus, the effective mean bubble-size is a constant for SBCM ($\bar{d}$), however for TBCM, it is assumed to have a functional form represented by Equation 2, where $\bar{d}_{G_{1,LB}}$ is the effective mean diameter of the "large" bubble phase and is obtained as part of the solution of the sub-model equations for estimating gas-liquid recirculation velocities. The effective mean bubble diameter of the "small" bubbles in TBCM is estimated from Equations 1 and 2 as shown later. This assumed distribution is justified in view of the similarity with the radial gas holdup profile with a relatively flat radial gas holdup profile implying that the effective mean bubble size is relatively homogeneous. On the other hand, a large gradient in the radial gas holdup profile implies greater concentration of gas in the column center resulting in relatively larger bubble voids coexisting with smaller sized bubbles, and only the "small" bubble phase present in the annular region. Therefore, this assumption on radial distribution of longtime averaged bubble size automatically reflects the non-uniformity in the radial gas holdup profile.

Table 1. Estimated gas holdup profile for the three operating conditions during the gas tracer experiments.

Experiment Number	Pressure (MPa)	Temperature (°C)	$\bar{U}_{G,sup}$ (cm/s)	Parameters of the Radial Gas Holdup Profile		
				$\bar{\varepsilon}_g$	m	c
Run 14.6	5.268	250	22.863	0.39	2	0.8444
Run 14.7	5.268	250	12.656	0.33	2	0.8908
Run 14.8	3.647	250	32.814	0.37	2	0.9433

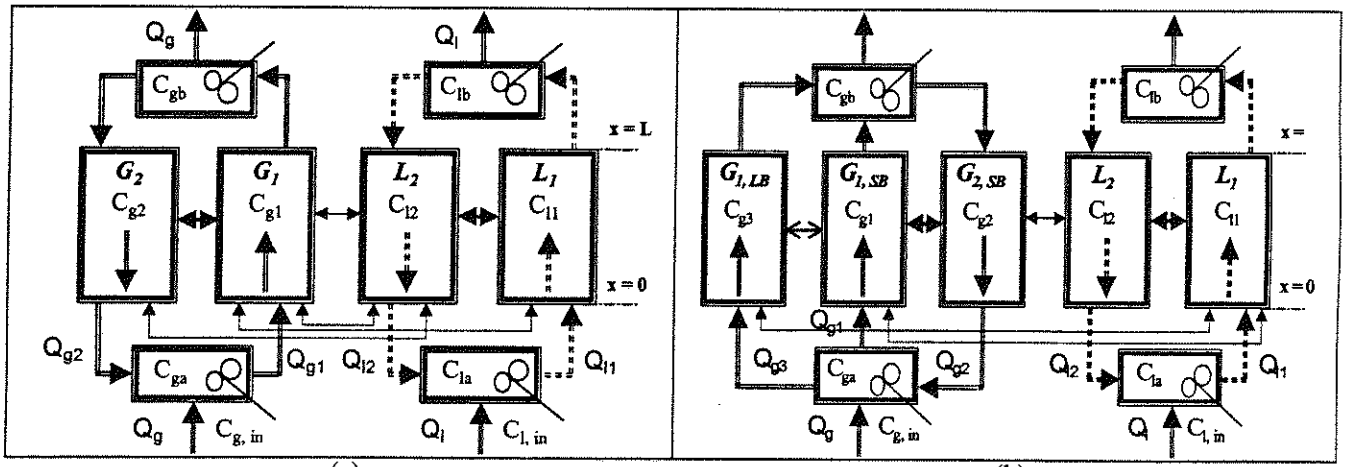

Figure 2. Schematic of bubble column reactor compartmentalization for
(a) Single Bubble Class Model (SBCM) (b) Two-Bubble Class Model (TBCM)

Figure 3 exhibits the radial profiles of the axial time-averaged liquid/slurry and gas velocity profiles computed from the hydrodynamic sub-model for the three operating conditions listed in Table 1. Clearly the computed gas velocity profile is not significantly affected by the nature of the radial distribution of the mean effective bubble diameter. In addition, the slip velocity between the gas and slurry phases could be as high as 50-60 cm/s in the column center depending on the superficial gas velocity. Based on these converged liquid & gas velocity profiles, the converged mean bubble size profile, and the known radial gas holdup profile, all the model parameters for the SBCM can be evaluated as shown by Gupta *et al.* (2000). However, some additional parameters need to be estimated for the TBCM as discussed below. From Equations 1 and 2, a bubble number density function defined as number of bubbles per unit reactor cross-sectional area is obtained.

$$n(\xi) = \frac{4\varepsilon_g(\xi)}{\pi d_B^2(\xi)} \qquad (3)$$

From Equation 3, the following four quantities are obtained by averaging over the core and annular regions the boundary between which is modeled by ξ'', the dimensionless radius where the radial gas velocity profile becomes zero.

$$\bar{n}_{G_{2,SB}} = \frac{2}{(1-\xi''^2)} \int_{\xi''}^{1} n_B(\xi)\xi\, d\xi \qquad \bar{d}_{G_{2,SB}} = \sqrt{\frac{4\bar{\varepsilon}_{g2}}{\pi \bar{n}_{B,S2}}} \quad (4)$$

$$\bar{n}_{G_{1,SB+LB}} = \frac{2}{\xi''^2} \int_{0}^{\xi''} n_B(\xi)\xi\, d\xi \qquad \bar{d}_{G_{1,SB+LB}} = \sqrt{\frac{4(\bar{\varepsilon}_{g1}+\bar{\varepsilon}_{g3})}{\pi \bar{n}_{B,S1-L}}} \quad (5)$$

As the holdups of the small bubbles in the core and annulus are assumed equal for TBCM, it implies that $\bar{n}_{B,S1}\,\bar{d}^2_{B,S1} = \bar{n}_{B,S2}\,\bar{d}^2_{B,S2}$. Therefore, the effective mean diameter of the small bubbles in the core is estimated as

$$\bar{n}_{G_{1,LB}} = \frac{\bar{n}_{G_{1,SB+LB}}\,\bar{d}^2_{G_{1,SB+LB}} - \bar{n}_{G_{2,SB}}\,\bar{d}^2_{G_{2,SB}}}{\bar{d}^2_{G_{1,LB}}} \quad (6)$$

$$\bar{d}_{G_{1,SB}} = \sqrt{\frac{\bar{n}_{G_{2,SB}}\,\bar{d}^2_{G_{2,SB}}}{(\bar{n}_{G_{1,SB+LB}} - \bar{n}_{G_{1,LB}})}}$$

In the above set of equations, the subscript "*S1-L*" refers to the small and large bubbles in the core. Knowing the mean "small" and "large" bubble diameters in the core, the mass transfer coefficients and specific interfacial areas for these two bubble phases are estimated in a similar manner as for the Single Bubble Class Model (Gupta *et al.*, 2000). Once all the hydrodynamic parameters for the two reactor models are estimated by the procedure described above, the reactor model equations are solved by a fully implicit finite difference scheme, which is robust and does not present problems related to stability and convergence.

4. Simulation Comparison with Experimental Data

Figures 4-7 present the comparison of the normalized experimental tracer response curves (detector level 7) with simulated responses computed from the two reactor models discussed above. The purpose of this comparative study is to evaluate the effect of some of the key model parameters as well as the two models against each other in their ability to predict tracer responses. From Figure 4, one can see that the effect of the axial dimension of the distributor and disengagement CSTs on the simulated tracer responses is negligible for both SBCM as well as TBCM. This result is similar to that of Degaleesan *et al.* (1996[b]) for liquid mixing studies in both laboratory as well as pilot-scale columns. Thus, for all subsequent simulations (Figures 5-7), the height of these regions was set to one column diameter.

The important parameters affecting the spread of the gas-phase tracer response curves are the Henry's constant and the volumetric mass transfer coefficients. As was shown by Degaleesan *et al.* (1996[a]), the tracer response curves simulated using the ADM were also very sensitive to these two parameters, however, no consistent trend was found in their estimated values. Figure 5 presents the comparison of the simulated and experimental responses for several values of the Henry's constant, which is ***dimensionless*** and is defined as the ratio of the concentration of Argon in the liquid to that in the gas when the gas and liquid phases are in equilibrium. One can see from the figure that for both the SBCM as well as for the TBCM, the value of the Henry's constant can significantly affect the peak arrival time, since a larger value of the Henry's constant implies that the tracer stays longer in the liquid/slurry phase resulting in a prolonged residence time. Except for Run 14.8, the simulated tracer curves assuming the thermodynamically estimated value of the Henry's constant (H^*=0.17) result in excellent match with the peak arrival time of the experimental curves with a little under estimation of the spreads in the tracer response curves about these peak arrival. It should however be noted that the measured tracer responses are a result of radiation measurement, which leads to additional broadening of the tracer responses due to practical limitations on detector shielding in a pilot-scale environment.

Figure 6 examines the effect of the small and large bubble interaction parameter for the Two-Bubble Class Model. It can be seen from the figure that the bubble-bubble interactions have a significant on the tracer curve only in absence of mass transfer (H=0.0 i.e., for an insoluble gas), and there is negligible effect of the bubble-bubble interactions on tracer responses when compared to the effect of the tracer solubility in the liquid/slurry, i.e., the magnitude of H. It should however be kept in mind that the average speeds at which the "small" and "large" bubbles travel do not differ by more than 30-45 cm/s as computed from the parameter estimation procedure. It is possible, therefore, that the velocities of the "small" and "large" bubble phases differ much more than assumed here, if computed using literature correlations (Krishna *et al.*, 1996). In that case, the bubble-bubble interaction parameter would have a more pronounced effect on the simulated tracer responses. However, as mentioned earlier, such correlations for bubble rise are developed without consideration of the inherent recirculatory nature of the flow, and may not provide good estimates for the bubble velocities.

The last effect evaluated in this study is the assumption of the existence of two-bubble classes. Figure 7 presents the result of such comparison, where the simulated responses have been computed using K=10. One can see from the figure that the two models do not exhibit any significant differences as far as comparison with tracer response data is concerned. This result is not too surprising as the "small" and "large" bubble phase equations for the TBCM when added together result in the equation describing the dynamics of the up-flowing gas in the SBCM. Therefore, one does not really need to make the assumptions about the bi-disperse bubble size distribution to characterize the gas-phase dynamics, as long as a reasonably accurate description of the recirculation in the gas and liquid phases is incorporated into the reactor model.

Table 2. Model equations for Single Bubble Class and Two-Bubble Class Models.

Single Bubble Class Model	Two Bubble Class Model
$\frac{\partial C_{g1}}{\partial t} = \left\{ \begin{array}{l} \overline{D}_{xx_1} \frac{\partial^2 C_{g1}}{\partial x^2} - \overline{u}_{g1} \frac{\partial C_{g1}}{\partial x} - \frac{4\left(\overline{D}_{rr}\varepsilon_g\right)_{r=r''}}{r'' R \overline{\varepsilon}_{g1}}\left(C_{g1} - C_{g2}\right) + R_{x,g1} \\ - \frac{k_{gulu} a_{gulu}}{\overline{\varepsilon}_{g1}}\left(HC_{g1} - C_{l1}\right) - \frac{k_{guld} a_{guld}}{\overline{\varepsilon}_{g1}}\left(HC_{g1} - C_{l2}\right) \end{array} \right\}$	$\frac{\partial C_{g1}}{\partial t} = \left\{ \begin{array}{l} \overline{D}_{xx_1} \frac{\partial^2 C_{g1}}{\partial x^2} - \overline{u}_{g1} \frac{\partial C_{g1}}{\partial x} - \left(\frac{4\left(\overline{D}_{rr}\varepsilon_g\right)_{r=r''}}{r'' R \overline{\varepsilon}_{g1}} + \frac{K_{SB_1-LB}}{\overline{\varepsilon}_{g1}} \right)\left(C_{g1} - C_{g2}\right) \\ - \frac{k_{sulu} a_{sulu}}{\overline{\varepsilon}_{g1}}\left(HC_{g1} - C_{l1}\right) - \frac{k_{suld} a_{suld}}{\overline{\varepsilon}_{g1}}\left(HC_{g1} - C_{l2}\right) + R_{x,g1} \end{array} \right\}$
$\frac{\partial C_{g2}}{\partial t} = \left\{ \begin{array}{l} \overline{D}_{xx_2} \frac{\partial^2 C_{g2}}{\partial x^2} + \overline{u}_{g2} \frac{\partial C_{g2}}{\partial x} - \frac{k_{gdld} a_{gdld}}{\overline{\varepsilon}_{g2}}\left(HC_{g2} - C_{l2}\right) \\ + \frac{4r''/R}{R^2 - r''^2} \frac{\left(\overline{D}_{rr}\varepsilon_g\right)_{r=r''}}{\overline{\varepsilon}_{g2}}\left(C_{g1} - C_{g2}\right) + R_{x,g2} \end{array} \right\}$	$\frac{\partial C_{g2}}{\partial t} = \left\{ \begin{array}{l} \overline{D}_{xx_2} \frac{\partial^2 C_{g2}}{\partial x^2} + \overline{u}_{g2} \frac{\partial C_{g2}}{\partial x} - \frac{k_{sdld} a_{sdld}}{\overline{\varepsilon}_{g2}}\left(HC_{g2} - C_{l2}\right) \\ + \frac{4r''/R}{R^2 - r''^2} \frac{\left(\overline{D}_{rr}\varepsilon_g\right)_{r=r''}}{\overline{\varepsilon}_{g2}}\left(C_{g1} - C_{g2}\right) + R_{x,g2} \end{array} \right\}$
	$\frac{\partial C_{g3}}{\partial t} = \left\{ - \overline{u}_{g3} \frac{\partial C_{g3}}{\partial x} - \frac{k_l a_l}{\overline{\varepsilon}_{g3}}\left(HC_{g3} - C_{l1}\right) + \frac{K_{SB_1-LB}}{\overline{\varepsilon}_{g3}}\left(C_{g1} - C_{g3}\right) \right\}$
$\frac{\partial C_{l1}}{\partial t} = \left\{ \begin{array}{l} \overline{D}_{xx_1} \frac{\partial^2 C_{l1}}{\partial x^2} - \overline{u}_{l1} \frac{\partial C_{l1}}{\partial x} + \left(\frac{r''}{r'}\right)^2 \frac{k_{gulu} a_{gulu}}{\overline{\varepsilon}_{l1}}\left(HC_{g1} - C_{l1}\right) \\ - \frac{4\left(\overline{D}_{rr}\varepsilon_l\right)_{r=r'}}{r' R \overline{\varepsilon}_{l1}}\left(C_{l1} - C_{l2}\right) + R_{x,l1} \end{array} \right\}$	$\frac{\partial C_{l1}}{\partial t} = \left\{ \begin{array}{l} \overline{D}_{xx_1} \frac{\partial^2 C_{l1}}{\partial x^2} - \overline{u}_{l1} \frac{\partial C_{l1}}{\partial x} - \frac{4\left(\overline{D}_{rr}\varepsilon_l\right)_{r=r'}}{r' R \overline{\varepsilon}_{l1}}\left(C_{l1} - C_{l2}\right) + R_{x,l1} \\ + \left(\frac{r''}{r'}\right)^2 \frac{1}{\overline{\varepsilon}_{l1}}\left[k_{sulu} a_{sulu}\left(HC_{g1} - C_{l1}\right) + k_l a_l\left(HC_{g3} - C_{l1}\right)\right] \end{array} \right\}$
$\frac{\partial C_{l2}}{\partial t} = \left\{ \begin{array}{l} \overline{D}_{xx_2} \frac{\partial^2 C_{l2}}{\partial x^2} + \overline{u}_{l2} \frac{\partial C_{l2}}{\partial x} + \frac{4r'/R}{R^2 - r'^2} \frac{\left(\overline{D}_{rr}\varepsilon_l\right)_{r=r'}}{\overline{\varepsilon}_{l2}}\left(C_{l1} - C_{l2}\right) \\ + \left(\frac{r''^2}{R^2 - r'^2}\right) \frac{k_{guld} a_{guld}}{\overline{\varepsilon}_{l2}}\left(HC_{g1} - C_{l2}\right) + R_{x,l2} \\ + \left(\frac{R^2 - r''^2}{R^2 - r'^2}\right) \frac{k_{gdld} a_{gdld}}{\overline{\varepsilon}_{l2}}\left(HC_{g2} - C_{l2}\right) \end{array} \right\}$	$\frac{\partial C_{l2}}{\partial t} = \left\{ \begin{array}{l} \overline{D}_{xx_2} \frac{\partial^2 C_{l2}}{\partial x^2} + \overline{u}_{l2} \frac{\partial C_{l2}}{\partial x} + \frac{4r'/R}{R^2 - r'^2} \frac{\left(\overline{D}_{rr}\varepsilon_l\right)_{r=r'}}{\overline{\varepsilon}_{l2}}\left(C_{l1} - C_{l2}\right) \\ + \left(\frac{r''^2}{R^2 - r'^2}\right) \frac{k_{suld} a_{suld}}{\overline{\varepsilon}_{l2}}\left(HC_{g1} - C_{l2}\right) + R_{x,l2} \\ + \left(\frac{R^2 - r''^2}{R^2 - r'^2}\right) \frac{k_{sdld} a_{sdld}}{\overline{\varepsilon}_{l2}}\left(HC_{g2} - C_{l2}\right) \end{array} \right\}$
$\frac{dC_{ga}}{dt} = \left\{ \begin{array}{l} \frac{\overline{\varepsilon}_{g2}\overline{u}_{g2}}{\overline{\varepsilon}_g \phi_{in} D_C} \frac{\left(R^2 - r''^2\right)}{R^2} C_{g2,0} - \frac{\overline{\varepsilon}_{g1}\overline{u}_{g1}}{\overline{\varepsilon}_g \phi_{in} D_C} \frac{r''^2}{R^2} C_{ga} \\ + \frac{U_G}{\overline{\varepsilon}_g \phi_{in} D_C} C_{g,in} - \frac{k_{CST} a_{CST}}{\overline{\varepsilon}_g}\left(HC_{ga} - C_{la}\right) + R_{x,ga} \end{array} \right\}$	$\frac{dC_{ga}}{dt} = \left\{ \begin{array}{l} \frac{\overline{\varepsilon}_{g2}\overline{u}_{g2}}{\overline{\varepsilon}_g \phi_{in} D_C} \frac{\left(R^2 - r''^2\right)}{R^2} C_{g2,0} - \frac{\left(\overline{\varepsilon}_{g1}\overline{u}_{g1} + \overline{\varepsilon}_{g3}\overline{u}_{g3}\right)}{\overline{\varepsilon}_g \phi_{in} D_C} \frac{r''^2}{R^2} C_{ga} \\ + \frac{U_G}{\overline{\varepsilon}_g \phi_{in} D_C} C_{g,in} - \frac{k_{CST} a_{CST}}{\overline{\varepsilon}_g}\left(HC_{ga} - C_{la}\right) + R_{x,ga} \end{array} \right\}$
$\frac{dC_{la}}{dt} = \left\{ \begin{array}{l} \frac{\overline{\varepsilon}_{l2}\overline{u}_{l2}}{\overline{\varepsilon}_l \phi_{in} D_C} \frac{\left(R^2 - r'^2\right)}{R^2} C_{l2,0} - \frac{\overline{\varepsilon}_{l1}\overline{u}_{l1}}{\overline{\varepsilon}_l \phi_{in} D_C} \frac{r'^2}{R^2} C_{la} \\ + \frac{U_L}{\overline{\varepsilon}_l \phi_{in} D_C} C_{l,in} + \frac{k_{CST} a_{CST}}{\overline{\varepsilon}_l}\left(HC_{ga} - C_{la}\right) + R_{x,la} \end{array} \right\}$	$\frac{dC_{la}}{dt} = \left\{ \begin{array}{l} \frac{\overline{\varepsilon}_{l2}\overline{u}_{l2}}{\overline{\varepsilon}_l \phi_{in} D_C} \frac{\left(R^2 - r'^2\right)}{R^2} C_{l2,0} - \frac{\overline{\varepsilon}_{l1}\overline{u}_{l1}}{\overline{\varepsilon}_l \phi_{in} D_C} \frac{r'^2}{R^2} C_{la} \\ + \frac{U_L}{\overline{\varepsilon}_l \phi_{in} D_C} C_{l,in} + \frac{k_{CST} a_{CST}}{\overline{\varepsilon}_l}\left(HC_{ga} - C_{la}\right) + R_{x,la} \end{array} \right\}$
$\frac{dC_{gb}}{dt} = \left\{ \begin{array}{l} \frac{\overline{\varepsilon}_{g1}\overline{u}_{g1}}{\overline{\varepsilon}_g \phi_{out} D_C} \frac{r''^2}{R^2} C_{g1,L} - \frac{\overline{\varepsilon}_{g2}\overline{u}_{g2}}{\overline{\varepsilon}_g \phi_{out} D_C} \frac{\left(R^2 - r''^2\right)}{R^2} C_{gb} \\ - \frac{U_G}{\overline{\varepsilon}_g \phi_{out} D_C} C_{gb} - \frac{k_{CST} a_{CST}}{\overline{\varepsilon}_g}\left(HC_{gb} - C_{lb}\right) + R_{x,gb} \end{array} \right\}$	$\frac{dC_{gb}}{dt} = \left\{ \begin{array}{l} \frac{\overline{\varepsilon}_{g1}\overline{u}_{g1}}{\overline{\varepsilon}_g \phi_{out} D_C} \frac{r''^2}{R^2} C_{g1,L} + \frac{\overline{\varepsilon}_{g3}\overline{u}_{g3}}{\overline{\varepsilon}_g \phi_{out} D_C} \frac{r''^2}{R^2} C_{g3,L} - \frac{U_G}{\overline{\varepsilon}_g \phi_{out} D_C} C_{gb} \\ - \frac{\overline{\varepsilon}_{g2}\overline{u}_{g2}}{\overline{\varepsilon}_g \phi_{out} D_C} \frac{\left(R^2 - r''^2\right)}{R^2} C_{gb} - \frac{k_{CST} a_{CST}}{\overline{\varepsilon}_g}\left(HC_{gb} - C_{lb}\right) + R_{x,gb} \end{array} \right\}$
$\frac{dC_{lb}}{dt} = \left\{ \begin{array}{l} \frac{\overline{\varepsilon}_{l1}\overline{u}_{l1}}{\overline{\varepsilon}_l \phi_{out} D_C} \frac{r'^2}{R^2} C_{l1,L} - \frac{\overline{\varepsilon}_{l2}\overline{u}_{l2}}{\overline{\varepsilon}_l \phi_{out} D_C} \frac{\left(R^2 - r'^2\right)}{R^2} C_{lb} \\ - \frac{U_L}{\overline{\varepsilon}_l \phi_{out} D_C} C_{lb} + \frac{k_{CST} a_{CST}}{\overline{\varepsilon}_l}\left(HC_{gb} - C_{lb}\right) + R_{x,lb} \end{array} \right\}$	$\frac{dC_{lb}}{dt} = \left\{ \begin{array}{l} \frac{\overline{\varepsilon}_{l1}\overline{u}_{l1}}{\overline{\varepsilon}_l \phi_{out} D_C} \frac{r'^2}{R^2} C_{l1,L} - \frac{\overline{\varepsilon}_{l2}\overline{u}_{l2}}{\overline{\varepsilon}_l \phi_{out} D_C} \frac{\left(R^2 - r'^2\right)}{R^2} C_{lb} \\ - \frac{U_L}{\overline{\varepsilon}_l \phi_{out} D_C} C_{lb} + \frac{k_{CST} a_{CST}}{\overline{\varepsilon}_l}\left(HC_{gb} - C_{lb}\right) + R_{x,lb} \end{array} \right\}$
$d_B = \overline{d}_B$	$d_B = \overline{d}_{LB}\left(1 - c\xi^m\right)$
Hydrodynamic Model	
$\varepsilon_g(\xi) = \overline{\varepsilon}_g \left(\frac{m+2}{m+2-2c}\right)\left(1 - c\xi^m\right)$	
Liquid Phase	**Gas Phase**
$0 = -\left(\rho_g \varepsilon_g + \rho_l \varepsilon_l\right) g - \frac{dP}{dz} + \frac{1}{r}\frac{d}{dr}\left(r \varepsilon_l \tau_{l,rz}\right)$	$0 = -\rho_g \varepsilon_g g - \varepsilon_g \frac{dP}{dz} + M_d$
$\tau_{l,rz}(\xi) = -\frac{\rho_l \nu_l^m}{R}\frac{du_l}{d\xi} - \frac{\rho_l l^2}{R^2}\left(\frac{du_l}{d\xi}\right)^2$	$M_d = -\frac{3\varepsilon_l \varepsilon_g \rho_l C_D}{4 d_B}\left(u_l - u_g\right)^2$
$\frac{l(\xi)}{R} = \frac{a(1-\xi)}{(\xi+b)^c} + d(1-\xi)^e$ *Kumar et al. (1995)*	$C_D = max\left[\frac{24}{Re}\left(1 + 0.15\,Re^{0.687}\right), \frac{8}{3}\frac{Eo}{Eo+4}\right]$ *Tomiyama et al. (1995)*

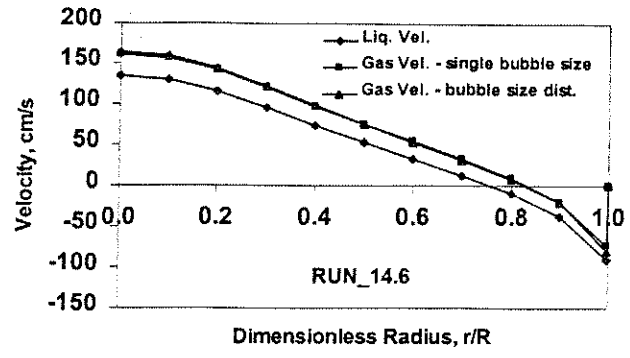

(a)

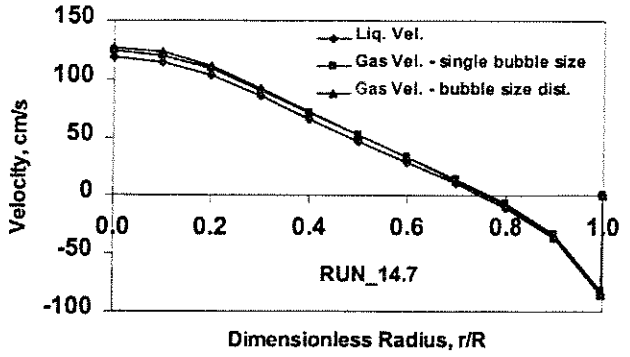

(b)

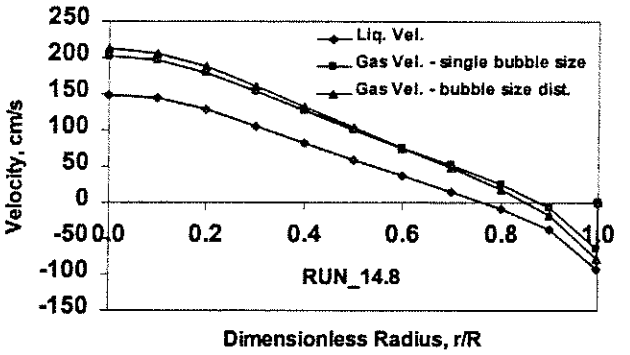

(c)

Figure 3. Liquid and gas radial velocity profiles for the three different operating conditions.

Lastly, we evaluate the assumption of the existence of two-bubble classes. Figure 7 presents the result of such comparison, where the simulated responses have been computed using K=10. One can see from the figure that the two models do not exhibit any significant differences as far as comparison with tracer response data is concerned. This result is not too surprising as the "small" and "large" bubble phase equations for the TBCM when added together result in the equation describing the dynamics of the up-flowing gas in the SBCM. Thus, one does not really need to make the assumptions about the bi-disperse bubble size distribution to characterize the gas-phase dynamics, as long as a reasonably accurate description of the recirculation in the gas and liquid phases is obtained.

5. Concluding Remarks

The comparison of the simulation results with gas tracer experiments reported in an earlier study (Degaleesan *et al.*, 1996) indicates that the TBCM does not present additional benefits over the SBCM. The TBCM does have an additional bubble-bubble interaction parameter, which has an effect on the gas phase tracer responses only in the absence of gas-liquid mass transfer. Coupled with a proper estimation of mass transfer effects, the simulated tracer responses are found to be in good agreement with experimental data; indicating reliable predictability from the solution of the model equations. Further, with incorporation of the reaction kinetics, the models provide the rational tools for scale-up and prediction of reactor performances.

6. Acknowledgements

The authors are grateful for the continued support of this research from the *Department of Energy* grant (DE-FC-22-95 PC 95051) via *Air Products and Chemicals, Inc.* and the industrial sponsors of the *Chemical Reaction Engineering Laboratory, Washington University.*

7. Nomenclature

a	interfacial area, cm^{-1}
C	concentration, moles/cm^3
C_D	drag coefficient
c	parameter in hold-up profile
Eo	Eotvos number
D_C	column diameter, cm
$D_{L,m}$	molecular diffusivity, cm^2/s
$\overline{D}_{rr}$	radial turbulent diffusivity, cm^2/s
$\overline{D}_{xx}$	axial turbulent diffusivity, cm^2/s
d	mean bubble diameter, cm
g	acceleration due to gravity, cm^2/s
H	Henry's constant
k	mass transfer coefficient, cm/s
L	dispersion height, cm
l	mixing length, cm
m	exponent in hold-up profile
Q	flow rate, cm^3/s
R	column radius, cm
R_x	reaction rate, moles cm^{-3} s^{-1}
t	time, s
$\overline{U}_{G,sup}$	gas superficial velocity, cm/s
u	velocity, cm/s
$\overline{u}$	radially averaged mean velocity, cm/s
V	volume of end zone CSTs, cm^3
x	axial position in the column, cm

Greek Symbols

ε	local phase hold-up
$\overline{\varepsilon}_g$	radially averaged phase hold-up
ϕ	fraction of the column diameter
ρ	density, g/cm^3
σ	surface tension of the liquid, dyne/cm
$\tau_{l,rz}$	total shear stress, dyne/cm^2
ν^m	kinematic viscosity, cm^2/s
ξ	dimensionless radius
ξ'	liquid velocity inversion point
ξ"	gas velocity inversion point

8. References

Chen, J., Gupta, P., Degaleesan, S., Al-Dahhan, M. H., Dudukovic', M. P., and Toseland, B. A., 1998, Gas Holdup Distributions in Large-Diameter Bubble Columns Measured by Computed Tomography, *Flow Measurement and Instrumentation*, **9**, 91-101.

Degaleesan, and Dudukovic', M. P., 1998, Liquid backmixing in bubble columns and the axial dispersion coefficient, *AIChE J.*, 44(11), 2369-2378.

Degaleesan, S., 1997, Fluid Dynamic Measurements and Modeling of Liquid Mixing in Bubble Columns, *D.Sc. Thesis*, Washington University.

Degaleesan, S., Dudukovic', M. P., Bhatt, B. L., and Toseland, B. A., 1996[a], Slurry bubble column hydrodynamics: Tracer studies of the La Porte AFDU Reactor during methanol synthesis, *Fourth quarterly report for Contract DOE-FC 2295 PC 95051.*

Degaleesan, S., Roy, S., Kumar, S. B. and Dudukovic', M. P., 1996[b], Liquid backmixing based on convection and turbulent dispersion in bubble columns, *Chem. Eng. Sci.*, **51**, 1967-1976.

Devanathan, N., Moslemian, D., and Dudukovic', M. P., 1990, Flow mapping in bubble columns using CARPT, *Chem. Eng. Sci.*, **45**, 2285-2291.

Kastanek, F., Zahradnik, J., Kratochvil, J. and Cermak, J., 1939, Chemical Reactions for Gas-Liquid Systems, Ellis Horwood, New York.

Gupta, P., Ong, B., Al-Dahhan, M.H., Dudukovic, M. P., and Toseland, B. A., 2000, Hydrodynamics of Churn-Turbulent Bubble Columns: Gas-Liquid Recirculation and Mechanistic Modeling, Accepted for publication in a topical issue of *Catalysis Today.*

Kumar, S. B., Moslemian, D., and Dudukovic, M. P., 1997, Gas Holdup Measurements in Bubble Columns Using Computed Tomography, *AIChE J.*, **43**(6), 1414-1425.

Kumar, S. B., Devanathan, N., Moslemian, D., and Dudukovic', M. P., 1994, Effect of scale on liquid recirculation in bubble columns, *Chem. Engng., Sci.*, **49**(24B), 5637-5652.

Shah, Y. T., Kelkar, B. G., Godbole, S. P., and Deckwer, W. D., 1982, Design parameters estimation for bubble column reactors, *AIChE J.*, **28**, 353-379.

de Swart, J. W. A., 1996, Scale-up of a Fischer-Tropsch slurry reactor, Ph.D. Thesis, University of Groningen, The Netherlands

Vermeer, D. J., and Krishna, R., 1981, Hydrodynamics and mass transfer in bubble columns operating in the churn-turbulent regime, *Ind. Engng. Chem. Process Design & Dev.*, **20**, 475-482.

Tomiyama, A., Kataoka, I., and Sakaguchi, T., 1995, Drag coefficients of bubbles (1st report, drag coefficients of a single bubble in a stagnant liquid), *Trans. JSME Part B*, **61**(587), 2357-2364.

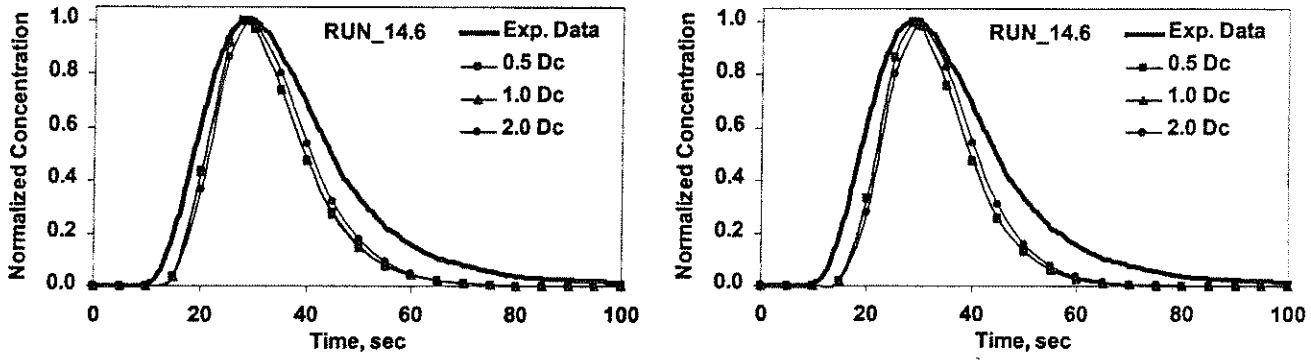

Figure 4. Effect of the axial dimension of the distributor and disengagement CSTs on the simulated gas tracer response curves computed using (a) SBCM (b) TBCM.

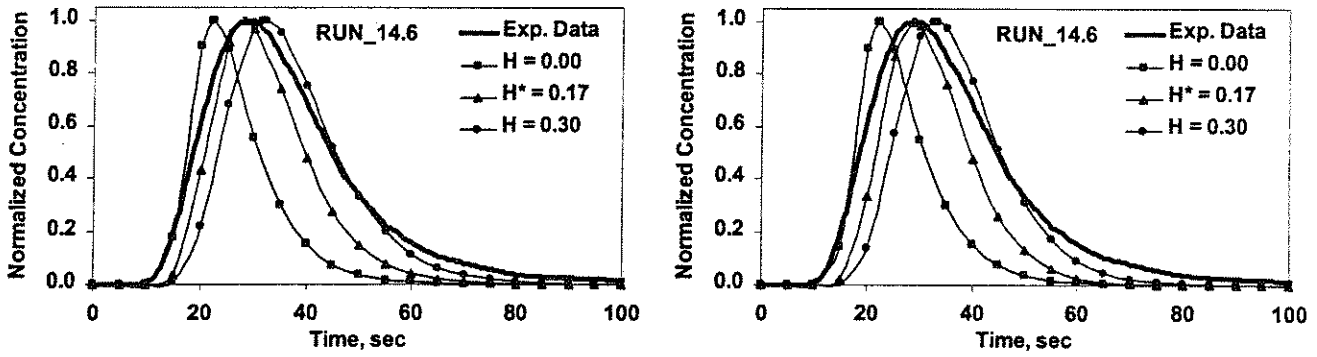

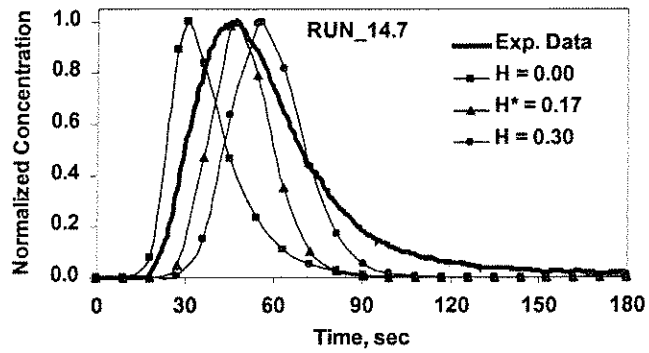

(b)

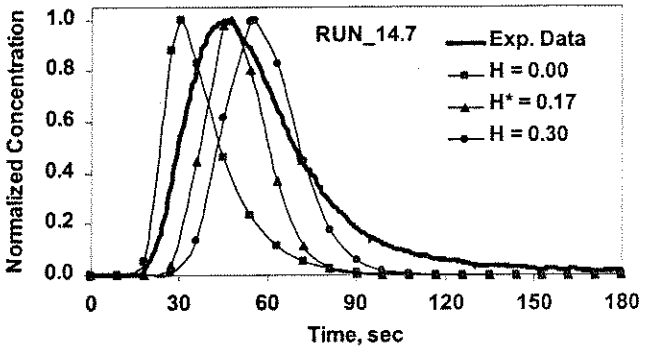

(e)

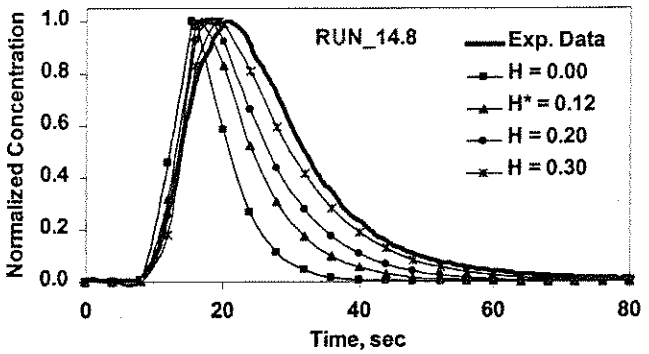

(c)

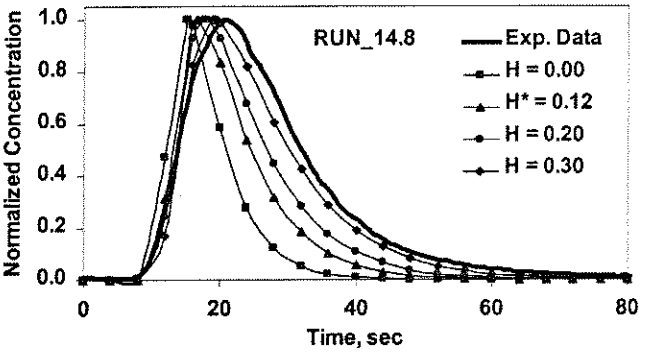

(f)

Figure 5. Effect of Henry's constant on simulated gas-tracer response curves (a)-(c) SBCM (d)-(f) TBCM.

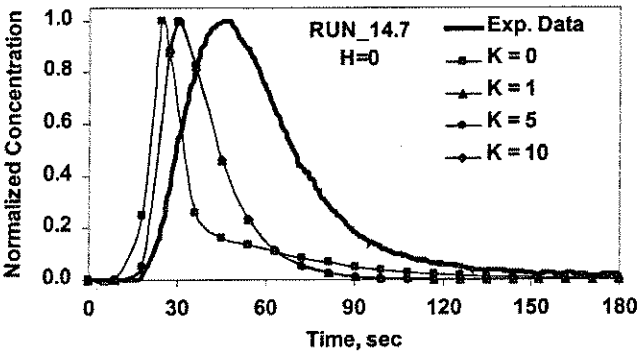

(a)

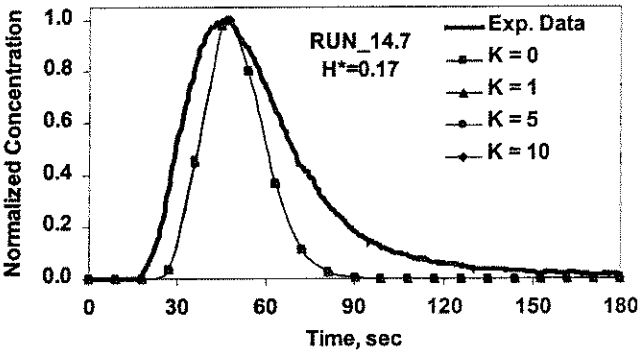

(b)

Figure 6. Effect of bubble-interaction parameter on simulated response curves (Run_14.7). (a) H=0 (b) H=H*.

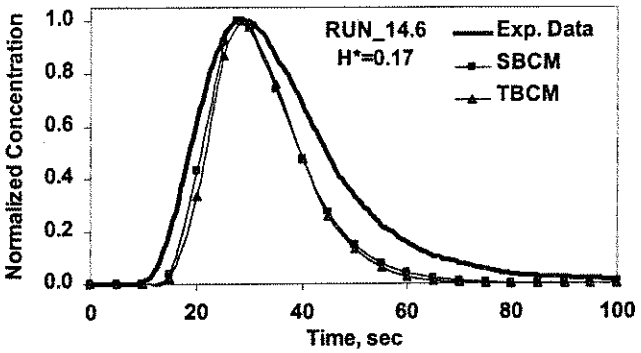

(a)

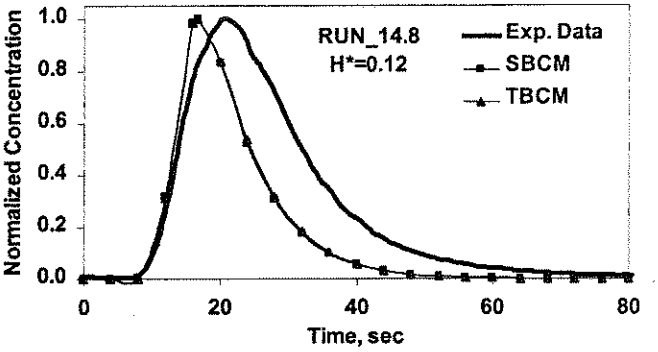

(b)

Figure 7. Comparison of simulated tracer response curves from SBCM and TBCM with experimental data (a) Run 14.6 (b) Run 14.8.

HYDRODYNAMICS OF CHURN TURBULENT BUBBLE COLUMNS: GAS-LIQUID RECIRCULATION AND MECHANISTIC MODELING

See the attached report for:

A. Problem Definition
B. Research Objectives
C. Research Accomplishments

Hydrodynamics of Churn Turbulent Bubble Columns: Gas-Liquid Recirculation and Mechanistic Modeling

Puneet Gupta, Booncheng Ong, Muthanna H. Al-Dahhan and Milorad P. Dudukovic'*

Chemical Reaction Engineering Laboratory

Department of Chemical Engineering, Campus Box 1198

1 Brookings Drive, Washington University St. Louis, MO 63130-4899

Bernard A. Toseland

Air Products & Chemicals, Inc.

PO Box 25780, Lehigh Valley, PA 18007, USA

* Corresponding Author Tel: (314) 935-7187

Fax: (314) 935-7211

E-mail: muthanna@wuche.che.wustl.edu

Abstract

A phenomenological (mechanistic) model has been developed for describing the gas and liquid/slurry phase mixing in churn-turbulent bubble columns. The gas and liquid phase recirculation in the reactor which are needed as inputs to the mechanistic reactor model are estimated via a sub-model which uses the two-fluid approach to solving the Navier Stokes equations. This sub-model estimates the effective bubble diameter in the reactor cross-section and provides a consistent basis for the estimation of volumetric mass transfer coefficients. A strategy for the numerical solution of the sub-model equations is presented along with simulation results for a few cases. The overall reactor model has been tested against experimental data from radioactive gas tracer experiments conducted at the Alternate Fuels Development Unit (AFDU), La Porte under conditions of methanol synthesis.

Keywords: Gas-liquid flow, slurry bubble column, computed tomography, radioactive particle tracking, gas-liquid recirculation, mechanistic reactor modeling, radioactive tracer studies.

1. Introduction

The abundance of natural gas in many remote areas has led to a continued interest in natural gas conversion to liquid fuels that can be easily and economically transported. The conversion of natural gas to value-added liquid chemicals is generally accomplished in two-stages. In the first stage, natural gas is converted to a mixture of hydrogen and carbon monoxide (synthesis gas), which in the second stage can be converted to a whole range of valuable chemicals depending on the catalyst and the employed process conditions. Liquid phase methanol synthesis, synthesis of Fischer-Tropsch (FT) liquids and a host of other processes based on syngas chemistries have been reported [1]. Traditionally, these processes were realized using fixed bed reactors, however, recently slurry bubble column reactors have become the reactors of choice. This change occurred owing to the excellent heat and mass transfer characteristics of slurry bubble column reactors and because this reactor type offers the possibility of greatly increased production capacities resulting from increased gas throughputs [2].

Conventional bubble column reactors have been in use for decades in many chemical processes, and consequently, a vast body of literature on bubble column reactors has grown since the 1950's [3-8]. Until the late 1980's only average hydrodynamic properties of these reactors, *viz.*, overall gas holdup, overall volumetric mass transfer coefficients, overall gas and liquid phase dispersion, were reported. However, with the advent of modern computing capabilities and advances in the sophisticated measurement techniques, characterization of the local hydrodynamics, both experimentally and numerically, has become possible during the last decade [9-18].

To predict reactor performance based on detailed hydrodynamic and mixing phenomena occurring in large-scale bubble column flows, mathematical modeling and numerical simulation using the two-fluid model has been frequently practiced. However, the choice of the correct closures and phase interaction terms needed to give accurate predictions of flow patterns from Computational Fluid Dynamic (CFD) simulations is still a matter of art. This arises because the phenomena governing these parameters occur on relatively small scales. However, measurement at these scales under actual operating conditions is still in its

infancy, with the common measurement techniques being limited to the characterization of the global and large scale properties only. Therefore, it is the modeling of the small scale phenomena and their coupled interactions with those at larger scales that limits the capability of Computational Fluid Dynamics (CFD) in serving as a stand-alone tool for prediction of bubble column reactor performance.

Given the state-of-the art, it is quite likely that reliable predicitions of reactor performance using multiphase CFD are a decade away. Therefore, for efficient design of slurry bubble column reactors, it is desirable to have models that are able to capture the majority of the physical phenomena and provide a reasonably reliable and fundamentally based method for design and scale-up. This goal is especially important for reactors involving complex chemistries in industrially relevant very large-scale systems such as Fischer-Tropsch. The most commonly used model of this type, the Axial Dispersion Model (ADM), has had only limited success in retrofitting experimental data. Mechanistic modeling offers the possibility of incorporating the relevant observable physics in describing liquid phase mixing [19-21] and offers a path to efficient design. We have used this approach to develop a mechanistic model that incorporates modeling the flow of not only the liquid, but also the gas phase.

Here, we present only a brief summary of the reactor model and focus on the development of a sub-model for predicting the long time-averaged gas and liquid recirculation velocities, which form the basis for the developed reactor model. Our approach is based on the Euler-Euler two-fluid representation of the momentum balance equations for the gas and liquid phases [11]. A number of investigators [22-26] have reported a similar model to describe liquid recirculation. However, we modify the model equations and closures used for the liquid phase turbulence. In particular, the momentum balance equations have been derived from the two-fluid equations, and the liquid recirculation model has been extended to calculate the radial profile of the axial gas phase velocity.

2. Phenomenological Reactor Model

The observed hydrodynamic phenomena in a typical bubble column operation are represented schematically in Figure 1 and form the basis of the mechanistic reactor model. In

the time average sense, the radial gas holdup distribution results in a single liquid recirculation loop with the liquid rising in the center and flowing downwards near the walls [21]. Most of the gas travels upwards through the column center and leaves the reactor; however, some small sized bubbles do not possess enough momentum to leave the reactor and recirculate along with the liquid. In addition to this convective recirculation, momentum transport is caused by the bubble wakes, bubble-bubble interactions and shear-induced turbulence – typically called 'eddy diffusion'. This physical picture is the result of numerous experimental studies on liquid recirculation reported in the literature [27-31], and of the extensive studies conducted by the non-invasive measurement techniques at the Chemical Reaction Engineering Laboratory (CREL) in Washington University-Saint Louis consisting of Computed Tomography-CT and Computer Automated Radioactive Particle Tracking-CARPT [21, 32-36]. CT provides non-invasive measurement of the long-time averaged, cross-sectional distribution of gas holdup in any reactor cross-section. The details of the γ-ray scanner and associated tomography reconstruction algorithms developed in CREL have been discussed elsewhere [34-35]. CARPT on the other hand provides information on the long-time averaged liquid velocity profile, turbulent stresses and eddy diffusivities. Details of the principles and methodology of the CARPT technique have also been discussed elsewhere [21, 32-33].

The compartmentalization of the mechanistic (phenomenological) model is shown in Figure 2, and is a modification and extension of the model proposed by Wang [37]. The net flow of liquid could be either zero (batch mode of operation) or a co-current upflow with the net flow of the gas. In either case, the liquid flow pattern inside the reactor consists of up-flow (L_1) in the core and down-flow (L_2) near the wall. The gas phase also has a similar recirculation pattern; with upflow in the center (G_1), and down flow by the wall (G_2) consisting of bubbles which do not possess sufficient momentum and get recirculated along with the liquid. The upward flowing gas usually consists of relatively small bubbles trapped in the wakes of the larger fast rising bubbles, and drags the liquid along with it. The top (disengagement) and the bottom (distributor) zones are modeled as being well mixed (Continuous Stirred Tanks - CSTs) and their height is taken to be the same as the column diameter, D_c. Changing the height of these zones between $0.5D_c$ and $2.0D_c$ does not have a

noticeable effect on the extent of liquid backmixing [20], provided the height of the gas-liquid mixture is much larger than the column diameter (L/D_c is at least 6). It has been found [38] that the effect of the height of these zones on the gas phase tracer responses is insignificant as well.

A differential element along the reactor length in the developed part of the flow, which occupies most of the column, consists of four zones into which the reactor cross-section is compartmentalized. By applying mass balances for a soluble species to each of these zones within the differential element, one obtains four transient convection-diffusion Partial Differential Equations (PDEs) with mass interphase transfer and radial exchange between the zones acting as source terms. Additional source terms appear in the form of reaction rates, if simulations are being carried out for a reactive species in a bubble column reactor operated under reaction conditions. On the other hand, the equations describing the dynamics of the perfectly mixed tanks representing the distributor and disengagement zones are only Ordinary Differential Equations (ODEs). Therefore, the reactor model results in an inter-coupled set of four PDEs and four ODEs as summarized below for a representative chemical species.

For the gas moving up-wards (G_1)

$$\frac{\partial C_{g1}}{\partial t}=\begin{Bmatrix}\overline{D}_{xx_1}\dfrac{\partial^2 C_{g1}}{\partial x^2}-\overline{u}_{g1}\dfrac{\partial C_{g1}}{\partial x}-\dfrac{4\left(\overline{D}_{rr}\varepsilon_g\right)_{r=r''}}{r''R\overline{\varepsilon}_{g1}}\left(C_{g1}-C_{g2}\right)+R_{x,g1}\\ -\dfrac{k_{gulu}a_{gulu}}{\overline{\varepsilon}_{g1}}\left(HC_{g1}-C_{l1}\right)-\dfrac{k_{guld}a_{guld}}{\overline{\varepsilon}_{g1}}\left(HC_{g1}-C_{l2}\right)\end{Bmatrix} \tag{1}$$

For the gas moving down-wards (G_2)

$$\frac{\partial C_{g2}}{\partial t}=\begin{Bmatrix}\overline{D}_{xx_2}\dfrac{\partial^2 C_{g2}}{\partial x^2}+\overline{u}_{g2}\dfrac{\partial C_{g2}}{\partial x}-\dfrac{k_{gdld}a_{gdld}}{\overline{\varepsilon}_{g2}}\left(HC_{g2}-C_{l2}\right)\\ +\dfrac{4r''/R}{R^2-r''^2}\dfrac{\left(\overline{D}_{rr}\varepsilon_g\right)_{r=r''}}{\overline{\varepsilon}_{g2}}\left(C_{g1}-C_{g2}\right)+R_{x,g2}\end{Bmatrix} \tag{2}$$

For the liquid moving up-wards (L_1)

$$\frac{\partial C_{l1}}{\partial t} = \left\{ \begin{array}{l} \overline{D}_{xx_1} \dfrac{\partial^2 C_{l1}}{\partial x^2} - \overline{u}_{l1} \dfrac{\partial C_{l1}}{\partial x} + \left(\dfrac{r''}{r'} \right)^2 \dfrac{k_{gulu} a_{gulu}}{\overline{\varepsilon}_{l1}} \left(HC_{g1} - C_{l1} \right) \\ - \dfrac{4 \left(\overline{D}_{rr} \varepsilon_l \right)_{r=r'}}{r' R \overline{\varepsilon}_{l1}} \left(C_{l1} - C_{l2} \right) + R_{x,l1} \end{array} \right\} \tag{3}$$

For the liquid moving down-wards (L_2)

$$\frac{\partial C_{l2}}{\partial t} = \left\{ \begin{array}{l} \overline{D}_{xx_2} \dfrac{\partial^2 C_{l2}}{\partial x^2} + \overline{u}_{l2} \dfrac{\partial C_{l2}}{\partial x} + \dfrac{4 r'/R}{R^2 - r'^2} \dfrac{\left(\overline{D}_{rr} \varepsilon_l \right)_{r=r'}}{\overline{\varepsilon}_{l2}} \left(C_{l1} - C_{l2} \right) + R_{x,l2} \\ + \left(\dfrac{r''^2}{R^2 - r'^2} \right) \dfrac{k_{guld} a_{guld}}{\overline{\varepsilon}_{l2}} \left(HC_{g1} - C_{l2} \right) + \left(\dfrac{R^2 - r''^2}{R^2 - r'^2} \right) \dfrac{k_{gdld} a_{gdld}}{\overline{\varepsilon}_{l2}} \left(HC_{g2} - C_{l2} \right) \end{array} \right\} \tag{4}$$

Gas in the distributor zone

$$\frac{dC_{ga}}{dt} = \left\{ \begin{array}{l} \dfrac{\overline{\varepsilon}_{g2} \overline{u}_{g2}}{\overline{\varepsilon}_g \phi_{in} D_C} \dfrac{\left(R^2 - r''^2 \right)}{R^2} C_{g2,0} - \dfrac{\overline{\varepsilon}_{g1} \overline{u}_{g1}}{\overline{\varepsilon}_g \phi_{in} D_C} \dfrac{r''^2}{R^2} C_{ga} \\ + \dfrac{U_{G,\sup}}{\overline{\varepsilon}_g \phi_{in} D_C} C_{g,in} - \dfrac{k_{CST} a_{CST}}{\overline{\varepsilon}_g} \left(HC_{ga} - C_{la} \right) + R_{x,ga} \end{array} \right\} \tag{5}$$

Liquid in the distributor zone

$$\frac{dC_{la}}{dt} = \left\{ \begin{array}{l} \dfrac{\overline{\varepsilon}_{l2} \overline{u}_{l2}}{\overline{\varepsilon}_l \phi_{in} D_C} \dfrac{\left(R^2 - r'^2 \right)}{R^2} C_{l2,0} - \dfrac{\overline{\varepsilon}_{l1} \overline{u}_{l1}}{\overline{\varepsilon}_l \phi_{in} D_C} \dfrac{r'^2}{R^2} C_{la} \\ + \dfrac{U_{L,\sup}}{\overline{\varepsilon}_l \phi_{in} D_C} C_{l,in} + \dfrac{k_{CST} a_{CST}}{\overline{\varepsilon}_l} \left(HC_{ga} - C_{la} \right) + R_{x,la} \end{array} \right\} \tag{6}$$

Gas in the disengagement zone

$$\frac{dC_{gb}}{dt} = \left[\begin{array}{l} \dfrac{\overline{\varepsilon}_{g1} \overline{u}_{g1}}{\overline{\varepsilon}_g \phi_{out} D_C} \dfrac{r''^2}{R^2} C_{g1,L} - \dfrac{\overline{\varepsilon}_{g2} \overline{u}_{g2}}{\overline{\varepsilon}_g \phi_{out} D_C} \dfrac{\left(R^2 - r''^2 \right)}{R^2} C_{gb} \\ - \dfrac{U_{G,\sup}}{\overline{\varepsilon}_g \phi_{out} D_C} C_{gb} - \dfrac{k_{CST} a_{CST}}{\overline{\varepsilon}_g} \left(HC_{gb} - C_{lb} \right) + R_{x,gb} \end{array} \right] \tag{7}$$

Liquid in the disengagement zone

$$\frac{dC_{lb}}{dt} = \left\{ \begin{array}{l} \dfrac{\bar{\varepsilon}_{l1}\,\bar{u}_{l1}}{\bar{\varepsilon}_l\,\phi_{out}\,D_C}\dfrac{r'^2}{R^2}C_{l1,L} - \dfrac{\bar{\varepsilon}_{l2}\,\bar{u}_{l2}}{\bar{\varepsilon}_l\,\phi_{out}\,D_C}\dfrac{\left(R^2 - r'^2\right)}{R^2}C_{lb} \\ -\dfrac{U_{L,\sup}}{\bar{\varepsilon}_l\phi_{out}\,D_C}C_{lb} + \dfrac{k_{CST}a_{CST}}{\bar{\varepsilon}_l}\left(HC_{gb} - C_{lb}\right) + R_{x,lb} \end{array} \right\} \tag{8}$$

Initial Conditions

The initial conditions in all zones of the reactor are those of zero initial concentration of the species to be introduced at time t = 0^+ at the reactor inlet.

$$t = 0; \quad C_{la} = C_{lb} = C_{ga} = C_{gb} = C_{l1} = C_{l2} = C_{g1} = C_{g2} = 0 \tag{9}$$

The inlet function for describing the introduction of a species at the reactor inlet depends on the simulation objectives. For simulating the distribution evolution of a reactant species under reaction conditions, one would typically have a step change in the concentration of the species at the reactor inlet. However, here we are interested in simulating the distribution of a non-reacting tracer. Additionally, this initial condition for the tracer at the inlet depends on the method of tracer injection, and whether it is an impulse tracer test, or a step-up/step-down tracer test. For the results presented in this study, the experimental impulse input for the tracer runs at AFDU, La Porte have been simulated using a Gaussian function with a tail [21].

$$t \rightarrow 0^+, t > 0; \quad C_{g,in} = \frac{\psi}{\sqrt{2\pi\kappa t}} exp\left\{-\frac{(\delta-\chi)^2}{2\kappa t}\right\} \qquad C_{l,in} = 0 \tag{10}$$

Boundary conditions for the fully developed region

Danckwerts boundary conditions are used at inlet and exit, guaranteeing preservation of mass for each phase. The bottom of the fully developed flow zone is the boundary with the CSTR representing the distributor zone, whereas the top of the fully developed flow zone is the boundary with the CSTR representing the disengagement zone. All the boundary conditions used are specified below.

Upflow section of the gas

$$x = 0; \qquad \overline{u}_{g1} C_{ga} = \overline{u}_{g1} C_{g1}\big|_{x=0} - \overline{D}_{xx_1} \left.\frac{\partial C_{g1}}{\partial x}\right|_{x=0} \tag{11}$$

$$x = L; \qquad \left.\frac{\partial C_{g1}}{\partial x}\right|_{x=L} = 0 \tag{12}$$

Downflow section of the gas

$$x = L; \qquad \overline{u}_{g2} C_{gb} = \overline{u}_{g2} C_{g2}\big|_{x=L} + \overline{D}_{xx_2} \left.\frac{\partial C_{g2}}{\partial x}\right|_{x=L} \tag{13}$$

$$x = 0; \qquad \left.\frac{\partial C_{g2}}{\partial x}\right|_{x=0} = 0 \tag{14}$$

Upflow section of the liquid

$$x = 0; \qquad \overline{u}_{l1} C_{la} = \overline{u}_{l1} C_{l1}\big|_{x=0} - \overline{D}_{xx_1} \left.\frac{\partial C_{l1}}{\partial x}\right|_{x=0} \tag{15}$$

$$x = L; \qquad \left.\frac{\partial C_{l1}}{\partial x}\right|_{x=L} = 0 \tag{16}$$

Downflow section of the liquid

$$x = L; \qquad \overline{u}_{l2} C_{lb} = \overline{u}_{l2} C_{l2}\big|_{x=L} + \overline{D}_{xx_2} \left.\frac{\partial C_{l2}}{\partial x}\right|_{x=L} \tag{17}$$

$$x = 0; \qquad \left.\frac{\partial C_{l2}}{\partial x}\right|_{x=0} = 0 \tag{18}$$

In the above set of equations, $\overline{D}_{xx}$ and $\overline{D}_{rr}$ are the average eddy diffusivities from CARPT, which are estimated from a scale-up methodology developed by Degaleesan [21]. For description of other symbols used in the equations above, the reader is referred to the nomenclature. For the simulation results presented in this study for a non-reactive soluble gas tracer, the above model equations have been solved by a completely implicit finite difference scheme (**FTCS** - first order **F**orward differences in **T**ime and second order **C**entral differences in **S**pace), which is robust and unconditionally stable. The treatment of the boundary conditions has been accomplished using ghost points. Since for simulation of tracer

responses, there are no non-linear terms in the equations, therefore, one needs to invert the matrix only once. This is accomplished by obtaining the LU decomposition of the matrix resulting from the application of the differencing scheme. The solution at successive times is simply obtained by matrix multiplication of the solution at previous time by repetitive LU back-substitution.

Before one can employ the numerical scheme discussed above for the solution of these reactor model equations, one needs as inputs the hydrodynamic model parameters. As mentioned before, a sub-model for gas and liquid recirculation is needed for this purpose and is being discussed below.

3. Two-Fluid Sub-Model for Gas and Liquid Phase Axial Momentum Exchange

The starting point in the derivation of the one-dimensional model for the radial liquid and gas-phase velocity profiles is the two-fluid model equations presented below. These equations are the result of the ensemble-averaged approach of Drew and Passman [11]. Here, the subscript '*l*' denotes the continuous liquid/slurry phase, whereas the subscript '*g*' denotes the dispersed gas phase, and both phases are considered incompressible.

Equations of Continuity

Liquid/Slurry
$$\frac{\partial \varepsilon_l}{\partial t} + \nabla.(\varepsilon_l \boldsymbol{u}_l) = 0 \tag{19}$$

Gas
$$\frac{\partial \varepsilon_g}{\partial t} + \nabla.(\varepsilon_g \boldsymbol{u}_g) = 0 \tag{20}$$

Momentum Equations

Liquid/Slurry
$$\rho_l \varepsilon_l \left(\frac{\partial \boldsymbol{u}_l}{\partial t} + \boldsymbol{u}_l.\nabla \boldsymbol{u}_l \right) = \rho_l \varepsilon_l \boldsymbol{g} - \varepsilon_l \nabla p - (\boldsymbol{M}_d + \boldsymbol{M}_{vm}) - \nabla.(\varepsilon_l \tau_l) \tag{21}$$

Gas
$$\rho_g \varepsilon_g \left(\frac{\partial \boldsymbol{u}_g}{\partial t} + \boldsymbol{u}_g.\nabla \boldsymbol{u}_g \right) = \rho_g \varepsilon_g \boldsymbol{g} - \varepsilon_g \nabla p + (\boldsymbol{M}_d + \boldsymbol{M}_{vm}) - \nabla.(\varepsilon_g \tau_g) \tag{22}$$

In the momentum balance equations, M_d is the drag force term, M_{vm} is the virtual mass term. The mathematical representation of these terms is shown in Equations 23 to 27.

$$\boldsymbol{M}_d = \frac{6\varepsilon_l \varepsilon_g}{\pi d_b^3} \boldsymbol{F}_d \tag{23}$$

$$\boldsymbol{F}_d = \frac{1}{8} \rho_l \pi d_b^2 C_D \left| \boldsymbol{u}_l - \boldsymbol{u}_g \right| \left(\boldsymbol{u}_l - \boldsymbol{u}_g \right) \tag{24}$$

$$C_D = max\left[\overbrace{\frac{24}{Re}\left(1 + 0.15\, Re^{0.687}\right)}^{C_{D,2}}, \overbrace{\frac{8}{3}\frac{Eo}{Eo+4}}^{C_{D,1}} \right] \tag{25}$$

$$\boldsymbol{M}_{vm} = \frac{1}{2} \varepsilon_l \varepsilon_g C_{vm} \left(\frac{D\boldsymbol{u}_l}{Dt} - \frac{D\boldsymbol{u}_g}{Dt} \right) \tag{26}$$

$$C_{vm} = 1 + 3.32\varepsilon_g + O(\varepsilon_g^2) \tag{27}$$

where C_D is the drag coefficient for sufficiently contaminated systems [39], $Eo = g\left(\rho_l - \rho_g\right) d_b^2 / \sigma$ is the Eotvos number based on the bubble diameter and the liquid surface tension, and $Re = d_b \left| \boldsymbol{u}_l - \boldsymbol{u}_g \right| / \nu_l^m$ is the bubble Reynolds number.

In the well-developed flow region of the column, the flow in the time-averaged sense is axisymmetric with only the axial velocities being non-zero. Hence, the time-averaged liquid flow pattern is represented by a single radial profile of the axial velocity. These assumptions are well justified in view of the holdup profile database available at CREL via CT; and the liquid velocity profile database via CARPT [21, 32-36].

Under these assumptions, the equations of continuity for both the phases (Equations 19 and 20) are identically satisfied and one cannot use the traditional approach of solving the Poisson equation for the pressure correction through the use of these continuity equations (as is done in 2-D and 3-D CFD codes). In addition, the left hand side of the momentum equations for both the gas and liquid phase becomes zero, and so does the virtual mass term. Finally, due to no flow in the radial and azimuthal directions, the pressure is assumed to be independent of the radial and azimuthal coordinates, and the pressure gradient term in the momentum equations reduces to *dp/dz*.

After retaining the non-zero gradients and velocity components in the momentum equations for the two phases, one gets the following simplified equations.

$$\textit{Liquid/Slurry}\quad 0=-\rho_l\varepsilon_l g-\varepsilon_l\frac{dp}{dz}-M_d-\frac{1}{r}\frac{d}{dr}\left(r\varepsilon_l\left\{\tau^m_{l,rz}+\tau^t_{l,rz}\right\}\right) \tag{28}$$

$$\textit{Gas}\quad 0=-\rho_g\varepsilon_g g-\varepsilon_g\frac{dp}{dz}+M_d-\frac{1}{r}\frac{d}{dr}\left(r\varepsilon_g\left\{\tau^m_{g,rz}+\tau^t_{g,rz}\right\}\right) \tag{29}$$

where

$$\tau^m_{l,rz}=-\mu^m_l\frac{du_l}{dr} \tag{30}$$

$$\tau^m_{g,rz}=-\mu^m_g\frac{du_g}{dr} \tag{31}$$

$$\tau^t_{l,rz}=\rho_l\overline{u'_{l,r}u'_{l,z}} \tag{32}$$

$$\tau^t_{g,rz}=\rho_g\overline{u'_{g,r}u'_{g,z}} \tag{33}$$

Since $\mu^m_g\approx O\left(10^{-1}\right)\mu^m_l$ and $\rho_g\approx O\left(10^{-1}-10^{-2}\right)\rho_l$, one can neglect both the molecular as well as the turbulent shear stresses in the gas phase as compared to those in the liquid/slurry phase. Therefore, upon addition of Equations 28 and 29 one obtains

$$0=-\left(\rho_g\varepsilon_g+\rho_l\varepsilon_l\right)g-\frac{dp}{dz}-\frac{1}{r}\frac{d}{dr}\left(r\varepsilon_l\left\{\overbrace{\tau^m_{l,rz}+\tau^t_{l,rz}}^{\tau_{l,rz}}\right\}\right) \tag{34}$$

In the above equation, the superscripts "*m*" and "*t*" refer to molecular (viscous) and turbulent contributions, and ε_g is the radial gas holdup profile, which is represented in terms of the following power law function which fits well the available experimental data.

$$\varepsilon_g(\xi)=\bar{\varepsilon}_g\left(\frac{m+2}{m+2-2c}\right)\left(1-c\xi^m\right) \tag{35}$$

where, $\xi = r/R$ is the non-dimensional radius. Substituting for the radial gas holdup (Equation 35) in Equation 34 and using $p' = -dp/dz/\rho_l g$, one gets, on integrating Equation 34 with boundary condition $\tau_{l,rz}=0$ at $\xi=0$,

$$(1-\varepsilon_g)\tau_{l,rz} = \frac{\rho_l g R \xi}{2}(p'-1) + \frac{(\rho_l - \rho_g) g R \bar{\varepsilon}_g \xi}{2} \frac{(m+2-2c\xi^m)}{(m+2-2c)} \tag{36}$$

After anticipating a downward maximum liquid velocity at dimensionless radius $\xi = \lambda$, one assigns $\tau_{l,rz}\big|_{\xi=\lambda} = 0$. Applying this condition to Equation 36 eliminates p' and yields Equation 37.

$$\tau_{l,rz}(\xi) = \frac{\rho_l (1-\gamma) g R c \bar{\varepsilon}_g \xi \lambda^m}{(m+2-2c)(1-\varepsilon_g(\xi))}\left(1-\left(\frac{\xi}{\lambda}\right)^m\right) = \rho_l g R \beta(\xi) \tag{37}$$

where $$\beta(\xi) = \frac{(1-\gamma) c \bar{\varepsilon}_g \xi \lambda^m}{(m+2-2c)(1-\varepsilon_g(\xi))}\left(1-\left(\frac{\xi}{\lambda}\right)^m\right) \tag{38}$$

and $\gamma = \rho_g / \rho_l$. To obtain the liquid velocity profile from the above shear stress profile, a constitutive relationship (closure) is needed relating the turbulent shear stresses to the mean liquid velocity profile. The simplest closure in terms of turbulent kinematic viscosity is employed in Equation 39.

$$\tau_{l,rz}(r) = -\rho_l (\nu_l^m + \nu_l^t)\frac{du_l}{dr} = -\rho_l \nu_l^m \frac{du_l}{dr} - \rho_l l^2 \left|\frac{du_l}{dr}\right| \frac{du_l}{dr} \tag{39}$$

The turbulent eddy viscosity, ν_l^t can be closed by a modified mixing length, $l(\xi)$, as given by Kumar *et al.* [22].

$$\nu_l^t = l^2 \left|\frac{du_l}{dr}\right| \tag{40}$$

$$l(\xi) = \left\{\frac{a(1-\xi)}{(\xi+b)^c} + d(1-\xi)^e\right\} R \tag{41}$$

The parameters *a*, *b*, *c*, *d* and *e* have been obtained by Kumar *et al.* [22] after considering extensive data on liquid recirculation velocities from CARPT, and results from experiments of other researchers who have made measurements of the liquid recirculation velocity by other experimental means. In this work, two other mixing length models are going to be used

to assess the effect of this parameter on the simulation results. These are the mixing length profile of Nikuradse [40] and that of Joshi [41].

Nikuradse $$l(\xi) = \{0.14 - 0.08\xi^2 - 0.06\xi^4\}R \tag{42}$$

Joshi $$l(\xi) = 0.16R \tag{43}$$

Therefore, Equation 39 becomes

$$\frac{du_l}{d\xi} = \begin{cases} \dfrac{\nu_l^m R}{2l^2}\left(1 - \sqrt{1 + \dfrac{4l^2 gR}{\nu_l^{m^2}}\beta(\xi)}\right) & for\ 0 \le \xi \le \lambda \\ -\dfrac{gR^2}{\nu_l^m}\beta(\xi) & for\ \lambda \le \xi \le 1 \end{cases} \tag{44}$$

Solution Procedure

The boundary conditions to be used for the solution of the above equations are $u_l = 0$ at $\xi = 1$, and $du_l/d\xi = 0$ at $\xi = 0$. Superimposed on this is the constraint that overall continuity for the liquid phase must be satisfied (Note that the integral is split at $\xi = \lambda$ which is not the point of inversion of the liquid velocity profile, rather the point of maximum downward liquid velocity).

$$U_{L,sup} = 2\int_{\xi=0}^{\xi=1}\{1-\varepsilon_g(\xi)\}u_l(\xi)\xi\,d\xi = 2\int_{\xi=0}^{\xi=\lambda}\{1-\varepsilon_g(\xi)\}u_l(\xi)\xi\,d\xi + 2\int_{\xi=\lambda}^{\xi=1}\{1-\varepsilon_g(\xi)\}u_l(\xi)\xi\,d\xi \tag{45}$$

It is this constraint that allows one to iterate on dp/dz and obtain a converged solution. The numerical scheme for the solution is as follows.

- Guess a value for λ (generally 0.9 is a good starting point)
- Calculate $u_{l,\lambda}$ by integrating Equation 43 from the boundary at $\xi = 1$ to $\xi = \lambda$

$$u_{l,\lambda} = -\frac{gR^2}{\nu_l^m}\int_{\xi=1}^{\xi=\lambda}\beta(\xi)d\xi \tag{46}$$

- To obtain the velocity of the liquid phase in the rest of the domain, integrate Equation 43 from $\xi = \lambda$ towards the column center using $u_{l,\lambda}$.

$$u_l = u_{l,\lambda} - \frac{\nu_l^m R}{2l^2} \int_{\xi=\xi}^{\xi=\lambda} \left(1 - \sqrt{1 + \frac{4l^2 gR}{\nu_l^{m^2}} \beta(\xi)} \right) d\xi \tag{47}$$

- Substitute the radial profile of the axial liquid velocity into Equation 45. If Equation 45 is satisfied within the tolerance criterion, then the converged solution has been obtained. If the tolerance criterion is not met then λ is incremented sequentially until convergence is achieved. A word of caution is in order at this point. The function defined by Equation 43 could have steep gradients and proper care must be taken while integrating to obtain an accurate solution.

Once the liquid velocity profile and *dp/dz* are determined as the converged solution to the one-dimensional liquid circulation model equations, we turn our attention back to the gas phase momentum equation. Combining Equations 23, 24 and 29, the expression for the slip velocity, u_s is obtained.

$$u_s = u_g - u_l = \sqrt{\frac{4d_b\left(-\frac{dp}{dz} - \rho_g g\right)}{3C_D \rho_l (1-\varepsilon_g)}} \tag{48}$$

Here, C_D is the drag coefficient and is a function of the slip velocity as well as the bubble diameter and has to be obtained through an iterative scheme for a prescribed bubble diameter. The effective bubble diameter for the entire domain is obtained by iteratively searching for that bubble diameter which satisfies the overall gas phase continuity

$$2\int_{\xi=0}^{\xi=1} \varepsilon_g(\xi)\, u_g(\xi)\xi\, d\xi = \overbrace{2\int_{\xi=0}^{\xi=1} \varepsilon_g(\xi)\, u_l(\xi)\xi\, d\xi}^{I_1} + \overbrace{2\int_{\xi=0}^{\xi=1} \varepsilon_g(\xi)\, u_s(\xi)\xi\, d\xi}^{I_2} = U_{G,sup} \tag{49}$$

The solution procedure for the gas phase velocity profile is based on adjusting the bubble diameter in the drag formulation via an iterative scheme to obtain a solution that satisfies gas phase continuity. The following steps are involved in this procedure.

- Guess a value for d_B (typically start with a very small value)
- Calculate $C_{D,1}$ as defined in Equation 25. Since $C_{D,1}$ is independent of the radial coordinate, ξ, as well as of the slip velocity, u_s, once d_B is known $C_{D,1}$ is simply evaluated based on the Eotvos number.
- Calculate $C_{D,2}$ as defined in Equation 25. Since $C_{D,2}$ is a function both of ξ and u_s, it has to be evaluated at each ξ by the following Newton-Raphson procedure

$$u_s^{k+1} = u_s^k - \frac{f\left(u_s^k\right)}{f'\left(u_s^k\right)} \tag{50}$$

$$f(u_s) = u_s - \sqrt{\frac{4d_b\left(-\frac{dp}{dz} - \rho_g g\right)}{3C_{D,2}\,\rho_l\left(1-\varepsilon_g\right)}} \tag{51}$$

$$f'(u_s) = \frac{df(u_s)}{du_s} = 1 - \frac{24}{u_s^2}\sqrt{\frac{\mu_l^{m^2}\left(-\frac{dp}{dz} - \rho_g g\right)}{3\rho_l^3 C_{D,2}^3\, d_b\left(1-\varepsilon_g\right)}} \tag{52}$$

- Calculate C_D as the maximum of $C_{D,1}$ and $C_{D,2}$ for each ξ, and subsequently calculate the radial profile of u_s from Equation 48.
- Evaluate the gas phase continuity using Equation 49. If the gas continuity is satisfied within the tolerance criterion, then the guessed bubble diameter is the correct one, otherwise d_b is incremented and the procedure is repeated until the tolerance criterion is met.

This solution procedure ensures that the gas phase continuity is satisfied as part of the solution. Additionally, it provides an estimation of the bubble diameter, which is subsequently useful for calculating mass transfer coefficients. It should, however, be noticed that the estimated bubble diameter depends on the drag formulation used, and therefore, it is

important to use a suitable drag correlation. In principle, any of the available drag forms could be used. This is an issue related to the sub-grid modeling of the phase interaction between the gas and liquid phases and beyond the scope of this work. However, this is important issue, as it is also relevant to the CFD simulations of flows in practical multi-phase systems. For the purposes of this study, we have adopted the formulation of Tomiyama *et al.* [39], as it is known to give reasonably good predictions over a wide range of bubble Reynolds numbers. It should also be mentioned that in its current form the solution of the equations from the sub-model requires the knowledge of the radial gas holdup profile; and, therefore, the model is not fully predictive.

Before proceeding further, a precautionary note has also to be made about the converged liquid velocity profile. From Equation 49, it can be seen that if the converged liquid velocity profile is such that the integral, I_1 is greater than $U_{G,sup}$, it implies that an unphysical result has been obtained, since it would mean that in the long-time average sense, the gas phase is moving slower than the liquid, which obviously cannot be the case. The converged liquid velocity profile should therefore be checked for consistency after a converged solution satisfying liquid phase continuity has been achieved. If I_1 greater than $U_{G,sup}$ does indeed occur, it is indicative of gross inaccuracies in the gas holdup profile being used for solution of the model equations for liquid recirculation.

Parameter Estimation

Once the radial profiles of the liquid/slurry and gas phase velocities are known, the various hydrodynamic input parameters for the mechanistic reactor model can be readily estimated. The liquid and gas velocity profiles obtained from the solution of the two-fluid recirculation model become zero at some radial locations. These are referred to as the inversion points with r' representing the inversion point for liquid velocity, and r'' that for the gas. The inversion points are important in parameter estimation, as they define the boundaries of the four zones in the reactor model, *viz.*, core and annulus flow regions for the gas and the liquid. The holdups of the gas and liquid/slurry in the various zones of the reactor are obtained from Equations 53 to 57 using the measured or estimated gas holdup profile.

Average liquid hold-up in the up-flowing liquid region

$$\bar{\varepsilon}_{l1} = \frac{2}{r'^2}\int_0^{r'}(1-\varepsilon_g)\,r\,dr \tag{53}$$

Average liquid hold-up in the down-flowing liquid region

$$\bar{\varepsilon}_{l2} = \frac{2}{R^2 - r'^2}\int_{r'}^{R}(1-\varepsilon_g)\,r\,dr \tag{54}$$

Average gas hold-up in the up-flowing gas region

$$\bar{\varepsilon}_{g1} = \frac{2}{r''^2}\int_0^{r''}\varepsilon_g\,r\,dr \tag{55}$$

Average gas hold-up in the down-flowing gas region

$$\bar{\varepsilon}_{g2} = \frac{2}{R^2 - r''^2}\int_{r''}^{R}\varepsilon_g\,r\,dr \tag{56}$$

Average gas hold-up in the up-flowing gas and down-flowing liquid region

$$\bar{\varepsilon}'_{g1} = \frac{2}{r''^2}\int_{r'}^{r''}\varepsilon_g\,r\,dr \tag{57}$$

From the converged solutions for the liquid and gas velocity profiles, the average velocities of the gas and liquid in the various zones are evaluated using Equations 58 to 61, and the mean slip velocity using Equation 62. From Equations 49 and 62, an important observation to be made is that the actual mean slip velocity is always less than the apparent slip velocity, which is usually defined as $U_{G,sup}/\bar{\varepsilon}_g - U_{L,sup}/\bar{\varepsilon}_L$.

Average liquid velocity in the up-flowing liquid region

$$\bar{u}_{l1} = \frac{2\int_0^{r'}(1-\varepsilon_g)\,|u_l|\,r\,dr}{r'^2\,\bar{\varepsilon}_{l1}} \tag{58}$$

Average liquid velocity in the down-flowing liquid region

$$\overline{u}_{l2} = \frac{\frac{2}{\overline{\varepsilon}_{l2}} \int_{r''}^{R} (1-\varepsilon_g)\, u_l\, r\, dr}{R^2 - r''^2} \tag{59}$$

Average gas velocity in the up-flowing gas region

$$\overline{u}_{g1} = \frac{R^2 U_{G,sup} + 2\int_{r''}^{R} |u_g|\, \varepsilon_g\, r\, dr}{r''^2\, \overline{\varepsilon}_{g1}} \tag{60}$$

Average gas velocity in the down-flowing gas region

$$\overline{u}_{g2} = \frac{\frac{2}{\overline{\varepsilon}_{g2}} \int_{r''}^{R} |u_g|\, \varepsilon_g\, r\, dr}{R^2 - r''^2} \tag{61}$$

Average actual slip velocity

$$U_{slip} = \frac{2\int_{\xi=0}^{\xi=1} \varepsilon_g(\xi)\, u_s(\xi)\, \xi\, d\xi}{\overline{\varepsilon}_g} \neq \frac{U_{G,sup}}{\overline{\varepsilon}_g} - \frac{U_{L,sup}}{\overline{\varepsilon}_l} \tag{62}$$

With the volumes and velocities associated with the various compartments of the reactor model having been estimated, the last set of parameters that need to be evaluated are the mass transfer coefficients and the interfacial areas for mass transfer. The volumetric mass transfer coefficient is widely studied and reported in the literature and numerous correlations are available for its estimation [7, 42]. However, most of these correlations are empirical in nature with little fundamental basis and therefore, usually work well only for systems similar to the ones from which data was obtained for their development. To incorporate some level of physics, in this study we have chosen to estimate the mass transfer coefficients based on the penetration theory by Higbie [43] and the interfacial areas have been evaluated using the bubble diameter that satisfies gas phase continuity. Following this methodology, one does not have to depend on empirical correlations for evaluating the mass transfer coefficients and

interfacial areas as they can be readily calculated using Equations 63 to 70. These expressions assume the bubbles to be spherical, but one can apply suitable shape factor corrections if needed [44].

Interfacial area for mass transfer from up-flowing gas to up-flowing liquid

$$a_{gulu} = \frac{6\left(\bar{\varepsilon}_{g1} - \bar{\varepsilon}_{g1}^{'}\right)}{d_b} \tag{63}$$

Interfacial area for mass transfer from up-flowing gas to down-flowing liquid

$$a_{guld} = \frac{6\bar{\varepsilon}_{g1}^{'}}{d_b} \tag{64}$$

Interfacial area for mass transfer from down-flowing gas to down-flowing liquid

$$a_{gdld} = \frac{6\bar{\varepsilon}_{g2}}{d_b} \tag{65}$$

Interfacial area for mass transfer in distributor and disengagement CSTRs

$$a_{CST} = \frac{6\bar{\varepsilon}_{g}}{d_b} \tag{66}$$

Mass transfer coefficient from up-flowing gas to up-flowing liquid

$$k_{gulu} = \frac{2}{\sqrt{\pi}}\sqrt{\frac{D_{L,m}(\bar{u}_{g1} - \bar{u}_{l1})}{d_b}} \tag{67}$$

Mass transfer coefficient from up-flowing gas to down-flowing liquid

$$k_{guld} = \frac{2}{\sqrt{\pi}}\sqrt{\frac{D_{L,m}(\bar{u}_{g1} + \bar{u}_{l2})}{d_b}} \tag{68}$$

Mass transfer coefficient from down-flowing gas to down-flowing liquid

$$k_{gdld} = \frac{2}{\sqrt{\pi}} \sqrt{\frac{D_{L,m}(-\bar{u}_{g2} + \bar{u}_{l2})}{d_b}} \tag{69}$$

Mass transfer coefficient in distributor and disengagement CSTRs

$$k_{CST} = \frac{2}{\sqrt{\pi}} \sqrt{\frac{D_{L,m} U_{slip}}{d_b}} \tag{70}$$

It should be noted that a constant bubble size has been used for estimating the "k_L" and "a" in the above equations, which is rarely the case in a real system. We therefore investigated the effect of a bubble-size distribution on these parameters using a log-normal distribution. It was found that the volumetric mass transfer coefficient calculated based on average bubble-size and an average slip-velocity, estimated using this average bubble-diameter, provided the upper bound for k_La as compared to k_La computed from the bubble-size and slip-velocity distributions. Moreover, as long as the normalized standard deviation for the chosen bubble size distribution remained within 0.25 (for the two mean bubble sizes investigated *viz.* 0.2 cm and 0.5 cm), this difference was within 10-15%. Therefore, for the high pressure conditions encountered in industrial applications where the bubble sizes are generally in the range from 1-5 mm, the assumption of a constant bubble size for calculation of mass transfer effects is reasonable.

The above estimation procedure provides all the hydrodynamic model parameters needed to solve the reactor model equations. In the next section, some results are presented both from simulation of the recirculation sub-model equations as well as from the reactor model mimicking gas tracer experiments in a pilot scale slurry bubble column under conditions of methanol synthesis.

4. Results and Discussion

For solution of the model equations for gas and liquid recirculation, one needs to know two important inputs - the radial gas holdup profile and the closure for liquid/slurry

phase turbulence. For the purposes of this study, the gas holdup profile is assumed known from experimental data, though some estimates for the average gas holdup could be obtained from correlations for systems where no experimental data exists [7, 45-46]. In such cases, the value of the exponent m in Equation 35 is usually assumed in the range of 2-5 [47] and c is assumed to be 1. On the other hand, the liquid phase turbulence in bubble column flows is usually assumed to be a superposition of the turbulence due to *shear* and that resulting from the highly oscillatory and dynamic bubble motion. The latter contributes to what is frequently referred to as the "bubble-induced" turbulence. Kumar *et al.* [22] investigated the existing literature on mixing length correlations relevant to bubble-column flows and found that none of the existing forms matched all the data well. Therefore, based on their own experimental database as well as other data from the literature, they developed a mixing length form as represented by Equation 40. This is a completely empirical form but is known to provide reasonable estimates of the level of liquid circulation in the column. Another very simple form for mixing length (Equation 42) has been proposed by Joshi [41], which also performs reasonably well in predicting the levels of liquid recirculation. Additionally, there is the mixing length correlation of Nikuradse [40] developed for describing turbulent single-phase pipe flows. We first compare the performance of these three mixing length forms against two data sets for which measured liquid recirculation profiles are available from CARPT experiments.

Figures 3 and 4 show the relative performance of the three mixing length forms in predicting experimental data for the liquid phase recirculation. The experimental data is from two different columns, one of diameter 10 cm and the other one of diameter 44 cm. The superficial gas velocity for the former was maintained at $U_{G,sup}$ = 12 cm/s while for the latter it was 10 cm/s. Nikuradse's mixing length always over-predicts the level of liquid since the effective turbulent viscosity from this formulation is only representative of the shear contribution to the total turbulence as in single-phase flows, and does not account for the increased turbulence generation and dissipation due to the presence of the bubbles. Therefore, for bubble column flows, use of Nikuradse's mixing length in solving for the liquid recirculation velocity profile is not recommended. Modifications to Nikuradse's mixing length could be sought to account for the bubble-induced turbulence, however, the

dependence of mixing length on bubble diameter and its velocity fluctuation is not well-established [23]. The correlations of Joshi [41] and Kumar *et al.* [22] give reasonable predictions for both the cases studied, though the correlation of Kumar *et al.* [22] seems to do somewhat better.

Next we demonstrate the use of the gas-liquid recirculation sub-model to obtain the hydrodynamic input parameters to the mechanistic reactor model; and subsequently, solve the bubble column model equations to predict radioactive gas tracer responses obtained in a 46-cm diameter pilot scale reactor undergoing liquid phase methanol synthesis. These experiments were conducted as part of the Department of Energy endeavor in developing slurry bubble column reactor technology for efficient conversion of synthesis gas (both from coal as well as natural gas) to alternate fuels and chemicals in the AFDU at La Porte, TX. The total dispersed phase height in the reactor was maintained at about 13.25 meters from the distributor, and the reactor was operated at a pressure of 50 atm and a temperature of 250 °C. The inlet superficial gas velocity was 25 cm/s. It decreased at the reactor exit due to a reduction in the total moles resulting from a consumption of the synthesis gas and production of methanol. The average superficial gas velocity in the reactor was calculated as 22.86 cm/s.

Radioactive Ar^{41} was injected at the bottom of the reactor into the gas inlet stream as the gas phase tracer. The evolution of its concentration inside the reactor was monitored at seven axial levels with the aid of scintillation counters. A sketch of the experimental setup for the tracer tests is shown in Figure 5 with details presented elsewhere [21]. For comparison of the simulation results with experimental tracer responses, detector level 7 has been chosen in this study. Since the intensity counts measured by a scintillation counter is a complex function of the photon interaction with matter and the detector solid angle, it is not straight-forward to relate the intensity counts to tracer concentration. Moreover, Ar^{41} has a finite solubility in the slurry mixture and has its residence time prolonged by dissolving in the liquid. As a result, when comparing simulated results with experimental data, one has to include the contribution of the dissolved tracer in the slurry phase towards total scintillation counts registered by the counters. Therefore, the total tracer concentration at a given axial location needs to be calculated by summing the tracer concentrations in the gas and the liquid after appropriately weighting them by their respective holdups. Since the detectors are

assumed to be reasonably shielded, it is justifiable to assume that at each detector level, the transient intensity counts when normalized by the maximum count, would provide the correct basis for comparing experimental data against normalized ***total*** concentration at that axial plane. Figure 6 shows the relative placement of the scintillation detectors with respect to the reactor insulation in one axial plane, as well as the various zones into which the reactor cross-section is compartmentalized. The normalized experimental tracer response curves shown in Figures 7 and 8 are obtained by averaging the intensity counts registered by the four detectors at the axial plane corresponding to detector-level 7. Since the gas as well as the entrained liquid move in a spiraling motion as the gas rises up the column after its introduction at the sparger, radial mixing of the tracer is rapid. This mixing is reflected in the responses observed by the four individual detectors at a given location. Moreover, since the reactor model is not a three-dimensional representation of the transient distribution of any chemical species inside the reactor, modeling the process of detector-scintillation due to the tracer, by employing sophisticated and computationally involved Monte Carlo techniques [48], is not sought in the present study. In view of this, the best strategy is to compare the normalized total tracer response with the normalized average intensity counts registered at a given detector level. The total tracer concentration, which is subsequently normalized by its maximum for comparison with experimental data, is given as:

$$C_{Total} = C_{g1}\left(r''^{2}\right) + C_{g2}\left(1 - r''^{2}\right) + C_{l1}\left(r'^{2}\right) + C_{l2}\left(1 - r'^{2}\right) \qquad (71)$$

Figures 7 and 8 exhibit the comparison of the normalized experimental and simulation data, obtained from the mixing lengths of Joshi [41] and Kumar *et al.* [22], respectively, for several values of the Henry's constant (representing the solubility of Argon[41] in the reactor slurry). The Henry's constant in this study is ***dimensionless*** and is defined as the ratio of the molar concentrations in the liquid and gas phases when the two phases are in equilibrium. The thermodynamically estimated value of the Henry's constant under the given operating conditions is about 0.17. This estimation procedure involves the assumption about the structure and mean molecular weight of the slurry mixture, and could deviate from the true value by ±25%-±50%. Therefore, one needs to examine the effect of this parameter on

the simulation results, which show high sensitivity to this parameter. The sensitivity to other parameters like the turbulent eddy diffusivities and volumes of the inlet and exit CSTRs is relatively insignificant as compared to the sensitivity with respect to the Henry's constant.

From the Figures 7 and 8, one can see that parameters estimated using the mixing length profile of Kumar *et al.* [22] in general provide better agreement with the measured tracer response, than those from the mixing length of Joshi [41]. Moreover, for a value of H = 0.3, and using the mixing length of Kumar *et al.* [22], one gets an excellent match of the simulated data with the experimental tracer response curve. Such is not the case when using the mixing length of Joshi [41]. This is to be expected since the mixing length formulation of Kumar *et al.* [22], as mentioned earlier, provides better predictions of the liquid recirculation profiles; which subsequently gets reflected in the predictions obtained from the overall model equations. Altogether, this implies that a consistent prescription of the hydrodynamic inputs to the reactor model should result in reliable predictions, and provides fundamentally based criteria for design and scale-up. It is also clear that mass transfer plays a significant role in governing the gas tracer distribution when one compares the simulation results for H = 0, and non-zero H with the experimental response.

5. Final Remarks

In this study, a self-consistent hydrodynamic sub-model has been developed from the two-fluid equations describing two-phase flow in the Euler-Euler framework. The results from the solution of the model equations provide accurate predictions of the levels of liquid and gas recirculation when a proper closure for turbulence is used in the model equations. The hydrodynamic sub-model has been integrated into the four-zone mechanistic reactor model describing the distribution, generation and consumption of the reactant species. Comparison of the results from the mechanistic model with experimental gas tracer data indicates a good agreement between the two, provided a correct estimate for the solubility of the gaseous component in the liquid/slurry is available. The integrated predictive capabilities of the gas-liquid recirculation sub-model and the mechanistic reactor model do not suffer from the empiricism of the Axial Dispersion Model, and therefore, provide a more reliable

and fundamentally based methodology for design, synthesis, analysis and scale-up of bubble column reactors.

6. Acknowledgements

The authors gratefully acknowledge the continued support of this research from the *Department of Energy* grant (DE-FC-22-95 PC 95051) through *Air Products and Chemicals, Inc.* and industrial sponsors of the *Chemical Reaction Engineering Laboratory, Washington University.*

Nomenclature

a	interfacial area, cm^{-1}
B	number of bubbles formed per unit volume per unit time, # cm^{-3} s^{-1}
C	concentration, moles/cm^3
C_D	drag coefficient
C_{vm}	virtual mass coefficient
c	parameter in the hold-up profile to allow non-zero hold-up at the wall
Eo	Eotvos number
D_C	column diameter, cm
$D_{L,m}$	molecular diffusivity, cm^2/s
$\overline{D}_{rr}$	radial turbulent diffusivity, cm^2/s
$\overline{D}_{xx_1}$	axial turbulent diffusivity of small bubbles and liquid going up, cm^2/s
$\overline{D}_{xx_2}$	axial turbulent diffusivity of small bubbles and liquid going down, cm^2/s
d_b	mean bubble diameter, cm
g	acceleration due to gravity, cm^2/s
H	Henry's constant
k	mass transfer coefficient, cm/s
L	dispersion height between the two CSTRs, cm
l	mixing length, cm
m	power law exponent in the radial gas hold-up profile
P	operating pressure, dyne/cm^2
Q	flow rate, cm^3/s
R	column radius, cm
R_x	reaction rate, moles cm^{-3} s^{-1}
r	radial position in the column, cm
r'	radius where the liquid velocity profile inverts
r"	radius where the gas velocity profile inverts
t	time, s
$U_{G,sup}$	gas superficial velocity, cm/s

$U_{L.sup}$	liquid superficial velocity, cm/s
u	velocity, cm/s
$\bar{u}$	radially averaged mean velocity, cm/s
V_a	volume of the CSTR representing the distributor zone, cm^3
V_b	volume of the CSTR representing the disengagement zone, cm^3
x	axial position in the column, cm

Greek Symbols

ε	local phase hold-up
$\bar{\varepsilon}$	radially averaged phase hold-up
$\tilde{\varepsilon}_g$	parameter in the gas holdup profile related to $\bar{\varepsilon}_g$
$\bar{\varepsilon}'_{g1}$	mean hold-up of up-flowing gas with down-flowing liquid
ϕ	fraction of the column diameter
μ_l^m	liquid/slurry viscosity, cP
ρ	density, g/cm^3
σ	surface tension of the liquid, dyne/cm
τ^m	viscous shear stress, $dyne/cm^2$
τ^t	turbulent shear stress, $dyne/cm^2$
ν^m	kinematic viscosity, cm^2/s
ν^t	turbulent viscosity, cm^2/s
ξ	dimensionless radius
ξ'	dimensionless radius where the liquid velocity profile inverts
ξ''	dimensionless radius where the gas velocity profile inverts

Subscripts

CST	well mixed distributor and disengagement zones, a and b
g	gas
ga	gas phase in the distributor zone, CST a

gb	gas phase in the disengagement zone, CST b
g1	up-flowing gas
g2	down-flowing gas
in	reactor inlet
l	liquid
la	liquid phase in the distributor zone, CST a
lb	liquid phase in the disengagement zone, CST b
l1	up-flowing liquid
l2	down-flowing liquid
gulu	gas flowing upwards with liquid going up as well
guld	gas flowing upwards with liquid going down
gdld	gas going down with liquid down as well
out	reactor outlet

References

[1] I. Wender, Fuel Processing Technology, 48 (1996) 189.

[2] S. T. Sie and R. Krishna, Applied Catalysis A, 186 (1999) 55.

[3] R. A. Mashelkar, Brit. Chem. Eng., 15 (1970) 1297.

[4] Y. T. Shah, ACS Symp. Ser. In Chem. React., 168 (1981) 203.

[5] W. -D. Deckwer, ACS Symp. Ser. (Chem. React.), 168 (1981) 213.

[6] M. A. Kohler, Appl. Catal., 22 (1986) 21.

[7] F. Kastanek, J. Zahradnik, J. Kratochvil and J. Cermak, Chemical Reactions for Gas-Liquid Systems, Ellis Horwood, New York, 1993, Chap. 4, p. 244.

[8] J. B. Joshi, U. Parasu Veera, Ch. V. Prasad, D. V. Phanikumar, N. S. Deshphande, S. S. Thakre and B. N. Thorat, PINSA-A, Proc. Indian Natl. Sci. Acad., Part A, 64 (1998) 441.

[9] M. Lopez de Bertodano, R. T., Jr. Lahey and O. C. Jones, Int. J. Multiphase Flow, 20 (1994) 805.

[10] F. Larachi, J. Chaouki, G. Kennedy and M. P. Dudukovic', in J. Chaouki, F. Larachi and M. P. Dudukovic' (Editors), Non-Invasive Monitoring of Multiphase Flows, Elsevier, New York, 1997, Chap. 11, p. 335.

[11] D. A. Drew and S. L. Passman, Theory of Multicomponent Fluids, Springer, New York, 1998, Chap. 11, p. 121.

[12] J. A. M. Kuipers and W. P. M. Van Swaaij, Adv. Chem. Eng., 24 (1998) 227.

[13] R. Krishna, M. I. Urseanu, J. M. van Baten and J. Ellenberger, Chem. Eng. Sci., 54 (1999) 4903.

[14] M. P. Dudukovic, Catal. Today, 48 (1999[a]) 5.

[15] M. P. Dudukovic, AIChE Symp. Ser. (Advanced Technologies for Fluid-Particle Systems), 321(1999[b]) 30.

[16] Y. Pan, M. P. Dudukovic' and M. Chang, Chem. Eng. Sci., 54 (1999) 2481.

[17] A. Sokolichin and G. Eigenberger, Chem. Eng. Sci., 54 (1999) 2273.

[18] S. S. Thakre and J. B. Joshi, Chem. Eng. Sci., 54 (1999) 5055.

[19] K. J. Myers, M. P. Dudukovic' and P. A. Ramachandran, Chem. Eng. Sci., 42 (1986) 2301.

[20] S. Degaleesan, S. Roy, S. B. Kumar and M. P. Dudukovic', Chem. Eng. Sci., 51 (1996) 1967.

[21] S. Degaleesan, Fluid Dynamic Measurements and Modeling of Liquid Mixing in Bubble Columns, D.Sc. Thesis, Washington University, Saint Louis, Missouri, USA, 1997.

[22] S. B. Kumar, N. Devanathan, D. Moslemian and M. P. Dudukovic', Chem. Eng. Sci., 49 (1994) 5637.

[23] N. W. Geary and R. G. Rice, AIChE J., 38 (1992) 76.

[24] H. Luo and H. F. Svendsen, Can. J. Chem. Eng., 69 (1991) 1389.

[25] R. G. Rice and N. W. Geary, AIChE J., 36 (1990) 1339.

[26] K. Ueyama and T. Miyauchi, AIChE J., 25 (1979) 258.

[27] R. Nottenkamper, A. Steiff and P. -M. Weinspach, Ger. Chem. Eng., 6 (1983) 147.

[28] T. Menzel, T. in der Weide', O. Staudacher, O. Wein and U. Onken, Ind. Eng. Chem. Res., 29 (1990) 988.

[29] B. P. Yao, C. Zheng, H. E. Gasche and H. Hofmann, Chem. Eng. Process., 29 (1991) 25.

[30] R. F. Mudde, J. S. Groen and H. E. A. Van Den Akker, Chem. Eng. Sci., 52 (1997) 4217.

[31] R. F. Mudde, J. S. Groen and H. E. A. Van Den Akker, Nucl. Eng. Des., 184 (1998) 329.

[32] N. Devanathan, D. Moslemian and M. P. Dudukovic', Chem. Eng. Sci., 45 (1990) 2285.

[33] N. Devanathan, 'Investigation of Liquid Hydrodynamics in Bubble Columns via a Computer Automated Radioactive Particle Tracking (CARPT)', D.Sc. Thesis, Washington University, Saint Louis, Missouri, USA, 1991.

[34] S. B. Kumar, D. Moslemian and M. P. Dudukovic', Flow Meas. Instr., 6 (1995) 61.

[35] S. B. Kumar, D. Moslemian and M. P. Dudukovic', AIChE J., 43 (1997) 1414.

[36] J. Chen, P. Gupta, S. Degaleesan, M. H., Al-Dahhan, M. P., Dudukovic' and B. A. Toseland, Flow Measurement and Instrumentation, 9 (1998) 91.

[37] Q. Wang, Modeling of Gas and Liquid Phase Mixing With Reaction in Bubble Column Reactors, M. S. Thesis, Washington University, Saint Louis, USA, 1996

[38] P. Gupta, M. H. Al-Dahhan, M. P. Dudukovic' and B. A. Toseland, Submitted, Chem. Eng. Sci. for presentation at ISCRE-16, Poland, 2000.

[39] A. Tomiyama, I. Kataoka and T. Sakaguchi, Trans. JSME Part B, 61 (1995) 2357.

[40] H. Schlichting, Boundary Layer Theory, McGraw Hill, New York, 1979, Chap. 20, p. 510.

[41] J. B. Joshi, Trans. Inst. Chem. Engrs, 58 (1980) 155.

[42] D. Azbel, Two-Phase Flows In Chemical Engineering, Cambridge University Press, Cambridge, 1981, Chap. 7, p. 157.

[43] P. V. Danckwerts, Gas-Liquid Reactions, McGraw Hill Co., New York, 1970, Chap. 5, p. 96.

[44] R. Clift, J. R. Grace and M. E. Weber, Bubbles, Drops, and Particles, Academic Press, New York, 1978, Chap. 7, p. 169.

[45] X. Luo, D. J. Lee, R. Lau, G. Yang and L. S. Fan, AIChE J., 42 (1999) 665.

[46] A. Kemoun, B. C. Ong, P. Gupta, M. H. Al-Dahhan and M. P. Dudukovic', Submitted, International Journal of Multiphase Flows, 2000.

[47] S. D. Gharat and J. B. Joshi, Chem. Eng. J. & Biochem. Eng. J., 48 (1992) 141.

[48] N. Tsoulfanidis, Measurement and Detection of Radiation, McGraw Hill, New York, 1983, Chap. 8, p. 247.

List of Figures

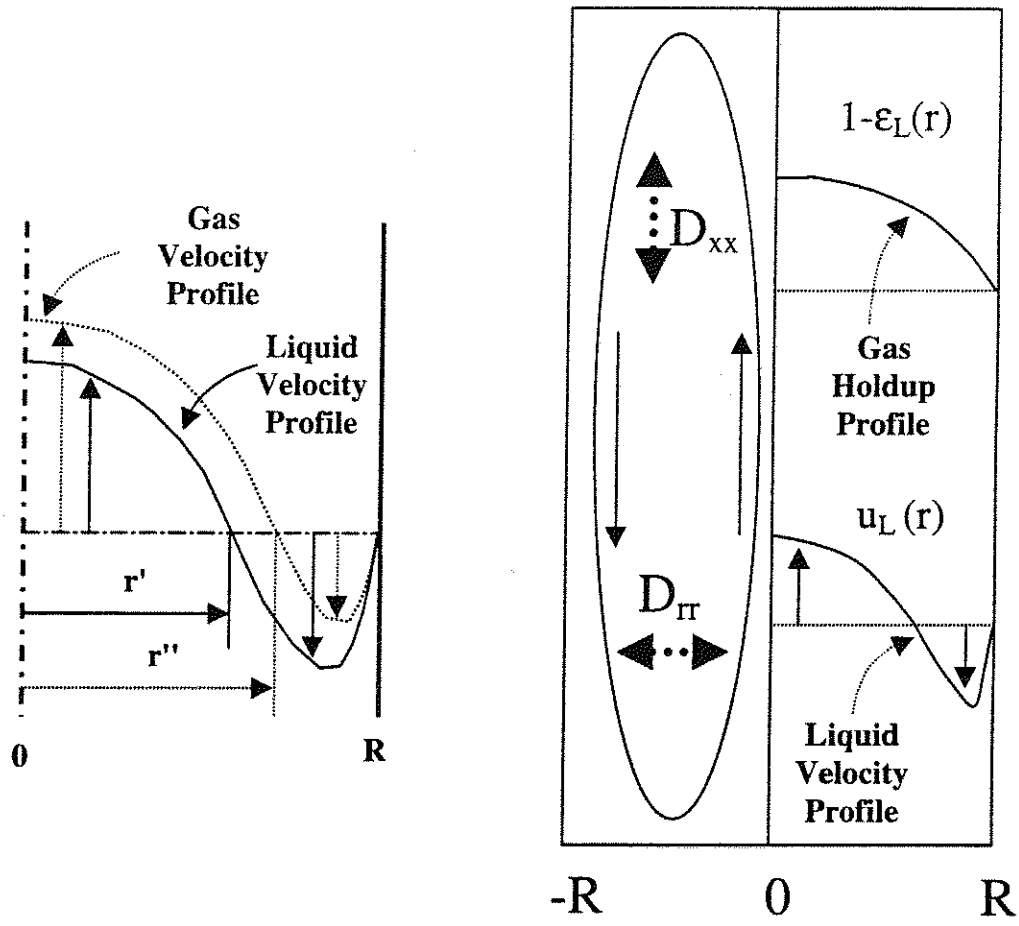

Figure 1. Schematic representation of the experimentally observed phenomena in bubble columns.

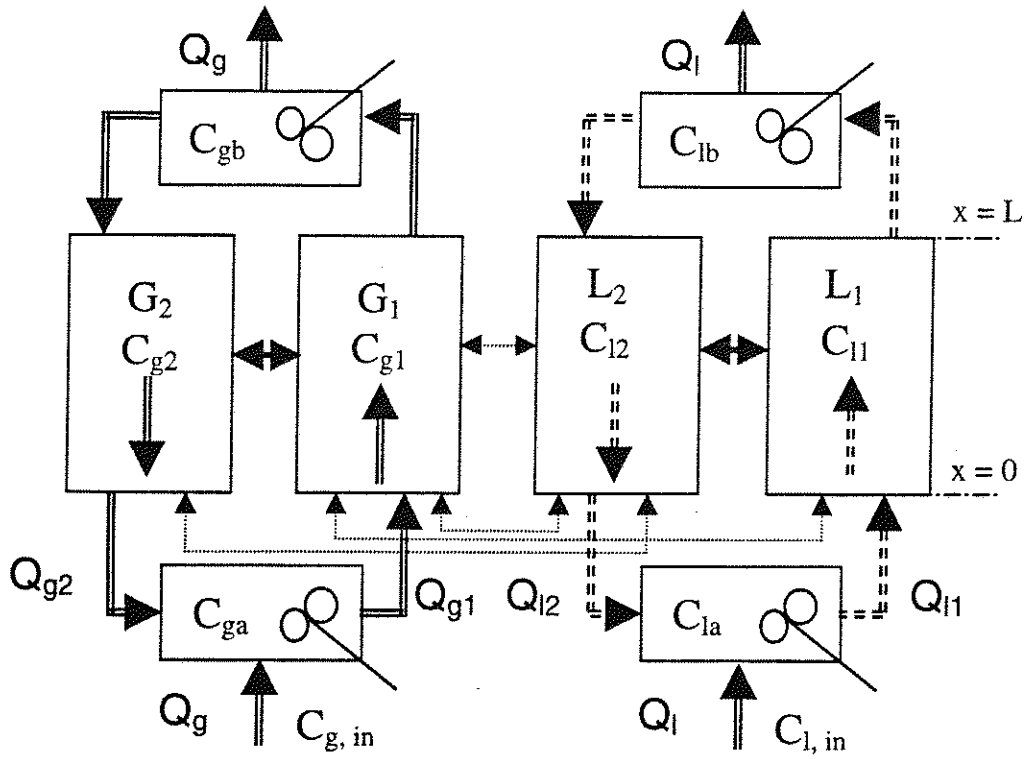

Figure 2. Schematic representation of the compartmentalization of the reactor.

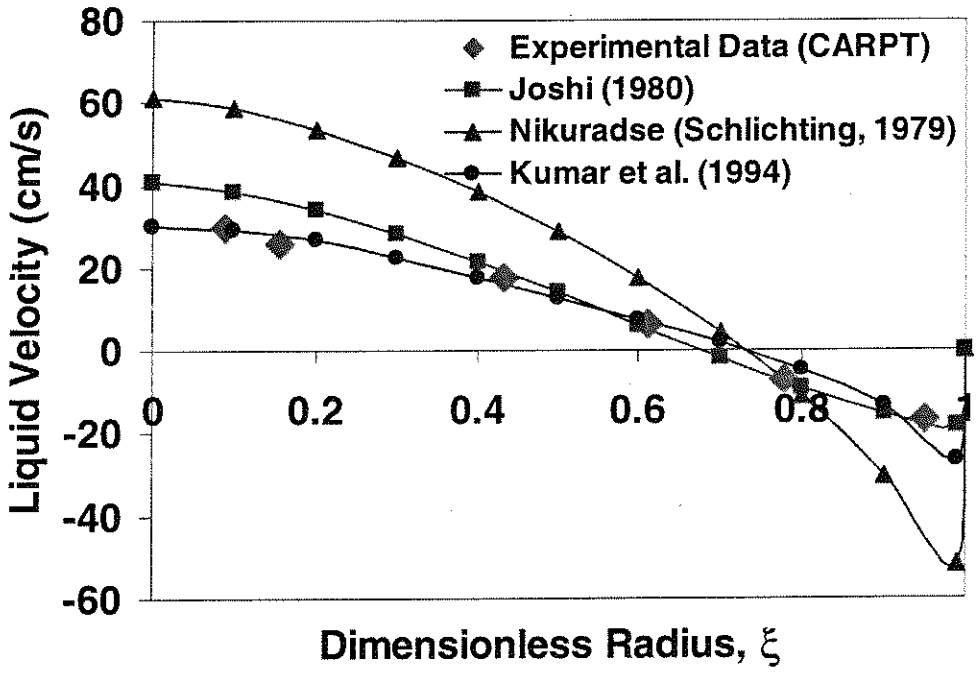

Figure 3(a)

Figure 3. Effect of mixing length profile on velocity profiles for 10 cm diameter bubble column operated at $U_{G,sup}$=12 cm/s. a) Liquid velocity b) Gas velocity.

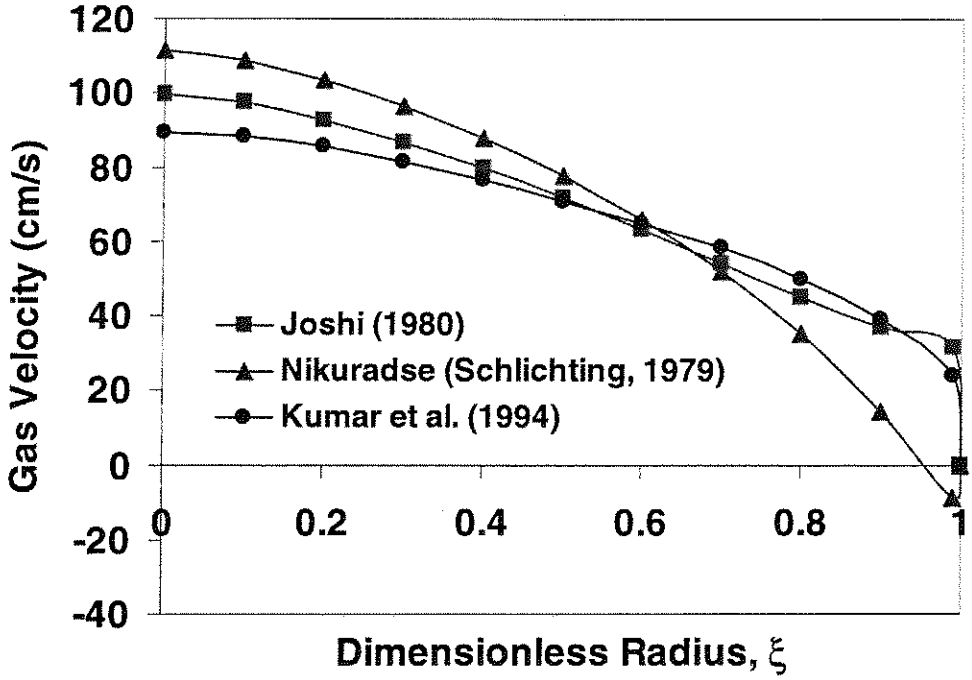

Figure 3(b)

Figure 3. Effect of mixing length profile on velocity profiles for 10 cm diameter bubble column operated at $U_{G,sup}$=12 cm/s. a) Liquid velocity b) Gas velocity.

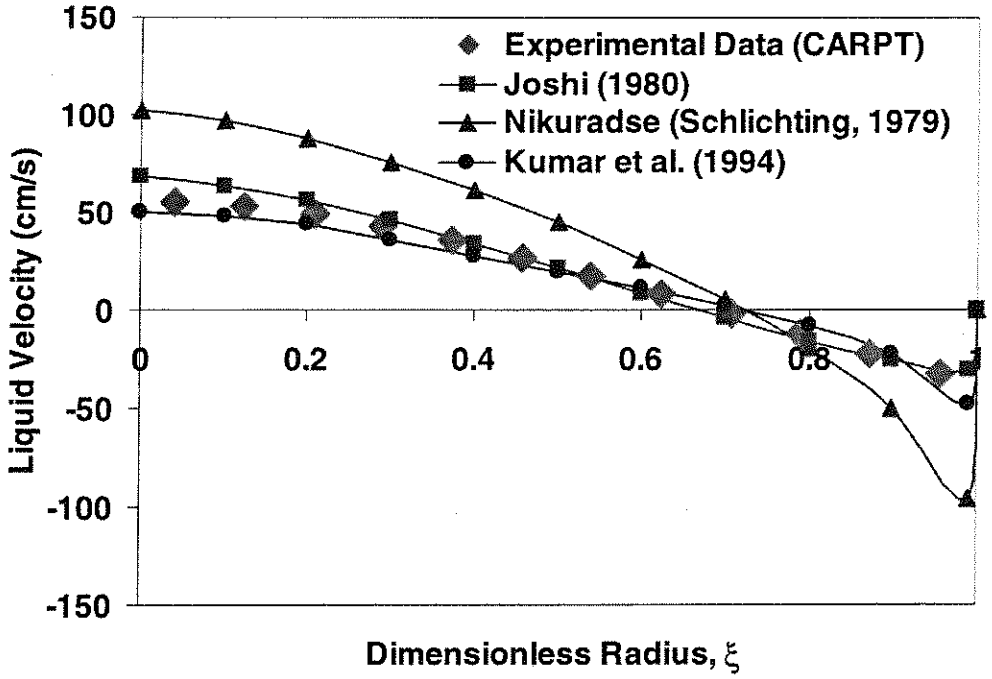

Figure 4(a)

Figure 4. Effect of mixing length profile on velocity profiles for a 44 cm diameter bubble column operated at $U_{G,sup}$=10 cm/s. a) Liquid velocity b) Gas velocity.

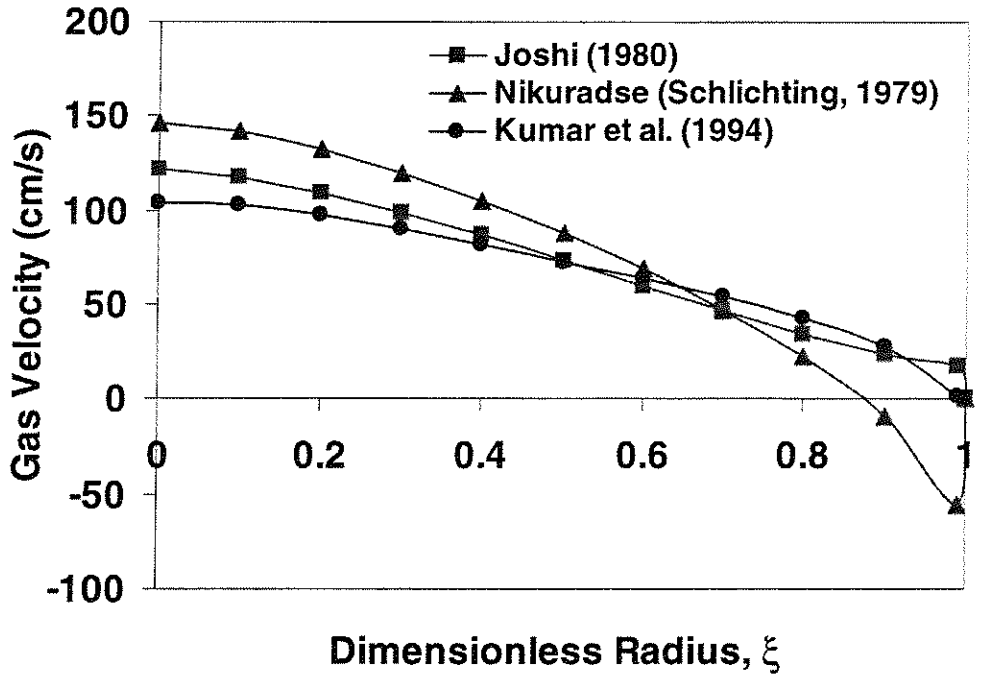

Figure 4(b)

Figure 4. Effect of mixing length profile on velocity profiles for a 44 cm diameter bubble column operated at $U_{G,sup}$=10 cm/s. a) Liquid velocity b) Gas velocity.

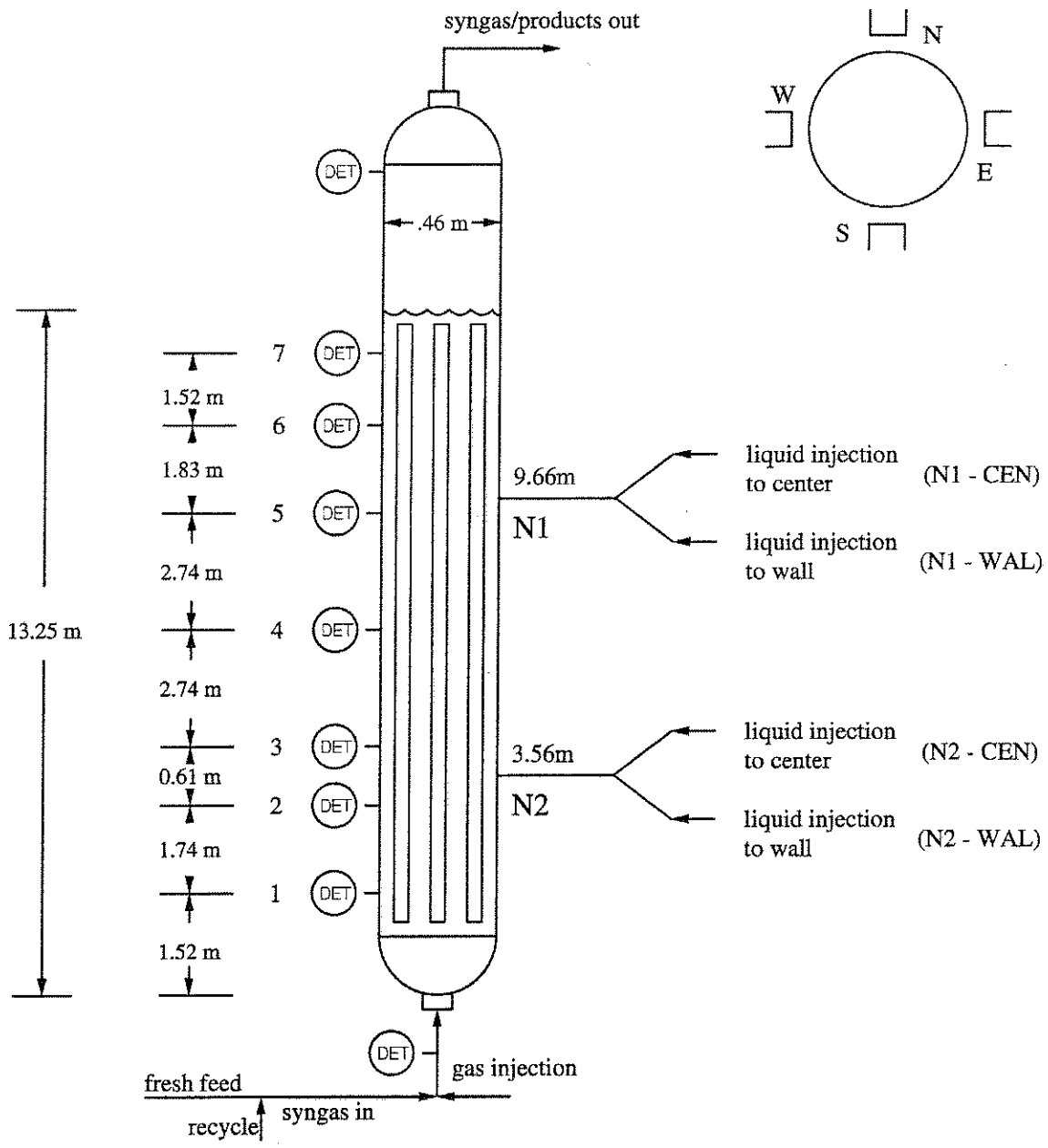

Figure 5. Schematic representation of the pilot-scale slurry bubble column at the Alternate Fuels Development Unit, La Porte indicating the detector levels for measurement of radioactive tracer responses [21].

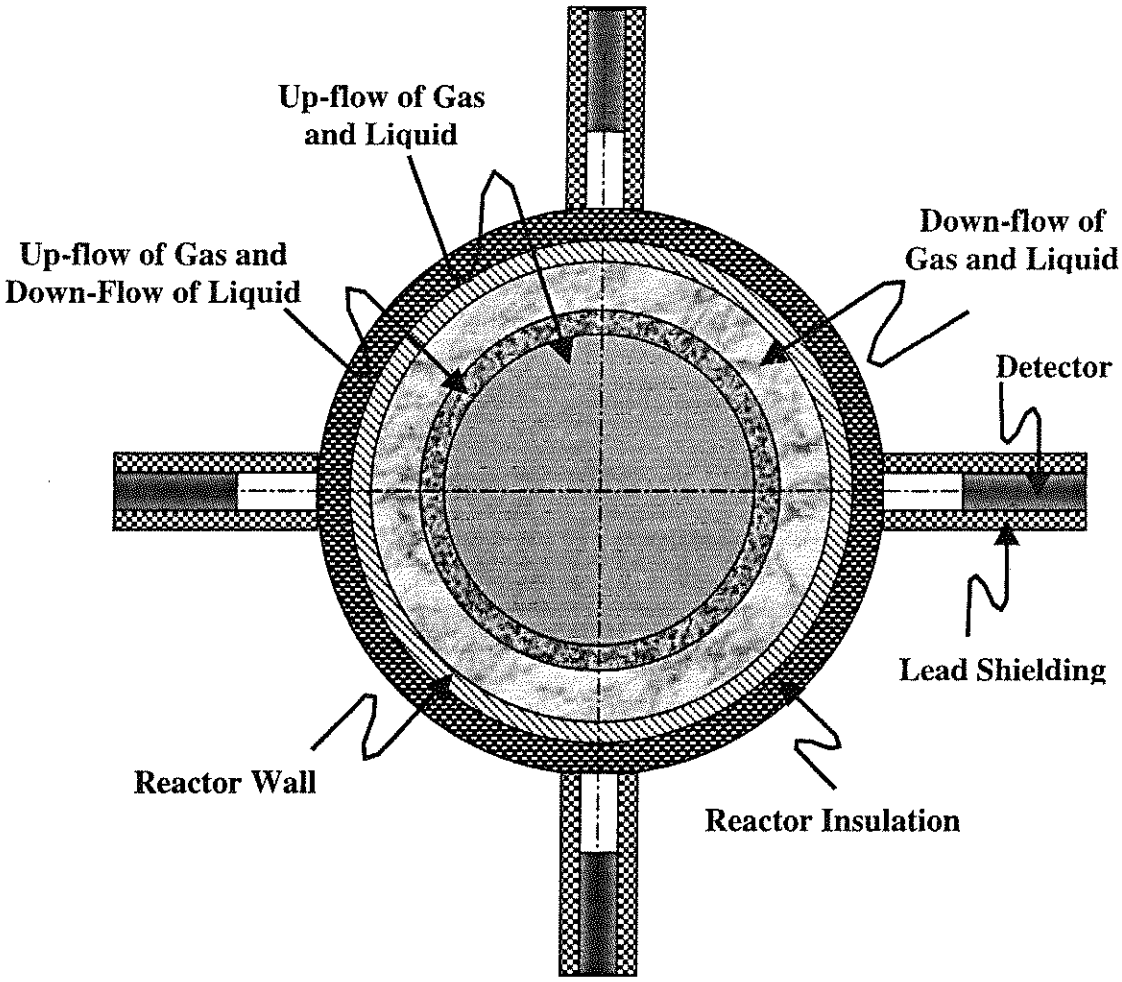

Figure 6. Schematic representation of the AFDU reactor cross-section along with scintillation detectors and their lead shielding.

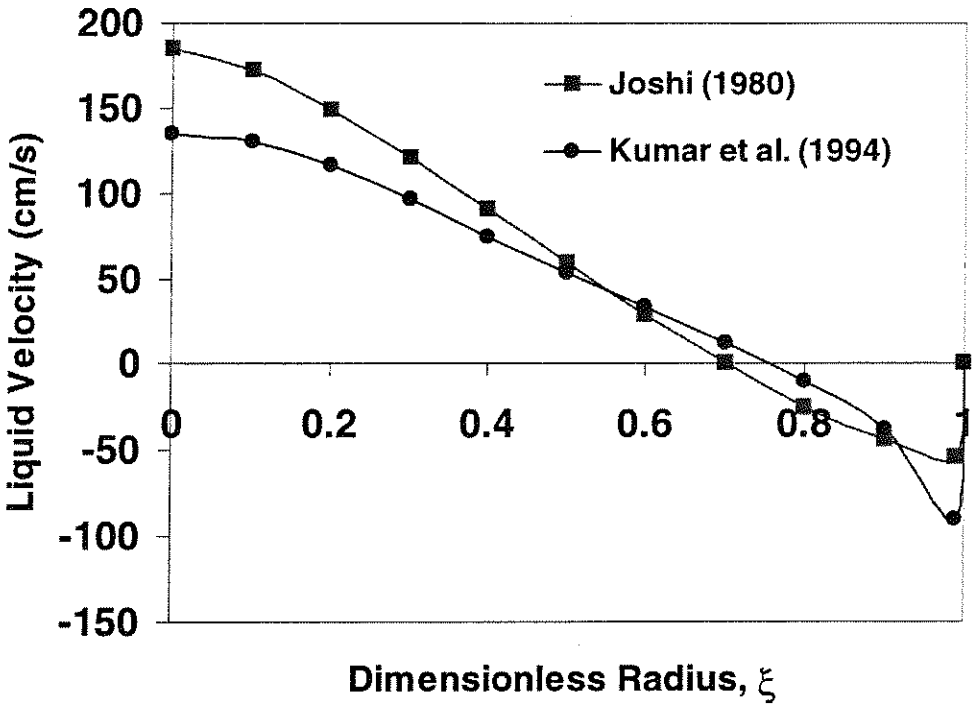

Figure 7(a)

Figure 7. Effect of mixing length profile on a) liquid and b) gas velocity profiles for a 46 cm diameter pilot scale slurry bubble column operated at $U_{G,sup}$=22.86 cm/s.

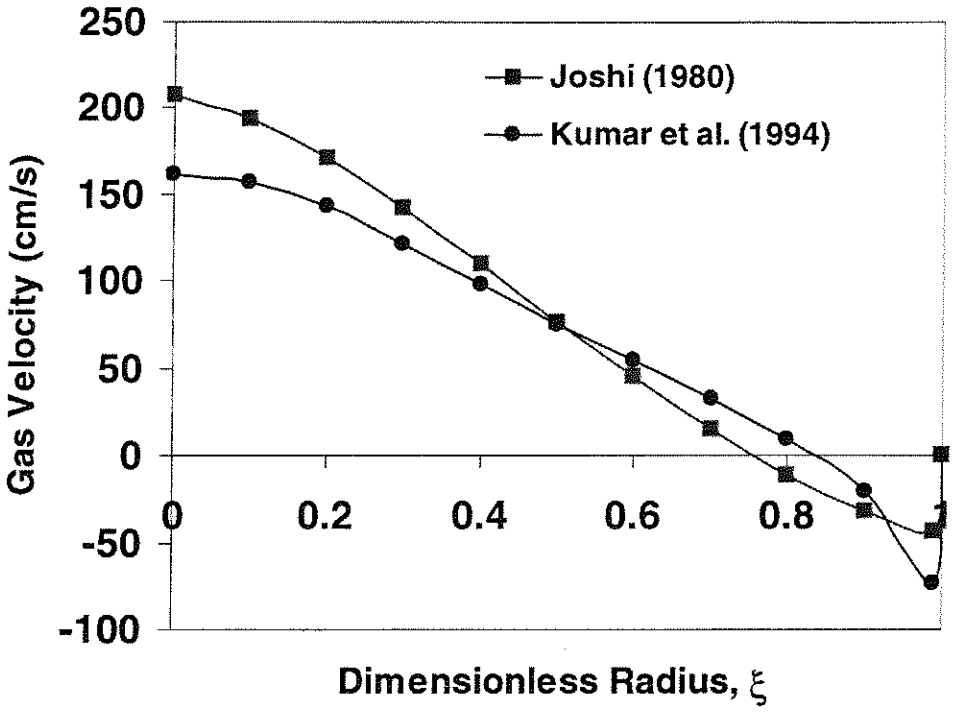

Figure 7(b)

Figure 7. Effect of mixing length profile on a) liquid and b) gas velocity profiles for a 46 cm diameter pilot scale slurry bubble column operated at $U_{G,sup}$=22.86 cm/s.

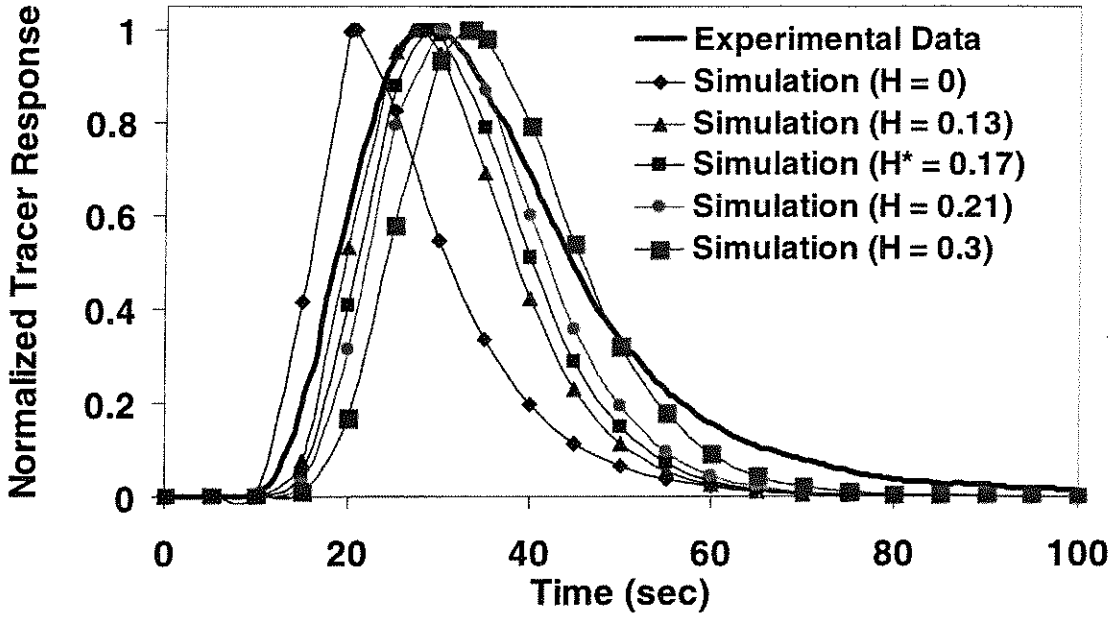

Figure 8(a)

Figure 8. Comparison of simulated and experimental radioactive gas tracer responses from a pilot scale slurry bubble column using mixing length formulations proposed by a) Joshi [41] b) Kumar *et al.* [22].

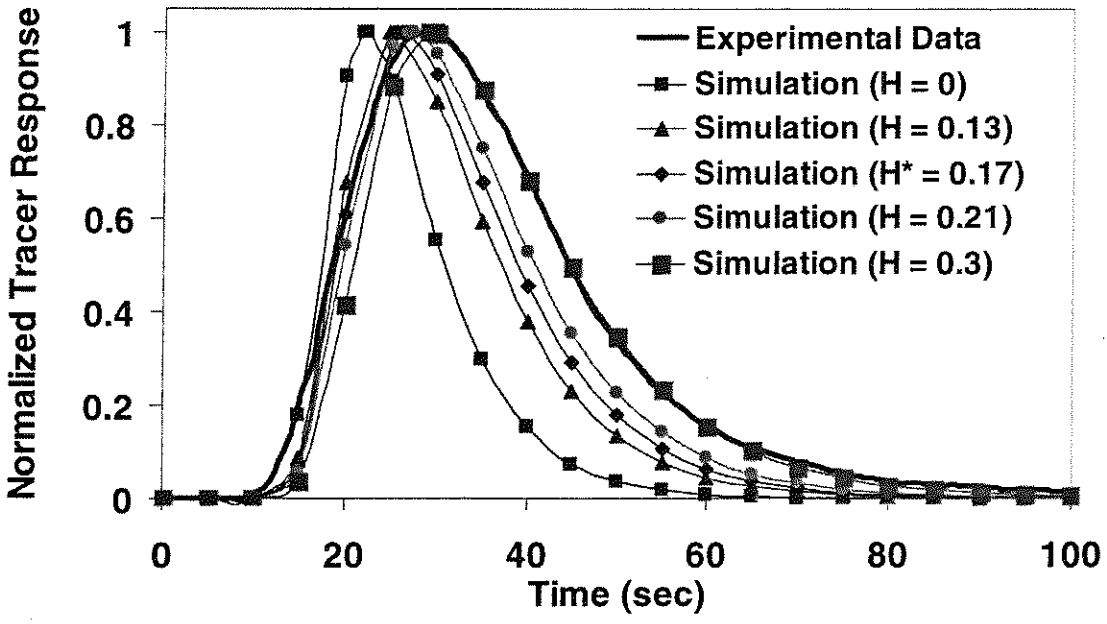

Figure 8(b)

Figure 8. Comparison of simulated and experimental radioactive gas tracer responses from a pilot scale slurry bubble column using mixing length formulations proposed by a) Joshi [41] b) Kumar *et al.* [22].

HIGH PRESSURE SLURRY BUBBLE COLUMN CONSORTIUM
for
HYDRODYNAMICS AND MODELING STUDIES OF HIGH PRESSURE SLURRY BUBBLE COLUMNS

"The following report summarizes the statement of work for the High Pressure Slurry Bubble Column Consortium, which consists of the following members: Air Products (USA), Conoco (USA), Sasol (South Africa) and Statoil (Norway). The consortium membership is open to additional companies."

A. Introduction

Slurry bubble columns are reactors of choice for a number of processes for gas conversion to fuels and chemicals such as Fischer-Tropsch synthesis and liquid phase methanol synthesis. These slurry bubble columns are usually operated at elevated pressure (up to 800 psi) and temperature (up to 280 C) and at high superficial gas velocities (up to 30 - 50 cm/s). It is known that the reactor performance and volumetric productivity and selectivity are affected significantly by the fluid dynamics which are not yet well understood due to the complexity of the flow field in such reactors. In addition, most of the current studies on bubble/slurry bubble columns hydrodynamics have been performed at atmospheric conditions. Therefore, it is essential to understand the effect of elevated pressure and high superficial gas velocity, the operating conditions of interest, on the fluid dynamics of slurry bubble columns. This should lead to improved design and scale-up/scale-down of these reactors.

It is known that in smaller diameter vessels column diameter may affect the observed hydrodynamics. However, it is argued that at high pressure even small diameter vessels can provide data indicative of large-scale operations. On the other hand an old rule of thumb suggests using a column at least 6" in diameter in order to eliminate wall effects. For this reason, at the Chemical Reaction Engineering Laboratory at Washington University a 6 inch diameter bubble/slurry bubble column facility has been developed for studies at elevated pressure (up to 175 psig). This facility is designed to be utilized with the Computer Radioactive Particle Tracking (CARPT) and Computed Tomograhy (CT), and is the only facility in the world that combines both of these techniques for non-invasive fluid dynamics measurements of velocity and holdup profiles, respectively, at elevated pressure. Only CARPT/CT can provide the needed data in churn turbulent flows at high volume fraction of the dispersed phase. In addition, pressure drop and pressure drop fluctuation measurements and optical probes for bubble sizes and bubble rise velocity measurements can be implemented in the developed facility.

B. Objectives

The overall objective of the proposed study is to quantify the effect of the key operating and design parameters such as elevated pressure, high superficial gas velocity, catalyst loading on the fluid dynamics of bubble column/slurry bubble columns via advanced diagnostic techniques (experimental investigations) and via modeling (theoretical and computational studies). The results should lead to a proper approach for scale-up/scale-down and design of Fischer-Tropsch slurry bubble column reactors. The detailed tasks are outlined below.

C. Members of the Consortium

Industrial Members:

The current members are:

Air Products and Chemicals – USA
Conoco – USA
Sasol – South Africa
Statoil – Norway

Each member provides funding in the amount of $50,000/year for 3 years.

Academic Members:

Washington University – Chemical Reaction Engineering Laboratory (CREL), Professors M.H. Al-Dahhan and M.P. Dudukovic: CREL responsible for achieving the goals set for the consortium.

Ohio State University, Professor L.S. Fan: CREL will subcontract work to Prof. Fan's laboratory regarding small-scale studies and physical property measurements at high-pressure operations.

D. Starting Date and Duration

The project duration is 3 years starting from the date of signing the contract (April 1, 1999)

E. Proposed Tasks (and Proposed Milestones)

The tasks and the timetable for the proposed study are listed below. Modifications will be tailored to meet the needs of the consortium members.

Task 1

1. Critically review and summarize the pertinent literature regarding the high-pressure bubble/slurry bubble columns. The specific goals are as follows:

   - Describe what is known regarding the effect of physicochemical properties, operating conditions (e.g. reactor pressure, high superficial gas velocity, temperature) and reactor internals on the following:

     * Hydrodynamics: overall gas holdup, gas holdup profile, interfacial area, bubble size distribution, flow pattern and turbulent parameters, solids distribution, gas mixing, flow regime and its transition with emphasis on the churn turbulent regime.
   - Other: heat and mass transfer. Discuss what is known for organic and water systems and illustrate the differences.

   - Review the state-of-the-art of scale-up and modeling and identify key scale-up issues.

Task 2

2. Identify a suitable solvent-air-solid system for the range of pressure available for 6" diameter column-cold flow set-up to mimic the conditions of hydrocarbon synthesis. The search for the solvent will be achieved by measuring, in small scale units (2" and/or 4"), the important intrinsic physicochemical properties such as density, viscosity and surface tension in the following solvents:

   - Standard FT wax provided by the industrial member(s) (suggested conditions: temperature = 200-250 C, Pressure = 20 bar, $\alpha > 0.9$-0.93; the wax properties at operating conditions of interest: density ~ 0.67 gm/cm3, viscosity ~ 0.3 cp., surface tension ~ 14-19 dyne/cm).

   - Hydrocarbon(s) of up to C20 or above to mimic FT waxes at the operating conditions of interest. Flammability and safety should be considered in the selection process.

Task 3

1. Investigate experimentally in a 6" diameter column, using a uniform distributor, the effects of elevated pressure, high superficial gas velocity and solids loading on the following:

   a. Gas holdup profiles via CT at two to three levels that include the fully developed flow and distributor regions.
   b. Overall gas holdup via pressure drop measurements.
   c. Radial and axial solids distribution at selected conditions via CT and pressure drop measurements.
   d. Flow field via CARPT (time averaged liquid velocity, turbulent stresses, kinetic energy and eddy diffusivity).

For the above investigations, the following systems are considered:

1. The system of water-air-glass beads will be used first because we have a database for it at atmospheric conditions and this will allow us to compare the results. The proposed conditions are:

   Solids size: 125 – 177 μm
   Solids loading: 7 to more than 40% wt.
   Pressure: 14.7 to 150 psig (3 pressures, 14.7, 30-40, 130-150 psig)
   Superficial gas velocity: 2 to 60 cm/s (5-8, 14, 25-30, 40-60 cm/s)
   Distributor: Uniform distributor or cross sparger with 0.15% open area or larger to provide a gas velocity at the holes lower than the sonic velocity for superficial gas velocities up to 50 cm/s.

2. The solvent-air-solid identified system in Task (2) will be used. The operating conditions will be identified with the consortium members based on the findings of (1) above. (Solids will be provided by the industrial members(s)).

NOTE: (1) For CARPT experiments, a radioactive particle size of 150 μm will be considered. This is based on the safety considerations that is related to the particle manufacturing and handling and the cost involved for irradiation which is increased tremendously as the particle diameter decreases. However, a test and evaluation will be considered to identify the largest size of the radioactive particle that can represent the solids of smaller sizes.

(2) The feasibility of implementing CARPT/CT techniques in high pressure (higher that 175 psig) and high temperature (up to 300 – 500 C) will be evaluated.

Task 4

Investigate experimentally on small scale units (2" and/or 4" diameter column) using the identified solvent, some key parameters such as (gas holdup via gas disengagement technique or pressure drop, bubble size and bubble rise velocity via optical probe, pressure drop and fluctuation) at selected operating conditions used in task 3. Evaluate the effect of reactor scale on the hydrodynamics at high pressure by comparing the findings with those obtained in 6" diameter column. Also use the small-scale results to provide input to models for prediction of larger scale results. These predictions will be compared with the experimental results obtained in a 6" diameter column [and the larger ones reported in the literature (if any)].

The developed phenomenological models, computational fluid dynamics (CFD) models, and scale-up methodology will be examined against the obtained experimental data.

Hydrodynamic Measurements in a Slurry Bubble Column

A. Problem Definition

Slurry bubble column reactors are presently used for a wide range of reactions in both chemical and biochemical industry. The successful design and scale up of bubble column reactors require a complete understanding of multiphase fluid dynamics and its influence on phase mixing and transport characteristics. Considerable effort has been directed towards phenomenological and computational fluid dynamics modeling. A major obstacle for advance in three phase modeling is a lack of reliable experimental data, particularly for holdup, velocity, turbulent kinetic energy and "Reynolds" sheer stress profiles. The existing experimental data is limited to systems operated under low superficial gas velocity and atmospheric pressure which are not industrially relevant. Most of these measurements were performed using probe techniques. Typically, liquid velocity was measured using Hot Film Anemometry or Pitot tube technique, while gas holdup was measured using conductivity or electro-resistivity probe techniques.

B. Research Objectives

Computer Automated Radioactive Particle Tracking (CARPT) and Computed Tomography (CT) are powerful and complementary noninvasive measurement techniques. They provide a full hydrodynamic picture of the flow, enable mass balance checkup and offer reliable experimental data that can be used in modeling. Over the past few years CREL laboratory adopted and improved both CARPT and CT technique. In this work we utilize both techniques and, together with differential pressure (DP) measurements, acquire data that is used to calculate holdups of all three phases, as well as the solids velocity and turbulent parameters profiles in a slurry system operated at industrially relevant high superficial gas velocities and pressures.

C. Research Accomplishments

This work represents a part of the tasks set for the high pressure slurry bubble column consortium sponsored by: Air Products and Chemicals, Conoco, Sasol and Statoil. The results are first reported to these companies and will be later released to other CREL sponsors. Hence, only a brief outline of used measurement techniques is presented here.

C1. CARPT Experiments

CARPT is a technique for tracking of a single radioactive tracer particle by detecting the distribution of emitted γ-rays. Collected data of the tracer particle location in time is used to compute the tracer particle velocity and "turbulent" parameters. Precise calibration and good radioactive particle tracking are essential in obtaining accurate and reproducible CARPT data. In this work the assessment of solids velocities and "turbulent" parameters is sought. Thus, the radioactive tracer particle should as closely as possible

track the solids present in the system. In this experiments a Scandium Sc-46 particle (half-life of 83 days, strength up to 300 μCi) with a total diameter of about 164 μm (within the solid phase particle size range of 105 to 175 μm) is used. Prior to irradiation the Sc-45 particle with diameter of 150 μm is protected against oxidation with a thin 7 μm coating of Parylene N, an extremely inert derivative of poly p-xylene with excellent mechanical properties. Nearly all types of Parylene polymer (family of the substituted poly para-xylylenes) are likely candidates. However, Chlorine derivatives should be avoided because of the activation cross section value of Chlorine that is comparable to the one of Scandium. In addition since processes for the production of the Flour based dimmers (starting reagent) are largely protected by the patents, availability of this derivatives is limited. Because of that after much thought and effort unsubstituted Parylene N is selected for coating of the tracer particles. Although with the high melting point of 410°C because of the lack of protection of hydrogen atoms by halogens (as in substituted derivatives) maximum working temperature of Parylene N in air is about 110 to 130°C. Since irradiation of Scandium by the high thermal flux of neutrons can cause significant heating of the material in excess of 100°C material must be sealed in a vial under helium (preferred than vacuum because of the better heat transfer) during irradiation. Coating process itself is rarely done on micro size particles. With the most common application being coating of electrical circuit boards. Process procedure and parameters have been custom developed for our application. The difference in the density between the coated radioactive tracer and the solid phase particles is, depending on the total diameter, less than few percents. This small difference in densities causes negligible difference in terminal settling velocities and consequently good solid phase tracking.

The detailed original procedure and setup for the CARPT experiment is given by Degaleesan (1997). Recently, improved in-situ calibration of the γ radiation detectors that employs the new automated calibration device and new tracer particle reconstruction procedures (including the Monte-Carlo method) have developed. The novel design of the CARPT calibration device enables in-situ calibration under high pressures without depressurizing the system for changing of axial or tangential radioactive particle position. Addition of the two stepper motors automate the movement in axial and tangential direction greatly reducing acquisition time (six fold compared to manual operation) and increasing the accuracy of placement of calibration points. Higher quantity of more accurate calibration points results in more accurate particle location reconstruction during the actual CARPT experiment.

CARPT data (Sc particle position in time) acquired over sufficiently long time (presently typically about 24 hours) to insure good time/ensemble averaging is used for calculation of time averaged solid:

a) velocities,
b) "Reynolds" stresses,
c) "turbulent" kinetic energy and
d) eddy diffusivities.

The basics of the calculation procedures are outlined by Degaleesan (1997).

Initial CARPT experiments using gas-liquid system have been conducted. Testing of the new tracer particle reconstruction algorithms is in progress.

C2. CT Experiments

CT is a technique for measurement of cross-sectional phase holdup distribution in multiphase systems. Single source CT is used for phase holdup reconstruction in two phase (e.g., gas-liquid) systems. Theoretically, dual source CT or ultrasonic technique are capable of resolving the holdups in three phase systems (e.g., gas-liquid-solid). However, because of numerical error accumulation dual source CT reconstruction of holdup profiles is still not practically possible, while the use of ultrasonic technique is, due to highly non-linear signal dependency, practically limited to bubbly flow regime and very low solids holdup (Warsito et al., 1997). An alternative approach is to calculate holdups of all three phases using combined experimental data from two or more "single mode" techniques. Sandia National Laboratories (Torczynski et al., 1998) were the first to utilize this approach to evaluate three phase holdup profiles in a "slurry column" (their solids of the diameter range d_P = 200 - 500 μm and density ρ_P = 1.04 correspond closer to those encountered in fluidized beds) using combined experimental data acquired by Electrical Impedance Tomography (EIT) and Gamma-Densitometry Tomography (GDT). However, the accuracy and reliability of EIT/GDT technique is questionable because of poor EIT spatial accuracy. In this work we present a new combination of measurement techniques CT/DP/CARPT that can be used to calculate holdup profiles of all three phases in a slurry system at all operating conditions.

For a single γ radiation source absorbance A_k (k = *L, GS, GLS*) over path l is equal to:

$$A_k = -\ln\frac{I_k - I_{k,bck}}{I_G - I_{G,bck}} = \sum_l \left[(\rho\mu)_k - (\rho\mu)_G\right] l_{ij} \tag{1a}$$

$$R_{k,ij} = (\rho\mu)_{k,ij} - (\rho\mu)_{G,ij} \tag{1b}$$

where I is the intensity of γ radiation, ρ is the phase density, μ is the phase specific attenuation coefficient and *ij* depicts a mesh cell along the path. For the column containing solids (holdup of ε_S^0) and gas in the voids between solid particles volumetric attenuation coefficient in cell *ij* is equal to:

$$(\rho\mu)_{GS,ij} = (\rho\mu)_{S,ij}\varepsilon_{S,ij}^0 + (\rho\mu)_{G,ij}\left(1 - \varepsilon_{S,ij}^0\right) \tag{2}$$

Using eq. (2) and eq. (1b) (written for gas-solid, k = *GS*) after some algebra local solids volumetric attenuation coefficient can be obtained as:

$$(\rho\mu)_{S,ij} = \frac{R_{GS,ij}}{\varepsilon_{S,ij}^0} + (\rho\mu)_{G,ij} \tag{3}$$

Similarly, for a slurry system:

$$(\rho\mu)_{GLS,ij} = (\rho\mu)_{G,ij}\varepsilon_{G,ij} + (\rho\mu)_{L,ij}\left(1 - \varepsilon_{G,ij} - \varepsilon_{S,ij}\right) + (\rho\mu)_{S,ij}\varepsilon_{S,ij} \tag{4}$$

From eq. (4) combined with eq. (1b) (written for liquid, $k = L$ and slurry, $k = GLS$) and eq. (3) yields the expression for local gas holdup (cell ij):

$$\varepsilon_{G,ij} = \frac{R_{GS,ij}\dfrac{\varepsilon_{S,ij}}{\varepsilon^{0}_{S,ij}} + R_{L,ij}\left(1-\varepsilon_{S,ij}\right) - R_{GLS,ij}}{R_{L,ij}} \tag{5}$$

Clearly in order to close the system of equations we need one more equation for local solids holdup $\varepsilon_{S,ij}$. In dual source CT one more equation of the form (1) can be written for the other γ source. In this work the additional equation is generated from DP and CARPT measurements:

$$-\frac{\Delta P}{\Delta z} = \rho_G \overline{\varepsilon_G} + \rho_L\left(1-\overline{\varepsilon_G}-\overline{\varepsilon_S}\right) + \rho_S \overline{\varepsilon_S} \qquad \text{DP} \tag{6}$$

$$\varepsilon_{S,ij} = \overline{\varepsilon_S}\frac{n_{S,ij}}{\overline{n_S}} \qquad \text{CARPT} \tag{7}$$

where $-\Delta P/\Delta z$ is the pressure drop from DP measurements, $n_{S,ij}$ is the number of the radioactive tracer particle occurrences in cell ij per unit volume and the over-bar depicts the cross sectional average value. Finally, the combination of eq. (6) and (7) yields the expression for the local solids holdup (cell ij):

$$\varepsilon_{S,ij} = \frac{-\dfrac{\Delta P}{\Delta z} - \rho_G \overline{\varepsilon_G} - \rho_L\left(1-\overline{\varepsilon_G}\right)}{\rho_S - \rho_L} \times \frac{n_{S,ij}}{\overline{n_S}} \tag{8}$$

Using the following iterative procedure the holdup profiles of all three phases can be calculated.

1) Guess the cross-sectional average solids holdup. The initial guess is based on the calculation of the cross-sectional average solids holdup from the overall gas holdup measurements and nominal solids loading (v_S, volume of solids per volume of slurry suspension initially charged into the column) using the equation $\overline{\varepsilon_S} = v_S(1-\overline{\varepsilon_G})$.
2) Using eg. (7) calculate the solids holdup in each cell.
3) Using eq. (5) calculate the gas holdup in each cell.
4) Calculate the cross-sectional average gas holdup.
5) Using eq. (8) calculate the solids holdup in each cell.
6) Calculate the cross-sectional average solids holdup.
7) Compare the calculated and previous values (initial guess in the first iteration) of the cross-sectional average solids holdup.
8) Using the solids holdups in each cell recalculated in step 5 repeat the steps 3 though 7 until convergence.

All experiments are conducted in a stainless steel (6" diameter, air-water-glass beads) slurry bubble column. The dynamic system height of around 180 cm (11 column

diameters) is maintained in all experiments. At each experimental condition (Rados, 1999) the column is scanned using CT at three axial positions:

1) Height ①, z = 34 cm (2 column diameters, beginning of fully developed region)
2) Height ②, z = 89 cm (5 column diameters, middle of fully developed region)
3) Height ③, z = 145 cm (9 column diameters, end of fully developed region).

So far we have completed experiments using four different sparger designs, wide range of superficial gas velocities from 8 to 60 cm/s, three pressures of up to 0.1 MPa and two different solids loadings of 20 and 35 wt%.

C3. DP Experiments

Differential pressure (pressure drop) data over the three axial positions where CT measurements are conducted and across the sparger are acquired. Also, absolute pressure at each of the four points is recorded. The primary reason for DP measurements is related to holdup measurements using CT/DP/CARPT technique at selected operating conditions. However in parallel we plan to evaluate applicability of the pressure signal time series for determining of the transition from bubbly to churn turbulent flow regime. Pressure measurement experiments required construction of the stainless steel column that is similar to the one that was used for CARPT/CT experiments but that has additional ports where the measurement probes (like the pressure transducer) can be mounted. After much effort this column has been designed and fabricated during the last year. The column has been installed in the new high pressure facility. Design of the column is given in Figure 1. Pressure measurement instrumentation has been installed, configured and together with the measurement procedure tested in an ambient pressure 8" Plexiglas gas-liquid bubble column. Initial experiments in the 8" column showed that regime transition is not characterized by the appearance of new or disappearance of existing dominant frequencies of the flow with increase in superficial gas velocity. Rather, increase in the magnitude of the dominant frequencies with increase of the superficial gas velocity has been observed. In addition it has been observed that the specific position of the dominant frequency peaks is position (height) dependent.

Transferring of the technique to the newly installed stainless steel 6" high pressure bubble column is in progress.

D. Conclusion

The numerical simulation tests of the proposed iterative holdup calculation procedure (eq. (5), (7) and (8)) showed that the procedure is stable for all tested solid loadings. Also, random noise artificially added to starting experimental gas holdup data (simulating experimental noise) didn't affect the stability of the procedure. The calculated cross sectional average solids holdup matched the starting experimental holdup with relative error less than 0.1%, well below the experimental accuracy of CARPT and CT techniques.

The CT experiments were used, assuming uniform solids holdup, to calculate the gas holdup profiles. The obtained cross sectional profiles looked reasonable and comparable to gas holdup profiles in corresponding gas-liquid systems.

The measurements and experiments conducted so far confirmed that the CT/DP/CARPT technique can be used for recalculation of holdup profiles of all three phases in slurry systems.

The calibration of the CARPT γ radiation detectors has been dramatically improved in speed and accuracy using newly developed automated CARPT calibration device. New tracer particle position reconstruction procedures have been recently developed. Preliminary results look very promising.

DP measurement technique has been tested in an 8" Plexiglas column. Additional probe measurement high pressure 6" stainless steel has been designed and machined. New high pressure facility for the new 6" column has been built.

E. Future Work

We have finished the planned CT experiments. Preliminary CARPT and DP experiments have been also conducted. The CARPT experimentation are scheduled for the Summer 2000. New high pressure facility and 6" column for probe measurements has been built. Initiation of the DP measurements in the 6" column is under way.

F. Bibliography

1. Degaleesan, S. Turbulence and Liquid Mixing in Bubble Columns. *D. Sc. Thesis* **1997**, Washington University, St. Louis, Missouri.

2. Rados, N. Slurry Bubble Column Hydrodynamics. *D.Sc. Proposal* **1999,** Washington University, St. Louis, Missouri.

3. Torczynski, J. R., K. A. Schollenberger, T. J. O'Hern and D. L. George. Reactor Hydrodynamics Portion of FETC Quarterly Report. *Sandia National Laboratories FEW-8616* **1998**, Albuquerque, New Mexico.

4. Warsito, M. Ohkawa, A. Maezawa, S. Uchida and S. Okamura. Non-Invasive and Simultaneous Measurement of Gas and Solid Holdups in A Slurry Bubble Column by A Novel Ultra-Sonic Technique. *AIChE J.* **1997,** submitted.

G. Acknowledgement

CREL gratefully acknowledges the support provided by the members of the high pressure slurry bubble column consortium, Air Products and Chemicals, Conoco, Sasol and Statoil, that made this work possible.

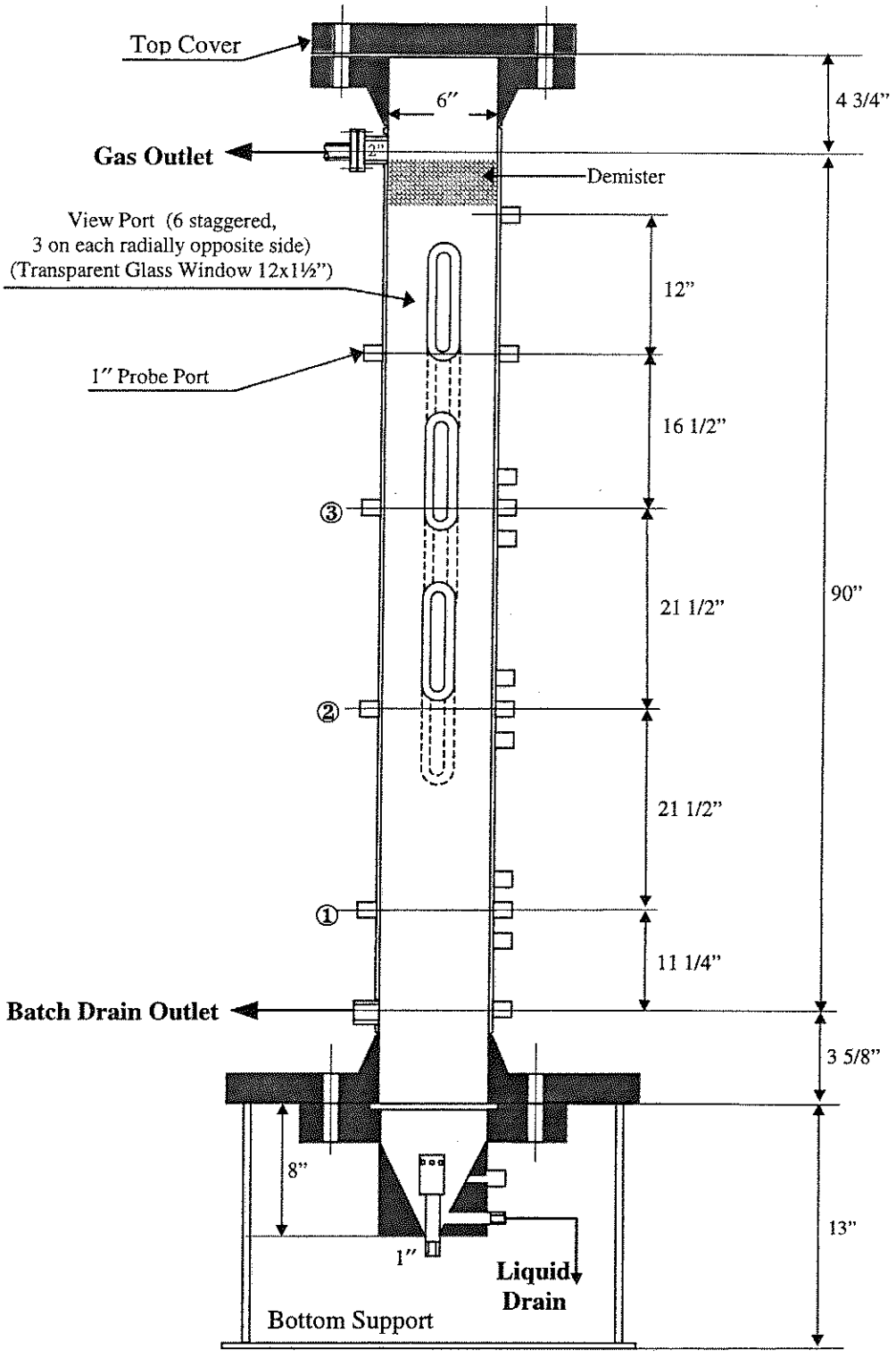

Figure 1. High pressure probe measurement bubble column design

PREDICTION OF RADIAL GAS HOLDUP PROFILES IN BUBBLE COLUMN REACTORS

See the attached report for:

A. Problem Definition
B. Research Objectives
C. Research Accomplishments

Predictions of radial gas holdup profiles in bubble column reactors

Yuanxin Wu*, Boon Cheng Ong and M.H. Al-Dahhan†

Chemical Reaction Engineering Laboratory,
Washington University, St. Louis, MO 63130, USA

Abstract

Gas holdup and its profile are important parameters to be characterized in bubble column reactors. Proper prediction of the radial gas holdup profiles is necessary for determining liquid mixing, flow regime transition, heat and mass transfer. In this study, the following gas holdup profile form, which can be fitted to the observed holdup profiles, is proposed: $\varepsilon_G = \bar{\varepsilon}_G(\frac{n+2}{n+2-2c})[1-c(r/R)^n]$

The parameters n and c needed to describe the gas holdup profile are correlated with appropriate dimensionless groups.

$$n = 2.188\times10^{3}\,\mathrm{Re}_G^{-0.598}\,Fr_g^{0.146}\,Mo_L^{-0.004}$$

$$c = 4.32\times10^{-2}\,\mathrm{Re}_G^{0.2492}$$

However, the cross-sectional average gas holdup, $\bar{\varepsilon}_G$, can be estimated using the available correlations for overall gas holdup.

The agreement between the correlation predictions and experimental data is reasonable over wide range of operating conditions.

Key words: bubble columns, gas holdup profiles, correlation

Introduction

Gas holdup profile is one of the most important parameters in bubble column reactors. The spatial variation of gas holdup gives rise to pressure variation, which results in liquid recirculation in the bubble column. This liquid recirculation governs the rate of mixing, heat transfer and mass transfer. The ability to predict radial gas holdup profiles in bubble column reactors would help us in determining the flow regimes, liquid mixing, heat and mass transfer better. This should make bubble column scale-up more reliable.

The existence of a pronounced radial holdup profile is the characteristic of the heterogeneous regime of flow in the column which generates strong liquid recirculation. The magnitude of gas holdup radial gradients and the magnitude of liquid velocity driven by the gas depend on superficial gas velocity, column diameter, the nature of the gas-liquid system and the operating conditions (pressure and temperature of the reactor).

During the past three decades, a number of experimental measurements of gas holdup and gas holdup profile have been reported in the literature and have been summarized by Joshi *et al.* (1998). A variety of techniques, such as optical fiber probes, gamma ray densitometry, particle image velocimetry, and gamma ray and X-ray attenuation together with computer tomography have been employed for the local gas holdup measurements. Due to the complexity of the system, no fundamental equation is available at present for prediction of the gas holdup profiles in bubble columns, There are a number of empirical equations, similar in form, that can be fitted to the observed holdup profiles.
Nassos and Bankoff (1967) proposed the following equation for the radial holdup profile:

$$\varepsilon_G = \tilde{\varepsilon}_G(\frac{n+2}{n})[1-(r/R)^n] \tag{1}$$

In eq. (1), $\tilde{\varepsilon}_G$, which is the radial chordal average gas holdup along the column diameter, and the exponent n are parameters and r/R is the dimensionless radial position. The value of parameter n is indicative of the steepness of the holdup profile. When n is large the profile is flat, for small n the profile is steep. The steepness of the holdup profile is reflected in the intensity of liquid circulation. Ueyama and Miyauchi (1979) reviewed the published literature and modified the above equation as follows to include the possibility of finite gas holdup close to the wall.

$$\varepsilon_G = \tilde{\varepsilon}_G(\frac{n+2}{n})[1-c(r/R)^n] \tag{2}$$

* Current Address: Wuhan Inst. Of Chem. Tech., Wuhan, Hubei 430073, P.R.China
Email: wyx4@public.wh.hb.cn
† Corresponding author: E-mail: muthanna@wuche.wustl.edu, Tel: 314-935-7187, Fax: 314-935-7211

In eq. (2), c is an additional parameter which is indicative of the value of gas holdup near the wall. If c =1 there is zero holdup close to wall, if c=0 holdup is constant with changing r/R.
Luo and Svendsen (1991) used eq.(2) rewritten in terms of mean cross-sectional holdup, $\bar{\varepsilon}_G$, as given below:

$$\varepsilon_G = \bar{\varepsilon}_G \left(\frac{n+2}{n+2-2c}\right)[1 - c(r/R)^n] \tag{3}$$

By applying eq.(3) to data, n was found to vary from 1.4 to11, and c from 0.5 to1 according to different authors (Joshi *et al.*, 1998) and based on different systems investigated. In the absence of a firm theoretical prediction of the radial gas hold up profile correlations are needed for evaluating n and c based on the knowledge of the general operating variables and physical properties of the system in order to estimate the gas holdup profile by eq. (3). In this work, such correlations have been developed as discussed below.

Correlation Development

Extensive gas holdup and gas holdup profile data have been acquired in the Chemical Reaction Engineering Laboratory (CREL) over the years under DOE contract DE2295PC95051 on the bubble column hydrodynamics, by employing gamma ray Computed Tomography (CT) over a range of superficial gas velocities (from 2 cm/s to 60 cm/s), at different pressures (0.1MPa to 1.0 MPa) with 5 different gas distributors and in columns ranging in diameter from 0.19-0.44 m. The majority of the gas holdup profiles were measured in air-water system. However, air-drakeoil (light mineral oil) and air-propanol systems were also used at different operating conditions. The reproducibility of the measured gas holdup profiles was within ± 3%. By analyzing the experimental results carefully it was found that the shape of holdup profiles changes most significantly with superficial gas velocities. However, Pressure affects the shapes of holdup profiles but it has less effect compared to superficial gas velocity within the range of pressure and superficial gas velocity that was examined. Gas distributor does affect holdup in a certain range of gas velocities but it has a minor effect on gas holdup profiles particularly in the fully developed region and at high gas velocity. The shape of the gas holdup profile at different column heights seems to be unchanged at a given gas velocity once the measurement has been taken at a certain distance from the distributor (2 L/D or higher). Column diameter has been reported to have an effect on gas holdup profile (Kumar *et al.*,1997).

Based on the experimental observations and dimensional analysis, the following functional dependence was proposed for parameters n and c:

$$n = af(\mathrm{Re}_G, Mo_L, Fr_G)\ ;$$

$$c = \beta\zeta(Re_G)$$

The above dimensionless groups, Re_G, Mo_L, Fr_G, which are defined below reflect the effect of velocity and pressure, which change the density of the gas and has an effect on gas holdup profile, and the effect of gas and liquid physical properties. By fitting roughly two thirds of the available experimental data from the database consisting of our experiments mentioned above and those in the literature (the remaining about one third of the experimental data set is used to evaluate the developed correlations), the correlations listed below are generated for n and c:

$$n = 2.188\times10^{3}\,\mathrm{Re}_G^{-0.598}\,Fr_g^{0.146}\,Mo_L^{-0.004} \tag{4}$$

$$c = 4.32\times10^{-2}\,\mathrm{Re}_G^{0.2492} \tag{5}$$

Where $\mathrm{Re}_G = \dfrac{DU_{Sg}(\rho_L - \rho_G)}{\mu_L}$, $Fr_G = \dfrac{U_{Sg}^2}{gD}$, $Mo_L = \dfrac{g\mu_L^4}{(\rho_L - \rho_G)\sigma_L^3}$

Equation (4) and (5) along with equation (3) are utilized for estimation of the gas holdup profiles for the whole set of the experiment data available. The cross sectional mean gas holdup, $\bar{\varepsilon}_G$, values used in this study were evaluated from the experimental data. However, a favorite correlation for the overall gas holdup can be used to estimate $\bar{\varepsilon}_G$ (Kemoun, et al., 2000).

As mentioned above, the majority of experimental data used were obtained by using an air-water system. Hence, based on the fitting performed in this study, n is almost independent of Mo_L $\left(n \propto Mo_L^{-0.004}\right)$. However, it was found that the liquid physical properties affect the overall gas holdup (Luo et al., 1999) and the holdup profile (Chen et al., 1998; Joshi et al., 1998). Therefore, at this stage, Mo_L is included in the correlation to be examined for any future necessary modification as gas holdup profiles become available for a wide enough range of liquid physical properties.

Due to the fact that most of the holdup profiles used were for air-water system, c was found to be only a function of Re_G. Liquid physical properties would affect the parameter c which need to be further examined.

Comparison of model predictions and experimental results

1. Effect of superficial gas velocity

As mentioned earlier, gas holdup profiles vary significantly with gas velocity. The results are shown in Figure 1.

One can see from Figure 1 that gas holdup profiles become steeper with increased gas velocity (n changes from 3.73 at 8 cm/s to 2.02 at 60 cm/s). The steeper holdup profile is, the faster liquid recirculation rate is, hence liquid mixing, heat transfer and mass transfer rate will be improved accordingly. From Figure 1, one can observe that model predicts the experimental results reasonably well (mean relative error is within 15%).

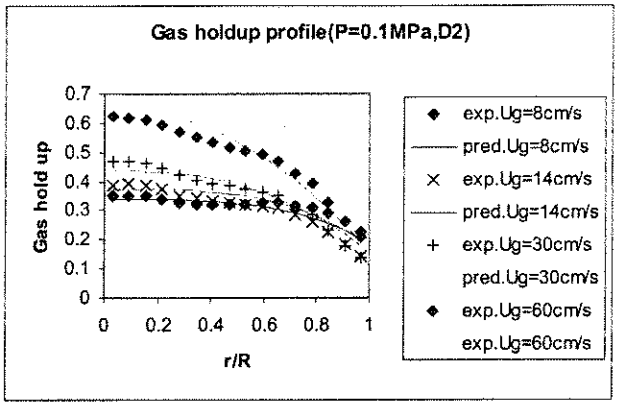

Figure 1 Effect of velocity on gas hold up profile
(Diameter of column: 0.15m, Distributor D2: Perforated plate, Hole diameter: 0.5mm,
Number of holes:163, Open area: 0.15%; P=0.1MPa;Water-air system)

2. Effect of reactor pressure

It is shown that pressure not only changes the gas hold up but also changes the gas holdup profile as well (Joshi *etal.*, 1998).

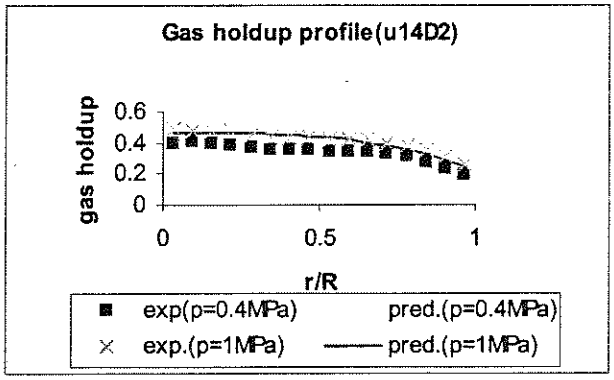

Figure 2 Effect of pressure on gas hold up profile in 0.15m reactor diameter
(Ug=14cm/s, Distributor D2:Perforated plate, Hole diameter: 0.5mm,
Number of holes: 163, Open area: 0.15%, Water-air system)

At higher pressure smaller bubbles are formed at the sparger due to high gas density (Luo et al., 1999). Small bubble size increases the overall gas holdup, and as pressure increases, gas bubble size distribution becomes narrow which results in a slightly flatter hold up profile due to the uniform distribution of small bubbles. As shown in Figure 2, at Ug=14cm/s as pressure varies from 0.4MPa to 1MPa there is no major difference in the shape of gas hold up profile (n values varies from 3.146 to 3.168). Unfortunately, currently there is no gas hold up profile available at higher pressure and higher gas velocity. For the operating condition studied, the model predicts the experimental results well (mean relative error is within 14%) .

3. Effect of physical properties

As mentioned earlier, both holdup distribution and liquid recirculation depend on liquid physical properties. A noncoalescing system and a coalescing systems have different overall gas holdup and gas holdup profiles as well. Figure 3 illustrates that the proposed correlations predict the experimental results reasonably well for liquids of different physical properties.

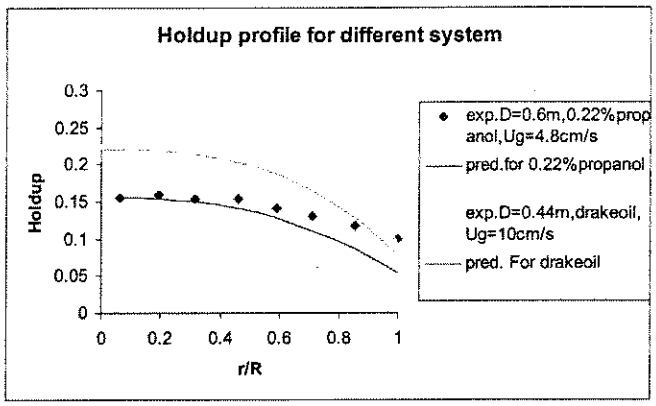

Figure 3 Effect of liquid physical properties on hold up profile
(Ug=4.8 cm/s, D=0.6m, air-0.22% propanol in water: Menzel *et al.*, 1990;
Ug=10cm/s, D=0.44m,air-drakeoil: Chen *et al.*, 1998)

It is noteworthy that two sets of the data presented in Figure 3 are taken from the literature (Menzel *et al.*, 1990; Chen *et al.*, 1998), and are predicted well by the developed correlations (mean relative error is within 17%). However, larger errors in the correlation predictions are obtained in the region near the wall for the data obtained from Menzel et al. (1990). This would be due to, as mentioned above, the majority of the measured holdup profiles used for the developed correlations (equations (4) and (5)) were obtained for air-water system which affect the dependency of the parameters n and c on the liquid physical properties.

4. Effect of column diameter

As reported in the literature (Joshi *et al.*, 1998) with increase in column diameter D, the liquid recirculation velocity increases as $V_c \propto D^{0.3to0.4}$. Hence, one would expect a steeper holdup profile in larger column diameter. This is not obvious from Figure 4 due to different superficial gas velocities used in columns of different diameter and this is the only available data at the moment.

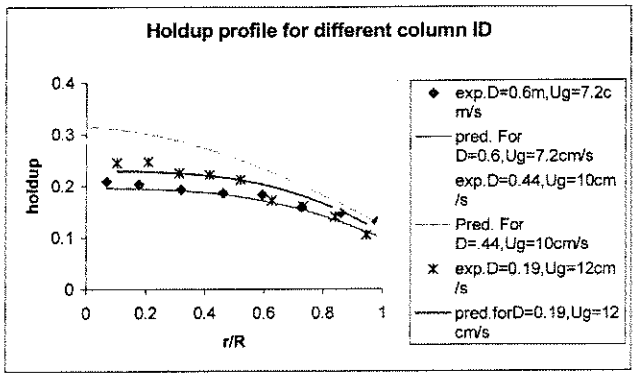

Figure 4 Effect of Column Diameter on the Holdup Profile
(Ug=7.2cm/s, D=0.6m: Menzel *et al*, 1990;Ug=10cm/s, D=0.44m: Chen *et al.*, 1998;
Ug=12cm/s, D=0.19m: Kumar, 1996)

Figure 4 shows the comparison of the correlations prediction and the experimental data at different column diameters. One can see that the prediction agrees with our experimental results and literature experimental data (mean relative error is within 15%).

Summary

It should be pointed out that in all the data presented here the cross sectional mean holdup $\bar{\varepsilon}_G$ was known. In a design situation, that would not be the case. Then a favorite correlation for the overall gas holdup can be used (Kemoun et al., 2000) to determine the mean holdup $\bar{\varepsilon}_G$ and the accuracy for our suggested radial holdup profile would naturally be affected by the accuracy of the correlation used to estimate $\bar{\varepsilon}_G$. A correlation is proposed for prediction of radial gas hold up profiles, which are important in driving liquid recirculation in bubble column. As Figure 1 to 4 illustrate the agreement between the correlation prediction and the experimental data is reasonable over a range of operating conditions (mean relative error is less than 17%). Further work considering gas-liquid-solid slurry system is still in progress.

References

Chen, J.W., Gupta, P., Sujatha, D., Al-Dahhan, M.H., Dudukovic, M.P. and Toseland, B.A.,1998, Gas Holdup Distribution in Large Diameter Bubble Columns, *Flow Measurement and Inst.*, 9(2), 91-101

Joshi, J.B., Veera, U Parasu, Parasad, Ch. V., Phanikkumar, D.V., Deshphande, N.S., Thakre, S.S. and Thorat, B.N., 1998, Gas Holdup Structure in Bubble Column Reactors *PINSA* 64,A, No4, 441-567

Kemoun, A., Ong, B.C., Gupta, P., Al-Dahhan, M.H., Dudukovic, M.P., 2000, Gas Holdup in bubble Columns at Elevated Pressure via Computed Tomography, (in press), *International Journal of Multiphase Flow*

Kumar, S. B., Moslemain D. and Dudukovic, M.P., 1997 Gas Holdup Measurement in Bubble Columns Using Computed Tomography, *AICHE J*, 43, 1414-1425

Luo, H. and Svendsen, H.F. 1991, Turbulent Circulation in Bubble Columns from Eddy Viscosity Distributions of Single-phase Pipe Flow, *Can. J. Chem.Eng.*, 69, 1389-1394

Luo, X., Lee, D.J., Lau, R., Yang, G., Fan., L.S., 1999, Maximum Stable Bubble Size and Gas Holdup in High-Pressure Slurry Bubble Columns, *AIChE J.*, 42, 4, 665-680

Menzel, Thomas, Thomas in der Weide, Staudacher, Oliver, Wein, Ondra and Onken, Ulfert, 1990, Reynolds Shear Stress for Modeling of bubble Column Reactors, *Ind.& Eng. Chem.Res.*, 29,988-994

Nassos, G.P. and Bankoff, S.G., 1967, Slip Velocity Ratios in An Air-water System under Steady-State and Transient Conditions, *Chem. Eng. Sci.* 22,667

Ueyama, K and Miyauchi, T., 1979, Properties and Recirculating Turbulent Two Phase flow in Gas Bubble Columns, *AICHE J,* 25,258

Nomenclature

c	Parameter in Eq(2)
D	Column diameter, m
Fr_g	Gas Froude number, dimensionless
g	Acceleration due to gravity, m/s^2
Mo_L	Liquid Morton number, dimensionless
n	Parameter in Eq(1)
r, R	Column radius, m
Re_G	Reynolds number, dimensionless
U_{Sg}	Superficial gas velocity, m/s
V_c	Liquid circulation velocity, m/s

Greek letters

$\varepsilon(r)$	Radial gas hold up profile
$\bar{\varepsilon}_G$	Cross-sectional average gas hold up
$\tilde{\varepsilon}_G$	Radial chordal average gas holdup
μ_L	Liquid viscosity, Pa.s
ρ_G	Gas density, kg/m^3
ρ_L	Liquid density, kg/m^3
σ_L	Liquid surface tension, N/m

Acknowledgement

The authors are thankful for the UCR-DOE grant (DE-FG26-99FT40594) which made this work possible. The support of CREL industrial sponsors and the Department of Energy via contract DE2295PC95051 is gratefully acknowledged as it made creation of the CREL database on holdup profiles possible.

PREDICTION OF AXIAL LIQUID VELOCITY PROFILE IN BUBBLE COLUMNS

See the attached report for:

A. Problem Definition
B. Research Objectives
C. Research Accomplishments

Prediction of Axial Liquid Velocity Profile in Bubble Columns

Yuanxin Wu* and M.H.Al-Dahhan†

Chemical Reaction Engineering Laboratory
Washington University, St.Louis, MO 63130, USA

Abstract

The liquid flow and mixing behavior in bubble columns is partially described by means of global liquid recirculation velocity profile. Due to the complex character of the flow in bubble columns, the prediction of the axial liquid circulation is still a difficult task. In this work the following correlation is proposed for the liquid recirculation profile:

$$\frac{V_L(r)}{V_{LO}} = 1 - 2.65 * n^{0.44} * c[\frac{r}{R}]^{2.65*n^{0.44}*c}$$

where n and c are the gas radial holdup parameters evaluated by the correlations proposed by Wu, Ong and Al-Dahhan (2000).

$$n = 2.188 \times 10^{3}\ Re_G^{-0.598}\ Fr_g^{\ 0.146}\ Mo_L^{-0.004}$$

$$c = 4.32 \times 10^{-2}\ Re_G^{0.2492}$$

The predictions of the developed liquid circulation correlation agree well with the experimental data obtained in our laboratory and reported in literature. The model is simple and is easy to use as an engineering tool to assess the liquid recirculation in bubble columns.

Key words: bubble columns, axial liquid velocity, correlation

Introduction

Bubble column reactors are widely used as gas-liquid and gas-liquid-solid contactors in industrial aerobic fermentations, hydrogenations and other chemical operations because of their simple construction and ease of maintenance. Bubble columns combine efficient gas transfer and mixing with low shear forces. The behavior of these reactors is determined by their hydrodynamic properties. The complex flow and mixing behavior found in bubble columns is often described by means of global parameters such as gas holdup and liquid circulation velocity. Due to the complex character of the flow in bubble columns, their design and scale up is still a difficult task.

Many models have been proposed to analyze and predict liquid circulation. Miyauchi and Shyu (1970) and Joshi and Sharma (1979) predicted liquid velocity in relation to the local gas holdup. However, the local gas holdup must be obtained from experimental data for both of these models. Zehner (1986) introduced a friction factor for liquid velocity prediction, but the value assigned by him to this parameter is not easy to justify. Kumar (1994) developed a one dimensional momentum balance based model which requires the holdup profile and eddy

* Current Address: Wuhan Inst. Of Chem. Tech., Wuhan, Hubei 430073, P.R.China
Email: wyx4@public.wh.hb.cn
†Corresponding author: Email: muthanna@wuche.wustl.edu, Tel: 314-935-7187, Fax: 314-935-7211

viscosity or mixing length profile to which the model is found to be very sensitive. Various attempts have been made at developing functional forms for the eddy viscosity (Ueyama and Miyauchi, 1979) and mixing length (Luo and Svendsen, 1991) which are required for solving the one dimensional model. However, Kumar (1994) showed that there is truly no universal expression for the mixing length or the eddy viscosity that can be successfully used under wide range of operating conditions, to predict the recirculating liquid velocity profile. In his mixing length correlation there are 5 parameters which are fitted to experimental data. Recently Krishna et al. (1999) proposed a computational fluid dynamics based model for prediction of holdup profile and axial velocity profile. CFD based model could be a powerful design and scale-up tool after it has been fully verified. This is not yet the case.

The objective of this work is to develop a simple model based on which axial velocity profile can be predicted in relation to the gas-input rate and the column dimensions without requiring as input the radial gas holdup profiles.

Model Development

A power law liquid velocity profile is widely accepted in the literature (Montserrat and Garcia-Calvo, 1996, Garcia-Calvo and Leton, 1994). The liquid rises with the bubbles in the central portion of the column and flows downward in the outer annular section. Hence, the liquid velocity distribution in a bubble column may be expressed as

$$\frac{V_L(r)}{V_{Lo}} = 1 - 2^{N/2}[\frac{r}{R}]^N \qquad (1)$$

N is the exponent of the liquid velocity profile and V_{Lo} is the liquid center line velocity. N varies from 2 - 2.3 or higher based on different reports (Kawase and Moo-Young 1986,1987, Montserrat and Garcia-Calvo, 1996). In fact, liquid circulation is due to the existence of the gas holdup radial profile, and the radial gas holdup profile and liquid circulation are intimately tied together. Both depend on superficial gas velocity, column diameter and the physical properties of the gas-liquid system investigated. The liquid according to the velocity profile of eq (1) is in central core region of the bubble column and flows downward in the wall zone.

A correlation of a similar form was proposed for prediction of the radial gas holdup profile (Luo and Svendsen, 1991):

$$\varepsilon_G = \bar{\varepsilon}_G \,(\frac{n+2}{n+2-2C})[1 - C(\frac{r}{R})^n] \qquad (2)$$

In eq. (2) n is indicative of the steepness of the gas holdup profile, and c determines the value of holdup near the wall. It provides for the possibility for both zero and non-zero gas volume fraction values at the wall which may affect the circulation of liquid as well. Possibly exponent N in eq. (1) also depends on the liquid properties and on the gas flow rates (Tobajas, 1996). Hence, it may be necessary to include both n and c in eq. (1) to predict the axial liquid velocity profile. To establish the needed relationship between the ga and liquid velocity profile, equation (1) is modified as:

$$\frac{V_L(r)}{V_{Lo}} = 1 - f(n,c)[\frac{r}{R}]^{g(n,c)} \qquad (3)$$

Correlations have been developed (Wu, Ong and Al-Dahhan, 2000) for calculation of parameters n and c as follows:

$$n = 2.188\times10^{3}\,\mathrm{Re}_G^{-0.598}\,Fr_g^{0.146}\,Mo_L^{-0.004} \qquad (4)$$

$$c = 4.32\times10^{-2}\,\mathrm{Re}_G^{0.2492} \qquad (5)$$

Where $\mathrm{Re}_G = \dfrac{DU_{Sg}(\rho_L - \rho_G)}{\mu_L}$, $Fr_G = \dfrac{U_{Sg}^2}{gD}$,

$$Mo_L = \frac{g\mu_L^4}{(\rho_L - \rho_G)\sigma_L^3}$$

By fitting our CARPT data, it was found that $f(n,c)=\xi(n,c)=2.65*n^{0.44}*c$. Therefore, eq. (3) becomes:

$$\frac{V_L(r)}{V_{LO}}=1-2.65*n^{0.44}*c[\frac{r}{R}]^{2.65*n^{0.44}*c} \quad (6)$$

As mentioned earlier, V_{Lo} is the axial liquid velocity in the center of the bubble column and can be obtained from either experiments or models reported by Zehner (1986) and Riquart (1981).

$$V_{LO}=0.737(U_G D)^{1/3} \quad \text{Zehaner (1986)} \quad (7)$$

$$V_{LO}=0.21(gD)^{1/2}(U_G^3\rho_L/g\mu_L)^{1/8} \quad \text{Riquart(1981)} \quad (8)$$

From eqs. (4) and (5), one can see that when the superficial gas velocity increases, c increases and n decreases. However n decreases with power 0.44 and c increases with power one, so that the overall effect is to render the axial velocity profile steeper with increased superficial gas velocity which is experimentally observed. The value of the term $f(n,c)=2.65*n^{0.44}*c$ is between 1.8 and 2.4 with column diameters of 0.1 to 0.63 m and for superficial gas velocity range of 0.02-0.6 m/s and different gas and liquid physical properties.

A predicted liquid velocity using eq. (6), with eqs. (4) and (5), is shown in Figure 1 and compared with experimental data. From Figure 1, it can be seen that the model matches experimental data well at different superficial velocities.

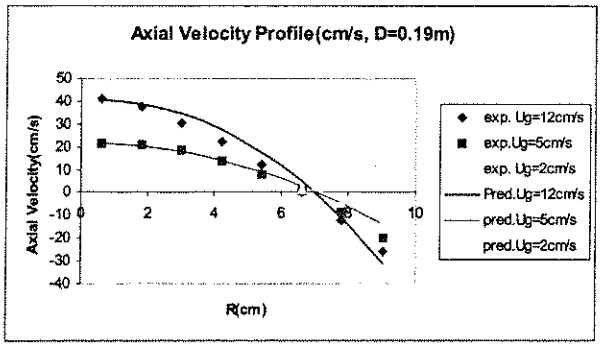

Figure 1 Comparison of model prediction and experimental data,
(CARPT Data for air-water system, Degaleesan, 1997)

Evaluation of model predictions

As mentioned above, eq. (6) was developed by only using part of our CARPT database, and it is necessary to determine whether eq. (6) can predict the experimental results from the literature to evaluate the capability of the modified model. We have compared the model predictions to the experimental data from very different sources reported in the literature and this comparison is illustrated below.

Figure 2 shows the comparison of model predictions and experimental data for small column diameter. It can been seen that for the column diameter equal to 0.172 m, the model can predict the axial velocity profile at different superficial gas velocity with reasonable accuracy. One can clearly see that the axial liquid velocity becomes steeper with the increase in superficial gas velocity, and the model predicts the point of zero velocity well. For the column diameter as big as 0.6 m, the comparison of model predictions and experimental data is plotted in Figure 3, from which it is evident that the similar predictions, as those represented in Figure 2, are observed.

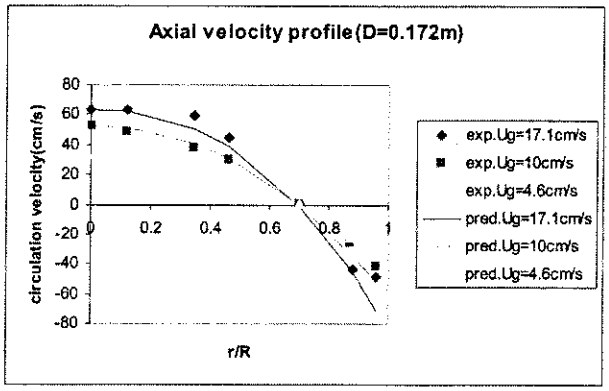

Figure 2 Comparison of model prediction and data of Pavlov (1969), Air-water system

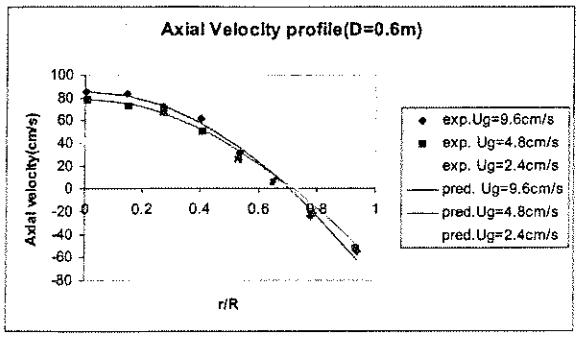

Figure3 Comparison of model prediction with the data of Menzel et al. (1990), Non-coalescence system.

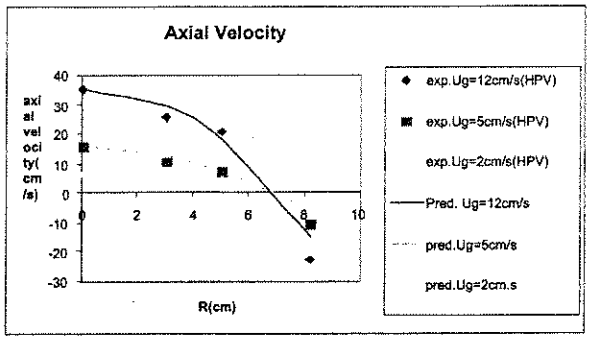

Figure 4 Comparison of model with the data from HPA (Heat Pulse Anemometry), Degaleeson, 1997

Figure 4 shows the model prediction of the data observed by Heat Pulse Anemometry techniques, and the comparison is good.

From Figure 2 to Figure 4, it is obvious that the model can predict the axial velocity profile of the experimental data within a range of conditions. This establishes that the proposed model could be used to predict axial velocity profile.

In order to compare the current model with the one dimensional model (Kumar, 1994, Luo and Svendsen, 1991), both predictions of the proposed model and the 1D model are plotted in Figure 5 and Figure 6 for comparison with experimental data.

One can see that the proposed model is in reasonable agreement with the one dimensional model prediction. However, it predicts the time averaged profile at superficial gas velocity of 0.17 m/s better than the 1D model prediction of Luo and Svendsen (1991).

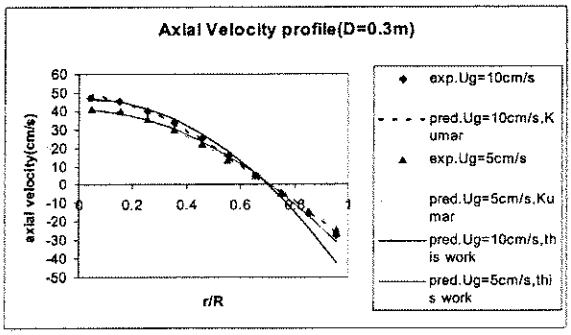

Figure 5 Comparison of this work with the CARPT data and one dimensional model (Kumar 1994)

It should be mentioned that the data in the above figures are not used in developing the model. In addition, with n and c developed under pressurized conditions, it may be possible for the model to predict the axial velocity profile in bubble columns operating at pressurized conditions. But this needs to be confirmed.

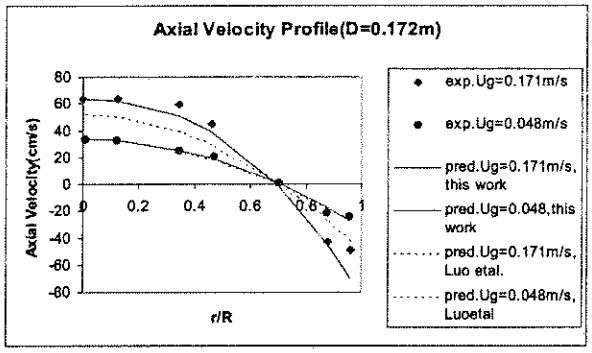

Figure 6 Comparison of this work and Luo and Svendsen (1991)
Model with experimental data

Summary

An existing model for prediction of the axial velocity profile is modified by using the correlations for the gas holdup n and c developed by Wu, Ong and Al-Dahhan (2000). The modified model can predict the experimental data reported in the literature well within a range of conditions. The model is simple and is easy to use as it requires as input only the superficial gas velocity, physical properties and column dimensions. The model can be readily used for prediction of the axial liquid velocity profile over a range of conditions, which should help the process engineers assess convective liquid mixing in bubble column rapidly.

Nomenclature

c	Parameter in Eq(2)
D	Column diameter, m
Fr_g	Gas Froude number, dimensionless
g	Acceleration due to gravity, m/s^2
Mo_L	Liquid Morton number, dimensionless
n	Parameter in Eq(2)
N	Parameter in Eq(1)
r, R	Column radius, m
Re_G	Reynolds number, dimensionless
U_{Sg}	Superficial gas velocity, m/s
V_c	Liquid circulation velocity, m/s
$V_L(r)$	Axial liquid velocity profile, m/s
V_{Lo}	Axial liquid velocity in the center of the column, m/s

Greek letters

$\varepsilon(r)$	Radial gas holdup profile
$\bar{\varepsilon}_G$	Cross-sectional average gas holdup
$\tilde{\varepsilon}_G$	Radial average gas holdup
μ_L	Liquid viscosity, Pa.s
ρ_G	Gas density, kg/m^3
ρ_L	Liquid density, kg/m^3
σ_L	Liquid surface tension, N/m

References

Degaleesan, Sujatha, Fluid dynamic measurement and modeling of liquid mixing in bubble columns, Ph.D. thesis, Washington University, St.louis, MO, USA, 1997

Garcia-Calvo, E., and Leton, P., 1994, Prediction of fluid dynamics and liquid mixing in bubble columns, Chem. Eng. Sci., 49(21), 3643-3649

Joshi, J.B. and Sharma, M.M., 1979, Circulation cells model for bubble columns. Trans. Inst. Chem. Eng., 57, 244-251

Kawase, Y. and Moon-Young, M., 1986, Liquid phase mixing in bubble column with Newtonian and non-Newtonian fluid, Chem.Eng.Sci., 41,1969-1977

Kawase, Y. and Moon-Young, M., 1987, Theoretical predictions of gas holdup in bubble column with Newtonian and non-Newtonian fluid, Ind.Eng.Chem.Res. 26,933-937

Krishna, R., Urseanu, M.I., van Baten, J.M., and Ellenberger J., 1999, Influence of scale on the hydrodynamics of bubble columns operating in the churn-turbulent regime: experiments vs. Eulerian simulations, Chem. Eng. Sci., 54(21), 4903-4911

Kumar, S.S., Computed Tomography measurements of void fraction and modeling of the flow in bubble columns, Ph.D. Thesis, Florida Atlantic University, Boca Raton, FL, USA, 1994

Luo H. and Svendsen H., 1991, Turbulent circulation in Bubble columns from eddy viscosity distributions of single-phase pipe flow, The Canadian Journal of Chemical Engineering, 69,1389-1394

Menzel, T., Weide, T., Staudacher, O., Wein, O., and Onken, U., 1990, Reynolds shear stress for modeling of bubble reactors, Ind. Eng. Chem. Res., 29, 988-994

Miyauchi, T., and Shyu, C.N. 1970, Flow of fluid in gas bubble columns, Kagaku Kogaku Ronbunshu, 34, 958-964

Montserrat, T., and Eloy Garcia-Calvo, 1996, Prediction of hydrodynamic behavior in bubble columns, J. chem. Tech. Biotechnol. 66, 199-205

Pavlov, V.P., 1965, Liquid circulation in a batch bubblier (in Russian) Khim. Promst. 9, 698-700

Riquarts, H.P., 1981, A physical model for axial mixing of the liquid phase for heterogeneous flow regime in bubble columns, German Chem.Eng., 4,18-23

Wu, Yuanxin, Boon Cheng Ong and M.H. Al-Dahhan, Prediction of gas holdup profiles in bubble column reactors, Chem. Eng. Sci., (2000), (ISCRE-16)

Zehner, P., 1986, Momentum, mass and heat transfer in bubble columns, Part1 Flow model of the bubble column and liquid velocities, Int. Chem. Eng., 41, 1969-1977

Acknowledgement

The authors are thankful for the UCR-DOE grant (DE-FG26-99FT40594) which made this work possible. The support of CREL Industrial sponsors and the Department of Energy via Contract DE2295PC95051 is gratefully acknowledge as it made creation of the CREL database on holdup and liquid velocity profiles possible.

GAS HOLDUP IN TRAYED BUBBLE COLUMNS

See the attached report for:

A. Problem Definition
B. Research Objectives
C. Research Accomplishments

Gas Holdup in a Trayed Cold-Flow Bubble Column

A. Kemoun[a], R. Novica[a], F. Li[a], M. H. Al-Dahhan[a], M. P. Dudukovic[a]
P. L. Mills[b,*], T. M. Leib[c], J. J. Lerou[d]

[a]Chemical Reaction Engineering Laboratory, Department of Chemical Engineering,
Washington University, St. Louis, MO 63130-4899, USA
[b]Chemical Science and Engineering Laboratory, DuPont Central Research and Development,
Experimental Station, E304/A204, Wilmington, DE 19880-0304, USA
[c]Reaction Engineering Consultants, DuPont Engineering Technology,
1007 Market Street/N6404, Wilmington, DE 19898-0001, USA
[d]DuPont Nylon Intermediates, Sabine River Laboratory, Orange, TX 77630, USA

Abstract

An experimental study was performed to investigate the effect of sieve trays on the time-averaged gas holdup profiles and the overall gas holdup in a cold-flow bubble column that was scaled-down from a commercial unit. γ-ray Computed Tomography (CT) was used to scan the column at several axial locations in the presence and absence of trays from which the local variation of the gas holdup was extracted. The overall gas holdup was also determined using the same configuration by comparing the expanded and static liquid heights. Air and water were used as the gas-liquid system. The superficial gas and liquid velocities were selected to span the range of the commercial system using gas spargers having multiple lateral distributors that were also scaled-down from the commercial design. To investigate the impact of sparger hole density on the local and overall gas holdup, two difference sparger designs were used in which the hole density per lateral was varied. The gas hole velocity was maintained constant at ca. 245 m/s, which approached that used in the commercial reactor.

It is shown that the local gas holdup determined by CT is generally higher in the tray down comer region and exhibits an asymmetric pattern when trays are present. The use of increased sparger hole density at a constant gas superficial velocity leads to steeper gradient in the gas holdup near the column centerline and a higher overall gas holdup. These findings suggest that the performance of bubble column reactors for various applications is sensitive to both sparger and tray design.

Keywords: Bubble column; Multiphase; Internals; Holdup; Tomography; Trays; Profiles; Spargers

1. Introduction

Stage-wise mass transfer operations, such as distillation, extraction, absorption, leaching, ion exchange, and drying, to name a few, typically utilize processing equipment with internals to promote intimate contacting between the various phases so that phase equilibrium can be approached for a given stage (cf., King, 1971; Sherwood *et al.*, 1975). When mass transfer is accompanied by chemical reaction in a multiphase contactor, the incorporation of internals is generally known to reduce the overall back mixing of each phase so that the benefits of reactor operation as an ideal cascade can be approached (Westerterp *et al.*, 1984). Besides modifying the microscale and macroscale flow patterns of the various phases, the addition of internals could alter various hydrodynamic and transport parameters that can potentially impact reactor performance, such as fluid holdups, multiphase flow pressure drop, phase voidage distributions, local fluid mixing, interphase mass transfer coefficients, and interfacial areas.

The ability to either scale-up new multiphase reactors, or to analyze the performance of existing ones, is clearly dependent upon understanding and quantifying local transport-kinetic interactions, flow and contacting patterns of the various phases, and how these change with operating conditions (Dudukovic *et al.*, 1999). For certain types of more common internals, such as trays and packing, used in staged mass transfer contactors, a significant body of literature exists on scale-up guidelines and methods for estimating hydrodynamic and transport parameters using empirical correlations (cf., Fair, 1985; Sloley, 1999). Information on the selection and performance of internals in gas-liquid catalytic reactors, such as trickle-beds, bubble-columns, and ebullated beds, is very limited in the open literature. For example, the use of perforated trays to reduce liquid-phase back mixing in bubble columns has been summarized by Deckwer (1992), while gas holdup and pressure drop data from two different tray designs has also been reported (Chen *et al.*, 1986). Most of the information on internals is usually confined to either patent teachings (cf., Nutter, 1995; Resetarits, 1992), or is maintained as company proprietary knowledge for a specific process. Hence, experimental data on such devices would be useful in certain multiphase reactor applications, as their performance is needed for rational selection and design purposes. With the continuing evolution of advanced fluid dynamic simulations of multiphase systems (Dudukovic *et al.*, 1999; Kuipers and van Swaaij, 1997), and invention of non-

invasive experimental methods for monitoring of multiphase flows (Chaouki *et al.*, 1997), the development of improved constitutive relationships for more accurate fluid dynamical predictions in complex geometries will continue to evolve. Hence, *a priori* prediction of how various internals affect the multiphase fluid dynamics in the absence of chemical reaction should eventually become more reliable. Experimental data that can be used for guiding the design and scale-up of reactors with the current state-of-the-art approaches is still required, however.

The primary objective of this work is to perform an experimental study on the hydrodynamics of a cold-flow bubble column reactor with trays that was scaled-down from a commercial unit, and to compare the results to those obtained for the empty reactor, *i.e.*, to the identical unit without any trays. Particular emphasis is placed upon the effect of the sparger design (hole density) and the trays on the local gas holdup profiles as measured by γ-ray Computed Tomography (Kumar *et al.*, 1995) and overall gas holdup as determined by the fast shutoff of the gas and liquid lines.

2. Cold-flow unit experimental system

The cold flow system is equipped with a column along with various sub-systems for feeding and controlling the volumetric flow rates of air and water. The liquid delivery system was connected to a centrifugal pump and the rotameter to control the liquid flow rate. The liquid was introduced to the top of the column through a shower-type distributor that was located about 13.9 cm above the top tray (Figure 1). The liquid exited the column bottom through a plenum, and then flowed into a surge tank. A second centrifugal pump was used to recycle the liquid back to the main feed tank. The air was supplied from the house supply system, which had a delivery pressure of about 841 kPa. After flowing through a filter, it was introduced to a rotameter and then connected to the sparger.

A schematic of the cold-flow column design is provided in Figure 1. It was constructed of clear acrylic tubing, and had a nominal diameter of 0.2-m and an overall height of 2.4-m. The column was divided into four sections where each section had an overall height of 0.52-m. Three sieve trays were located between each section. The top and bottom trays were used to account for entrance and exit effects.

Several ports were installed in the middle stage and also across the trays so that pressure transducers and liquid conductivity probes could be inserted for local measurement of the pressure fluctuations and liquid-phase tracer concentrations. Another identical column without these ports was also constructed and used for the γ-ray Computed Tomography (CT) measurements. The ports were omitted to reduce the interference of the nuclear radiation that might otherwise occur during collection of the tomographic data.

A schematic of the tray design and hole layout is shown in Figure 2. The trays were constructed of 6.35 mm thick acrylic sheet and contained 42 holes having a diameter of 6.35 mm each that were laid out on a triangular pitch. The down comer occupied about 10% of the total tray cross-sectional area. The latter was a copy of the one used in the commercial system, which was mounted flush with the top of the tray.

The dimensions for the column diameter, tray spacing, tray geometry, and tray hole diameter were determined by applying scaling principles to a commercial-scale system. The key concepts that were used included equality of gas and liquid mass velocities, hydrodynamic head, tray hole velocity and pressure drop, and phase residence times on a stage. The details are omitted for brevity but appeared to provide a reasonable first basis for scale-down of the commercial system.

The spargers in the cold-flow unit were scaled down using operating conditions and mechanical data extracted from the commercial-scale sparger design. To obtain gas mass velocities in the cold-flow unit that were in the same range as those used on a given tray in the commercial system, a gas jet velocity of ca. 180 to 245 m/s from each respective sparger hole was required.

Details on the sparger design are shown in Figure 3. Ten laterals were welded to the main gas distribution manifold with the lateral lengths being selected so the sparger fits into the column with a clearance of 6 to 12 mm. As shown in Figure 4, each lateral was drilled with either 40 or 200 holes with a hole diameter of 350 μm. The total number of holes in a lateral was varied to maintain nearly the same gas hole velocity as the gas volumetric flow rates were varied from 0.944, 2.36, and 4.72 liters/s at STP. The holes were drilled to give an offset angle of 30 degrees from the vertical and were arranged so they pointed downward. The sparger assembly was mounted 0.41 m below the first tray from the bottom of the column. The gas was introduced to the main sparger supply line through a 9.5-mm o.d. manifold.

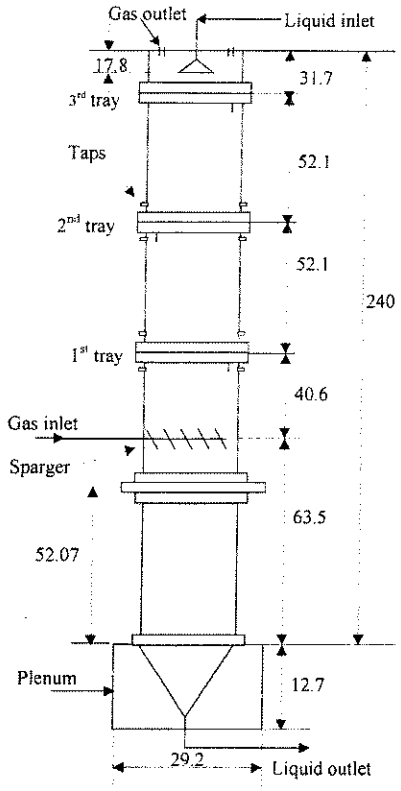

Figure 1. Schematic diagram of the column used for the cold-flow studies. (all dimensions are given in cm).

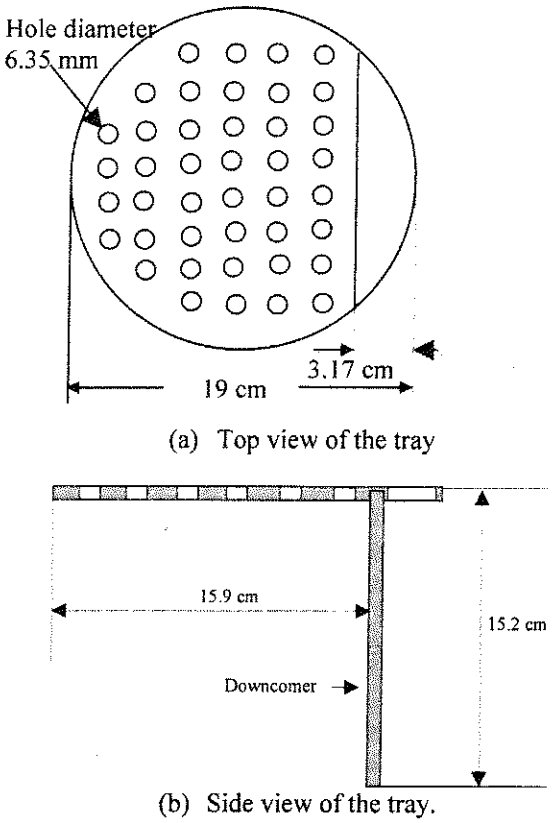

Figure 2. Schematic of the tray design.

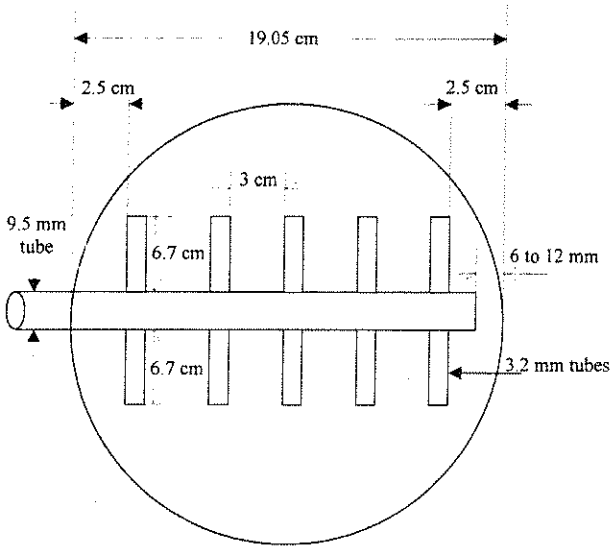

Figure 3. Design of the gas sparger.

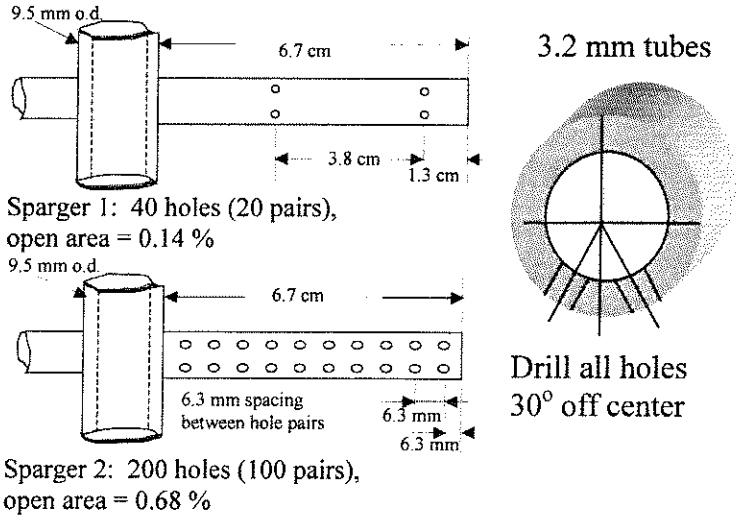

Figure 4. Details on the hole schedule for the gas sparger laterals.

The operating conditions, which were scaled down from the commercial reactor system, used in this study are summarized below in Table 1.

Table 1. Range of Operating Conditions

Liquid flow rate (liters/s)	0.13 - 0.41
Gas flow rate (liters/s)	1.98 – 4.75
Gas velocity through the sparger holes:Sparger #1 Gas velocity through the sparger holes:Sparger #2	$U_h \cong 245.24$ m/s at superficial gas velocity U_g=3.33 cm/s $U_h \cong 245.24$ m/s at U_g=16.65 cm/s
Gas and liquid phases	Air and water
Liquid superficial velocity U_l (cm/s)	0.4 – 1.42
Gas superficial velocity U_g (cm/s)	1.6 – 16.7

3. γ-ray computed tomography

Computed Tomography (CT) was used to determine the time-averaged cross-sectional variation of the gas holdup at various axial column locations. The particular axial positions where CT scans were made are shown in Figure 5. These were selected to provide gas holdup profiles both above and below the first tray, below the second tray, and halfway between the first and second trays. To assess the effect of sparger hole density on the gas holdup profile, the CT scans were performed at levels 2 - 4 using the sparger having the lowest hole density (sparger no. 1, Fig. 4), at a superficial gas velocity of 3.33 cm/s and superficial liquid velocity of 0.44 cm/s and 0.88 cm/s, respectively. The CT scans were then repeated at all axial locations shown in Figure 5 using the sparger having the greatest hole density (sparger no. 2, Fig. 4) at U_g=16.65 cm/s and U_l=0.44 cm/s and U_l=1.1 cm/s, respectively. To assess the effect of the trays on the local gas holdup profiles, the trays were removed and the scans were repeated at the latter set of conditions as well a U_l=0 cm/s corresponding to a batch liquid.

The scanner used here is based upon a third generation fan-beam configuration developed at Washington University. Details of the hardware and software have been described in previous work (Kumar *et al.*, 1995 and 1997). The scanner design consists of an array of NaI (TI) detectors with a diameter of 5 cm as well as an encapsulated 92 mCi Cs^{137} source located opposite to the center of the array of detectors. Five detectors were used for the present study, which can cover the whole cross section of the column. The detectors and the source are mounted on a plate, which can be rotated around the axis of the column by a stepping motor that is controlled through a microprocessor. Moreover, the whole assembly can be moved in the axial direction along the column to scan different axial levels of the column. This design of the CT scanner yields a spatial resolution of ca. 0.35 cm in the horizontal direction and 1.0 cm in the vertical direction.

The tomographic attenuations were measured along a number of beam paths through the column from different coordinates. Once a set of attenuation measurements was completed, the density distribution image was reconstructed by using a suitable reconstruction algorithm. In this work, the Estimation-Maximization (Kumar, 1994) was used since it has the following advantages: (1) it accounts for statistical variations associated with radiation measurements; (2) it readily incorporates non-uniform beam effects; and (3) it ensures that the final reconstruction will contain positive values. To obtain statistically significant results, and to reduce the effect of position, the CT scans were conducted around the column using a total scanning time of two hours.

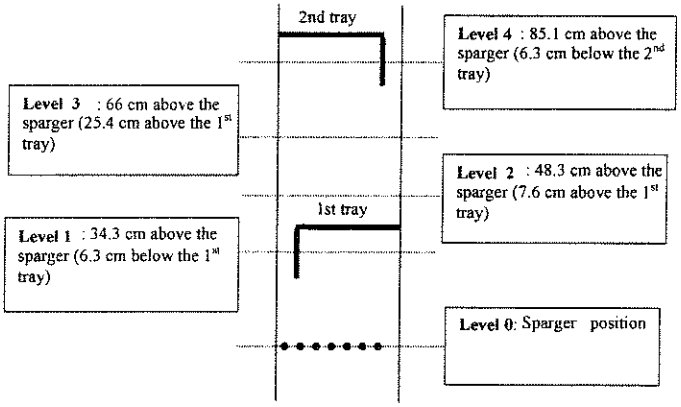

Figure 5: Axial positions of the CT scans

4. Results and discussion

Both the local and overall gas holdups obtained in the presence and absence of the trays as determined by Computed Tomography and the simultaneous shutoff of the gas and liquid lines technique are compared in this section for the two different types of sparger designs.

4.1. Computed tomography results

Figure 6a shows that the gas holdup distribution at level 2, which is 7.62 cm above the 1st tray, is asymmetric,. Figure 6b shows that when the superficial liquid velocity is increased to 1.1 cm/s, the asymmetry is more pronounced. The region of high gas holdup contours show that the maximum gas holdup at level 2 is ca. 11% at U_l=0.44 cm/s (Figure 6a) and ca. 10.5% at U_l=1.1 cm/s (Figure 6b).

Figure 7a is similar in concept to Figure 6a, except it shows the gas holdup distribution at level 3, which is 25.4 cm above the 1st tray. The gas holdup distribution between the trays is now symmetric at both superficial liquid velocity of 0.44 and 1.1-cm/s, respectively. This differs from the results in Figure 6a corresponding to level 2 (7.6 cm above the 1st tray), where the gas holdup distribution was asymmetric at the same liquid flow rates. Inspection of the gas holdup distribution contours shows that the maximum gas holdup decreases from 13.3% at U_l=0.44 cm/s (Figure 7a) to 12.1% at U_l=1.1 cm/s (Figure 7b).

Figure 8 shows the gas holdup distribution at level 4, which is 6.35 cm below the 2nd tray. A region of reduced gas holdup occurs in the tray down comer region. The regions of higher gas holdup are positioned in the center of the column for U_l=0.44 cm/s. This region of increased gas holdup moves further from the down comer when the superficial liquid velocity is increased from 0.44 cm/s to 1.1 cm/s.

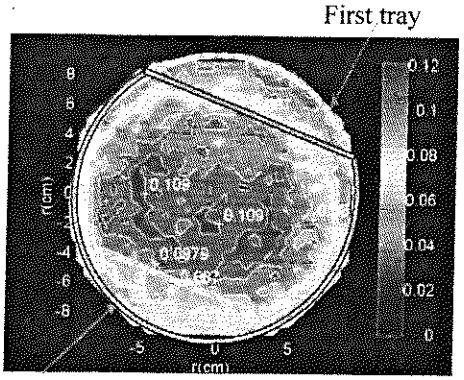

(a) U_g=3.3 cm/s and U_l=0.44 cm/s.

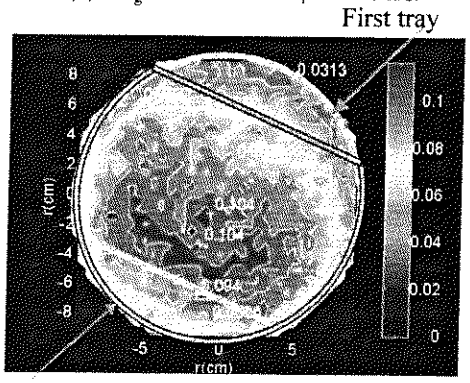

(b) U_g=3.3 cm/s and U_l=1.1cm/s.

Figure 6. Gas holdup distribution for sparger no. 1 at level 2.

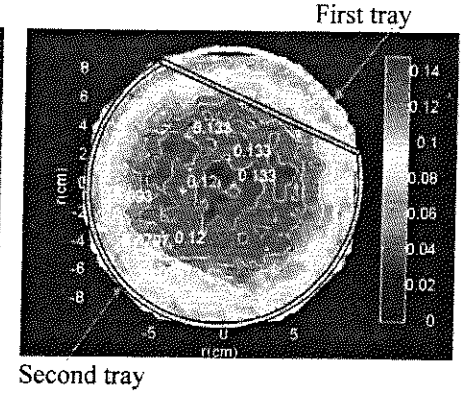

(a) U_g=3.3 cm/s and U_l=0.44 cm/s.

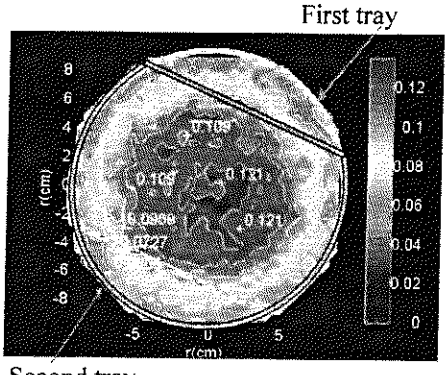

(b) U_g=3.3 cm/s and U_l=1.1cm/s.

Figure 7. Gas holdup distribution for sparger no. 1 at level 3.

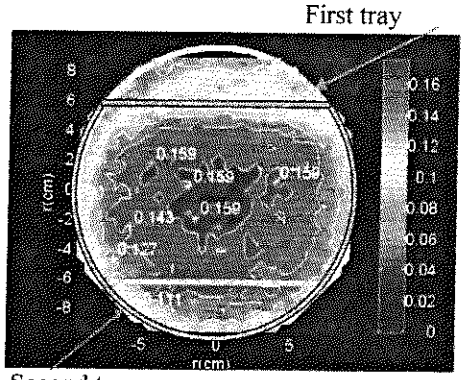

(a) U_g=3.3 cm/s and U_l=0.44 cm/s.

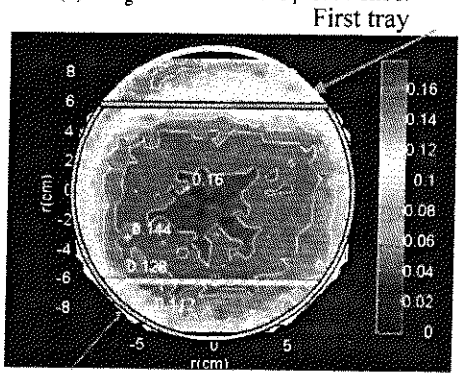

(b) U_g=3.3 cm/s and U_l=1.1cm/s.

Figure 8. Gas holdup distribution for sparger no. 1 at level 4.

The experiments described above, which correspond to the sparger having a low hole density, were repeated using the sparger having the highest hole density. The same superficial liquid velocities were used (0.44 cm/s and 1.1 cm/s, respectively), but the superficial gas velocity was increased from 3.3 cm/s and 6.6 cm/s to 16.6 cm/s so that the same gas jet velocity was maintained through the sparger holes. A comparison between the gas holdup profiles for the two different spargers shows that at level 1, which is just 6.35 cm below the 1st tray, the highest gas holdup occurs in the center of the column at both liquid flow rates. The holdup is relatively insensitive as the superficial liquid velocity is increased from 0.44 cm/s to 1.1 cm/s at U_g=16.6 cm/s, which is the highest rate used. The same behavior is also noted at level 2, which is 7.62 cm above the first tray, except a region of lower gas holdup occurs closest to the column wall.

The symmetry of the cross-sectional gas holdup at level 3 allows the azimuthally time-averaged radial gas holdup profiles to be determined. The results are compared in Figure 9 at various gas and liquid flow rates. At the highest superficial gas velocity (U_g=6.7 cm/s), the gas holdup profile increases as the superficial liquid velocity is increased from U_l=0.44 cm/s to U_l=1.1 cm/s. At the lowest superficial gas velocity used (U_g=3.3 cm/s), the opposite behavior occurs, i.e., the gas holdup profile decreases when the liquid flow rate increases. At level 3 which is halfway between the two trays, and level 4, which lightly below the second tray, the gas holdup is relatively insensitive to variations in liquid flow rate. The region of the lowest gas holdup is in the down comer or slightly below it.

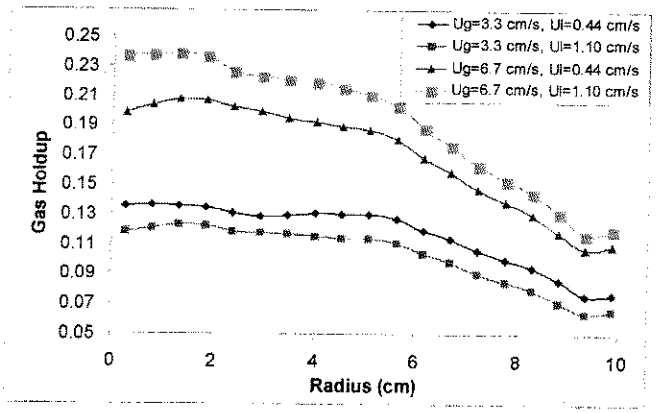

Figure 9. Azimuthally time-averaged radial gas holdup at the middle of the stage obtained with sparger no. 1.

CT scans were also conducted by removing the trays to create an open column interior. The superficial liquid velocities used were 0 cm/s (batch liquid), 0.44 cm/s and 1.1 cm/s, while the superficial gas velocity was set at U_g=16.6 cm/s. The scanner was positioned halfway between the first and second trays, which corresponds to level 3 in Figure 5.

A comparison between the gas holdup profiles obtained in the presence and absence of trays is given in Figure 10. The CT data for the situation where trays were removed was first processed to evaluate the azimuthally time-averaged radial gas holdup associated with uniform bubbles whose diameters were visually estimated to be about 5 to 10 mm (upper set of data points). Next, the azimuthally time-averaged radial gas holdup was also determined for the experiment associated with the large bubbles of 30 to 50 mm bubble sizes that mainly exist in the center of the column (lowest set of data points). This difference in these two experiments was the result of different surface tension due to the impurity of the water, which infected the system as for example one-drop of oil can generate formation of large bubbles. These large bubbles rise quickly and lead to a decreased gas holdup. The gas holdup profiles obtained for the column with trays is seen to fall between the gas holdup of the uniform bubbles and large bubbles. The highest gas holdup for this case is obtained at the lowest superficial liquid velocity used (0.44 cm/s). The presence of both the uniform and large bubbles in the empty column suggests that two different hydrodynamic regimes exist in the same column due to the purity of the water.

Figure 10 also shows that the gas holdup profiles obtained in the empty column without trays are only slightly affected by the liquid flow rate over the range of superficial liquid velocities (0, 0.44 cm/s and 1.1 cm/s) that were studied. The gas holdup profiles for the empty column have a larger gradient than those obtained in the column with trays. This finding suggests that one function of the trays is to create an obstacle for the uniform bubbles, and to induce bubble coalescence to produce some large bubbles. These larger bubbles eventually escape the stage through the down comer and are captured by the second tray. The flow visualization also reveals the appearance of large bubbles that are about 20 to 30 mm in diameter in the trayed column. The CT scans also confirm that a high concentration of gas exists below the trays, which seems to induce bubble coalescence.

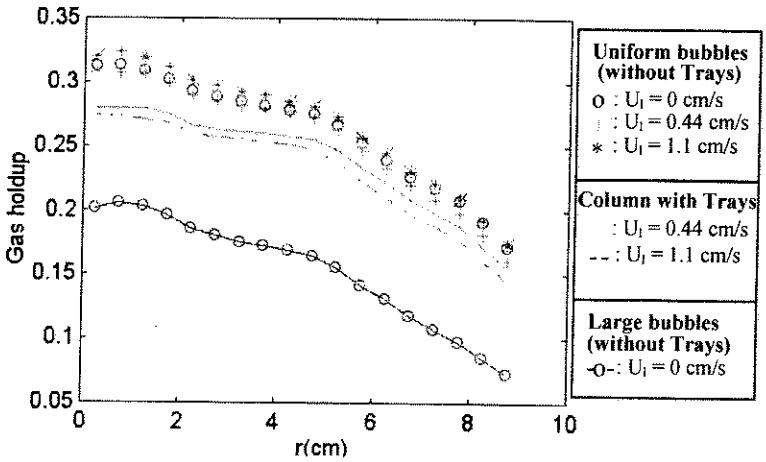

Figure 10. Comparison of the gas holdup profiles at a superficial gas velocity Ug=16.6 cm/s at various liquid flow rates in a column with and without trays.

4.2. Overall gas holdup

The combined effects of the sparger hole density, gas flow rate, liquid flow rate, and presence or absence of sieve trays on the overall gas holdup were determined using the simultaneous shut-off of the air, input and output water lines. The difference between the expanded height (before the shut-off) and the static height (after the shut-off) leads to the overall gas holdup

It is well accepted that gas sparger design and performance can have a significant effect on both the local and overall gas holdups in bubble column reactors. Use of fundamental mass and momentum conservation principles to provide detailed *a priori* predictions of performance for typical commercial-scale spargers using computational fluid dynamics is not possible using existing knowledge. This is mainly due to the existence of a large number of sparger holes that are typically present in commercial-scale gas-sparger designs, and difficulties associated with modeling high velocity, multiple interacting gas jets into a gas-liquid dispersion. Another complicating feature is that the gas sparger performance is also dependent on the column aspect ratio as well as the liquid physical properties, both of which influence coalescence and breakup of the gas bubbles (Kumar, 1994).

The sparger designs used here were identical except for the total number of sparger holes, which translates into a difference in the hole density or the number of holes per unit column cross-sectional area. The total number of holes per lateral and hole diameter was selected so that the same gas velocity through the holes could be obtained when the superficial gas velocity changed from U_g=3.3 cm/s to 16.6 cm/s. This particular range for the superficial gas velocity produced a gas velocity that approached the commercial system, namely, u_h = 245 m/s.

Figure 11 compares the effect of the number of sparger holes on the overall gas holdup as a function of the gas flow rate at a constant liquid volumetric flow rate. The sparger with the greatest number of holes per unit column cross-sectional area (sparger no. 2) always provides a larger overall gas holdup over the indicated range of gas and liquid volumetric flow rates. The same trend in the gas holdup was observed at other liquid flow rates. For a given sparger, the gas velocity through the sparger holes was variable owing to the use of variable gas volumetric flow rates.

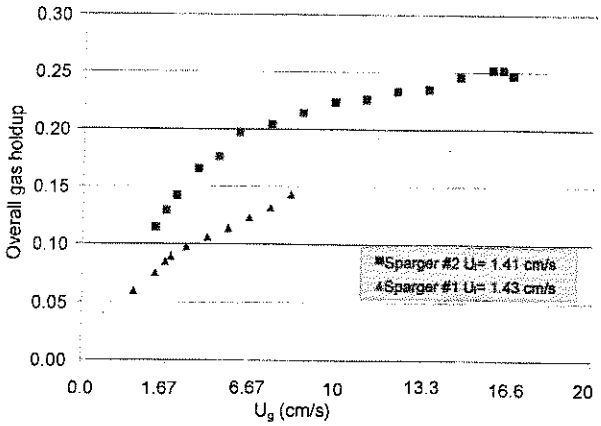

Figure 11. The effect of sparger no.2 hole density on the overall gas holdup.

The results for sparger having the lowest density of holes are shown in Figure 12. When the superficial gas velocity exceeds U_g=4.2 cm/s, the overall gas holdup increases when the superficial liquid velocity is increased from U_l=0.44 cm/s to U_l=1.1 cm/s for a fixed value of the superficial gas velocity. However, when the superficial liquid velocity is increased further from U_l=1.1 cm/s to U_l=1.43 cm/s, the overall gas holdup undergoes a reduction for a fixed value of the superficial gas velocity. This behavior could be due to the formation of larger bubbles by coalescence of smaller bubbles. It should also be noted that when the sparger is operated at a superficial gas velocity of 3.3 cm/s, the gas velocity through the sparger holes is nearly the same as that used in the commercial unit (u_h = 245 m/s).

The overall gas holdup data obtained using the sparger having the greatest density of holes per unit cross-sectional area of the column are illustrated in Figure 13. When superficial gas velocities exceed 4.16 cm/s, the overall gas holdup decreases as the superficial liquid velocity is increased from 0.44 cm/s to 0.77 cm/s, and from 1.1 cm/s to 1.41 cm/s. However, at a superficial gas velocity of U_g=16.65 cm/s, which translates into a gas hole velocity for the commercial unit (u_h = 245 m/s) for this particular sparger hole density, the overall gas holdup slightly increases when superficial liquid velocity is increased from 0.44 cm/s to 0.77 cm/s. The overall gas holdup then decreases slightly when the superficial liquid velocity is increased further to 1.41 cm/s.

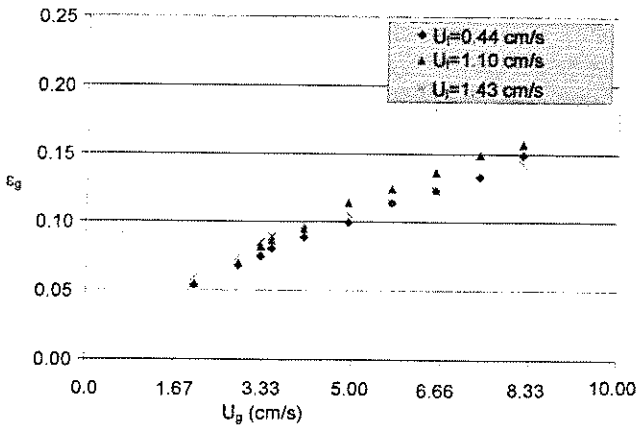

Figure 12. Overall gas holdup using the sparger no.1

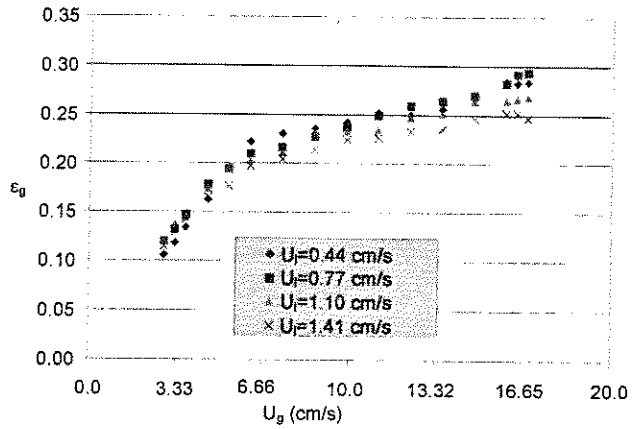

Figure 13. Overall gas holdup using the sparger no.2

The CT-based results for the time-averaged cross-sectional gas holdup profiles that were obtained between trays 1 and 2 (middle of the stage) with sparger no. 1 show that when $U_g < 5$ cm/s, the gas holdup decreases slightly when the superficial liquid velocity is increased from 0.44 cm/s to 1.10 cm/s. However, when $U_g > 5$ cm/s, the gas holdup increases when the superficial liquid velocity is increased from 0.44 cm/s to 1.10 cm/s. This agrees with the trend for the overall gas holdup that is illustrated in Figure 12, which provides some partial confirmation between the two independent experimental methods.

The effect of column internals on the overall gas holdup was also investigated by removing the trays and repeating the measurements using identical values for the superficial gas and liquid velocities. It was found that the overall gas holdups were nearly the same, even though the axial and radial profiles were not. For the geometry and conditions studied in this work, this appears to contradict arguments suggesting that the trays reduce bubble coalescence and produce higher overall gas holdups.

5. Summary and conclusions

An experimental system was developed to study the local and overall gas holdup in a trayed bubble column reactor under cold-flow conditions. Many commercial bubble column reactors employ trays and other types of internals to control gas-liquid contacting, but limited design information is available.

The gas holdup profiles were determined using γ-ray Computed Tomography. Measurements were made at different axial locations using two different gas spargers. The gas holdup profiles are generally affected by the superficial velocities of the gas and liquid, the gas sparger geometry, and the presence or absence of the trays. The gas holdup distribution can be either symmetric of asymmetric depending upon various hardware and operational variables. The gas holdup generally decreases from the column center toward the column wall, and the region of higher gas holdup can shift toward the wall with an increase in the superficial velocity of the liquid. The effect of the number of sparger holes per lateral on the gas holdup cannot be neglected and needs to be carefully considered for a given set of process conditions.

The gas holdup profile in bubble column reactors is affected by the presence of internal trays that provide a staging effect, as well as by the sparger design. The use of available engineering correlations for prediction of gas holdup can lead to incorrect estimates since they are based on empty bubble columns without any internals.

The overall gas holdup was also measured using spargers having a different hole density over a range of gas and liquid superficial velocities. The holdup was relatively unaffected by the liquid superficial velocity for the range studied ($0.46 \leq U_l$ (cm/s) < 1.52 cm/s), but it increased with increasing gas superficial velocity. The effect of column internals on the overall gas holdup was also investigated by removing the trays and repeating the measurements using identical values for the superficial gas and liquid velocities. It was found that the overall gas holdups were nearly the same, even though the axial and radial profiles were not. For the geometry and conditions studied in this work, this appears to contradict arguments suggesting that the trays reduce bubble coalescence and produce higher overall gas holdups.

6. References

Chaouki, J., Larachi, F., and Dudukovic, M. P. (Eds.) 1997. Non-invasive Monitoring of Multiphase Flows. Elsevier, Amsterdam.

Chen, B. H. 1986. Axial dispersion and heat transfer in gas-liquid bubble columns. In Handbook of Heat and Mass Transfer, Volume 2: Mass Transfer and Reactor Design (N. P. Cheremisinoff, Ed.), pp. 1005-1028. Gulf Publishing, Houston.

Dudukovic', M. P., Larachi, F. and Mills, P. L. 1999. Multiphase reactors – revisited. Chemical Engineering Science 54, pp. 1975-1995.

Fair, J. R. 1985. Stagewise mass transfer processes. In Scaleup of Chemical Processes (A. Bisio and R. L. Kabel, Eds.), pp. 431-503. Wiley-Interscience, New York.

King, C. J. 1971. Separation Processes, pp. 146-211. McGraw-Hill, New York.

Kuipers, J. A. M. and van Swaaij, W. P. M. 1997. Application of computational fluid dynamics to chemical reation engineering. Reviews in Chem. Engg 3, 1.

Kumar, S. B. 1994. Computer tomographic measurements of void fraction and modeling of the flow in bubble columns. Ph.D. Thesis, Florida Atlanta Unviersity, Boca Raton, FL.

Kumar, S. B., Moslemian, D. and Dudukovic', M. P. 1995. A gamma-ray tomographic scanner for imaging void fraction distribution in bubble columns. Flow Meas. Instr. 6, 61.

Kumar, S. B., Dudukovic', M. P. and Toseland, B. A. 1997. Measurement techniques for local and global fluid dynamic quantities in two and three-phase systems. In Non-invasive Monitoring of Multiphase Flows (J. Chaouki, F. Larachi and M. P. Dudukovic', Eds.), pp. 1-46. Elsevier, Amsterdam.

Nutter, D. E. Nov. 21, 1995. Gas-liquid contacting apparatus including trays with vapor apertures in overlapping panel margins. US Patent 5,468,425.

Resetarits, M. R. Mar. 24, 1992. Multiple down comer contacting tray with fluid-directing baffles. US Patent 5,098,615.

Sherwood, T. K., Pigford, R. L., and Wilke, C. R. 1975. Mass Transfer, pp. 593-666. McGraw-Hill, New York.

Sloley, A. W. 1999. Should you switch to high capacity trays?. Chemical Engineering Progress 94, pp. 23-35.

Westerterp, K. R., van Swaaij, W. P. M. and Beenackers, A. A. C. M. 1987. Chemical Reactor Design and Operation, pp. 160-226. Wiley, Chicester.

A NOVEL SIGNAL FILTERING METHODOLOGY FOR OBTAINING LIQUID PHASE TRACER RESPONSES FROM CONDUCTIVITY PROBES

See the attached report for:

A. Problem Definition
B. Research Objectives
C. Research Accomplishments

A Novel Signal Filtering Methodology for Obtaining Liquid Phase Tracer Responses from Conductivity Probes

Puneet Gupta[a], Muthanna H. Al-Dahhan[a†], Milorad P. Dudukovic'[a], Patrick L. Mills[b]

[a] Chemical Reaction Engineering Laboratory
Department of Chemical Engineering
Campus Box 1198
One Brookings Drive, Washington University
St. Louis, Missouri 63130-4899, USA

[b] DuPont Central Research and Development Experimental Station
E304/A204
Wilmington, DE 19880-0304, USA

† Corresponding Author
Tel: (314) 935-7187
Fax: (314) 935-7211
E-mail: muthanna@wuche.wustl.edu

Abstract

Local conductance measurements using a conductivity cell, consisting of electrode plates encased in plastic tubing, have been employed for point conductance measurements in two-phase gas-liquid flows. It is shown that such measurements can provide local liquid mixing information in gas-liquid flows such as those encountered in bubble and staged bubble columns either with an upward flow of gas in a batch liquid, or with co-current or counter-current flow of gas and liquid. This requires the characterization of the liquid phase conductance from the electrical signals acquired by such a conductivity probe (cell) in the presence of bubbles, which is non-trivial due to the systematic lowering of the conductance of the probe measurement volume when a bubble contacts or pierces the probe tip. Thus, application of standard digital filtering techniques to signals masked by frequent bubble passage results in an inaccurate representation of liquid conductance by filtered signals. A special purpose software filtering technique has been developed in this work to address this issue and to cleanly extract the actual liquid phase conductance from response signals representing the instantaneous point conductance of a bubbling two-phase gas-liquid mixture. The implementation of the new filtering algorithm has been achieved through coupling with standard Butterworth filters in MATLAB™ Ver. 5.

Keywords: Gas-liquid flow, bubble column, conductivity probes, signal filtering.

Introduction

Bubble columns are extensively used in hydrogenation, oxidation, hydroformylation, chlorination, fermentation and natural gas conversion processes to fuels and chemicals. Often it is important to assess the state of mixing of the liquid phase. In bubble columns without baffles or trays, it is typically assumed that the liquid is perfectly mixed. When departure from complete backmixing is desired, staging of the bubble columns via trays/baffles is required (Shah *et al.*, 1982). Since information in the open literature on liquid backmixing in bubble columns with trays is very sparse, we undertook to study it experimentally. In order to accomplish this, we had to determine a suitable method for measuring tracer concentration in the liquid phase, unmasked by the presence of the gas, and to evaluate what state of mixing frequencies can be captured by the selected conductivity measurement equipment. We found that the solution to this problem was non-trivial and decided to share our findings in this manuscript.

Electrical conductance/capacitance probes have been frequently used for the estimation of bubble properties in gas-liquid/gas-solid flows as well as in gas-liquid-solid fluidized beds (Svendson *et al.*, 1998; Gunn and Al-Doori, 1985; Buchholz *et al.*, 1981; Werther and Molerus, 1973). In addition, signals from conductivity probes, which are calibrated to provide instantaneous point phase holdup information, have been used for experimental characterization of regime transitions in multi-phase flows from time-series data utilizing sophisticated numerical tools (Briens *et al.*, 1996). In several other studies, where the quantity of interest is just the time-averaged phase holdup, probe designs (plate and ring-shaped electrodes) different than those employed for instantaneous conductance

measurements have been used (Hu *et al.*, 1985; Andreussi, *et al.*, 1988; Fossa, 1998; Zrymiak and Hill, 1986; Cartellier and Achard, 1991; Tsochatzidis, *et al.*, 1992; Hassan and Rush, 1985).

The conductivity probes can also be utilized to estimate liquid phase velocities and to study local liquid mixing in single as well as two-phase systems by the measurement of liquid phase electrolytic tracer concentrations (Choi, 1996; Boddem and Mewes, 1996; Sokolov and Mashaal, 1990; Rustemeyer *et al.*, 1989; Shah *et al.*, 1978). Traditional application of conductivity measurements involved the characterization of the liquid phase concentrations of tracer ionic species in solutions devoid of gas. When such measurements are used to obtain the overall liquid phase residence time distribution (RTD) in single-phase flow, little ambiguity is encountered in the interpretation of conductivity-probe signals, as they are free from *biased-noise* contributions, which due to bubble passage, are inevitable in two-phase flow. However, the usual noise contributions associated with the electronics etc. are present irrespective of whether the signals were measured in a single or a two-phase system. Such noise components are readily removed by using appropriate filters, *viz.*, the filters available in the Signal Processing Toolbox (MATLAB™ Ver. 5).

Experimental evidence indicates that signals acquired using conductivity probes in two-phase gas-liquid flows are corrupted due to significant systematic lowering of the measured conductivity when a bubble hits the probe. This systematic bias in the measured conductance in gas-liquid flows has frequently limited the use of such probes for tracer experiments. As the conductivity of the gas is appreciably smaller than that of the liquid containing an electrolyte as tracer, one observes frequent dips in the measured

electrical conductance signal as bubbles pass over the probe measurement volume. If one were to apply standard filtering techniques, one obtains a filtered signal that is always an underestimate of the actual signal, which one would measure if there were no bubbles (gas) present in the system. This is because the noise component, which one is trying to remove, has a non-zero mean and this causes the filtered signal to under-predict the actual value.

Rustemeyer *et al.* (1989) tried to avoid the signal corruption due to bubble passage by mechanically screening the probe tips. However, the screening of the probe tips to avoid completely the presence of gas can never be perfect, and the signals shown in their article still seem to carry some information due to bubble interaction with the probe tips. Other researchers have tried to resolve the signal corruption due to bubble passage by standard data filtering techniques (Boddem and Mewes, 1996). However, the filtered tracer response seems to have lost some information for the very reasons mentioned above. Standard digital signal filtering procedures assume that the signal component to be filtered has a zero mean, which happens to be the case only with random noise associated with either the measuring device or fluctuations in the electrical signals. As mentioned earlier, the interaction of the bubbles with the conductivity probes causes a systematic lowering (bias) of the measured signals. If this systematic lowering of the signals were to be considered as noise, the mean of such a noise component is not zero, and standard filtering algorithms do not work very well in removing them out. Therefore, interpretation of data from the tracer experiments in gas-liquid flows becomes non-trivial as standard filtering techniques for removing un-biased noise (with zero mean) from the conductivity probe signals are not applicable.

An in-house special purpose software filtering technique has been developed that can effectively tackle the problem of extracting meaningful information about the liquid phase conductance alone, from data with systematic corruption obtained in two-phase gas-liquid systems. The advantage of using a software-based filter over a hardware filter is that the acquired signal can be tested against several software filters, whereas a hardware filter permanently filters the original signal, which is no longer accessible for further processing. The filtering technique developed in this work is first demonstrated on numerically generated signals and is subsequently applied to experimental data sets acquired in a counter-current staged bubble column.

Experimental Setup

Figure 1 shows the experimental setup of an 8" diameter counter-current staged bubble column, which was used to acquire the experimental data sets on which the developed filtering technique is demonstrated. The column is made of clear acrylic using air as the gas phase and tap water serving as the liquid medium. A liquid distributor at the top and a gas distributor at the bottom maintain counter-current flow of liquid and gas, respectively. The column is sectioned by the use of three trays each having 42 holes ¼" in diameter. The air sparger has 40 holes of 0.35 mm in diameter, which are evenly distributed as shown in Figure 2. The conductivity probes (MI-900 Series conductivity electrodes) used in this study were obtained from Microelectrodes Inc. Each probe is interfaced to a 486 PC via a data acquisition board (AT-MIO-16E-10 with a 12-bit resolution and a sampling rate of 100 kS/sec) from National Instruments. The probes

consist of two electrodes (platinum black coated) approximately 3 mm apart, which are encased in plastic tubing. The probes are connected to conductance meters (YSI Model 35), and the output from the meters is sent to the data acquisition board.

A pair of conductivity probes was used to acquire the experimental data with the two probes spatially configured as shown in Figure 3. In this configuration, the first probe (Probe_0) was positioned in the downcomer region of Tray 2, whereas, the other probe (Probe_1) was placed in the center of the column just below Tray 1. To assess the ability of the developed filtering technique to reliably extract the liquid phase conductance in response to an impulse tracer injection, three different operating conditions of the gas and liquid flow rates were used as summarized in Table 1. Impulse tracer injections were made in the liquid inlet stream before the liquid distributor for each of the three operating conditions. The injected tracer consisted of 10-ml of 0.2-gm/ml KCl solution and was introduced at the top of the column into the showerhead with the aid of a syringe. The start of the injection was controlled to the accuracy of a tenth of a second with the help of a stopwatch. The data acquisition system was initiated exactly a minute before the actual injection of tracer was made. This was done to aid in filtering the data later as well as to get an in-situ baseline measurement. The tracer injection time was 2.5 ± 0.5 seconds for all the runs.

Problem Description

Figure 4 shows the signals obtained from the conductivity probe exposed to three different media, specifically air, water and air-water. The sampling frequency for data

acquisition was 100 Hz with a total sampling time of 60 seconds. It can be clearly seen from the figure that the signals obtained from measurements in air and in water (single-phase measurements) have minimal un-biased noise associated with fluctuations in the supply voltage. However, the signals from the gas-liquid system with turbulent bubbling of gas in batch liquid, show significant systematic lowering of the signal when bubbles interact with the probe surface. Our objective is to be able to extract, from signals acquired in gas-liquid systems, the liquid phase conductance devoid of biased noise resulting from frequent bubble passage over the probe tips. As mentioned earlier, if standard filtering algorithms are employed for data filtering, then the filtered signal is systematically under-predicted. This is shown in Figure 5, where a second order Butterworth filter (MATLAB™ Ver. 5) was used to filter the signal from the gas-liquid system, and obtain filtered responses. Two cut-off frequencies (0.5 Hz and 0.05 Hz) were used to filter the signals. It can be seen from Figure 5 that in spite of a very low cut-off frequency of 0.05 Hz, the filtered signal is an under-prediction of the signal measured in water. To overcome the difficulty associated with standard filtering techniques explained above, it was realized that some kind of threshold criterion has to be resorted to so that one is able to get the uncorrupted signal. The details of the developed filtering algorithm and its ability to filter out the biased noise due to bubble passage from the conductivity probe signal are presented below.

Description of the Filtering Algorithm

The filtering algorithm developed as part of this work involves the steps below and presented as a flow chart in Figure 6. Coupled with the thresholding criterion is the use of Butterworth filters from the Signal Processing Toolbox (MATLAB™ Ver. 5) in the procedure to filter the conductivity-probe signals to remove the biased noise due to bubble passage. The steps involved in this procedure are:

1. The raw signal, RS(t), is first subjected to a regular Butterworth filter to obtain the filtered signal FS(t).
2. The filtered signal, FS(t), is further processed as follows. At each time instant, if the filtered signal, $FS(t_i)$, is lower than the raw signal, $RS(t_i)$, then the transformed response is made equal to the raw signal. However, if at that instant, the filtered signal is higher or equal to the raw signal, the filtered signal, $FS(t_i)$, is accepted as the transformed signal without any modifications. This procedure is referred to as thresholding. The resulting transformed signal, FST(t), is the filtered plus thresholded signal.
3. A residual (RES) is calculated, which is equal to the square root of the sum of the squares of the differences between the raw (RS) and filtered plus thresholded (FST) signals, divided by the total number of data points in the time-series.
4. If this residual is less than a certain tolerance (TOL - 5×10^{-6} volts in this case), then the filtered plus thresholded response is taken to be the final filtered response,

otherwise the filtered plus thresholded signal replaces the raw signal, RS(t) = FST(t), and the process is repeated by returning to Step 1.

5. This procedure is continued until the tolerance criterion is met.

The choice of the tolerance (TOL) in general will depend upon the system being studied, and can be estimated from a few test runs in the specific gas-liquid system under investigation. Too strict a tolerance could however, result in over-smoothing of the signal, and consequently, a loss of information.

Results and Discussion - Implementation of the Filtering Algorithm

Figure 7 shows the results of the above algorithm applied to the raw signal in Figure 4. Here we coupled a Butterworth filter of order 2 with the new filtering procedure and performed the filtering operation, using the same two cutoff frequencies (0.5 Hz and 0.05 Hz) to compare the performance of the new technique with that of the standard filter. One can immediately see from the figure that the new filtering algorithm has performed much better in extracting a very reasonably smooth signal from the raw data, and that the final filtered signal is relatively independent of the cutoff frequency. However, this observation may not be general, as the desired final signal is obvious from visual inspection and is relatively easy to extract as it has insignificant amplitude variation. Therefore, the most important question that remained to be answered was whether this technique could be applied to a signal, which resembles a signal similar to one that one would obtain while measuring the impulse response of an electrolytic tracer in the liquid (water) phase.

To answer this important question, a numerically generated signal resembling a typical response to an impulse tracer injection, was created. This signal was then added to the raw signal (shown in Figure 4) acquired in a bubbling air-water system. The numerically generated signal was created using the following expression:

$$\left.\begin{aligned} y_{num} &= y_{raw} && t \le 5 \\ y_{num} &= y_{raw} + 4.0 * \left\{ (t-5) * exp\left(-\frac{t}{2}\right) + (t-5)^3 * exp\left(-\frac{3t}{2}\right) \right\} && t \ge 5 \end{aligned}\right\} \qquad (1)$$

where y_{raw} is the air-water signal in Figure 4.

The performance of the standard and new filtering algorithms on the signal obtained from this numerical tracer test is shown in Figure 8a. Upon visual observation again, one can see that the new technique has been able to extract the equivalent liquid phase conductance much better than standard Butterworth filters. Two different cutoff frequencies were tested to study their effect on the final filtered signals. As before, even with a higher cutoff frequency, the new algorithm has performed better than the standard filtering procedure. To test the algorithm on an experimental data set, the filtering procedure was applied to raw conductivity signal of Probe_0 obtained under operating conditions of Experiment 1 as shown in Table 1. From Figure 8b, one can see that the algorithm has been successful in producing the desired level of data reduction, and standard filtering algorithm results in loss of information specially near the peak of the experimental response. Thus, by the above filtering plus thresholding procedure, we are retaining frequencies less than or equal to the cutoff frequency as the successively filtered signal relaxes to the final filtered plus thresholded signal.

Characteristic Response Time of the Conductivity Probes

When acquiring point liquid phase tracer responses, another important issue that needs to be addressed is that of the probe response time. At a sampling frequency of 100 Hz and a total sampling time of eleven minutes needed for the tracer (electrolytic KCl solution) to completely exit the system, it was anticipated that enormous amount of raw data would be acquired. This might not provide any additional information than if the data were acquired at a lower sampling frequency; as a high sampling frequency only results in storage of non-significant data. A sampling frequency of 100 Hz would imply by the Nyquist criterion that one is capturing actual phenomena with the frequency-content up to 50 Hz. This would only be true if the conductivity measurement system has an overall response time approximately 3-5 times faster than 20 milliseconds to ensure that the measured signal relaxes to 95-99% (assuming first order response) of the final value when a step change in conductance occurs.

The details of the experimental procedure to determine the probe response time are discussed in the next section. The characteristic response time of the probes is around 75 milliseconds (assuming first order response), which corresponds approximately to a frequency of 13 Hz. A characteristic probe response time of ~ 75 milliseconds implies that with such a probe one could confidently monitor a process having a characteristic time of greater than ~ 400 milliseconds. In other words, one cannot expect to capture reliably any phenomena that have characteristic frequencies higher than 2-3 Hz. The characteristic frequency of the tracer washout curves, for typical bubble column experiments, is in the range $1x10^{-3}$ - $1x10^{-2}$ Hz. This range is two orders of magnitude

lower than the highest frequencies that these probes can capture, implying that the use of these probes for the current work is well justified. Therefore, a sampling frequency 3-5 times the highest characteristic frequency that can be captured with these probes (2-3 Hz) would be approximately 10 Hz. Hence, 10 Hz was chosen as the sampling frequency for all the tracer experiments on the counter-current staged bubble column.

The approximate characteristic-response time of the probes was determined experimentally by modeling the time for the probe signal to rise from that in air to that in tap water by a first order process with zero dead-time. The experiment was repeated five times by dipping the conductivity probe into tap water (with the aid of a stopwatch) and the characteristic response time taken as an average from these five repetitions. The results of such an experiment are shown in Figure 9. Unfortunately, due to the relatively poor de-wetting characteristics of the probes, the reverse experiment to determine the fall time of the probe signal, when the probe is withdrawn out of tap water into air did not yield any useful information.

In general, the choice of the cut-off as well as of the sampling frequencies will depend on the smallest characteristic time-scale that one is trying to capture from these experiments. It should be pointed out that this method (or for that matter any other) will lead to significant errors when the smallest characteristic frequency that one wants to capture is of the same order as that corresponding to bubble passage, breakup and coalescence. It has recently been reported by Letzel *et al.* (1997) that in bubble columns of industrial importance, characteristic frequencies of O (10^0 Hz) are related to overall liquid circulation; those of O (10^1 Hz) are related to bubble passage, coalescence and breakup; while those of O (10^2 Hz) are associated with the turbulence microscale in the

system. Therefore, a natural question to ask was if similar information could be obtained from the conductivity probe signals acquired in a gas-liquid turbulent bubbling system. If bubbles are expected to exhibit a similar frequency response in this system as well, then to satisfactorily capture the characteristic frequency due to bubble passage with the conductivity probes, one has to have the characteristic response time of the probe to be at the most 20–30 milliseconds. This obviously is not the time resolution of the probes we are currently using. Thus, one would not be able to distinctly see a frequency corresponding to bubble-passage with these probes; and probes with a better time resolution are required for such a purpose.

Results and Discussion – Tracer Tests in Counter-Current Staged Bubble Column

To test the feasibility of the developed filtering technique on experimentally acquired data as opposed to a numerically generated one, impulse tracer injections were made as described in the section on 'Experimental Setup'.

Figure 10 shows the tracer response curves for the two probes utilized in studying the inter-stage mixing at the three operating conditions. One can immediately see that the developed filtering technique has been successful in cleanly extracting the liquid phase impulse tracer responses. As can be seen from Table 1, experiments 1 and 2 were performed to examine the effect of the liquid flow rate, while experiments 2 and 3 were conducted to characterize the effect of the gas flow rate. Since the liquid flow rate for experiments 2 and 3 was the same, one can see from the Figures 10(b) and 10(c) that the impulse responses of the two probes in these experiments are very similar even though

the gas holdups under these two operating conditions were significantly different. From Figure 10, one can also see that the liquid flow rate has a significant effect on the tracer response curves. This comes as no surprise as the tracer response curves have to get washed out approximately three times as fast for a liquid flow rate of 6.5 GPM vs. a flow rate of 2.0 GPM. Also, a higher liquid flow rate enhances the radial mixing on the stage and hence, the tracer response curves get washed out almost uniformly throughout the stage.

From Figure 10, one can also see that the trays provide the desired effect of staging for the liquid phase in the bubble column which inherently results in reduced backmixing. When one calculates the cross-correlation of the two signals, the maximum occurs with the signal from Probe_1 lagging the signal from Probe_0. Table 2 shows the characteristic time by which the signals arriving at Probe_1 lag those that arrive at Probe_0 under different operating conditions. The characteristic lag time provides a good estimate of the mean residence time of the liquid phase between the two probes. Knowing the distance between the probes (20 inches in this case), one can estimate the average interstitial liquid velocity between the two probes (which takes into account the average gas holdup between the two probes) by dividing the distance between the probes by the above time lag or lead (Table 2). However, the obtained information about the velocity is only a long-time average between the two points, and not an instantaneous velocity.

Conclusions

A new filtering methodology has been developed to extract liquid phase tracer responses from conductance measurements obtained in two-phase gas-liquid systems undergoing turbulent bubbling. By properly choosing a cut-off frequency, and coupling that with the thresholding algorithm described above, one is able to extract reliable information from conductivity probe signals regarding liquid macro-mixing in gas-liquid media. The new filtering approach has been demonstrated through experimental measurements characterizing liquid mixing in a trayed bubble column operated with counter-current flow of gas and liquid. This new filtering methodology opens up the possibility of its use in many potential industrial and research applications.

Acknowledgments

The authors acknowledge the financial support from DuPont Central Research and Development for this work.

Nomenclature

FS	filtered signal, volts
FST	filtered plus thresholded signal, volts
RES	residual in the filtering algorithm, volts
RS	raw signal, volts
t	time, sec
TOL	tolerance criterion in the filtering algorithm, volts
y_{num}	numerically generated raw signals for Figure 8, volts
y_{raw}	air-water raw signals in Figure 4, volts

References

Andreussi, P., Di Donfrancesco, A., and Messia, M., 1988, An impedance method for the measurement of liquid hold-up in two-phase flow, *Int. J. Multiphase Flow*, **14**(6), 777-785.

Boddem, M., and Mewes, D., 1996, Two-phase flow in the upper plenum of a PWR during ECC, International Conference on Nuclear Engineering, **1**, Part B, 813-823, ASME 1996.

Briens, C. L., Hudson, C. and Briens, L. A., 1996, Rapid characterization of flow regimes in multiphase reactors through box-counting dimensions with an embedding dimension of two, *Chem. Eng. J.*, **64**, 169-178.

Buchholz, R., Zakrzewski, W. and Schügerl, K., 1981, Techniques for determining the properties of bubbles in bubble columns, *Int. Chem. Eng.*, **21**(2), 180-187.

Cartellier, A., and Achard, J. L., 1991, Local phase detection probes in fluid/fluid two-phase flows, *Rev. Sci. Instrum.*, **62**(2), 279-303.

Choi, K. H., 1996, Circulation liquid velocity in external-loop airlift reactors, *Korean J. Chem. Eng.*, **13**(4), 379-383.

Fossa, M., 1998, Design and performance of a conductance probe for measuring the liquid fraction in two-phase gas-liquid flows, *Flow Meas. Instrum.*, **9**(2), 103-109.

Gunn, D. J. and Al-Doori, H. H., 1985, The measurement of bubble flows in fluidized beds by electrical probe, *Int. J. Multiphase Flow*, **11**(4), 535-551.

Hassan, Y. A., and Rush, G. C., 1985, A new technique for estimation of void fraction from conductivity probe signals in a small break loss-of-coolant accident test facility, *The American Society of Mechanical Engineers*, Presented at the Winter Annual Meeting, Miami Beach, Florida – Nov. 17-21, 1985.

Hu, Z., Yu, B. and Wang, Y., 1985, Studies on the local hold-up and liquid velocity distribution in G-L-S three phase fluidized bed, *Chem. Reaction Eng. Tech.*, **1**(3), 66-73.

Letzel, H. M., Schouten, J. C., Krishna, R. and van den Bleek, C. M., 1997, Characterization of regimes and regime transitions in bubble columns by chaos analysis of pressure signals, *Chem. Eng. Sci.*, **52**(24), 4447-4459.

MATLAB, 1997, Version 5, The MATH WORKS Inc., Boston, MA.

Rustemeyer, U., Pauli, J., Menzel, T., Buchholz, R., and Onken, U., 1989, Liquid-Phase Mixing Model for Hydrodynamics of Bubble Columns, *Chem. Eng. Process.*, **26**, 165-172.

Schibler, J. A., December 1997, Improving precision and accuracy with software-based signal filtering, *American Laboratory*, 52-54.

Shah, Y. T., Kelkar, B. G., Godbole, S. P., and Deckwer, W. D., 1982, Design Parameter Estimations for Bubble Column Reactors, *AIChE J.*, **28**(3), 353-379.

Shah, Y. T., Stiegel, G. J., and Sharma, M. M., 1978, Backmixing in Gas-Liquid Reactors, *AIChE J.*, **24**(3), 369-400.

Sokolov, M., and Mashaal, M., 1990, Velocity measurements in slow flow by the conductance-tracer method, *Experiments in Fluids*, **9**, 252-256.

Svendson, H. F., Luo, H., Hjarbo, K. W. and Jakobsen, H. A., 1998, Experimental determination and modeling of bubble size distributions in bubble columns, *Chinese J. of Chem. Eng.*, **6**(1), 29-41.

Tsochatzidis, N. A., Karapantsios, T. D., Kostoglou, M. V., and Karabelas, A. J., 1992, A conductance probe for measuring liquid fraction in pipes and packed beds, *Int. J. Multiphase Flow*, **18**(5), 653-667.

Werther, J. and Molerus, O., 1973, The local structure of gas fluidized beds – I. A statistically based measuring system, *Int. J. Multiphase Flow*, **1**, 103-122.

Zrymiak, T. L. and Hill, G. A., 1986, Probe for measuring local gas holdups in saline potash pulps, *Can. J. Chem. Eng.*, **64**(2), 341-345.

List of Figures

List of Tables

Table 1. Operating Conditions for Various Tracer Experiments.

Experiment Number	Gas Flow Rate (SCFH)	Liquid Flow Rate (GPM)	Gas Superficial Velocity (cm/sec)	Liquid Superficial Velocity (cm/sec)
1	118	2.0	3.25	0.44
2	118	6.5	3.25	1.44
3	236	6.5	6.51	1.44

Table 2. Characteristic Lag/Lead times of Probe_1 signals w.r.t. Probe_0 signals.

Experiment Number	Gas Flow Rate (SCFH)	Liquid Flow Rate (GPM)	τ_{LAG} (sec)
1	118	2.0	73.4
2	118	6.5	40.1
3	236	6.5	30.7

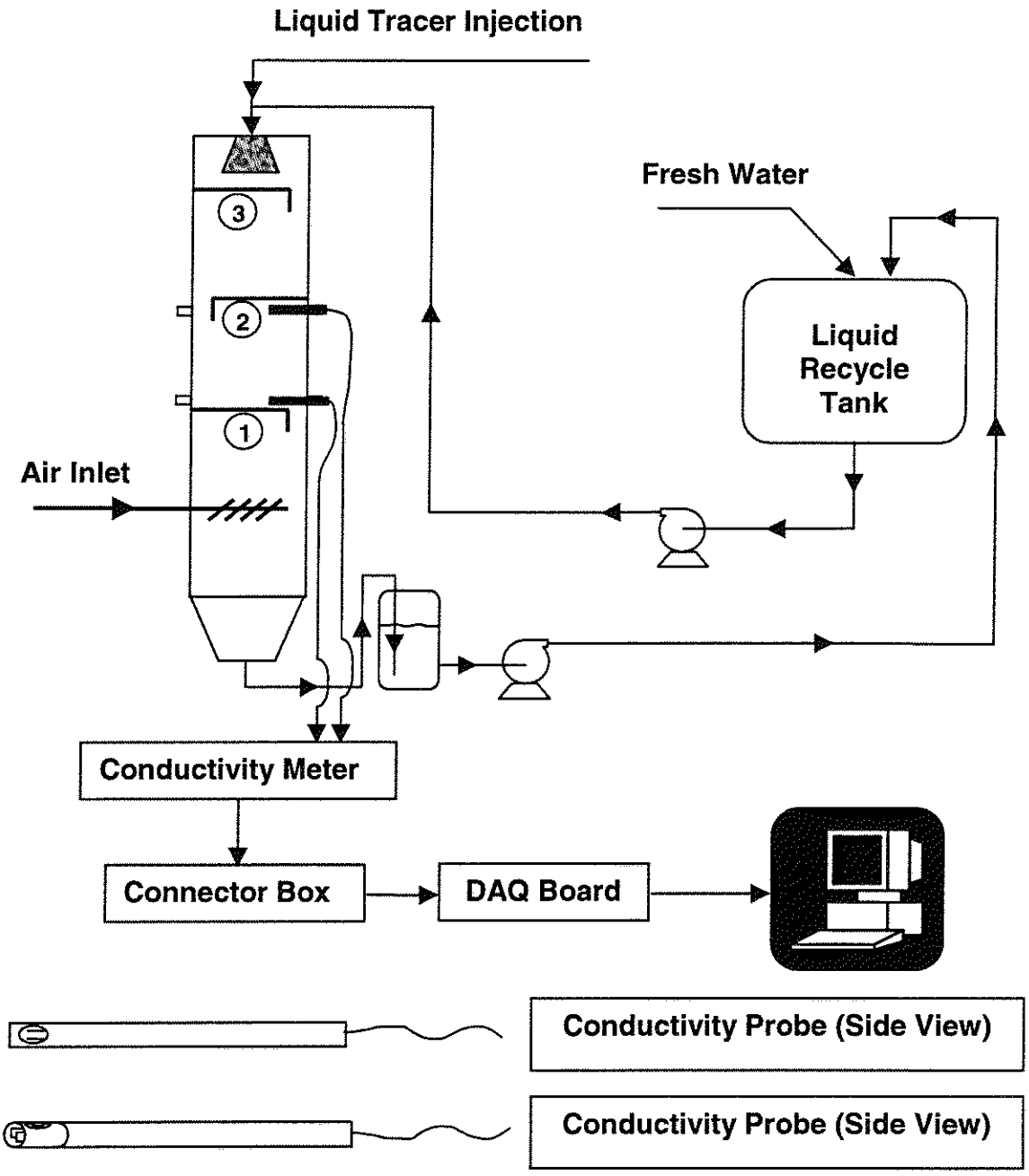

Figure 1. Schematic of the counter-current staged bubble column process loop and the data acquisition set-up with a sketch of the conductivity probes.

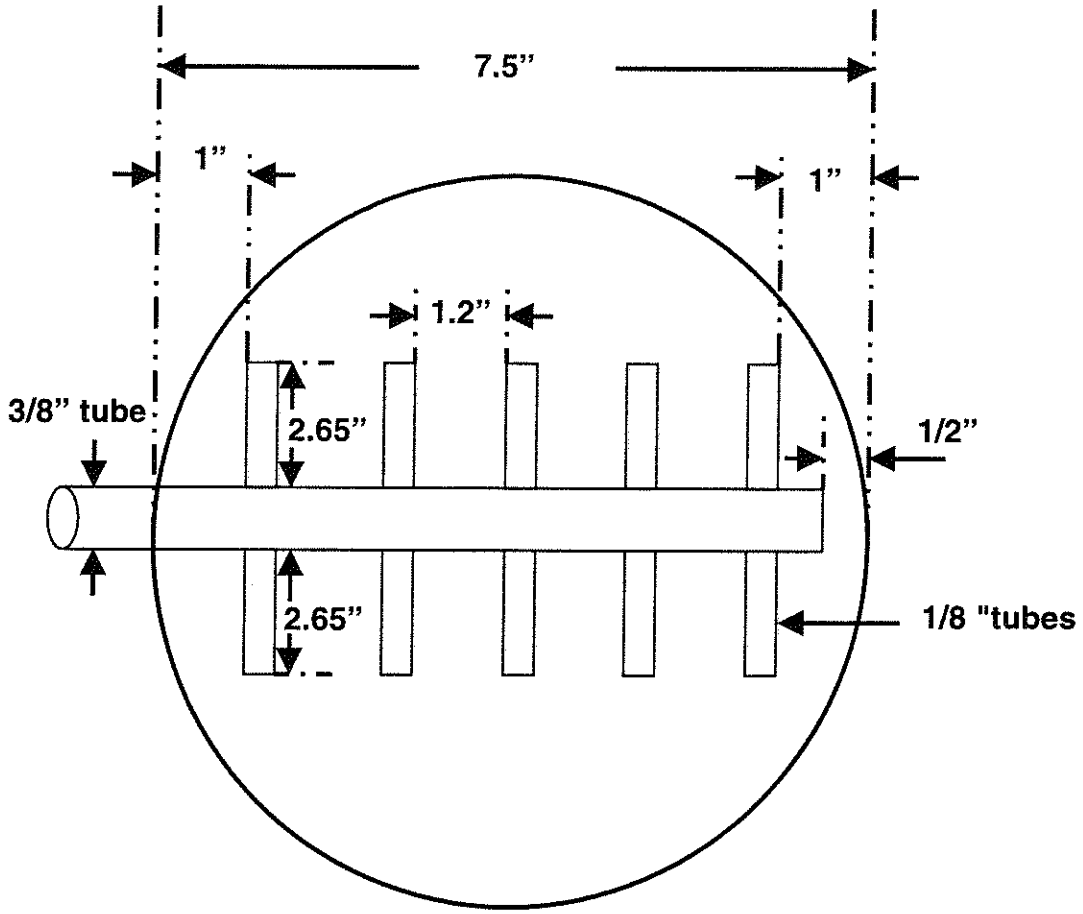

Figure 2. Details of the sparger used in the experimental set-up.

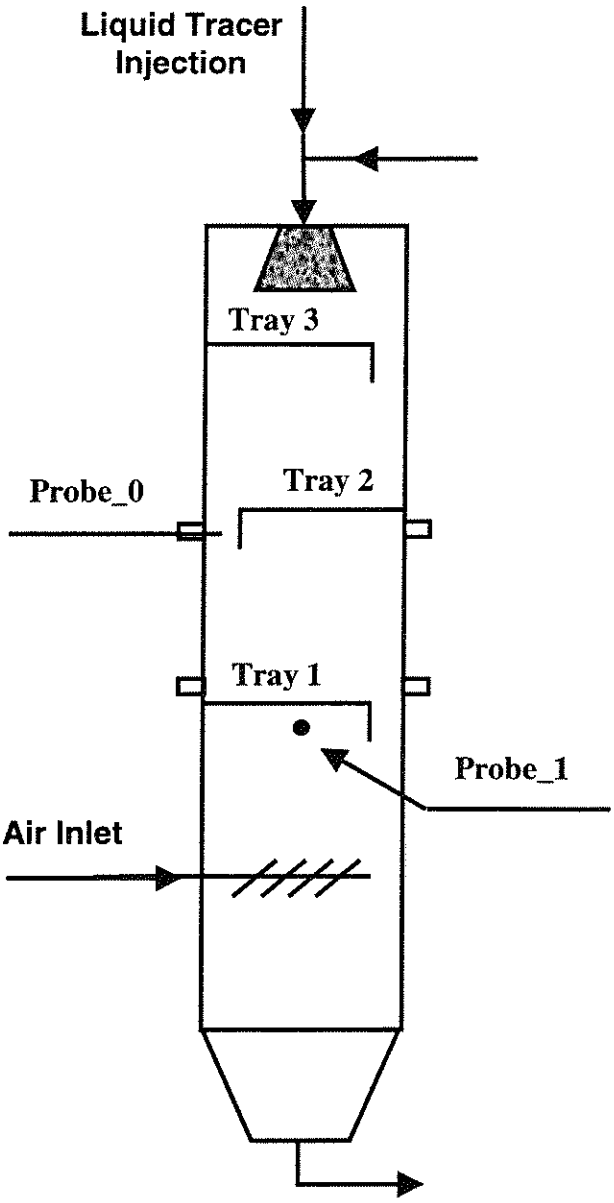

Figure 3. Location of the conductivity probes during tracer response measurements.

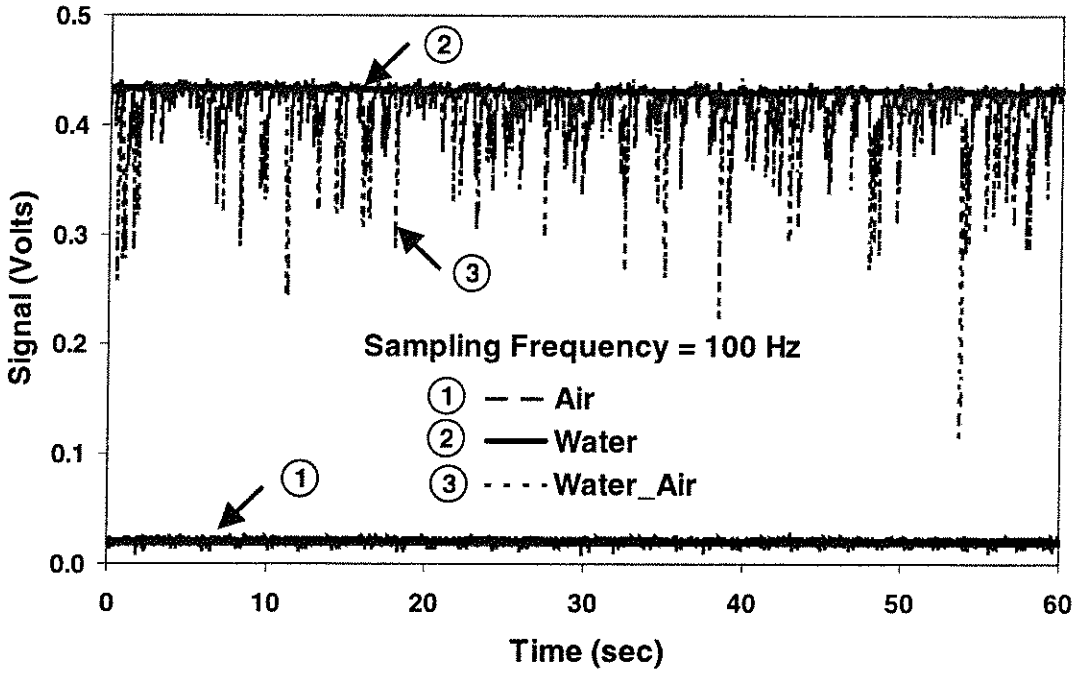

Figure 4. Typical signals measured by the conductivity probe in single and two-phase media.

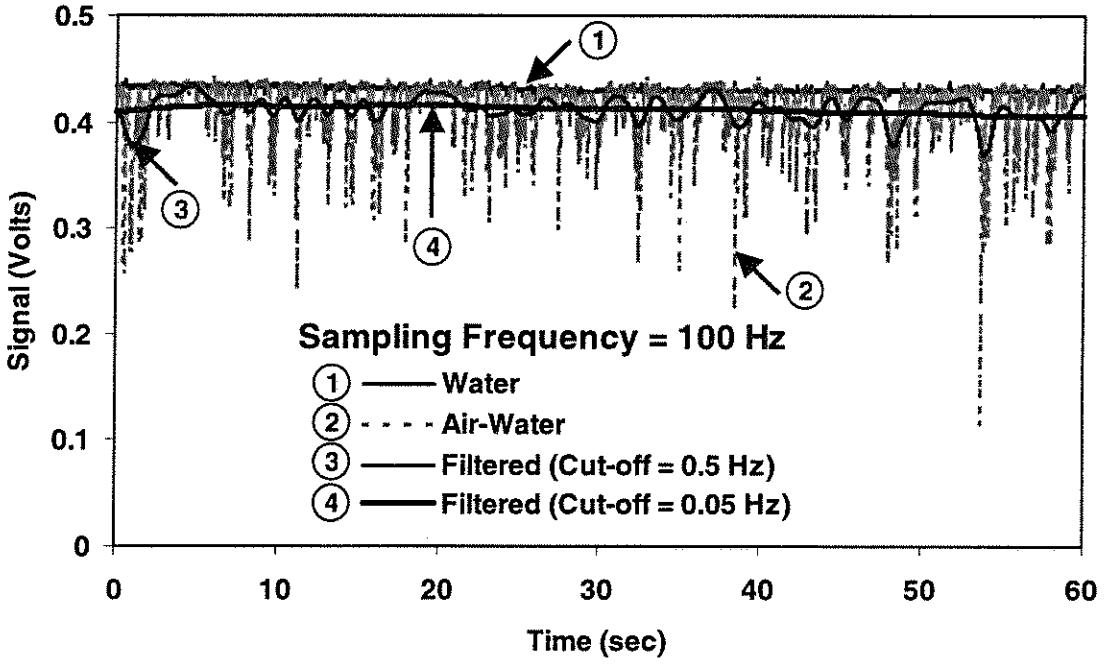

Figure 5. Performance of a standard Butterworth filter of order 2 in filtering conductivity probe signals.

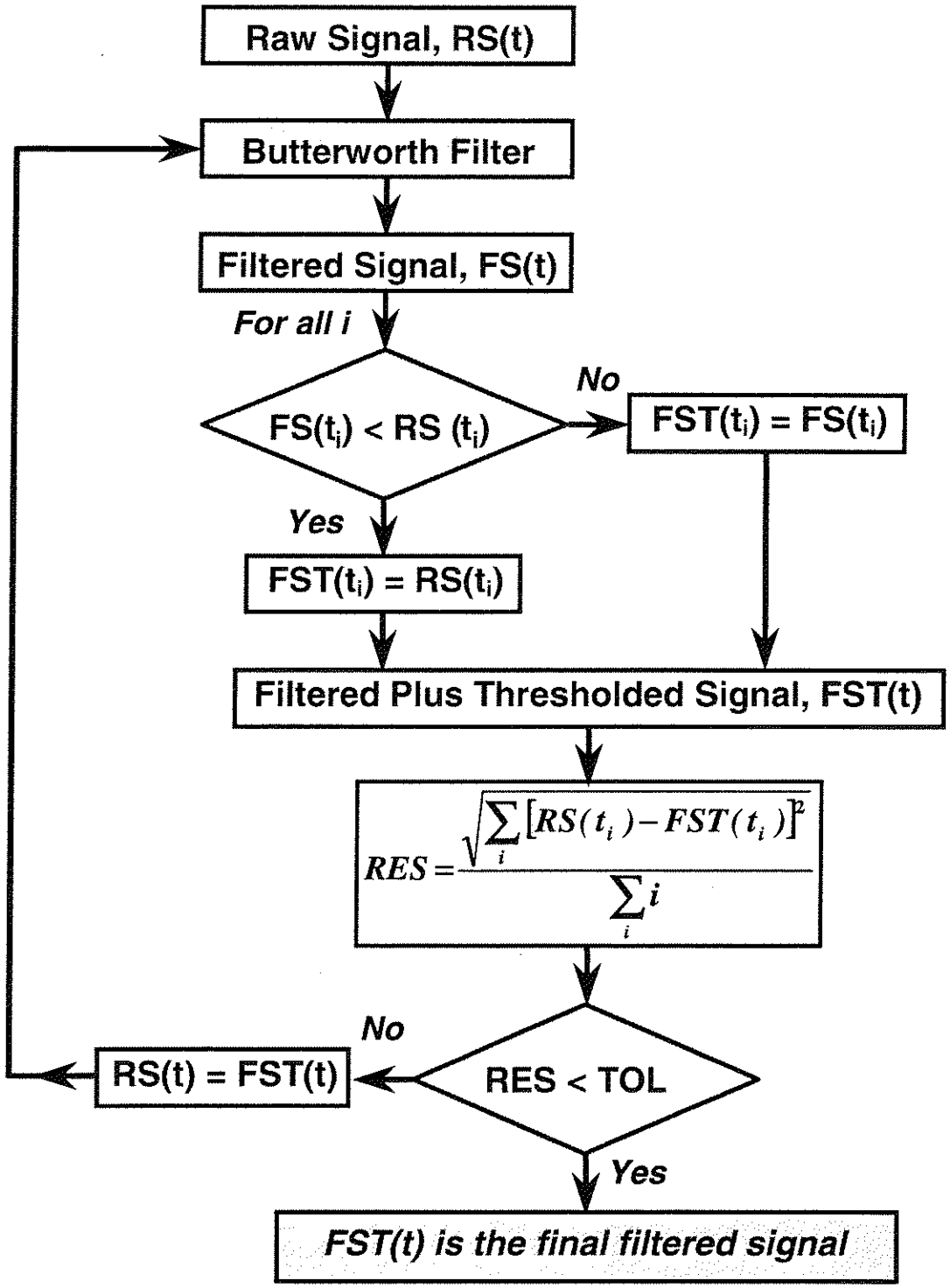

Figure 6. Flow chart for the developed filtering algorithm.

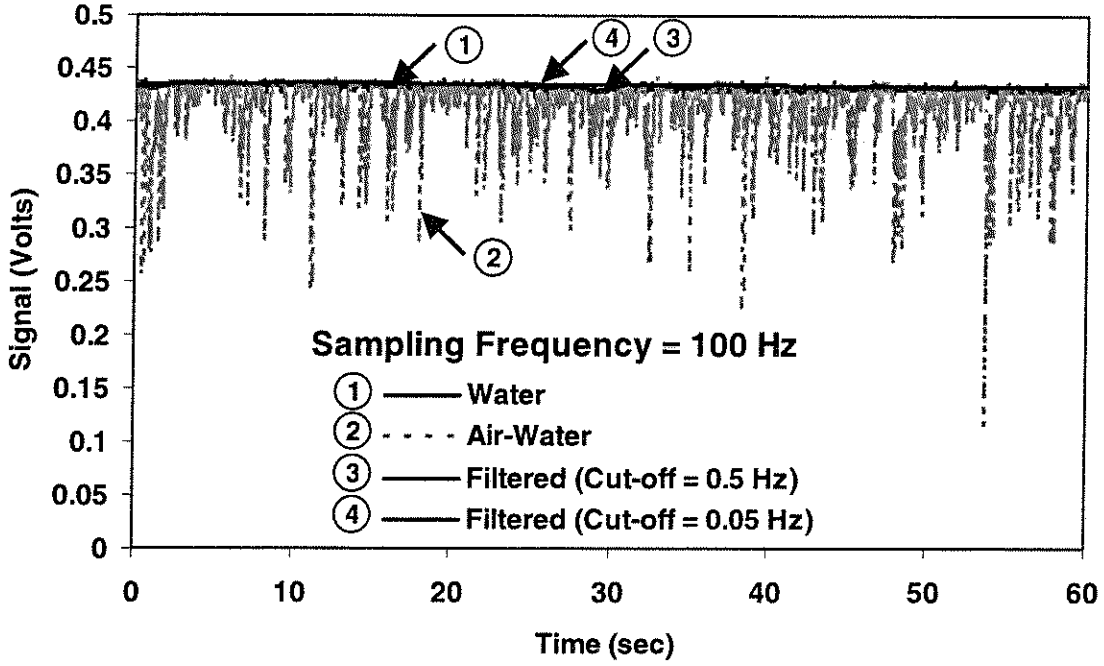

Figure 7. Performance of the new filtering technique, in conjunction with a Butterworth filter of order 2, in filtering conductivity probe signals.

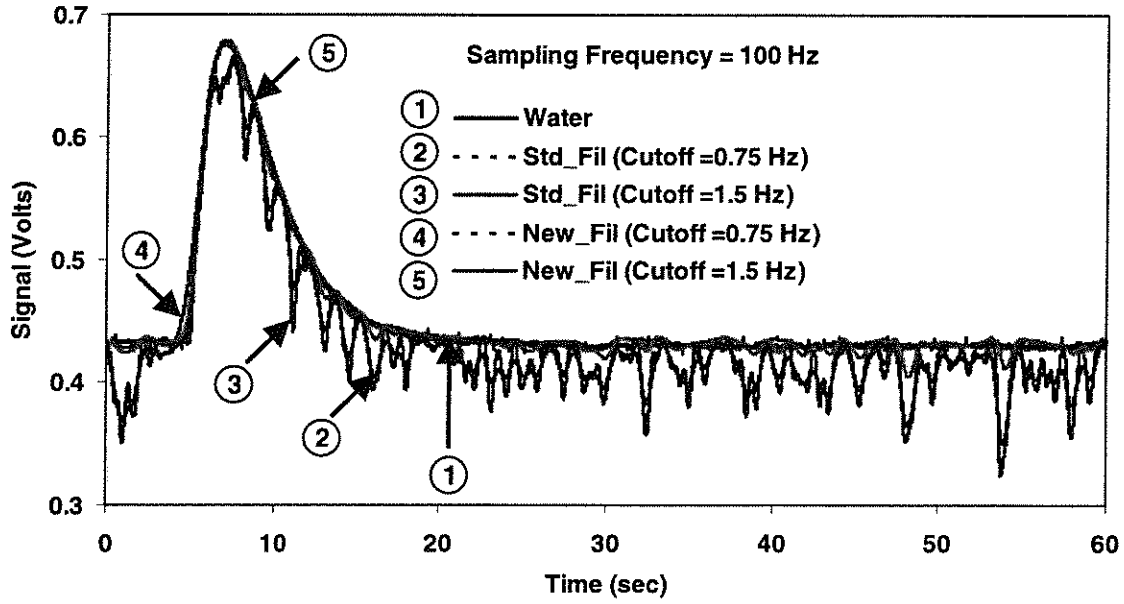

(a)

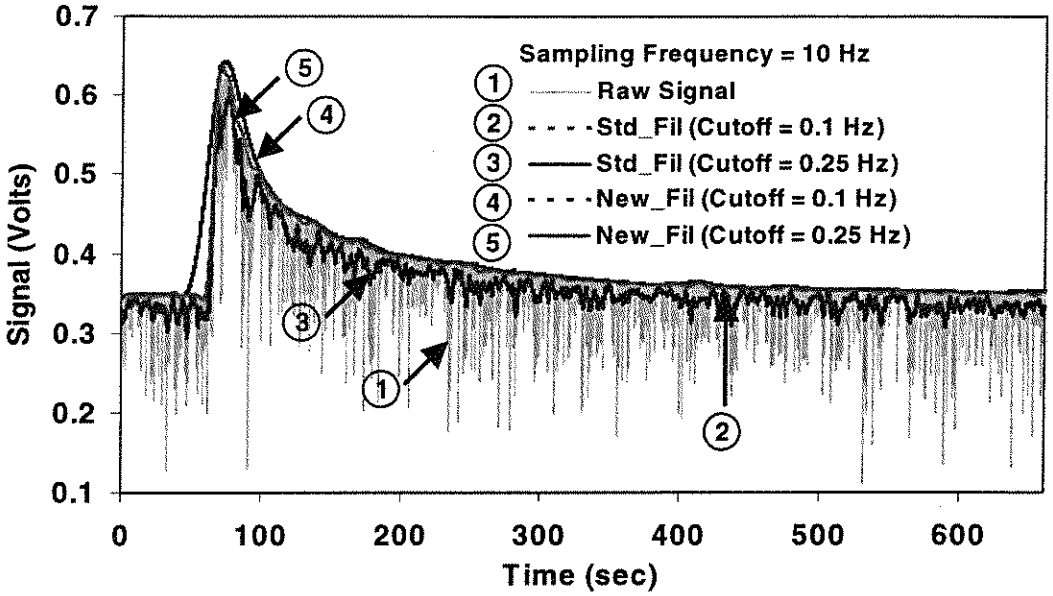

(b)

Figure 8. Performance of the standard and new filtering techniques in filtering (a) the numerically generated signal, and (b) raw signal from experimental data.

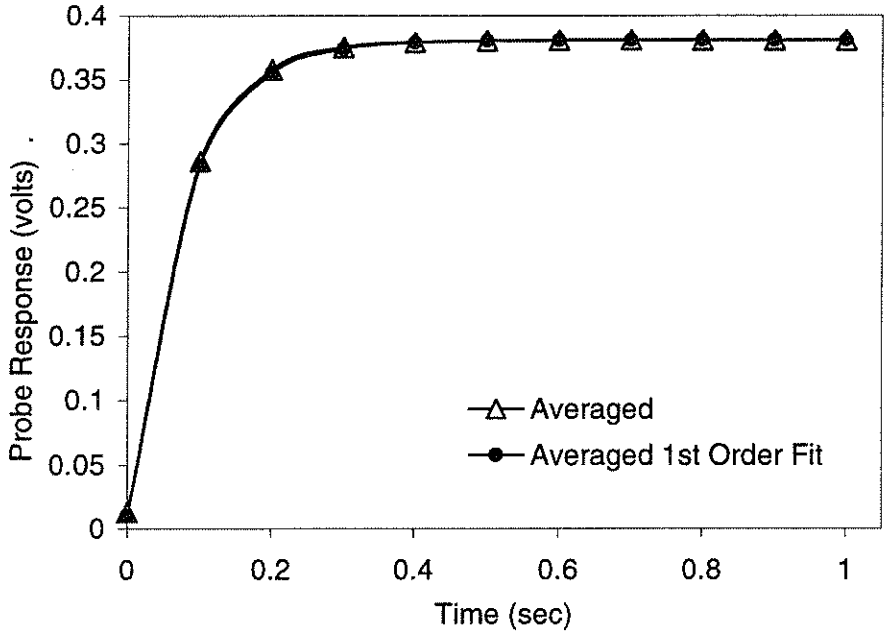

Figure 9. First order model fit of the rise of the conductivity probe signal from the one detected in air to that in tap water.

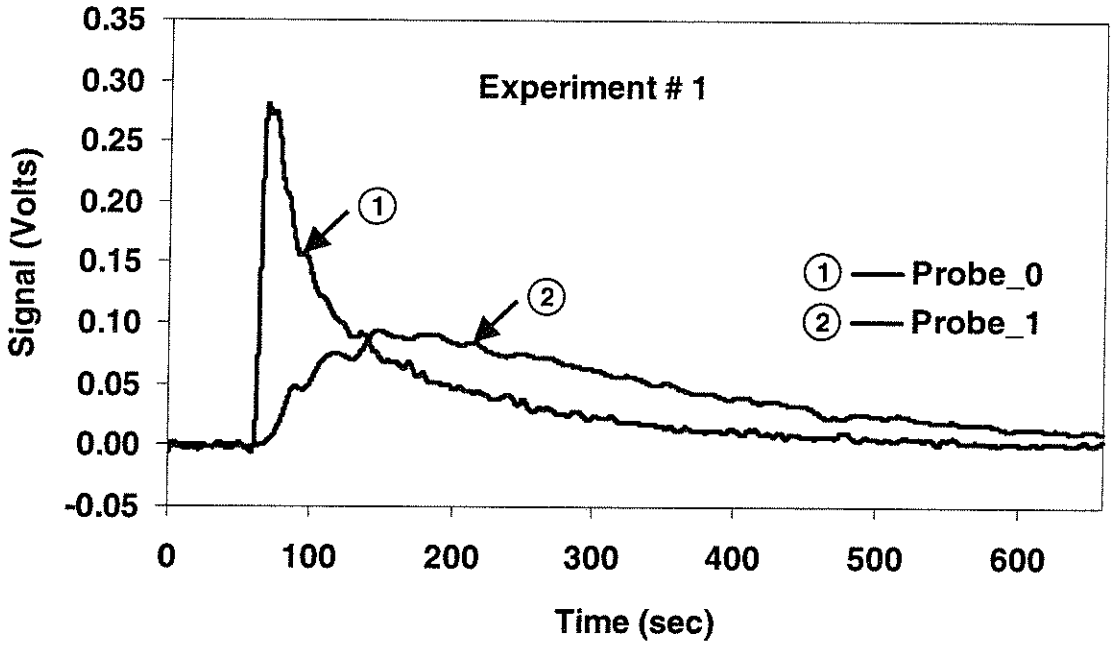

(a) $U_G = 3.25$ cm/s, $U_L = 0.44$ cm/s

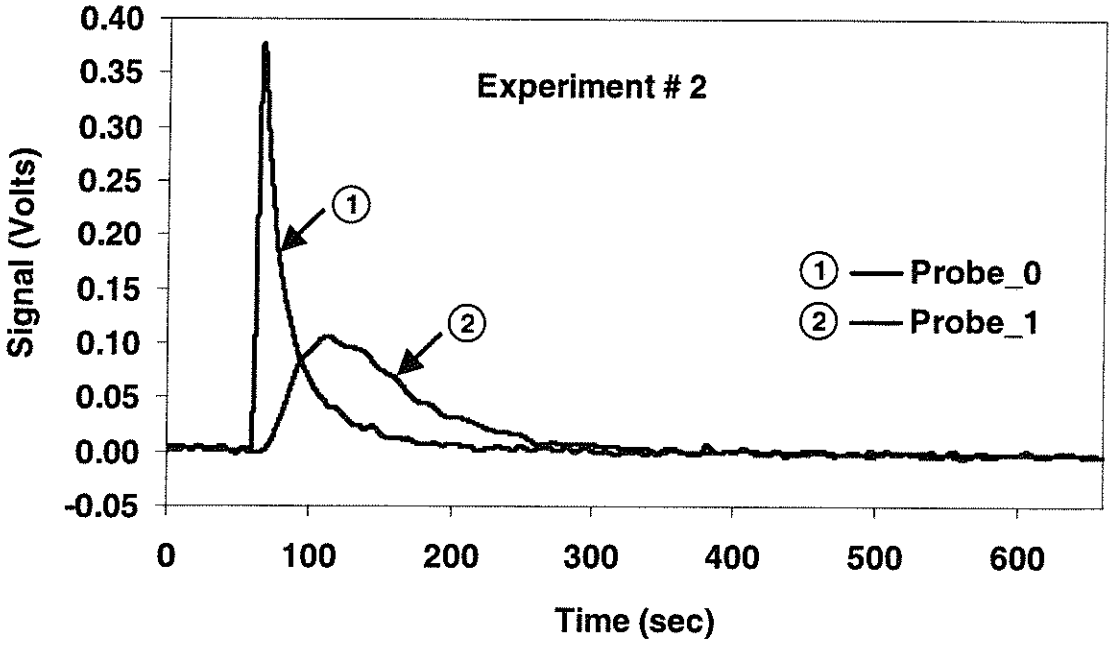

(b) $U_G = 3.25$ cm/s, $U_L = 1.44$ cm/s

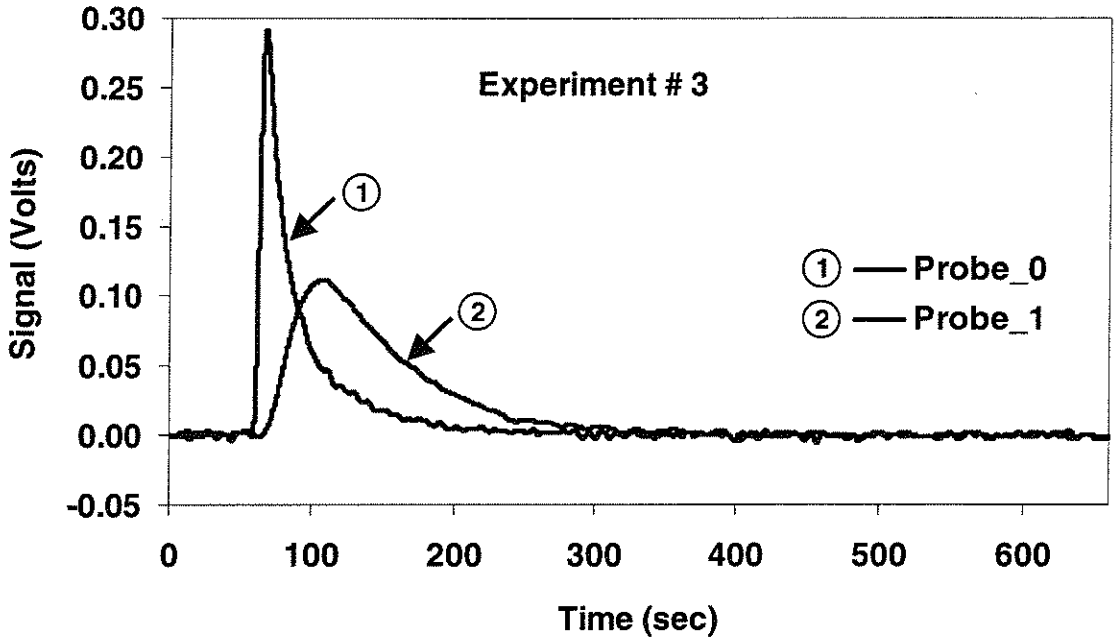

(c) $U_G = 6.51$ cm/s, $U_L = 1.44$ cm/s

Figure 10. Tracer response curves for the experiments at different operating conditions listed in Table 1 with the two probes positioned as in Figure 3.

HYDRODYNAMICS OF TRAYED BUBBLE COLUMNS

A. Problem Definition

Multistage bubble columns are conventional bubble columns sectionalized using horizontal perforated plates of chosen geometry into a number of stages with no moving parts inside the column. The hydrodynamic performance of multistage bubble columns strongly depends on the construction of the plate internals as well as the gas sparger desing.

B. Research Objectives

The objective of this work is primarily to study the effect of the trays and gas sparger on the overall gas holdup, and axial gas holdup profile at a range of superficial gas and liquid velocities. In bubble columns with internals, one should also be aware of the rate of energy that gets dissipated by the trays. Therefore, the pressure drop across the tray will be measured at selective conditions.

C. Research Accomplishments

C1. Experimental Setup

A trayed co-current bubble column set-up has been developed. The column is 8 inches in diameter, made of Plexiglas, and has a total height of 240 cm. Four stages and three different tray configurations are used (see figure 1). The distance between trays is 20 inches. Water and compressed air are used to run at atmospheric conditions. A set of superficial gas and liquid velocities has been chosen in such way that the bubbly and churn turbulent regimes are covered. Two different gas spargers have been studied, a single nozzle of 3/8" in diameter, and a perforated plate (0.019" hole size). Overall gas holdup is measured by the gas disengagement technique, whereas differential pressure drop measurements determined at four axial locations provide us with the gas holdup within the stage. Pressure drop across the tray is measured in three out the four tray locations using differential pressure transducers.

C2. Effect of Tray Design, Superficial Gas and Liquid Velocities on the Overall Gas Holdup

Superficial liquid velocity slightly affects the overall gas holdup. When superficial liquid velocity is tripled, the overall gas holdup never increases by more than 15 % of its value at the lowest liquid velocity. There is a significant increment on the gas holdup, enhanced by increasing superficial gas velocities, when trays are used (see figure 2). It has been observed an improvement of 15 % in the bubbly regime, and 30 % in the churn turbulent as compared to the column without trays, when trays of 10.2 % open area, and 0.6 cm hole diameter are used.

Hole diameter, which directly determines bubble size and liquid interstitial velocity across the trays, is the key factor in the design of the trays, e.g. 0.6 cm in diameter holes yielded gas holdups 15 % larger than 1.74 cm holes.

The tray open area does not play such an important role in the increment on the gas holdup as the hole diameter. Nevertheless, one would expect to see a small reduction when the open area is increased, due to the fact that the energy dissipation in the trays is now smaller. This work shows the unexpected opposite effect, which has to be further studied.

C3. Effect of the Gas Sparger on the Overall Gas Holdup

The bubble size generated when the perforated sparger is used, is smaller than the one generated by the nozzle, and therefore in the absence of internals (figure 3) the increase on the gas holdup is evident. The perforated sparger extends the gas holdup linear growth region, making the transition from bubbly to churn-turbulent regime to appear at a higher superficial gas velocity.

On the other hand, the trays redistribute and adjust the bubble size in each of the stages, and therefore (figure 4) similar gas holdups are now measured. However, it still can be noticed the difference in the trends for the spargers studied. Somehow the bubbles "remember" how they were initially formed at the gas inlet.

C4. Pressure Drop across the trays.

There are two opposite effects that need to be considered for increasing superficial gas velocities: 1st a reduction of the hydrostatic pressure due to the decrease on the density of the gas-liquid mixture, and 2nd an increase in the rate of energy dissipation (dynamic pressure drop) in the trays. From figures 5 and 6, one can observe that at low superficial gas velocities the hydrostatic term is predominant, due to the linear decrease on the density of the gas-liquid mixture. On the other hand, at larger superficial gas velocities the influence of the dynamic pressure drop term and the slower decrease on the density of the mixture slows down the decrease on the overall pressure drop.

Higher superficial liquid velocities (figure 5), smaller cross sectional open areas (figure 6) and smaller hole diameters, increase the rate of energy dissipation in the trays and thereby contribute to the increase on the dynamic pressure drop.

C5. Gas Holdup axial profile.

The axial gas holdup trend (figure 7) is qualitatively similar to that when trays are not used, with a flat profile at low superficial gas velocities, and a maximum at the sparger region at larger velocities.

The relative increment on the gas holdup (figure 8) when trays of smaller hole diameter are used, reconfirm the fact that the key parameter of design is the hole diameter.

D. Future Work

Conduct experiments at selective conditions of gas and liquid superficial gas velocities in order to determine the role of the liquid phase on the hydrodynamics of the TBC. The physical properties of the liquid phase (density, surface tension, viscosity, etc..) will be chosen in such a way to match those of real reacting systems such as heavy oils in hydrocracking processes.

The experimental data collected in this work, in addition to the reported in the literature will be used to construct a correlation for the overall gas holdup in co-current trayed bubble columns.

Moreover, tracer injection experiments will be conducted to learn about the unique liquid mixing characteristics that the sectionalization brings along.

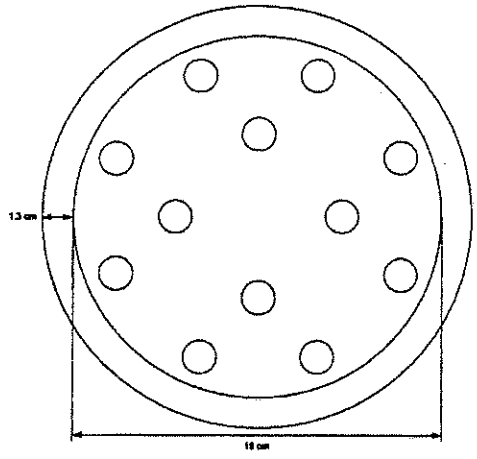

1st Design: 12 holes, 1.74 cm Diameter hole, 10.2 % O.A.

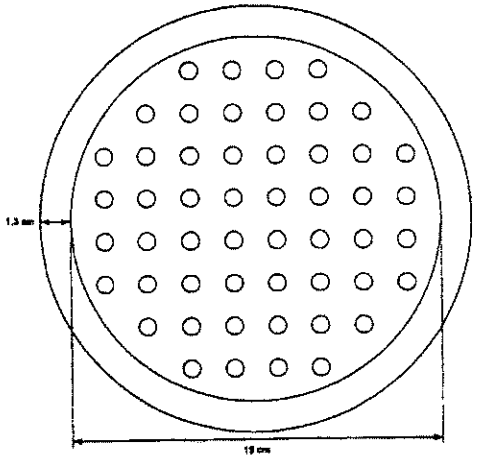

2 nd Design: 52 holes, 0.6 cm Diameter hole, 5.2 % Open Area

3rd Design: 101 holes, 0.6 cm Diameter hole, 10.2 % Open Area

Figure 1. Trays used throughout this study in the TBC.

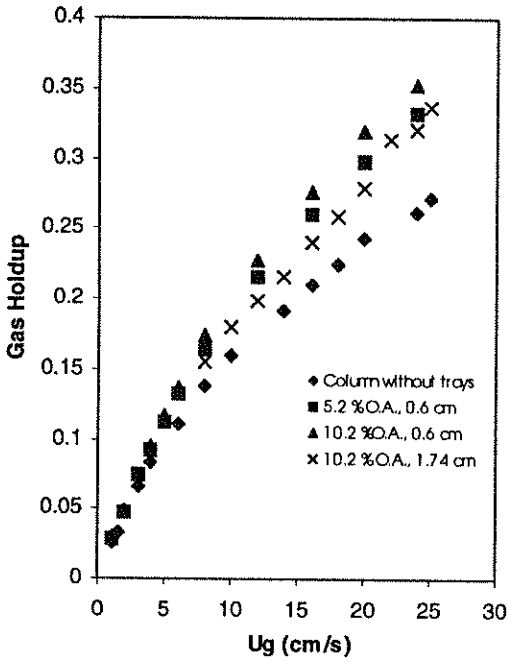

Figure 2. Effect of tray design and superficial gas velocity on the overall gas holdup at ul=0.5 cm/s, using a single nozzle sparger.

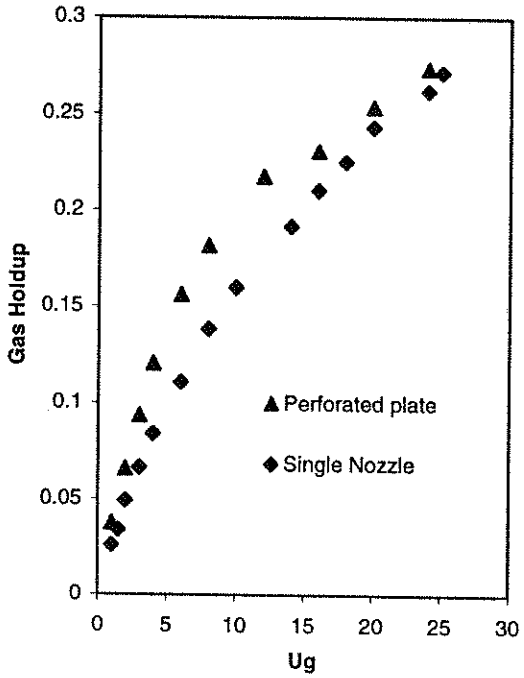

Figure 3. Effect of gas sparger on the overall gas holdup in BC without trays at ul= 0.5 cm/s.

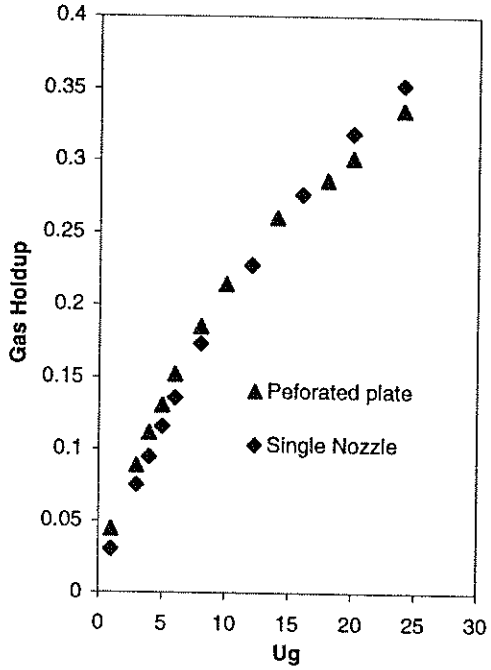

Figure 4. Effect of gas sparger on the overall gas holdup in TBC with 10.2 % O.A., and 0.6 cm in diameter trays at ul=0.5 cm/s.

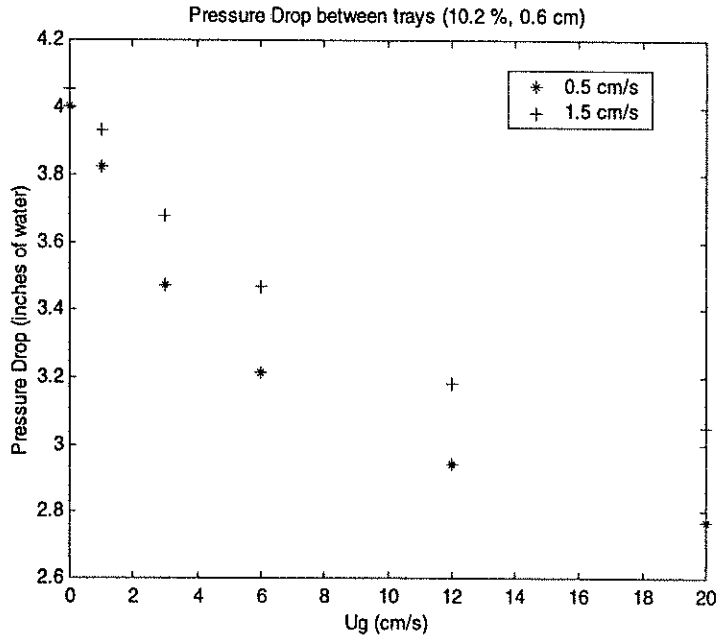

Figure 5. Effect of superficial liquid velocity on the pressure drop across the trays at a range of superficial gas velocities, 10.2 % O.A., and 0.6 cm in diameter trays are used.

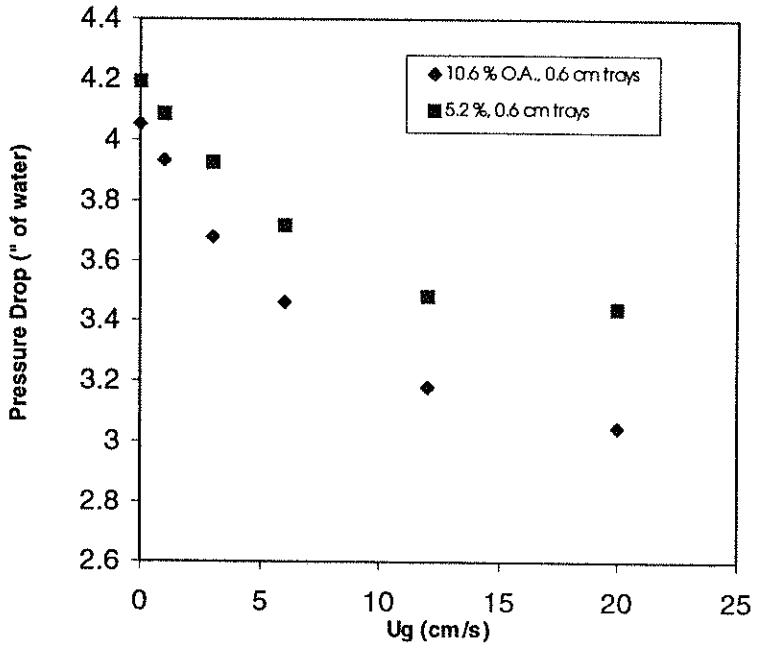

Figure 6. Effect of tray geometry on the pressure drop across the trays at a range of superficial gas velocities, ul=1.5 cm/s.

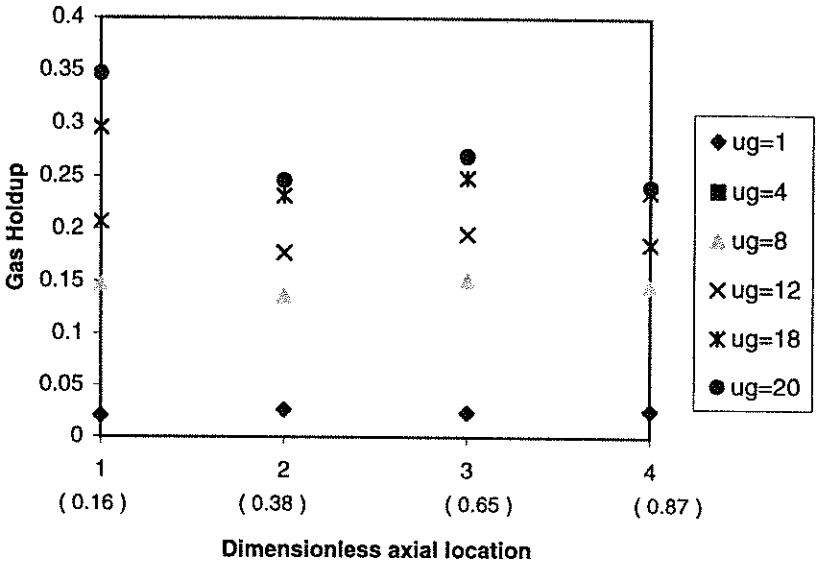

Figure 7. Gas holdup axial profile at a range of superficial gas velocities, 5.2 % O.A., and 0.6 cm in diameter trays, ul=1 cm/s.

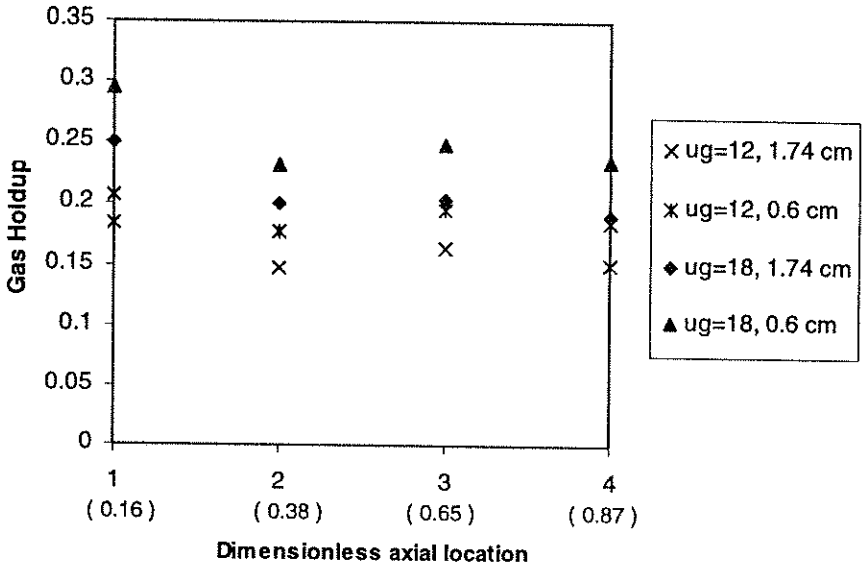

Figure 8. Effect of tray hole diameter on the axial gas holdup profile at ug=12 and 18 cm/s. Trays of 10.2 % O.A., 0.6 cm, and 1.74 cm in diameter are used.

HYDRODYNAMIC MODEL

OF A TRAYED BUBBLE COLUMN

A. Problem Definition

Understanding kinetics and hydrodynamics is essential to develop improvements in industrial reactor performance. Within this concept, Washington University and a chemical company cooperate together to study the hydrodynamics of a trayed bubble column used in a specific process application.

B. Research Objectives

The objectives are in the short term to develop a hydrodynamic model, which could enable one to simulate an actual industrial trayed bubble column; and in the long term one would expect to suggest some changes which would provide better yield for the process.
The present report deals with the first part of the objectives. A series of N stirred tanks is used as a primary model for the trayed bubble column. The aim is to develop and improve this hydrodynamic model in order to simulate correctly the actual reactor. The corresponding program is expected to be general enough so that it could be used for other similar applications studied in CREL.

C. Research Accomplishments

The regarded trayed bubble column layout is given in the Figure below. As shown in this sketch, the liquid and gas streams are in counter-current flow and the gas sparger is oriented upward. In this particular operation, part of the component present in the gas phase transfers to the liquid phase where it reacts with liquid reactants to yield the desirable product, which remains in solution.

C1. Assumptions

The assumptions used for the present hydrodynamic model follow:

- The liquid and gas stream enter the column at the top and bottom, respectively, and leave it at the bottom and top, respectively. Thus, there is countercurrent flow in the column and no liquid nor gas is fed or withdrawn at intermediate trays.
- The gas and liquid phases are well mixed on each tray, which allows one to model each phase (gas and liquid) on the tray as a stirred tank.

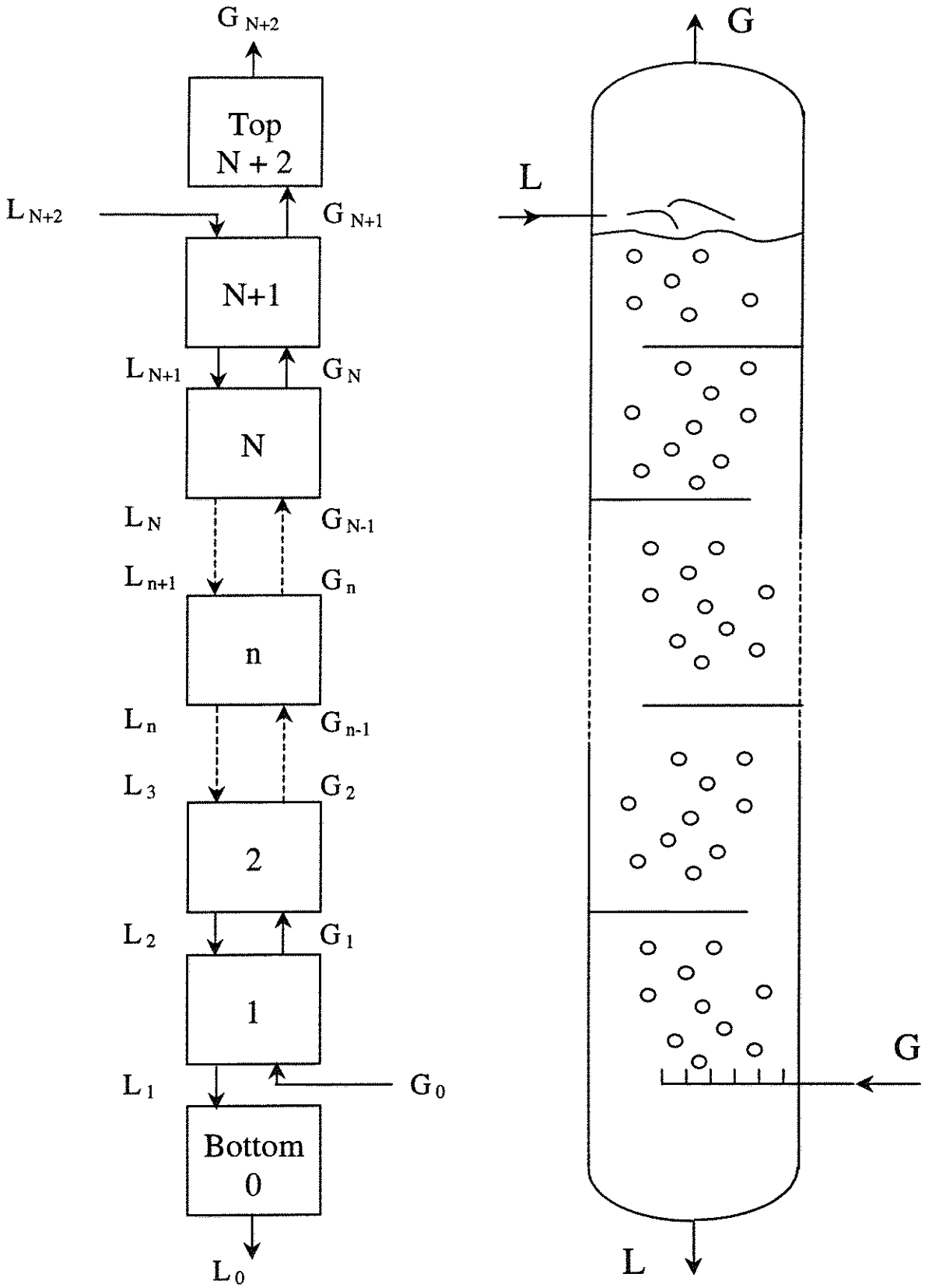

Figure 1: Hydrodynamic Model for a Trayed Bubble Column

- The top of the column is modeled as a stirred tank for the gas phase on the top.
- The bottom of the column is well mixed and is represented by a stirred tank for the liquid phase (the sparger is oriented upward).
- The column is adiabatic that is to say no heat is exchanged through the wall.
- Heat of mixing is neglected on each tray.
- There is equal temperature of the gas and liquid on each tray. The temperature variation from tray to tray is obtained by the energy balance for the adiabatic column.
- The change in gas and liquid molar flow rates is taken into account through transfer and reaction (the change due to accumulation is neglected).
- Parameters such as pressure on the tray, gas holdup... are evaluated from approximate equations or correlations. These quantities can vary from tray to tray but remain constant with time on each tray.
- The reaction takes place in the liquid phase, most probably in the liquid bulk.
- The mass transfer resistance in the gas phase is negligible and thus: $y_n^{i*} \approx y_n^i$.

C2. Modeling

The composition of the liquid phase, gas phase and the temperature in each tank (trays, top and bottom of the column) are evaluated when solving the following system of differential equations including mass balances, phase equilibrium equation and energy balances, via Matlab software.

Mass Balance for component i on tray n

Gas Phase

$$F_{G,n-1}.y_{n-1}^i = \frac{d}{dt}\left(y_n^i.N_{G,n}^{Total}\right) + \left(k_L a\right)_{mol,n}^i \left(x_n^{i*} - x_n^i\right) + F_{G,n}.y_n^i$$

with

$$y_n^i = \frac{N_{G,n}^i}{N_{G,n}^{Total}} \qquad \left(k_L a\right)_{mol,n}^i = \left(k_L a\right)_{vol,n}^i \cdot \frac{N_{L,n}^{Total}}{\left(1-\varepsilon_{G,n}\right)V_n}.V_n$$

$$N_{G,n}^{Total} = \sum_{i=1}^{C} N_{G,n}^i \qquad N_{L,n}^{Total} = \sum_{i=1}^{C} N_{L,n}^i \qquad F_{G,n} = G_n \cdot \frac{N_{G,n}^{Total}}{\varepsilon_g.V_n}$$

Liquid Phase

$$F_{L,n+1}.x_{n+1}^i + \left(k_L a\right)_{mol,n}^i \left(x_n^{i*} - x_n^i\right) = \frac{d}{dt}\left(x_n^i.N_{L,n}^{Total}\right) + R_n^i.\left(1-\varepsilon_{G,n}\right)V_n + F_{L,n}.x_n^i$$

with

$$x_n^i = \frac{N_{L,n}^i}{N_{L,n}^{Total}} \qquad \left(k_L a\right)_{mol,n}^i = \left(k_L a\right)_{vol,n}^i \cdot \frac{N_{L,n}^{Total}}{\left(1-\varepsilon_{G,n}\right)V_n}.V_n$$

$$N_{L,n}^{Total} = \sum_{i=1}^{C} N_{L,n}^i \qquad F_{L,n} = L_n \cdot \frac{N_{L,n}^{Total}}{\left(1-\varepsilon_g\right)V_n}$$

Phase equilibrium equation at the interface

$$y_n^{i*} = K_n^i . x_n^{i*} \approx y_n^i \qquad \text{where} \qquad K_n^i = \frac{\rho_{L,n}}{M_{L,n}} . \frac{v_{mol}}{P_{Total,n}} . S_n^i$$

$\rho_{L,n}$ and S^i_n will be determined from industrial data and $M_{L,n}$ from the following equation: $M_{L,n} = \sum_{i=1}^{C} M^i$, where M^i is the molecular weight of component i.

Energy Balance on tray n

$$\sum_{i=1}^{C} F_{G,n-1} . y^i_{n-1} . \overline{H}^i_{G,n-1} + \sum_{i=1}^{C} F_{L,n+1} . x^i_{n+1} . \overline{H}^i_{L,n+1} = \frac{dU_n}{dt} + \sum_{i=1}^{C} F_{G,n} . y^i_n . \overline{H}^i_{G,n} + \sum_{i=1}^{C} F_{L,n} . x^i_n . \overline{H}^i_{L,n}$$

with

- $\overline{H}^i_{G,n} = \left(\overline{H}^i_G\right)_0 + \int_{T_0}^{T_n} C^i_{p,G}(T).dT \qquad \overline{H}^i_{L,n} = \left(\overline{H}^i_L\right)_0 + \int_{T_0}^{T_n} C^i_{p,L}(T).dT$
- Since

$$\frac{dU_n}{dt} = \frac{d(H_n - P_{Total,n} . V_n)}{dt} = \frac{dH_n}{dt} \quad \text{(because } P_{Total,n} \text{ and } V_n \text{ are constant with time)}$$

and $$H_n = H_{R,n} + \sum_{i=1}^{C} y^i_n . N^{Total}_{G,n} . \overline{H}^i_{G,n} + \sum_{i=1}^{C} x^i_n . N^{Total}_{L,n} . \overline{H}^i_{L,n} \text{ , then}$$

$$\frac{dU_n}{dt} = \frac{dH_{R,n}}{dt} + \sum_{i=1}^{C} \left[y^i_n . N^{Total}_{G,n} . \frac{d\overline{H}^i_{G,n}}{dt} + \overline{H}^i_{G,n} . \frac{d}{dt}\left(y^i_n . N^{Total}_{G,n}\right) \right]$$

$$+ \sum_{i=1}^{C} \left[x^i_n . N^{Solvent}_{L,n} . \frac{d\overline{H}^i_{L,n}}{dt} + \overline{H}^i_{L,n} . \frac{d}{dt}\left(x^i_n . N^{Solvent}_{L,n}\right) \right]$$

with $$H_{R,n} = \left(H_R\right)_0 + \int_{T_0}^{T_n} m_{R,n} . C_R(T).dT$$

When one applies the ideality hypothesis for the specific heats i.e. one assumes them constant for the range of temperature in the column, then:

$$\overline{H}^i_{G,n} = \left(\overline{H}^i_G\right)_0 + C^i_{p,G,mean} . (T_n - T_0) \qquad \overline{H}^i_{L,n} = \left(\overline{H}^i_L\right)_0 + C^i_{p,L,mean} . (T_n - T_0)$$

where $C^i_{P,G,mean}$ and $C^i_{P,:L,mean}$ represent the specific heat of component i in gas and liquid respectively, determined at the mean temperature T_{mean} of the column

and $$H_{R,n} = \left(H_R\right)_0 + m_{R,n} . C_{R,mean} . (T_n - T_0)$$

where $C_{R.mean}$ is the specific heat of the tank and trays evaluated at the mean temperature of the tank and trays. However, the enthalpy of the reactor is often negligible and this assumption will be used in the present work.

C3. Results

Let us model a column with 7 trays, in which the following reaction takes place in the liquid phase:

$$A\ (l) + B\ (g) \rightarrow C\ (l) + D\ (l)$$

The solution initially includes reactant A and a solvent E, while the gas phase contains an inert F and reactant B, which is transferred to the liquid phase. The following operating conditions were considered:

Table 1: Composition of the inlet gas and liquid streams for three different runs.

	Gas Fraction			Liquid Fraction		
	Run 1	***Run 2***	***Run 3***	***Run 1***	***Run 2***	***Run 3***
Component A	0	0	0	**0.069**	**0.069**	**0.035**
Component B	0.21	0.21	0.21	0	0	0
Component C	0	0	0	0.046	0.046	0.046
Component D	0	0	0	0	0	0
Component E	0	0	0	**0.877**	**0.877**	**0.911**
Component F	0.79	0.79	0.79	0.008	0.008	0.008

Table 2: Inlet gas and liquid temperatures for three different runs.

	Run 1	***Run 2***	***Run 3***
Inlet Gas Temperature, K	308.15	**283.15**	308.15
Inlet Liquid Temperature, K	318.15	**283.15**	318.15

After computation, the liquid and gas molar fractions are obtained as well as the temperature in each tank. The evolution of reactants and products molar fractions and of the temperature is shown in Figures 2, 3, 4, 5 and 6 for Run 1 to Run 3.

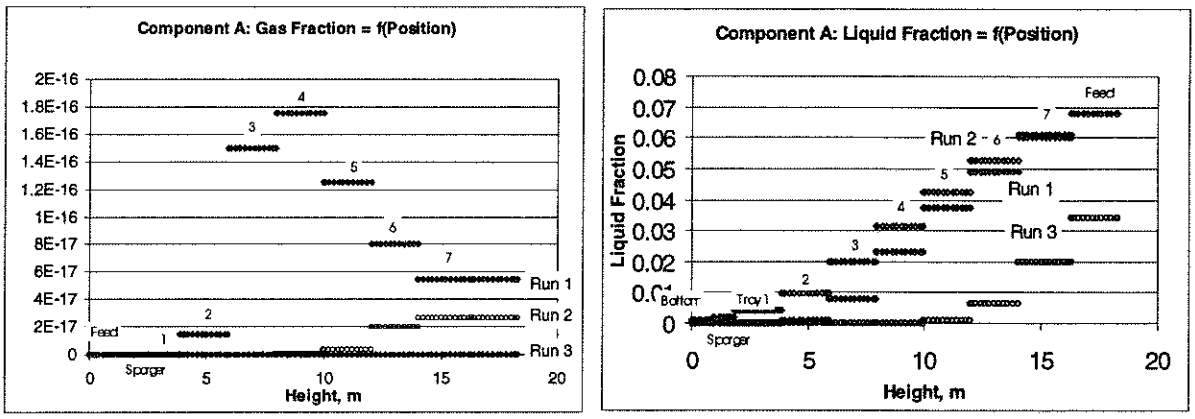

Figure 2: Component A

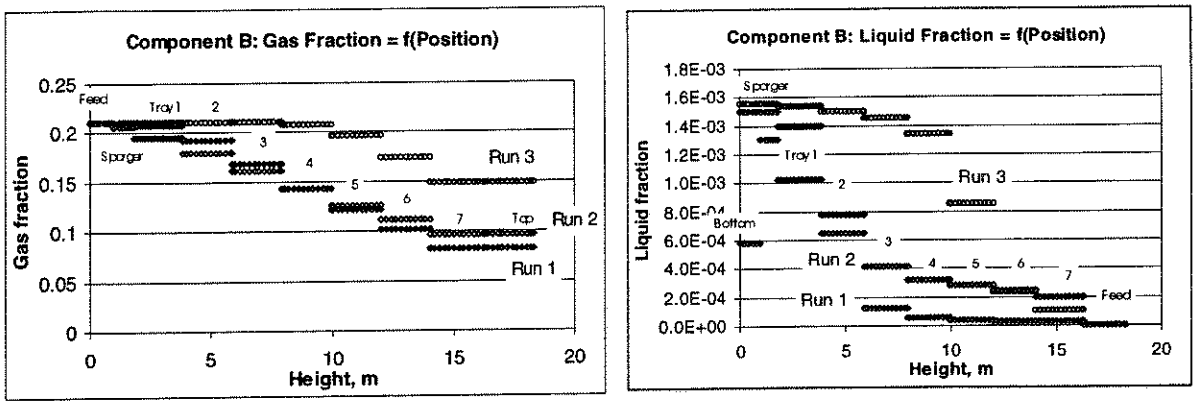

Figure 3: Component B

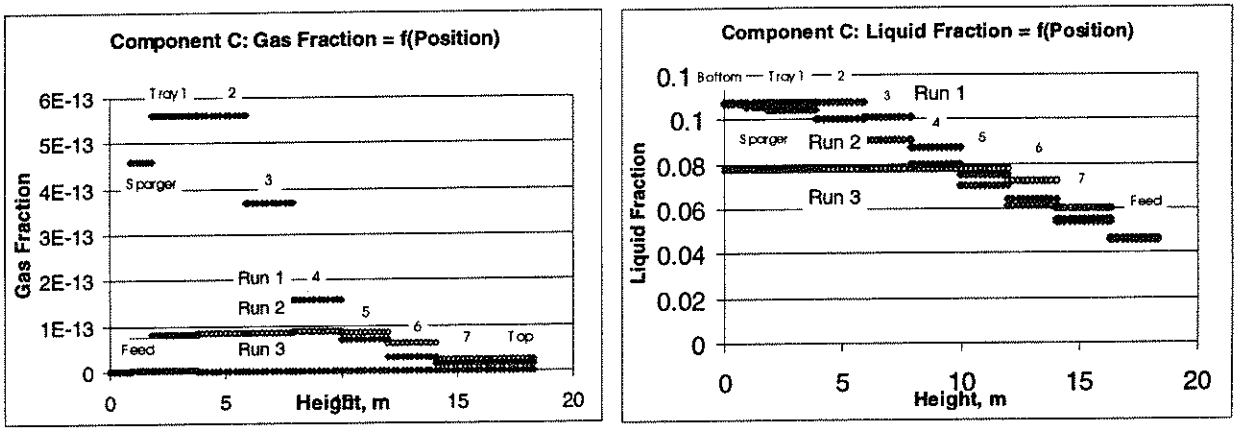

Figure 4: Component C

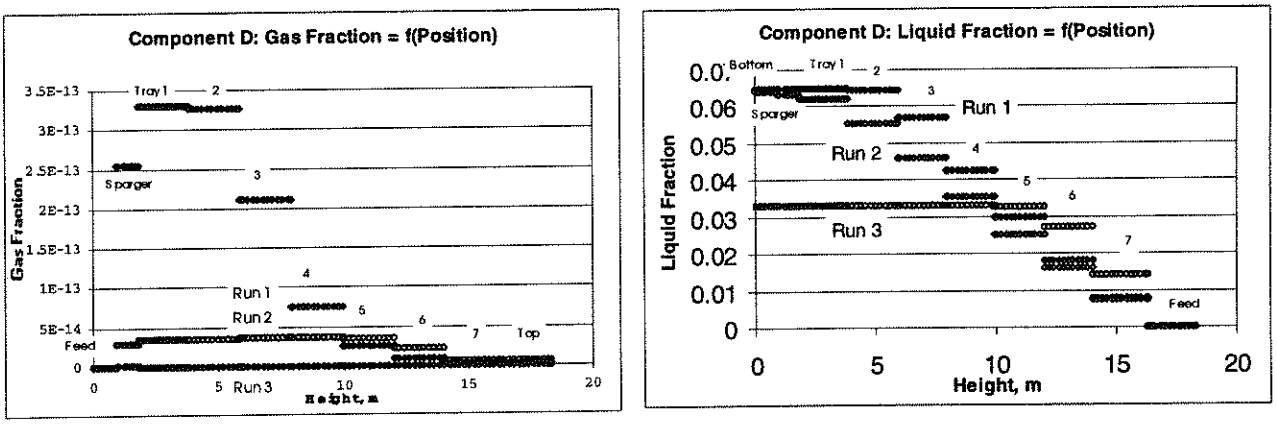

Figure 5: Component D

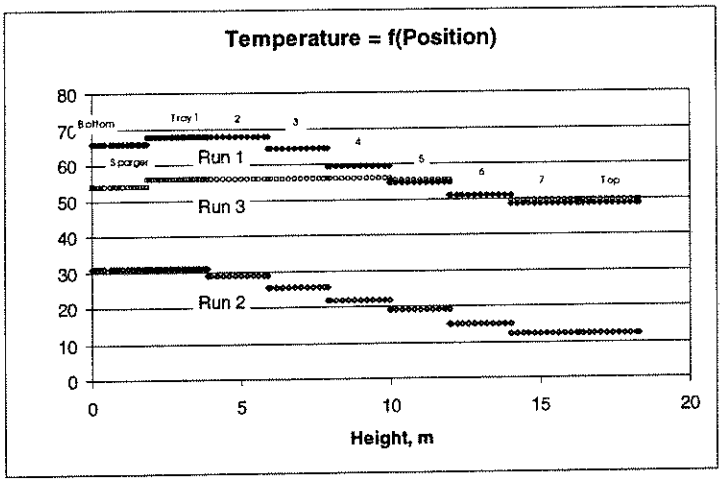

Figure 6: Temperature

Run 2 requires the same composition as Run 1 but includes lower inlet temperatures for both the liquid and gas phases. Thus, the reaction is slower and the final conversion is obtained in the very bottom of the column whereas it is already reached in Tray 2 for Run 1 (the liquid fraction for component A reaches zero only in the bottom of the column whereas this reactant is already totally consumed in Tray 2). The temperature profile follows the same evolution in both Runs 1 and 2 but that for Run 2 shows much lower values due to the respective inlet temperatures.
Run 3 differs from Run 1 only in the amount of liquid reactant A introduced in the column. Since less A enters the reactor, it is consumed faster than in Run 1 and the final conversion is reached in Tray 5 (instead of Tray 2 for Run 1). The temperature remains also almost the same from the bottom to Tray 4 since there is no reaction anymore (the small decrease in temperature for the sparger and the bottom regions is due to the introduction of colder inlet gas).

D. Future work

The model will be run with industrial data and compared to some measurements performed on the regarded actual trayed bubble column. It will then be improved and modified according to the accuracy of the simulation.

E. Notation

C	Number of components	
$C^{i}_{P,G}$	Specific heat of component i in the gas phase	$J.mol^{-1}.K^{-1}$
$C^{i}_{P,L}$	Specific heat of component i in the liquid phase	$J.mol^{-1}.K^{-1}$
C_R	Specific heat of the tank and tray	$J.Kg^{-1}.K^{-1}$
$F_{G,n}$	Molar gas flow rate from the nth tray	$mol_{Gas}.s^{-1}$
$F_{L,n}$	Molar liquid flow rate from the nth tray	$mol_{Liquid}.s^{-1}$
G_n	Volumetric gas flow rate from the nth tray	$m^3_{Gas}.s^{-1}$

H_n	Total enthalpy on tray n	J
$H_{R,n}$	Enthalpy of the tank and tray at tray n	J
$\overline{H}^i_{G,n}$	Partial molar enthalpy of component i in the gas phase, on tray n	$J.mol^{-1}$
$\left(\overline{H}^i_G\right)_0$	Standard partial molar enthalpy of i in the gas phase, on tray n	$J.mol^{-1}$
$\overline{H}^i_{L,n}$	Partial molar enthalpy of component i in the liquid phase, on tray n	$J.mol^{-1}$
$\left(\overline{H}^i_L\right)_0$	Standard partial molar enthalpy of i in the liquid phase, on tray n	$J.mol^{-1}$
K^i_n	Equilibrium ratio at the interface for component i on tray n	
$(k_L a)^i_{mol,n}$	Molar mass transfer coefficient for component i, on tray n	$mol_{Liquid}.s^{-1}$
$(k_L a)^i_{vol,n}$	Volumetric mass transfer coefficient for component i, on tray n	$m^3_{Liquid}.m^{-3}_{Mixture}.s^{-1}$
L_n	Volumetric liquid flow rate from the nth tray	$m^3_{Liquid}.s^{-1}$
$m_{R,n}$	Mass of the tank and tray at tray n	kg
$M_{L,n}$	Liquid molecular weight on tray n	$kg_{Liquid}.mol^{-1}_{Liquid}$
$N^i_{G,n}$	Moles of component i in the gas phase on tray n	mol
$N^i_{L,n}$	Moles of component i in the liquid phase on tray n	mol
$N^{Total}_{G,n}$	Total number of moles in the gas phase on tray n	mol
$N^{Total}_{L,n}$	Total number of moles in the liquid phase on tray n	mol
$P_{Total,n}$	Absolute pressure on tray n	Pa
R^i_n	Reaction rate for component i on tray n	$mol.m^{-3}_{Liquid}.s^{-1}$
S^i_n	Solubility of component i on tray n	$m^3_{NTP\ of\ i\ dissolved}.m^{-3}_{Liquid}.Pa_{partial\ pressure\ of\ i}$
t	Time	s
T_0	Standard temperature	K
T_n	Temperature on the nth tray	K
U_n	Total internal energy on tray n	J
v_{mol}	Normal molar volume ($v_{mol} = 0.0224\ m^3.mol^{-1}$)	$m^3.mol^{-1}$
V_n	Volume of the nth reactor	$m^3_{Mixture}$
x^i_n	Mole fraction of component i in the liquid phase on tray n	$mol_i.mol^{-1}_{Total\ Liqu}$
x^{i*}_n	Mole fraction of component i in the liquid at the interface, tray n	$mol_i.mol^{-1}_{Total\ Liqu}$
y^i_n	Mole fraction of component i in the gas phase on tray n	$mol_i.mol^{-1}_{Total\ Gas}$
y^{i*}_n	Mole fraction of component i in the gas at the interface, tray n	$mol_i.mol^{-1}_{Total\ Gas}$
$\varepsilon_{G,n}$	Gas holdup of the nth reactor	$m^3_{Gas}.m^{-3}_{Mixture}$
$\rho_{L,n}$	Liquid density on tray n	$kg_{Liquid}.m^{-3}_{Liquid}$

STUDY OF PARTICLE MOTION IN PACKED/EBULLATED BEDS BY CT AND CARPT

See the attached report for:

A. Problem Definition
B. Research Objectives
C. Research Accomplishments

STUDY OF PARTICLE MOTION IN PACKED/EBULLATED BEDS BY CT AND CARPT

Jinwen Chen*, Novica Rados, Muthanna H. Al-Dahhan, Milorad P. Dudukovic

Department of Chemical Engineering

Washington University in St. Louis

One Brookings Drive

St. Louis, MO 63130-4899, USA

Duyen Nguyen, Krishniah Parimi

Chevron Research and Technology Company

100 Chevron Way

Richmond, CA 94802-0627, USA

* Currently in National Center for Upgrading Technology, 1 Oil Patch Drive, Devon, AB T9G 1A8 Canada

ABSTRACT

In this study, Computed Tomography (CT) and Computer Automated Radioactive Particle Tracking (CARPT) were used to study the gas distribution and the incipient particle motion in a packed/ebullated bed in which gas and liquid are in co-current up flow. CT scans were performed to evaluate the gas-liquid distributor and the gas sparger used for the experiments. The results show that with the use of a perforated plate gas-liquid distributor (with 96 1-mm holes, open area of 0.1%) and a gas sparger (cross shaped, with 16 3-mm holes), the cross sectional gas holdup distribution in the packed/ebullated bed is relatively uniform with gas holdup of about 0.11 in the center and 0.09 near the wall of the bed (with superficial gas and liquid velocities of 2 cm/s and 0.3 cm/s, respectively). The cross sectional averaged gas holdup was 0.095. CARPT experiments were utilized in an air-water-ethanol (10% ethanol by weight)-solids system to identify the operating conditions at which solid particles first start to move in the bed. It was found that at a gas superficial velocity of 1.7 cm/s and superficial liquid velocity of 0.3 cm/s, solids particles in the bed start to move and travel long distances in the axial direction. CARPT experiments were then conducted in the same system at superficial gas velocity of 2.0 cm/s and superficial liquid velocity of 0.3 cm/s. It was found that at these conditions the solid particles in the bed are moving significantly throughout the column with up flow in the center and down flow near the wall of the column. The time averaged maximum upward and downward velocity of the tracer particle is about 0.47 mm/s and 0.57 mm/s, respectively.

Keywords: Particle motion, packed/ebullated beds, CARPT, CT

1. INTRODUCTION

Gas-liquid-solid packed/ebullated beds are widely used in petroleum, chemical, food and environmental processes. One of the operation modes in these processes is that gas and liquid flow upward through a packed bed of solids particles which is essentially stationary. In some cases, the bed is subject to periodic withdrawals of a small batch of particles and replenishment with fresh ones. Stationary particles, during normal operation of the bed, and plug flow of solids, during withdrawal and replenishment, are most desirable from the operational point of view. It is thus necessary to determine whether any backmixing of solids occurs in the bed during normal operation. It is important to identify the operating conditions at which incipient particle fluidization occurs and when the catalyst particles start to migrate throughout the bed. It is also of interest and importance to determine the magnitudes of the traveling velocity of solid particles when migration occurs. This type of study has not been accomplished before due to the lack of reliable experimental techniques.

In the past decade, a number of advanced techniques for noninvasive monitoring of multiphase flows have been developed. For velocity measurements, the techniques include particle image velocimetry (PIV) (Chen and Fan, 1992), laser Doppler anemometry (LDA) (Gross and Quhlman, 1992; Mudde *et al.*, 1997), radioactive particle tracking (RPT) (Bascoul, *et al.*, 1993; Larachi *et al.*, 1995) or computer automated radioactive particle tracking (CARPT) (Devanathan *et al.* 1990; Moslemian *et al.* 1992; Yang *et al.*, 1993; Degaleesan, 1997). Various kinds of densitometry and tomography/radiography have been applied to phase density measurements, such as X-ray computed tomography (X-ray CT) (Kantzas, 1994), X-ray radiography (Yates *et al.*, 1994; Yates, 1997), gamma-ray densitometry (Shollenberger *et al.*, 1997, Mudde, *et al.*, 1999) and gamma-ray computed tomography (gamma-ray CT) (Kumar *et al.*, 1995, 1997), and electronic impedance tomography (Halow, 1997). A detailed review on the applications of noninvasive techniques in monitoring of multiphase flow can be found in Chaouki *et al.* (1997).

The Chemical Reaction Engineering Laboratory (CREL) at Washington University in St. Louis has developed unique experimental facilities for quantification of phase density and velocity patterns in multiphase flow systems. These include computer automated radioactive particle tracking (CARPT) and computed tomography (CT). CARPT provides experimental data on instantaneous positions, time averaged velocity profiles and turbulent parameters in the entire flow fields (Davanathan *et al.*, 1990; Moslemian *et al.*, 1992; *Yang et al.*, 1993), while CT yields the time averaged density profiles at discrete cross sectional planes of the reactor (Kumar, 1994; Kumar *et al.* 1995, 1997). The combination of CARPT with CT has been used to produce unique data in multiphase systems such as bubble columns (Degaleesan, 1997; Degaleesan *et al.*, 1997, Chen *et al.*, 1998, 1999), liquid-solid and gas-liquid-solid fluidized beds (Limtrakul, 1996) and liquid-solid risers (Roy *et al.*, 1997). CARPT and CT are especially useful in providing information on opaque flow systems such as the ebullated bed.

The objective of this work was to determine if the incipient particle migration could be identified using CARPT. Specifically, it was desired to: 1) evaluate by CT scans if the gas-liquid distributor and sparger used could achieve relatively uniform gas holdup distribution in the packed bed, 2) use the evaluated distributor and sparger to determine by CARPT the conditions at which solid particles first start to move in the bed, i.e., identify the conditions for incipient particle motion, 3) determine particle trajectories, mean velocities and motion patterns when significant particle motion occurs.

2. EXPERIMENTAL SETUP AND OPERATING CONDITIONS

2.1 Experimental Setup

The packed bed reactor used in this study is made of a Plexiglas pipe with an inner diameter of 30.5 cm. The solids phase consists of 3.2 mm alumina particles (Activated Alumina, ALCOA Industrial Chemicals). During the experiments, the packed height of the bed was kept at about 90 to 100 cm above the distributor (L/D = 3~3.3). The schematic of the experimental setup is shown in Figure 1. The flowrates of both the gas phase (compressed air) and liquid phase (tap water or solution of 10% wt ethanol in tap

water) are measured by rotameters. The gas and liquid phase, which are in co-current up-flow in the bed, are introduced to a plenum which is located below the distributor. Both air and water flow upward through the holes in the distributor. The distributors investigated are perforated plates. Distributor I has 204 holes of 0.77 mm, of which 180 are distributed in 9 rings of 1.5 cm apart with 20 holes in each ring. The other 24 holes are equally distributed in the outer ring which is also 1.5 cm apart from the adjacent ring. This yields a total open area of 0.13%. Distributor II has 96 holes of 1 mm in diameter, yielding an open area of 0.1%. The holes are distributed with a trianglular pattern. In addition, a gas sparger is used in the plenum with distributor II to improve the gas distribution before the gas flows up with the liquid to the bed through the distributor. The gas sparger consists of four stainless steel tubes arranged as a cross. In each tube, there are two pairs of 3 mm holes which are located at 53 mm and 118 mm from the center of the cross. The two holes for each pair are positioned at 180 degrees. During the experiments, all the holes in the gas sparger were pointing in the horizontal direction to get a more uniform gas distribution. An expanded section of the column (45.7 cm in diameter and 45.7 cm in height) was used on the top to separate the gas from the liquid. The gas is vented while the liquid flows to a tank for recycle.

2.2 CT Facility

The CT scanner in CREL is a third generation fan-beam in house gamma-ray scanner. The details of the hardware and software have been described elsewhere (Kumar, 1994; Kumar *et al.*, 1995; 1997) and will be summarized here. The scanner consists of an array of collimated NaI (Tl) detectors of 5 cm in diameter (9 detectors were used for the present study which can cover the whole cross section of the column) and a gamma-ray source (an encapsulated Cesium-137 with activity of about 92 mCi). The detectors and the source are mounted on a plate that can be rotated, which makes it possible to get a 360° scan around the column. The whole assembly can be moved up and down to scan different axial levels of the column. This design of the CT scanner yields a spatial resolution of 0.35 cm in the horizontal direction and 1.0 cm in the vertical direction. In order to get statistically significant results and in order to reduce the position effect on the

scans, CT scans were conducted around the whole cross section (360 degrees) with total scanning time of about 2 hours.

The intensity of a beam of monoenergetic radiation that is transmitted through a homogeneous material can be expressed by the Beer-Lambert's law:

$$T = \frac{I}{I_0} = e^{-\rho\mu l} \tag{1}$$

where T is the transmission ratio, I_0 is the incident radiation, I is the detected radiation, μ is the mass attenuation coefficient, ρ is the medium density, and l is the path length through the medium. If the medium is made of two materials with mass attenuation coefficients μ_1 and μ_2, densities ρ_1 and ρ_2, and thickness l_1 and l_2, respectively, the net attenuation A is:

$$A = \rho_1\mu_1 l_1 + \rho_2\mu_2 l_2 \tag{2}$$

If $l_1 = \varepsilon_1 L$ and $l_2 = \varepsilon_2 L$, where $L = l_1 + l_2$, then

$$A = [\rho_1\mu_1\varepsilon_1 + \rho_2\mu_2(1-\varepsilon_1)]L \tag{3}$$

The measured quantity $ln(I_0/I)$ is equal to the integral sum of the attenuation through the material along the beam path. For tomography, attenuations are measured along a number of such beam paths through the object from different directions around it. Given a set of attenuation measurements, the density distribution (image) can be reconstructed by using a suitable reconstruction algorithm. In this work, the Estimation-Maximization (EM) algorithm is used for image reconstruction. The details of the algorithm are provided elsewhere (Kumar, 1994).

As discussed above, with a single source CT scanner, one can quantify the individual phase holdup only for a two phase flow system. A dual source CT scanner is needed to quantify the individual phase holdups for a three phase flow system. However, for a gas-liquid-solid three phase flow system, if the gas and liquid superficial velocities are not so high that fixed bed state can be assumed in the column (except at the very top of the bed), one can still evaluate the individual phase holdups (volumetric fraction) for each of the three phases by using several scans as discussed below.

For a three phase system, Equation (2) can be written as

$$A_{g-l-s,ij} = [\rho_g \mu_g \varepsilon_{g,ij} + \rho_l \mu_l (1 - \varepsilon_{g,ij} - \varepsilon_{s,ij}) + \rho_s \mu_s \varepsilon_{s,ij}] L_{ij} \quad (4)$$

where A_{ij} is the total attenuation in the pixel ij, ρ_g, ρ_l, ρ_s are the densities, μ_g, μ_l, μ_s are the linear attenuation coefficients and $\varepsilon_{g,ij}$, $\varepsilon_{l,ij}$, $\varepsilon_{s,ij}$ are the holdups (volumetric fractions) for the gas, liquid and solids phase, respectively. L_{ij} is the length along which a particular gamma ray beam passes through this pixel.

Similarly, for the same column containing a pure liquid, the column containing gas and solids, and the column containing liquid and solids, for the same pixel and the same beam, the following relationships hold for the total attenuation:

$$A_{l,ij} = \rho_l \mu_l L_{ij} \quad (5)$$

$$A_{g-s,ij} = [\rho_g \mu_g (1 - \varepsilon_{s,ij}) + \rho_s \mu_s \varepsilon_{s,ij}] L_{ij} \quad (6)$$

$$A_{l-s,ij} = [\rho_l \mu_l (1 - \varepsilon_{s,ij}) + \rho_s \mu_s \varepsilon_{s,ij}] L_{ij} \quad (7)$$

Since $\rho_g << \rho_l$ *or* ρ_s , and μ_g, μ_l, μ_s are of the same order of magnitude, the attenuation caused by the gas phase is negligible. Thus, combining Equation (5), (6) and (7) one can get an estimate of solids holdup in the pixel ij:

$$\varepsilon_{s,ij} = 1 - (A_{l-s,ij} - A_{g-s,ij}) / A_{l,ij} \quad (8)$$

Combining Equations (4), (5), (6), (7) and (8) yields an estimate of local gas holdup:

$$\begin{aligned} \varepsilon_{g,ij} &= 1 - \varepsilon_{s,ij} - (A_{g-l-s,ij} - A_{g-s,ij}) / A_{l,ij} \\ &= (A_{l-s,ij} - A_{g-l-s,ij}) / A_{l,ij} \end{aligned} \quad (9)$$

Liquid holdup is obtained from:

$$\varepsilon_{l,ij} = 1 - \varepsilon_{g,ij} - \varepsilon_{s,ij} \quad (10)$$

Therefore, by scanning the same column filled with pure liquid phase, with a packed bed consisting of gas and solid phase only, with a packed bed consisting of liquid and solid phase only, and finally scanning the gas-liquid-solid system at the same position, the holdups for all the three phases can be obtained. This is only possible since the solids are assumed not to move and to preserve the same packed bed configuration for each scan.

2.3 CARPT Facility

The CARPT facility in CREL has been successfully applied in the studies of liquid motion in bubble columns (Devanathan *et al.*, 1990; Moslemian *et al.*, 1992; Yang, *et al.*, 1993; Degaleesan, 1997; Degaleesan *et al.*, 1997; Chen *et al.*, 1998, 1999), solids motion in gas-solid fluidized beds (Moslemian *et al.*, 1992), solids motion in liquid-solid and gas-liquid-solid fluidized beds (Limtrakul, 1996) and liquid-solid risers (Roy *et al.*, 1997). Details about the software and hardware can be found elsewhere (Devanathan, 1991, Degaleesan, 1997). For the present study, a radioactive Scandium-46 particle (about 0.5 mm in diameter and 2.89 g/cm^3 in density with activity of 450 μCi) was embedded into an aluminum particle with a diameter of 3.2 mm. In order to match the density of the solid phase (alumina) which is to be monitored, an air void is created inside the aluminum particle so that the composite density (scandium-aluminum-air) is equal to the density of the solid particle (alumina) which is 1.6 g/cm^3 when saturated with water. With the particle size and density the same as that of the solids, the radioactive tracer particle is able to successfully mimic the dynamic behavior of the solids phase. The intensity of the gamma rays emitted by the tracer particle is continuously monitored (frequency =50) by 16 NaI (Tl) scintillation detectors (5 cm in diameter) which are strategically located around test section. In order to determine the exact position of the tracer particle at each instant in time, calibrations are performed for each detector, providing a relationship between the distance from the detector to the particle and the intensity count received by the detector. Using this calibration information and the intensities of radiation received by detectors at each sampling period, the instantaneous position of the particle is calculated by an inverse mapping algorithm. The moving velocities of the particle could then be obtained by time differentiation (Devanathan, 1991, Degaleesan, 1997).

As mentioned above, calibrations for all the detectors are needed prior to the experiments to get the relationship between the intensity count received by a detector and the distance between the detector and the tracer particle. For a given source strength, the intensity of radiation (radiation counts) received by a detector from the radioactive source decays exponentially with the distance between the detector and the source, due to factors such

as attenuation and build up. This is also a complex function of column geometry and the medium being traveled, hence, the holdups of the three individual phases. Therefore calibration must be conducted under the operating conditions (in-situ calibration). In this study, 16 detectors were used to get the instantaneous positions of the particle in the whole packed bed. The detectors were arranged around the column in such a way that, wherever the radioactive particle is, there are at least 3 - 4 detectors in different directions that are close to the particle except near the bottom of the column where no detectors were mounted. Calibration experiments for CARPT involve positioning the radioactive tracer particle at several hundred known locations throughout the column and measuring the intensity counts received by the detectors. A specially designed calibration device was used for calibration in this study. The details of the calibration device is described elsewhere (Degaleesan, 1997). It is essentially consists of a hollow frame that is fixed on to the top flange of the expansion part of the column. The center of the frame is aligned with the axis of the column. Placed on this frame is a circular plate that is positioned between four guiding wheels that allow rotation of the plate around the axis of the column. Marks on the frame are made to indicate various angular positions. A slot is machined on the plate that passes through the center of the plate, extending from one end of the plate to the other. Fixed on the plate, in alignment with this slot, is a UniSlide control. Mounted on the UniSlide is a clamping device to hold a stainless steel rod of 12 mm in diameter. The entire rod consists of two sections that can be screwed together with perfect alignment. Along the rod, scaling marks are made to indicate the axial position of the particle. The radioactive particle is held on the tip of another smaller aluminum rod, 15 cm long and 6 mm in diameter, screwed into one end of the rod. Vertical movement of the rod allows for the axial positioning of the radioactive particle, while the UniSlide control knob determine the radial position of the particle and the rotation of the plate provides for the azimuthal movement. The above device allows for the precise movement of the radioactive particle to known locations in the column without changing the loading of the solids phase during the calibration.

In this study, a total of 901 calibration positions were employed to generate a fine three dimensional mesh in the column. These 901 positions were equally distributed at 17 axial levels with 53 points for each level. For each of the detectors, the radiation counts (intensity counts) and the distance between the radioactive particle and the detector were acquired for all the calibration points. A cubic spline fitting method was used to get the calibration curves which are used to reconstruct the instantaneous positions of the tracer particle.

3. EVALUATION OF THE DISTRIBUTORS/SPARGER

Since gas holdup distribution in the column is believed important to the solids motion, it was necessary to check, whether the gas holdup distribution in the bed is uniform. CT scans were conducted at the following conditions to evaluate the cross sectional gas holdup distribution obtained with distributor I and II.

Liquid: Tap water

Gas: Compressed air

Total height of packed bed: 91 cm from the distributor

Superficial gas velocity: 2 cm/s

Superficial liquid velocity: 0.3 cm/s

Axial levels for scanning: 1) 56 cm above the distributor

2) 20 cm above the distributor

At first, distributor I was investigated. CT scanning results show that the cross sectional gas holdup distribution obtained with this distributor is not quite uniform, with gas holdup of 0.13 in the center and 0.08 near the wall of the bed. This non-uniform distribution of gas holdup is not desired in the particle tracking study. Therefore distributor II, together with the cross-shaped sparger, is further evaluated with CT scanning.

Figures 2a and 2b represent the cross sectional gas and solids holdup distributions obtained with distributor II at axial levels of 56 cm from the distributor, respectively.

Figure 3a shows the azimuthally averaged radial gas holdup profiles at the two axial positions, 56 and 20 cm from the distributor, while Figure 3b shows the azimuthally averaged radial solids holdup profiles at the same axial positions. The gas and solids holdups are quite uniformly distributed in the cross section of the bed as seen from Figure 2a and 2b. The gas holdup profiles are relatively flat with about 0.11 in the center and 0.09 at the wall of the column (see Figure 3a), giving a cross sectional averaged gas holdup of about 0.095. The solid holdup (volumetric fraction) profiles are also relatively flat except near the wall where some artifact may exist due to wall effect. The cross sectional averaged solid holdup is about 0.66, which is very close to the value commonly reported in the open literature.

It should be mentioned that no solids motion was observed visually under the conditions mentioned above, which is also confirmed by monitoring the radiation counts using a radioactive particle. However, with ethanol-water solution (10% ethanol by weight), which is used in the particle tracking experiments, and at the same gas and liquid superficial velocities, significant solids motion was observed. This will be discussed shortly. For simplification and convenience of experimental operation (no liquid recycle is needed), tap water, instead of the ethanol-water solution, was used in the evaluation of distributors. Since the bubbles in the water-solution are much smaller than in water, it can be safely assumed that even under the ebullition conditions, the solids particles are still uniformly distributed in the cross section of the bed. Therefore, CT scans were not repeated with the ethanol solution.

4. PARTICLE TRACKING STUDY USING CARPT

To identify the conditions (gas and liquid superficial velocities) at which the solid particles start to move in the packed bed with two-phase upflow, CARPT experiments were performed. The liquid phase used was ethanol (AAPER Alcohol and Chemical Co., 190 Proof -95%) - water solution (10% ethanol by weight) unless otherwise indicated. The concentration of ethanol in the solution was measured by an optical reflex meter (2WA-J, Shanghai, China) every 30 minutes and some ethanol was periodically added to

the solution in order to keep the ethanol concentration constant during the experiments. Moreover, a fresh ethanol solution was always prepared and used after 24 hours. The total height of the solids packed bed was kept at 97 cm from the distributor for all the CARPT experiments.

4.1 Preliminary CARPT Experiments

There are 16 detectors mounted around the column (the lowest two detectors were 44 cm above the distributor). If the radioactive particle is not moving in the bed, the radiation counts detected by the detectors should be constant with time. In other words, if the radiation counts received by the detectors vary with time, the particle must be moving in the bed. This was verified by checking the radiation counts received by the detectors for a water filled packed bed in which the radioactive particle, fixed at the tip of a 12.7 mm stainless steel rod, was placed at three different positions. The three positions used were as follows (see Figure 4a and 4b):

Position 1: center of the column, 10 cm below the solids free surface

Position 2: center of the column, 12.5 cm below the solids free surface

Position 3: 2.5 cm from the center of the column, 12.5 cm below the solids free surface

Figures 5a and 5b illustrate the radiation counts received over 30 minutes for the three radioactive particle positions for detector 3 and detector 8, respectively, which were placed at different axial and azimuthal positions. It is obvious that: 1) the intensity counts are constant with time and 2) both of the two detectors can easily distinguish different positions of the particle. In other words, if the tracer particle moves by 2.5 cm from its original position, there will be a significant change in intensity counts for the same detector.

In order to identify the conditions at which the solids particles start to move in the bed experiments were conducted by releasing the particle into the bed, and collecting the radioactive emissions at all detectors. Different runs were performed by reducing the superficial gas velocity while keeping the liquid superficial velocity the same (0.3 cm/s).

The radioactive particle was originally placed at the position which is 47 cm above the distributor and 8 cm from the center of the column. Figures 6a and 6b display the intensity counts received by the detectors over one hour at superficial gas velocities of 1.5 cm/s and 1.7 cm/s, respectively. At 1.5 cm/s superficial gas velocity (Figure 6a), the intensity counts received by the four detectors are essentially constant. Only slight oscillations are observed at closer scrutiny (by expanding the time scale) but there is no long time drift in intensities. This implies that while the particle may be periodically moving, its movement is oscillatory in character and confined to at most one or two particle positions around its center. However, long term changes in intensity counts with time can be observed at gas superficial velocity of 1.7 cm/s for the same detectors as shown in Figure 6b, indicating that the particle is now moving slowly but definitely. Clearly, a long time drift in the intensity counts indicates that the particle is now moving away from its original location. Thus, this operating condition can be considered as the one at which incipient long distance particle movement occurs. It was expected that at liquid superficial velocity of 0.3 cm/s and gas superficial velocity of 2.0 cm/s the particles will move significantly inside the bed, which was confirmed by a similar experiment conducted at these conditions. As seen in Figure 6c the particle is moving noticeably after 15 minutes of the experiment. Hence, CARPT experiments were conducted at these conditions to track the particle movements inside the bed.

4.2 Results and Discussion of CARPT Experiments

Once the calibration is properly conducted, CARPT experiments can be run to get the information regarding particle motion. This was done by placing the radioactive particle in some position in the bed and running the experiment for many hours to get sufficient data. Two different initial particle positions were used: one was in the center of the column and 20 cm below the solid free surface, and the other one was 4 cm from the column wall and 20 cm below the solid surface. It should be noted that the original position of the particle is not important since the particle can move anywhere in the column during the experiments. In this study, CARPT data was collected for 20 hours. However, since the particle moves very slowly in the bed, the particle cannot visit most parts of the column even in 20 hours. This is different from normal CARPT experiments

for bubble columns conducted in CREL, in which the particle moves fast and can visit every location in the column many times so that ensemble averaged information can be obtained.

Figures 7a and 7b show typical trajectories of the particle over 1 hour. The particle original position was in the center of the column and 20 cm below the free solids surface. Figure 7a represents the z trajectory (axial position) of the particle while Figure 7b presents the x and y trajectories (cross sectional position) of the particle. The origin of the coordinates is the center of the distributor. It is obvious that the particle is moving throughout the column. It takes about 30 minutes for the particle to move from the top to the bottom (20 cm above the distributor) of the bed, indicating an axial migrating velocity of about 2.6 cm/min during this particular time period. Compared with axial movement, the radial movement of the particle is much less pronounced as evident from Figure 7b.

In order to get the particle velocity, the whole bed was divided into fictitious cells, and particle position at each sample time was identified and assigned to a cell using the CARPT calibration curves. An instantaneous velocity was assigned to a cell that contains the mean particle position between two successive locations. The instantaneous velocities were then averaged in each cell over the whole time span of the CARPT experiments to get time averaged particle velocities. Figures 8a and 8b are the axially and azimuthally time averaged (over 20 hours) axial and radial velocity profiles. One can see from the figures that solids particles move upwards in the center of the column and move downwards near the wall. The maximum up flow velocity is about 2.8 cm/min occurring near the center of the column, while the maximum down flow velocity is about 3.4 cm/s occurring at dimensionless radius of 0.78 (Figure 8a). The flow inversion point is at dimensionless radius of about 0.42. This flow pattern is similar to those observed in gas solid fluidized beds (Moslemian *et al.*, 1992), in bubble columns (Devanathan *et al*; Franz *et al.*, 1984; Menzel *et al.*, 1990; Mudde *et al.*, 1997; Chen *et al.*, 1998a, 1998b), in liquid solid and gas liquid solid fluidized beds (Limtrakul, 1996; Larachi, *et al.*, 1995) and in liquid-solids risers (Roy *et al.*, 1997) although in the present case the results are

not based on ensemble averaging. Compared to the axial velocity, the radial velocity of the particle is much smaller as evident from Figure 8b, with maximum velocity of 0.4 cm/min. In the first approximation, it can be assumed that solid particles in the bed are basically moving in the axial direction at the employed operating conditions.

Figure 9 presents the side view of the azimuthally averaged two dimensional velocity vector plot. The arrows represents the direction and magnitude of the velocity vectors. It should be noted that in some regions/positions there is no arrow since the radioactive particle never visited those regions/positions. Therefore the velocities (directions and magnitudes) are unknown in these regions/position, which does not imply that the velocities are zero. From the vector plot, one can see that the radioactive particle was traveling axially and radially throughout the bed except the bottom (up to 20 cm above the distributor).

5. CONCLUSIONS

CT scans were conducted to evaluate the cross sectional gas holdup distribution in the air-water-solids (alumina particles of 3.2 mm diameter) system at superficial gas velocity of 2.0 cm/s and superficial liquid velocity of 0.3 cm/s, and it was found that at these conditions the solids are essentially in the fixed bed. The gas holdup distribution obtained with distributor II (perforated plate with 96 holes of 1 mm in diameter uniformly distributed in triangular pattern, open area of 10%) with a cross-shape sparger in the plenum is relatively uniform with gas holdup of about 0.11 in the center and 0.09 near the wall of the column. The cross sectional averaged gas and solids holdups in the bed are about 0.095 and 0.66, respectively.

In the air-water-ethanol (10% ethanol in weight)-solids system, at gas superficial velocity of 1.7 cm/s and superficial liquid velocity of 0.3 cm/s, solids particles in the bed start to move and travel long distance. These gas and liquid velocities correspond to the minimun fluidization conditions for this system.

In the air-water-ethanol (10% ethanol by weight)-solids system, at superficial gas velocity of 2.0 cm/s and superficial liquid velocity of 0.3 cm/s, the solid particles in the bed exhibit significant axial movement throughout the column with up flow in the center and down flow near the wall of the column. The time averaged maximum upward and downward velocities of the particles are about 2.8 cm/min and 3.4 cm/min, respectively. The radial movement of the solids particles is negligible.

CARPT and CT can be used to provide a valuable data base for establishing a correlation or verifying a model for the onset of incipient two phase flow fluidization of packed beds.

6. NOTATION

A = net attenuation

$A_{l,\,ij}$, $A_{g\text{-}s\,ij}$ $A_{l\text{-}s,\,ij}$ $A_{g\text{-}l\text{-}s,\,\mathrm{ij}}$ = net attenuation of pure liquid phase, gas solid phase, liquid solid phase and gas liquid solid phase in the *ij* pixel

D = column diameter, cm

I = detected radiation

I_0 = incident radiation

l = path length

L = total path length through the composite material

L_{ij} = total path length through the ij pixel

R = radius of column, cm

r = radial position, cm

T = transmission ratio

U_g = superficial gas velocity, cm/s

U_l = superficial liquid velocity, cm/s

Greek Letters

ε = phase holdup

ε_1, ε_2 = holdup of phase 1 and phase 2

$\varepsilon_{g,ij}$, $\varepsilon_{l,ij}$, $\varepsilon_{s,ij}$ = holdup of gas, liquid and solids in the ij pixel

μ = attenuation coefficient, g/cm^2

μ_1, μ_2 = attenuation coefficient of phase 1 and phase 2, cm^2/s

μ_g, μ_l, μ_s = attenuation coefficient of gas, liquid and solid phase, g/cm^2

ρ = density of material, g/cm^3

ρ_1, ρ_2 = density of phase 1 and phase 2, g/cm^3

ρ_g, ρ_l, ρ_s = density of gas, liquid and solid phase, g/cm^3

Subscripts

1, 2 = phases 1 and 2, respectively.

7. REFERENCES

Bascoul, A., J. P. Couderc, and H. Delmas, "Solids Motion in Liquid-Solid Fluidization (Mouvement des particules solides en fluidisation liquide-solide)", Chem. Eng. J. **52**, 235 (1993)

Chaouki, J., F. Larachi, and M. P. Dudukovic′, "Noninvasive Tomographic and Velocimetric Monitoring of Multiphase Flows", *Ind. Eng. Chem. Res.* **36**(11), 4476 (1997)

Chen, R. C. and L.-S. Fan, "Particle Image Velocimetry for Characterizing the low Structure in Three-Dimensional Gas-Liquid-Solid Fluidized Beds", *Chem. Eng. Sci.* **47**, 3615 (1992)

Chen, J., P. Gupta, M. H. Al-Dahhan, M. P. Dudukovic′, and B. A. Toseland, "Gas Holdup Distributions in Large Diameter Bubble Columns Measured by Computed Tomography", *Flow Meas. Instr.* **9**, 91 (1998)

Chen, J., F. Li,, S. Degaleesan, P. Gupta, M. H. Al-Dahhan, M. P. Dudukovic′, and B. A. Toseland, "Fluid Dynamic Parameters in Bubble Columns with Internals, *Chem. Eng. Sci.* (Proceedings of the 1998 15th International Symposium on Chemical Reaction Engineering, ISCRE 15, Sep 13-16 1998, Newport Beach, CA, USA) **54** (13-14), 2187 (1999)

Degaleesan, S., "Fluid Dynamic Measurements and Modeling of Liquid Mixing in Bubble Columns", *Ph. D. Thesis*, Washington University in St. Louis, St. Louis, USA, (1997)

Degaleesan, S., M. P. Dudukovic′, B. A. Toseland, and B. L. Bhatt, "A Two-Compartment Convective-Diffusion Model for Slurry Column Reactors", *Ind. & Eng. Chem.* **36**(11), 4670 (1997)

Devanathan, N., D. Moslemian, and M. P. Dudukovic′, 1990, "Flow Mapping in Bubble Columns Using CARPT", *Chem. Eng. Sci.* **45**, 2285 (1990)

Devanathan, N., "Investigation of Liquid Hydrodynamics in Bubble Columns via Computer Automated Radioactive Particle Tracking", *Ph.D. Thesis*, Washington University in St. Louis, St. Louis, USA, (1991)

Franz, K., T. Borner, H. J. Kantorek, and R. Buchholz, "Flow Structures in Bubble Columns", *Germany Chem. Eng.* **7**, 365 (1984)

Gross, E. W., and J. M. Kuhlman, "Three-component Velocity Measurements in a Turbulent Recirculating Bubble-driven Liquid Flow" *Int. J. Multiphase Flow* **18**, 413 (1992)

Halow, J. S., "Electrical Capacitance Imaging of Fluidized Beds, in *"Non-Invasive Monitoring of Multiphase Flows"*, Chaouki, J., Larachi, F., Dudukovic, M. P., Eds, Elsevier: Amsterdam, The Netherlands, Chapter 9, p 263 (1997)

Kantzas, A., "Computation of Holdups in Fluidized and Trickle Beds by Computer-Assisted Tomography", *AIChE Journal* **40**(7), 1254 (1994)

Kumar, B. S., "Computer Tomographic Measurements of Void Fraction and Modeling of the Flow in Bubble Columns", *Ph.D. Thesis*, Florida Atlantic University, USA, (1994)

Kumar, B. S., D. Moslemian, and M. P. Dudukovic, "A Gamma Ray Tomographic Scanner for Imaging Void Fraction Distribution in Bubble Columns" *Flow Meas. Instr.* **6**(1), 61 (1995)

Kumar, S. B., D. Moslemian, and M. P. Dudukovic′ , "Gas Holdup Measurements in Bubble Columns Using Computed Tomography", *AIChE Journal* **43**(6), 1414 (1997)
Larachi, F., G. Kennedy, and J. Chaouki, "3-D Mapping of Solids Flow Fields in Multiphase Reactors with RPT", *AIChE Journal* **41**(2), 439 (1995)

Limtrakul, S., "Hydrodynamics of Liquid Fluidized Beds and Gas-Liquid Fluidized Beds. *Ph.D. Thesis*, Washington University in St. Louis, St. Louis, USA, (1996)

Menzel, T., T. in der Weide, O. Staudacher, O. Wein, and U. Onken, "Reynolds Shear Stress for Modeling of Bubble Column Reactors", *Ind. Eng. Chem. Res.* **29**(6), 988 (1990)

Moslemian, D., N. Devanathan, and M. P. Dudukovic′, "Radioactive Particle Tracking Technique for Investigation of Phase Recirculation and Turbulence in Multiphase Systems" *Rev. Sci. Instrum.* **63**(10), 4361 (1992)

Mudde, R. F., J. S. Groen, and H. E. A. van den Akker, "Liquid Velocity Field in a Bubble Column: LDA Experiments", *Chem. Eng. Sci. (Proceedings of the 1997 3rd International Conference on Gas-Liquid-Solid Reaction Engineering,)* **52**(21-22), 4217 (1997)

Mude, R. F., W. K. Harteveld, H. E. A. van den Akker, T. H. J. J. van der Hagen, and H. van Dam, "Gamma Radiation Densitometry for Studying the Dynamics of Fluidized Beds", *Chem. Eng. Sci. (Proceedings of the 1998 15th International Symposium on Chemical Reaction Engineering, ISCRE 15, Sep.13-16, 1998, Newport Beach, CA, USA)*, **54** (13-14), 2047 (1999)

Roy, S., J. Chen, S. Kumar, M. H. Al-Dahhan, and M. P. Dudukovic′, "Tomography and Particle Tracking Studies in a Liquid-Solid Riser", *Ind. Eng. Chem. Res.* **36**(11), 4666 (1997)

Shollenberger K. A., J. R. Torczynski, D. R. Adkins, T. J. O'Hern, and N. B. Jackson, "Gamma-Densitometry Tomography of Gas Holdup Spatial Distribution in Industrial Scale Bubble Columns", *Chem. Eng. Sci.* **52** (13), 2037 (1997)

Yang, Y. B., N. Devanathan, and M. P. Dudukoviç, "Liquid Backmixing in Bubble Columns via Computer-Automated Radioactive Particle Tracking (CARPT)", *Experiments in Fluids* **16**, 1 (1993)

Yates, J. G., D. J. Cheesman, Y. A. Sergeev, "Experimental methods in Fluidized Research", *Int. J. Multiphase Flow* **20**, 297 (1994)

Yates, J. G., "Experimental Observations of Voidage in Gas Fluidized Beds", *In "Non-invasive Monitoring of Multiphase Flows"*, Chaouki, J., Larachi, F., Dudukovic, M. P., Eds.; Elsevier: Amsterdam, The Netherlands, Chapter 4, p141 (1997)

FIGURE CAPTION LIST:

Figure 8. Axially and azimuthally time averaged particle axial and radial velocities (U_g = 2 cm/s, U_l =0.3 cm/s, air-water+ethanol, two phase upflow)

(a) Axial velocity

(b) Radial velocity

Figure 9. Two dimensional velocity vector plot of azimuthally averaged particle velocity (U_g = 2 cm/s, U_l =0.3 cm/s, air-water+ethanol, two phase upflow. Note: The radioactive particle never visited the regions/positions where there is no arrow)

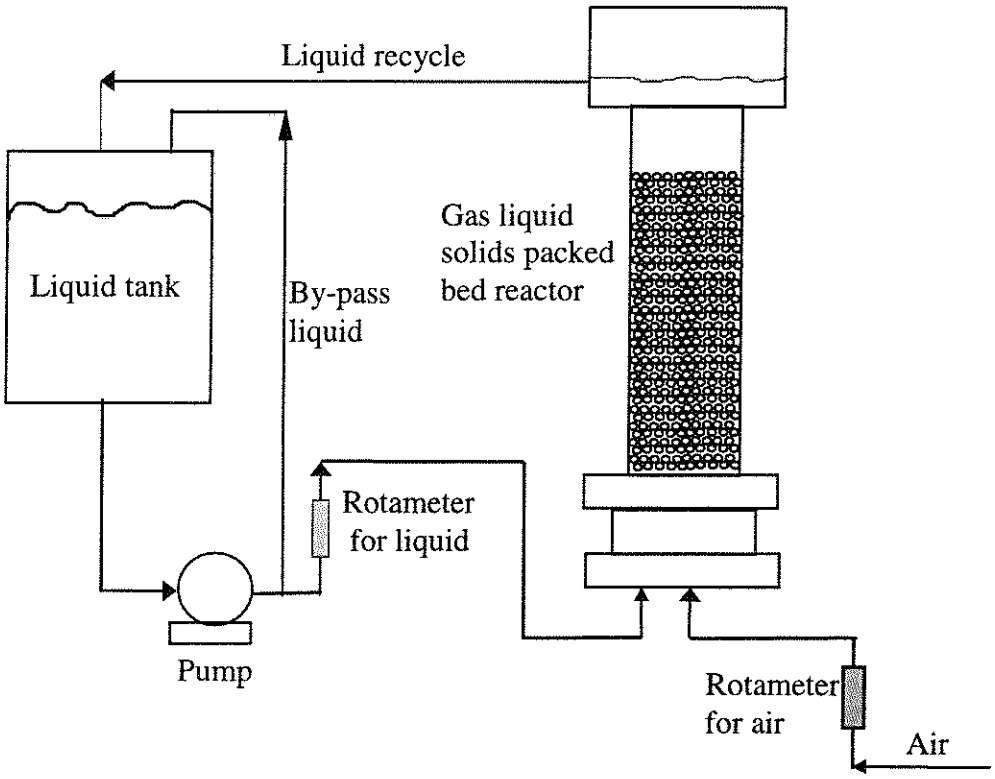

Figure 1. Schematic of the experimental setup

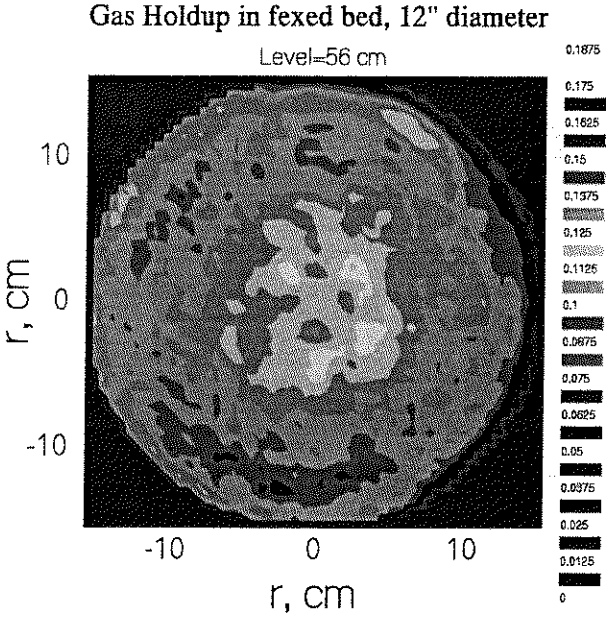

(a) Cross sectional gas holdup distribution

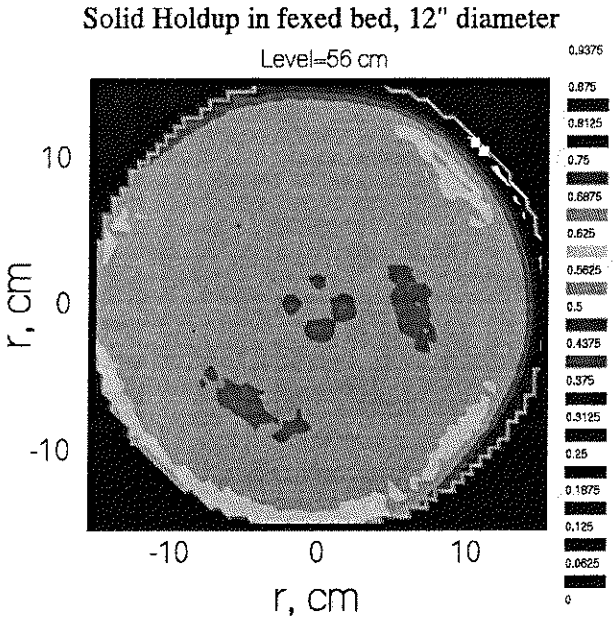

(b) Cross sectional solids holdup distribution

Figure 2. Time averaged gas and solids cross sectional distribution in the 30.5 cm diameter packed bed reactor (Distributor II, U_g = 2 cm/s, U_l =0.3 cm/s, air-water, two phase upflow)

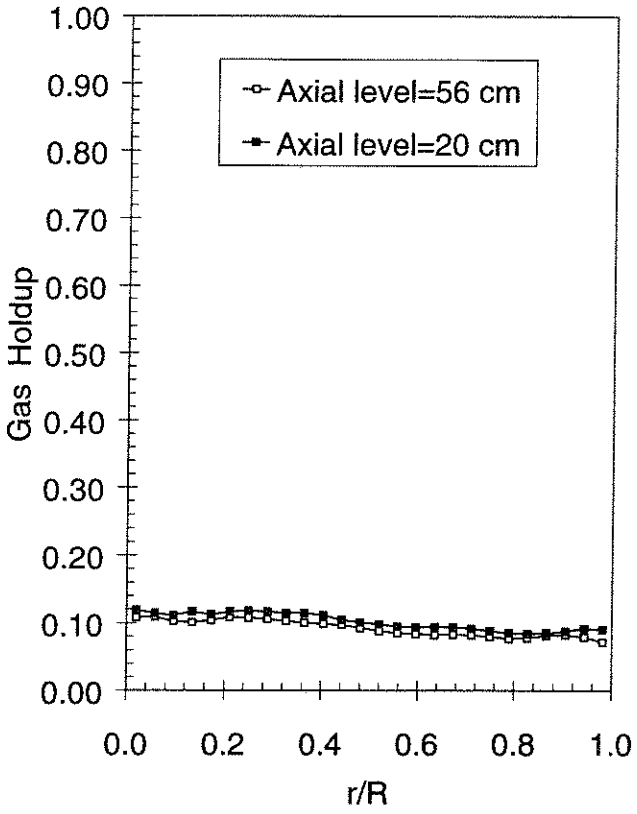

(a) Radial gas holdup profiles

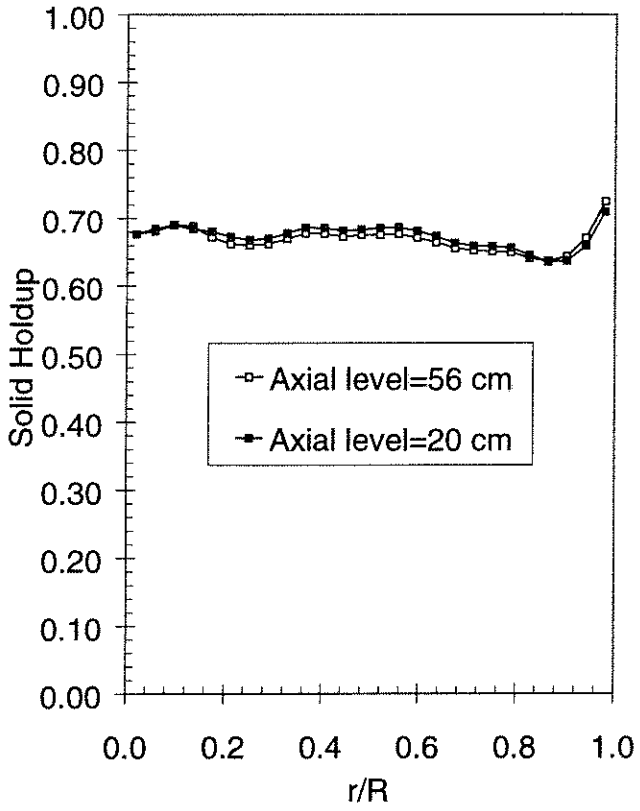

(b) Radial solids holdup profiles

Figure 3. Radial gas and solids holdup (Volumetric fraction) profiles in the 30.5 cm diameter packed bed reactor (Distributor II, U_g = 2 cm/s, U_l =0.3 cm/s, air-water, two phase upflow)

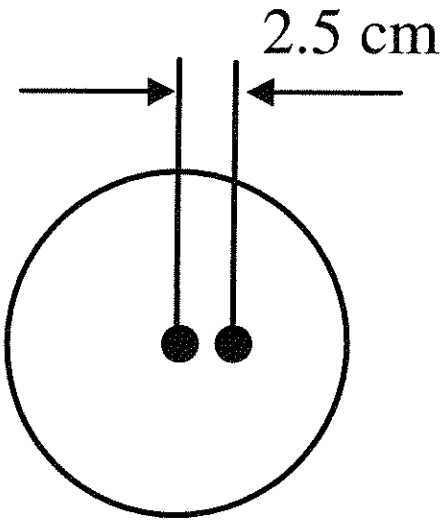

(a) Top view of the three positions

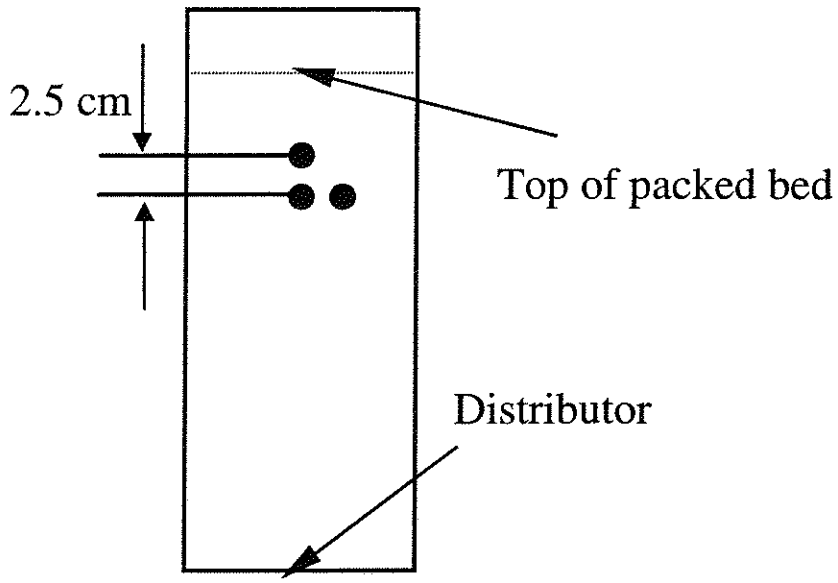

(b) Side view of the three positions

Figure 4. Diagram of the three particle positions

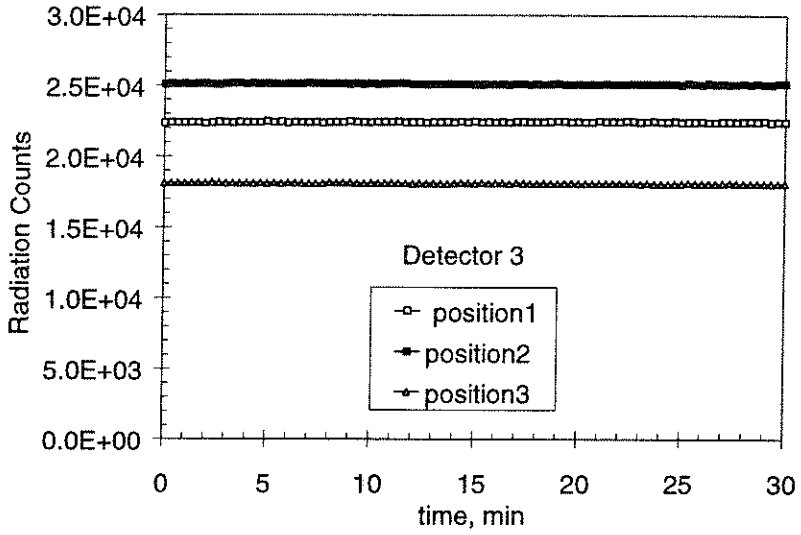
3.0E+04
2.5E+04
2.0E+04
1.5E+04
1.0E+04
5.0E+03
0.0E+00
Radiation Counts
Detector 3
position1
position2
position3
0
5
10
15
20
25
30
time, min

(a) Detector 3

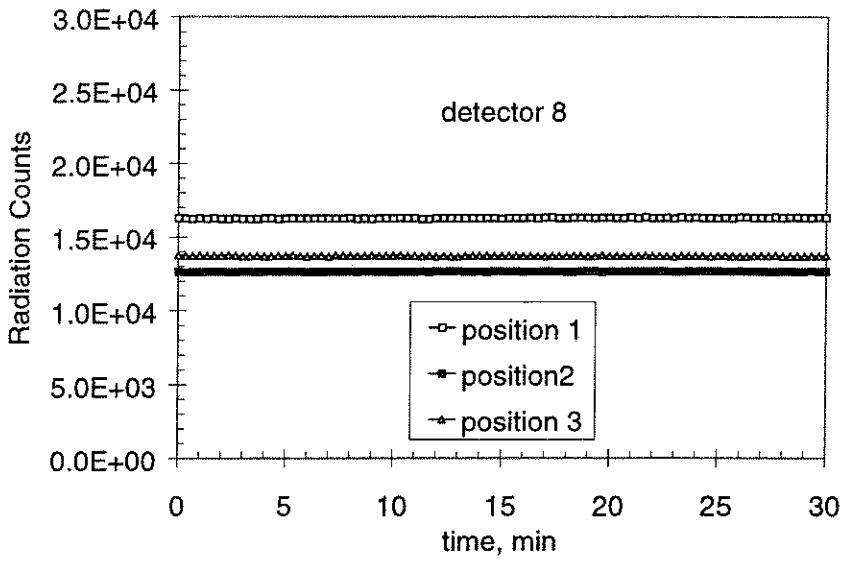

(b) Detector 8

Figure 5. Radiation counts with time for different particle positions obtained with air-water-solids system

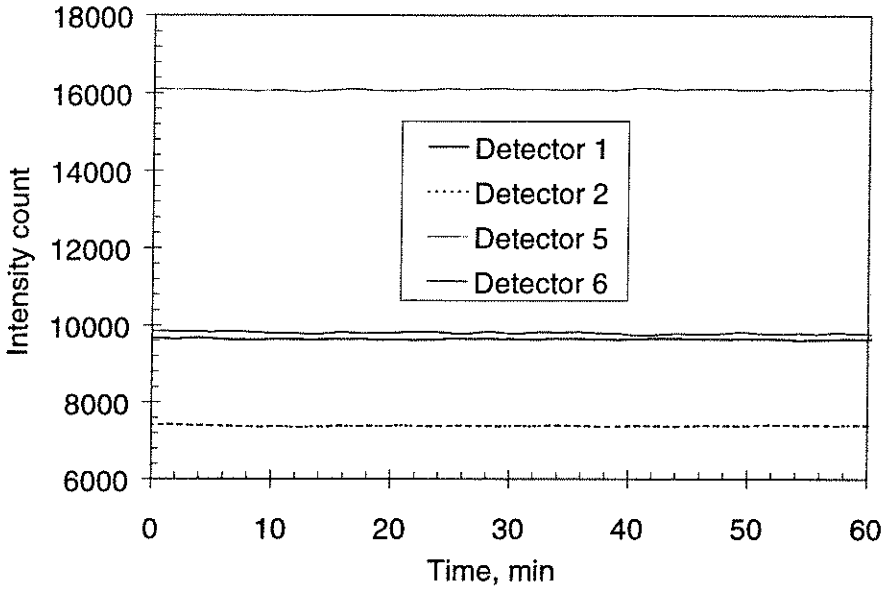

(a) Superficial gas velocity = 1.5 cm/s

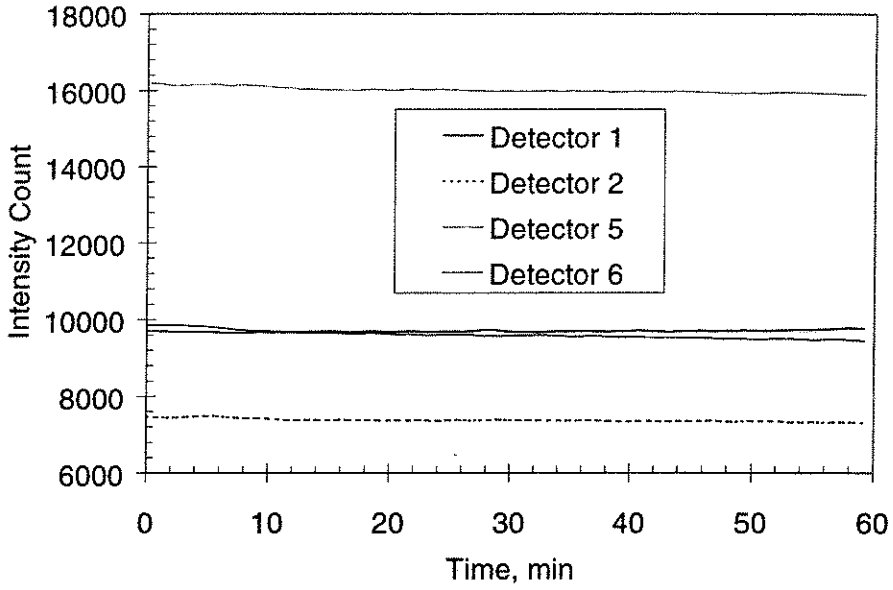

(b) Superficial gas velocity = 1.7 cm/s

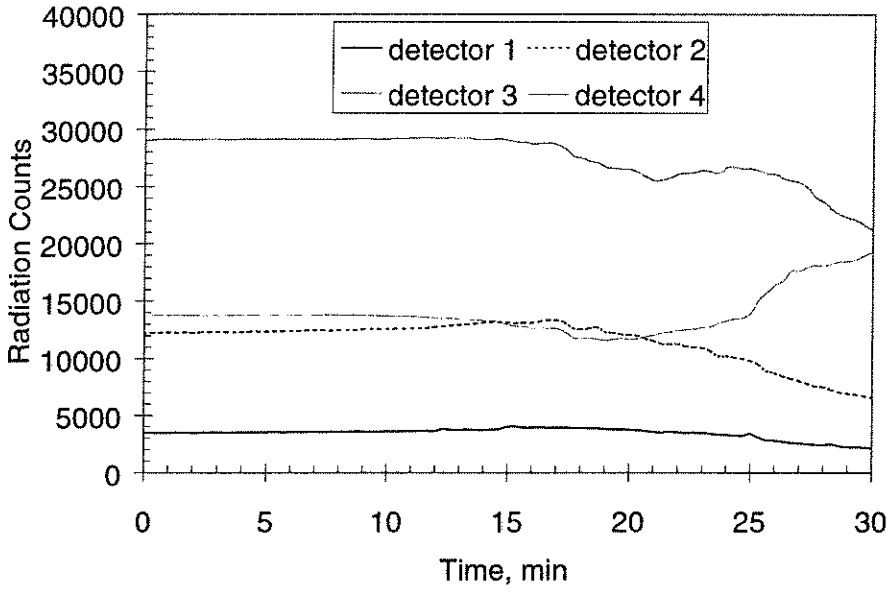

(c) Superficial gas velocity = 2.0 cm/s

Figure 6. Intensity counts with time (Distributor II, U_l =0.3 cm/s, air-water+ethanol, two phase upflow)

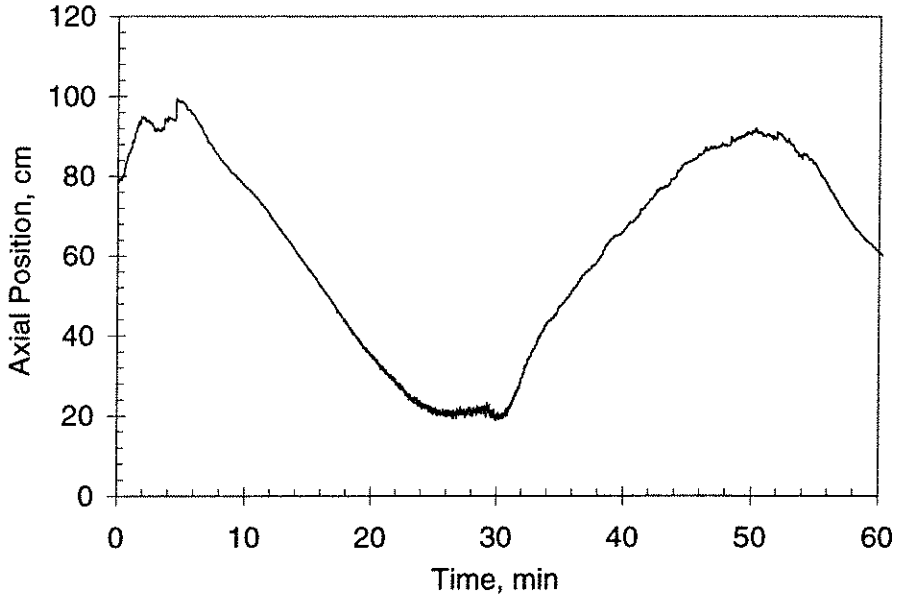

(a) Trajectory in z direction

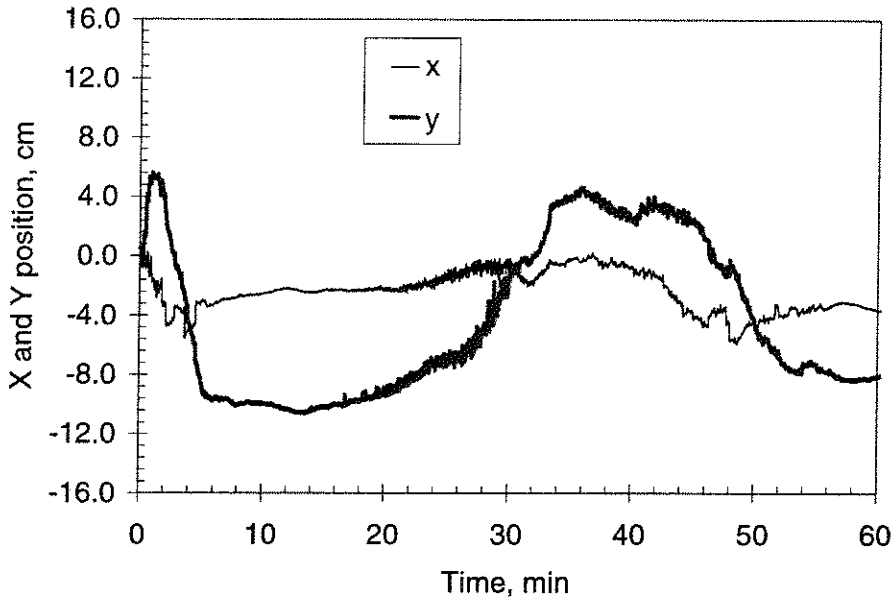

(b) Trajectories in x and y direction

Figure 7. Trajectories of the particle

(U_g = 2 cm/s, U_l =0.3 cm/s, air-water+ethanol, two phase upflow)

(Particle original position: center of the column and 20 cm below the solids free surface)

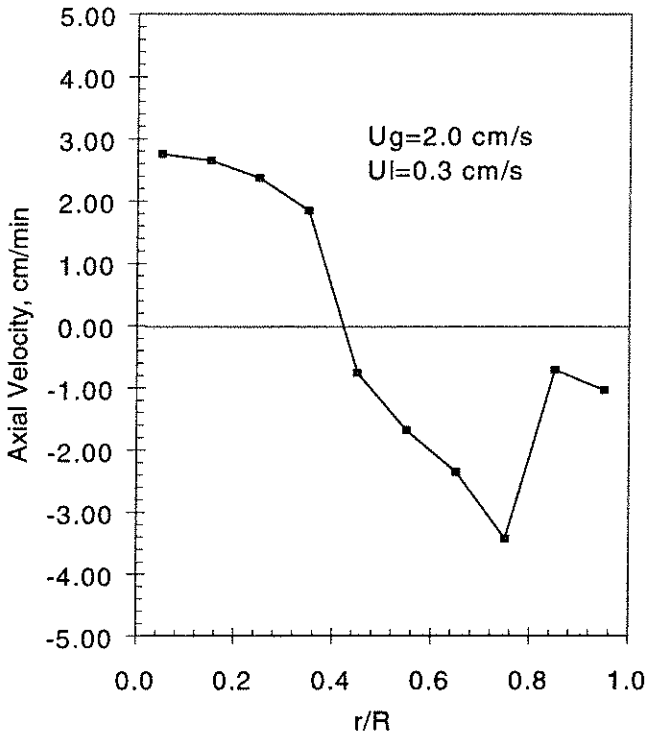

(a) Axial velocity

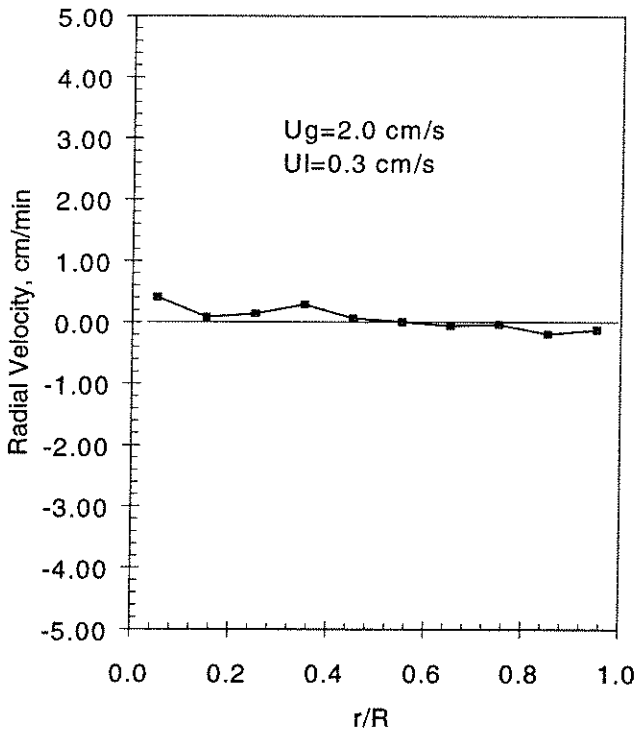

(b) Radial velocity

Figure 8. Axially and azimuthally time averaged particle axial and radial velocities (U_g = 2 cm/s, U_l =0.3 cm/s, air-water+ethanol, two phase upflow)

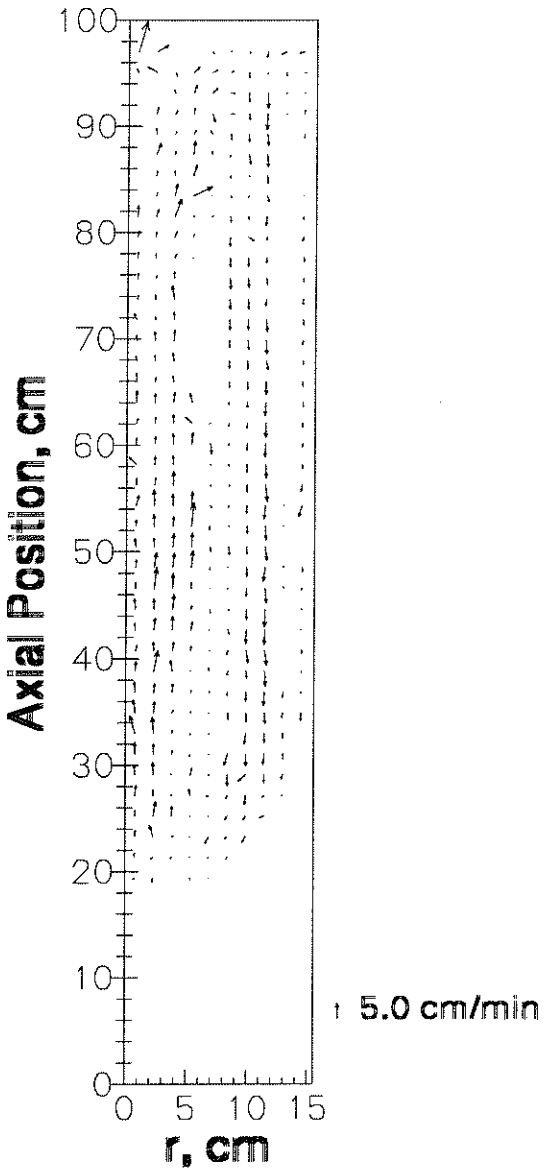

Figure 9. Two dimensional velocity vector plot of azimuthally averaged particle velocity (U_g = 2 cm/s, U_l =0.3 cm/s, air-water+ethanol, two phase upflow)

(Note: The radioactive particle never visited the regions/positions where there is no arrow)

A METHOD FOR ESTIMATING THE SOLIDS CIRCULATION RATE IN A CLOSED-LOOP CIRCULATING FLUIDIZED BED

See the attached report for:

A. Problem Definition
B. Research Objectives
C. Research Accomplishments

A Method for Estimating the Solids Circulation Rate in a Closed-Loop Circulating Fluidized Bed

Shantanu Roy*, Abdenour Kemoun,

Muthanna Al-Dahhan and M. P. Dudukovic

Chemical Reaction Engineering Laboratory
Department of Chemical Engineering
Washington University
St. Louis, MO 63130-4899

Paper Submitted to
Powder Technology

June 2000

* Present Address: Corning Incorporated, Process Engineering and Modeling, SP TD 01 2, Corning, NY 14831

Abstract

We propose a simple method for accurately estimating the solids circulation rate in a closed-loop liquid-solid circulating fluidized bed. The technique is based on the use of radioactive isotopes for estimating the solids velocity and volume fraction distribution in a chosen section of the circulating fluidized bed loop. The method is demonstrated for a liquid-solid circulating fluidized bed, and is readily applicable in other systems such as gas-solids circulating fluidized beds or closed-loop pneumatic and hydraulic transport lines. With minor modifications, the method can be used for industrial systems as well.

1. Introduction

Gas-solid circulating fluidized beds (Fan and Zhu, 1998; Kunii and Levenspiel, 1991) find wide application in the chemical and process industry, such as in fluidized catalytic cracking (FCC) (Kunii and Levenspiel, 1991), combustion (Engstrom and Lee, 1991), alumina calcining (Reh, 1986), and synthesis of fine chemicals like maleic anhydride (Statig, 1992). More recently, liquid-solid circulating fluidized beds are also finding applications in the process industry, such as the synthesis of aromatic and olefinic alkylates (Jin et al., 1998). In either of these systems, the fluid phase (gas or liquid) operates in a "flow-through" mode, while the solid phase (usually a catalyst) circulates in a closed loop formed between the riser (where the principal reaction is effected) and the regenerator (where the deactivated catalyst is regenerated). A schematic diagram of the typical configuration is shown in Figure 1.

One of the primary variables that determines the performance of the riser as a reactor is the mean solids circulation rate in the system, since together with the solids inventory in the riser it dictates the time of contact between the flowing fluid phase (containing the reactants) and the solid catalyst. For any given solids inventory charged to the system, circulating fluidized beds could be run in either a "fixed inventory mode" or a "variable inventory mode" (Berruti et al., 1995). In the former case, the solids circulation rate is not an independent variable and depends on the fluid flow rate. In other words, the fluid flow rate is controlled externally and the solids flux and circulation rate is allowed to reach an unknown steady state value depending on the total solids inventory, the flow resistances in the system, and the carrying capacity of the fluid. In the variable inventory setup, the solids flow control devices (such as mechanical devices like L-valves and

screw feeders or non-mechanical devices like venturis) are used to set the solids flow rate so that both the solids flux and the fluid flow rate are independent variables. However, even in this case the solids circulation rate may not be precisely known because the performance characteristics of the solids flow control devices are often unreliable and there is a need for their calibration.

From a reaction engineering viewpoint, it is of prime importance to know the solids circulation rate because that determines the fluid-solids contact times and the performance of the system as a reactor. Also of consequence in reactor performance is the backmixing in the phases. One may be erroneously led to believe that it should be possible to quantify the solids circulation rate and the backmixing by simple tracer-response experiments, and consequently use models from residence time distribution (RTD) theory (e.g., Nauman and Buffham, 1983) for predicting reactor performance. Unfortunately, for "closed loop" circulating systems (such as circulating fluidized beds, blood circulation in the human body, etc.), it has been shown by several researchers through rigorous theory that interpretation of a tracer impulse-response experiment, and extraction of the mean time of circulation based on a single injection and single measurement, is not unique (Fu, 1970; Naor et al., 1972; Nauman, 1974). Thus, determination of the mean circulation rate of solids is not a trivial problem, and techniques other than attempts at assessment of the first passage time distributions are required. The most obvious method to bypass the non-uniqueness problem is to "break-the-loop" and estimate the time-averaged solids flow rate across a given section assuming it to be an estimate of the overall solids circulation rate in the closed loop. It would be

preferable if the experimental method employed for this were "non-intrusive", i.e., it should not change the flow itself in any way.

Numerous studies in the open literature address this problem. Burkell et al. (1988) present an excellent review of some of the techniques that have been tried. These include: closing a permeable valve in the return leg and timing the solids accumulation rate; recording the force imparted by returning particles as they flow downwards from the cyclone/hopper into the solids standpipe; timing the descent of identifiable particles using visual inspection; measuring the pressure drop across a constriction in the loop; and estimating the solids flow rate by making a heat balance across a calorimetric section of the loop. Patience and Chaouki (1991) presented an approximate method for estimating solids circulation rate based on pressure drop measurements. Milne (1992) presented a method in which a rigid horizontal screen attached to a vertical rod is dropped into the bulk of the moving packed bed of solids in the return leg, and the time required for the tip of the rod to travel a prescribed distance is determined.

Most of the methods described above are intrusive, *i.e.*, they involve the introduction of one or more devices into the flow, which may in turn change the flow itself leading to a systematic error in the measurement. Some methods, such as estimating solids flow rate using wall pressure drop measurement, are non-intrusive but involve some *ad hoc* assumptions about the nature of the flow itself, which may not be borne out in reality. Further, some of these methods need *a-priori* calibration that is often difficult to perform *in-situ*.

In this paper, we present a method for measurement of solids circulation rate in a closed loop circulating fluidized bed that can be used in opaque systems as well without

introduction of any probes or other internals into the system. Thus, the method is non-intrusive, i.e., it does not alter the flow pattern of the solids in any way, and is relatively inexpensive as well. The method requires, however, a section in which the solids move in closed packed condition, and preferably in plug flow as well.

2. Experimental

The present method for measuring solids circulation rate was developed during our experimental work to study the flow pattern in liquid solid risers. A schematic diagram of the liquid solid riser setup is shown in Figure 2. Water is used at the continuous phase and 2.5 mm glass beads are used as the dispersed phase in the experiments. The setup consists of a vertical 6 in. diameter, 11 ft. riser with a downleg consisting of a hopper for storing solids inventory and a 2 in. diameter standpipe. The solid particles are fluidized and transported by upward flowing liquid in the riser and into the solids hopper wherein the solids inventory is maintained. A specially designed wire mesh separates the solids and liquid in the hopper. Solids flow down vertically through the vertical standpipe while the liquid flows out from the top of the hopper. A venturi eductor connecting the standpipe and the riser is used to recycle back the solids into the riser. Motive water, passing through the eductor, sucks the solids from the standpipe into the horizontal line connecting the eductor and the riser. The eductor thus functions like a non-mechanical solids flow directing device. Water can also be supplied to the riser through the line at the riser bottom. Thus, by varying the amount of liquid flow through the two lines, the riser can be run in variable inventory mode. The critical point to note is that while the eductor can be used to drive the solids into the riser, the exact flow rate of

solids for a certain eductor liquid flow rate is an unknown function that must be determined. Knowledge of this function is critical and a primary requirement for any kind of quantitative or comparative study of solids hydrodynamics in the riser section itself.

It may be noted here that in other kinds of circulating fluidized bed systems, *viz.* gas-solid systems which may be run in fixed inventory or variable inventory mode, solids flow is directed into the riser section in a similar fashion with the possible use of some other mechanical or non-mechanical device. The method of solids measurement discussed in this paper is readily applicable in such systems as well without any significant modification. Our system of interest, the liquid-solid circulating fluidized bed, serves as an example in which the method for estimating solids flow rate has been employed successfully.

2.1 Theory

The basic idea is to view the flow rate of solids as a function of the velocity of the solids ensemble in any section of the circulating loop as well as the volume fraction of solids in that section. Thus, if Q_s represents the solids volumetric flow rate in any section, v_s the velocity of solids in that section, ε_s the solids volume fraction in that section, and A the mean cross-sectional area of flow in that section of the loop, then:

$$Q_s = \int_A \varepsilon_s v_s dA \tag{1}$$

In general, in circulating fluidized beds the flow rate could be fluctuating in various zones of the loop and a representative estimate of solids circulation rate should be based only on

a time averaged measurement (where the time of averaging is greater than the largest time scale of fluctuation). Thus, time (ensemble) averaging the above equation (1) and recognizing that the time-average of the fluctuations in either v_s or ε_s is zero, yields:

$$\langle Q_s \rangle = \int_A \langle v_s \rangle \langle \varepsilon_s \rangle dA + \int_A \langle v_s' \varepsilon_s' \rangle dA \qquad (2)$$

The second term in equation (2), $\langle v_s' \varepsilon_s' \rangle$ could have contributions from two sources. First, there may be random fluctuations is both v_s' and ε_s' which may be correlated. Second, these quantities may not have any random fluctuations but may deviate in a deterministic and time-invariant (steady-state) fashion from the plug flow profile, and their profiles may be correlated. In either case, the second term above could contribute to the solids flow rate, $\langle Q_s \rangle$.

The key to our method is to identify a region in the circulation loop where the solid volume fraction is the highest and close to complete packing. Normally, in circulating fluidized beds, such regions often exist in the narrow pipelines connecting various units that need to allow a large solids flow rate. Standpipes that feed the solids to the riser often have this kind of flow (Fan and Zhu, 1998). For example, in the liquid-solid riser example presented here, the solids flow in the standpipe (Figure 2) was much like a moving packed bed.

Two facts are notable about such a section in which the solids move closed to packed bed condition. First, the fluctuations in both the solids velocity v_s' and the solids volume fraction ε_s' are negligibly small. Thus, the only contribution to the second term

on the right hand side of equation (2) can be from correlation between the time-invariant (steady state) solids volume fraction and velocity profiles. Second, in narrow tubes with a high solids flow rate, the cross-sectional variation of holdup is minor so that the right hand side of equation (2) may be approximated by writing the solids flow rate in terms of the cross-sectional average solids holdup and velocity:

$$\langle Q_s \rangle \approx \overline{\langle v_s \rangle}.\overline{\langle \varepsilon_s \rangle}.A \tag{3}$$

It is of interest, therefore, to assess the relative error incurred in using equation (3) instead of equation (2) in estimating the solids flow rate. This is done in the following manner.

When the standpipe flow is close to steady state packed flow, theoretical models for solids volume fraction distribution and velocity profiles can be invoked. The radial solids volume fraction distribution is estimated using the model proposed by Mueller (1991). The model predicts the radial solids volume fraction distribution in a tube of diameter D packed with uniform-sized particles of diameter d_p as a function of the dimensionless radial distance from the tube wall, r^*. The model equations can be summarized as:

$$\tilde{\varepsilon}_s(r^*) = (1-\varepsilon_b)\left(1 - J_0(ar^*)e^{-br^*}\right) \tag{4}$$

where:

$$r^* = \frac{D/2 - r}{d_p} \quad \text{, for} \quad 0 \le \frac{D/2 - r}{d_p} \tag{4a}$$

$$a = 8.243 - \frac{12.98}{\left(D/d_p + 3.156\right)} \quad \text{, for} \quad 2.61 \le D/d_p \le 13.0 \tag{4b}$$

$$a = 7.383 - \frac{2.932}{\left(D/d_p - 9.864\right)} \quad \text{, for} \quad 13.0 \le D/d_p \tag{4c}$$

$$b = 0.304 - \frac{0.724}{D/d_p} \tag{4d}$$

$$\varepsilon_b = 0.379 + \frac{0.078}{\left(D/d_p - 1.80\right)} \tag{4e}$$

ε_b represents the porosity (1.0-solids volume fraction) of the packed bed in the bulk region (i.e., away from the walls), and J_0 is the Bessel function of the first kind of order zero. Next, the radial solids velocity profile is assumed to be of the form:

$$\tilde{v}_s(r) = \left(\frac{n+2}{n}\right)\overline{v_s}\left[1 - \left(\frac{r}{R}\right)^n\right] \tag{5}$$

where n=2,3,4,5,6,7 represents the convexity of the velocity profile (n=2 being a parabolic profile and n=7 corresponding to the universal flat single-phase turbulence profile). In each of the profiles represented by equation (5), the steady state cross-sectional average solids velocity is the same, $\overline{\langle v_s \rangle}$.

The percentage error incurred in calculating the solids flow rate using the cross-sectional average quantities (equation (3)) is:

$$Error = \frac{\int_A \tilde{v}_s(r)\tilde{\varepsilon}_s(r)dA - \overline{\langle v_s \rangle}.\overline{\langle \varepsilon_s \rangle}.A}{\overline{\langle v_s \rangle}.\overline{\langle \varepsilon_s \rangle}.A} \times 100\% \tag{6}$$

The results from such a calculation, with five different particle sizes (d_p = 0.1 mm, 0.5 mm, 1.0 mm, 2.5 mm and 5.0 mm) flowing vertically in a 2 in. (5.08 cm) diameter tube are shown in Table 1. Clearly, the maximum error incurred in ignoring the profile of solids velocity and using the cross-sectional average instead is less than 4%. The error is considerably smaller when the velocity profile is flat (n=7) as compared to a parabolic velocity profile (n=2).

The conclusion from the above analysis is that in the event that the solids flows in close to packed bed condition, random fluctuations in solids volume fraction are absent, an error of less than 4% is made in using the cross-sectionally averaged solids velocity and holdup values for estimation of the total solids flow rate (equation (3)). The error is even smaller if in addition, the solids flow is close to plug flow. Our goal, therefore, is to use some simple but accurate means to estimate the cross-sectional average solids holdup and solids velocity in the standpipe.

2.2 *Densitometry Measurements*

For our specific setup of the liquid-solid riser, the region of most uniform (least fluctuating) solids flow was found to be the standpipe connecting the solids hopper and the eductor (Figure 2). Visual inspection of the flow pattern in the Plexiglas® standpipe (2 in. diameter) showed that the solids were moving downwards in a plug or piston flow like a moving packed bed.

In order to estimate the solids volume fraction in the piston flow of solids in the standpipe, the principle of densitometry was used. In this method, we make use of the

Beer-Lambert's Law which states that if I_0 is the intensity of a collimated beam of radiation in free space, and I the intensity when there is a medium of mass attenuation coefficient μ_{eff} and effective density ρ_{eff}, then the attenuation in the intensity of the beam is given by:

$$\frac{I}{I_0} = \exp\left(-\mu_{eff}\rho_{eff}l_{eff}\right) \tag{7}$$

where l_{eff} is the intervening distance between the source and the detector. Thus, if the intervening length and intensities can be measured, then equation (7) can be used to back-calculate the line-averaged effective attenuation coefficient. For a two-phase system, the effective attenuation coefficient is an average of the attenuation coefficients of the individual phases, each weighted by its respective volume fraction.

A schematic diagram of the experimental setup for the densitometry measurements is shown in Figure 3. A thick lead cylinder of around 5 in. diameter was positioned perpendicular to the standpipe and a hole of 2.7mm. diameter was drilled in the center. A small radioactive 2.5 mm diameter particle (of 300 μCi strength, Sc-46 isotope) was placed in this thick lead shielding so that the beam of gamma radiation ensuing from the 2.7 mm aperture was collimated. A NaI(Tl) scintillation detector was placed at a diametrically opposite location across the standpipe, in the same plane as that of the collimated tracer particle (densitometry source). The detector was connected in line to electronic hardware consisting of a photomultiplier tube, pre-amplifier, amplifier, scaler, discriminator and finally the signal is acquired on-line using a computerized data

acquisition system. The electronics used is standard for any kind of photon counting application and has been discussed elsewhere (Larachi et al., 1997; Tsoulfanidis, 1994).

This being a liquid-solid system, the photon counts (intensity of radiation *I)* are first acquired with the standpipe full of water. This serves as a background measurement for the system, I_w, and includes the attenuation properties of the wall of the standpipe and water. Thereafter, the system is run at a desired condition of interest and the photon counts I are recorded. It can be shown readily using equation (7), and the fact that the effective attenuation coefficient is the sum of individual phase attenuation coefficients weighted by their respective volume fractions, that:

$$-\ln\left(\frac{I}{I_w}\right)=\overline{\varepsilon_{s,l}}(\mu_s\rho_s-\mu_w\rho_w)l_{eff} \tag{8}$$

l_{eff} is the effective distance between the source and the detector center. In our case, the detector and source were placed along a diameter of the standpipe, though in general it can be placed along any other chord and the l_{eff} should be used accordingly.

It may be noted here that the $\overline{\varepsilon_{s,l}}$ calculated above is a "line-averaged" measurement (i.e. average solids holdup along the line connecting the source and the detector). In general, if the standpipe flow is not close to packed-bed condition, the cross-sectional solids holdup distribution in the standpipe could be different from the cross-sectionally averaged value. In order to experimentally verify this fact, the experiment described above could be repeated along various chords and the $\overline{\varepsilon_{s,l}}$ value calculated for

each. If these values are very close, then the assumption of close packing is verified. If the values are not close, and there are some differences in the measurements of $\overline{\varepsilon_{s,l}}$ along various chords, then the individual measurements could still be used to obtain a circularly symmetric "cross-sectional distribution" using the proceudre of Abel inversion (Kumar and Dudukovic, 1997). Cross-sectional averaging of that distribution would yield the true cross-sectionally averaged solids volume fraction. As shown later, in the present set of experiments the latter procedure was not deemed necessary since visual observation as well as measuring $\overline{\varepsilon_{s,l}}$ along various chords verified the existence of closed-packing of solids.

2.3 *Time-of-Flight Measurements*

Following equation (3), the other part of our solids flow measurement strategy involves the measurement of the mean solids streamwise velocity in the section of the standpipe being monitored. For this measurement, we follow a procedure similar to that employed in the Computer Automated Radioactive Particle Tracking (CARPT) technique (e.g. Devanathan et al., 1991; Larachi et al., 1997). For this a tracer particle is prepared by introducing a radioactive isotope (such as Sc-46) into a small metal or plastic sphere that has the same diameter as the solid phase particles, and also the same effective density as the solid particles. Thus, hydrodynamically this particle is exactly the same as the solid phase particles, though its presence in the system can be detected because it emits gamma ray photons.

For actual implementation of the experiment, the particle is left to move by itself in the closed loop circulating fluidized bed. Its flow behavior is deemed to be exactly similar to any other solid particle, since they have the same size and density. For measurement, two detectors are fixed perpendicular to and along the vertical standpipe. The schematic diagram of the arrangement is shown in Figure 5. Instead of a single detector as in Section 2.2, now two identical scintillation detectors are positioned along the standpipe and held a known distance apart. The electronics and hardware used are the same as discussed in Section 2.2 and shown in Figure 4.

As the solids circulate, the tracer particle makes multiple sojourns through the standpipe. The data acquisition is switched on and the gamma photon rates are counted continuously. In every visit the tracer particle makes to the standpipe, when the particle is the closest to Detector 1 (Figure 5), a peak is recorded in its counts time series, and similarly for Detector 2 when the particle is the closest to it. Since the data acquisition is performed at a constant frequency, the time difference between these peaks is found. This represents the residence time of the particle in one visit to the standpipe.

In multiple visits, the tracer particle traces out tortuous paths between the two detector planes because of some internal dispersion within the standpipe. Sometimes it passes close to the wall of the standpipe and sometimes through the center. For that reason, it is advisable to let the particle circulate with the solids in the system for a long time and trace many realizations so that a statistically significant and ergodic mean residence time may be evaluated, along with its variance:

$$\bar{t} = \frac{1}{N}\sum_{i=1}^{N} t_i \tag{9}$$

$$\sigma^2 = \frac{1}{N-1}\sum_{i=1}^{N}\left(t_i - \bar{t}\right)^2 \tag{10}$$

Finally, since the distance between the centers of the detectors, L, is known, the mean velocity, $\overline{v_s}$, can be evaluated:

$$\overline{v_s} = \frac{L}{\bar{t}} \tag{11}$$

The variance in equation (10) can be used to estimate the discrepancy in the solids velocity measurement.

It may be noted here that the procedure outlined above for estimating the mean flow rate does not suffer from any indeterminacy constraints that are known to exist in closed-loop circulating systems (Naor et al., 1972; Mann and Crosby, 1973). In our method, we are tracking a single particle to extract the RTD between two well-defined planes, which is distinct from measuring the circulation time distribution by injecting an ensemble of tracer particles in the system. From the latter approach, a unique flow rate cannot be extracted with two measurement points (Naor et al., 1972); while in our approach that is possible without any ambiguity.

3. Results and Discussion

As was discussed earlier, our primary interest in developing the above procedure was to estimate the solids circulation rate in the liquid-solid circulating fluidized bed shown in Figure 2. Solids flow rate through the eductor, and hence the overall circulation rate, could be varied through the eductor (Figures 3 and 5) by varying the motive water

flow rate but the nature of this variation had to be quantified, *i.e.,* the eductor had to be calibrated. The methods outlined in sections 2.1 and 2.2 were used for that purpose. The motive water flow rate through the eductor (Figures 3 and 5) was varied and the corresponding change in $\overline{\langle v_s \rangle}$ and $\overline{\langle \varepsilon_s \rangle}$ were recorded using the methods described in Section 2 to construct the calibration curve for the eductor.

Figure 5 presents the results from the solids volume fraction (holdup) measurements as a function of motive water flow rate through the eductor. As was stated earlier, for the range of operation studied, the back-calculated solids volume fraction in the standpipe was constant at a value of 0.52 ± 0.01. Experiments were also performed for a selected number of cases at different chords of the standpipe, but the solids volume fraction calculated from all those experiments were found within 2% of the mean value. Thus, there was no need for any further data processing using Abel inversion or other techniques for calculating the true cross-sectional average of solids volume fraction (Kumar and Dudukovic, 1997). The line average estimated with the present method was found to be satisfactory.

The solids holdup determined, the next step was to find out the residence time distribution of the solid phase between two horizontal planes in the eductor standpipe, as outlined in Section 2.2. Typical raw data is shown in Figure 7(a) for the first 640 s in an experiment with a liquid flow of 47 gpm through the eductor and 20 gpm through the bottom of the riser (thus making up a total of 67 gpm at a liquid superficial velocity of 23 cm/s through the riser). The peaks in Figure 7(a) indicate the times at which the tracer particle was the closest to either of the detectors and hence the detectors recorded a

maximum in counts. Figure 7(b) shows the same data zoomed in around such a peak that occurred around 10 s from starting the run. It is clear that the peak in counts for the two detectors are very well defined (above 1500) as compared to the background measured by the detectors (less than 100). The time lag between the two peaks can thus be accurately calculated and used to develop a histogram of residence times in multiple sojourns of the tracer particle.

A typical residence time histogram for the flow conditions of Figure 7 is shown in Figure 8. From that data, it is possible to calculate the mean and variance of the residence time distribution, using equations (6) and (7). These values, for the various operating conditions that were studied, are tabulated in Table 1. Given that the centerline spacing between the detectors is 16 cm, equation (8) and the mean residence time values from Table 1 were used to evaluate the mean velocity of solids at each operating condition. Together with the mean solids volume fraction shown in Figure 6, the mean velocity values were used to find the mean solids circulation rate for each condition. The results are plotted, as a function of liquid superficial velocity in the riser and solids to liquid flow ratio, in Figure 9. Figure 9 thus serves as the operating calibration chart for the eductor that expresses the mean solids circulation rate in the system as a function of motive water flow rate in the eductor.

It is interesting to note from the readings in Figure 7(a) that the same detector (with the same settings) records a different maximum value in counts for different passes of the tracer particle. The reason for this is that the particle passes at different positions in the cross section of the standpipe (thus representing statistically all the possible solid particles in the system), and hence the radiation gets attenuated differently in different

passes. Further, lateral dispersion of the tracer particle could in principle, in an extreme case of radial flow in a cross section, lead to a maximum in counts recorded by a given detector at a time that is different from the time the particle first hits the central plane of the detector. Indeed, this is a potential problem with this method and is really another manifestation of the classical problem of measuring RTD in a system with open boundaries. However, in this particular case of eductor calibration, since the velocities are very high, the flow is essentially convective with a large Peclet number. This fact was also verifiable *post facto*, by evaluating the dimensionless variance values from the RTD data (Table 1). The small variance of the solids RTD also suggest that the dispersion is low, so that the solid particles move through the standpipe in a "first in – first out" basis. This clearly is possible only if the standpipe is packed with moving solids, so that the particles have very little freedom to move in the off-streamwise directions. This corroborates our observations from the densitometry measurements.

4. Summary

The ideas presented in the preceding paragraphs have been known in the past and have been used for sophisticated non-invasive flow monitoring methods, *viz.* radioactive particle tracking and computed tomography (densitometry). Earlier work with these experimental tools has been directed towards evaluating flow patterns (e.g. Devanathan et al. (1991), Larachi et al., 1997) and volume fraction distributions (Kumar et al., 1997) in batch systems. Our novel contribution in this paper has been to combine the principles of the two methods for estimating with accuracy the solids circulation rate in circulating fluidized bed systems, which is a problem of fundamental interest in the chemical and

process industry. We have also been able to produce proof of concept in a laboratory scale liquid-solid circulating fluidized bed. In that system, we were able to develop an *in situ* calibration for the solids circulation rate as a function of the operating conditions.

Since the method does not make any *a priori* assumptions about the flow or the properties of the phases in the system, the method presented here can be readily used in any other situation in which other phases or different geometries are involved. Use in industrial systems should also be possible, except that depending on the thickness of the vessel walls, a stronger radioactive source may be required for a good signal-to-noise ratio. The radioactive particle can then be selected of sufficiently short half-life so that it is harmless when the time comes to replace the batch of the catalyst, and the tracer particle itself need not be recovered after the suggested flow rate measurement.

References

[1] L. S. Fan and C. Zhu, *Principles of Gas-Solid Flows*, Cambridge University Press (1998).

[2] D. Kunii and O. Levenspiel, *Fluidization Engineering*, 2nd Ed., Butterworth-Heinemann (1991).

[3] M. E. Dry, *CHEMTECH 12* (1982) 744.

[4] F. Ensgtrom and Y. Y. Lee, in P. Basu, M. Horio and M. Hasatani (eds.), *Circulating Fluidized Bed Technology III*, Pergamon Press, NY (1991) 15.

[5] L. Reh, in P. Basu (ed.), *Circulating Fluidized Bed Technology,* Pergamon Press, New York (1986) 105.

[6] W. Statig, *Chem. Process* (August 1992) 18.

[7] Y. Jin, Y., W. Liang, Z. Wang, Z. Yu, E. Min, M. He and Z. Da, *US Patent 5789640* issued to *China Petrochemical Corporation, Beijing, China; Tsinghua University, Beijing, China; Research Institute of Petroleum Processing Sinopec, Beijing, China* (1998).

[8] J. J. Burkell, in P. Basu and J. F. Large (eds.) *Circulating Fluidized Bed Technology II*, Pergamon Press, New York (1988) 501.

[9] G. S. Patience and J. Chaouki, in P. Basu, M. Horio and M. Hasatani (eds.) *Circulating Fluidized Bed Technology II*, Pergamon Press, New York (1991) 627.

[10] B. J. Milne, F. Berruti and L. A. Behie, in O. E. Potter and D. J. Nicklin (eds.) *Fluidization VII*, Engineering Foundation, New York (1992) 235.

[11] F. Berruti, J. Chaouki, L. Godfroy, T. S. Pugsley and G. S. Patience, *Can. J. Chem. Engng.* **73** (1995), 579.

[12] G. E. Mueller, *Chem. Engng. Sci.* **46(2)** (1991) 706.

[13] F. Larachi, J. Chaouki, G. Kennedy and M. P. Dudukovic, in J. Chaouki, F. Larachi and M. P. Dudukovic (eds.) *Non-Invasive Monitoring of Multiphase Flows* (1997) 335.

[14] N. Tsoulfanidis, *Measurement and Detection of Radiation*, Hemisphere Publishing Corporation (1983).

[15] S. B. Kumar and M. P. Dudukovic, in J. Chaouki, F. Larachi and M. P. Dudukovic (eds.) *Non-Invasive Monitoring of Multiphase Flows*, Elsevier (1997) 47.

[16] N. Devanathan, D. Moslemian and M. P. Dudukovic, (1990) *Chem. Engng. Sci.* **45** (1990) 2285.

[17] G. S. Patience and J. Chaouki, in P. Basu, M. Horio and M. Hastani (eds.) *Circulating Fluidized Bed Technology III,* Pergamon Press, New York (1991) 627.

[18] Mueller, G. E. in *Chem. Engng. Sci.* **46** (1991) 706.

[19] P. Naor, R. Shinnar and S. Katz, *Int. J. Engng. Sci.* **10** (1972) 1153.

[20] U. Mann and E. J. Crosby, *Chem. Engng. Sci.* **28** (1973) 623.

List of Figures

List of Tables

Particle Size, d_p (mm)	Mean Solids Holdup, ε_s	n=2*	n=3*	n=4*	n=5*	n=6*	n=7*
0.1	0.5972	3.17	3.01	2.85	2.69	2.54	2.40
0.5	0.5963	3.26	3.11	2.96	2.81	2.67	2.53
1.0	0.5914	3.98	3.82	3.66	3.49	3.34	3.18
2.5	0.5962	2.67	2.52	2.37	2.22	2.07	1.93
5.0	0.5911	2.67	2.52	2.37	2.22	2.08	1.94

* Percentage error.

Table 1

Liquid Superficial Velocity, cm/s	Eductor Liquid Flow Rate, gpm	Liquid Flow Rate in Main Line, gpm	Mean Residence Time of Solids, s	Variance, s^2	Dimensionless Variance
15	25	19	1.232	0.186	0.123
	30	14	0.667	0.009	0.020
	35	9	0.526	0.006	0.022
	44	0	0.375	0.004	0.028
20	20	38	2.046	0.407	0.097
	30	28	0.772	0.041	0.069
	40	18	0.449	0.004	0.019
	47	9	0.351	0.005	0.041
	58	0	0.261	0.002	0.029
23	20	47	1.943	0.112	0.030
	30	37	0.727	0.009	0.017
	40	27	0.465	0.003	0.014
	50	17	0.333	0.001	0.009
	58	9	0.276	8.53×10^{-4}	0.011
	67	0	0.211	3.48×10^{-4}	0.008

Table 2

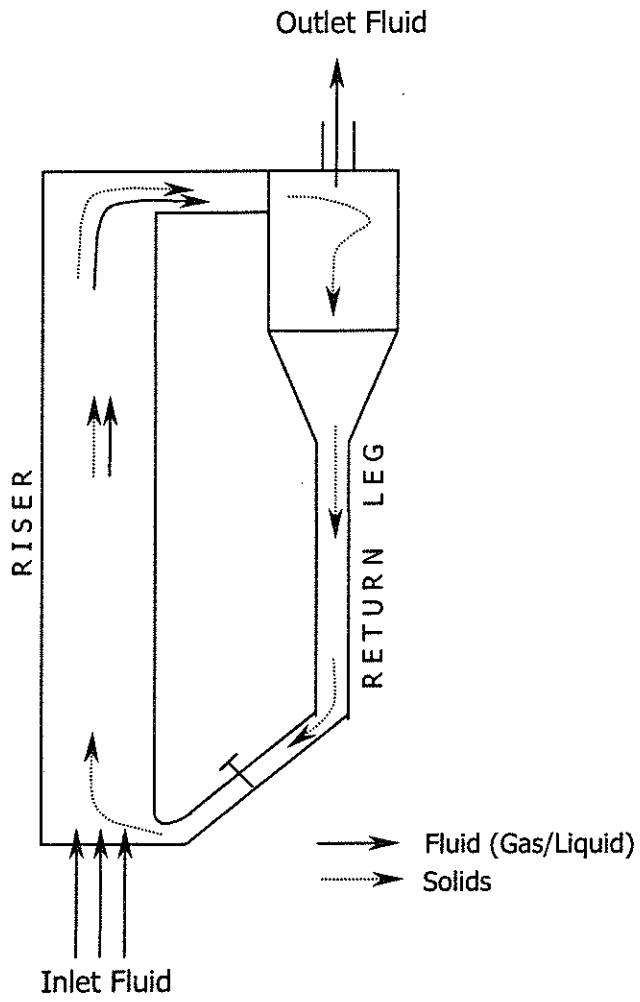
Outlet Fluid
RISER
RETURN LEG
Fluid (Gas/Liquid)
Solids
Inlet Fluid

Figure 1

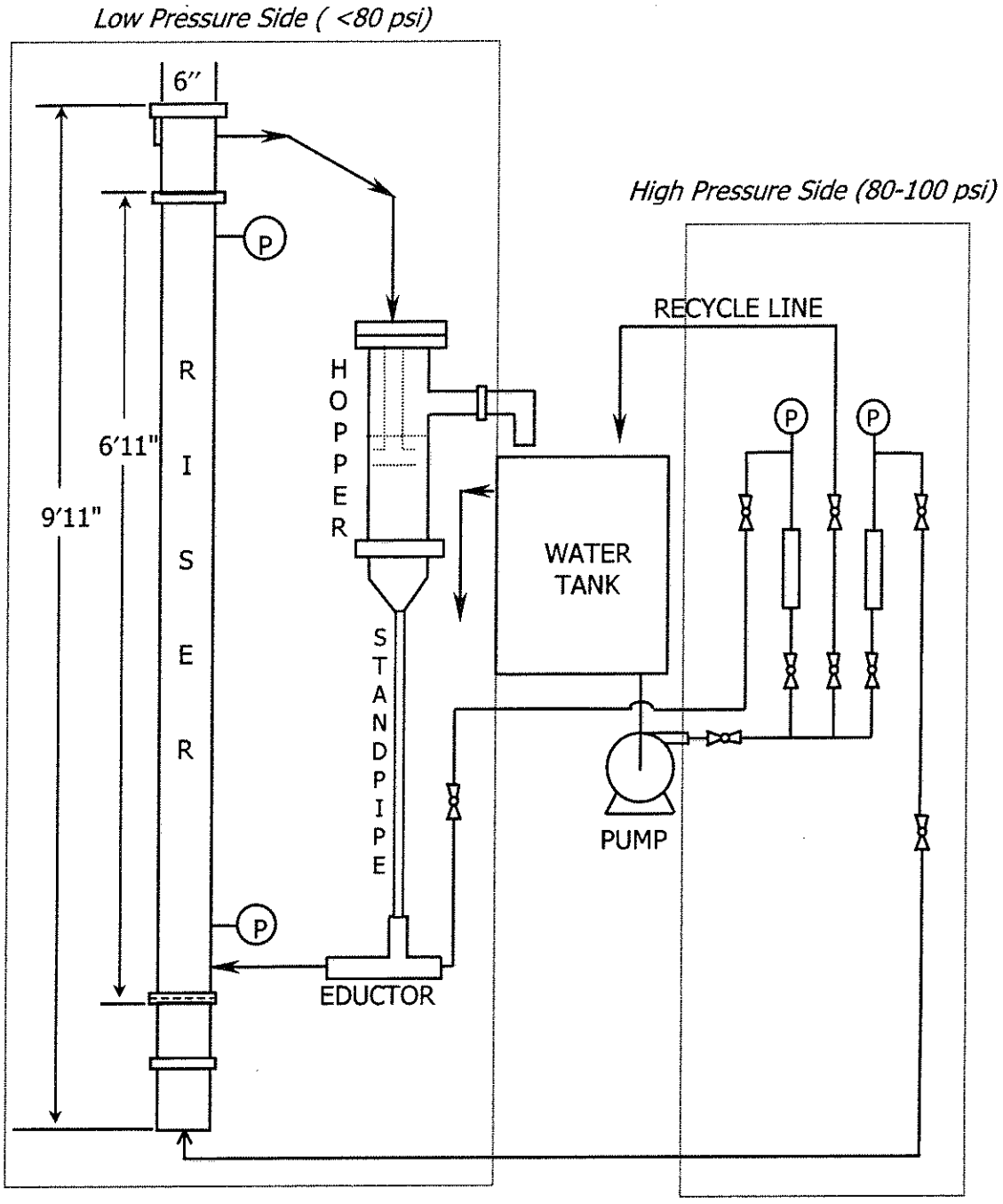
Low Pressure Side (<80 psi)
High Pressure Side (80-100 psi)
6"
6'11"
9'11"
RISER
HOPPER
STANDPIPE
EDUCTOR
RECYCLE LINE
WATER TANK
PUMP
P

Figure 2

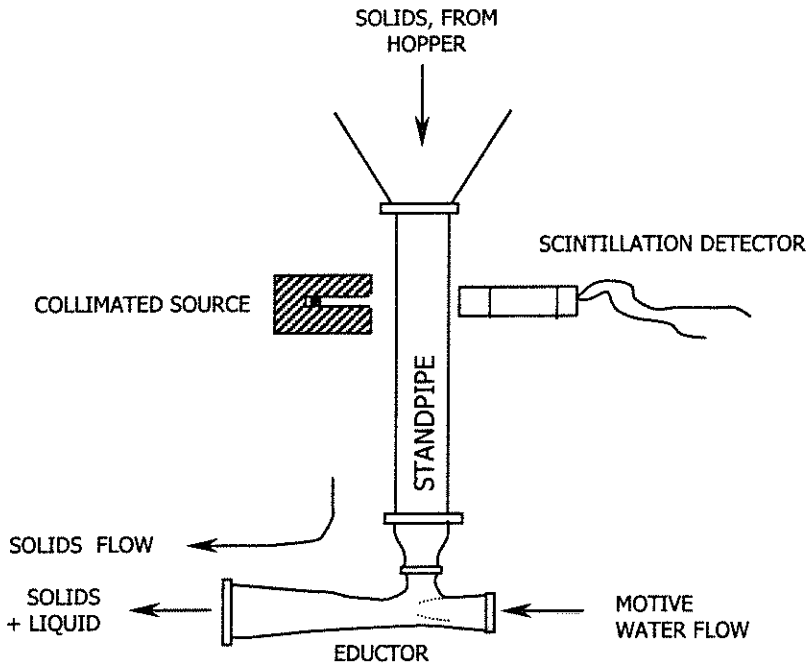
SOLIDS, FROM
HOPPER
SCINTILLATION DETECTOR
COLLIMATED SOURCE
STANDPIPE
SOLIDS FLOW
SOLIDS
+ LIQUID
MOTIVE
WATER FLOW
EDUCTOR

Figure 3

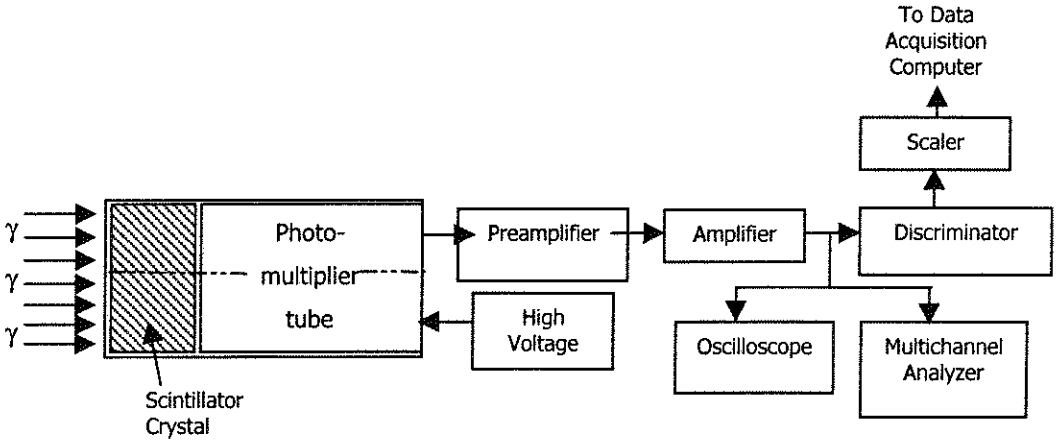
To Data
Acquisition
Computer
Scaler
γ
γ
γ
Photo-
multiplier
tube
Preamplifier
Amplifier
Discriminator
High
Voltage
Oscilloscope
Multichannel
Analyzer
Scintillator
Crystal

Figure 4

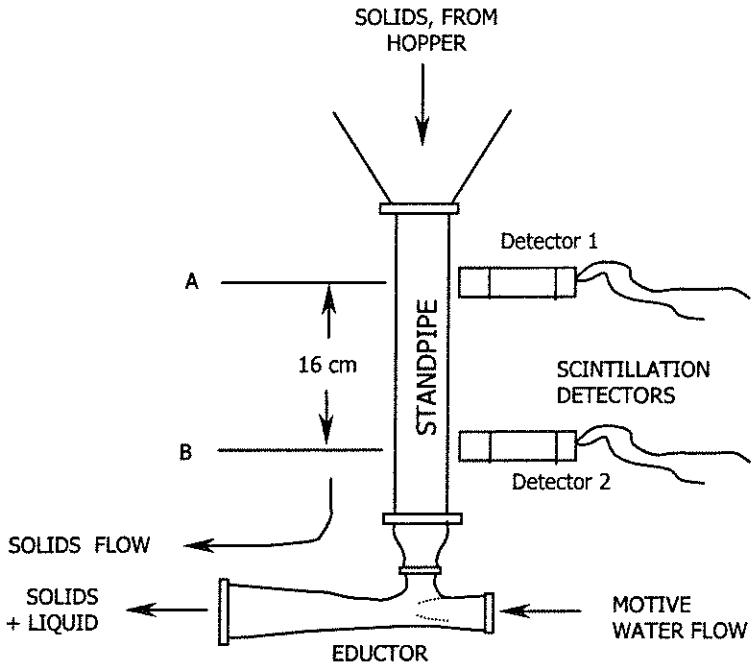
SOLIDS, FROM
HOPPER
Detector 1
A
16 cm
B
STANDPIPE
SCINTILLATION
DETECTORS
Detector 2
SOLIDS FLOW
SOLIDS
+ LIQUID
MOTIVE
WATER FLOW
EDUCTOR

Figure 5

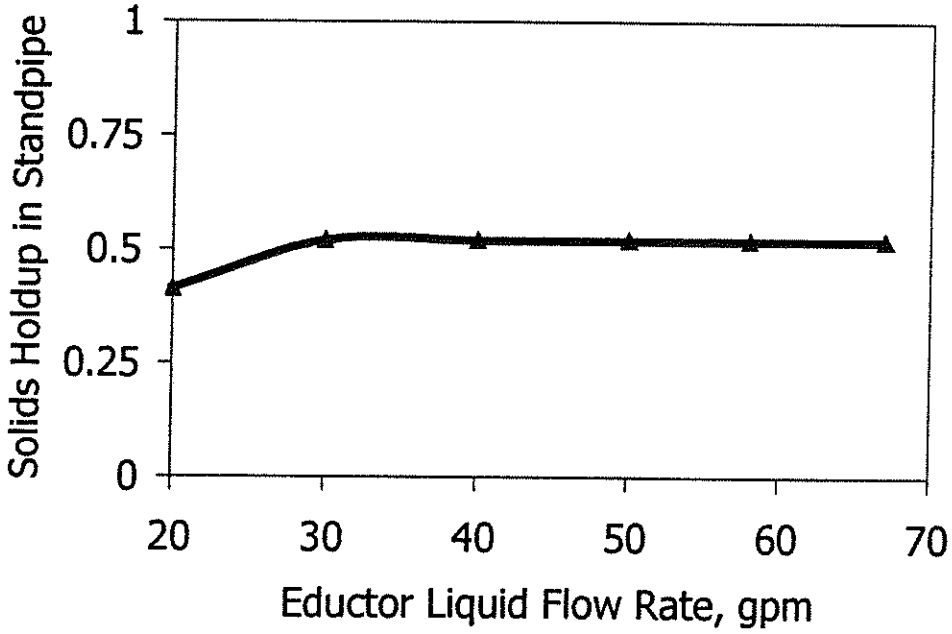
Solids Holdup in Standpipe
1
0.75
0.5
0.25
0
20
30
40
50
60
70
Eductor Liquid Flow Rate, gpm

Figure 6

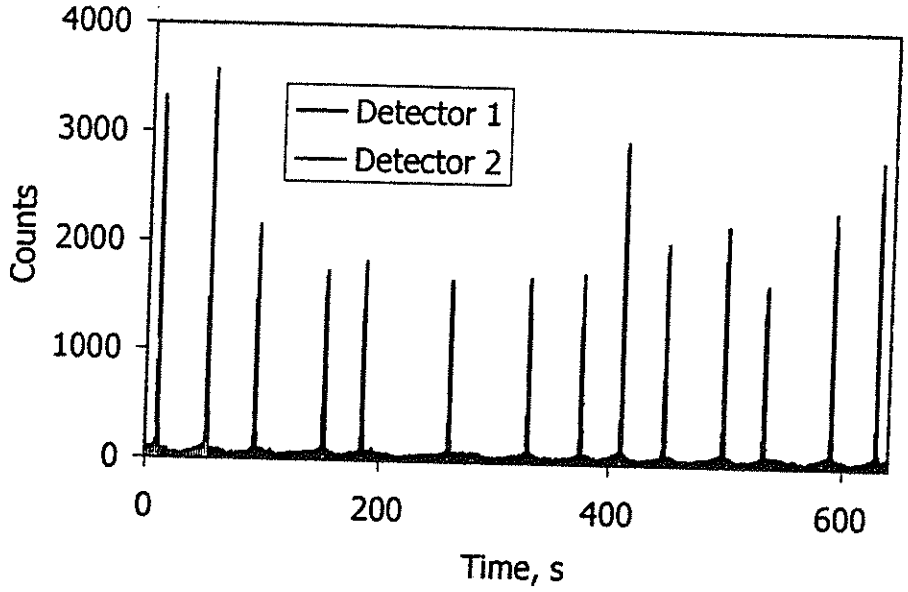
4000
3000
2000
1000
0
Counts
Detector 1
Detector 2
0
200
400
600
Time, s

(a)

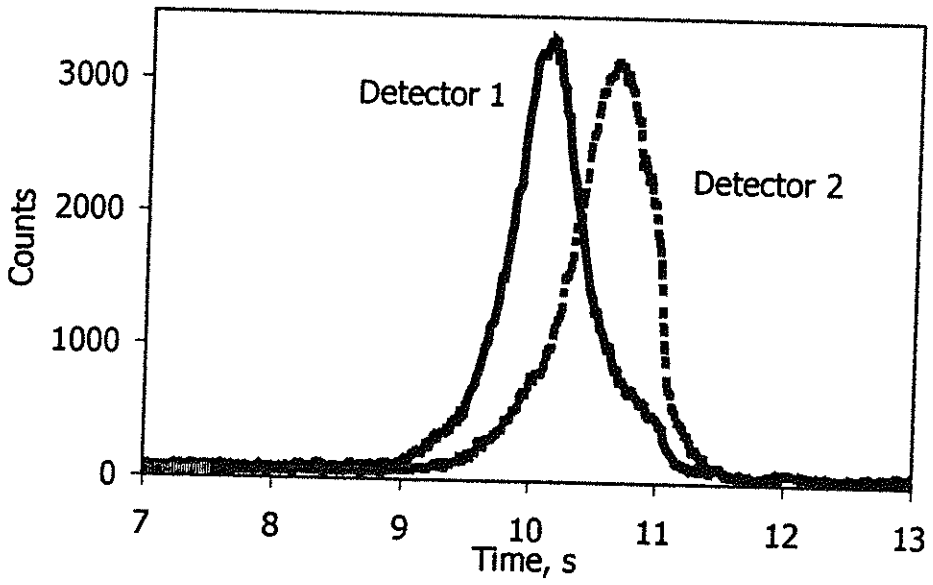
3000
2000
1000
0
Counts
Detector 1
Detector 2
7
8
9
10
11
12
13
Time, s

(b)

Figure 7

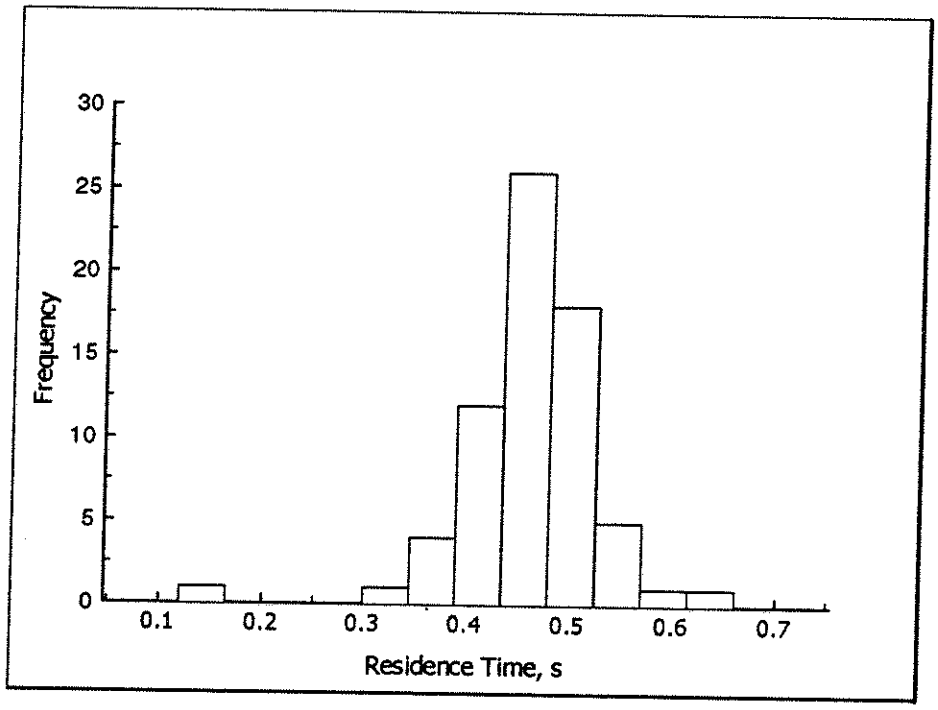

Figure 8

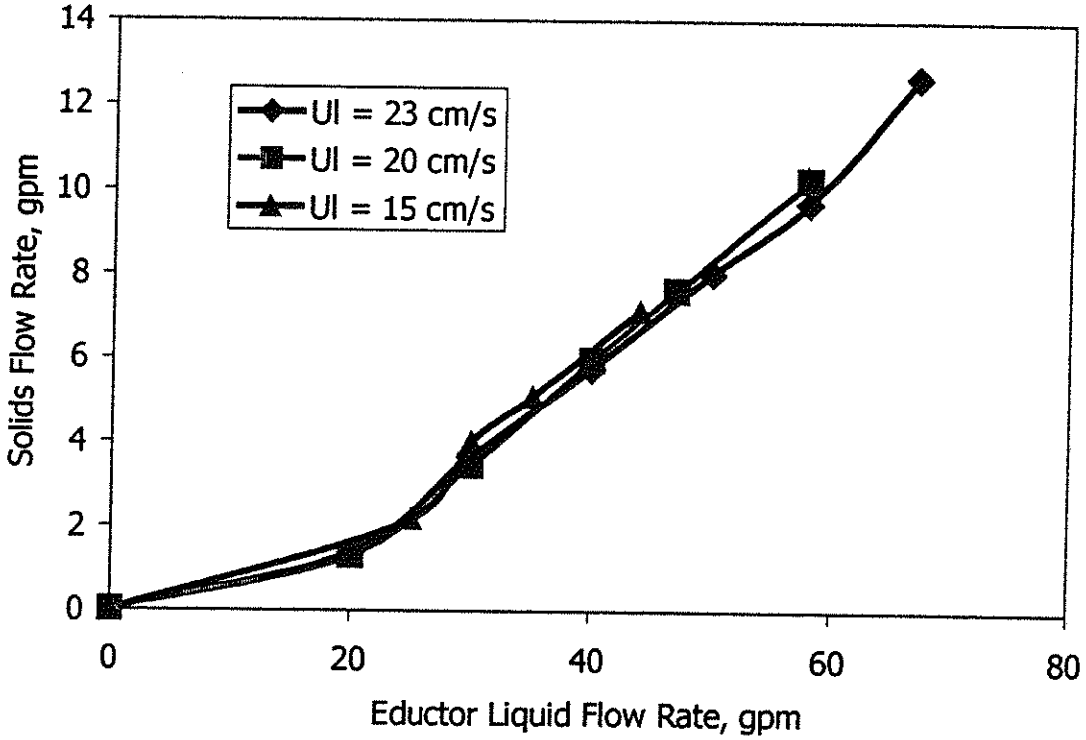
14
12
10
8
6
4
2
0
Solids Flow Rate, gpm
Ul = 23 cm/s
Ul = 20 cm/s
Ul = 15 cm/s
0
20
40
60
80
Eductor Liquid Flow Rate, gpm

Figure 9

OPTIMAL DESIGN OF RADIOACTIVE PARTICLE TRACKING EXPERIMENTS FOR FLOW MAPPING IN OPAQUE MULTIPHASE REACTORS

See the attached report for:

A. Problem Definition
B. Research Objectives
C. Research Accomplishments

Optimal Design of Radioactive Particle Tracking Experiments for Flow Mapping in Opaque Multiphase Reactors

Shantanu Roy[†], Faical Larachi[*], M. H. Al-Dahhan and M. P. Duduković

Department of Chemical Engineering
Campus box 1198
Washington University
One Brookings Drive
St. Louis, MO 63130, USA

[*]*Department of Chemical Engineering*
Université Laval
Quebec, Sainte-Foy
Canada G1K 7P4

Paper Submitted to
Nuclear Instruments and Methods in Physics A

June 2000

[†] Current Address: Corning Incorporated, Process Engineering and Modeling, SP TD 01 2, Corning, NY 14831, USA.

Abstract

In the past decade, radioactive particle tracking techniques have emerged in the field of chemical engineering and have become increasingly popular for *non-invasive* flow mapping of the hydrodynamics in multiphase reactors. Based on γ-ray sensitization of an array of scintillation detectors, the computer automated radioactive particle tracking (CARPT) technique measures flow fields by monitoring the actual motion path of a single discrete radioactive flow follower which has the physical properties of the phase whose motion is being followed. A limitation to the accuracy of CARPT lies in the error associated with the reconstruction of the tracer particle position which affects the space-resolution capability of the technique. It is of interest, therefore, to minimize this error by choosing wisely the best hardware and an optimal configuration of CARPT detectors' array. Such choices are currently based on experience, without firm scientific basis.

In this paper, through theoretical modeling and simulation, we describe how the accuracy of a radioactive particle tracking setup may be assessed *a priori*. Through an example of a proposed implementation of CARPT on a gas-solids riser, we demonstrate how this knowledge can be used for choosing the hardware required for the experiment. Finally, we show how the optimal arrangement of detectors can be effected for maximum accuracy for a given amount of monetary investment for the experiment.

Keywords: CARPT, particle tracking, resolution, sensitivity

1. Introduction

Measurement of velocity of a phase in a multiphase flow system is a problem of fundamental interest that concerns both physicists and engineers. In particular, for chemical engineering applications, it is of primary importance to accurately estimate the time-averaged velocity fields, turbulence parameters and eddy diffusivities of phases in a reactor in order to predict their performance.

In pursuit of this goal, the last decade has witnessed important progress in the area of non-invasive flow mapping in complex multiphase systems, through the method of radioactive particle tracking (e.g. [1-5]). Most multiphase systems of interest to the chemical industry have a large volume fraction of the dispersed phase and are thus opaque because of scattering of visible light. This rules out the use in such systems of conventional non-invasive techniques such as Laser Doppler Anemometry and Particle Image Velocimetry [5]. Further, introduction of invasive probes is not desirable because their presence changes the flow pattern itself, and poses several practical limitations in interpreting the experimental data. Computer automated radioactive particle tracking (CARPT) has emerged as a technique of choice because it does not suffer from such limitations [1-5].

The CARPT technique is based on the principle of tracking the motion of a single particle (Figs. 1a,b) as a marker of a typical element of the phase whose velocity field in a flow vessel is to be mapped. For tracking liquids, e.g. [3,18], a small, encapsulated radioactive tracer particle is designed which is made neutrally buoyant with respect to the liquid phase. For tracing particulate solids (e.g. [4], [15]), the tracer particle is designed to be of exactly the same dimensions as the solids inventory and has the same effective density as the solid particles. The tracer isotope chosen is normally a highly penetrative γ-ray emitter, so that it is possible to probe high volume

fraction flow structures that are confined within the *opaque* vessels. An array of strategically positioned scintillation detectors (Fig. 1b) around the vessel records the photon counts emitted by the tracer as it freely wanders and follows the phase of interest. By noting the photon counts as a function of time recorded by the entire array of detectors, it is possible to reconstruct the "*Lagrangian*" tracer particle position time series ([1], [4]). Since the tracer particle is "designed" to mimic the motion of the phase of interest, by collecting the tracer flow path over a wide observation time window it is possible to approximate the ensemble-average flow fields and mixing patterns of the whole phase ([1-5], [15]). The process of tracking the tracer particle is completely automated and the data is acquired at high enough frequency so that successive instantaneous positions of the particle are recovered with fidelity. The time-series of positions and velocities can be further processed to yield local and global mixing information and dispersion coefficients (e.g. [1-5]). The versatility of the CARPT technique opens up possibilities of its use not only in laboratory scale multiphase systems, but for small to medium scale industrially relevant pilot plant units in the near future.

Given the immense possibilities that CARPT offers, it is also prudent to recognize that it is not an "off-the-shelf" technique that can be implemented at will. In order to use it on a relatively large pilot plant scale gas-solids riser, or even on a new system in the laboratory, careful and systematic planning is required to identify all the issues that must be resolved before the actual experiment is designed and executed. Unfortunately, the complexities associated with the process of photon detection and extraction of tracer particle position from γ-ray photon counts recorded at the scintillation detectors (Fig. 1b) precludes an easy assessment of the "optimal experimental protocol" *a priori.* Consequently, with every new system to be studied, a

laborious trial and error experimental procedure has to be undergone before a good experimental run can be implemented.

In this study, we develop theoretical tools for assessing the optimal protocol for implementing CARPT, i.e. maximize accuracy, minimize cost and maximize implementation feasibility. The decisions to be taken for an optimal design are twofold. First, one needs to choose the right hardware for the experiment. Second, an "optimal configuration" of the chosen hardware has to be selected. An example of a 6 in. pilot-plant gas-solids riser serves to illustrate the concepts, which can be readily implemented in any new system of interest.

2. The Monte Carlo Model

Nuclear radiation models based on Monte-Carlo algorithms (discrete photon models) are common and well documented in nuclear physics (e.g. [6-12]). Use of this method in the context of CARPT experiments is also well studied and documented in a variety of different systems [11,12]. The approach is based on estimating the total efficiency of a scintillation detector for photons emitted from a point radioactive source. It forms the basis of this study, in that all the computations necessary for ascertaining the optimal CARPT configuration use the Monte-Carlo algorithm for generating the photon counts.

The number of photo-peak photon counts C recorded by a detector during a sampling interval T from a point radioactive source of strength A positioned at (x,y,z) in the system (here a riser, Fig. 1a,b), is given by the following relationship [11,15]:

$$C = \frac{T\nu A\varepsilon_{abs}\phi}{1+\tau\nu A\varepsilon_{abs}\phi} \tag{1}$$

ν is the number of γ-ray photons emitted per disintegration (characteristic of the radioactive isotope). In a typical CARPT configuration (Fig. 1), at any given instant of time, the tracer position is a point source and the counts recorded at each detector are given by Eq.1. The absolute efficiency ε_{abs} is given by the following equation [11,15] :

$$\varepsilon_{abs} = \iint_{\Omega} \frac{\vec{r}.\vec{n}}{r^3} \exp\left(-\sum_{j=1}^{N} \mu_j l_j \right) \left(1 - \exp(-\mu_D d)\right) d\Sigma \tag{2}$$

In the above expression, $\vec{r}$ is the radius vector from the source to the detector and $\vec{n}$ is the unit normal vector to the curved surface of the detector. μ_D is the mass attenuation coefficient of the detector crystal material (for the energy of the γ-ray photon) and d is the penetration depth of photons in the detector crystal. μ_j is the mass attenuation coefficient of all the materials that are in the path of the photons between the source and the detector, and l_j is the penetration depth in each, respectively.

The expression for the absolute detector efficiency, given by Eq.2, is a complex two-dimensional surface integral that is difficult to estimate. First, one does not have any *a priori* information about the solid angle itself (hence the limits of the integral in three dimensional space). Second, the "penetration depth" of the photon in the detector crystal, travelling along "each ray" within the solid angle, is not known. It is therefore imperative to use some tractable numerical method to evaluate the integral, and hence the counts recorded at the detector as a function of relative distance from the tracer particle.

One possible way to estimate the solid angle, the absolute efficiency (Eq.2) and hence the photon counts (Eq.1) is to use a Monte-Carlo algorithm [5,7,10,11]. In this algorithm, photons are randomly generated at the source, and their individual paths from between the source and the

detectors are traced. The calculations yield approximations to two quantities: the solid angle Ω and the depth of penetration d in the detector crystal. Thus, an approximation to the total detector efficiency ε_{abs} is calculated. The photo-peak efficiency, i.e., the fraction of photons above a minimum threshold energy that contribute to the photo-peak in the spectrum of the radioactive isotope is estimated using standard correlations [14]. With this knowledge, the photon counts (Eq.1) are estimated for each location of the tracer particle and detector position. Details of the algorithm and its implementation for a typical CARPT configuration is given elsewhere [7,10,11].

Fig. 2a-c shows typical distribution of counts for various locations of the source (tracer particle). Fig. 2a shows a typical configuration inside a column in which the tracer particle is being moved along the axis of the column. The detector is positioned close to the column wall and perpendicular to the axis of the column. When the tracer particle is moved along the axis, the typical counts recorded at the detectors are shown in Fig. 2b. Fig. 2c shows an analogous two-dimensional contour plot, in which the tracer is moved inside the column in a vertical plane perpendicular to the detector and containing the axis of the column. The counts are generated using Eqs.1,2. The maximum in recorded photon counts occurs, as expected, when the tracer particle is closest to the detector and located along the axis of the detector. As the tracer particle is moved away, the photon counts recorded at the detector fall off rapidly. Very far from the detector, the anisotropy effects of solid angle and detector shape are small, and the recorded counts fall off with distance according to the expected inverse square relationship.

3. CARPT Performance Indicators

In CARPT, assuming that the tracer particle follows the phase being tracked with fidelity, it is our goal to reconstruct with accuracy the exact position of the tracer particle as a function of time. There are sources of error which pose a limitation to accurate position reconstruction, of which the important ones are:

- statistical fluctuations in the intensity of source (number of photons emitted in a given time);
- poor relative orientation of source and detector causing detector to be "blinded" by excessive counts or receiving very low counts (low signal-to-noise ratio);
- flow-induced fluctuations in volume fraction of the dispersed phase in the reactor (e.g. solid volume fraction fluctuations in the riser).

In order to quantify the "goodness" of a CARPT setup, we propose two "performance indicators", namely resolution and sensitivity, which can be used to assess the uncertainty in position reconstruction caused by the above and other less important sources of error.

Resolution. Resolution refers to the sphere of uncertainty around the exact particle position. It can also be viewed as the minimum distance between two neighboring positions of the tracer particle that can be discriminated as two *different* particle positions. Mathematically, allowing tracer particle movement only in the z-direction, this is expressed as:

$$R(z)=\sigma(z)=\sigma_C \frac{dz}{dC} \tag{3}$$

σ_C refers to the variance in photon counts due to source fluctuations. The derivative represents the rate of change of reconstructed position as a function of recorded photon counts.

Sensitivity. Resolution tells us about the accuracy of reconstruction of a single location of the tracer. Another way to look at the fidelity of the CARPT experiment is to define the sensitivity as the fractional (or percent) change in counts recorded at the detector with a small change in position of the tracer particle. For unidirectional movement in z-direction of the tracer particle, sensitivity can be defined as:

$$S(z)=\frac{1}{C}\frac{dC}{dz}=\frac{d\ln C}{dz} \tag{4}$$

Comparing Eqs. 3 and 4, it is clear that the two quantities are related:

$$R(z)=\frac{1}{S(z)\sqrt{C}} \tag{5}$$

The advantage of studying both resolution and sensitivity functions gives a better physical interpretation to the experimentalist. In any experimental setup, it is desirable to maximize sensitivity and resolution, i.e., maximize the value of *S(z)* and minimize the value of *R(z)*. It is also clear that if it were possible to measure or predict the counts recorded at any detector as a function of distance, then both the sensitivity and resolution functions could be calculated. It is also noteworthy that resolution and sensitivity are specific to a given detector and are a function of detector distance from the source tracer. The independent variable, *z*, is the position of the *tracer* in the reactor, and is the distance with reference to the detector axis. Thus,

the functions are naturally defined in a reference frame that is fixed to the detector (and is different for each detector) while the tracer is free to move around in the reactor of interest, in a reference frame fixed to the reactor column.

Resolution and Sensitivity in Multiple Dimensions. The definitions of sensitivity and resolution stated in Eqs. 3, 4 above assume tracer particle motion in only one dimension with respect to the detector. Without any loss of generality, these definitions may be directly extended to polar (radial) coordinates by simply replacing z by r in the equations (Fig. 2a). It can be readily shown, through simple geometrical arguments, that in such a case the radial functions $\sigma_r(r)$ and $S_r(r)$ are related to the corresponding Cartesian functions by:

$$\frac{1}{\sigma_r(x,y,z)} = \frac{\cos\alpha}{\sigma_x(x,y,z)} + \frac{\cos\beta}{\sigma_y(x,y,z)} + \frac{\cos\gamma}{\sigma_z(x,y,z)} \tag{6}$$

$$S_r(x,y,z) = S_x(x,y,z).\cos\alpha + S_y(x,y,z).\cos\beta + S_z(x,y,z).\cos\gamma \tag{7}$$

In the above Eqs. 6 and 7, β and γ are the direction cosines of the point (x,y,z). Clearly, sensitivity and resolution are functions of all three-dimensions with a value associated (for each detector) with each point in three-dimensional space in the reactor column.

As such, it is very difficult to analyze these three-dimensional functions (Eq. 6,7) and make any kind of qualitative or quantitative conclusions about desirable detector configurations for CARPT. For purposes of the present study, we consider the two-dimensional sensitivity and resolution functions at critical planes in the column. On a 2-D plane, we can see a "slice" of the three-dimensional functions presented in Eqs. 6,7. If a cut off plane is taken vertically (i.e., a plane vertically aligned along the axis of the reactor column) then Eqs. 6,7 reduce to:

$$\frac{1}{\sigma_r^{2D}} = \frac{\cos\theta}{\sigma_y} + \frac{\sin\theta}{\sigma_z} \tag{8}$$

$$S_r^{2D} = S_x \cos\theta + S_y \sin\theta \tag{9}$$

where θ, the angle which the position vector of the tracer location *on* the plane makes with the x-axis, replaces the direction cosines in Eqs. 6, 7. Details of the equivalence and derivations have been presented by Roy [15]. It has also been shown [15] that it is *sufficient* to consider the two-dimensional functions to understand the complete behavior of the three dimensional functions.

Resolution and Sensitivity in Multiple Detector Scenarios. In CARPT, we have a number of detectors which are arranged at certain positions around the column (Fig. 1b). The theory introduced above refers to the resolution and sensitivity in space for a single detector. It is therefore important to be able to combine the functions due to several detectors at each point in space (in the column).

We recognize here that the resolution function (defined by Eq. 5) refers to the uncertainty in location of the tracer particle, i.e., the expected mean position of the particle. It may thus be viewed as the error (or variance) in calculating the mean position of the tracer particle. It is known in theory of statistics [16] that if σ_i is the uncertainty in determining a series of independent observations x_i, then the uncertainty in the mean of x_i is given by:

$$\frac{1}{\sigma_\mu^2} = \sum_{i=1}^{N} \frac{1}{\sigma_i^2} \tag{10}$$

In the present case, the three-dimensional resolutions obtained at any point (x,y,z) in space can be viewed as uncertainties obtained from N independent observations (N detectors). Hence, the resolutions can be added to yield the overall resolution function:

$$\frac{1}{\sigma_T^{\,2}(x,y,z)} = \sum_{i=1}^{N} \frac{1}{\sigma_i^{\,2}(x,y,z)} \tag{11}$$

Using Eq.11, the overall sensitivity may be defined as:

$$S_T^{\,2}(x,y,z) = \sum_{i=1}^{N} S_i^{\,2}(x,y,z) \tag{12}$$

For scenarios in which multiple detectors are being used, Eqs. 11 and 12 provide means of estimating the overall performance of the CARPT setup. In the next section, different scenarios of detector configurations will be studied and compared based on these quantities.

4. Single Detector Analysis

As discussed earlier, we use the sensitivity and resolution functions as indicators of performance. In this and the following section, we show how the CARPT operating parameters can be used for choosing the optimal detector characteristics and also the optimal orientation and positioning of detectors. In order to serve as an illustration, we take the example of a gas-solids riser reactor (Fig. 1a). Such a reactor consists of a closed loop in which small solid phase particles circulate, driven upwards by a high gas-flow rate in the "riser" section. The gas flows out continuously at the top while the solids (often a catalyst) is recirculated back into the system.

Performance of such systems is critically determined by the solids phase velocity field and recirculation patterns, and therefore it is proposed to perform CARPT on the system by tracking a single radioactive solid particle that is designed to follow the solid phase flow pattern. Prior to actual implementation, it is necessary to choose the right hardware and arrangement. Thus, we apply the theoretical results presented earlier in this paper to narrow down a "good" configuration, and also estimate the spatial distribution of inaccuracies of the proposed configuration.

In this section, the discussion is restricted to choosing the right hardware: tracer isotope, source strength, detector crystals, and their size and shape. It suffices to make this decision by simulating one-dimensional motion of the tracer particle and analyzing the counts, and associated performance parameters of a single detector. Whatever conclusions are drawn for a single detector is readily applicable for all the detectors.

The arrangement shown for single detector analysis is the same as shown in Fig. 2a. The exact dimensions of the riser column, and the parameters of the simulation are presented in Table 1. The tracer particle is moved along the axis of the riser column. A scintillation detector (2 in. diameter) is placed horizontally (perpendicular to the column axis) such that the detector crystal center is 12.24 cm from the column axis (center of the disk is 1.4 cm from the riser wall). This location of detector is chosen because if the tracer particle was placed flush the wall, then at this location the detector would record counts slightly below saturation. Hence, placing the detector at this location amounts to "using the full scale" of the detector crystal, i.e., when the tracer particle is closest, the detector records its maximum allowable counts. This forms a natural basis for all our computations in this section.

Tracer Isotope. There are two variables that should determine the choice of a radioactive isotope for a CARPT experiment. First, the number of photons that reach the detector depends on the density (and hence the attenuation) of the intervening medium of the vessel and the column wall. Second, a lower energy of the γ-ray photons implies a higher attenuation coefficient of the *crystal*, since there is a higher probability of the photon to be absorbed (and cause eventual emission of a photo-electron) in the crystal [13,17]. In general, different radioisotopes emit γ-rays at one or more different energies, corresponding to the nuclear transitions in the isotopes. For example, molybdenum (^{99}Mo) emits at four characteristic energies (0.181 MeV, 0.740 MeV, 0.778 MeV and 0.140 MeV), cobalt (^{66}Co) emits at two energies (1.173 MeV and 1.332 MeV) while gold (^{198}Au) emits at a single energy (0.412 MeV). In order to discriminate between different sources from a CARPT perspective, in Figs. 3a,b the resolution and sensitivity have been plotted as a function of distance of the tracer particle from the detector axis for different photon energies. Note the typical shape of the sensitivity and resolution functions. Owing to a very high count rate for tracer locations near the axis of the detector, the gradient is small (Figs. 2b,c), leading to sensitivity loss in detecting the exact tracer location. In this region, the sensitivity grows linearly with distance. Such a "blinding" of the detectors in the "near view" of the detector also causes lack of resolution (the resolution function grows as the reciprocal of distance from the detector axis for short distances and tends to infinity). In the intermediate range, the sensitivity function goes through a maximum and the resolution through a minimum. At large distances between the tracer particle and the detector, the counts fall according to an inverse square law, so that the resolution increases as a cubic function of distance and the sensitivity falls as the reciprocal of distance.

Figs. 3a shows that decreasing the photon energy from 1.0 MeV (approximately the mean photon energy of radioactive scandium - ^{46}Sc) to 0.4 MeV (approximately the mean photon energy of radioactive gold – ^{198}Au), the minimum in the variance of determining the particle position decreases from about 5 mm to about 3 mm. Accordingly, the maximum resolution (due to a single detector *alone*) is doubled (σ_z is halved). For lower energy photons, the detector crystal absorbs more of them so that the photon count is high. Photon emission and counting being Poisson statistical processes (thus mean counts is equal to the variance), the standard deviation in photon counts is consequently higher. Since the detector geometry is the same for all the photon energies studied, the only factor that affects the counts recorded at the detector is the attenuation coefficient of the detector crystal material itself for the given energy of the photon. Thus, the resolution function varies inversely as the square root of recorded counts, and consequently increases (σ_z decreases) with decreasing photon energy.

Detector sensitivity (Fig. 3b) is not so strongly affected, however, and is marginally *lower* for lower energy photons. The reason for this behavior can be understood by inspecting the energy-sensitivity relationship, derived by using the chain-rule on Eq.5:

$$\frac{\partial S}{\partial E} = -S\left(\frac{1}{2C}\frac{\partial C}{\partial E} + \frac{1}{\sigma_z}\frac{\partial \sigma_z}{\partial E}\right) \tag{13}$$

The first term on the RHS is negative while the second is positive. Fig. 3b suggests that the first and second terms are commensurate, and therefore cancel each other for short and long-range distances. For intermediate range, and according to Fig. 3b, the resolution diminishes as the energy is reduced faster than does the counts, and thus the 2nd term dominates the 1st slightly.

It is thus prudent to choose an isotope for the CARPT tracer particle such that the resolution obtained is the highest. In the particular case of a gas-solids riser, a favorable aspect in this regard is the small density of the vessel walls and vessel contents. Thus, even if the energy of the γ-rays is low, they do not get appreciably attenuated in the column and are effectively captured by the detector crystal leading to high resolution. In denser systems, like liquid-solid or gas-liquid-solid reactors, such a choice need not necessarily be the best because most of the photons would get attenuated in the vessel itself.

Source Strength. The choice of the radioactive strength of the source is dictated by considerations similar to those outlined in the previous section. It is logical to assume that the stronger the source, the better is the signal-to-noise ratio and hence the better resolution and sensitivity of CARPT. What is of greater consequence is to know whether there is some *optimal* source strength beyond which increasing the source strength has no significant impact.

In Figs. 4a,b, the resolution and sensitivity functions are plotted by varying the source strength. Higher source strength implies almost proportionally higher photon counts. For precisely the same reasons as elucidated earlier, the sensitivity function is essentially invariant with source strength variation. Analogously, the resolution is improved (σ_z decreases) with increasing source strength.

However, it is interesting to note that beyond a source strength of 300 μCi, there is no *significant* improvement in *maximum* resolution of the detector with further increase in source strength. σ_z varies as the inverse square root of photon counts, as explained earlier. When the source strength is very high and a large number of photons reach the detector for any given position of the tracer particle, σ_z decreases asymptotically (and slowly) to its lower bound, which

is zero (corresponding to "perfect" resolution). Therefore, the conclusion is that it is good to use a strong source, but using anything beyond 300 μCi is overkill. (The gross assumption is that dead-time effects are marginal.) If these are no longer negligible, then even 300 μCi is conservative.

It may also be noted that a consideration against using strong sources is the possibility of detector saturation. Even though a strong source produces better resolution, there is the possibility that when the tracer particle is very close to the wall (and hence the detectors), the count rate may be so high that the detectors get saturated. This occurs because the number of photons arriving at the detector is too large for the crystal and associated electronic hardware to respond to them and record their number. In CARPT, since the tracer particle is free to move in the vessel, there is no *a priori* information when the particle is close to the wall and is saturating the detectors in its vicinity. It is thus necessary to choose a strength of tracer particle such that it does not saturate the detectors, yet maintains high resolution when the tracer particle is far from the detector. 300 μCi seems like an optimal choice.

Crystal Size. Crystal size is an important variable determining the resolution and sensitivity of the detector. The size of the crystal (and detector) contributes in two ways to the overall performance of the detector. First, a larger crystal implies longer penetration lengths of the photons, leading to more probability of attenuation of photons and a larger photon count. Second, a larger crystal implies larger surface area and, hence, more anisotropy due to the shape of the crystal.

Figs. 5a,b show the resolution and sensitivity functions when the detector crystal size is varied from 0.5 in. to 3.0 in. It is assumed that all detectors have a L/D ratio of unity and the

nominal size of the detector crystal is equal to the diameter as well as the length of the crystal. Most commercially available scintillation crystals have this shape, although more expensive crystals are available in different shapes. The effect of crystal shape on CARPT performance is investigated later.

Sensitivity is seen to be worst for the largest crystal (3 in.) while the resolution is seen to be the best. With a larger crystal, probability of photon capture is much higher. Thus even if the same number of photons were to enter the crystal, the larger volume of the crystal implies that photons will get absorbed in the crystal with higher probability. Further, the larger surface area of the larger crystal implies that the solid angle subtended by the source at the detector crystal surface is higher. Thus, in general, a larger number of photons hit the surface and eventually get absorbed. Thus, the number of photons absorbed by the 3 in. crystal is considerably higher than that by a 0.5 in. crystal. Also, the larger solid angle for the larger detector causes a lower spatial gradient of the count distribution $\partial C/\partial z$. Consequently, sensitivity is considerably lower for a large crystal, while the resolution is higher (Eqs.3, 4). Resolution deals with the number of photons counted by the detector; this number is proportional to the crystal bulkiness. An increase by a factor of 6 in size makes the 3 in. crystal 6^3=216 times bigger than the 0.5 in. one. This explains the corresponding dramatic improvement in resolution. On the contrary, due to the crystal bulkiness there is a net deterioration in sensitivity for the intermediate range distances as the crystal size increases. It is noteworthy, however, that the improvement in resolution from a 2 in. to a 3 in. crystal is not significant. The loss in sensitivity is appreciable, however, in moving from a 2 in. to a 3 in. crystal.

Crystal Shape. It is instructive at this point to investigate the effect of aspect (L/D) ratio of the crystal on the resolution and sensitivity functions, and hence the accuracy of CARPT. Commercially available detector crystals of aspect ratios other than 1.0 are usually expensive, and for that reason would not be the preferred choice of CARPT. Our motivation for these sets of simulations was to investigate whether the choice of crystals of L/D=1.0 causes some significant improvement/loss of accuracy or not.

For these sets of simulations, a 2 in. NaI crystal was considered as the basis, and two other crystals were simulated of L/D of 0.5 and 2.0 such that the total volume of the crystals (and hence the total amount of NaI material) was conserved. Simple volume basis calculations show that the three crystals should have the following dimensions: L=3.17 in., D=1.59 in. (L/D=2); L= 2 in., D=2 in. (L/D=1); L=1.26 in., D=2.52 in. (L/D=0.5). The resolution and sensitivity plots for crystals of these dimensions are shown in Figs. 6a,b.

Clearly, the "slender" crystal (L/D=2) has the highest sensitivity but the lowest resolution. The "flat" crystal (L/D=0.5) has the lowest sensitivity but the highest resolution. For "slender" crystals, the probability of photons entering from the flat surface is minimum (because diameter is lowest), and the average penetration length even when the photons enter from the curved surface is less (owing to lesser crystal diameter). Thus, photons counted are lower, and the resolution is lower.

Why the sensitivity is high for a "slender" crystal can be understood by referring back to Fig. 2b. The variation of photon counts with distance has a flat maximum region above the flat disk of the detector, then drops rapidly in the near vicinity of the detector and then asymptotically decreases according to an inverse square relationship. For a crystal with high L/D, the diameter being small causes the flat region of the photon counts-distance curve to be

smaller and the drop to the asymptotic region faster. Consequently, a relatively higher sensitivity is observed.

The message from Figs. 6a,b is that "flat" crystals are best suited for applications like CARPT, because they provide improved resolution when compared with "slender" ones, even though sensitivity is marginally less. However, we also note that the percentage improvement in maximum resolution between a crystal with L/D=0.5 and one with L/D=2 is around 20% (i.e., from 5 mm to 4 mm). Since in CARPT, any "single-detector resolution" is further improved by packing detectors all around the riser column, this marginal improvement in resolution over a L/D=1 crystal does not justify the extra cost incurred (around 1.5 times) for purchasing "flat" detectors for our purpose for the given scenario.

Crystal Material. NaI(Tl) detectors are most commonly available from commercial vendors of scintillation detectors. Other than NaI(Tl), another material popularly used in detector crystals is bismuth germanate (BGO). BGO is a denser material and hence it is of interest if any substantial improvement in accuracy is obtained with its use. The two types of detectors are compared in Figs. 7a,b. In performing these simulations, the fact that the BGO total attenuation coefficient is 2.5 times that of NaI has been incorporated. Furthermore, it has been assumed that the photopeak fraction is the *same* as that for NaI, since no correlations for calculating this quantity could be found in the open literature. The actual photo-fraction for the BGO detectors may be somewhat higher. Finally, the dead time of 230 ns for NaI and 320 ns for BGO has been incorporated.

Fig. 7a shows that the improvement in resolution by the BGO detector, as compared to the NaI detectors is only marginal. Higher dead time for BGO partially offsets the increase in

counts due to higher density of the crystal when compared to NaI. The sensitivity is slightly higher for the NaI detector. The simulations seem to indicate that there is no substantial improvement in using BGO, hence we would like to restrict ourselves to the use of NaI detectors.

Detector Elevation. Finally, for completeness, we also simulated the resolution and sensitivity functions for varying detector elevation, i.e, the distance between the riser wall and the front disk of the detector. From heuristic and experimental experience, it is well recognized [1-5] that for the best CARPT implementation it is advisable to mount the detectors flush with the vessel walls, as long as one ensures that detectors do not get saturated. With the current set of studies, it was possible to verify this fact and provide quantitative guidelines about how far from the riser wall the detectors can be allowed to be positioned without substantially sacrificing accuracy.

The results are presented in Figs. 8a,b. The distances mentioned in the legend refer to the distance between the detector front face and the riser axis. The outer radius of the riser is 8.26 cm. The plots show that both sensitivity and resolution is best when the detector is closest to the column wall. When the tracer particle is far from the detector, naturally the "elevation" of the particle with respect to the detector becomes small as compared to the lateral distance (distance between the particle and detector axis) so that both the sensitivity and resolution curves collapse into asymptotes. It can also be stated, from Figs. 8a,b, that in order to assure that the detectors do not get saturated when the tracer particle is near the wall, it is advisable to keep the detector within around 1 cm of the column wall in order to achieve optimal resolution and sensitivity.

Conclusions. From all the theory and results presented in this section, the following conclusions emerge regarding effective implementation of CARPT on the gas-solids riser.

- If possible, it is advisable to use a tracer isotope that emits low energy photons, and has a short half-life. Gold (^{198}Au) seems like such a choice.
- Tracer particle source strength of 300 μCi is sufficient for the dimensions of the gas-solids riser considered.
- 2 in. cylindrical NaI(Tl) detectors, with an L/D of 1, are sufficient for purposes of CARPT on the riser under consideration.
- Detectors should be mounted such that their flat surfaces are within 1 cm of the outer wall.

It is important to reiterate that while the techniques demonstrated above can be readily applied in finding the right hardware for CARPT implementation of any kind of reactor. Some of the conclusions that are very specific to the case of gas-solids riser may get modified, but the general framework of analysis and the deductions made from there will be along similar lines.

5. Multiple Detector Analysis

In CARPT, our objective is to monitor the motion of the tracer particle as it moves around in the reactor vessel. In principle, three detectors positioned in space are sufficient to monitor the motion of the tracer. The number of photons registered by a given detector is a measure of the radius of an approximately spherical surface with the detector at its center and the particle located at the surface. An instantaneous position of the tracer particle can be thought of as the point where the surfaces intersect, and clearly three such surfaces (i.e., corresponding to three detectors) will determine any point in three-dimensional space uniquely. However, it has

been shown (e.g. [1-5]) and is also part of the expertise developed in CARPT implementation over the last decade, that statistical fluctuations in the photon emission and their counting introduces errors which can be minimized if redundancy in number of detectors is introduced, i.e., use many more than the suggested minimum of three. Using larger number of detectors, and associated electronic hardware, multiplies the cost of implementing CARPT and the returns in terms of accuracy must justify the extra monetary investment.

We note here that it is *not* sufficient merely to add detectors around the column of interest, but to arrange them in an *optimal* manner, such that one is able to achieve the best accuracy with using the minimum number of detectors. It may be possible to have a large number of detectors that are not optimally placed, so that position reconstruction will be in error whenever the tracer particle visits a region that is not of high enough resolution and sensitivity. In general, the resolution and sensitivity functions are spatially distributed, hence particle position reconstruction is not uniformly accurate everywhere.

This essentially defines an "optimization problem", wherein the objective function is to maximize the *overall* resolution and sensitivity subject to constraints on the number of detectors. The idea is to use minimum number of detectors, owing to economic considerations and "*steric*" limitations, i.e., problem of physically fitting too many solid detectors in limited space. The complete optimization problem is of course a topic of extensive research in itself, but in this section we will investigate several practical scenarios that are of interest to us and propose a few that would meet the desired requirements.

Resolution and Sensitivity Distribution: Single Plane of Detectors. In the analysis that follows, we have followed the "best" hardware as ascertained in Section 4, so that the most desirable

contribution from each detector may be obtained in any given arrangement of the whole array of detectors. The relevant parameters of the simulation are as reported in Table 1. All simulations have been performed with the detectors positioned such that the front surface is 9.7 cm from the riser column axis (1.44 cm from the column wall). When the detector is in this position, the counts recorded by it are just below saturation level when the tracer particle (of 300 μCi strength) is closest to it near the vessel wall. Such a positioning is like using the "full scale" of the detector, i.e., the maximum "counting ability" of the detector is being utilized.

We will present our systematic investigation by comparing first the effect of having one or more scintillation detectors on a single plane. First, the case of single detector is shown in Fig. 9a,b. Fig. 9a shows the resolution distribution in space, at 0^0 (reference), 30^0 rotation and 60^0 rotation of the 2-D vertical planes through the axis of the riser column (the planes are marked in red as I, II and II in Figs. 9-12). Fig. 9b shows the sensitivity function distribution for the same planes. The tracer particle was placed in 3267 (=27×121) points in the planes and counts simulated at the detector. The counts from each of the tracer particle positions were then interpolated using 2D-spline interpolation on the plane. The directional resolution and sensitivity functions were calculate and then recomposed to yield σ_r and S_r. This process was repeated for *all* the configurations presented in this section, for each of three planes shown. The contour plot of resolution in Fig. 9a-I, and that of sensitivity in Fig. 9b-I, when viewed from the position of the detector (marked in red) shows a completely symmetric distribution. An interesting observation is that the region in which the detector is located is clearly "visible" in the contour plot, even though no information was provided in the contour plots about the boundaries of the detector disk.

On rotating the plane of analysis, the right half of the plane is closer to the detector while the left half moves away. This leads to higher resolution (note the difference in contour color scale) in the vicinity of the detector and lesser resolution on the edge of the plane away from the detector. Also, the narrow annular region of very low resolution (in dark red or brown color in Fig. 9a) that is encountered very close to the detector axis (Fig. 9a), is also visible. Similar observations can be made about Fig. 9b, on which sensitivity contours have been plotted. The first plot of Fig. 9a shows a spatially symmetric distribution of sensitivity, with very low sensitivity in the central axis of the detector. At different angular orientations the asymmetry (with respect to the detector location and the plane orientation) is clearly visible. We would like to point out here that for each of the contour plots in Figs. 9-12, the scales are *not* the same and inspection of the plots needs to be done with the contour legend next to it. Use of different scales became necessary in order to make all the plots "visible" with clear distribution of spatial resolution and sensitivities.

On adding extra detectors in around the riser column, both the sensitivity and resolution is expected to improve. Using the equations developed in Section 3, the "composite" sensitivity and resolution by adding 2, 3 and 4 detectors in the same plane is noted. Figs. 10a,b shows an example contour plot when 4 detectors are put in the single horizontal plane, at right angles to each other. The objective of this analysis is to find out the optimal number of detectors *per* plane. Of interest are the regions of maximum resolution (minimum σ_r), and maximum sensitivity. Table 2 the minimum value of σ_r and maximum sensitivity is tabulated for each view. "Best resolution" refers to minimum value of σ_r, while "best sensitivity" refers to maximum S_r value.

The primary conclusion from Table 2 is that while there is a substantial improvement in both sensitivity and resolution in using two detectors in the plane instead of one, the

improvement for adding the third (which notably, is not "symmetrically" placed because the three detectors are placed at right angles to each other with the fourth vertex of the square vacant) and thereafter a fourth is only marginal. Naturally, the absolute value of sensitivity or resolution depends on the relative location of the detector and the view being considered, but the broad conclusion can be drawn anywhere in the column. It maybe noted that ~~the~~ Table 2 *does not* have any information of spatial distribution of the sensitivity and resolution functions, which can only be discerned by actual inspection of the contour plots like Fig. 9 and 10.

Resolution and Sensitivity Distribution: 3-D Array of Detectors. In the discussion that follows, we investigate four alternative scenarios of arranging the detectors around the riser column. Normally, between 8 and 32 detectors are used for a single CARPT experiments, depending on the size and geometry of the column being studied. Each detector enclosure is slightly more than 2 in. in diameter and about 12 in. long, so that there is a limitation of space ("steric" limitation) of arranging two detectors any closer than 5 cm.

In Table 3, details of four different configurations are listed. Arrangement 1 uses only one detector but adjacent layers are closely packed, i.e., at a distance of 5 cm. Adjacent detectors (in adjoining layers) are azimuthally separated by 45^0. The array of detectors thus looks like a single helix winding around the riser column, and is arguably the favorable arrangement with *only one* detector per plane. Arrangements 2 and 3 (Table 3) are two alternative distributions of two detectors per plane. These configurations are expected to produce better "per plane" resolution and sensitivity. The two configurations differ in their "stagger angle", i.e., the angle between the detectors in adjacent planes. Adjacent planes are separated by 10 cm (which seems optimal since we have seen earlier in single detector analysis that 10–15 cm is roughly the

distance from any detector at which its resolution and sensitivity is the maximum). Both of these arrangements have been used in the past in CARPT implementation [1-5,15]. Finally, in arrangement 4, three detectors per plane are used. On any given plane, the three detectors are arranged in an equilateral triangle, with side of about 16 cm. Adjacent planes are separated by 10 cm, and the detector planes are staggered so that the vertices of the equilateral triangles of two adjacent planes are directed opposite to each other.

Figs. 11, 12 show two example sets of contour plots for arrangements 1 and 4, respectively. (Note that the contour legend is specific to each plot). Naturally, it is difficult to visualize exactly how each detector contributes to the overall resolution and sensitivity patterns, but some general observations can be made. First, the edges of the zones of interrogation (i.e., the top and bottom of the contour plots) have relatively low resolution (high σ_r) and low sensitivity. Second, the nature of the sensitivity function (i.e., zero very close to the detector, maximum at intermediate range, and asymptotically decreasing at long range) and of the resolution function (i.e., asymptotically unbounded at the detector center, minimum and intermediate range, and asymptotically increasing at long range) is evident in three dimensions as well. This leads to pockets of very high resolution and high sensitivity on a background of *relatively* low resolution and sensitivity.

It is also interesting to note that typically there are regions near the very central plane of the column that have *relatively* low resolution and sensitivity. This seems counter-intuitive but is nevertheless true, for the following reason. Recall the asymptotic long-range tail of the sensitivity and resolution functions in one dimension (Figs. 3-8). In all detector arrangements we have discussed here, the central plane of the column always has one or more detectors. Thus, due to these detectors alone, parts of the central plane have low resolution and sensitivity.

Furthermore, the central plane is the only zone in the entire column where the long-range tails of *all* the other (i.e., off-central plane) detectors superpose "destructively" with each other as well the near-detector "bad" zone of the central plane detectors. This effect is not pronounced in situations in which the central plane does not have detectors, or has very few of them, because in that case any plane of the column is equivalent. It may be noted that this unfavorable "central detector plane phenomenon" is only relative when compared to other regions of the column and the loss of resolution is marginal when compared to regions which have no detectors in the vicinity, or in the regions of the column outside the zone of interrogation of the detectors.

Inspection of Figs. 9-12 provides qualitative guidelines for detector placement but it is difficult to discern any quantitative indicators. For that reason, we have attempted to tabulate some of the key indicators learned from the Figures in Table 4. The quantities tabulated are the mean values, maximum values, minimum values and standard deviations of the resolution and sensitivity functions for each view of each detector arrangement. The numerical values of the various quantities seem to indicate that arrangements 1 and 3 are comparable, i.e., keeping one detector per plane and staggering adjacent planes by 90^0 and 5 cm separation works out to be similar to having two detectors per plane, and staggering 10 cm apart planes by 45^0. In both cases, the resolution is *relatively* poor and the distribution of high resolution and sensitivity regions is *relatively* non-uniform (higher standard deviation). Staggering adjacent two-detector planes by 90^0 provides *relatively* better symmetry.

Finally, arrangement 4, which is entirely symmetric, provides very good resolution and sensitivity and also a very uniform distribution all around the column including the azimuthal direction (compare different views). We also reiterate that other such symmetrical distributions of detectors could provide the same or better resolution, although having more than three per

plane is not recommended. The substantial improvement in arrangement 4 (Fig. 12) is, however, at the cost of seven additional detectors when compared to arrangements 2 and 3.

Conclusions. The basic conclusions that can be drawn from the preceding discussion are as follows.

- On a single plane, three is the optimal number of detectors to be used.
- As far as possible, arrange detectors in a way so that they are symmetrically distributed around the riser column.
- Stagger adjacent planes alternately so that detectors on alternate planes are farthest from each other.
- One recommended choice is to have three detectors per plane arranged in an equilateral triangle. Adjacent planes are 10 cm apart and the triangles are staggered.
- The edges of interrogation of the detectors have relatively poor resolution and sensitivity, so it may be advisable to "upgrade" those regions by placing a few more detectors in the vicinity.
- Although of secondary importance, the central plane of the column may develop *relatively* poor resolution and sensitivity. This effect can be offset by putting more detectors off the central plane.

6. Summary

For practitioners of radioactive particle tracking experiments, a technique increasingly becoming popular for probing opaque multiphase flow reactors non-invasively, accurate implementation of the experiment has always been a major bottleneck. In the past, choice of

hardware and detector arrangement has been an art, dependent on the experience and intuition of the experimentalist. While this approach suffices for smaller laboratory units, this clearly cannot work when CARPT needs to be implemented on medium-scale pilot plant units and large-scale reactors. From an engineer's perspective, experiments on larger-scale systems are the ones of practical importance. CARPT offers possibilities for studying the flow patterns in larger units but the necessary theory for scientific implementation was lacking.

In the light, the present work provides a satisfactory approach for a more "systematic" implementation of a CARPT experiment. With the example of a gas-solids riser, we have shown the nature of the calculations and the kind of performance indicators that can be extracted. These may not be, arguably, the only indicators of performance of the setup. For example, in a subsequent publication, we intend to investigate the role of frequency of photon counting at the detectors. However, the present communication is complete in itself in that the choice of the hardware and the arrangement of detectors can be totally determined based on the study. A rigorous inspection of the "CARPT performance parameters" also offers the possibility of improvement in the position reconstruction algorithm itself.

References

[1] J. S. Lin, M. M. Chen, B. T. Chao, AIChE J. 31 (1985) 465.

[2] D. Moslemian, M. M. Chen, B. T. Chao, Part. Sci. Tech. 7 (1989) 335.

[3] N. Devanathan, D. Moslemian, M. P. Dudukovic, Chem. Engng. Sci. 45 (1990) 2285.

[4] F. Larachi, G. Kennedy, J. Chaouki, AIChE J. 41 (1995) 439.

[5] F. Larachi, J. Chaouki, G. Kennedy and M. P. Dudukovic, in Non-Invasive Monitoring of Multiphase Flows, Elsevier, 1997, Chapter 11, 335.

[6] L. Wielopolski, Nucl. Instru. and Meth. 143 (1977) 577.

[7] G. B. Beam, L. Wielopolski, R. P. Gardner, K. Verghese, Nucl. Instr. and Meth. 154 (1978) 501.

[8] S. N. Kaplanis, Int. J. Appl. Radiat. Isot. 29, (1978) 543.

[9] S. N. Kaplanis, Nucl. Instru. and Meth. 188, (1981) 353.

[10] L. Moens, J. de Donder, X. L. Lin, F. de Corte, A. de Wispelaere, A. Simonits and J. Hoste, Nucl. Instr. and Meth. 187 (1981) 451.

[11] F. Larachi, G. Kennedy, J. Chaouki, Nucl. Instr. and Meth. A338, (1994) 568.

[12] L. Godfroy, F. Larachi, G. Kennedy, B. Grandjean, J. Chaouki, Appl. Radiat. Isot. 48 (2) (1997) 225.

[13] N. Tsoulfanidis, Measurement and Detection of Radiation, Hemisphere Publishing Corporation, 1983.

[14] F. T. Avignone III, J. A. Jeffreys, Nucl. Instru. Meth. 179 (1981) 159.

[15] S. Roy, Flow Patterns in Liquid-Solid Risers, D. Sc. Thesis, Washington University in St. Louis, Missouri, USA (2000).

[16] Bevington, P. R. (1969) *Data Reduction and Error Analysis in the Physical Sciences.* McGraw-Hill, New York.

[17] Knoll, G. F. (2000) *Radiation Detection and Measurement*, 3rd edition, John Wiley and Sons.

List of Tables:

List of Figures:

Figure 8. Effect of variation of distance between column wall and detector face center.

Figure 9. Resolution and sensitivity functions for a single detector (a) Resolution (top) (b) Sensitivity (bottom). At 0^0, 30^0 and 60^0 planes respectively. Red dot shows the detector location.

Figure 10. Resolution and sensitivity functions for a four detectors in a plane (a) Resolution (top) (b) Sensitivity (bottom). At 0^0, 30^0 and 60^0 planes respectively. Red dots show detector locations.

Figure 11. Resolution and sensitivity functions for Arrangement I (Table 3) (a) Resolution (top) (b) Sensitivity (bottom). At 0^0, 30^0 and 60^0 planes respectively.

Figure 12. Resolution and sensitivity functions for Scenario IV (Table 3) (a) Resolution (top) (b) Sensitivity (bottom). At 0^0, 30^0 and 60^0 planes respectively.

Table 1. Parameters used in detector resolution and sensitivity calculations.

Parameter	Value
Detector Crystal Material	NaI (Tl)
Detector Nominal Size	2 in.
Detector Aspect Ratio (L/D)	1
Detector Decay Time	230 ns
Riser Column Outer Radius	8.26 cm
Riser Wall Thickness	2.54 cm
Riser Wall Material	Plexiglas®
Source	Scandium-46 (^{46}Sc)
Mean Photon Energy	1 MeV
Source Strength	300 μCi
Detector Elevation (distance between column axis and detector flat disk)	1.4 cm

* For each set of computations, one of the parameters was varied and the rest were kept constant at the above values.

Table 2. Resolution and sensitivity analysis with detectors on a single plane.

Number of Detectors in Plane	View I		View II		View III	
	Best Resolution, mm	Best Sens., %/mm	Best Resolution , mm	Best Sens., %/mm	Best Resolution , mm	Best Sens. %/mm
1	5.0	0.9	3.8	1.1	1.8	1.5
2	3.5	1.3	2.9	1.3	1.7	2.0
3	0.7	3.2	1.5	1.9	1.6	2.2
4	0.6	3.3	1.3	2.3	1.5	2.3

Table 2

Table 3. Details of detector arrangements simulated.

Arrangement	Total Number of Detectors	Number of Detectors per Plane	Number of Planes	Distance between Adjacent Planes	Angle of Stagger between Adjacent Planes
1	13	1	13	5 cm	45^0
2	14	2	7	10 cm	90^0
3	14	2	7	10 cm	45^0
4	21	3	7	10 cm	60^0

Table 4. Distribution indices of resolution and sensitivity patterns for the detector arrangements simulated.

		Resolution (mm)				Sensitivity (%/mm)			
		Mean	Max.	Min.	Std. Dev.	Mean	Max.	Min.	Std. Dev. ($\times 10^{-2}$)
Arrangement 1	View I	1.87	2.70	0.55	0.11	2.73	3.98	2.01	7.09
	View II	1.99	2.88	1.24	0.05	2.64	3.34	1.96	5.64
	View III	1.96	2.81	1.25	0.05	2.67	3.39	1.96	5.64
Arrangement 2	View I	1.74	2.61	0.59	0.10	2.90	4.28	1.81	4.61
	View II	1.87	2.82	1.25	0.06	2.77	3.34	1.89	3.93
	View III	1.92	2.62	1.26	0.10	2.72	2.17	1.84	6.97
Arrangement 3	View I	1.83	3.04	0.71	0.08	2.81	3.94	1.34	7.19
	View II	1.86	2.96	0.76	0.12	2.80	3.99	1.865	8.33
	View III	1.91	2.73	0.77	0.09	2.76	3.77	2.03	7.65
Arrangement 4	View I	1.50	2.13	1.08	0.01	3.39	4.10	2.53	4.32
	View II	1.50	2.13	1.08	0.01	3.39	4.10	2.53	4.32
	View III	1.50	2.13	1.08	0.01	3.39	4.10	2.53	4.32

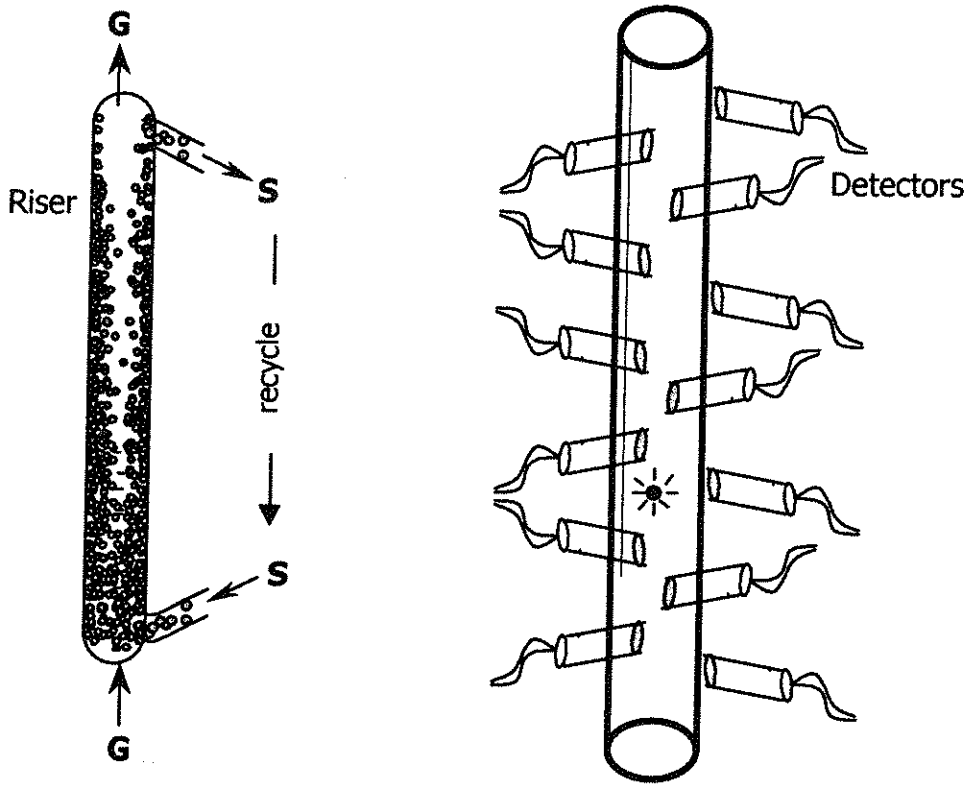

(a) (b)

Figure 1

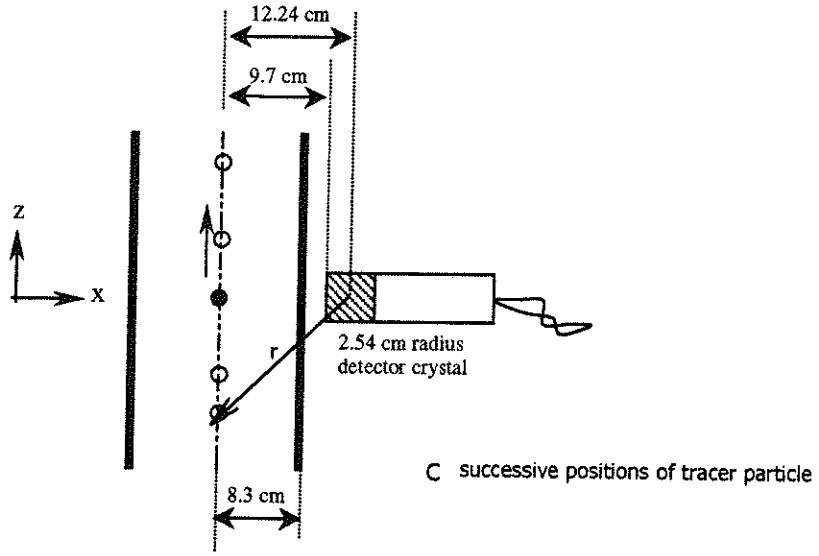
12.24 cm
9.7 cm
z
x
r
2.54 cm radius
detector crystal
C successive positions of tracer particle
8.3 cm

(a)

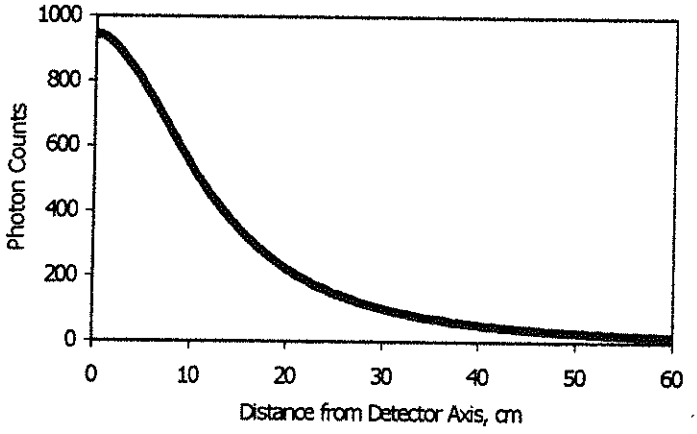
Photon Counts
1000
800
600
400
200
0
0
10
20
30
40
50
60
Distance from Detector Axis, cm

(b)

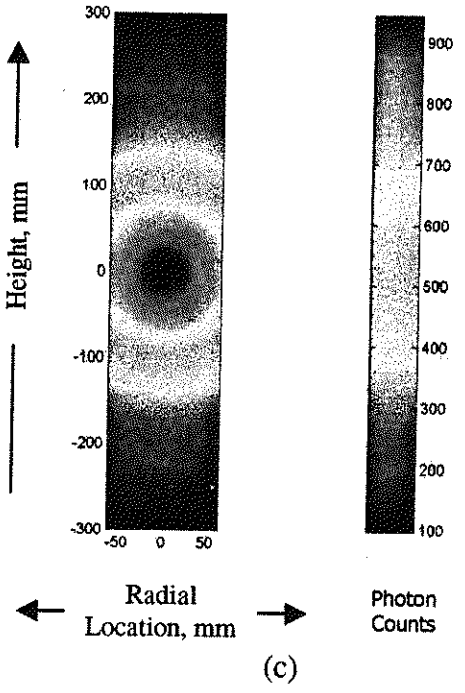
Height, mm
300
200
100
0
-100
-200
-300
-50
0
50
Radial
Location, mm
900
800
700
600
500
400
300
200
100
Photon
Counts

(c)

Figure 2

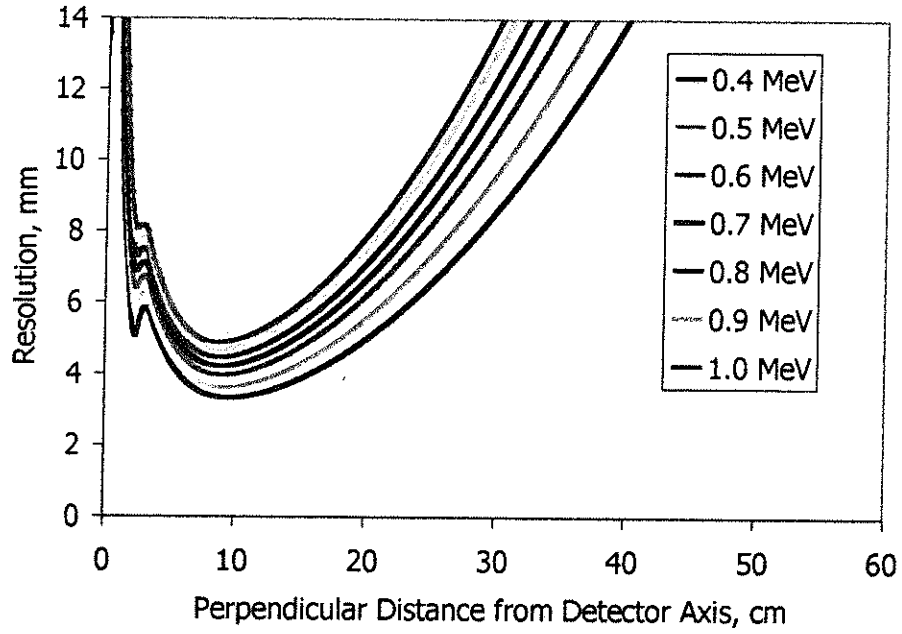
Resolution, mm
14
12
10
8
6
4
2
0
0
10
20
30
40
50
60
Perpendicular Distance from Detector Axis, cm
0.4 MeV
0.5 MeV
0.6 MeV
0.7 MeV
0.8 MeV
0.9 MeV
1.0 MeV

(a)

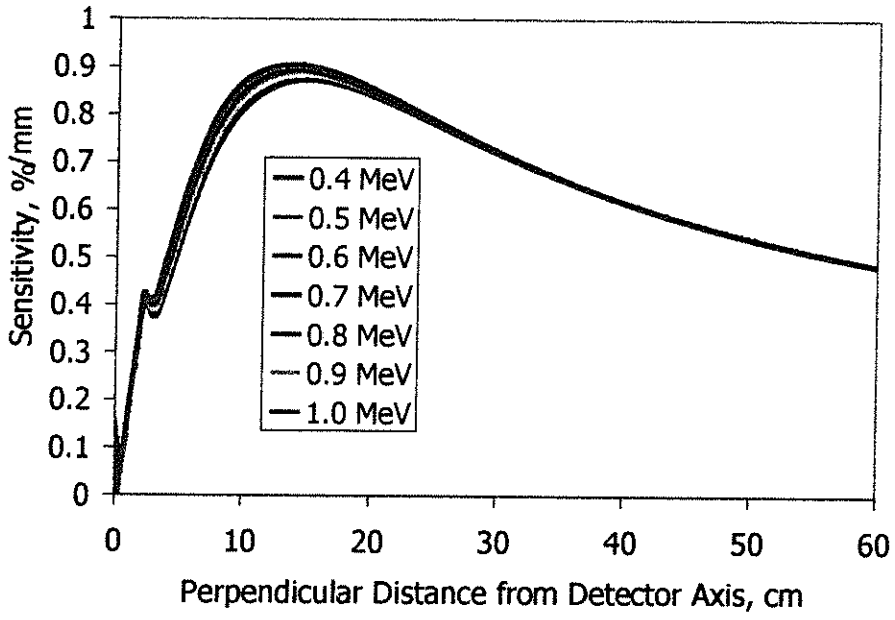
Sensitivity, %/mm
1
0.9
0.8
0.7
0.6
0.5
0.4
0.3
0.2
0.1
0
0
10
20
30
40
50
60
Perpendicular Distance from Detector Axis, cm
0.4 MeV
0.5 MeV
0.6 MeV
0.7 MeV
0.8 MeV
0.9 MeV
1.0 MeV

(b)

Figure 3

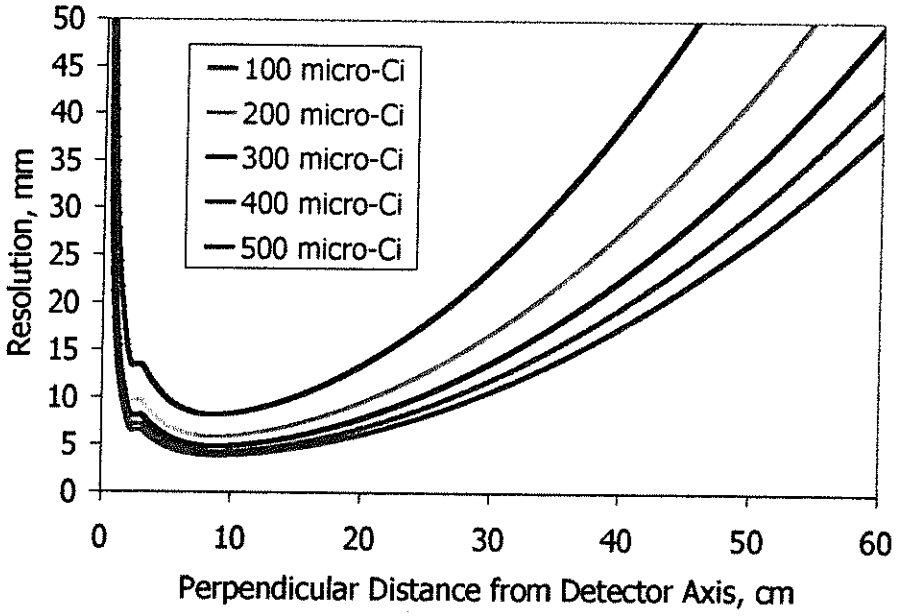
100 micro-Ci
200 micro-Ci
300 micro-Ci
400 micro-Ci
500 micro-Ci
Resolution, mm
Perpendicular Distance from Detector Axis, cm

(a)

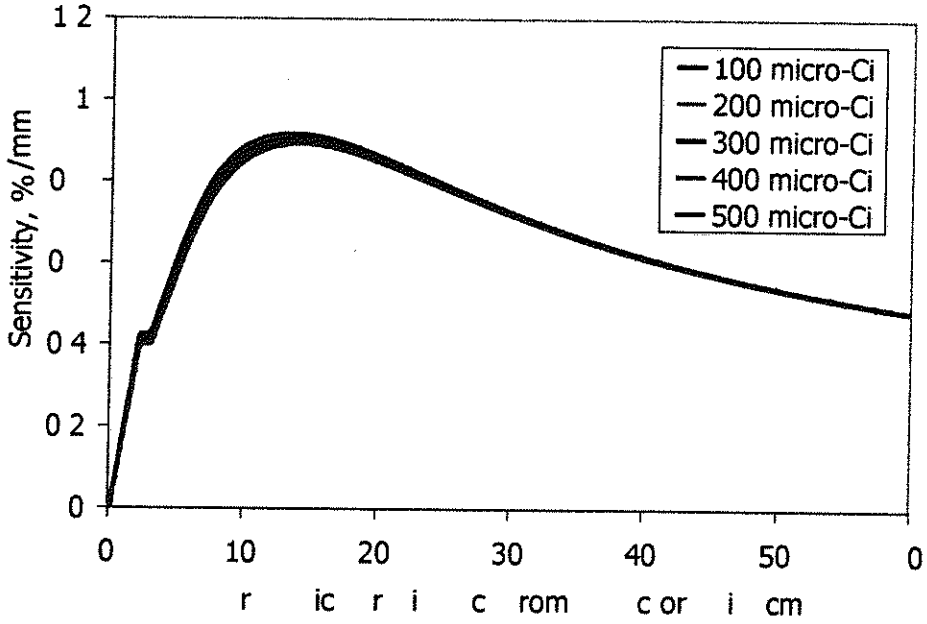
100 micro-Ci
200 micro-Ci
300 micro-Ci
400 micro-Ci
500 micro-Ci
Sensitivity, %/mm

(b)

Figure 4

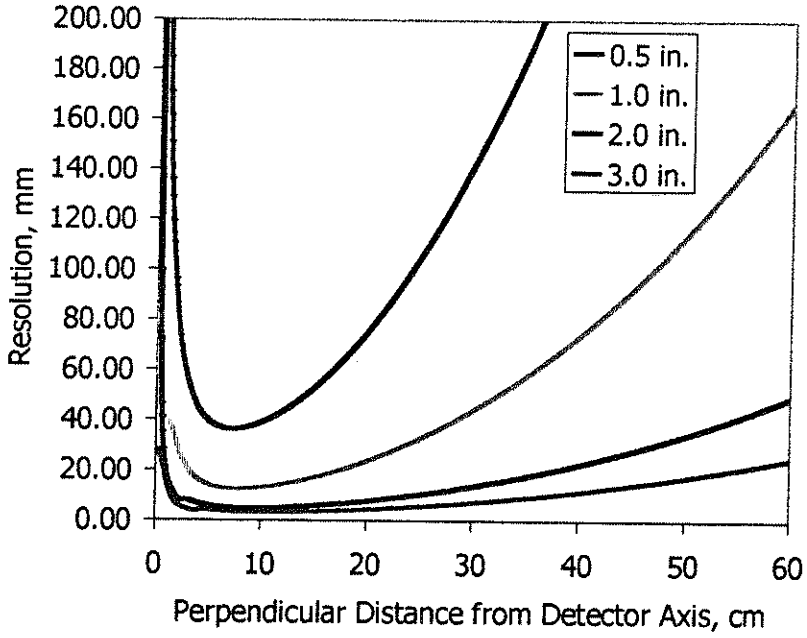
200.00
180.00
160.00
140.00
120.00
100.00
80.00
60.00
40.00
20.00
0.00
Resolution, mm
0.5 in.
1.0 in.
2.0 in.
3.0 in.
0
10
20
30
40
50
60
Perpendicular Distance from Detector Axis, cm

(a)

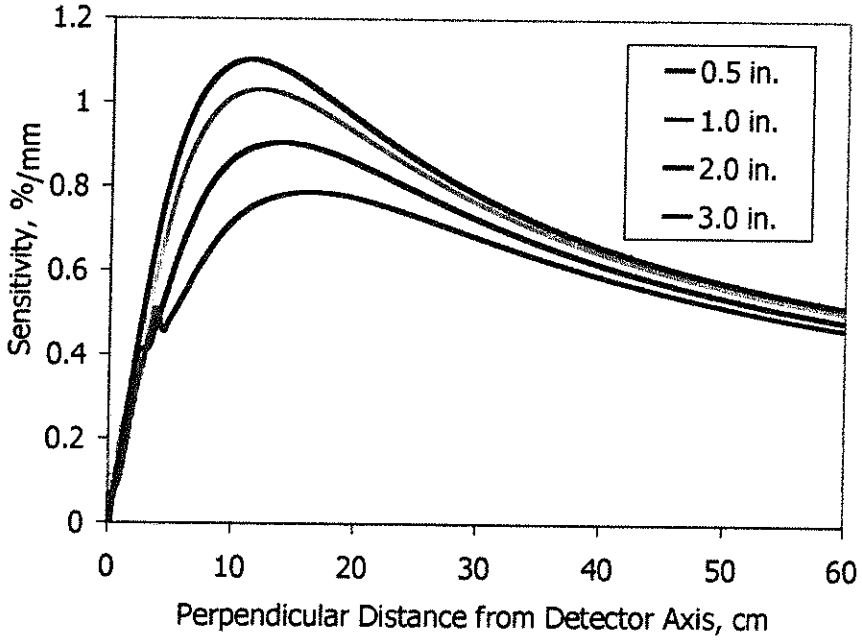
1.2
1
0.8
0.6
0.4
0.2
0
Sensitivity, %/mm
0.5 in.
1.0 in.
2.0 in.
3.0 in.
0
10
20
30
40
50
60
Perpendicular Distance from Detector Axis, cm

(b)

Figure 5

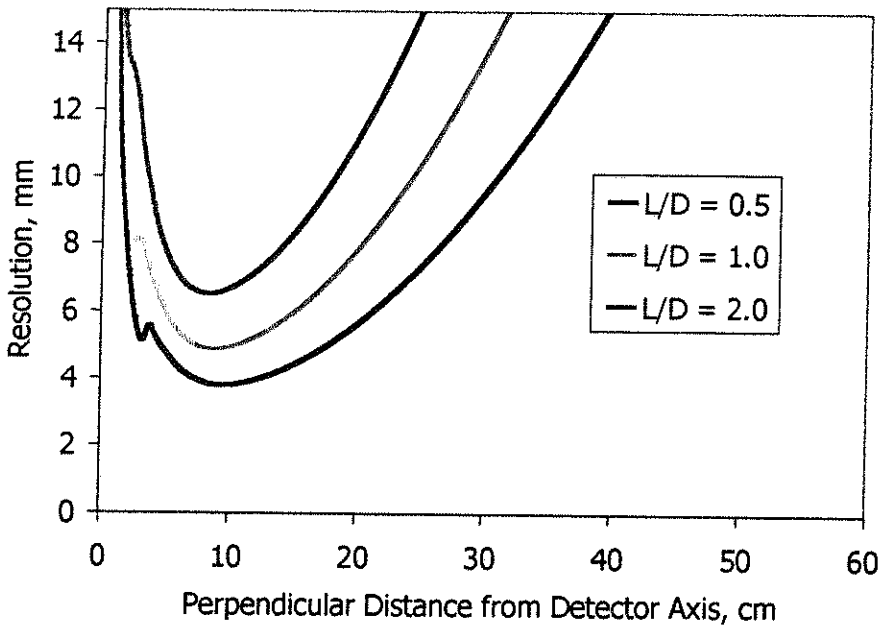
Resolution, mm
0
2
4
6
8
10
12
14
0
10
20
30
40
50
60
Perpendicular Distance from Detector Axis, cm
L/D = 0.5
L/D = 1.0
L/D = 2.0

(a)

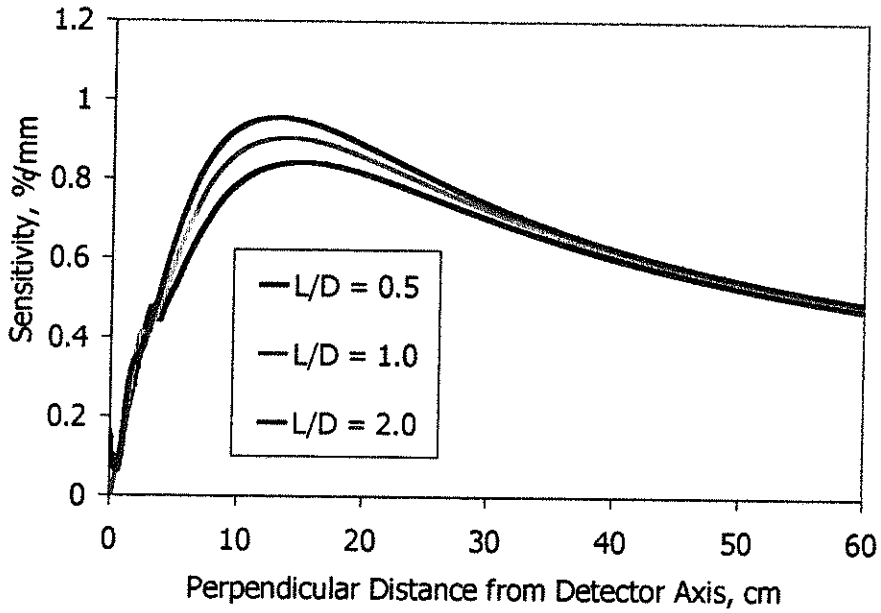
Sensitivity, %/mm
0
0.2
0.4
0.6
0.8
1
1.2
0
10
20
30
40
50
60
Perpendicular Distance from Detector Axis, cm
L/D = 0.5
L/D = 1.0
L/D = 2.0

(b)

Figure 6

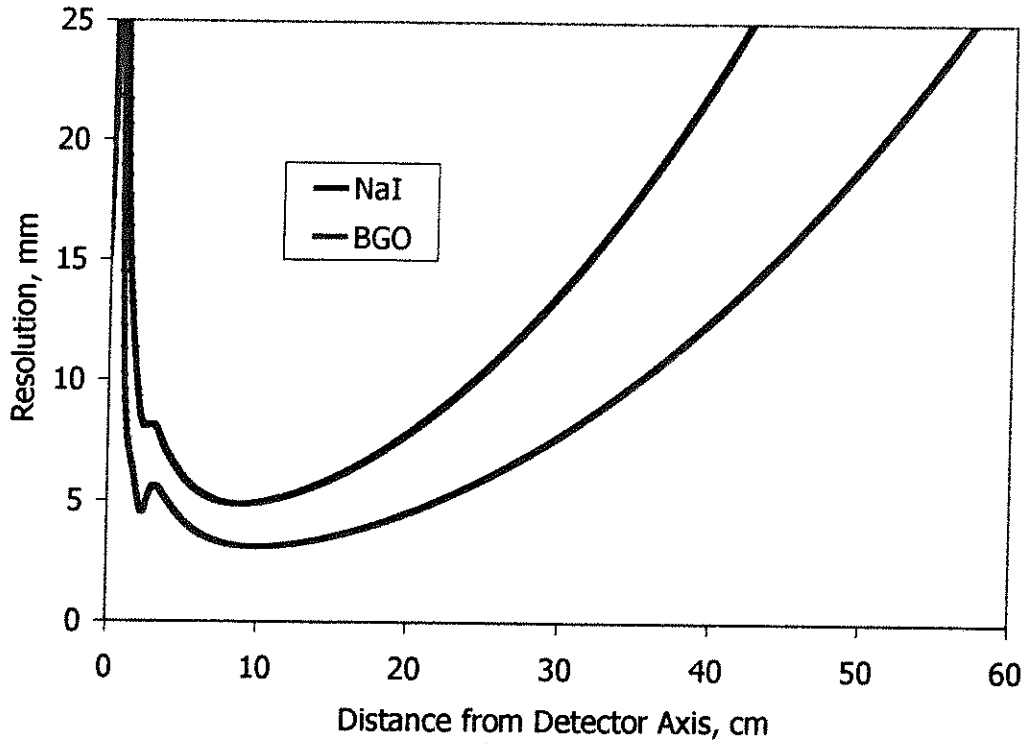
25
20
15
10
5
0
Resolution, mm
NaI
BGO
0
10
20
30
40
50
60
Distance from Detector Axis, cm

(a)

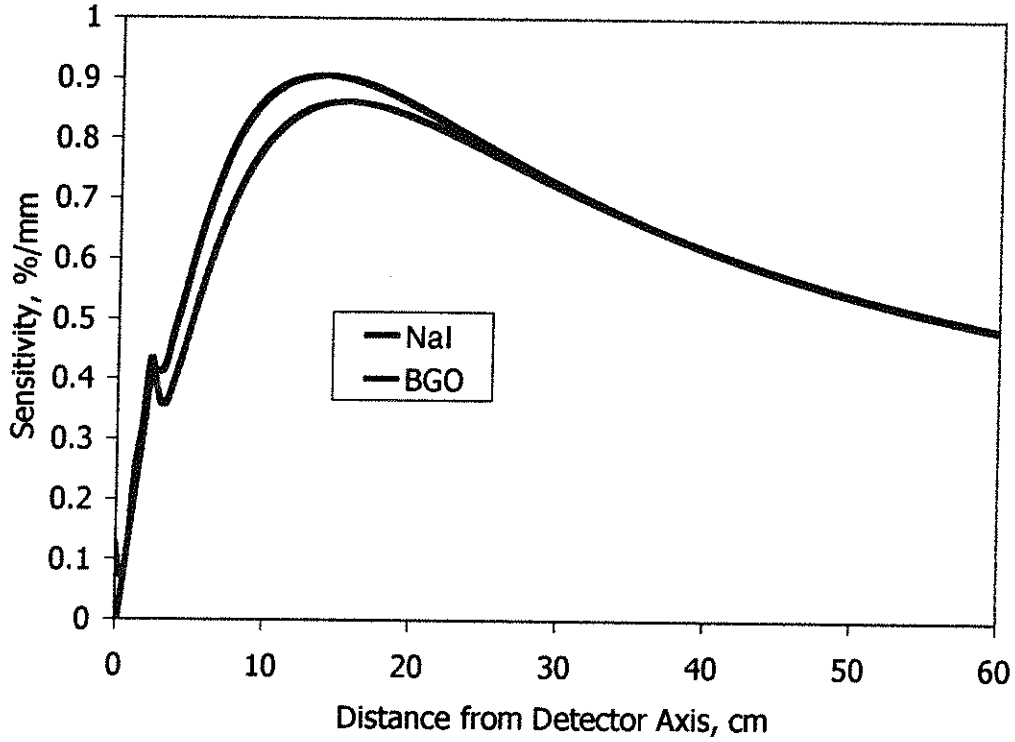
1
0.9
0.8
0.7
0.6
0.5
0.4
0.3
0.2
0.1
0
Sensitivity, %/mm
NaI
BGO
0
10
20
30
40
50
60
Distance from Detector Axis, cm

(b)

Figure 7

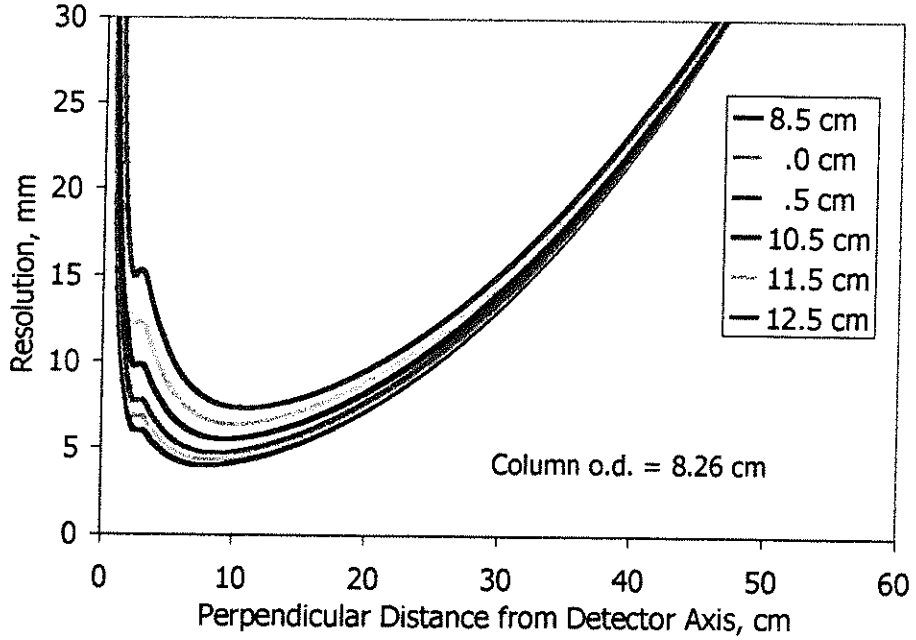
Resolution, mm
30
25
20
15
10
5
0
0
10
20
30
40
50
60
Perpendicular Distance from Detector Axis, cm
8.5 cm
.0 cm
.5 cm
10.5 cm
11.5 cm
12.5 cm
Column o.d. = 8.26 cm

(a)

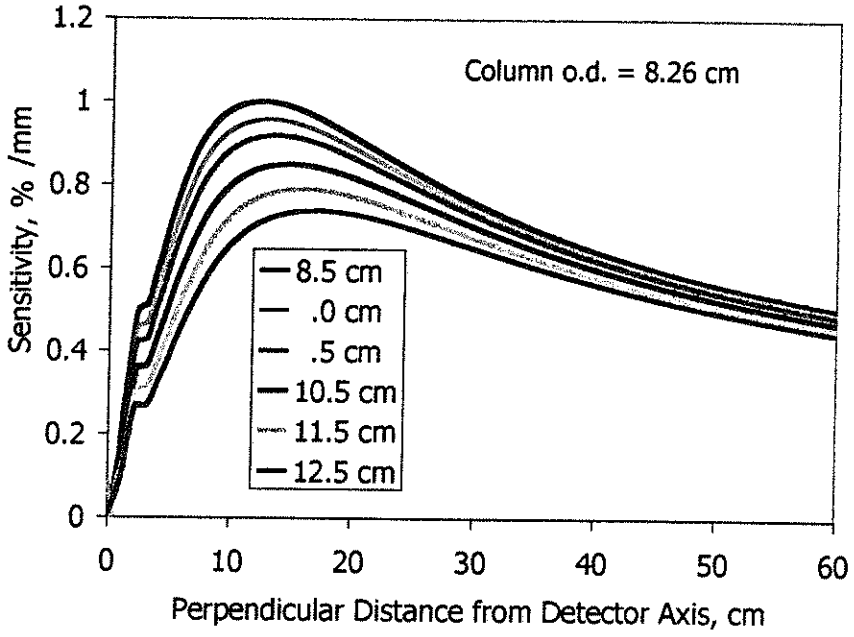
Sensitivity, % /mm
1.2
1
0.8
0.6
0.4
0.2
0
0
10
20
30
40
50
60
Perpendicular Distance from Detector Axis, cm
Column o.d. = 8.26 cm
8.5 cm
.0 cm
.5 cm
10.5 cm
11.5 cm
12.5 cm

(b)

Figure 8

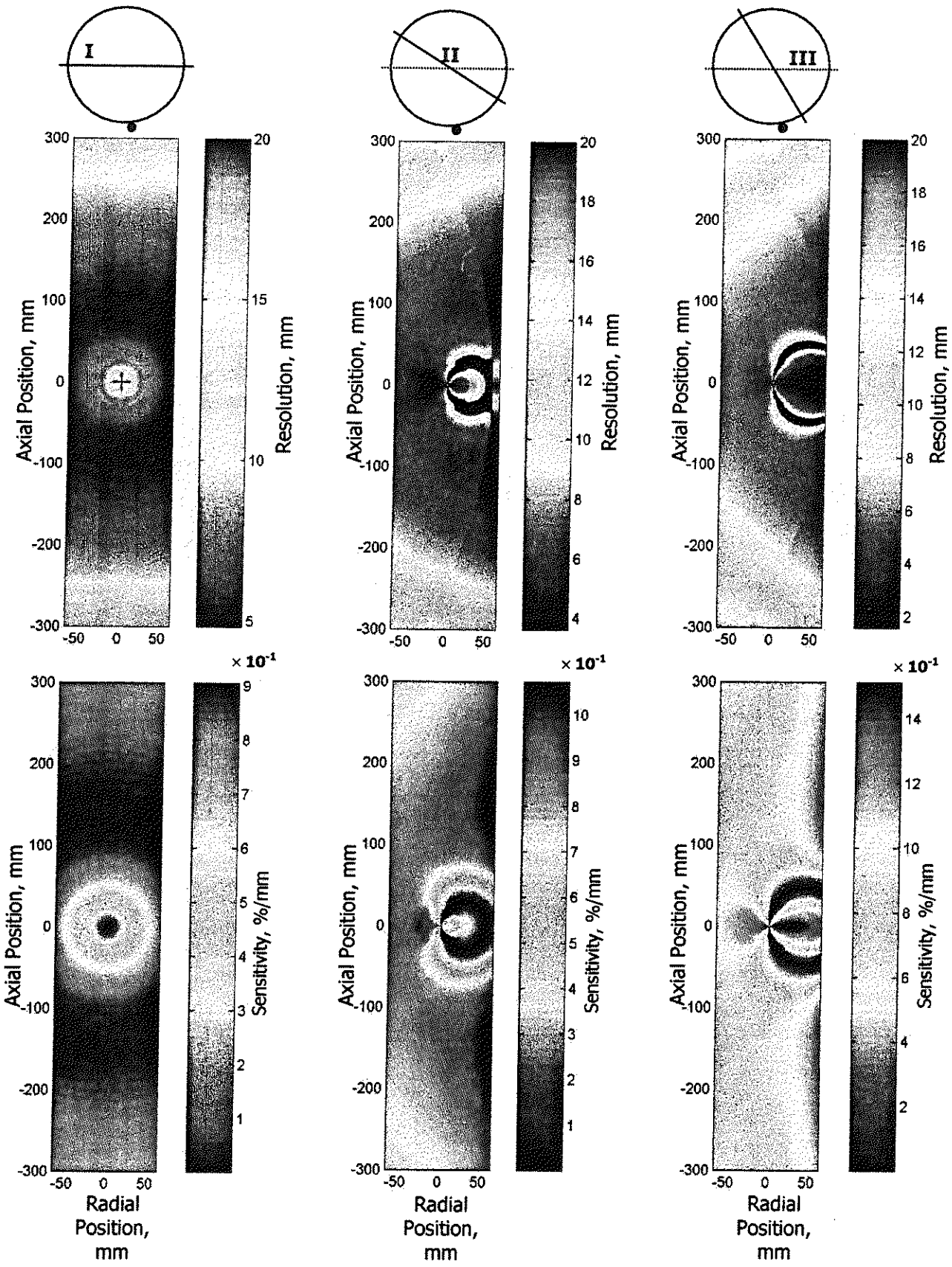
I
II
III
Axial Position, mm
Resolution, mm
Sensitivity, %/mm
× 10⁻¹
Radial Position, mm

Figure 9

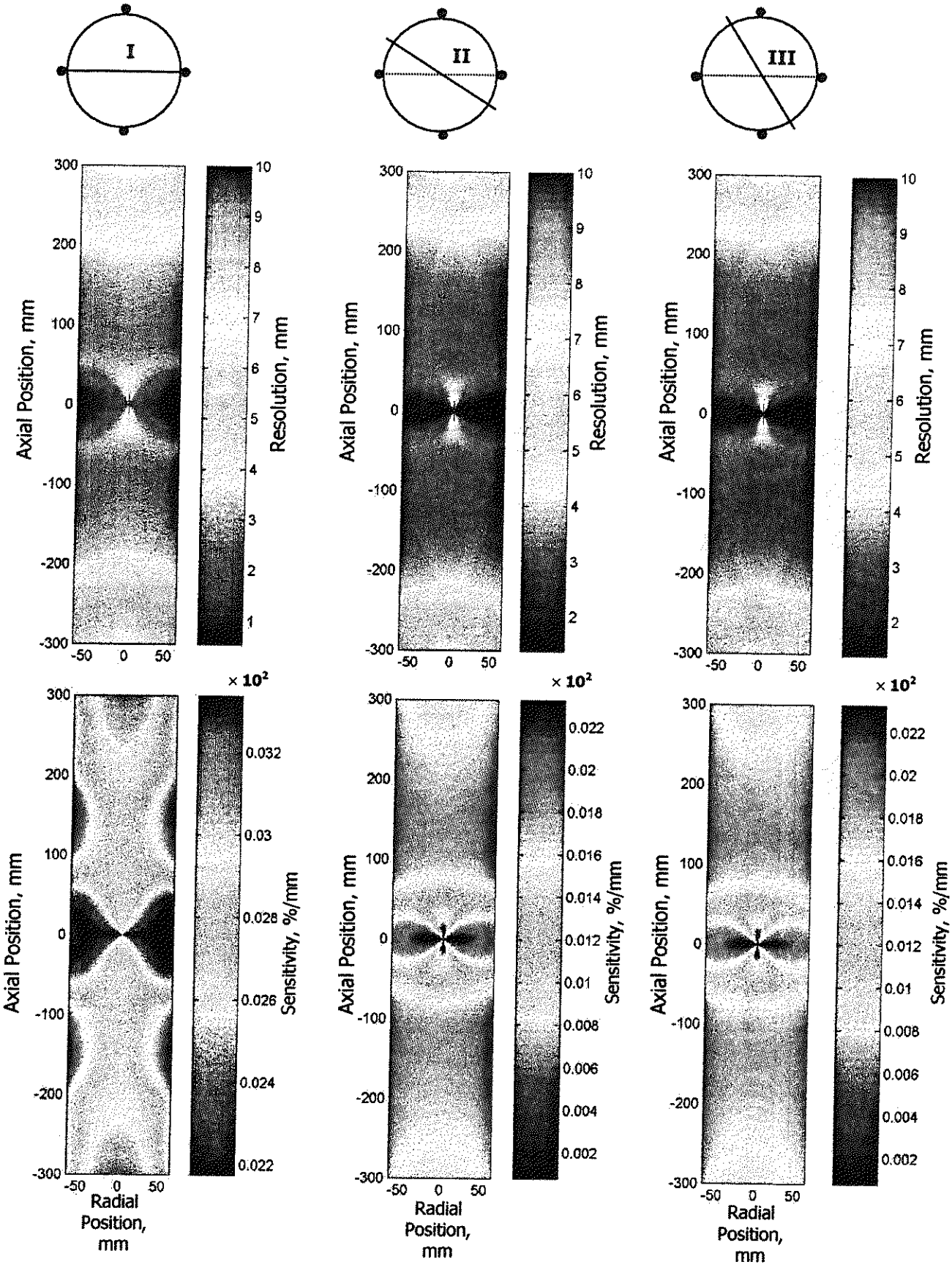
I
II
III
Axial Position, mm
Resolution, mm
Sensitivity, %/mm
× 10²
Radial Position, mm

Figure 10

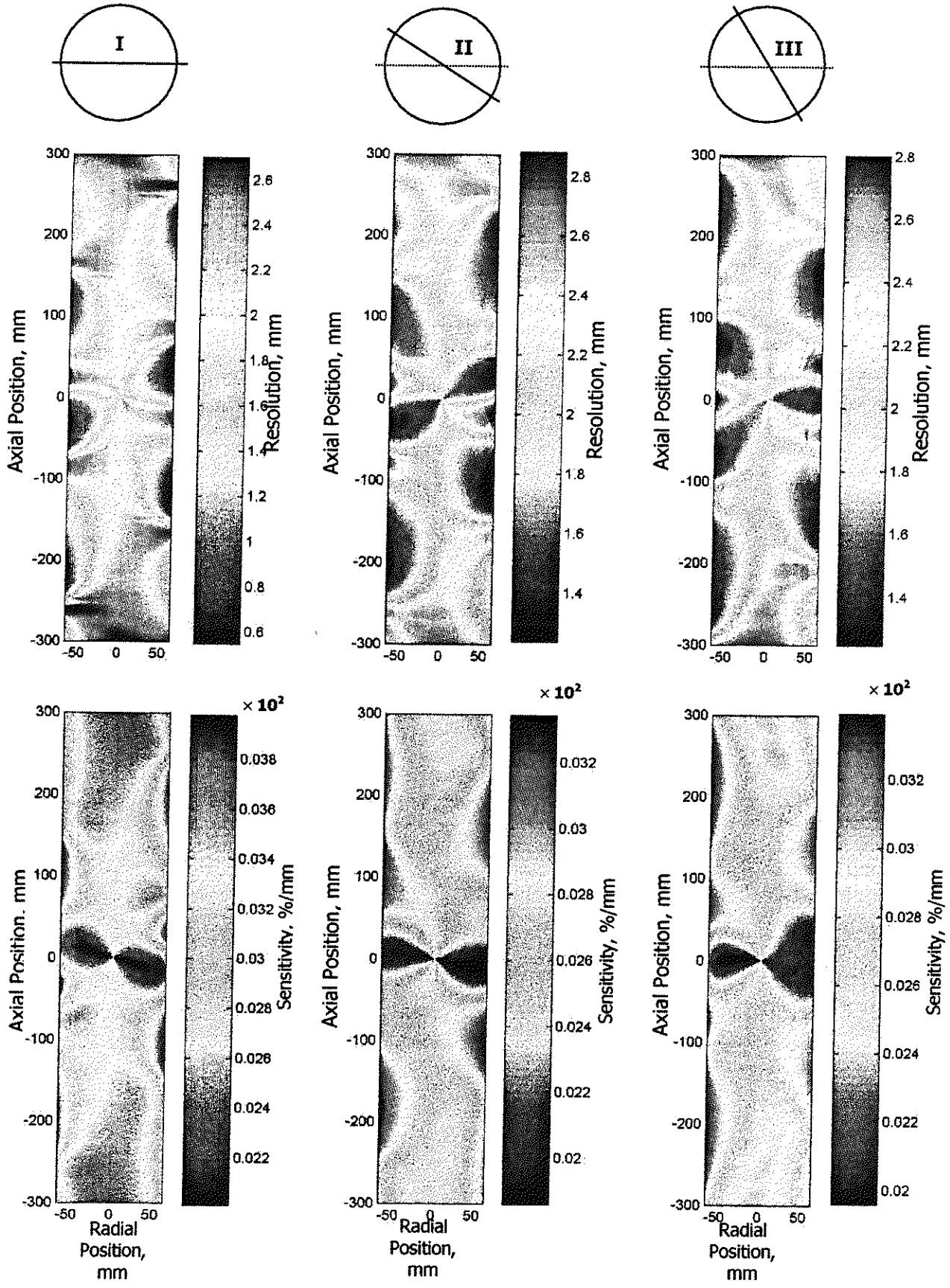
I
II
III
Axial Position, mm
Resolution, mm
Sensitivity, %/mm
× 10²
Radial Position, mm

Figure 11

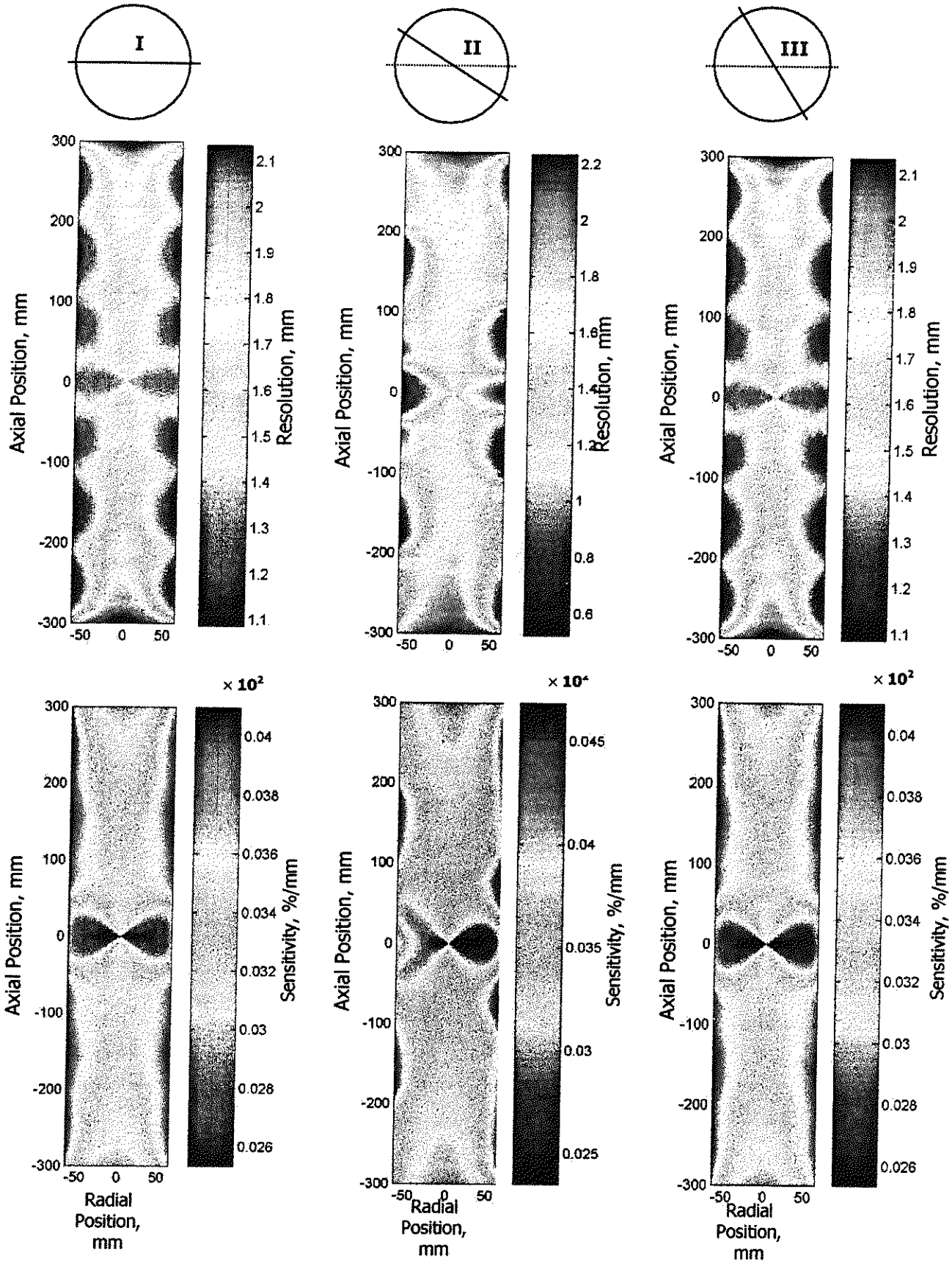
I
II
III
Axial Position, mm
Resolution, mm
Sensitivity, %/mm
× 10²
× 10⁴
Radial Position, mm

Figure 12

A LAGRANGIAN DESCRIPTION OF FLOWS IN STIRRED TANKS VIA COMPUTER AUTOMATED RADIOACTIVE PARTICLE TRACKING (CARPT)

See the attached report for:

A. Problem Definition
B. Research Objectives
C. Research Accomplishments

A Lagrangian Description of Flows in Stirred Tanks Via Computer Automated Radioactive Particle Tracking (CARPT)

A.R.Rammohan, A.Kemoun, M.H. Al-Dahhan and M.P.Dudukovic'*

Chemical Reaction Engineering Laboratory (CREL), Washington University, St.Louis, MO-63130

Abstract

In this study Computer Automated Radioactive Particle Tracking (CARPT) is implemented for the first time in characterization of flows in stirred tanks. Both the experimental technique and the experimental set up are discussed. The CARPT technique is seen to capture some of the important qualitative flow phenomena observed in such flows like the two recirculating loops above and below the impeller and the dead zones at the bottom of the tank. The CARPT data is also used to extract 'Sojourn' time distributions in different zones of the reactor. These distributions are used to partially quantify the observed dead and the active zones in the tank.

Keywords: Hydrodynamics; Mixing; Multiphase flow; Visualisation; Particle tracking; Non-invasive technique

Nomenclature

D, T, D_T	Tank Diameter (cms)
Di	Impeller Diameter (cms)
H_T	Height of Liquid in tank (cms)
N	Rpm
r, R	radial distance (cms)
V_r	mean radial velocity (cms/s)
V_θ	mean tangential velocity (cm/s)
V_z	mean axial velocity (cm/s)
Z	Axial Distance
Re	Reynolds Number
t	time in seconds

Greek symbols

Δ	Incremental change
μ	First moment of the STD
σ^2	Second moment of the STD
γ_1	Third moment of the STD
γ_2	Fourth moment of the STD

---

1. Introduction

Stirred tank reactors (STR) are widely used in the manufacture of fine chemicals, pharmaceuticals and in paper and pulp, polymer and food industry. Most of these operations involve mixing of two or more phases. The design of stirred tanks requires the knowledge of the flow field (like velocity, turbulence intensity, holdup distribution of the dispersed phase, etc.) and the understanding of the effects of various system parameters, like impeller type, power input, numbers of baffles, etc., on mixing efficiency. Detailed experimental data characterizing single-phase flows in stirred tanks exists in the literature (Van't Reit and Smith, 1975; Yianneskis, Popilek and Whitelaw, 1987; Wu and Patterson, 1989; Ranade and Joshi, 1990; Yianneskis and Whitelaw, 1993; Stoots and Calabrese, 1995; Zhou and Kresta, 1996; Kemoun, Lusseyran, Mallet and Mahoust, 1998; and Schaeffer and Hofken, 1999). This data has been collected using existing popular measurement techniques such as Laser Doppler Anemometry (LDA), Digital Particle Imaging Velocimetry (DPIV), etc. all of which provide Eulerian data only that must then be related to mixing times and mixing efficiency (Wittmer, Falk, Pitiot and Vivier, 1998). For multiphase flows which are of considerable interest, "optical" techniques like LDA, DPIV etc. are limited to low volume fractions of the dispersed phase (Rousar and Van den Akker, 1994; Morud and Hjertager, 1996; and Deen and Hjertager, 1999) and cannot be used to discern any information regarding the phase holdup distributions.

In contrast, Computer Automated Radioactive Particle Tracking (CARPT) and Computed Tomography (CT) are powerful non –invasive monitoring techniques capable of providing information in 'opaque' multiphase flows that have not been employed in stirred tanks so far. CARPT and CT have been used extensively to characterize multiphase flows at high volume fractions successfully in a variety of other multiphase reactors such as bubble columns, liquid solid risers, etc (Chaouki, Larachi and Dudukovic', 1997; Kumar and Dudukovic', 1997; Devnathan, Moslemian and Dudukovic', 1990; Degaleesan and Dudukovic', 1995; and Roy, Chen, Kumar, Al-Dahhan and Dudukovic', 1997). CARPT provides the actual trajectories of a tracer particle and can be readily used in both single phase and multiphase systems. It yields Lagrangian information about the velocity vector along the particle trajectory from which the complete three dimensional velocity distributions, turbulence parameters and

dispersion coefficients can be obtained. Such information can be used to validate Computational Fluid Dynamic (CFD) simulations in a STR. It also provides visualization and insight into the complex swirling flows in STRs. In this work the implementation of CARPT in STRs is described. A qualitative assessment of the CARPT results obtained in a STR using water as the fluid is provided. The objective of this study is to establish the type of information that CARPT can provide in single phase flows in stirred tanks. This is to be followed by quantitative comparison with data obtained by established techniques like LDA and DPIV. The ultimate objective is to use CARPT in opaque multiphase flows in stirred tanks at conditions inaccessible to other measurement techniques.

2. Experimental set-up

2.1 The stirred vessel

The stirred vessel used is of the standard Holland and Chapman type (1966) consisting of a cylindrical tank with four baffles and a stirrer (Figure 1). All the parts are made of a transparent material (clear plexi glass). The diameter of the vessel is D=0.2m. The baffles are D/10 in width and D/125 in thickness, vertical and flush with the wall. The agitator is a Rushton turbine composed of a disc of D_I= D/3 overall diameter with six rectangular radial blades of w=D/15 height and thickness D/125. The turbine is located at a distance D_I from the bottom of the tank, which is filled with water to a height equal to the tank diameter. The shaft diameter is D/31.5 and the disc thickness is D/67.

2.2 The CARPT setup

The CARPT set up consists of 16 scintillation detectors (Figure 2) mounted on aluminum supports, which are arranged on an octagonal base. There are eight aluminum supports placed around the tank at 45 degrees to each other. Each support has two holes of diameter 2.2'' (5.6 cms). The axial location of the center of the holes from the octagonal base plate is as follows: The lowest hole is at a distance of Z_1=2.86 cms, then Z_2=7.72 cms, Z_3=12.59 cms and Z_4=17.45 cms. Every aluminum support has the holes placed, either at Z_1 and Z_4 or at Z_2 and Z_3. Every consecutive support has alternate locations of the holes. This configuration optimizes the extent to which the particle can be seen by each detector in the tank (Degaleesan, 1997). Each detector unit is a cylinder 2.125''(5.4 cms) in diameter and 10.25'' (26.0 cms) long, and contains an active cylindrical Sodium Iodide crystal (2'' X 2'' i.e. 5.08 cms X 5.08 cms). Every axial level has four detectors each at right angles with the others. These detectors are placed at the above mentioned four different axial levels. The detectors at each axial level are staggered by 45 degrees with respect to the previous level. The radioactive particle (Figure 3), the position of which is tracked, is about 2.3 mm in diameter, made of polypropylene with radioactive Scandium embedded in it (Sc-46, 80 μCi) and with an air pocket so that the effective density of the particle is equal to that of water (or the fluid tracked). In spite of the fact that the tracer particle is neutrally buoyant its size is too large to enable it to follow all the energy containing eddies in the flow. This particle was chosen because it was readily available to test the CARPT technique in stirred tanks.

Once feasibility is established one can search for a more suitable tracer size while compromising between size and density mismatch. We discuss the limitations of the current tracer particle in the subsequent section.

2.3 The CARPT technique

Devanathan (1991) adapted the Computer Automated Radioactive Particle Tracking (CARPT) technique to study the motion of the liquid phase in bubble columns. A single radioactive particle that is neutrally buoyant with respect to the liquid being tracked (the isotope employed was radioactive Scandium, Sc-46, emitting γ radiation) was used. During an experiment, as the particle moves about in the vessel tracking the liquid phase, the position of the particle is determined by an array of scintillation detectors that monitor the γ radiation emitted by the particle. The radiation intensity recorded at each detector decreases exponentially with increasing distance between the particle and the detector. In order to estimate the position of the particle from the radiation intensities, calibration is performed prior to a CARPT experiment by placing the particle at various known locations and monitoring the radiation recorded by each detector (Figure 4). Using the information acquired, calibration curves are established that relate the intensity received at a detector to the distance between the particle and the detector (Figure 5). Once the distance of the particle from the set of detectors is evaluated, a weighted regression scheme is used to estimate the position of the particle at a given sampling instant in time. Thereby a sequence of instantaneous position data is obtained that yields the position of the particle at successive sampling instants (Figure 6). In our experiments the sampling frequency was 50 Hz, i.e. particle position is identified at 0.02 seconds intervals. Time differentiation of the successive particle positions yields the instantaneous Lagrangian velocities of the particle, i.e., velocities as a function of time and position of the particle. From the Lagrangian particle velocities, ensemble averaging is performed to calculate the average velocities and thereafter the various turbulence parameters of the liquid.

2.4 Measurement errors

2.4.1 Tracer Ability to Follow the Liquid

The accuracy of determining the liquid velocity using the particle tracking technique depends in part on the ability of the tracer particle to follow the liquid. Close matching of the density of the particle with that of the liquid ensures that the particle is neutrally buoyant. However, the finite size of the particle makes it differ from a liquid element, unable to sample the small scale eddies. Devanathan (1991) showed that for a particle of size 2.36 mm, and a difference of 0.01 gm/cm^3 in density between the particle and the liquid, the maximum difference in the velocities (between particle and liquid) is 1cm/s. Degaleesan (1997) showed that the maximum frequency at which the 2.36 mm particle can be taken to follow the liquid up to 99.0% is 30Hz. She also showed that for frequencies less than 30 Hz, which represent the large scale eddies, the particle will be able to closely follow the liquid phase, and the measured particle fluctuating velocities

can be considered to be those of the liquid phase. Higher frequency eddies cannot be followed by the current particle.

2.4.2 Statistical Nature of Gamma Photons

The emission of gamma photons from a radioactive source follows a Poisson distribution (Tsoulfanidis, 1983). Therefore every mean count reported in the calibration curve is associated with a distribution of counts. When reconstructing the particle position from the instantaneous counts registered by each detector only the mean values are used, while in reality the counts measured will be but one value from the distribution seen around the mean. Hence, the reconstructed particle position will not be the exact instantaneous position. The error in reconstructing the particle position along a known trajectory (a circular one when placed in the impeller disc at r=6.0 cms, Z=6.67 cms) is found to be less than 3mm.

2.4.3 Solid Angle Effect

Devanathan (1991) showed that the solid angle has a significant effect on the intensity and that the side face of the detector Sodium Iodide (NaI) crystal is more effective than the front face from the standpoint of detection. If many detectors see the particle, each with a different solid angle, then the errors introduced by some detectors are partially compensated for by other detectors resulting in better accuracy. To obtain higher accuracy in tracer location, solid angle effects have to be considered in the calibration. To some extent this has been implemented by Degaleesan (1997), by using a two step method in reconstructing the particle position. Further improvements can be accomplished by modeling the various interactions of the radiation with the medium and the detector crystal. Modeling of the gamma ray interactions using Monte Carlo simulations has been successfully performed by Larachi et al. (1994) who has used radioactive particle tracking to study the behavior of solids in ebullated beds.

Given the above possible sources of errors in reconstructing the particle position and measurements of the liquid velocity, in a stirred tank we find the accuracy in reconstructing particle position to be good. This can be seen from the fact that the reconstructed particle positions are hardly ever located in the region of the baffles which are about 1.5 mm thick (Figure 7).

2.5 Experimental Conditions

Water is used as the fluid whose motion is tracked by the radioactive particle. Experiments were conducted at 150 rpm (Re_{imp} =12,345). The height of the liquid in the tank was 20.0 cm (equal to tank diameter). The experiments were conducted at room temperature.

3. Results and Discussion

3.1 Validity of Experimental Data

As a first step in establishing the validity of their experimental data, different researchers have reported mass balance verifications. The balance is usually verified in a control volume containing the impeller. These results have been summarized in Table 1. It can be seen that mass balances are usually satisfied within 1-10% accuracy. Table 1 suggests that the CARPT 's accuracy in closing the mass balance within 7% is comparable to other techniques.

Table 1: Accuracy of Mass Balance Closure

Researcher	Technique Used	Region Considered	Accuracy
Gunkel and Weber (1975)	HFA	0<z/D<.16, 0<r/D<1	Within 4%
Yianneskis, Popilek and Whitelaw (1987)	LDA	C.V. around impeller	Within 1%
Wu and Patterson (1989)	LDA	-.22<z/D<.22, 0<r/D<0.55	Within 1%
Ranade and Joshi (1990)	LDA	C.V. around impeller	Within 5%
Yianneskis and Whitelaw (1993)	LDA	C.V. around impeller	Within 1%
Zhou and Kresta (1996)	LDA	-.15<z/D<.23, 0<r/D<.525	Within 5-10%
This work	CARPT	C.V. around the impeller	Within 7%

3.2 Location of the Eye of the Recirculating Loops

The azimuthally averaged velocity in the r-z plane is displayed in Figure. 8. The velocity vector plot captures the key qualitative features expected in this stirred tank configuration (Van Molen and Van Maanen, 1978; Yianneskis, Popilek and Whitelaw, 1987; Costes and Couderc, 1988; Wu and Patterson, 1989; and Ranade and Joshi, 1990). There is a clear radial jet in the plane of the impellers, which goes right to the walls. This high-speed radial jet entrains the surrounding fluid and slows down as it approaches the tank wall. Near the tank wall, the jet stream splits into two portions, one of which then circulates through the upper and the other through the lower portion of the tank and is finally drawn back into the impeller region. These two streams result in the two recirculation loops seen in Figure 8. One loop is above the impeller and the other below the impeller. Both circulation loops exhibit what is conventionally called the eye of the loop. The vertical position of the eye of the upper loop is found to be around D/2 and the eye of the bottom loop is at an elevation around D/5 (where D is tank diameter) with the radial location of both loops at 2D/5. This compares well with the dimensionless locations reported by the other researchers as evident from Table 2.

Table 2: Location of the Eye of Circulation Loops (T= D= tank diameter)

Researcher	Lower r/T	Lower z/T	Upper r/T	Upper z/T	Clearance Hc/T
Yianneskis, Popilek and Whitelaw (1987)	0.3	0.20	0.30	0.48	0.33
Costes and Couderc (1988)	0.4	0.25	0.4	0.75	0.50
Schaefer, Hofken and Durst (1997)	0.4	0.20	0.4	0.5	0.33
Kemoun, Lusseyran, Mallet and Mahoust (1998)	0.4	0.20	0.4	0.5	0.33
Current work	0.4	0.20	0.4	0.5	0.33

3.3 Mapping the Dead Zones in the Stirred tank

At the bottom of the stirred tank the influence of the impeller is not as pronounced as in the rest of the tank. This results in regions of very low velocities at the bottom of the tank where fluid elements (or dispersed phase like solid particles) tend to spend greater time than in the other portions of the tank. The presence of such regions can lower the mixing efficiency. The existence of such zones has been identified by flow visualization studies (Kemoun, 1995). He introduced a number of polypropylene beads (of d_P=0.3 mm and ρ_P=0.8 gm/cc.) into the flow and illuminated the bottom of the tank with a laser sheet. The regions with higher number of particles reflect more light and appear as the bright regions in the photograph. We reproduce here one such snapshot taken by Kemoun (1995) in Figure 9a where the bright spots can be seen to be in the form of a starfish like pattern. These bright regions correspond to the dead zones where velocities are lower causing more particles to accumulate and settle. A similar plot has been generated from the CARPT data where the vector plot of the resultant of the radial and the tangential velocity at the bottom of the tank is shown in Figure 9b. The plot is colored with the contours of the total velocity vector in this plane. The blue regions show the regions of very low velocity. The yellow regions show the regions of high velocity. At the bottom the dead zone can be seen clearly and it seems to resemble a starfish.. The interesting thing is that these dead zones seem to be due to a swirling tornado like structure, which starts just below the impeller plane and is entirely three dimensional in nature. The instability seems to begin at the baffles and slowly propagates downward until the starfish like pattern is observed at the bottom. This comparison of CARPT obtained results with direct flow visualisation illustrates CARPT's potential in capturing important flow phenomena.

3.4 Partial Quantification of Dead Zones Using Sojourn Time Distributions (STDs)

In this study we extract the Sojourn Time Distribution (STD) i.e. strictly speaking the probability density function for different regions in the tank, from the CARPT experiment. For illustrative purposes we have divided the tank only in the axial (vertical)

direction into ten regions each 2cms in height. For each of these zones we compute the STD, as illustrated below, and we display the STD;s in Figure 10. It is important to note that any additional compartmentalization in the angular (θ) and radial (r) direction is possible. Thus, STDs can be calculated from the experimental CARPT data for any region of interest in the stirred tank. We obtain the STD for an axial slice of the tank, defined above, as follows. From the CARPT experiment the record of the particle trajectory as a function of time is available with the time starting at zero and with every subsequent particle location recorded at intervals of Δt= 0.02 seconds (corresponding to f_{sample}= 50Hz). Hence, the N^{th} particle position corresponds to the time $N\Delta t$ seconds since the start of the experiment. To generate the STD curve for each zone the records of the particle positions are scanned until the particle is found in the zone of interest (i.e. the axial co-ordinate of the tracer is between Z_{lower} and Z_{upper} of that zone). Now the particle position is tracked until the tracer leaves the zone of interest. The number of consecutive occurences (say N) from the time the tracer particle entered the zone until the time the tracer particle leaves the zone of interest is noted. From this the sojourn time of the tracer particle during that pass through the zone of interest can be calculated as

$$t_{res1} = N \bullet \Delta t \quad - \quad -(1)$$

This procedure is repeated every time the particle enters and leaves the zone of interest. For a typical CARPT run of 16 hours the particle enters and leaves the bottom most zone (Z=0-2cms) more than 20,000 times and each of those visits contributes to the STD curve. The above procedure is repeated for all the other zones. All STDs are then calculated. In addition, the STD, like any other probability density function, can be characterized in terms of its moments like the mean value, standard deviation, skewness and kurtosis and this is also done. The definition of each of these statistical quantities is reviewed below.

The mean of the STD in the i^{th} zone is denoted by μ_i and is defined by

$$\mu_i = \sum_{j=1}^{N_{tot}} t_{resj_i} E_i(t_{resj}) \Delta t \quad - \quad -(2)$$

Here N_{tot} corresponds to the number of particle occurences (20000 for the bottom zone), t_{resji} is the sojourn time of the tracer particle during the j^{th} trip to zone I of interest as given by (1) and $E_i(t_{resj})$ is the STD for that zone. The first moment (μ_i) about the mean provides an insight as to whether the region experiences low or high through flow. A region where the mean residence times are higher can be thought of as a region of lower velocities and ultimately as dead zones.

The variance of the STD in the i^{th} zone is denoted by σ_i^2 and is defined by the formula

$$\sigma_i^{\,2} = \sum_{j=1}^{N_{tot}} (t_{resj_i} - \mu_i)^2 E_i(t_{resj}) \Delta t \quad - \quad -(3)$$

The positive square root of the variance is the standard deviation denoted by σ_i. σ_i^2 is also referred to as the second moment about the mean value and it indicates how "spread out" the STD is.

Skewness is the third moment about the mean, and is defined for the STD of the

i^{th} zone as

$$\gamma_{1i} = \sum_{j=1}^{N_{tot}} \left(\frac{t_{resj_i} - \mu_i}{\sigma_i} \right)^3 E_i(t_{resj}) \Delta t \quad - \quad -(4)$$

It is a measure of asymmetry of the distribution. If $\gamma_{1i} > 0$, the distribution is said to be skewed to the right and if $\gamma_{1i} < 0$, the distribution is said to be skewed to the left. If the p.d.f. of the variable is symmetric about the mean then $\gamma_{1i} = 0$.

The fourth moment about the mean is called kurtosis, and is defined for the STD of the i^{th} zone as

It reflects the degree to which the population is distributed in the tail of the distribution.

$$\gamma_{2i} = \sum_{j=1}^{N_{tot}} \left(\frac{t_{resj_i} - \mu_i}{\sigma_i} \right)^4 E_i(t_{resj}) \Delta t - 3 \quad - \quad -(5)$$

$\gamma_{2i} > 0$ means that the data is concentrated around the mean (it is leptokurtic); $\gamma_{2i} < 0$ means that the data is concentrated in the tails of the distribution (it is platykuritic).

The CARPT data in the stirred tank have been processed as discussed above to generate the STD curves shown in Figure 11. Inspection of the STD's in various zones reveals that there is a definite similarity in the shape of the STDs in the zones above and below the impeller (E_2 ,E_3 , E_5 and E_6). It is also evident from Figure 11 that the STD in the very bottom region (E_1) is almost the same as that in the top most region (E_{10}). Moreover, the mean residence times and the standard deviations (variances) are the largest in these zones as shown in Figure 12. As discussed earlier flow visualisation with polystyrene particles revealed stagnant zones in the bottom zones which were confirmed by CARPT. CARPT data interpreted in terms of STDs and their moments reveal that the stagnant zones can then also be expected in the top region in the tank where the standard deviation of the STD is even somewhat higher than in the zone at the bottom of the tank (see figure 12). Further compartmentalization of the tank for CARPT data processing can identify the precise location of such dead zones. Clearly, compartmentalization the θ and r direction would allow examination of the regions around the baffles etc.

From the STD curves the different moments were extracted as per equations (2)-(5) and are summarized in Table 3.

Table 3: Different Moments of the STD Curves in various Axial Zones in a Batch Stirred Tank

Zone	Z (cms)	Tmean (sec)	Tstd (sec)	Skewness	Kurtosis
1	0-2	0.4777	0.4999	1.9428	6.6237
2	2-4	0.2946	0.2727	2.4113	10.019
3	4-6	0.2978	0.2599	2.4038	9.7555
4	6-8	0.3146	0.219	1.304332	3.91227
5	8-10	0.3381	0.2693	2.6062	10.804
6	10-12	0.3389	0.278	2.9137	13.056
7	12-14	0.3714	0.2918	2.6403	13.276
8	14-16	0.4255	0.349	1.8961	6.053
9	16-18	0.4758	0.4894	2.0202	6.859

10	18-20	0.5113	0.6182	1.9364	5.153

In Figure 12 the axial variation of the mean and the standard deviations of the STD curves for the axially distributed compartements are shown. This figure indicates that the mean residence time is the highest at the bottom and the top of the tank which was also evident from Figure 11. This trend is as expected since both at the bottom and the top of the tank the velocities are very low and hence once the particle enters these regions it tends to remain longer in these regions than in the impeller plane where the velocities are the highest. The mean residence time reaches a minimum in zone 2 (Z=2-4 cms) and then increases progressively until it reaches its maximum value in the topmost zone. The axial variation of the standard deviation of the sojourn times reaches a minimum in the zone containing the impeller (Zone 4) and then increases exhibiting the same trend as the mean sojourn times. The lowest standard deviation in the impeller plane would seem to suggest that the flow in this region is the closest to plug flow with the deviation from plug flow increasing as we move away from this zone. This confirms the presence of an almost unidirectional radial jet in the impeller zone and regions of lower velocity near the bottom and top of the tank. The axial variation of the third and the fourth moment of the STD's are shown in Figure 13. The skewness (third moment) is seen to be greater than zero in the entire tank which indicates that the distribution is skewed to the right throughout the tank. This skewness to the right is seen to be smallest in the zone containing the impeller and at the bottom and the top portion of the tank. The kurtosis in the entire tank is greater than zero which suggests that the sojourn times are concentrated around the mean (i.e. it is leptokurtic) as evident from Figure 11. It should be reemphasized that we have compartmentalized the stirred tank into equal segments in the axial direction without partitioning in radial or azimuthal direction only as a matter of convenience and to illustrate the STD concept and demonstrate how CARPT data can be used to obtain STDs. The stirred tank could readily be divided into a two dimensional or three dimensional compartmental sections as demonstrated by Mann and coworkers (Mann, Williams, Dyakowski, Dickin and Edwards, 1997) and CARPT data can be used to provide STD's of such compartments and to provide "connectiveness" i.e. flow exchange between the compartments which is needed for mixer and reactor performance calculations.

In addition, various quantities for comparison with computational fluid dynamic codes (CFD) predictions can be evaluated from CARPT data.

4. Summary and Conclusions

In this work CARPT has been introduced as a technique for measuring the flow field in single-phase flow in a stirred tank. The striking feature of CARPT is that upon calibration data that take months to collect with conventional laser based techniques can be obtained in 16-20 hours! Moreover it is the only Lagrangian data available. It has been shown that the CARPT technique can qualitatively capture many of the important flow structures observed in stirred tanks. The full three dimensional Lagrangian measurements obtained by CARPT also provide both better visualization and quantitative measures of the specific features of the flow pattern like the location of the eye of the recirculating loops and the shapes of the dead zones at the bottom of the tank. CARPT allows a direct

assessment of the sojourn time distributions in different parts of the stirred tank. A partial quantification of the dead zones and active zones was achieved by examining the obtained STD curves. A more detailed quantitative comparison of the mean and turbulent velocity profiles obtained in different regions of the tank by CARPT to the values reported by conventional LDA and DPIV techniques is currently in progress. Such comparison will enable us to ascertain the limitations and the accuracy of the CARPT measurements in single phase flows before we embark on multiphase flow studies in stirred tanks.

Acknowledgement

The authors would like to thank the sponsors of the Chemical Reaction Engineering Laboratory (CREL) for making this research possible.

References

Costes, J. and Couderc, J.P., 1988, Study by LDA of the turbulent flow induced by a Rushton turbine flow induced by a Rushton turbine in a stirred tank influence of the size of the units –I . Mean flow and turbulence, *Chemical Engineering Science*, 43(10), pp.2751-2764.

Costes, J. and Couderc, J.P., 1988, Study by LDA of the turbulent flow induced by a Rushton turbine flow induced by a Rushton turbine in a stirred tank influence of the size of the units –II . Spectral analysis and scales of turbulence, *Chemical Engineering Science*, 43(10), pp.2765-2772.

Chaouki, J., Larachi, F., Dudukovic', M.P., 1997, Non-Invasive Monitoring of flows, Eds.: Elsevier, Amsterdam, The Netherlands, chapter 2, p48.

Deen, N.G. and Hjertager, B.H., 1999, Multiphase Particle Image Velocimetry Measurements in an Aerated Stirred Tank, Paper prepared for presentation at the 1999 Annual Meeting of AIChE, Dallas, Tx, Oct 31-Nov 5, Session 06005 : Solid- Liquid & Gas- Liquid Mixing, Unpublished.

Degaleesan, S., 1997, Fluid dynamic measurements and modeling of liquid mixing in bubble columns, D.Sc. Thesis, Washington University, St.Louis, MO.

Degaleesan, S., and Dudukovic', M.P., 1995, Measurement of turbulent dispersion coefficients in bubble columns using CARPT, Mixing X, Banff, Canada, June.

Devanathan, N., 1991, Investigation of liquid hydrodynamics in bubble columns via Computer Automated Radioactive Particle Tracking (CARPT), D.Sc. Thesis, Washington University, St.Louis, MO.

Devanathan, N., Moslemian, D., Dudukovic', M.P., 1990, Flow mapping in bubble columns using CARPT, *Chemical Engineering Science*, 45(8), pp. 2285-91.

Gunkel, A.A. and Weber, M.E., 1975, Flow phenomena in stirred tanks- I, Impeller stream, *A.I.Ch.E. Journal,* 21(5), pp. 931-949.

Holland, F.A. and Chapman, F.S., 1966, Liquid mixing & processing in stirred tanks, New York, Reinhold publns, pp. 11 –14.

Kemoun, A., 1995, Experimental Characterization of the structures in a stirred tank reactor, PhD thesis, Institut National polytechnique de Lorraine, Nancy, France.

Kemoun, A., Lusseyran, F., Mallet, J., Mahoust, M., 1998, Experimental scanning for simplifying the model of a stirred tank flow, *Experiments in Fluids*, 25, pp. 23-36.

Kumar, S.B., and Dudukovic', M.P., 1997, Computer assisted gamma and X-ray tomography: Application to multiphase flow. In Non-Invasive monitoring of multiphase flows, Eds.: Elsevier, Amsterdam, The Netherlands.
Larachi, F.G., G.Kennedy and J.Chaouki, 1994, A gamma ray detection system for three dimensional Particle Tracking in Multiphase Reactors, *Nuclear Instruments and Methods in Physics Research*, A338, pp 568 –576
Mann, R.; Williams, R. A.; Dyakowski, T.; Dickin, F. J. and Edwards, R. B., 1997, Development of mixing models using electrical resistance tomography, *Chemical Engineering Science*, 52(13), pp. 2073-2085.
Morud, K.E. and Hjertager, B.H., 1996, LDA measurements and CFD modeling of gas – liquid flow in a stirred vessel, *Chemical Engineering Science*, 51(2), pp.233-249.
Ranade, V.V. and Joshi, J.B., 1990, Flow generated by a disc turbine, *Transactions of Instituion of Chemical Engineers*, 68(A), pp. 19-50.
Rousar, I. and Van den Akker, H.E.A., 1994, LDA measurements of liquid velocities in sparged agitated turbines with single and multiple Rushton turbines, *Instituion of Chemical Engineers Symposium Series*, 136, pp. 89-96.
Roy, S., Chen, J., Kumar, S.B., Al Dahhan, M.H., and Dudukovic', M.P., 1997, Tomographic and Particle Tracking studies in a Liquid – Solid Riser, *Industrial and Engineering Chemistry Research*, 36(11), pp 4666-4669.
Schaeffer, M., Hofken, M. and Durst, F., 1997, Detailed LDV measurements for visualization of the flow field within a stirred tank reactor equipped with a Rushton turbine, *Transactions of Instituion of Chemical Engineers*, 75(A), pp. 729-736.
Schaefer, M., and Hofken, M., 1999, Experimental study of trailing vortices around impeller blades, Presented at Mixing XVII, August 15-20th, Banff, Alberta, Canada.
Stoots, C.M. and Calabrese, R.V., 1995, Mean velocity field relative to a Rushton turbine blade, *A.I.Ch.E. Journal*, 41(1), pp. 1-11.
Tsoulfanidis, N., 1983, Measurement and detection of radiation, McGraw Hill, NewYork.
Van't Reit, K. and Smith, J.M., 1975, The trailing vortex system produced by Rushton turbine agitators, *Chemical Engineering Science*, 30, pp. 1093-1105.
Van der Molen, K. and van Maanen, H.R.E., 1978, Laser Doppler measurements of the turbulence flow in stirred vessels to establish scaling rules, *Chemical Engineering Science*, 33, 1161-1168.
Wu, H. and Patterson, G.K., 1989, LDA measurements of turbulent flow parameters in a stirred mixer, *Chemical Engineering Science*, 44 (10), pp.2207-2221.
Wittmer, S., Falk, L., Pitiot, P., Vivier, A., 1998, Characterization of Stirred vessel hydrodynamics by three dimensional trajectography, *Canadian Journal of Chemical Engineering*, A7(6), pp. 600 – 610.
Yianneskis, M., Popilek, Z. and Whitelaw, J.H., 1987, Steady and unsteady flow characteristics of stirred reactors, *Journal of Fluid Mechanics*, 175, pp. 537-555.
Yianneskis, M. and Whitelaw, J.H., 1993, On the structure of the trailing vortices around Rushton turbine blades, *Transactions of Institution of Chemical Engineers*, 71 (A), pp.543-550.
Zhou, G. and Kresta, S.M., 1996, Distribution of energy between convective and turbulent flow for three frequently used impellers, *Transactions of Instituion of Chemical Engineers*, 74 (A), pp.379-389.

Captions for the Figures

Figure. 1. Stirred Tank of the Holland –Chapman type used for the CARPT Experimental Study
Figure. 2. CARPT Setup for the Stirred Tank
Figure 3. Details of the CARPT Tracer Particle
Figure 4. Details of the Calibration Procedure
Figure. 5. Calibration Map for Detector #1
Figure. 6. Projection of the Particle Trajectory in a Veritcal Plane at N=150 rpm for 30 seconds
Figure. 7. Projection of the Reconstructed Particle Position at N=150 rpm, top view for 1 hr of the 16 hour run
Figure. 8. Azimuthally Averaged Velocity Vector Plot at N=150 rpm
Figure. 9a. Dead Zones from Flow Visualization Studies (Kemoun, 1995)
Figure. 9b. Map of Dead Zones from CARPT
Figure.10. Compartmentalization of the Stirred Tank into Axial Zones
Figure 11. Sojourn Time Distributions in Different Axial Zones of the STR from CARPT Data
Figure 12. Axial Variation of the mean and the standard deviation of the STDs
Figure 13. Axial Variation of the Skewness and the Kurtosis of the STDs

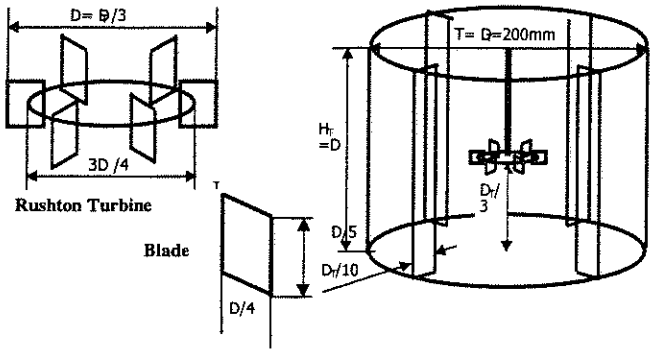

Figure 1

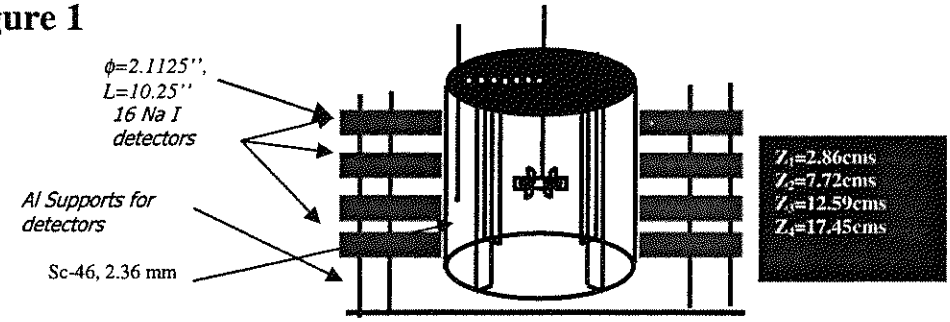

Figure 2

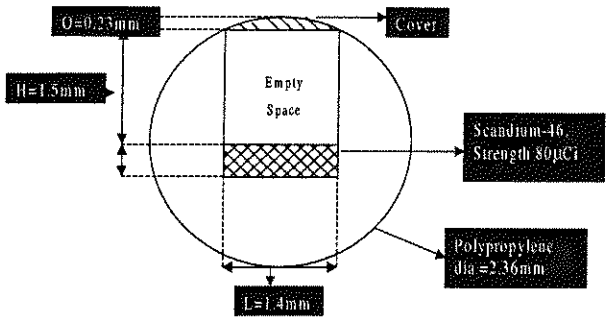

Figure 3

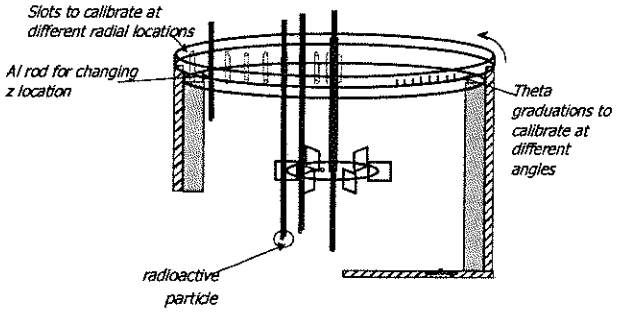

Figure 4

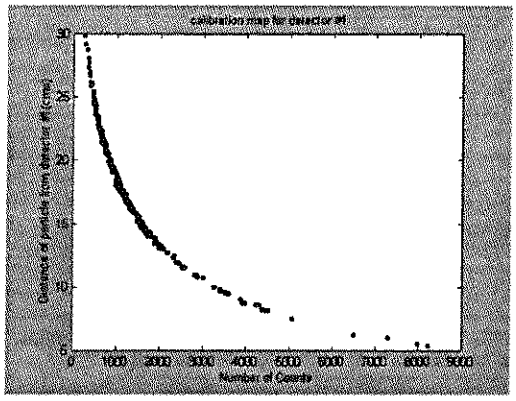

Figure 5

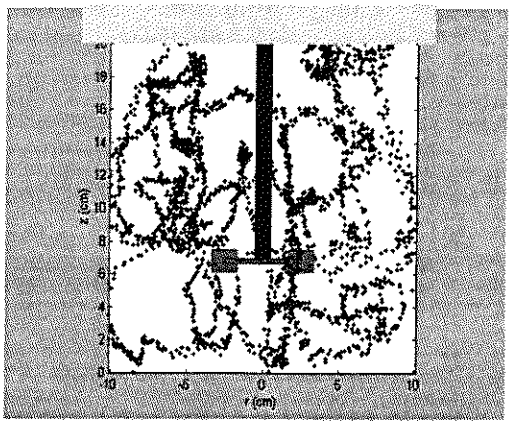

Figure 6

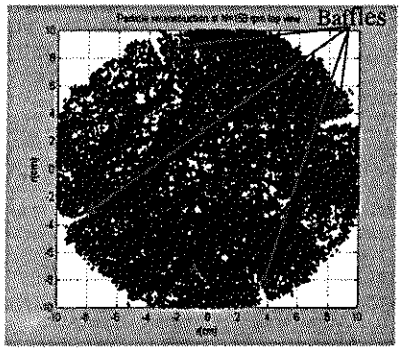

Figure 7

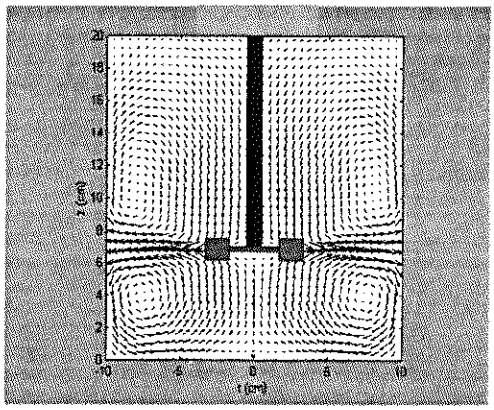

Figure 8

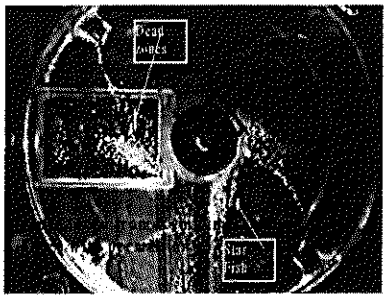

Figure 9a

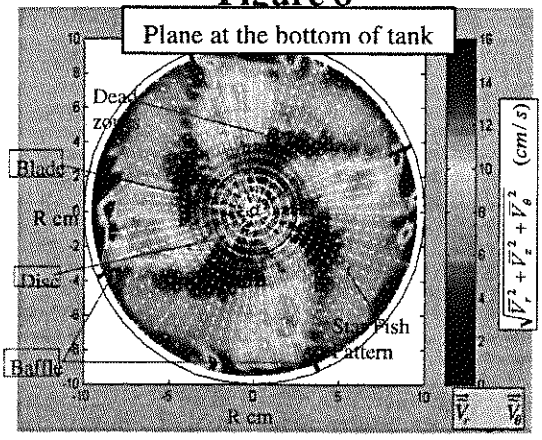

Figure 9b

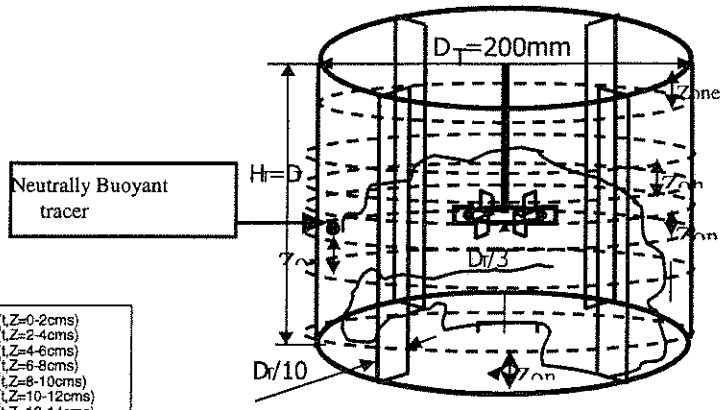

Figure 10

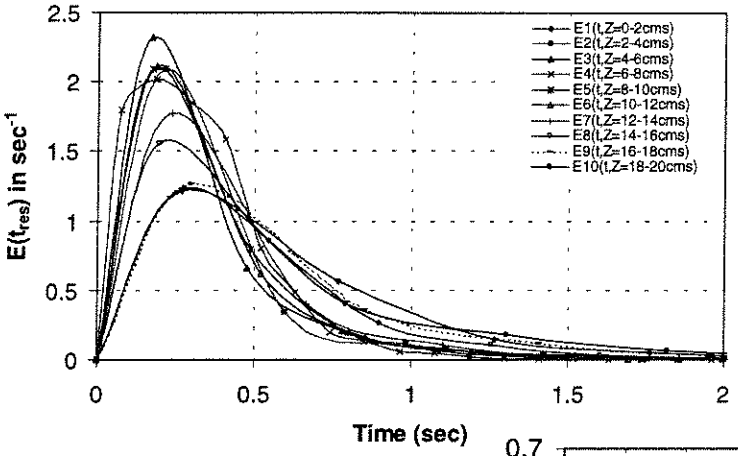

Figure 11

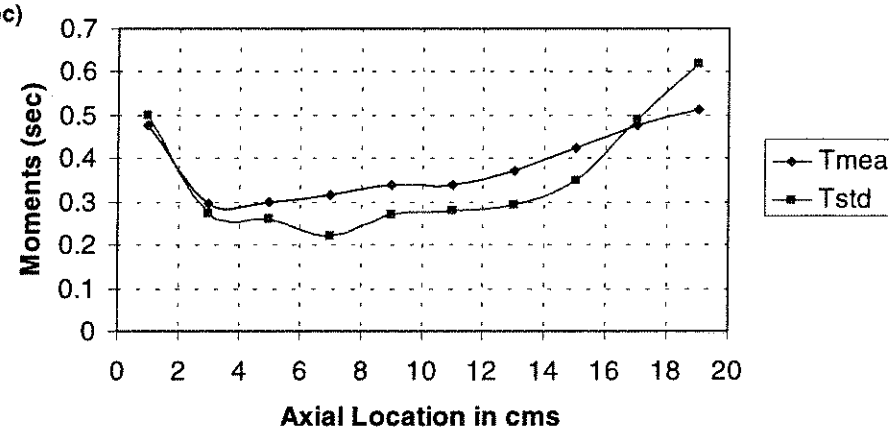

Figure 12

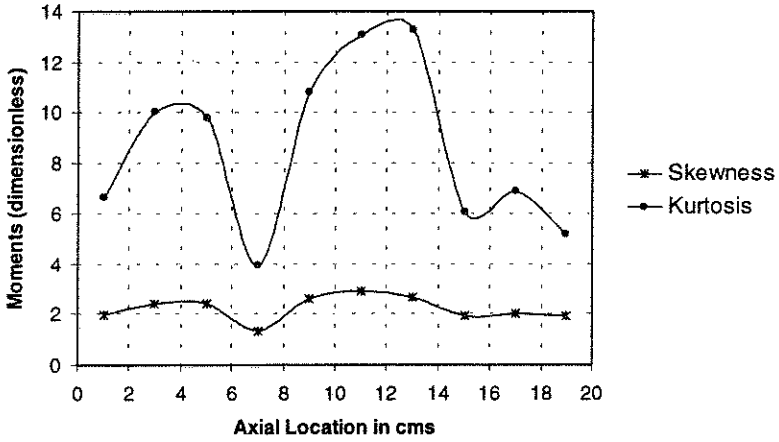

Figure 13

STATISTICAL CHARACTERIZATION OF MACROSCALE FLOW TEXTURES IN TRICKLE BEDS

A. Problem Definition

For the proper scale-up and design of trickle beds, it is important to understand and predict the complex fluid dynamics. Hence, there is a need to know how fluid dynamics quantities such as phase holdup, gas and liquid velocities and phase pressure are distributed spatially and temporally in the multi-dimensional packed beds. The description of steady state hydrodynamics requires the information on global quantities (i.e. overall phase holdup and pressure drop), which can be calculated primarily by empirical or phenomenological models (Saez and Carbonell, 1985; Holub et al, 1992, 1993), and information on velocity distribution and phase holdup distribution. Both experiments (Lutran et al., 1991; Ravindra et al 1997) and numerical simulations (Jiang et al., 1999) have demonstrated concluded that fluid flow distribution under steady state conditions is a function of bed structure (i.e. porosity distribution), initial wetting state of particles and inlet superficial velocities of the two fluids. To utilize the flow distribution information in the scale-up and design of trickle beds, it is necessary to quantify the flow distribution in terms of physical parameters such as bed structure parameters, particle wetting factors and operating conditions. Recent advanced experimental measurements revealed that the velocity distribution (Sederman et al., 1997, 1998; Volkov et al., 1986) and porosity distribution (Chen, et al., 1998) in a cylindrical column are pseudo random in nature. This implies that a statistical method of moments could be used as a tool to characterize the flow and structure distributions.

The goal of this study is to develop useful correlations of interest to trickle-bed design, which bridge the gap between physical bed structure parameters, operating conditions and the resultant two phase flow distribution in terms of statistical variables (i.e. moments). The approach used to pursue this goal relies on a series of numerical fluid dynamics simulations. The recent advances in understanding of multiphase flow and development of robust codes, that can simulate multi-fluid and multi-dimensional problems, have made simulation of complex flows such as those observed in trickle beds feasible. For instance, a tool such as CFDLIB (developed by the Los Alamos National Laboratory), which is capable of simulating transient multiphase flows (Kashiwa et al., 1994; Kumar 1995; Khadilkar, 1996; Jiang et al., 1999), is available for understanding the characteristics of flow distributions and for developing such structure-flow correlations.

In this report, we present how to implement these physical phenomena into CFDLIB code, and how the local interfacial forces affect statistical quantities of the simulated flow distribution. To quantify the relationship of bed structure, particle wetting and resultant flow distribution, through a series of numerical two phase flow simulations, we correlate these distributions in terms of statistical parameters (i.e. standard deviation, std) at given flow input conditions.

B. Research Objectives

The research objectives for this study are:

1. Examine the effects of capillary pressure (wetting) on two-phase flow distribution in trickle beds.
2. Develop the relationship between bed structure, particle wetting and flow distribution.

C. Research Accomplishment

The research accomplishments are discussed in the attached manuscript accepted by the 16th International Symposium on Chemical Reaction Engineering (ISCRE16), September, Poland.

1. Introduction

For successful scale-up and design of trickle beds, it is important to understand and predict the complex multiphase fluid dynamics. In other words, one needs to know how the hydrodynamic quantities such as phase holdup, gas and liquid velocities and phase pressure are distributed spatially and temporally in the multi-dimensional reactors. Even the precise description of the steady-state hydrodynamics requires not only the information on global quantities (i.e., overall holdup and pressure drop), which can be calculated primarily by empirical or phenomenological models (Saez and Carbonell, 1985; Holub et al, 1992, 1993), but also the information on the distribution of these quantities. Both experimental studies (Lutran et al., 1991; Ravindra et al 1997) and numerical simulation (Jiang et al., 1999) lead to the conclusion that fluid flow distribution under steady-state condition is a function of bed structure (i.e., porosity distribution), particle wetting and the inlet superficial velocities of the two phases. However, there is no quantitative relationship available in the literature to describe the state of the bed and its effect on reactor performance.

To develop such a model, one needs to first understand the nature of the system. Fortunately, recent experiments revealed that the fluid velocity distribution (Sederman et al., 1997, Volkov et al., 1986), liquid holdup distribution (Toye et al., 1997) and porosity distribution (Chen, et al., 2000) in packed beds are pseudo-random in nature. This means that the local hydrodynamic quantities (such as holdups and velocities as well as particle external wetting efficiency) and local porosity can be considered as random variables. The global hydrodynamics then can be described by the local hydrodynamic parameters through a proper probability density function (Crine et al., 1992). The goal of this study was to search for such a probability function and to describe the function parameters in terms of measurable parameters such as bed dimensions, particle size and shape, operating conditions, etc.

The logical way to pursue this goal is to conduct extensive measurements of the bed-scale hydrodynamics and of the local-scale hydrodynamic parameters, simultaneously. This requires the determination of bed structure characteristics, such as porosity distribution, with the same spatial resolution as achieved in flow measurements. Although the non-invasive tomography techniques are available for such high-cost

experiments (Toye et al., 1997; Sederman et al., 1997; Reinecke et al., 1998), the numerical flow simulation provides also a rational way, with good cost-effectiveness, to obtaining useful preliminary results needed to guide the future experimental validation study.

To effectively model the gas and liquid distributions in trickle beds, one should resolve two critical issues: (i) how to implement the complex geometry of the packed bed in the flow equations (*structure problem*); (ii) how to take into account the gas-liquid-solid interactions (*closure problem*). Most previous approaches 'solved' these two problems in a simplistic manner. For bed structure problem one used either the mean porosity, or the longitudinally averaged porosity profile (i.e. an oscillating radial porosity profile, $\varepsilon(r)$) or the mean porosity with some empirical quantities (e.g. radial spreading factor, effective viscosity, effective diffusivity) (Song et al., 1998; Bey and Eigenberger, 1997). Recently, for the purpose of heat-transfer study of gas flow in a single tube fixed-bed with low tube-to-particle diameter ratio (2~3), a 3-D computational fluid dynamics (CFD) simulation was performed by generating the fine mesh within the interstitial void space between particles of large size (~5 cm) (Logtenberg and Dixon, 1998; Nijemeisland et al., 1998). It is impossible, however, for a massive commercial column, or even for a bench-scale trickle bed with small particle size (0.5 - 3 mm) to use such fine-mesh approach. Moreover, it is also not necessary because the exact porosity structure is completely changed with re-packing even with the same particles and the same packing method. However, we should be able to obtain the same or similar statistical quantities of the bed porosity distribution even after re-packing. Thus, one can generate a porosity distribution with same statistical characteristics under certain constraints , and then use such porosity distribution section by section in further numerical flow simulation.

Closure problem is the second tough issue in multiphase flow simulation. The existence of microscopic turbulence in porous media has been detected by several experiments by point-wise probes (Jolls and Hanratty, 1966; Latifi et al., 1989); therefore, one has to take Reynolds stress term into consideration in the fine-mesh CFD modeling with high gas flow rate (see Nijemeisland et al., 1998). For the macroscale flow modeling in packed beds, however, the contribution of the Reynolds stress term to the fluid momentum equation is not important (Jiang et al., 2000) because when averaging a number of local (random) signals within a representative elementary volume (e.g., a cubic section containing a cluster of particles), the microscopic turbulence is smoothed out. In fact, the interfacial momentum exchange terms play a significant role in multiphase flow simulations. The capillary pressure caused by the gradient of phase holdup and particle partial wetting can generate pressure differences between the gas and the liquid phase. Such pressure difference can affect the fluid flow distribution significantly, as confirmed by experimental observations of liquid distribution (Ravindra et al., 1997; Jiang et al., 1999) and flow simulation by the extended discrete cell model (DCM) (Jiang et al., 1999).

In this paper, we focus on modeling the macroscale flow distribution in trickle beds by implementing the statistical porosity structure and by modeling the complex multiphase interacting forces in the flow equations. By analyzing a series of bed

structures and flow simulation results, we develop the preliminary statistical correlations for the structure-flow relationship.

2. Statistical Nature of Bed Structure and Flow

2.1 Bed Structure

The porosity and its distribution in a packed bed are the key parameters in determining the flow distribution. The effective implementation of porosity distribution in the flow simulation model is the critical point, which affects the capability and applicability of the developed flow model. To achieve a quantitative understanding of the porosity distribution in packed beds, numerous research efforts have been made during the past several decades. For instance, measurements of the longitudinally averaged radial porosity profiles (Benenati and Brosilow, 1962), correlations of radial porosity distribution (Mueller, 1991; Bey and Eigenberger, 1997) and sphere-packing computer simulation of 3-D porosity structure (Jodrey and Tory, 1981), etc. have been reported. It was found that the mean porosity and porosity distribution are determined largely by particle size, shape, and particle surface properties (i.e. roughness and hardness) as well as the method of packing the bed.

The recent advances in computer tomography (CT) and magnetic resonance imaging (MRI) techniques can provide the 3-D structure in packed beds in a non-invasive way (Reinecke et al., 1998; Baldwin et al., 1996). Depending on the spatial resolution of the techniques used, different types of porosity distributions were found. For instance, the porosity data obtained from γ-ray CT scans of a cylindrical column packed with 3-mm monosize spheres has definitely exhibited a Gaussian distribution of the pixel porosity values at a pixel size (i.e., spatial resolution) of 4 mm (Chen et al., 2000). However, it has been found by MRI that there are two peaks in the distribution of voxel porosity values of the bed with 3mm particles if the voxel size is reduced to 180 μm (Sederman, 2000): one with low value due to voxels filled with solid and one high value due to voxels filled with pore space. This implies that the type of porosity distribution depends on the size of voxel (or pixel size) chosen in the measurements. In general, the porosity distribution is certainly Gaussian if the voxel size is larger than the particle diameter. In this study we focus on the modeling of macroscale flow texture, which is on the scale of a cluster of particles.

2.2 Multiscale Flow and Multi-Force Actions

Due to the mixed definitions encountered in the literature, it is necessary to clearly define each spatial scale referred to in this paper.

- *Microscale level*: the scale of interstitial space (< particle diameter), also called 'local scale' or 'particle scale'
- *Mesoscale level*: The scale of a cluster of particles, also called 'section scale'
- *Macroscale level*: the scale of an elementary volume large enough to be representative of the bed (Crine et al., 1992), also called 'large scale' or 'bed scale'

The experimental observations in packed beds have also shown that the fluid flow distribution is multiscale in nature, and flow distribution/maldistribution can be observed from the macroscale to the microscale (Hoek et al., 1986; Melli et al., 1990; Wang et al.,

1998). From flow modeling point of view, it means that, to describe the different scales of flow textures, one needs to implement the governing flow equations with the different details of basic-forces (i.e., inertial, viscous, capillary, and gravitational force etc.). As we found earlier (Jiang et al., 2000), the contribution of the Reynolds stress term to the fluid momentum equations is not important for the 'macroscale' flow modeling, but it should be very important for the 'microscale' flow simulation (Nijemeisland et al., 1998). On the other hand, also depending on the scale of packing elements used in the packed beds, which essentially determine the scale of flow passages, the contributions of each basic-force on liquid flow distribution are of different magnitudes (Melli et al., 1990). In the beds packed with large packing elements (e.g., separation packing: 10 ~ 30 mm Pall rings and Rasching rings etc.) the liquid distribution patterns are not sensitive to the wetability of the packing surface (Bemer and Zuiderweg, 1978). For the trickle-bed packing: typically, 0.5 ~ 3 mm spherical or cylindrical particles, however, the influences of particle wetting on liquid distribution are significant (Levec et al., 1986; Lutran et al., 1991; Ravindra et al., 1997; Jiang et al., 1999). This implies that even for the same macroscale flow texture (e.g. macroscale flow distribution), the contribution of each basic-force is of different magnitude depending on the different characteristic radius of the flow passages.

2.3 Link of Macroscale and Cell-Scale Hydrodynamics

Because the multiscale spectrum of flow fluid textures exists in multiphase flow packed beds, two critical questions are raised accordingly: (i) *'what is the fundamental mechanism that links those different scales of flow textures in packed beds*?' (ii) *'Is it realistic to develop a universal flow model which can capture the whole spectrum of flow structures*?'

The experimental evidence (Melli et al., 1990) and relevant theoretical study (Melli et al., 1991) have shown that in a nearly 2-D network, the macroscale flow regimes can be described in terms of different combination of microscale flow regimes. That means that the microscale and meso-scale hydrodynamics in packed beds are the roots of global hydrodynamics. Theoretically, one can link the macroscale and micro- or meso-scale flow textures through certain rules. Crine et al (1992) introduced the concept of statistical hydrodynamics, in which all the local hydrodynamic quantities were considered as random variables, like the packing properties discussed in Section 2.1. Then the link of the bed scale, section scale and local scale hydrodynamics is the probability density function (pdf) of the random variables, through which the global hydrodynamic quantities can be determined at the bed scale.

In this paper we start from 'section scale' (i.e., meso-scale) flow and structure elements, and examine how the section scale flow hydrodynamics is affected by the section scale bed structure and relevant basic-forces. We then seek the link when bridge the bed scale (i.e., global) and section scale hydrodynamics in a statistical manner.

2.4 Statistical Quantities

Since the section scale flow and porosity are random in nature in packed beds, one can use certain statistical methodology to characterize such randomness of the system. The relevant quantities can be described by a probability density function (p.d.f.)

characterized by its moments such as mean (μ), variance (σ^2), skewness (γ_1) and kurtosis (γ_2). The definitions of these are readily available in the literature (Roussas, 1997). In this work, we will use the mean, μ

$$\mu = \sum_j x_j p(x_j) \tag{1}$$

where $p(x_j)$ is the probability density function of the random variable x_j of the system, and the variance, σ^2

$$\sigma^2 = \sum_j (x_j - \mu)^2 p(x_j) \tag{2}$$

can be used to characterize the spread around the mean. We examine the effect of skewness and kurtosis on the results also, since the two values of these would indicate the changes caused by a non-Gaussian probability density function.

3. Multiphase Flow Modeling in Trickle Beds

In this work the ensemble averaged k-fluid model in the computational fluid dynamics code, CFDLIB, developed by Los Alamos National Laboratory (Kashiwa et al., 1994), is used as a transient multiphase flow simulation tool, which has been adopted for trickle beds, and can handle gas and liquid two phase flow with stationary solid phase (Kumar 1995, Khadilkar, 1998; Jiang et al., 1999). Here we provide only the key aspects of the flow equations and the relevant closure formulations for the case of trickle-bed reactors.

Equation of continuity:

$$\frac{\partial \rho_k}{\partial t} + \nabla \cdot \rho_k u_k = 0 \tag{3}$$

Equation of momentum:

$$\frac{\partial \rho_k u_k}{\partial t} + \nabla \cdot \rho_k u_k u_k = F_{D(k-l)} + \rho_k g + \theta_k \nabla p - \nabla \cdot < \alpha_k \rho_0 u_k' u_k' > \tag{4}$$

The momentum exchange term, $F_{D(k-l)}$ is expressed as a product of the exchange coefficient, X_{kl}, phase volume fractions, and relative velocity of the two phases k and l as shown below

$$F_{D(k-l)} = \theta_k \theta_l X_{kl} (u_k - u_l) \tag{5}$$

X_{kl} is calculated by the modified two-phase flow Ergun equation (Holub et al., 1992) in which constant Ergun parameters are used (E_1=180, E_2=1.8). The discussion regarding choosing constant Ergun parameters is given elsewhere (Jiang et al., 2000a). Therefore, the exchange coefficient between the liquid and solid phase (X_{ls}) and the gas and solid phase (X_{gs}) can be written as

$$X_{ks} = \left(A_{ks} \mu_k V_k + B_{ks} \rho_k V_k^2\right) \frac{1}{(1-\varepsilon)|u_k|} \tag{6a}$$

$$A_{ks} = 180 \frac{(1-\varepsilon)^2}{\theta_k^3 d_p^2} \tag{6b}$$

$$B_{ks} = 1.8\frac{(1-\varepsilon)}{\theta_k^3 d_p} \tag{6c}$$

For gas-liquid drag, either no interaction is assumed for the low interaction regime or the drag coefficient derived from two-fluid interaction model (Attou et al., 1999) is used:

$$X_{gl} = \frac{\theta_g}{\varepsilon}\left(A_{gl}\mu_g V_r + B_{gl}\rho_k V_r^2\right)\frac{1}{(1-\varepsilon)\left|u_g - u_l\right|} \tag{7a}$$

$$A_{gl} = 180\frac{(1-\theta_g)^2}{\theta_g^3 d_p^2}\left(\frac{1-\varepsilon}{1-\theta_g}\right)^{2/3} \tag{7b}$$

$$B_{gl} = 1.8\frac{(1-\theta_g)}{\theta_g^3 d_p}\left(\frac{1-\varepsilon}{1-\theta_g}\right)^{1/3} \tag{7c}$$

$$V_r = \theta_g\left|u_g - u_l\right| \tag{7d}$$

The influence of phasic pressure differences due to the interfacial tension and the gradient of liquid volume fraction, which reflects the contribution of the capillary force on the liquid flow distribution, is also taken into account in pressure calculations by Equation (8). This equation was proposed by Grosser et al., (1988) and modified by Jiang et al. (1999) by introducing the particle external wetting factor, *f*, which can be evaluated by the correlation for particle external wetting efficiency (Al-Dahhan and Dudukovic, 1995).

$$p_L = p_G - (1-f)\frac{(1-\varepsilon)E_1^{0.5}}{\varepsilon d_p}\sigma_s\left[0.48 + 0.036\ln\left(\frac{\varepsilon-\theta_L}{\theta_L}\right)\right] \tag{8}$$

The Reynolds stress term ($\nabla\cdot\langle\alpha_k\rho_0 u'_k u'_k\rangle$) is negligible for the case discussed in this paper.

4. Numerical Simulation Results and Discussions

As discussed in Sections 1 and 2, the observed flow textures in trickle beds result from a combination of interstitial structure (porosity distribution), interaction of between the fluids and particles and the interaction of between the gas and the liquid phase. In this study, we examine each individual contribution to two phase flow distribution by performing a series of numerical experiments. The following issues are addressed: (i) how does the capillary force affect the flow distribution? (ii) how is the flow distribution affected by porosity distribution? (iii) what is the influence of superficial velocities at the inlet?

4.1 Model Packed Beds

Recall that the type of porosity distribution in packed beds is scale-dependent. A pseudo-Gaussian distribution of porosity at a section scale (5-10 mm) can be considered as a reasonable assumption for section-scale flow simulation in trickle beds.

A 2D rectangular model bed of dimensions 50 cm × 10 cm was considered with pre-assigned porosity values to different sections (50 sections in the vertical (z) direction and 10 sections in the horizontal (x) direction as shown in Figure 1).

The generated pseudo-Gaussian porosity distributions have the same mean value ($\mu \sim 0.40$) but have different standard deviation (std), skewness (γ_1) and kurtosis (γ_2) as listed in Table 1. The gas and liquid flow were introduced at the top of the bed at certain superficial velocities. The fluid system used in the simulations is air and water, but any type of system such as hydrogen and hydrocarbons can be simulated by changing physical properties of the fluids. Atmospheric pressure is considered in this study but high-pressure can be handled by using different physical properties and high-pressure formulations for the drag coefficients.

4.2 Capillary Force Effect

To examine the effect of capillary force on the two phase flow distribution in a packed bed, a series of CFDLIB simulations have been performed by incorporating a particle wetting factor (f) in the k-fluid pressure calculation (see Eq.8). Two limiting wetting conditions are defined, namely, 'complete prewetting' and 'complete non-prewetting'. The actual situation of particle wetting in trickle beds is somewhere between these two limits. The 'complete prewetting' means that there is always a liquid film covering all the particle surfaces, this results in the negligible effect of capillary force on liquid flow. Correspondingly, capillary pressure is not accounted for in flow computation by assigning a value of unity for f. Strictly speaking, this does not happen in practice, even if one pre-wets the bed at high gas and liquid flow rates before starting to operate the trickle bed. One often drains the liquid from the bed after terminating the liquid and gas flow (Levec et al., 1988). On draining, the liquid films over the particles, connecting the pendular rings, might rupture, leaving isolated pendular rings at the contact points of the particles. It is argued by Ravindra et al (1997) that the bed with isolated pendular rings, especially with large diameter particles, could behave as a nonprewetted bed. On the other hand, 'completely non-prewetted' bed means there is no liquid film over the particles, then capillary force fully contributes to the liquid flow distribution. Accordingly, capillary pressure is fully incorporated into CFDLIB computation by assigning to f the value of zero. By changing the wetting factor (f) from 0.0 to 0.5 and 1.0, one can study the effect of capillary force on flow distribution in completely nonprewetted, partially prewetted and completely prewetted beds, respectively.

Figure 2 shows the simulated longitudinal profiles of porosity, liquid holdup and liquid saturation at different wetting factors (f = 0, 0.5 and 1.0). Here the section liquid saturation is defined as the ratio of the section liquid holdup and section porosity. In the completely nonprewetted bed (f = 0.0), the liquid saturation profile and porosity profile in the longitudinal direction (z) have similar trends. Lower liquid saturation occurs in lower porosity regions (see Fig 2a). This can be explained by higher capillary force occurring at smaller interstice when the particle surface is nonprewetted. Because the section liquid holdup is a product of the section porosity and section liquid saturation, the variation of liquid holdup is more pronounced than the variation of porosity. When the wetting factor, f, increases, the capillary force effect becomes less significant.

For the case of completely prewetted particles, liquid occupies the low porosity regions with higher liquid saturation. The liquid saturation profile and the porosity profile now have opposite trends as shown in Figure 2c. The variation of liquid holdup in the

longitudinal direction, then, becomes small. Similar results are obtained for the lateral profiles of liquid saturation at different wetting factors indicating that completely prewetted particles can diminish the effect of local porosity variation on liquid distribution and improve liquid holdup distribution.

Histograms showing the distribution of the gas and liquid velocity components are displayed in Figure 3. The distribution in horizontal velocity components V_x (L) and V_x (G) in a prewetted bed (upper row in Fig 3) and non-prewetted bed (lower row in Fig 3) are, as expected, symmetric about zero velocity, but higher standard deviations of V_x (L) and V_x (G) are found in the non-prewetted bed. The distribution for vertical velocity components, V_z (L) and V_z (G), are Gaussian in nature, and almost symmetric about the mean value. The observed zero velocities of the vertical velocity components V_z (L) and V_z (G) are due to the no-slip boundary condition used for left and right walls of the model beds. As the Z-axis points upward the axial downward velocities are negative. It is of interest to note that in the case of nonprewetted beds some positive axial velocity component V_z (G) exist, indicating counter-current gas flow is observed locally (see Fig 3-up-right). This may be explained by the high heterogeneity of liquid holdup which occurs in the nonprewetted bed due to capillary force. This implies that the effect of liquid maldistribution on gas flow distribution in trickle bed can be significant, especially in nonprewetted beds. The positive local gas velocity leading to local counter-current flow of gas and liquid may explain why in the high interaction regime the slit model of Holub et al (1992) needed to be modified by Al-Dahhan et al., (1998) to include a 'negative' slip between gas and liquid at the gas-liquid interface.

4.3 Porosity Distribution Effect

To examine the porosity distribution effect, the beds with the same mean porosity but with different standard deviations (std) of the porosity distribution (see Table 1) are used in the k-fluid model simulation at given operating conditions (U_l = 0.3 cm/s; U_g = 6.0 cm/s) and wetting conditions. Figures 4 and 5 show contours of solid volume fraction distribution in the model beds (II, III, IV) and the corresponding liquid volume fraction (i.e., *holdup*) distributions. It is clear that the effect of porosity distribution on liquid holdup distribution is significant in the case of non-prewetted beds ($f = 0$). The higher the std of the porosity distribution, the higher the std of liquid holdup distribution. Even for the case of partial particle external wetting this effect still exists, which often occurs in deep trickling flow regime. However, further simulations indicate that such porosity effect could be reduced if the packed-bed operates with completely prewetted particles.

4.4 Correlation Development

Based on the presented k-fluid model simulation results, it can be concluded that high heterogeneity of the porosity distribution and high capillary force result in high heterogeneity of liquid holdup and two phase flow velocities. To quantify this relationship of bed structure, particle wetting and resultant flow distribution, we correlate these distribution results in terms of statistical parameters (e.g., standard deviation). For example, we can develop a correlation between the standard deviation of the holdup distribution σ_l, external wetting efficiency, f, and the standard deviation of the bed porosity, σ_B, as given in Equations (9) ~ (10c). Figure 6 shows the comparison of the k-

fluid model computed value of the holdup standard deviation, σ_l, with the value calculated from the correlation below

$$\sigma_l = a_1(\sigma_B) f^2 + a_2(\sigma_B) f + a_3(\sigma_B) \quad (9)$$

$$a_1(\sigma_B) = -0.1696\sigma_B - 0.0002 \quad (10a)$$

$$a_2(\sigma_B) = -0.2593\sigma_B + 0.0012 \quad (10b)$$

$$a_1(\sigma_B) = 0.5002\sigma_B + 0.0019 \quad (10c)$$

With respect to its two limits of the prewetting states (i.e. f = 0.0 and f = 1.0), it is possible to establish Eqs (11a) and (11b) which correspond to the non-prewetted case and the prewetted case, respectively.

$$\sigma_l = 0.5002\sigma_B + 0.0019 \qquad (f = 0.0) \quad (11a)$$

$$\sigma_l = 0.0713\sigma_B + 0.0029 \qquad (f = 1.0) \quad (11b)$$

The ratio of the slopes of the two straight linear lines (Eqs 11a and 11b) is about 7.0 for the given operating condition as plotted in Figure 7. A higher degree of particle external wetting diminishes the effect of bed structure on two phase flow distribution.

The choice of fractional wetting (*f*-value) in the k-fluid model simulation is very important due to the major effect of fractional wetting on flow distribution. Since the fractional wetting (f) can be described as the percentage of particle external surface covered by continuous liquid film (*unbroken*) in whole packed beds, the particle external wetting efficiency developed in trickle-bed literature can be used as a good approximation of the fractional wetting. One may use the correlation of overall liquid holdup (e.g., Holub et al., 1992) to calculate the mean liquid holdup, and use the correlation for particle external wetting efficiency (e.g., Al-Dahhan et al., 1995) to evaluate *f*, then use Equation (9) to calculate σ_l, the standard deviation of the holdup distribution if σ_B, the standard deviation of porosity is available for given inflow condition, and eventually establish the Gaussian probability density function (p.d.f.) for liquid holdup distribution in trickle beds.

4.5 Superficial Velocities at the Inlet

The above simulation results are given for certain inlet conditions (U_l = 0.3 cm/s; U_g = 6.0 cm/s). Figure 8 shows the dependence of the global liquid holdup and particle external wetting efficiency on liquid superficial velocity at gas superficial velocity of 3 cm/s. Particle partial-wetting occurs at the liquid superficial mass velocity less than 6 kg/m^2/s where both porosity distribution and partial wetting contribute to the two phase flow distribution.

Figure 9 shows the CFDLIB simulated liquid holdup (*mean + std*) at different liquid superficial mass velocities. The holdup values calculated by Holub et al (1992) correlation are also plotted (filled square). Clearly, the global holdup correlation gives higher values than those from k-fluid model simulations particularly at high liquid flow rate. One of the reasons could be the use of the global correlation from 3D beds on the current 2D model bed which was simulated.

It is interesting to note that the higher values of liquid holdup standard deviation are obtained at low and high liquid superficial mass velocities, and a minimum holdup standard deviation exists at L of 6 $kg/m^2/s$ where a complete particle external wetting is just reached. Similar experimental observation was reported earlier (Jensen, 1977). In the partial particle external wetting regime, a decrease in liquid superficial velocity a lower in f, and further enhances the capillary force effect, and eventually results in more liquid nonuniformity (e.g. higher standard deviation of liquid holdup). In the fully wetted regime, however, the flow passage size decreases with increasing inlet liquid velocity and, it causes more significant gas-liquid interactions which result in nonuniformities.

5. Concluding Remarks

Because of the statistical nature of section-scale porosity distribution in packed-beds, the section-scale gas and liquid distributions in trickle-beds has been characterized by pseudo-Gaussian function in which the mean value is evaluated by the global correlation (e.g. Houlb et al., 1992), and the standard deviation (std) is estimated based on the std-correlation developed in this study provide that the std of porosity is known. Capillary pressure partially contributes to the liquid distribution if particles are partially wetted by liquid flow. The effect of porosity nonuniformity on liquid distribution is diminished if the particles are fully wetted. CFD is shown to be an efficient numerical tool for developing quantitative relationships among bed structure, particle wetting and operating conditions. Although the present numerical study was limited to a 2D rectangular bed, the extension to 3D cylindrical packed-column simulations is in progress. The extensive experimental validations of numerical results using CT and MRI techniques are proposed as future work to establish the final structure-flow correlation.

6. Nomenclature

d_p = particle diameter, m
E_1, E_2 = Ergun constants ($E_1 = 180$; $E_2 = 1.8$)
f = fractional wetting value
$f(x_j)$ = probability density function
F_D = Drag force
g = gravity, cm/s^2
P_0 = pressure, dyn/cm^2
u_0 = material velocity, (cm/s)
$|u_{kl}|$ = slip interstitial velocity between phase k and phase l, cm/s
$\bar{u}_k$ =material k interstitial velocity vector, cm/s
$\bar{u}'_k$ = fluctuating part of k interstitial velocity vector, cm/s
Vr = Superficial relative velocity based on gas flow, as defined in Eq (7d), cm/s
V_x, V_z = interstitial velocity components, cm/s
U_0 = input superficial velocity, cm/s
X_{kl} =momentum exchange coefficient between phase k & l
x_j = variable of system

Greek Letters

α_1, α_2, α_3 = parameters

α_k = material indicator (=1 if k is present; =0 otherwise)

$\dot{\alpha}_k$ = material derivative

ε_B = bed porosity

ε = section porosity

θ_k = material k volume fraction ($\theta_k = < \alpha_k >$)

τ_0 = deviatiric stress

ρ = density of fluid, kg/m^3 (gas: 1.2; liquid: 1000)

ρ_k = density of material k, g/cm^3 ($\equiv < \alpha_k \rho_0 >$)

μ = mean value

μ_α = viscosity of phase α

σ_s = surface tension

σ_B = standard deviation of porosity distribution

σ_l = standard deviation of liquid holdup

γ_1 = Skewness of statistical data

γ_2 = Kurtosis of statistical data

< > = ensemble averaged

References

Al-Dahhan, M. H. & Dudukovic, M. P. (1995). Catalyst wetting efficiency in trickle-bed reactors at high pressure. *Chem. Engng. Sci.*, 50, 2377-2389.

Al-Dahhan, M. H., Khadilkar, M.R., Wu, Y. & Dudukovic, M. P. (1998). Prediction of pressure drop and liquid holdup in high-pressure trickle-bed reactors. *Ind. Engng Chem. Res.*, 37, 793-798.

Attou, A., Boyer, C. & Ferschneider, G. (1999). Modeling of the hydrodynamics of the cocurrent gas-liquid trickle flow through a trickle-bed reactor. *Chem. Engng Sci.*, 54, 785-802.

Bemer G. G. & Zuiderweg, F. J. (1978). Radial liquid spread and maldistribution in packed columns under different wetting conditions. *Chem. Engng Sci.*, 33, 1637-1643.

Benenati, R. F. & Brosilow, C. B. (1962). Void fraction distribution in beds of spheres. *A. I. Ch. E. J.*, 8, 359.

Bey, O. & Eigenberger, G. (1997). Fluid flow through catalyst filled tubes. *Chem. Engng Sci.*, 52, 1365-1376.

Chen, J., Rodas, N., Al-Dahhan, M. H. & Dudukovic, M. P. (2000). Study of particle motion in packed/ebullated beds by CT and CARPT. accepted by *I&EC Res.*

Crine, M., Marchot, P. & L'Homme, G. (1992). Statistical hydrodynamics in trickle flow columns.
A.I.Ch.E. J., 38, 136-147.

Grosser, K. A., Carbonell, R. G. & Sundaresan, S. (1988) Onset of pulsing in two-phase cocurrent downflow through a packed bed. *A.I.Ch.E. J.*, 34, 1850.

Hoek, P. J., Wesselingh, J. A. & Zuiderweg, F. J. (1986). Small scale and large scale liquid maldistribution in packed columns. *Chem. Engng Res. Des.*, 64, 431-449.

Holub, R. A., Dudukovic, M. P. & Ramachandran, P.A. (1992). A phenomenological model for pressure-drop, liquid holdup, and flow regime transition in gas-liquid trickle flow. *Chem. Engng. Sci.*, 47, 2343-2348.

Holub, R. A., Dudukovic, M. P. & Ramachandran, P.A. (1993). Pressure drop, liquid holdup, and flow regime transition in gas-liquid trickle flow. *A.I.Ch.E. J.*, 39, 302-321.

Jensen, R. H. (1977). Optimum liquid mass flux for two phase flow through a fixed bed of catalyst. US4039430.

Jiang, Y., Khadilkar, M.R., Al-Dahhan & Dudukovic, M. P. (1999). Two phase flow distribution in 2D trickle bed reactors. *Chem. Engng Sci.*, 54, 2409-2419.

Jiang, Y., Khadilkar, M.R., Al-Dahhan & Dudukovic, M. P. (2000). Single phase flow modeling in packed beds: A discrete cell approach revisited. *Chem. Engng Sci.*, 55, 1829-1844.

Jodrey, W. S. & Tory, E. M. (1981) Computer simulation of isotropic, homogeneous, Dense random packing of equal spheres. *Power Technology*, 30, 111-118.

Jolls, K. R. & Hanratty, T. J. (1966). Transition to turbulence for flow through a dumped bed of spheres. *Chem. Engng Sci.*, 21, 1185-1190.

Kashiwa, B. A., Padial, N. T., Rauenzahn, R. M. & W. B. Vander Heyden. (1994). A cell centered ICE method for multiphase flow simulations. *ASME Symposium on Numerical Methods for Multiphase Flows*, Lake Tahoe, Nevada.

Khadilkar, M. R. (1998). Performance studies of trickle-bed reactors. Doctoral thesis, Washington University, St. Louis, Missouri, USA.

Kumar, S. (1995) Simulation of multiphase flow system using CFDLIB code. *CREL Annual Meeting Workshop*, St. Louis, MO., USA.

Latifi, M. A., Midoux, N. & Storck, A. (1989) The use of micro-electrodes in the study of the flow regimes in packed bed reactor with single phase liquid flow. *Chem. Engng Sci.*, 44, 2501-2508.

Levec, J., Saez, A. E. & Carbonell, R. G. (1986). The hydrodynamics of trickling flow in packed beds: Experimental observations. *A.I.Ch.E. J.*, 32, 369.

Logtenberg, S. A. & Dixon, A. G. (1998). Computational fluid dynamics studies of the fixed bed heat transfer. *Chem. Engng Process.*, 37, 7-21.

Lutran, P. G., Ng, K. M. & Delikat, E. P. (1991). Liquid distribution in trickle beds. An experimental study using computer-assisted tomography. *Ind. Eng. Chem. Res.*, 30, 1270.

Melli, T. R., Santos, J. M., Kolb, W. B. & Scriven, L. E. (1990). Cocurrent downflow in networks of passages: Microscale roots of macroscale flow regimes. *Ind. Engng. Chem. Res.*, 29, 2367-2379.

Melli, T. R. & Scriven, L. E. (1991) Theory of two-phase cocurrent downflow in networks of passages. *Ind. Eng. Chem. Res.*, 30, 951-969.

Mueller, G. E. (1991). Prediction of radial porosity distribution in randomly packed fixed beds of uniformly sized spheres in cylindrical containers. *Chem. Engng Sci.*, 46, 706.

Ravindra, P. V., Rao, D. P. & Rao M. S. (1997). Liquid flow texture in trickle-bed reactors: an experimental study. *Ind. Engng Chem. Res.*, 36, 5133.

Nijemeisland, M., Logtenberg, A. A. & Dixon, A. (1998). CFD studies of wall-region fluid flow and heat transfer in a fixed bed reactor. *AIChE Annual Meeting*, Paper 311f, Miami, FL.

Reinecke N., Petritsch, G. Schmitz, D. & Mewes, D. (1998) Tomographic measurement techniques: visualization of multiphase flows. *Chem. Engng Tech.*, 21, 7-18.

Roussas, G. G. (1997). *A Course in Mathematical Statistics*, 2nd Edition, Academic Press.

Saez, A. E. & Carbonell, R. G. (1985). Hydrodynamic parameters for gas-liquid cocurrent flow in packed beds. *A.I.Ch.E. J.*, 31, 52-62.

Sederman, A. J. (2000). PDF of voxel porosity distribution. *Personal Communication*, from University of Cambridge.

Sederman, A. J., Johns, M. L., Bramley, A. S., Alexander, P. & Gladden, L. F. (1997). Magnetic resonance imaging of liquid flow and pore structure within packed beds. *Chem. Engng Sci.*, 52, 2239-2250.

Song, M., Yin, F. H., Chuang, K. T. & Nadakumar, K. (1998). A stochastic model for the simulation of the natural flow in random packed columns. *The Canadian J. of Chem. Engng*, 76, 183-189.

Toye, D., Marchot, P., Crine, M. & L'Homme, G. (1997). Computer-assisted tomography for liquid imaging in trickle flow columns. In: J. Chaouki, F. Larachi and M. P. Dudukovic (Eds), *Non-invasive monitoring of multiphase flows* (p. 105) Amsterdam: Elsevier.

Wang, Y-F., Mao, Z-S. and Chen, J. (1998). Scale and variance of radial liquid maldistribution in trickle beds. *Chem. Engng Sci.*, 53, 1153-1162.

Volkov, S. A., Reznikov, V. I., Khalilov, K. F., Zel'vensky, Yu. V. & Sakodynsky, K. I. (1986) Nonuniformity of packed beds and its influence on longitudinal dispersion. *Chem. Engng Sci.*, 41, 389.

Table 1. Statistical quantities of porosity distribution

Beds	Mean (μ)	Std (σ)	Skewness (γ_1)	Kurtosis (γ_2)
I	0.399	0.0082	0.2736	0.1335
II	0.399	0.0118	-0.2093	0.6746
III	0.399	0.0217	0.0351	0.0203
IV	0.404	0.0439	-0.1128	-0.2972

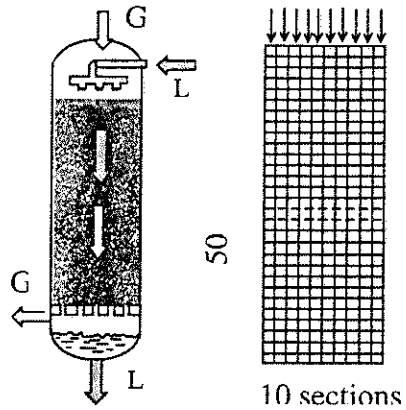

Figure 1 Trickle bed and model bed with 500 sections (d_p = 3 mm)

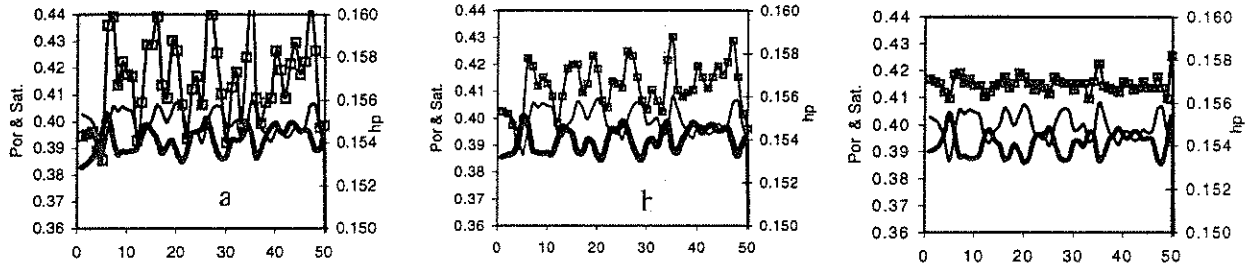

Figure 2. Transverse averaged profiles of porosity (hard line), liquid holdup (line with square) and liquid saturation (least line) vs. longitudinal position (z) at different wetting states (a) f = 0.0; (b) f = 0.5; (c) f = 1.0 at U_l = 0.3 cm/s, U_g = 6.0 cm/s

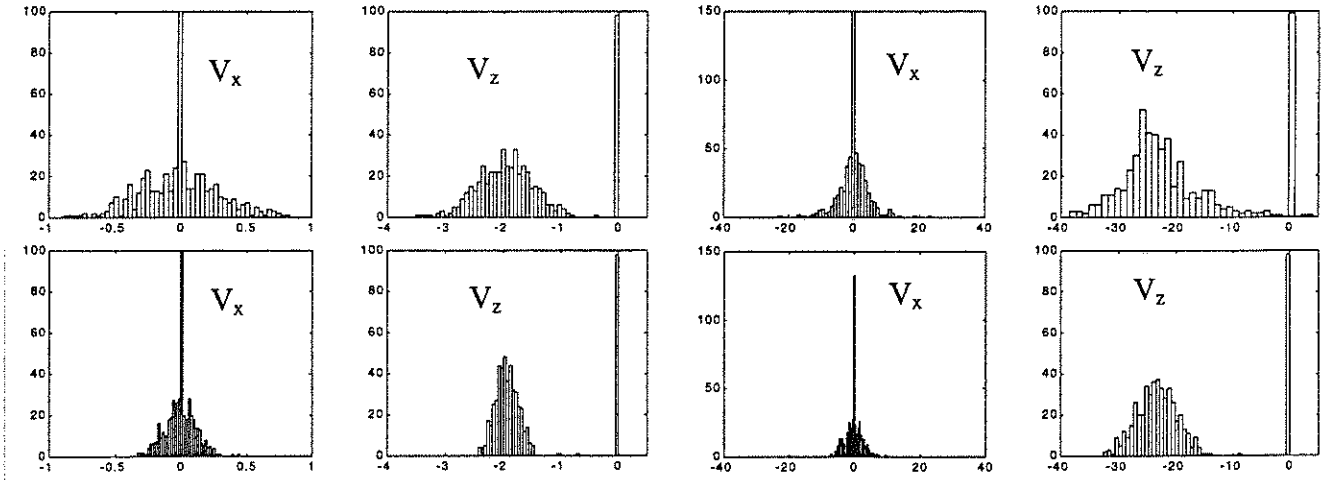

Figure 3. Distribution of gas and liquid interstitial velocity components in non-prewetted bed (f = 0) (up-row plots) and in prewetted bed (f = 1) (low-row plots) at U_{l0} = 0.3 cm/s, U_{g0} = 6.0 cm/s (G-gas, L-liquid) (unit in cm/s)

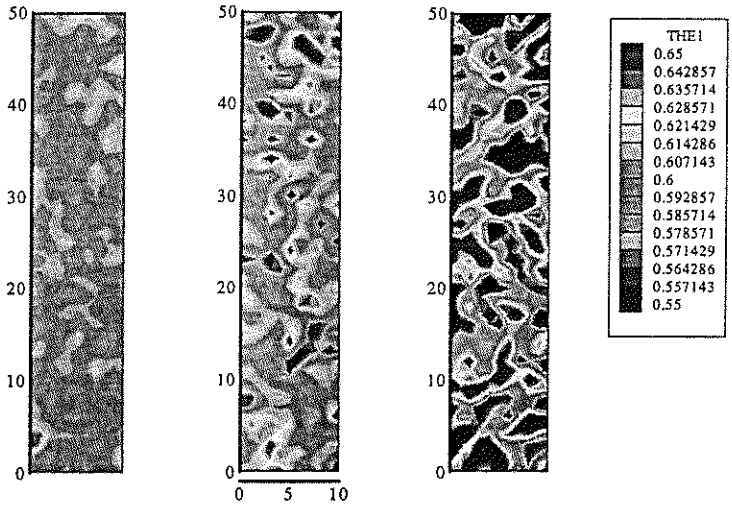

Figure 4 Contours of solid volume fraction (=1.0-porosity) distribution of model beds (II, III, IV) for k-fluid model simulations

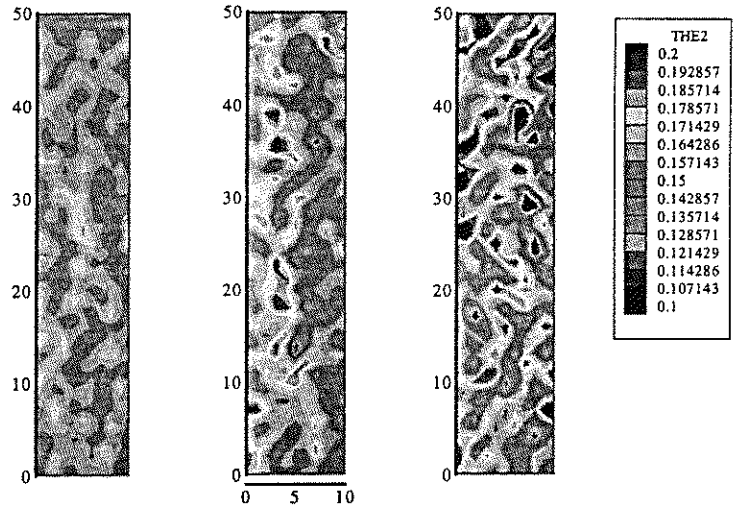

Figure 5 Contours of k-fluid model simulated liquid volume fraction (holdup) distribution in model beds (II, III, IV)

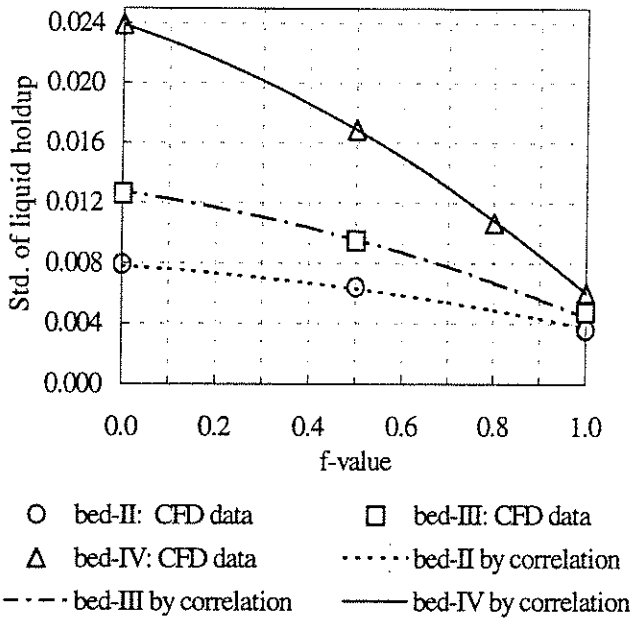

Figure 6. Standard deviation of liquid holdup distribution from k-fluid model simulations and from Eq (9) calculations vs. bed wetting factor (f) in model Bed-II, III, IV

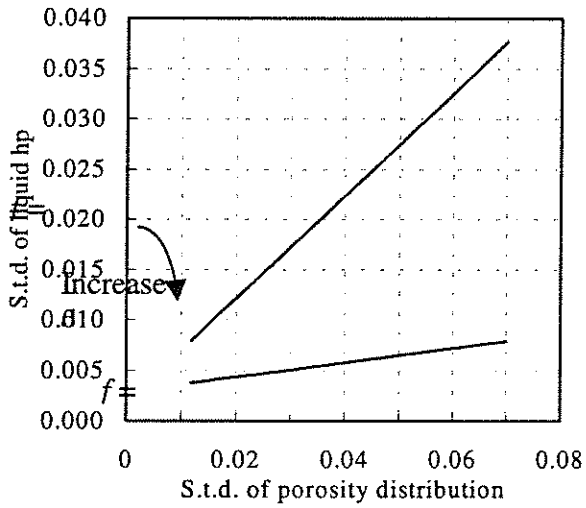

Figure 7 Standard deviation of liquid holdup distribution vs. standard deviation of bed porosity at two wetting limits at $U_{l0} = 0.3$ cm/s, and $U_{g0} = 6.0$ cm/s

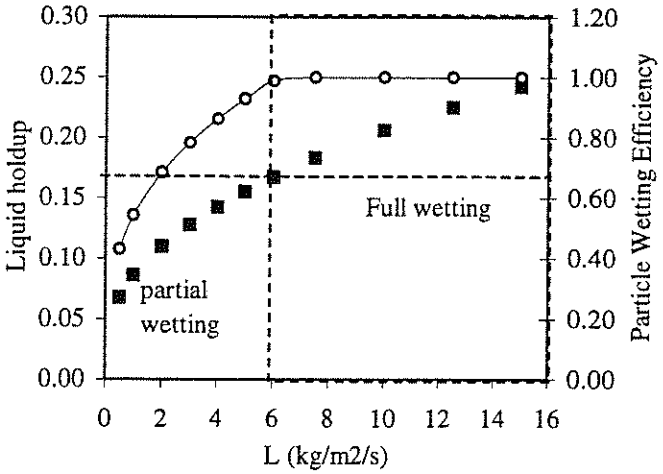

Figure 8. Liquid holdup (filled square) (Holub et al., 1992) and particle external wetting efficiency from correlation (empty circle) (Al-Dahhan & Dudukovic, 1995)

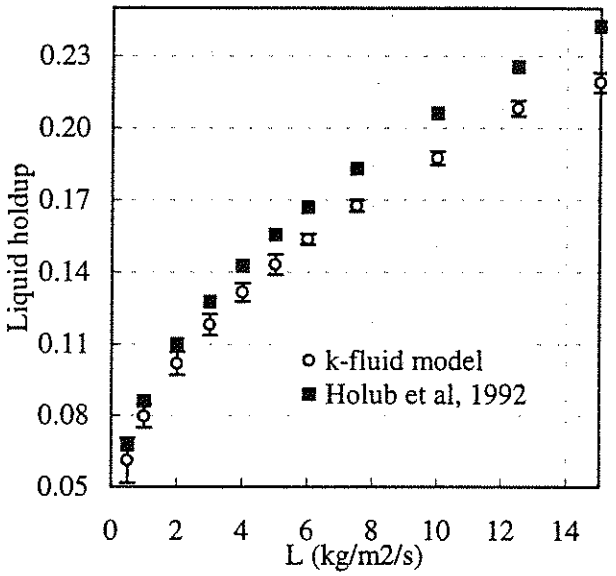

Figure 9. Liquid holdup values from k-fluid model (mean + std) and Holub's slit model (1992):
$\varepsilon_B = 0.399$; $d_p = 3$ mm; $U_g = 0.03$ m/s. Plus and minus bars are the standard deviation of 500 sectional liquid holdup.

A PARALLEL APPROACH TO CATALYST AND REACTOR SELECTION FOR A FINE CHEMICAL PROCESS

A. Problem Definition

Multiphase flow reactors of various configurations are used in numerous chemical processes. A systems approach for multiphase reactor selection in the petroleum and petrochemical industries has been developed by Krishna (1994). The general selection methodology for multiphase reactors as suggested by Krishna (1994) consists of the assessment of the most desirable volume-to-surface area of each phase, best contacting flow pattern of the phases and the most desirable multiphase flow regime for the process under consideration. This then leads to optimal reactor type selection. The discussion of the reactor selection in systems approach, however, is often based on the premise that the most appropriate catalyst form was first identified by a chemist who focused on developing better chemistry and surface properties of the catalyst. In other words, the conventional paradigm is that catalyst and reactor selection occur generally in a sequential manner. Recently, a new paradigm is evolving in the chemical engineering community, that of simultaneous development of catalyst and reactor selection and design (Villermaux, 1993; Krishna and Sie, 1994; Lerou and Ng; 1996; Dudukovic, 1999; Dudukovic et al., 1999). It is believed that the simultaneous consideration and evaluation of the optimal conditions for best yield, selectivity and volumetric productivity, both from the perspective of the catalyst as well as the reactor type selection and operation, is the most desirable approach for achieving optimal process economics. This is particularly necessary since the catalyst with the best yield and selectivity developed in exploratory work without consideration of reactor scale up is not always able to find a perfect playground in the process commercialization (Roy et al., 2000). To adopt a new approach of simultaneous catalyst and reactor development, it is required that the chemist and chemical engineer work in coordination and pursue a global optimum in terms of the efficiency and profitability of the whole process. The use of such a "parallel" approach in the petroleum and petrochemical industries is beneficial and clearly possible since the time for development of the processes is normally long and this approach can shorten it. For the fine chemicals industry it is urgent for project management to pursue such an approach, which should result in quicker process development. This should allow time plans of the business to be met and should make companies more competitive in the current climate of intensified economic pressure, primarily due to the globalization of the world economy (Lerou and Ng, 1996).

B. Research Objectives

The objective of this report is to explore the applicability of the aforementioned parallel approach of catalyst and reactor selection in the development of a fine chemical process. The system we have chosen to study is a three-phase catalytic partial oxidation reaction. The use of semi-batch stirred-tank slurry reactor is most popular for commercial practice in such processes but often leads to low productivity and inefficient operation as a whole because of the adverse back-mixing effect on selectivity (Khadilkar et al., 1998; Jiang et al., 1998) and because of the time-consuming catalyst separation associated with the batch slurry process.

Because the advantages of a packed bed over a semi-batch stirred-tank slurry reactor are numerous, we proposed to develop a packed bed process for such a typical three-phase catalytic system in which the parallel approach is to be implemented. The case study discussed in this report is based on an actual oxidation process in the fine chemicals industry but does not reveal the names of actual species and catalyst used due to constraints of proprietary nature.

C. Research Accomplishments

The research accomplishments are discussed in the attached manuscript accepted by *3rd International Symposium in Catalysis in Multiphase Reactors*, May 28-31, Naples, Italy (2000).

1. INTRODUCTION

Multiphase flow reactors of various configurations are used in numerous chemical processes. A systems approach for multiphase reactor selection in the petroleum and petrochemical industries has been advocated by Krishna (1994). The general selection methodology, as suggested by Krishna (1994), consists of the assessment of the most desirable volume-to-surface area of each phase, best contacting flow pattern of the phases and the most desirable flow regime for the process under consideration. This then leads to optimal reactor type selection. The relevant scale-up strategies were given in the review paper by Sie and Krishna (1998). The discussion of the reactor selection is often based on the premise that the most appropriate catalyst form was identified by a chemist who focused on developing better chemistry and surface properties of the catalyst. In other words, the conventional paradigm is that catalyst and reactor selection occur generally in a sequential manner. Recently, a new paradigm is evolving in the chemical engineering community, that of simultaneous development of catalyst and reactor selection and design (Villermaux, 1993; Krishna and Sie, 1994; Lerou and Ng; 1996; Dudukovic, 1999; Dudukovic et al., 1999). It is believed that the simultaneous consideration and evaluation of the optimal conditions for best yield, selectivity and volumetric productivity, both from the perspective of the catalyst as well as the reactor type selection and operation, is the most desirable approach for achieving optimal process economics. This is particularly necessary since the catalyst with the best yield and selectivity developed in exploratory work without consideration of reactor scale up is not always able to find a perfect playground in the process commercialization (Roy et al., 2000). To adopt a new approach of simultaneous catalyst and reactor development, it is required that the chemist and chemical engineer work in coordination and pursue a global optimum in terms of the efficiency and profitability of the whole process. The use of such a "parallel" approach in the petroleum and petrochemical industries is beneficial and clearly possible since the time for development of the processes is normally long and this approach can shorten it. It is believed that adoption of this approach in the fine chemicals industry would also result in quicker process development. This should allow the time plans of the business to be met and should make companies more competitive in the current climate of intensified economic pressure, primarily due to the globalization of the world economy (Lerou and Ng, 1996).

The objective of this paper is to explore the applicability of the aforementioned parallel approach to catalyst and reactor selection in the development of a process for fine chemicals production. The system we have chosen to study is a three-phase catalytic liquid phase oxidation reaction. The use of semi-batch stirred-tank slurry reactor is most popular for commercial practice in such processes but often leads to low productivity and inefficient operation as a whole because of the adverse back-mixing effect on conversion or selectivity (Khadilkar et al., 1998; Jiang et al., 1998) and most of all because of the time-consuming catalyst separation associated with the batch slurry process. For instance, frequently in a stirred-tank slurry reactor the reaction product is in the liquid phase solution from which it must be separated in crystallized form. Considerable amount of time is spent on filtering the catalyst, then on evaporating the solvent to crystallize the product. Moreover, if the temperature drops before the catalyst is filtered, the product crystallizes and sticks with the catalyst. All of these problems may be avoided by choosing instead a continuous flow packed-bed reactor operated at the desired temperature. The advantages of a packed bed over a semi-batch stirred-tank slurry reactor are numerous. A packed bed certainly provides a much higher catalyst to liquid volume ratio than the slurry reactor and thus suppresses the undesired homogeneous reactions, if such are present, and in addition leads to more cost effective and safer designs for high-pressure operation (Ramachandran and Chaudhari, 1983).

Packed beds provide versatility of operation as the different operating modes (e.g., cocurrent downflow, cocurrent upflow and counter-current flow) in gas-liquid packed beds can result in large differences of reactor performance because local hydrodynamics depends on the operating mode and flow regime (Wu et al., 1996). To achieve optimal reactor performance special care is required in choosing the proper operating mode and flow regime. In addition, particle-scale incomplete wetting is always a concern in trickle-bed reactor (TBR) operation although it is reasonably well predicted through empirical correlations for contacting efficiency (Al-Dahhan and Dudukovic, 1995). The effect of particle partial wetting on reactor performance can only be determined by first identifying the limiting reactant. It has been established that for liquid limiting reactions increased catalyst wetting improved conversion, while for the gas limiting ones exactly the converse is true (Khadilkar et al., 1996; Wu et al., 1996).

The potential problem in packed bed design with small catalyst particles is the high pressure-drop. A possible remedy is to use larger-sized particles. This, however, can result in low catalyst utilization due to larger inter-particle diffusion resistance. The catalyst particles, however, can be tailored to meet the demands of the reaction as aforementioned. For a fast reaction, for example, the catalyst needs not be uniformly distributed throughout the particle and it is often an advantage to place all active material in a thin shell close to the outer surface. The advantage of this is the ability to use larger-sized particles (2~3 mm) without internal diffusional problems.

In the design of packed beds, for given productivity and feed condition, one needs to determine the required reactor volume and dimensions. By varying the column diameter, the gas and liquid superficial velocities are changed accordingly, which can cause the column to operate in different flow regimes (e.g., trickling, pulsing flow etc.) with different magnitudes of the mass transfer rate. Bed-scale flow maldistribution may also be encountered when varying the H/D ratio and the superficial velocities, which further causes additional deviation of reactor performance from model prediction. The

development scenario we proposed for the considered liquid phase oxidation reaction includes three stages. The first stage focuses on determining a suitable catalyst form by considering the internal particle diffusion and kinetics; identifying the limiting reactant and choosing the proper operating mode as well as flow regime. The second stage requires solving a suitable reactor model for the chosen catalyst form and flow pattern and estimating the needed reactor size. The third stage is needed to experimentally test and verify the issues associated with the scale up of the process discovered in the second stage and develop more accurate reactor model for design. The case study discussed here is based on an actual oxidation process in the fine chemicals industry but does not reveal the names of the actual species and the catalyst used due to constraints of proprietary nature.

2. PRELIMINARY MODEL FOR CHOOSING THE CATALYST AND REACTOR OPERATING MODE

The oxidation reaction of interest $aA(g) + bB(l) \rightarrow P(l)$ is first order with respect to dissolved oxygen and is gas reactant limited at operating pressure of 0.79 MPa. Current production takes place in an aqueous solution in a slurry reactor. To evaluate TBR performance at the first stage of development, an *isothermal plug flow* model with partial external wetting of catalyst particles, and with no reactor scale maldistribution, is used. It considers reaction, gas-liquid-solid (G-L-S) mass transfer of species *A* on wetted catalyst surface and gas-solid (G-S) transport of species *A* to the dry catalyst surface (which is much faster compared to the G-L-S mass transfer). Internally porous uniformly impregnated catalyst particles are assumed completely wetted by liquid due to capillary force. The model is simplified so as to avoid solving the differential equations of species mass balances and energy balance by utilizing the mean oxygen gas phase concentration between the inlet and outlet and constant temperature. Hence, the average consumption rate of nonvolatile liquid reactant *B* per unit reactor volume is given by

$$\frac{Q_L C_{B0} X_B}{V_R} = \left(\frac{b}{a}\right)\frac{\overline{C}_{Ag}}{m_A}(1-\varepsilon_b)k_1\rho_{Pa}\times\left[\frac{\eta_{CE}}{\frac{1}{\eta}+\frac{(V_P/S_{ex})(k_1/\rho_P)}{k_{gls}}}+(1-\eta_{CE})\eta\right] \qquad (1)$$

where $k_1 = 3.0\times10^{10}\exp(-2.0\times10^4/RT)$ $(m^3/kg.cat/s)$ (2)

The reactor development calculations are based on a production rate of 2.27×10^7 kg/year at 100 °C and with $C_{B0} = 0.5$ kmol/m^3.

2.1 Internal particle diffusion and gas-liquid-solid mass transfer

For the given productivity and assigned column diameter D, one can solve Equation (1) by adjusting the reactor volume (V_R) using 'trial and error', to satisfy both sides of the Equation (1). As evident from the right hand side of Equation (1), three factors affect reactor performance: G-L-S overall mass transfer coefficient, k_{gls}, internal particle diffusion effects via the catalyst effectiveness factor, η, and the catalyst wetting efficiency, η_{CE}. The increase in k_{gls} and η improves the reaction rate. However, the effect of η_{CE} is not as obvious, it depends on the combination of factors. Such as what is the limiting reactant, what is the effectiveness factor and how do transport rates on wet and dry area compare. By varying the particle diameter (e.g., 1mm, 2mm and 3mm), it is found that the value of η is very small even for the smallest-sized particle (η = 0.128 for

d_p = 1mm). To eliminate or minimize the internal particle diffusion, an inert particle coated with the active catalyst component would improve the catalyst utilization. The typical way to do this is to deposit a thin layer of the active component onto the support particle. This layer is called a *washcoat* and is typically 20-100μm in thickness (Edvisson, et al., 1994). For an inert porous sphere of 2mm, the value η for the given reaction can reach 0.992 when the thickness of the washcoat layer is 20μm. It is evident that using inert coated particles can significantly improve catalyst utilization. One should note that these evaluations are based on the assumption that both the dry and wetted particle external surface can contribute to the reaction due to the inert *porous* particle used. The liquid inside the internal pores can get in contact with the gas phase directly through the dry surface region on the particle. If instead inert non-porous particles are used for coating with the catalyst, the dry surface region cannot contribute to the reaction at all because no liquid exists in that region. In this particular case, improved k_{gls} and η_{CE} will definitely improve the reaction rate because the second term (dry part) on the right hand side of Equation (1) disappears. Therefore, we have two options for catalyst forms to choose from. Option-I is to use porous coated particles (called *Packing-I*), and Option-II is to employ non-porous coated particles (called *Packing-II*). The optimal operating conditions for packing-I and II can then be determined for the given kinetics.

2.2 Packing-I and Packing-II

For packing-I, both wetted and dry particle surfaces can contribute to the reaction. Moreover, the contribution of the dry surface is pronounced due to lesser mass transfer resistance for the gaseous reactant. Hence, less external wetting in the trickling flow regime is preferred for high liquid conversion although the k_{gls} value on the wetted surface is low. The suggested operating mode for packing-I is a TBR with a low height to diameter H/D ratio (i.e. pan-cake reactor) operated deep in the trickling flow regime. For nonporous packing-II, however, the liquid can only externally wet the active catalyst film. Only the wetted surface sees the liquid reactant and can contribute to the reaction. Complete external wetting and pulsing flow regime with high k_{gls} value are preferred. That means a cigar-shaped TBR is a preferred option. Fig 1 shows the required reactor volume, V_R and the dimensions, height H and diameter D for different reactor H/D ratios to achieve the assigned production rate (2.27×10^7 kg/year). The required gas and liquid superficial mass flow velocities are given in Fig 2. Transport coefficients were evaluated from the appropriate correlations (see Ramachandran and Chaudhari, 1983) and the correlation of Al-Dahhan and Dudukovic (1995) was used for estimation of contacting efficiency. The contacting efficiency as a function of H/D is shown in Figure 3. The calculation has all performed assuming gas feed 20% in excess of stoicheometric requirements. A complete conversion of liquid reactant species B (X_B = 1.0) has been assumed in these calculations. Apparently, the smallest required reactor volume for the given production rate occurs at the lowest H/D ratio (e.g. pan-cake TBR) for packing-I, and at the highest H/D ratio (cigar shape TBR) for both packing-I and packing-II. However, a high pressure-drop occurs at very high H/D ratio due to the high superficial velocity (e.g., H/D = 46.5; ΔP > 6.0 atm). In any event using the above analysis one can identify the preferred flow modes for the new catalyst forms (packing-I and packing-II) to achieve a distinct advantage of TBR over the current slurry reactor. The utilization of the active catalyst component can be improved by 400 ~500 % by coating the active

component on inert particles in comparison with the regular uniformly impregnated catalyst particles.

Because of the exothermic nature of the oxidation reaction, the released heat of reaction can be estimated by a simplified energy balance equation to ensure the stability of the developed packed beds. Table 1 gives the maximum adiabatic temperature rise as well as an optimistic estimation of the effect of volatilization of the inert solvent. The estimated adiabatic temperature rise of 73.3 C in absence of solvent volatilization is high by industry standards. However, the solvent in this application is truly inert and inflammable and increased temperature has no adverse effect on the process as selectivity issues do not arise. Clearly 10% and 18% solvent volatilization can reduce significantly the temperature rise, but may not be achievable with a high boiling point solvent. The estimates given in Table 1 show promise of heat removal by solvent volatilization based on the simple energy balance. The operating pressure, feed temperature and reaction rate are the key parameters that may affect the volatilization rates of inert solvent, which further affect the profiles of temperature and reaction rate by heat removal. Significant heat removal can be expected by the use of more volatile inert solvent instead of the current solvent, which boils at high temperature. In fact, one should note that these arguments are based on the very simple energy balance without accounting for the heat dispersion and the concentration reduction of gaseous reactant due to the temperature rise. To judge these arguments in a more quantitative sense, a more detailed reactor model that considers solvent volatilization and axial dispersion effects of mass and heat is needed.

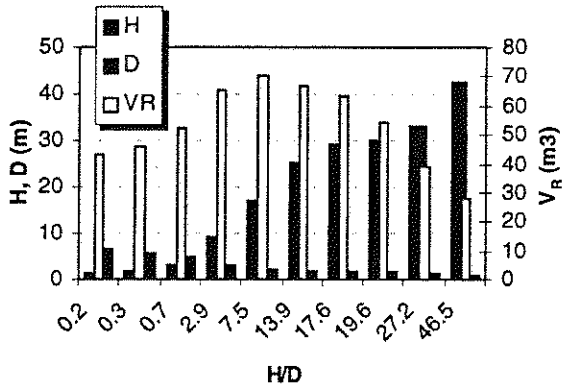

Fig 1. Required reactor volume as a function of reactor H/D ratio (all H/D range for packing-I; H/D >= 17.6 for packing-II) $X_B = 1.0$

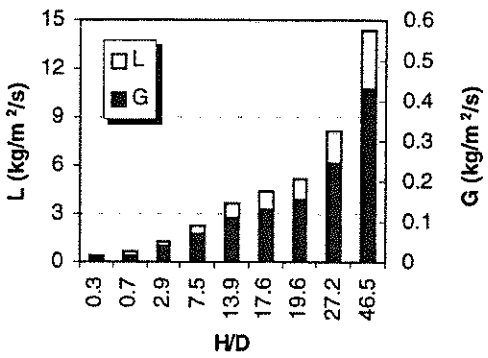

Fig 2. Superficial velocity as a function of reactor H/D ratio (all H/D range for packing-I; H/D >= 17.6 for packing-II) $X_B = 1.0$

Table 1. Estimation of maximum adiabatic temperature rise in TBRs

Flow regimes	Trickling flow (Packing-I)	Pulsing flow (Packing-II)
Reactor size (m):	H=8.93m; D = 3.48m 0.79	H=33.21m; D = 1.22m 0.79
Pressure (MPa) G/L	0.0389/1.290	0.243/8.063
Heat generated	3.138×10^5 kJ/m^3	3.138×10^5 kJ/m^3
$(\Delta T)_{Ad\text{-}NSV}$, °C	73.3	73.3
$(\Delta T)_{Ad\text{-}SV}$, °C	37.0 (10%wt volatilization) 3.1 (18%wt volatilization)	37.0 (10%wt volatilization) 3.1 (18%wt volatilization)

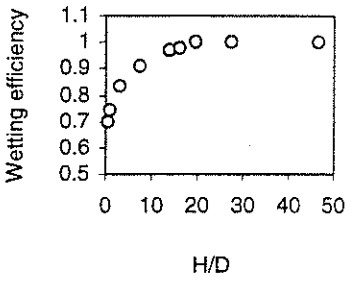

Fig. 3 Catalyst external wetting efficiency as a function of H/D ratio

* The formulas used in the estimation given below

$$(\Delta T)_{Ad-NSV} = \frac{(-\Delta H_r) C_{B,0} X_B}{\rho_l C_{P,l} (1 + G C_{P,g} / L / C_{P,l})} \quad \text{(Without volatilization)}$$

$$(\Delta T)_{Ad-SV} = \frac{(-\Delta H_r) C_{B,0} X_B}{\rho_l C_{P,l} (1 + G C_{P,g} / L / C_{P,l})} - \frac{(-\Delta H_V) F_V}{L C_{P,l} (1 + G C_{P,g} / L / C_{P,l})} \quad \text{(With volatilization)}$$

3. MORE DETAILED MODEL FOR PREDICTING TBR PERFORMANCE

For the two chosen TBR configurations shown in Fig 4, a transient pseudo-homogeneous model is written by accounting for mass and energy balances with accumulation, convection, and axial dispersion terms along with chemical reaction as well as the heat removal due to inert solvent volatilization. The contribution of particle partial wetting on reactor performance for porous packing-I in a pan-cake TBR is considered based on the correlation of Al-Dahhan and Dudukovic (1995). The heat release and the temperature rise cause partial solvent volatilization that lowers the temperature rise. As the first approximation, we neglect the variations of gas phase pressure, P and total 'gas' superficial velocity, U_g along the reactor. Final reactor design equations would have to consider these variations. Regarding solvent volatilization we assume that it is not mass transfer limited, but that the solvent is always distributed according to the local equilibrium requirements between the gas and liquid phase. This means that local temperature dictates the mole fraction of the solvent in the vapor phase. With these assumptions, the volatilization rate of inert solvent, F_V can be estimated by equation (8) in which F_v is a function of temperature T and gas superficial velocity U_g. The parameters used in reactor modeling are given in Table 2. The Danckwerts type boundary conditions are chosen for both mass and energy balance equations at reactor inlet and exit.

Mass balances:

$$\frac{\partial}{\partial t}(\varepsilon_g C_{Ag}) = D_{gA}\frac{\partial^2}{\partial z^2}(\varepsilon_g C_{Ag}) - \frac{\partial(U_g C_{Ag})}{\partial z} - (ka)_{gl}(C_{Ae} - C_{Al}) - \eta(1-\varepsilon_B)(1-\eta_{CE})\rho_{pa}k_0 C_{Ae}e^{-E_a/T_R} \quad (3)$$

$$\frac{\partial}{\partial t}(\varepsilon_l C_{Al}) = D_{lA}\frac{\partial^2}{\partial z^2}(\varepsilon_l C_{Al}) - \frac{\partial(U_l C_{Al})}{\partial z} + (ka)_{gl}(C_{Ae} - C_{Al}) - (ka)_{ls}(C_{Al} - C_{As}) \quad (4)$$

$$\frac{\partial}{\partial t}(\varepsilon_l C_{Bl}) = D_{lB}\frac{\partial^2}{\partial z^2}(\varepsilon_l C_{Bl}) - \frac{\partial(U_l C_{Bl})}{\partial z} - (ka)_{ls}(C_{Bl} - C_{Bs}) \quad (5)$$

Energy balances:

$$[\varepsilon_g C_{pg}\rho_g + \varepsilon_l C_{pl}\rho_l + (1-\varepsilon_b)C_{pb}\rho_P]\frac{\partial T}{\partial t} = \lambda_{ax}\frac{\partial^2 T}{\partial z^2} - [U_g\rho_g C_{pg} + U_l\rho_l C_{pl}]\frac{\partial T}{\partial z} + \frac{b}{a}\eta(1-\varepsilon_b)\rho_{pa}k_0[\eta_{CE}C_{As} + (1-\eta_{CE})C_{Ae}](-\Delta H_r)e^{-E_a/RT} - F_V\Delta H_v \quad (6)$$

Reaction:

$$(ka)_{ls}(C_{Al} - C_{As}) = \eta(1-\varepsilon_b)\eta_{CE}\rho_{pa}k_0 C_{As}e^{-E_a/RT} \quad (7a)$$

$$(ka)_{ls}(C_{Bl} - C_{Bs}) = \frac{b}{a}\eta(1-\varepsilon_b)\rho_{pa}k_0[\eta_{CE}C_{As} + (1-\eta_{CE})C_{Ae}]e^{-E_a/RT} \quad (7b)$$

Volatilization rate: $$F_V \approx U_g\frac{C_{g0}T_{in}}{P}\cdot\frac{d}{dz}\left(\frac{P_V}{T}\right) \quad (8)$$

Initial conditions: $$t=0:\ T=T_{in};\ C_{Ag} = C_{Al} = C_{Bl} = 0 \quad (9)$$

Boundary conditions:

Inlet $z=0$:

$$U_g C_{Ag,0} = U_g C_{Ag} - \varepsilon_g D_{gA}\frac{\partial C_{Ag}}{\partial z};\quad U_l C_{Al,0} = U_l C_{Al} - \varepsilon_l D_{lA}\frac{\partial C_{Al}}{\partial z}$$

$$U_l C_{Bl,0} = U_l C_{Bl} - \varepsilon_l D_{lB}\frac{\partial C_{Bl}}{\partial z};\quad \lambda_{ax}\frac{dT}{dz} = (U_g\rho_g C_{pg} + U_l\rho_l C_{pl})(T - T_{in}) \quad (10)$$

Outlet $z=H$: $$\frac{\partial C_{Ag}}{\partial z} = 0;\quad \frac{\partial C_{Al}}{\partial z} = 0;\quad \frac{\partial C_{Bl}}{\partial z} = 0;\quad \frac{\partial T}{\partial z} = 0 \quad (11)$$

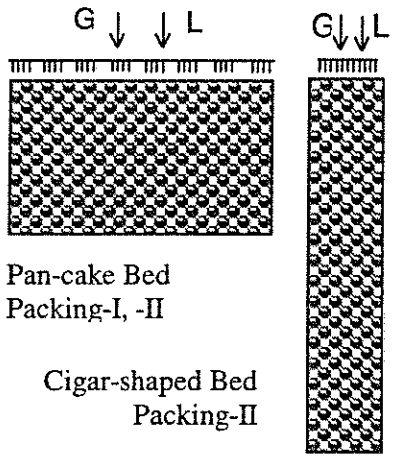

Pan-cake Bed
Packing-I, -II

Cigar-shaped Bed
Packing-II

Fig 4 Two chosen TBRs with different packing (not to scale)

Table 2 Parameters and operating conditions used

Pan-cake TBR	Cigar-shaped TBR
$U_l = 0.367\times10^{-3}$ m/s	$U_l = 8.063\times10^{-3}$ m/s
$U_g = 1.357\times10^{-3}$ m/s	$U_g = 29.79\times10^{-3}$ m/s
D = 5.72 m; H = 1.80 m	D = 1.22 m; H = 33.21 m
$\rho_l = 1000$ kg/m^3; $\rho_{cat} = 1250$ kg/m^3	
$\mu_l = 3.0\times10^{-3}$ Pa s; $\mu_g = 2.43\times10^{-5}$ Pa.s	
$\varepsilon_B = 0.37$; $d_p = 0.002$ m; $L_s = 20$ μm	
$D_A = 8.9\times10^{-9}$ m^2/s; $C_{B,0} = 0.5$ kmol/m^3	
$(-\Delta Hr) = 627.6\times10^3$ kJ/kmol	
$P_v = \exp(73.65-7258.2/T-7.304\ln T+4.1653\times10^{-6}T^2)$ Pa	
$H_v = 5.205\times10^4(1-T/647.13)^{[0.32-0.212T/647.13+0.258(T/647.13)^2]}$ kJ/kmol	
P = 0.50~2.0 MPa; T_{in} = 50~200 °C; C_{B0} = 0~1.5 kmol/m^3	

This set of partial differential equations (3-11) with respect to time (t) and space (z) was solved using the collocation algorithm implemented in subroutine PDECOL. Both dynamic and steady state results for the temperature and species concentration profiles are obtainable for various bed dimensions, operating pressure and feed

conditions. In this paper, the steady-state simulation results are presented for a cigar-shaped TBR and a pan-cake TBR (see Fig 4) at the conditions specified in Table 2.

Since the Peclet number for heat dispersion is very small for the short reactor, the calculated temperature profiles are rather flat along the pan-cake TBR (see Figs 5 and 7). Because of the gas-limited mass transport behavior of the process at relatively high temperature, the effects of operating pressure on the conversion and exit temperature are obvious. Increasing the gas pressure increases the conversion and causes a larger temperature rise in the reactor as displayed in Figs 5 and 6. Although solvent volatilization can remove some heat, as shown in Figure 7, it is not an efficient way to lower the temperature rise significantly because the boiling point of the solvent is relatively high. From Equation (8), one may expect to enhance the heat removal through solvent volatilization by increasing the feed temperature. However, at a given feed pressure, this also results in the decrease in gaseous concentration, which further reduces the conversion as shown in Figure 8. Hence, the pan-cake reactor exhibits the maximum conversion at a particular feed temperature for a given operating pressure. When the feed temperature is lower than 62 C, the conversion, X_B becomes sensitive to the feed temperature because the contribution of the kinetic resistance to the total reaction resistance becomes important. On the other hand, when the feed temperature is higher than 62 C, the contribution of the kinetic resistance compared to the total mass transport resistance is not significant (see Table 3). Obviously, an increase in feed temperature causes the increase in exit temperature. From the process point of view, certain optimal feed temperature exists.

Similar computational results are obtained for the cigar-shaped TBR except that the temperature profile along the cigar-shaped reactor is significant, in particular, at high pressure as shown in Figure 9. An increase of the feed temperature to 160 C can cool down the exit temperature by ~10 C by solvent volatilization compared to the no solvent volatilization case. It is not surprising to have a temperature rise of 70 C for a tall reactor of 33.2 m under adiabatic conditions. The operating pressure effect on conversion is significant due to the gas-limited reaction rate and is as displayed in Figure 10. Figures 11 and 12 again show how the feed temperature can affect the temperature rise and the exit temperature. It is apparent that the feed temperature around 100 C is most desirable for the cigar-shaped TBR for the conditions given in Table 3.

To assess the viability of the original plug flow assumption used in the preliminary evaluation, we compared the required reactor-lengths of cigar-shaped TBRs for achieving a complete conversion at a constant diameter by both simplified plug flow model of Equation (1) and the detail model (Eqs 3-11). The comparison at different feed temperatures is shown in Figure 13. As expected, the exit temperature increases with increasing feed temperature. The constant temperature equal to the feed temperature, however, is assumed in the plug flow model. Hence, the plug flow model yields an over-prediction of reactor-length at feed temperature less than 100 C and an under-prediction when the feed temperature is higher than 100C. This is because the overall conversion is sensitive to temperature in the low temperature range due to the importance of the kinetic term; however, it becomes more sensitive to the gaseous concentration in the high temperature range in which relative lower temperature benefits the reaction in the plug flow model.

During the simulation work, two other issues drew our attention:

- For the low H/D ratio reactor (e.g., pan-cake TBR) using the feed concentration and temperature at the reactor inlet as a boundary condition can lead to large errors in the computer results since the Peclet number is much smaller than that in the high H/D ratio reactor (e.g., cigar-shaped TBR). Danckwerts type boundary condition must be used for the pan-cake TBR wherein the axial heat dispersion is dominant.
- Since the pan-cake TBR has a large column diameter (e.g., 5.72 m in this case), the effect of flow maldistribution on performance may also be important. A more detail two-dimensional flow model is needed for obtaining accurate results in the pan-cake TBR. Moreover, the careful design of liquid and gas distributor for large diameter column becomes also essential for the success of pan-cake TBR scale up.

4. REQUIRED EXPERIMENTAL STUDY AND FINAL REMARKS

One should note that the present results and discussion rest on the numerical simulations. That means we have only accomplished the first stage and the second stage of the proposed process development scenario. The third stage consists of the experimental validation part that mainly focuses on the scale-up concerns from both catalyst and reactor perspectives of the process.

We can conclude that Packing-I can be operated in both trickling and pulsing regimes whereas packing II should only be used in pulsing regime. High conversion can be achieved at high operating pressure in both types of TBRs. The pan-cake TBR gives a more uniform temperature distribution than the cigar-shaped TBR. Both pan-cake and cigar-shaped reactors exhibit maximum conversion at a particular feed temperature. Solvent volatilization can help in reducing the temperature rise, but it is not effective with a high boiling point solvent. Experimental validation is necessary and a more accurate reactor model for the selection and optimization of the final configuration and design.

The critical scaleup issue associated with the pan-cake TBR is flow maldistribution whereas the high mechanical energy consumtion due to high pressure-drop in the cigar-shaped TBR is of concern in the third stage of process development.

NOTATION

a, b	stoichiometric coefficients of liquid and gas reactants (a =1.5; b = 1.0)
C_{A0}	concentrations of species *A* in gas feed, kmol/m^3
C_{Ag}	concentrations of species *A* in gas bulk phase, kmol/m^3
C_{Al}	concentrations of species *A* in liquid bulk phase, kmol/m^3
C_{As}	concentrations of species *A* at catalyst surface, kmol/m^3
C_{Asls}	concentrations of species *A* in stagnant liquid phase in the pores, kmol/m^3
C_{B0}	concentration of species *B* in liquid feed, kmol/m^3
C_{Bl}	concentration of species *B* in liquid bulk, kmol/m^3
C_{Bs}	concentration of species *B* at catalyst surface, kmol/m^3
C_{pg}	heat capacities of gas, kJ/kg.K
C_{pl}	heat capacities of liquid, kJ/kg.K
C_{pb}	heat capacities of catalyst particle,
D_{gA}	dispersion coefficient of *A* in gas phase, m^2/s
D_{lA}	dispersion coefficient of *A* in liquid phase, m^2/s
D_{lB}	dispersion coefficient of *B* in liquid phase, m^2/s

d_p particle diameter, m
D_r reactor diameter, m
E_a activation energy, kJ/mol
F_v vaporization rate of inert solvent, kmol/m^{3}reactor/s
G gas superficial mass velocity, kg/m^2/s
H length of reactor, m
k_0 exponential factor
k_{gls} gas-liquid-solid mass transfer coefficient, m/min,
$k_{gls} = \left[1/k_{ls} + \eta_{CE}(1-\varepsilon_b)/(ka)_{gl}/(V_P/S_{ex})\right]^{-1}$
$(ka)_{gl}$ volumetric gas liquid mass transfer coefficient, 1/s
k_{gsl} gas to stagnant liquid mass transfer coefficient, m/s
$(ka)_{ls}$ volumetric liquid to solid mass transfer coefficient, 1/s
k_r rate constant, cm^3/gcat/s
$(-\Delta H_r)$ heat of reaction, kJ/kmol
ΔH_V heat of solvent volatilization, kJ/kmol
L liquid superficial mass velocity, kg/m^2/s
Ls thickness of active coated layer, m
m_A Henry's constant of species *A* in liquid phase
Q_L liquid volumetric flow rate, m^3/min
S_{ex} external surface area of particle, m^2
t time, s
T temperature, K
T_{in} feed temperature, K or °C
U_g liquid and gas superficial velocities, m/s
U_l liquid superficial velocities, m/s
V_p volume of particle, m^3 ($V_p / S_{ex} = d_p/6$, for spheretic particle)
X_B, X_b conversion of species *B*
z axial position, m
ε_g gas holdup
ε_l liquid holdup
ε_b bed porosity
ρ_P particle density, kg cat./m^3 particle
ρ_{pa} density based on the active lay component, g cat./m^3 $\rho_{pa} = \rho_P\left(1-\left(Ls/d_p\right)^3\right)$
η effectiveness factor, $\eta = \frac{1}{\phi_P}\left(\frac{1}{\tanh 3\phi_P} - \frac{1}{3\phi_P}\right)$ and $\phi_P = \frac{V_P}{S_{ex}}\left(\frac{\rho_P k_1}{D_A}\right)^{0.5}$
η_{CE} particle wetting efficiency
λ_{ax} heat dispersion coefficient

REFERENCES

Al-Dahhan, M. H., Dudukovic, M.P., *Chem. Engng Sci.*, 50, 2377-2389 (1995)
Dudukovic, M. P., Larachi, F., and Mills, P. L., *Chem. Engng Sci.*, 55, 1975-1995 (1999)
Dudukovic, M. P., *Catalyst Today*, 48, 5-15 (1999)
Edvisson, R.K. and Cybulski, A, *Chem. Engng Sci.*, 49, 5653-5666 (1994)

Jiang, Y., Khadilkar, M. R., Al-Dahhan, M. H., Dudukovic, M. P., Chou, S. K., Ahmed, G. and Hahney, R. I., *A.I.Ch.E J.*, 44, 921-926 (1998)
Khadilkar, M. R., Wu, Y., Al-Dahhan, M. H., Dudukovic, M. P. and Colakyan, M., *Chem. Engng Sci.*, 51, 2721 (1996)
Khadilkar, M. R., Jiang, Y., Al-Dahhan, M. H., Dudukovic, M. P., Chou, S. K., Ahmed, G. and Hahney, R. I., *A.I.Ch.E. J.*, 44, 912-920 (1998)
Krishna, R., *Advanced in Chem. Engng.*, 19, 200-249 (1994)
Krishna, R. and Sie, S. T., *Chem. Engng Sci.*, 49, 4029 (1994)
Lerou, J. J. and Ng, K. A., *Chem. Engng Sci.*, 51, 1595-1614 (1996)
Ramachandran, P. A. and Chaudhari, R.V., *Three Phase Catalytic Reactors*, Gorden Breach (1983)
Roy, S., Mills, P. L. and Dudukovic, M. P., accepted for publication by *Catalysis Today* (2000)
Sie, S. T. and Krishna, R., *Reviews in Chem. Engng*, 14, 203-252 (1998)
Villermaux, J., *Chem. Engng Sci.*, (1993)
Wu, Y., Khadilkar, M. R., Al-Dahhan, M. H., Dudukovic, M. P., *I &EC Res*, 35, 397 (1996)

Table 3. Mass Transfer Resistances (unit: hr)

T_{in}, C	$\frac{1}{ka_{gl}a_P\eta_{CE}}$	$\frac{1}{ka_{gs}a_P(1-\eta_{CE})}$	$\frac{1}{k_1\rho_{Pa}(1-\varepsilon_B)}$	$\frac{1}{k_1\rho_{Pa}(1-\varepsilon_B)} / \frac{1}{ka_{gl}a_P\eta_{CE}}$
60	0.1125	2.49×10^{-5}	0.0323	0.29
100	0.1062	2.14×10^{-5}	0.0013	0.012

P = 0.79 MPa, C_{B0} = 0.525 kmol/m3 at pan-cake TBR

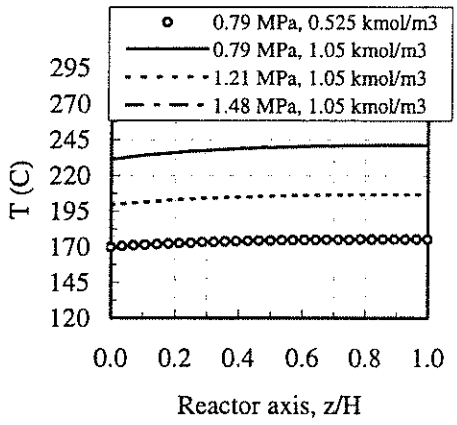

Fig 5. Operating pressure effect on temperature profiles along the pan-cake TBR:
T_{in} = 100 C. H = 1.8 m, H/D = 0.31.

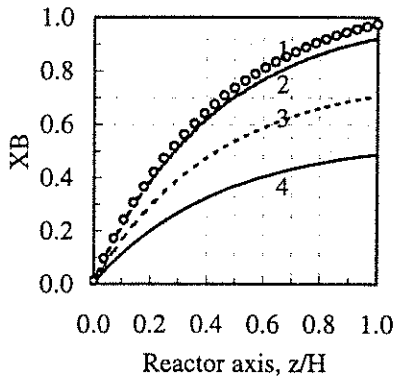

Fig 6. Operating pressure effect on conversion profiles along the pan-cake TBR:
T_{in} = 100 C. H = 1.8 m, H/D = 0.31.
1-0.79 MPa, 0.525 kmol/m^3; 2-1.48 MPa, 1.05 kmol/m^3; -3-1.21 MPa, 1.05 kmol/m^3;
4-0.79 MPa, 1.05 kmol/m^3.

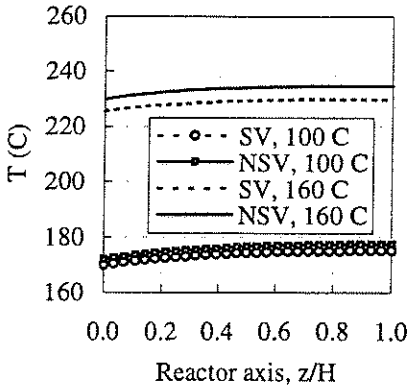

Fig 7. Temperature profiles with and without solvent volatilization in pan-cake TBR: Dash line-with solvent volatilization, line-without solvent volatilization, C_{B0} = 0.525 kmol/m^3, X_B = 1.0, H = 1.8 m, H/D = 0.31.

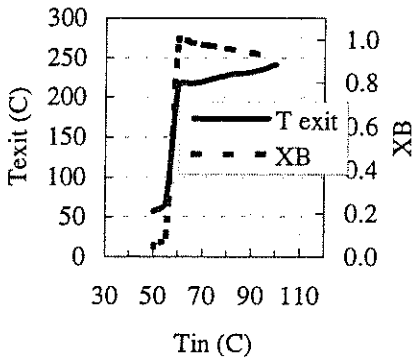

Fig 8. Effect of feed temperature on exit temperature and conversion in pan-cake TBE: H = 1.8 m, H/D = 0.31, C_{B0} = 1.05 kmol/m^3, P = 1.48 MPa.

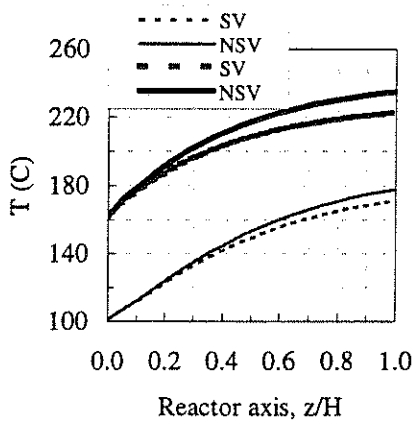

Fig 9. Temperature profiles with and without solvent volatilization in the cigar-shaped TBR:
Thick lines: Tin = 100 C, P = 0.79 MPa;
Thin lines: Tin = 160 C, P = 0.83 MPa.
C_{B0} = 0.525 kmol/m^3, X_B = 1.0, H/D = 27.2.

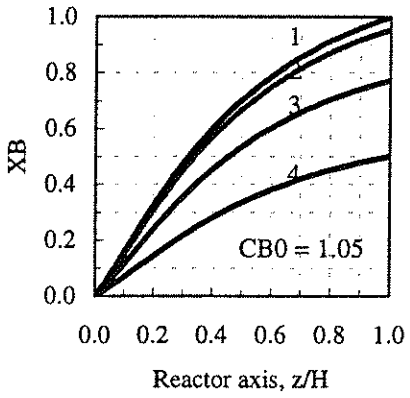

Fig 10. Operating pressure effect on conversion profiles along the cigar-shaped TBR:
T_{in} = 100 C. H/D = 27.2
(1-1.52 MPa, 2-1.48 MPa, 3-1.21 MPa, 4-0.79 MPa)

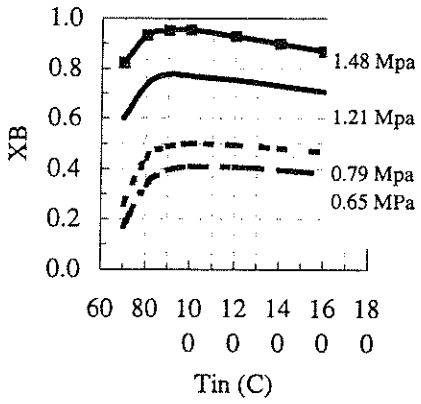

Fig 11. Conversion and exit temperature at different operating pressures in cigar-shaped TBR: C_{B0} = 1.05 kmol/m^3, H = 33.2 m, H/D = 27.2.

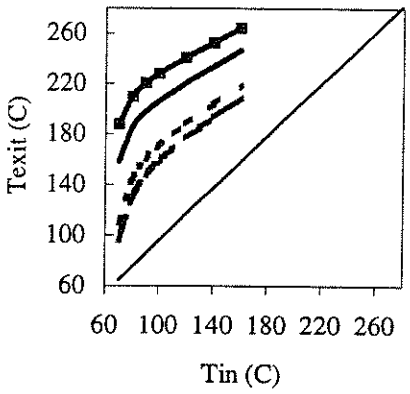

Fig 12. Feed temperature and exit temperature at different operating pressures in cigar-shaped TBR: C_{B0} = 1.05 kmol/m^3, H = 33.2 m, H/D = 27.2.

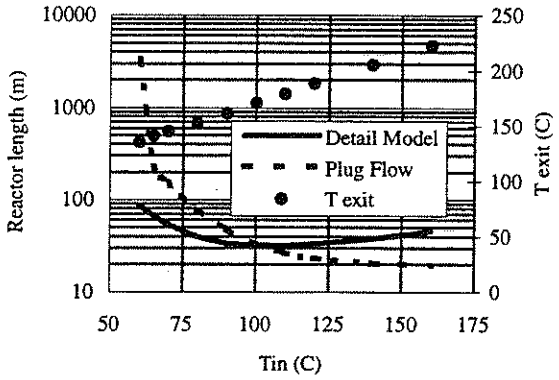

Fig 13. Comparison of the calculated required reactor length of cigar-shaped reactors from plug flow model and the detail model for complete conversion: D = 1.22 m, C_{B0} = 0.525 kmol/m^3, P = 0.79 MPa, X_B = 1.0

DRAWBACKS OF THE DISSOLUTION METHOD FOR THE MEASUREMENT OF LIQUID-SOLID MASS TRANSFER COEFFICIENT IN TWO-PHASE FLOW PACKED BED REACTORS OPERATED AT LOW AND HIGH PRESSURES

See the attached report for:

A. Problem Definition
B. Research Objectives
C. Research Accomplishments

DRAWBACKS OF THE DISSOLUTION METHOD FOR THE MEASUREMENT OF LIQUID-SOLID MASS TRANSFER COEFFICIENT IN TWO-PHASE FLOW PACKED BED REACTORS OPERATED AT LOW AND HIGH PRESSURES

RESEARCH NOTE

*Wes HighFill, Boon Tee Ong, Muthanna Al-Dahhan**

Chemical Reaction Engineering Laboratory (CREL)
Chemical Engineering Department
Washington University
One Brookings Drive
St. Louis, MO 63130

* Corresponding Author Tel: (314) 935-7187
Fax: (314) 935-4832
E-mail: muthanna@wuche.che.wustl.edu

ABSTRACT

Dissolution method was used predominantly at atmospheric conditions to measure liquid-solid mass transfer coefficient in two-phase flow packed bed reactors. In an attempt to investigate the effect of reactor pressure and gas flow rate on the liquid-solid mass transfer coefficient in a trickle bed rector using the dissolution method, difficulties were encountered in implementing this method at low to high pressure operation. Noticeable loses in the dissolved material were observed due to flashing/stripping from the liquid phase to the atmosphere and the effluent gas stream. This leads to misinterpret the effect of reactor pressure and to improper conclusion. In this note, we intend to alert the researchers about such drawbacks, which would be encountered at atmospheric to low pressures and to provide suggestions to overcome such problems.

INTRODUCTION

Packed bed reactors are catalyst beds contacted by cocurrent downflow (trickle beds), cocurrent upflow (packed bubble beds) or countercurrent flow of gas and liquid. They are used widely in various processes in petroleum, petrochemical, chemical, biochemical and environmental industry. Packed bed reactors, particularly trickle beds; are usually operated at elevated pressure (up to about 30 MPa). Liquid-solid mass transfer coefficient is one of the important parameters for design, scale-up and performance characterization of these reactors.

A variety of methods have been used in numerous studies to measure liquid-solid mass transfer coefficients in two phase flow packed bed reactors (e.g. dissolution, electrochemical, chemical reaction, dynamic adsorption, ion exchange followed by instantaneous reaction) (1,2)

Dissolution and electrochemical methods predominantly are used to measure liquid-solid mass transfer coefficients. The dissolution method measures an average volumetric liquid-solid mass transfer coefficient ($k_{ls}a$) for an entire bed or for a section of a bed based on the liquid saturation limit of the dissolved material (i.e., integral measurement), while the electrochemical method measures the local liquid-solid mass transfer coefficient (k_{ls}) for a single particle in a bed (i.e., local measurement). In addition, the dissolution method has been used to measure liquid-solid wetting efficiency in two-phase flow packed beds (3).

Despite the operating condition of interest is high pressure all the previous investigations on the liquid-solid mass transfer coefficient were performed under atmospheric conditions (4). Few studies have been conducted to investigate and to predict the effect of reactor pressure on pressure drop, liquid holdup, wetting efficiency, gas-liquid interfacial area and flow regime transition in trickle bed and packed bubble bed reactors (5). Recently Highfill and Al-Dahhan (1999) (2) and Highfill (1998) (1) have studied the effect of high pressure on the liquid-solid mass transfer coefficient (k_{ls}) in a trickle bed reactor using electrochemical method. The cathode particle was placed in the center of the middle section of the bed. They found that k_{ls} increases with the increase in pressure and in gas flow rate. The effects of the reactor pressure and gas flow

rate were described based on the analysis of five limited cases presented by Al-Dahhan and Dudukovic (1994), 1995) (6,7) and Al-Dahhan et al. (1997) (5). Since, as mentioned earlier, the electrochemical method provides a local measurement of k_{ls}, it is of interest to examine the effects of reactor pressure and gas flow rate on the mass transfer measured in a section of the bed or in the entire bed using the dissolution method.

Therefore, in this study the dissolution method is utilized in an attempt to investigate the effect of reactor pressure and gas flow rate on the $k_{ls}a$ on a section of the bed and in the entire bed. Unfortunately, difficulties were encountered in implementing the dissolution method measurements in a trickle-bed reactor operated at low to high pressures, which can lead to misinterpret the effect of reactor pressure, and to improper conclusion. Since the current trend of research on the two-phase flow packed beds is at elevated pressure (the operating conditions of interest to that number of industrial applications), the purpose of this note is to alert the researchers about such drawbacks which would be as well encountered at atmospheric to low pressures and to provide suggestions to address such problems.

EXPERIMENTAL WORK

The dissolution method employs particles made from a solid material that is sparingly soluble in the liquid phase in order to prevent the change in the bed characteristics during the measurement. Different types of packing material have been used which are benzoic acid (8,9,10,11,12,13,14), benzoic acid mixed with a fluorescent dye (15), naphthalene (3,16) and β-naphthal (17). During the dissolution method one must be careful not to saturate the liquid exiting the column. To avoid this, previous investigators have either used short beds consisting of only active particles (dissolved particles), or they have used longer beds of inert particles with a short section of active particles packed within. In addition, the active particles can be dispersed along the bed within the inert particles in amount equivalent to a short section required to maintain the dissolved material under 60-75% of the liquid saturation limit (1).

Assuming plug flow and performing steady state mass balance, yield the following equation to evaluate $k_{ls}a$:

$$k_{ls}a = \frac{Q}{AZ}\ell n\left(\frac{C^L_{A,sat} - C^L_{A,in}}{C^L_{A,sat} - C^L_{A,out}}\right)$$

where Q is the volumetric liquid flow rate (m^3/s), A is the bed cross-sectional area (m^2), Z is the packed bed length (m), $C^L_{A,sat}$ is the saturation concentration of the dissolved material, $C^L_{A,in}$, is the concentration of the dissolved material in the inlet flow and $C^L_{A,out}$, is the concentration of the dissolved material in the outlet flow. Usually $C_{A,in}$ is equal to zero. Hence, by measuring Q and $C_{A,out}$, $k_{ls}a$ can be evaluated.

In this work, naphthalene as the packing material and a system of water-nitrogen were used to measure $k_{ls}a$. A stainless steel mold was designed and constructed to manufacture 0.32 cm x 0.32 cm (1/8 inch x 1/8 inch) cylindrical naphthalene particles using a heat press (1).

Figure 1 shows the high-pressure trickle bed reactor facility (2,6,7) which was used to measure $k_{ls}a$ by a dissolution method. The facility can be operated up to 7 MPa (1000 psi). It consists of the reactor and gas-liquid distributor, the liquid delivery system, the gas delivery system, the separator, the gas and liquid exit systems and the data acquisition system. The reactor used was of 2.2 cm diameter and 50 cm in height. The height of the bed packed with naphthalene cylindrical particles (0.32 cm x 0.32 cm) was ~ 3.2 cm (1.25 inches) that resulted in an outlet concentration of 25-75% of the saturation level for the range of liquid and gas flow rates used. This active bed was either placed in the middle height of the reactor or dispersed along the bed. For the former case, the bed below and above the naphthalene particles was packed with 0.32 cm x 0.32 cm (1/8 inch x 1/8 inch) cylindrical glass particles.

Samples from the reactor outlet stream were drawn from the separator via a 0.16 cm (1/16 inch) needle valve mounted on a 0.16 (1/16 inch) tubing as shown in Figure 1. U.V. spectrophotometer (Bausch & Lomb Spectronic 21 Model U.V.-D) was used to measure the concentration of naphthalene in water. For the range of light necessary for naphthalene

(ultraviolet region), quartz cuvettes were utilized. It was found that a wave length of 274 nm gives the maximum absorbency (1,3) and hence, it was used for the measurement of naphthalene concentration in water.

Table 1 shows the experimental conditions used to measure $k_{ls}a$ by dissolution of naphthalene particles which represent trickle flow regime (7,18,19).

RESULTS AND DISCUSSION

At all pressures, the measured $k_{ls}a$ values increases with the increase in liquid flow rate as shown in Figure 2 (a,b). All of the previous studies showed such a trend. At constant pressure and liquid flow rate, $k_{ls}a$ increases with gas flow rate for the pressures investigated. This trend of $k_{ls}a$ with gas velocity coincides with the findings reported in the literature (2,3,9,11,13,14,15,20,21,22). However, in this work, $k_{ls}a$ values obtained at 30 psig (0.31 MPa) are larger than those obtained at 500 psig (3.55 MPa) where the gas density is larger (see Figures 2 a and b). This is not consistent with the findings of Highfill and Al-Dahhan (1999) (1) where the $k_{ls}a$ measured by electrochemical method increases with the reactor pressure at constant liquid and gas flow rates and with the trend of the effect of reactor pressure on particle wetting efficiency, liquid holdup and pressure drop. In addition, Bliss (1976) (14) in experiments covered trickle and pulse flow regimes, found that $k_{ls}a$ measured by dissolution of benzoic acid particles increased with gas velocity and gas density using helium, nitrogen and argon gases.

It was found that the measured outlet naphthalene concentration decreases as the pressure increases at fixed flow rates of gas and liquid. Figure 3 shows that the measured molar flow of the naphthalene,$Q_L C_L$ exp. (mol/s), decreases with pressure. Such a decrease is larger at higher liquid flow rates where more naphthalene is dissolved. It is obvious from equation (1), that if $C^{L}_{A,out}$ decreases at constant liquid and gas flow rates, then the evaluated value of $k_{ls}a$ decreases.

It is believed and confirmed experimentally in the following section that the reason for the decrease in the naphthalene concentrations with pressure is that the naphthalene is being

flashed/stripped from the liquid phase during the sampling process. As shown in Figure 1, the samples were drawn from the high pressure gas-liquid separator (which is under the same pressure of the reactor) via a 1/16 inch needle valve which is opened to the atmospheric conditions (room environment). Therefore, the drop in the pressure across the sampling valve caused flashing, thereby inducing naphthalene to transfer from the liquid to the atmosphere. As the reactor pressure was increased, the pressure drop across the sampling valve was increased causing more flashing and hence more naphthalene transfers from the liquid to the atmosphere. Therefore, at higher reactor pressures, a lower liquid effluent concentration was found at constant liquid and gas flow rate, which yields a lower $k_{ls}a$ value according to eq (1). Since the molar flow rates of naphthalene in the saturated air $\left(Q_g C_g^*\right)$ and liquid $\left(Q_L C_L^*\right)$ at the operating conditions used are comparable and of the same order of magnitude as shown in Table 2 (23), there would be a possibility of the naphthalene to be stripped from the liquid phase inside the reactor, separator and from the collected samples to the atmosphere. Similar case would happen to the benzoic acid as shown in Table 2 where the estimated $Q_g C_g^*$ is of order of magnitude larger than the estimated $Q_L C_L^*$. To confirm experimentally the loss of the dissolved material to the atmosphere and/or to the gas effluent stream by flashing/stripping, the following test was performed.

Experimental confirmation for the loss of the dissolved material

The same facility described earlier (Figure 1) has been used to quantitatively characterize the loss of the dissolved naphthalene and benzoic acid by flashing/stripping. In this experimental test, no active particles (i.e. naphthalene or benzoic acid particles) were used. Instead, the reactor was packed only with 0.32 cm x 0.32 cm (1/8 inch × 1/8 inch) cylindrical glass beads. Solutions with known concentrations of the naphthalene and another one of benzoic acid were prepared and charged into the feed tanks. The set-up was operated using the same operating procedure for the measurement of liquid-solid mass transfer coefficient. The concentrations of naphthalene (when naphthalene solution was used) and benzoic acid (when benzoic acid solution was used) in the

feed tank were measured for each operating condition used. As mentioned earlier, the samples were analyzed using Bausch & Lomb U.V. Spectrophotometer at wavelengths of 274 nm for naphthalene and 268 nm for benzoic acid concentrations.

At steady state operating conditions (i.e. maintaining for a few minutes for constant system pressure, gas and liquid flow rates, liquid level in the separator), samples were drawn from the sampling valve connected to the separator (Figure 1) where the concentrations were measured by the U.V. Spectrophotometer. The differences between the measured concentrations of the exit of the reactor (withdrawn from the gas/liquid separator) and of the feed tank represent the loss occurred for the dissolved material by flashing/stripping in the reactor, separator and to the atmosphere via the sampling procedure. The reproducibility of the measurements has been evaluated and found to be within ± 3%.

Tables 3 and 4 summarize the experimental results obtained for the naphthalene and benzoic acid experiments, respectively. It is obvious that the outlet concentrations of the dissolved materials decreases as the reactor pressure increases. It is noteworthy that the percentage differences for benzoic acid concentrations are larger than those of naphthalene despite the percentage saturation of the benzoic acid solution is much lower than that of the naphthalene solution in the feed tank. This is due to the differences in solubility, vapor pressure and Henry's law constant as indicated in Table 2. Moreover, noticeable decrease in the concentrations was observed even at low pressures (30 psig) particularly for benzoic acid solution. This indicates that some losses of the dissolved benzoic acid to the effluent stream would occur even at atmospheric pressure and to room atmosphere where most of the previous studies were performed (as mentioned earlier) using benzoic acid particles to measure liquid-solid mass transfer coefficient at atmospheric pressure. In all these studies, no attempt was performed to *a priori* characterize whether there is a noticeable loss of the dissolved material to account for. Based on the results of this work, such evaluation should be performed for each operating condition used whether the operation is at elevated or atmospheric pressure.

CONCLUDING REMARKS

According to these findings, a careful consideration needs to be given to the problems discussed above in implementing the dissolution method for measuring liquid-solid mass transfer coefficient and catalyst wetting efficiency in two-phase flow packed beds under high and atmospheric pressures. One way to remedy such problems is by using high-pressure on-line analytical equipment to analyze the liquid effluent stream under similar reactor pressure. This is not straight-forward and high pressure analytical equipment is commonly not available. In addition, the gas effluent stream needs to be analyzed to close the mass balance and to check whether really naphthalene or benzoic acid is stripped in the reactor and gas-liquid separator to the gas stream. It is also found that the equipment and the method to analyze the gas phase for very low concentration of naphthalene and benzoic acid are not handy and/or straight forward (1).

In the absence of the above-mentioned analytical techniques, it is suggested that a priori calibration of the system at the operating conditions of interest should be performed to identify a correction factor for the loss of the dissolved material from the withdrawn samples. This can be done by performing the following steps:

1) fill the reactor with glass particles of the similar shape and dimensions as those of the active bed.
2) use feed solution of known concentrations of naphthalene or benzoic acid.
3) operate the system at the same operating conditions that need to be used for $k_{ls}a$ measurements (i.e similar pressure, gas and liquid flow rates and temperature).
4) withdraw samples and measure the naphthalene concentrations by following the same procedure used for $k_{ls}a$ measurements.
5) repeat 2 to 4 using a suitable range of naphthalene or benzoic acid concentrations that cover the range of concentrations obtained during the $k_{ls}a$ measurements.

6) develop a calibration curve and/or correction factors for the operating condition of interest that represent the measured concentrations versus the inlet feed concentrations. The differences between them represent the correction factors that need to be added to the measured naphthalene or benzoic acid concentrations during $k_{ls}a$ measurement in order to account for the loss of naphthalene or benzoic acid during the sampling procedure.

Moreover, it is recommended even at atmospheric conditions to conduct similar procedure to check if there is noticeable loss of the dissolved material by flashing/stripping that may occur.

References

1. HighFill, W. Liquid-Solid Mass Transfer Coefficient in High-Pressure Trickle-Bed Reactor. MS Thesis, Washington University in Saint Louis, Missouri, 1998.
2. Al-Dahhan, M.; HighFill. W. Liquid-Solid Mass Transfer Coefficient in High Pressure Trickle Bed Reactors. Submitted to *Intl. J. of Heat & Mass Transfer* 2000.
3. Lakota, A.; Levec, J. Solid-Liquid Mass Transfer in Packed Beds with Cocurrent Downward Two-Phase Flow. *AIChE J,* 36, 1444,1990.
4. Al-Dahhan, M.; HighFill, W.; Friedman, M. Assessment of the Effects of High-Pressure Operation on the Liquid-Solid Mass Transfer Coefficient in Trickle-Bed Reactors. *Ind. Eng. Chem. Res.* 36, 4421, 1997a.
5. Al-Dahhan, M.H.; Larachi, F.; Dudukovic, M.P.; Laurent, A. High Pressure Trickle-Bed Reactors: A Review. *Ind. Eng. Chem. Res.* 36, 3292, 1997.
6. Al-Dahhan, M.H.; Dudukovic, M.P. Pressure Drop and Liquid Holdup in High Pressure Trickle-Bed Reactors. *Chem. Eng. Sci.* 49, 5681, 1994.
7. Al-Dahhan, M.H.; Dudukovic, M.P. Catalyst Wetting Efficiency in Trickle-Bed Reactors at High Pressure. *Chem. Eng. Sci.* 50, 2377, 1995.

8. Huang, C.-C.; Podrebarac, G.G.; Ng, F.T.; Rempel, G.L. A Study of Mass Transfer Behaviour in a Catalytic Distillation Column. *The Canadian Journal of Chemical Engineering* 76, 323, 1998.
9. Ruether, J.A.; Yang, C.; Hayduk, W. Particle Mass Transfer During Cocurrent Downward Gas-Liquid Flow in Packed Beds. *Ind. Eng. Chem. Proc. Des. Dev.* 19, 103, 1980.
10. Satterfield, C.N.; Van Eek, M.W.; Bliss, G.S. Liquid-Solid Mass Transfer in Packed Beds with Downward Concurrent Gas-Liquid Flow. *AIChE J.* 24, 709, 1978.
11. Specchia, V.; Baldi, G.; Gianetto, A. Solid-Liquid Mass Transfer in Concurrent Two-Phase Flow through Packed Beds. *Ind. Eng. Chem. Proc. Des. Dev.* 17, 362, 1978.
12. Hirose, T.; Mori, Y.; Sato, Y. Liquid-to-Particle Mass Transfer in Fixed Bed Reactor with Cocurrent Gas-Liquid Downflow. *J. Chem. Eng. Japan* 9, 220, 1976.
13. Sylvester, N.D.; Pitayagulsarn, P. Mass Transfer for Two-Phase Cocurrent Downflow in a Packed Bed. *Ind. Eng. Chem. Proc. Des. Dev.* 14, 421, 1975.
14. Bliss, G.S. Effects of the Gas Phase on Liquid-Solid Mass Transfer in a Trickle Bed. Master of Science Thesis, Massachusetts Institute of Technology, Boston, Massachusetts, 1976.
15. Lemay, Y.; Pineault, G.; Ruether, J.A. Particle-Liquid Mass Transfer in a Three-Phase Fixed Bed Reactor with Cocurrent Flow in the Pulsing Regime. *Ind. Eng. Chem. Proc. Des. Dev.* 14, 280, 1975.
16. Goto, S.; Levec, J.; Smith, J.M. Mass Transfer in Packed Beds with Two-Phase Flow. *Ind. Eng. Chem. Proc. Des. Dev.* 14, 473, 1975.
17. Goto, S.; Smith, J.M. Trickle-Bed Reactor Performance. *AIChE J.* 21, 706, 1975.
18. Fukushima, S.; Kusaka, K. Interfacial Area and Boundary of Hydrodynamic Flow Region in Packed Column with Cocurrent Downward Flow. *J. Chem. Eng. Japan* 10, 461, 1977a.
19. Fukushima, S.; Kusaka, K. Liquid Phase Volumetric and Mass Transfer Coefficient, and Boundary of Hydrodynamic Flow Region in Packed Column with Cocurrent Downward Flow. *J. Chem. Eng. Japan* 10, 468, 1977b.

20. Rao, Y.G.; Drinkenburg, A.A.H. Solid-Liquid Mass Transfer in Packed Beds with Cocurrent Gas-Liquid Downflow. *AIChE J.* 31, 1059, 1985.

21. Yoshikawa, M.; Iwai, K.; Goto, S.; Teshima, H. Liquid-Solid Mass Transfer in Gas-Liquid Cocurrent Flows Through Beds of Small Packings. *J. Chem. Eng. Japan* 14, 444, 1981.

22. Chou, T.S.; Worley, F.L.; Luss, D. Local Particle-Liquid Mass Transfer Fluctuations in Mixed-Phase Cocurrent Downflow through a Fixed Bed in the Pulsing Regime. *Ind. Eng. Chem. Fundam.* 18, 279, 1979.

23. Lide, D.R. CRC Handbook of Chemistry and Physics. *CRC Press* 72nd ed, 1992.

List of Tables

List of Figures

Table 1: Operating Conditions and Bed Characteristics

system	water-nitrogen
liquid velocity	0.036 - 0.28 cm/s
gas velocity	1.0 - 7.9 cm/s
pressure	0.3 1- 3.55 MPa (30 - 500 psig)
bed diameter	2.2 cm
cross sectional area of the bed	3.8 cm^2
bed length	49.7 cm
equivalent active bed, height of naphthalene	3.2 cm
bed porosity	0.334
average naphthalene particle size	0.33 cm (diameter) x 0.43 cm
average glass particle size	0.25 cm (diameter) x 0.31 cm

Table 2: Molar flow rate of naphthalene and benzoic acid in the air that is equilibrium with water saturated with these materials for the conditions shown in Table 1 (23)

Naphthalene

	$Q_g C_g^*$		$Q_L C_L^*$
low gas velocity	2.6×10^{-8}	low liquid velocity	7.8×10^{-8}
1.1 cm/s (4.2 cm^3/s)		0.09 cm/s (0.33 cm^3/s)	
high gas velocity	1.8×10^{-7}	high liquid velocity	2.27×10^{-7}
7.8 cm/s (29.6 cm^3/s)		0.25 cm/s (0.96 cm^3/s)	

Solubility = 0.03 g/L

Henry's constant = 4.9×10^{-4} (bar m^3/mol)

Benzoic Acid

low gas velocity	3.1×10^{-5}	low liquid velocity	7.3×10^{-6}
1.1 cm/s (4.2 cm^3/s)		0.09 cm/s (0.33 cm^3/s)	
high gas velocity	2.14×10^{-4}	high liquid velocity	2.12×10^{-5}
7.8 cm/s (29.6 cm^3/s)		0.25 cm/s (0.96 cm^3/s)	

Solubility = 2.7 g/L

Henry's constant = 7.1×10^{-8} (bar m^3/mol)

Table 3: Naphthalene concentrations measured at the inlet and outlet of the trickle-bed reactor system

Pressure = 30 psig (0.31 MPa)

$$\% \text{ difference between inlet and outlet concentration} = \frac{|\,inlet\ conc. - outlet\ conc.\,|}{inlet\ conc.} \times 100\%$$

Inlet concentration (ppm)	% saturation	V_g (cm/s)	V_L (cm/s)	Outlet concentration (ppm)	% difference between inlet and outlet concentration
9.34	28.02	2.37	0.32	8.06	13.69
9.36	28.08	2.37	0.05	8.60	8.15
10.14	30.42	7.95	0.27	9.04	10.80
10.09	30.27	7.95	0.05	8.20	18.74

Pressure = 300 psig (2.17 MPa)

Inlet concentration (ppm)	% saturation	V_g (cm/s)	V_L (cm/s)	Outlet concentration (ppm)	% difference between inlet and outlet concentration
9.00	27.00	1.05	0.07	4.74	47.33
9.17	27.51	1.05	0.27	4.40	52.06
9.11	27.33	4.72	0.33	3.31	63.69
9.40	28.20	4.72	0.06	4.45	52.62

Table 4: Benzoic acid concentrations measured at the inlet and outlet of the trickle-bed reactor system

Pressure = 30 psig (0.31 MPa)

$$\% \text{ difference between inlet and outlet concentration} = \frac{|\,inlet\ conc. - outlet\ conc.\,|}{inlet\ conc.} \times 100\%$$

Inlet concentration (ppm)	% saturation	V_g (cm/s)	V_L (cm/s)	Outlet concentration (ppm)	% difference between inlet and outlet concentration
9.94	0.28	1.05	0.24	3.16	68.15
9.84	0.27	1.05	0.06	2.07	79.01
10.03	0.28	4.55	0.07	3.16	68.45
9.66	0.27	4.55	0.24	4.17	56.83

Pressure = 300 psig (2.17 MPa)

Inlet concentration (ppm)	% saturation	V_g (cm/s)	V_L (cm/s)	Outlet concentration (ppm)	% difference between inlet and outlet concentration
6.09	0.17	1.01	0.05	1.52	75.10
9.48	0.26	1.01	0.23	0.97	89.79
8.47	0.24	6.77	0.04	4.81	43.21
10.94	0.30	6.77	0.24	4.90	55.20

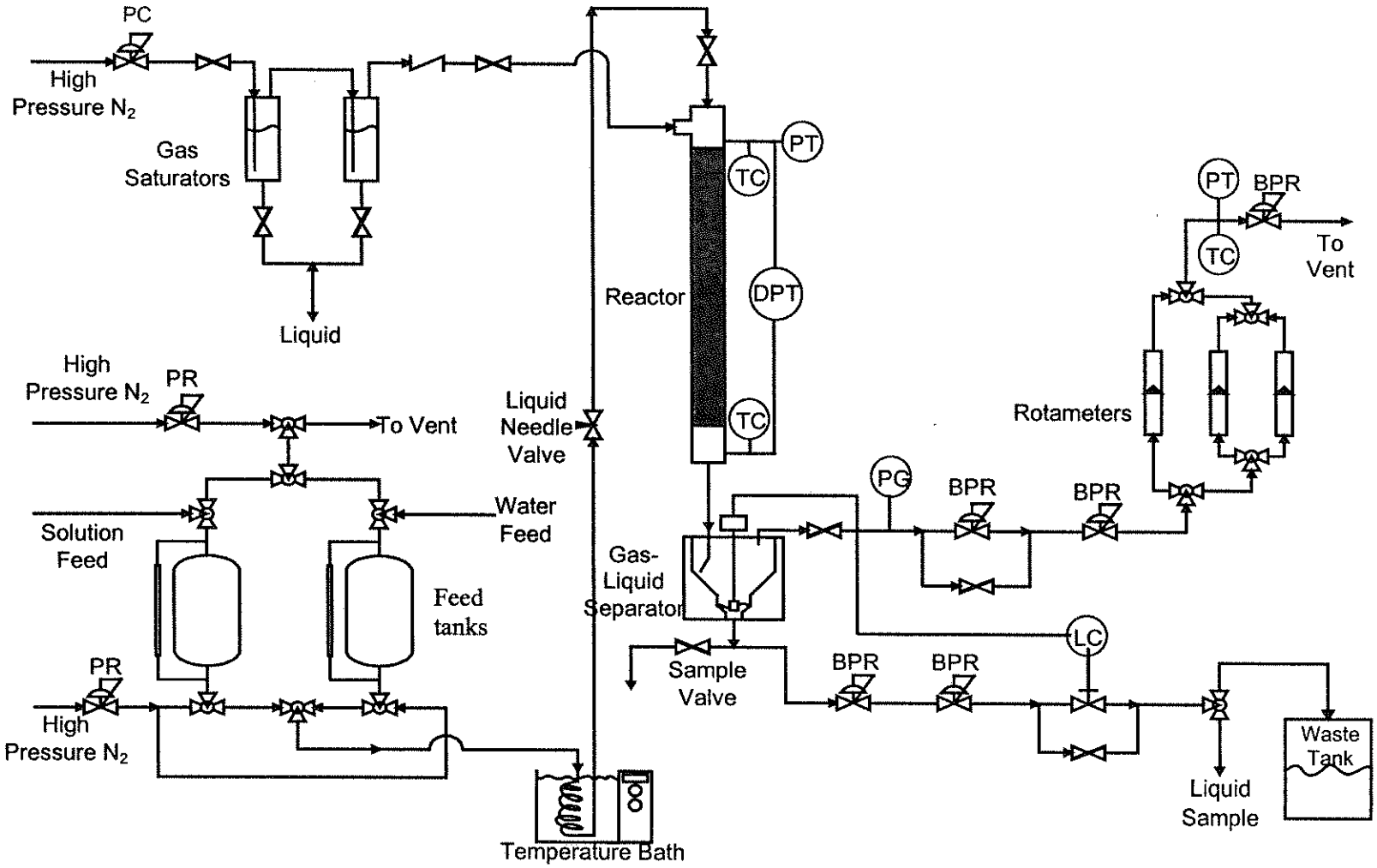

Figure 1. Schematic diagram of the High Pressure Trickle Bed Reactor facility. PR: Pressure regulator, BPR: Back pressure regulator, LC: Level control, TC: Thermocouple, PT: Pressure transducer, DPT: Differential pressure transducer.

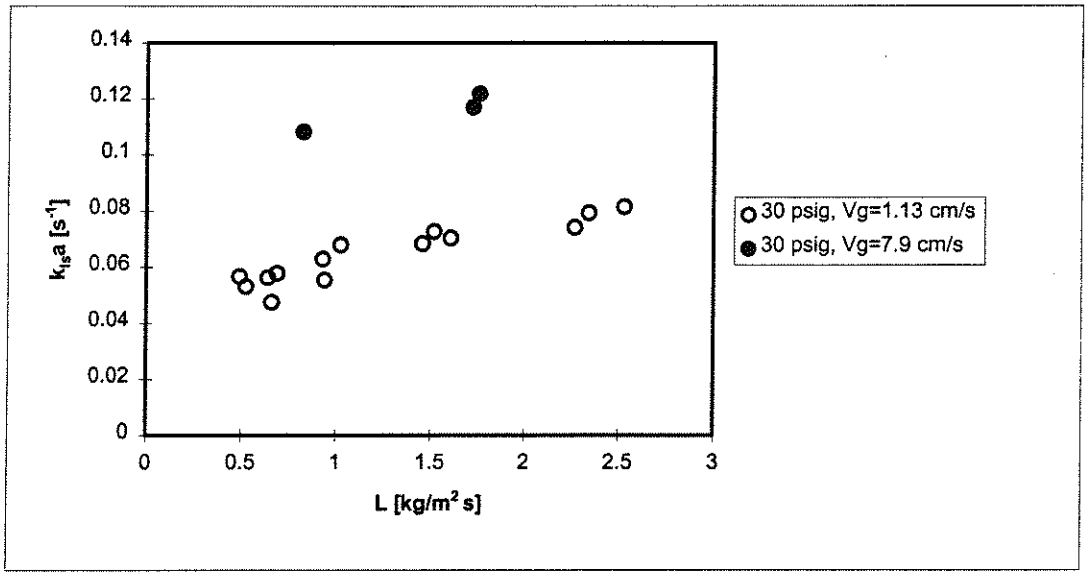

Figure 2(a). Volumetric liquid-solid mass transfer coefficients ($k_{ls}a$) vs. liquid mass velocity (L), measured at 30 psig (0.31 MPa) operating pressure. (For high V_g data: V_g = 7.9 cm/s, ε_B = 0.3339, Z = 49.7 cm, equivalent active section length = 3.204 cm; For low V_g data: V_g = 1.13 cm/s, ε_B = 0.3343, Z = 49.7 cm, equivalent active section length = 3.207 cm).

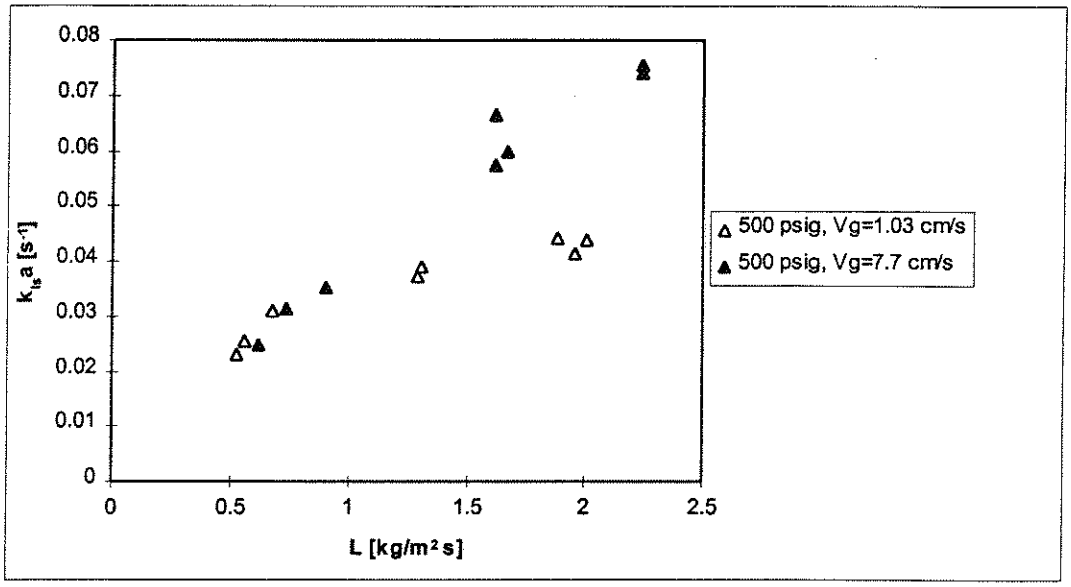

Figure 2(b). Volumetric liquid-solid mass transfer coefficients ($k_{ls}a$) vs. liquid mass velocity (L), measured at 500 psig (2.17 MPa) operating pressure. (For high V_g data: V_g = 7.7 cm/s, ε_B = 0.3339, Z = 49.7 cm, equivalent active section length = 3.204 cm; For low V_g data: V_g = 1.03 cm/s, ε_B = 0.3339, Z = 49.7 cm, equivalent active section length = 3.204 cm).

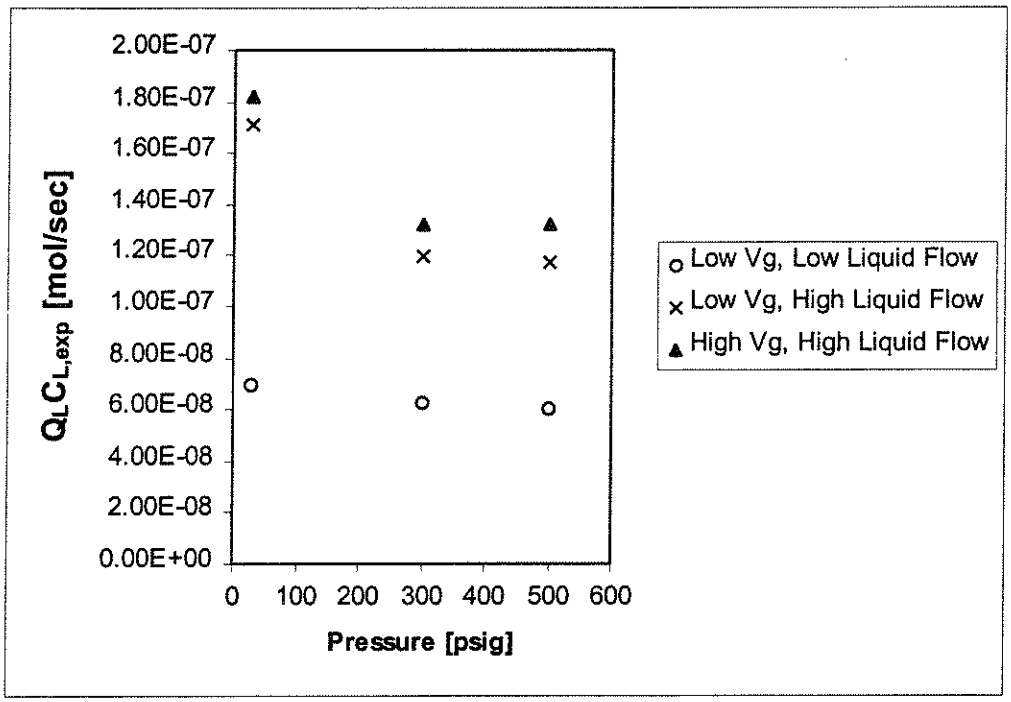

Figure 3: Molar flow rate of naphthalene in the liquid phase found during the dissolution experiments (conditions are listed in Figure 2 and Table 1).

THE EFFECT OF PARTICLE DILUTION ON THE WETTING EFFICIENCY AND LIQUID FILM THICKNESS IN SMALL TRICKLE BEDS

See the attached report for:

A. Problem Definition
B. Research Objectives
C. Research Accomplishments

THE EFFECT OF PARTICLE DILUTION ON WETTING EFFICIENCY AND LIQUID FILM THICKNESS IN SMALL TRICKLE BEDS

*D. Tsamatsoulis♣, M.H. Al-Dahhan#, F. Larachi© and N. Papayannakos♣**

♣ N.T.U.A., Department of Chemical Engineering, 9, Heroon Polytechniou, GR 157 80 Zografos, Greece

Washington University in St Louis, Department of Chemical Engineering, 1 Brooking Drive, St Louis MO 63130

© University of Laval, Department of Chemical Engineering, Quebec, Sainte-Foy, G1K 7P4, Canada

* *Author to whom correspondence should be addressed*

Abstract : Partial wetting in small scale trickle bed reactors results in incorrect determination of intra-particle apparent kinetic parameters as well as in erroneous reactor scale-up. Although a dilution of catalyst particles with inert fines improves the catalyst wetting efficiency, it does not guarantee full external catalyst wetting at all superficial liquid mass velocities. In this work, a method is presented to relate the wetting efficiency obtained at different operating conditions and at different laboratories for diluted and non-diluted beds. Liquid film thickness in diluted and non-diluted beds is estimated. The effect of the operating conditions on partial wetting and liquid film thickness is discussed.

INTRODUCTION

Pilot plant and laboratory-scale trickle bed reactors, which are fixed beds of catalyst contacted by cocurrent gas-liquid downflow, are usually utilized to conduct investigations needed for the design, scale-up and scale-down of industrial reactors (e.g., testing commercially used catalyst or an alternative feedstock, etc.). Low liquid hourly space velocity (LHSV) and low reactor-to-particle diameter ratio (d_r/d_p <20) are prevalent in small-scale trickle beds. These conditions often cause poor catalyst utilization due to partially wetted catalyst, non-negligible wall effects, high liquid back-mixing (i.e., axial dispersion) and/or maldistribution. Since the hydrodynamics and reaction kinetics are closely interlinked, the above mentioned hydrodynamic problems influence drastically the performance of pilot plant and laboratory-scale trickle bed reactors (Al-Dahhan et al., 1997; Al-Dahhan and Dudukovic, 1996; Tsamatsoulis and Papayannakos, 1993; Gierman, 1988; Van Klinken and Van Dongen, 1980).

Diluting the catalyst beds with fines (small, inert, and nonporous particles of about 0.2 – 0.3 mm diameter) has been utilized to overcome the shortcomings encountered with the conventional non-diluted small-scale reactors. Although the hydrodynamics of the diluted beds differ from that of commercial reactors, fines allow the small scale reactors to approach kinetically the performance of the commercial units by improving the plug flow character of the pilot plant and laboratory reactors (i.e. improving catalyst wetting and utilization, homogenizing liquid distribution, reducing wall effect and minimizing axial dispersion). As a matter of fact, this allows decoupling of the hydrodynamics and the intra-particle "apparent" kinetics (Al-Dahhan and Dudukovic, 1996). It is generally considered that the dilution of the catalyst particles

with fines would virtually eliminate partial wetting as well as dispersion effects. However, full catalyst wetting cannot be achieved at all superficial liquid mass velocities (Al-Dahhan and Dudukovic, 1996; Tsamatsoulis and Papayannakos, 1996).

The existing experimentally measured values of catalyst wetting efficiency in trickle bed reactors are scanty and in most cases are not related to each other due to large contrasts in operating conditions explored by different investigators. This poses a serious obstacle in using literature data for different applications. Two recent studies by Al-Dahhan and Dudukovic (1996) and Tsamatsoulis and Papayannakos (1996) reported catalyst wetting efficiency data in two totally non-overlapping ranges of operating conditions. They found that the wetting efficiency improves and approaches unity at different range of superficial liquid mass velocities Hence, this work presents a new unifying method to relate the wetting efficiency data measured at different conditions in different laboratories for diluted and non-diluted small-scale beds. The effects of operating conditions on catalyst wetting efficiency and liquid film thickness are discussed as well.

EXPERIMENTAL CONDITIONS

The wetting efficiency values used in this work were obtained experimentally for commercial porous catalysts at different operating conditions. Table 1 summarizes the bed characteristics and the experimental conditions, as reported by Al-Dahhan and Dudukovic (1996) (cold flow experiments) and Tsamatsoulis and Papayannakos (1996) (hot flow experiments). The liquid phase density was very close for both the hot and cold flow experiments. The ratio of nitrogen density at 0.31 MPa and room temperature to

hydrogen density at working conditions (Table 1) is 1.85, while the nitrogen density ratio at 0.31 MPa and at 1.83 MPa was about 6. The tracer in the hot flow experiments (Tsamatsoulis and Papayannakos, 1996) was made up of sulphur-containing compounds in one of the liquid feeds. In the cold flow experiments (Al-Dahhan and Dudukovic, 1996) heptane was used to trace the hexane flow.

Liquid tracer technique was used in both hot and cold flow experiments. In the hot flow experiments a step increase of tracer concentration was suddenly imposed by switching the liquid feed from a low to a high sulphur concentration feed (Tsamatsoulis and Papayannakos, 1993). The liquid holdups and effective tracer diffusivities values were determined by fitting to the experimental tracer response data the solution of the advection-diffusion parabolic partial differential equation for mass balance (Tsamatsoulis and Papayannakos, 1996). A pulse injection of heptane tracer into the steady hexane flow was used in the cold flow experiments. The method of moments was utilized to evaluate the hold-up and effective tracer diffusivities (Al-Dahhan and Dudukovic, 1995, 1996). In both cases, the wetting efficiency values were estimated by the form $a_w = (D_{e,pw}/D_e)^{0.5}$ for both diluted and non-diluted beds.

DISCUSSION

The dependence of wetting efficiency values on superficial liquid velocity for the diluted beds, as shown in Figure 1, indicates that the data of the hot and cold flow experiments do not overlap. Higher wetting efficiencies were obtained in the hot experiments compared to those obtained in the cold experiments at the same liquid mass velocities.

Wetting efficiency should be affected by the liquid holdup and the extent of the liquid spreading over the external surface of the catalyst. As the liquid holdup increases, wetting efficiency increases and the actual liquid mass velocity (L/ε_L) decreases. Hence, the variation of the ratio a_w/ε_L with (L/ε_L) indicates the compatibility of different experimental data. In Figure 2, it is observed that both hot and cold flow experimental data obtained for the diluted and non-diluted beds at the conditions listed in Table 1 appear to follow the same trend. Figure 2 also shows that the same trend was observed for the data obtained using different ratios of fines/particles. This implies that a careful dilution procedure can be effective for dilution values (λ_ε = the ratio of the fines bed volume to the volume of the catalyst bed voidage) from 0.6 to 1.5. However, $\lambda_\varepsilon = 1$ along with the packing procedure proposed by Al-Dahhan et al. (1995) are recommended to ensure reproducibility of the diluted beds.

The liquid film thickness over the catalyst external surface, which affects both gas and liquid mass transfer, is a hydrodynamic parameter, that depends on the wetting efficiency. Assuming that the liquid film thickness over the catalyst particles and fines is uniform, the film thickness can be evaluated as follows based on the wetting efficiency, holdup and shape and size of the bed particles:

$$\delta = \frac{\varepsilon_L}{a_w}\frac{V_R}{S_{ext}} \tag{1}$$

$$V_R = \frac{V_{RS}}{1-\varepsilon_{bed}} \tag{2}$$

Assuming fully wetted fines, yields:

$$a_w S_{ext} = a_w S_p + S_f \tag{3}$$

Substituting equations (2) and (3) into equation (1) gives:

$$\delta = \frac{\varepsilon_L}{1-\varepsilon_{bed}} \frac{1}{a_w \frac{S_p}{V_{Rs}} + \frac{S_f}{V_{Rs}}} \tag{4}$$

where,

$$V_{Rs} = V_{Rf} + V_{Rp}$$

$$\lambda = \frac{V_{Rf}}{V_{Rp}} \qquad \text{for diluted bed}$$

$$\lambda = 0 \qquad \text{for non-diluted bed.}$$

By geometrically evaluating S_p/V_{Rs} and S_f/V_{Rs} for different shapes of particles and for spherical fines, respectively, the uniform liquid film thickness can be estimated for different beds as follows:

Bed of spheres diluted with spherical fines:

$$\delta = \frac{\varepsilon_L}{3(1-\varepsilon_{bed})} \left[\frac{1}{\frac{a_w}{R_p(1+\lambda)} + \frac{1}{R_f(1+1/\lambda)}} \right] \tag{5}$$

Bed of non-diluted spheres:

$$\delta = \frac{\varepsilon_L}{3(1-\varepsilon_p)} \frac{R_p}{a_w} \tag{6}$$

Bed of cylindrical extrudates diluted with spherical fines:

$$\delta = \frac{\varepsilon_L}{(1-\varepsilon_{bed})} \left[\frac{\lambda+1}{2a_w\left(\frac{1}{R_p} + \frac{1}{L_p}\right) + \frac{3\lambda}{R_f}} \right] \tag{7}$$

Bed of non-diluted cylindrical extrudates:

$$\delta = \frac{\varepsilon_L}{(1-\varepsilon_p)}\left[\frac{1}{2a_w(\frac{1}{R_p}+\frac{1}{L_p})}\right] \qquad (8)$$

In Figure 3, the dependence of liquid film thickness on the superficial liquid mass velocity is presented for diluted and non-diluted beds. It is obvious that in both diluted and non-diluted beds the thickness of the liquid film does not change with liquid velocity when the particles are not completely wetted (Figure 1). The same trend has been observed for the static liquid thickness in diluted and non-diluted beds (Tsamatsoulis and Papayannakos, 1995). This implies that at these conditions the increase in liquid holdup with liquid flow rate results in improving the effective wetting by spreading the liquid over the external surface of the particles, while the liquid film thickness remains unchanged. Furthermore, it is found that the film thickness in a diluted bed depends on the degree of dilution (λ_ε) and gas velocity. Without a significant increase in liquid holdup the liquid film thickness decreases with the increase in the degree of dilution where the ratio of the external surface of fines to external surface of particles increases and, hence, the wetted surface per reactor volume increases. In addition, as the gas velocity increases the liquid film decreases due to better spreading of the liquid over the external surface of the particles. Such trend is similar to the trend of the effect of gas velocity on the liquid holdup presented by the five cases proposed in Al-Dahhan and Dudukovic (1994, 1995, 1996). Hence, the liquid film thickness could be emperically correlated with the degree of dilution and superficial gas velocity. As a preliminary attempt, the following correlation (eq. 9) fits well the film thickness values evaluated by

equations (5) to (8). However, detailed experimental work and analysis are needed to develop an extended correlation based on dimensionless groups.

$$\delta = 0.0025(\lambda_\varepsilon u_{gs}^{0.35})^{-0.77} = 0.0025\lambda_\varepsilon^{-0.77} u_{gs}^{-0.27} \tag{9}$$

where

$$\lambda_\varepsilon = \lambda \frac{1-\varepsilon_p}{\varepsilon_p(1-\varepsilon_f)} \tag{10}$$

Figure 4 illustrates that the developed correlation predicts properly the liquid film thickness and its trend with $\left(\lambda_\varepsilon\ u_{gs}{}^{0.35}\right)$. A parity plot of the film thickness is presented in Figure 5. The correlation values of the liquid film are within ±20%.

CONCLUDING REMARKS

Dilution of the catalyst beds with inert fines improves catalyst wetting efficiency. However, fully wetted catalyst cannot be considered a priori at all operating conditions. The variation of the ratio of catalyst wetting efficiency to liquid holdup $(a_w/\varepsilon_L)$with the actual liquid mass velocity (L/ε_L) can be used to relate the experimental data obtained at different operating conditions.

Liquid film thickness over the external surface of the catalyst particles decreases with the increase in the degree of dilution and superficial gas velocity. In a partially wetted catalyst bed, as superficial liquid velocity increases liquid holdup increases while liquid film thickness remains unchanged. As a result, catalyst wetting efficiency improves due to better spreading of the liquid phase over the external surface of the particles.

ACKNOWLEDGEMENTS

The authors are thankful to the Fulbright Foundation for the support of one of the authors (Dr. N. Papayannakos) during his stay at the Chemical Reaction Engineering Laboratory (CREL) at Washington University in St Louis.

NOTATION

a_w wetting efficiency as the ratio of the wetted external surface area to the total particle external area

δ liquid film thickness, mm

D_e effective diffusivity of the fully wetted particles, m^2/s

$D_{e,pw}$ effective diffusivity of the partially wetted particles, m^2/s

ε_L liquid holdup defined as the ratio of the liquid volume in the bed to the total bed volume

ε_{bed} diluted bed void fraction

ε_p bed void fraction of spherical or cylindrical particles

ε_f bed void fraction of fines

L liquid superficial mean velocity based on empty tube cross section, $Kg.m^{-2}.s^{-1}$

L_p mean length of cylindrical particles, mm

λ ratio of the fine particle volume to the sphere or extrudate particle volume, in diluted beds

λ_e ratio of fine bed volume to particle bed void volume

R_p radius of cylindrical or spherical particles, mm

R_f mean diameter of fines, mm

S_{ext} external area of the particles in the bed, cm^2

u_{gs} gas superficial velocity, cm/s

V_R bed volume, cm^3

V_{Rf} fines bed volume, cm^3

V_{RP} catalyst bed volume, cm^3

V_{RS} total solids volume in the reactor ($V_{Rf} + V_{RP}$), cm^3

LITERATURE CITED

Al-Dahhan M.H. and Dudukovic M.P., 1994. Pressure Drop and Liquid Holdup in High Pressure Trickle Bed Reactors, *Chem. Eng Sci.*, **49**(24B), 5681.

Al-Dahhan, M.H., Wu, Y. and Dudukovic M.P., 1995. Reproducible Technique for Packing Laboratory Scale Trickle Bed Reactors with a Mixture of Catalyst and Fines, *Ind. Eng. Chem. Res.*, **34**, 741.

Al-Dahhan, M. H. and Dudukovic M.P., 1995. Catalyst Wetting Efficiency in Trickle-Bed Reactors at High Pressure, *Chem. Eng. Sci.*, **50**(15), 2377.

Al-Dahhan, M.H. and Dudukovic M.P., 1996. Catalyst Bed Dilution for Improving Catalyst Wetting in Laboratory Trickle-Bed Reactors, *AIChE J.*, **42**(9), 2594.

Al-Dahhan, M.H., Larachi, F., Dudukovic, M.P. and Laurent, A., 1997. High Pressure Trickle Bed Reactors: A review, *Ind. Eng. Chem. Res.*, **36**, 3292.

Gierman, H., 1988. Design of Laboratory Hydrotreating Reactors: Scaling Down of Trickle Flow Reactors, *Appl. Catal.*, **43**, 285.

Tsamatsoulis, D. and Papayannakos, N., 1993. Axial Dispersion and Holdup in a Bench-Scale Trickle Bed Reactor at Operating Conditions, *Chem. Eng. Sci.*, **49**(4), 523.

Tsamatsoulis, D. and Papayannakos, N., 1995. Simulation of Non-Ideal Flow In A Trickle Bed Hydrotreater By The Cross-Flow Model, Chem. Engg Sci., **50**(23), 3685.

Tsamatsoulis, D. and Papayannakos, N., 1996. Partial Wetting of Cylindrical Catalytic Carriers in Trickle-Bed Reactors, *AIChE J.*, **42**(7), 1853.

Van Klinken, J. and van Dongen, R.H., 1991. Catalyst Dilution For Improved Performance of Laboratory Trickle Bed Reactors, *Chem. Engg Sci.*, **14**, 406.

Table 1. Bed Characteristics and Experimental Conditions

Cold experiments (Al-Dahhan and Dudukovic, 1995, 1996)

	Data (1)	Data (1,2)	Data (1)	Data (1,2)	Data (1)
Experimental Conditions					
Pressure, MPa		0.31, 3.55	0.31, 1.82	0.31, 3.55	0.31, 1.82
Temperature, K		293	293	293	293
Gas Feed		Nitrogen	Nitrogen	Nitrogen	Nitrogen
Superficial Gas Velosity, cm/s		1.02, 8.7	1.02, 8.6	1.02, 8.5	1.02, 8.6
Liquid Feed		Hexane	Hexane	Hexane	Hexane
Liq. sp. gr. at exp. cond., g/cm^3		0.68	0.68	0.68	0.68
Fine Properties	SCF				
Non-porous Silicon Carbide					
Mean Particle diameter, mm	0.21				
Material density, g/cm^3	3.21				
Bed density, g/cm3	1.51				
Bed porosity	0.53				
Particle Properties		PA		PB	
Type		Cyl. Ex. *		Sph. **	
Diameter/Length, mm/mm		1.57/4.3		1.52	
Particle Porosiy		0.599		0.697	
Particle density, g/cm^3		1.189		0.697	
Bed Charactiristics		**PA**	**BA**	**PB**	**BC**
Particles / Fines		PA	PA/SCF	PB	PB/SCF
Bed diameter, cm		2.19	2.19	2.19	2.19
Bed length, cm		51.61	53.8	51.63	53.5
Bed Porosity		0.36	0.22	0.41	0.31
Vol Fin Bed/Vol Part Bed Void			0.96		0.57
Vol Fin Bed/Vol Part			0.54		0.4
Vol Fine Part/Vol Part			0.25		0.19

* : Porous Cylindrical Extrudates
** : Porous Spheres
Data (1) : Al-Dahhan and Dudukovic, 1996
Data (2) : Al-Dahhan and Dudukovic, 1995
Data (1, 2) : Al-Dahhan and Dudukovic, 1996, 1995
SCF: Fines for cold experiments
PA: Cylindrical particles - non-diluted bed
PB: Spherical particles - non-diluted bed
BA: Diluted bed of cylindrical particles
BC: Diluted bed of spherical particles

Hot experiments (Tsamatsoulis and Papayannakos, 1996)

	Data (3)	Data (3)	Data (3)	Data (3)
Experimental Conditions				
Pressure, MPa		5	5	5
Temperature, K		623	623	623
Gas Feed		Hydrogen	Hydrogen	Hydrogen
Superficial Gas Velosity, cm/s		0.16	0.16	0.16
Liquid Feed		VGO1	VGO1	VGO2
Liq. sp. gr. at exp. cond., g/cm^3		0.71	0.71	0.71
Fine Properties	SP			
Non-porous Silica Powder				
Mean Particle diameter, mm	0.35			
Material density, g/cm^3	2.64			
Bed density, g/cm3	1.59			
Bed porosity	0.4			
Particle Properties		P1		
Type		Cyl. Ex. *		
Diameter/Length, mm/mm		1.40/3.8		
Particle Porosiy		0.59		
Particle density, g/cm^3		1.36		
Bed Charactiristics		**P1**	**B1**	**B2**
Particles / Fines		P1	P1/SP	P1/SP
Bed diameter, cm		2.54	2.54	2.54
Bed length, cm		47	47	47
Bed Porosity		0.44	0.36	0.31
Vol Fin Bed/Vol Part Bed Void			0.53	1.59
Vol Fin Bed/Vol Part			0.42	1.25
Vol Fine Part/Vol Part			0.25	0.75

* : Porous Cylindrical Extrudates

Data (3) : Tsamatsoulis and Papayannakos, 1996

SP: Fines for hot experiments

P1: Cylindrical particles - non-diluted bed

B1: Diluted bed of cylindrical particles with volume of fines / volume of particles = 0.25

B2: Diluted bed of cylindrical particles with volume of fines / volume of particles = 0.75

Figure Captions

Figure 1. Dependence of the diluted beds effective wetting on the superficial liquid mass velocity (Table 1).

Figure 2. a_w/ε_L vs. L/ε_L for the diluted (BA, BC, B1, B2) and the corresponding non-diluted (PA, PB, P1) beds.
Dashed lines : boundaries of ± 20% around the solid line (Table 1).
With diluted beds BA and BC data was collected at : P=0.31 MPa, u_{gs} =1.02 cm/sec and P=1.82 MPa, u_{gs} = 8.7 cm/sec.
With non-diluted beds PA and PB data was collected at : P=0.31 MPa, u_{gs} =1.02 cm/sec and P=3.55 MPa, u_{gs} = 8.7 cm/sec.

Figure 3. The effect of superficial liquid mass velocity on the liquid film thickness in partially wetted beds (Table 1).
(I): P= 0.31 MPa, u_{gs} =1.02 cm/sec, and (II) : P=1.82 MPa, u_{gs} = 8.7 cm/sec.

Figure 4. Comparison between the prediction of the liquid film thickness using the developed correlation (eq. 9) (dash line) and the mean values estimated using equations (5) to (8) (symbols) (Table 1).

Figure 5. Parity plot of the film thickness values predicted by the developed correlation (eq. 9) and those estimated using equations (5) to (8)
(I) : P= 0.31 MPa, u_{gs} =1.02 cm/sec, and (II) : P=1.82 MPa, u_{gs} = 8.7 cm/sec (Table 1).

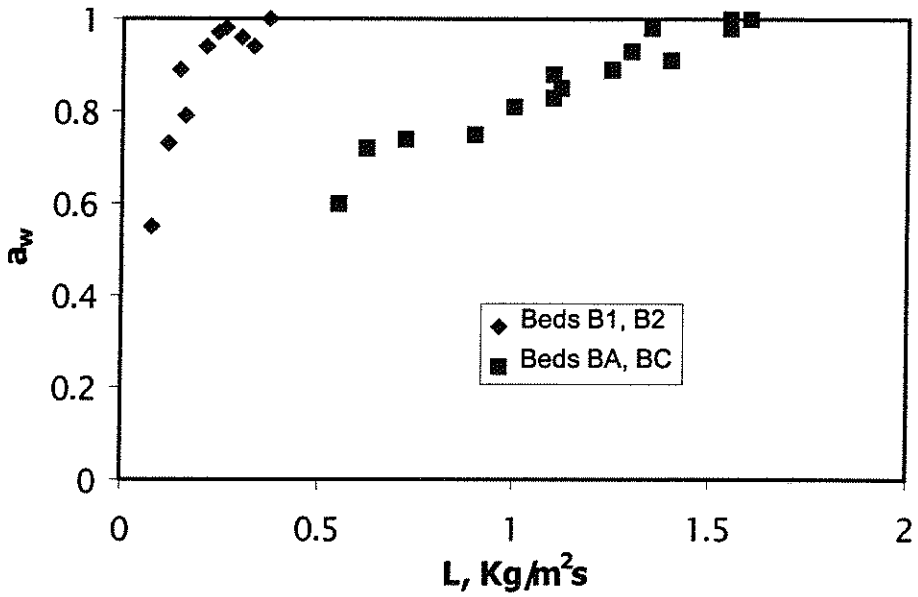

Figure 1

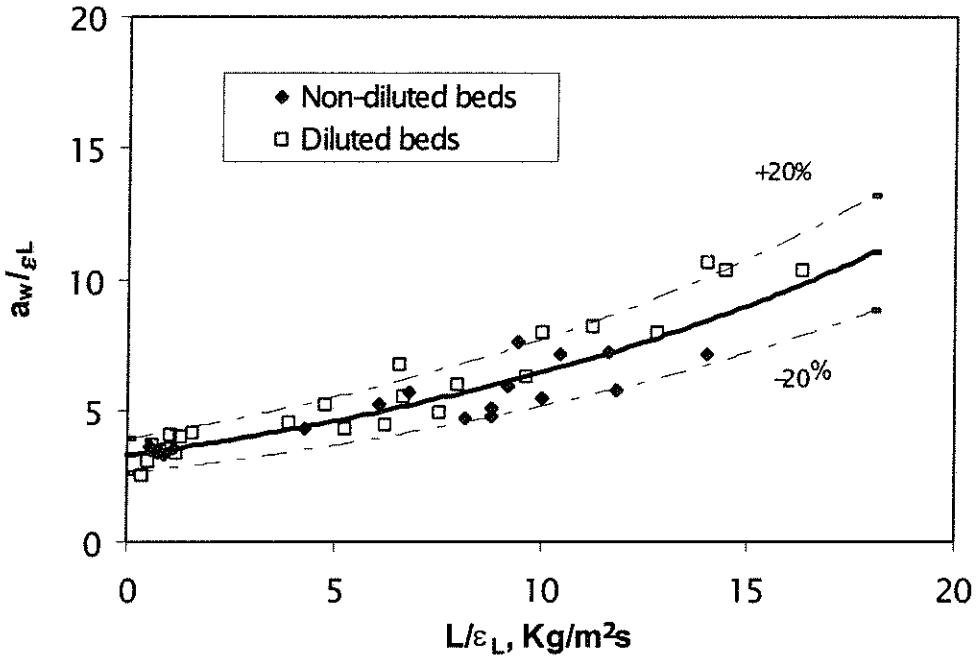
Non-diluted beds
Diluted beds
+20%
-20%
a_w/ε_L
L/ε_L, Kg/m²s
0
5
10
15
20

Figure 2

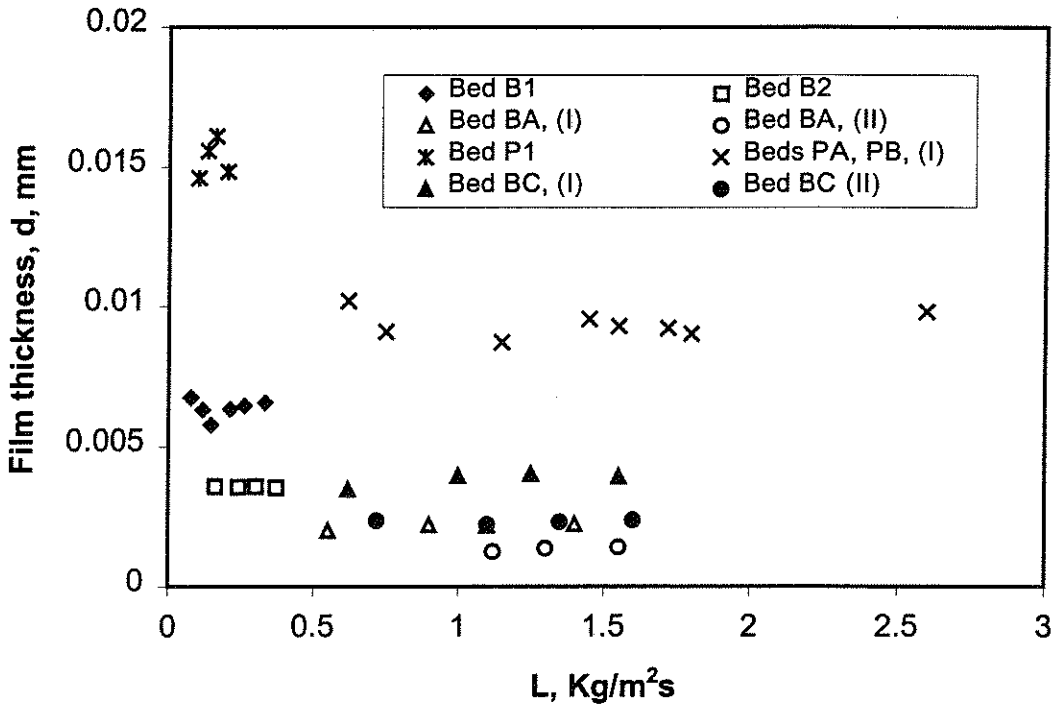
0.02
0.015
0.01
0.005
0
Film thickness, d, mm
0
0.5
1
1.5
2
2.5
3
L, Kg/m²s
Bed B1
Bed B2
Bed BA, (I)
Bed BA, (II)
Bed P1
Beds PA, PB, (I)
Bed BC, (I)
Bed BC (II)

Figure 3

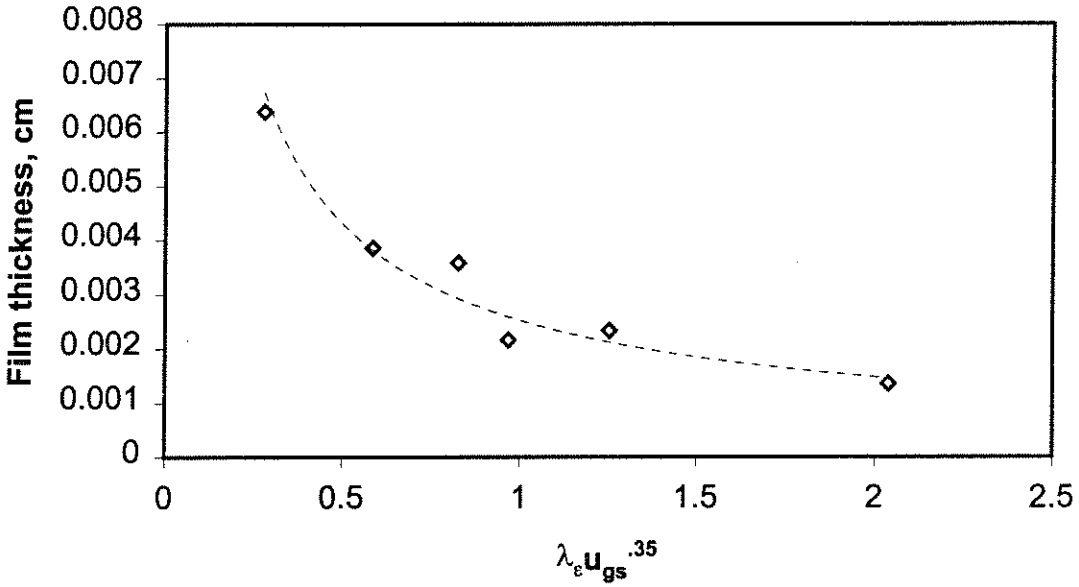
Film thickness, cm
0.008
0.007
0.006
0.005
0.004
0.003
0.002
0.001
0
0
0.5
1
1.5
2
2.5
$\lambda_\varepsilon u_{gs}^{.35}$

Figure 4

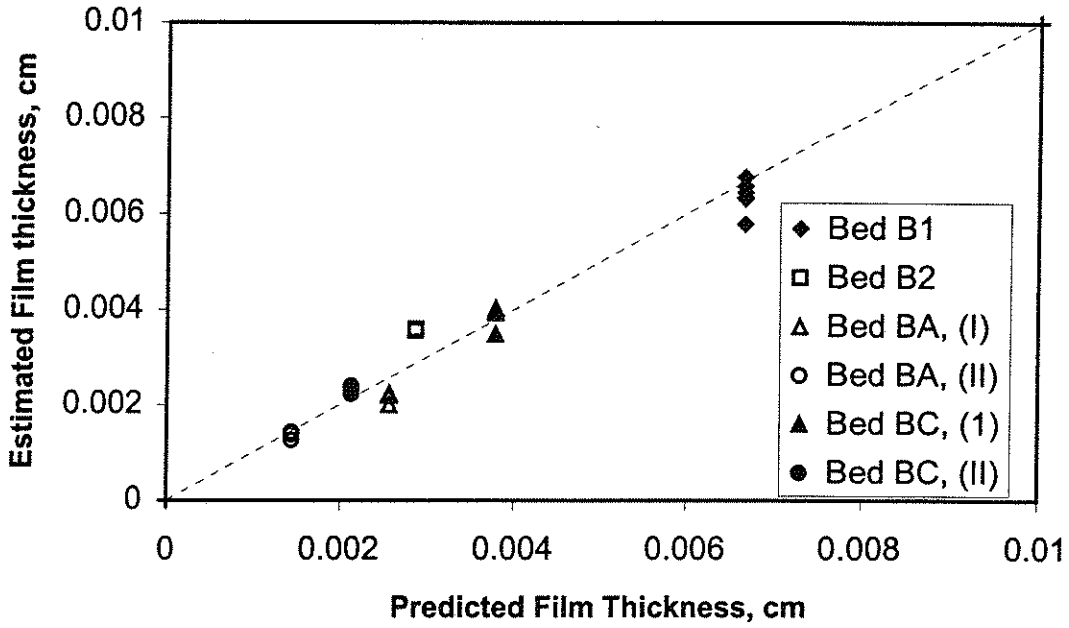
Estimated Film thickness, cm
0.01
0.008
0.006
0.004
0.002
0
0
0.002
0.004
0.006
0.008
0.01
Predicted Film Thickness, cm
Bed B1
Bed B2
Bed BA, (I)
Bed BA, (II)
Bed BC, (1)
Bed BC, (II)

Figure 5

AREA I: MULTIPHASE REACTORS AND SYSTEMS

B. COMPUTATIONAL FLUID DYNAMICS AND COMPUTATIONAL REACTION ENGINEERING

Our work in this important area focused on:

i) Utilizing Computational Fluid Dynamics (CFD) codes such as CFDLIB and FLUENT to predict the hydrodynamic parameters (velocity, turbulence parameters, etc.) in bubble/slurry bubble column, trickle beds, liquid-solid riser, stirred tanks, etc. Verification of these codes versus the measured parameters by CARPT/CT is one of the current goals.

ii) Development of boundary element based algorithms for reaction engineering problems. Faster, robust algorithms that can handle more complex problems of diffusion and multiple reactions are the desired goal.

iii) Development of a robust method for calculation of steep moving fronts in packed bed reactors, heat regenerators, reactor-generators and similar applications.

Project summaries are included for:

B1. Computational Fluid Dynamics (CFD)

B1-1. Two-Dimensional Axisymmetric Simulation of Gas-Liquid Flow in Cylindrical Bubble Column Reactor by Fluent and Comparison with CARPT/CT Measurements. **(P. Chen)**

B1-2. CFD Modeling of Multiphase Flow Distribution in Catalytic Packed-Bed Reactors: Scale Down Issues. **(Y. Jiang, M. Khadilkar)**

B2. Computational Reaction Engineering

B2-1. Computational Reaction Engineering. **(P.A. Ramachandran)**

B2-2. Osculatory Interpolation in the Method of Fundamental Solutions for Non-Linear Poisson Problems. **(K. Balakrishnan)**

TWO DIMENSIONAL AXISYMMETRIC SIMULATION OF GAS-LIQUID FLOW IN CYLINDRICAL BUBBLE COLUMN REACTOR BY FLUENT AND COMPARISON WITH CARPT/CT MEASURMENTS

A. Problem Definition

The design and scale-up of bubble column reactors rely on understanding of the hydrodynamics of gas-liquid flow. The need to establish a rational basis for the interpretation of the interaction of fluid dynamic variables is the primary motivation for bubble column modeling based on computational fluid dynamics (CFD). A commercial CFD package, **FLUENT**, is used to run the simulations. The purpose is to validate the capability of FLUENT by comparing the numerical predictions with the CARPT/CT measurements for liquid velocity field and gas holdup profile.

B. Research Objectives

1. Compare the mean axial velocity and gas holdup with CARPT/CT data.
2. Compare the Reynolds stress with CARPT data.
3. Implement two bubble class model into FLUENT and validate the code.

C. Research Accomplishment

C1. Model Equations

In the Eulerian two-fluid approach, the different phases are treated mathematically as interpenetrating continua. The derivation of the conservation equations for mass, momentum and energy for each of the individual phases is done by ensemble averaging the local instantaneous balances for each of the phases.

Continuity (k^{th} phase):

$$\frac{\partial}{\partial t}(\alpha_k \rho_k) + \nabla \cdot (\alpha_k \rho_k \vec{u}_k) = \sum_{p=1}^{n} \dot{m}_{pk} \tag{1}$$

Volume Fraction

$$\sum_{k=1}^{n} \alpha_k = 1 \tag{2}$$

Momentum (k^{th} phase):

$$\frac{\partial}{\partial t}(\alpha_k \rho_k \vec{u}_k) + \nabla \cdot (\alpha_k \rho_k \vec{u}_k \otimes \vec{u}_k) = -\alpha_k \nabla p + \nabla \cdot \bar{\bar{\tau}}_k + \vec{F}_k + \sum_{p=1}^{n} (K_{pk}(\vec{u}_p - \vec{u}_k) + \dot{m}_{pk}\vec{u}_{pk}) \quad (3)$$

where $\bar{\bar{\tau}}_k$ is the k[th] phase stress strain tensor, whose components are given by:

$$\tau_{k,ij} = \alpha_k \mu_k \left(\frac{\partial u_{k,i}}{\partial x_j} + \frac{\partial u_{k,j}}{\partial x_i} \right) - \frac{2}{3} \alpha_k \mu_k \delta_{ij} \frac{\partial u_{k,l}}{\partial x_l} \quad (4)$$

Inter-Phase Momentum Exchange Coefficient

The exchange coefficient for gas-liquid mixture is

$$K_{pq} = \frac{3}{4} C_D \frac{\alpha_p \alpha_q \rho_q \left| \vec{u}_p - \vec{u}_q \right|}{d_p} \quad (5)$$

where the subscript 'p' and 'q' indicate the properties for the secondary phase (bubble) and the primary phase (liquid), respectively. C_D is the drag force coefficient for sufficiently contaminated systems (Tomiyama, 1995)

$$C_D = \max\left[\frac{24}{\mathrm{Re}} \left(1 + 0.15\,\mathrm{Re}^{0.687}\right), \frac{8}{3} \frac{Eo}{Eo + 4} \right] \quad (6)$$

where

$Eo \equiv$ Eotvos Number $\equiv g\rho_q d_p^2/\sigma$

$Re \equiv$ Bubble Reynolds number $\equiv d_p|\mathbf{u}_p\text{-}\mathbf{u}_q|/\nu_q$

The turbulence in the continuous phase is modeled through a set of modified k-ε equations with extra terms that include interphase turbulent momentum transfer.

The numerical simulation was performed on a 300 (axial) × 19 (radial) rectangular grid. A case of 8-in (19 cm in diameter) column operated at superficial gas velocity U_{sup} = 12 cm/s has been simulated. The column contained a batch liquid with unexpanded height of 95.0 cm. The boundary condition, on the side wall of the column is set as no-slip. The injection of the small bubble phase was uniformly done over the central 16 bottom cells. The large bubble phase was injected uniformly over the central 9 bottom cells. For air-water system, $C_D/d_p \cong$ constant, for bubble size within 2 to 8 mm. Thus the momentum exchange term between water and small bubble phase is not sensitive to small bubble size. In the simulation, small bubble size is set to be 3 mm and the big bubble size was calculated by Krishna's correlation (1996).

$$d_{p,large} = 0.069(U-U_{trans})^{0.376}$$

where U_{trans} is regime transition velocity, which is set to be U_{trans} = 0.035 m/s. At the distributor the large bubbles constitute a fraction $(U-U_{trans})/U$ of the total incoming volumetric flow, whereas the samll bubble constitute a fraction (U_{trans}/U) of the total incoming flow.

C2. Quantitative Comparison with CARPT/CT Measurements

Figures 1, 2, 3 are the comparisons of the mean axial liquid velocity, gas holdup and liquid kinetic energy with the CARPT and CT data at H = 53 cm (Dagaleesan, 1997), respectively. While the velocity and kinetic energy profiles are quite close, there are significant discrepancies between the numerical gas holdup profile and the experimental one. At the present, we postulate there is mainly due to the assumption that there is no breakup or coalescence. In fact, in a column operated at this high gas flow rate (12 cm/s), such behavior is dominant. Also, when axisymmetric simulation is performed, there is no inward force exert on the bubbles such that the peak value of gas holdup is not in the centerline.

D. Future Work

1. Perform three-dimensional simulation using two bubble class model.
2. Develop a bubble population balance model by incorporating coalescence and breakup models within the CFD framework.

E. Bibliography

Dagaleesan, S., *D. Sci. thesis*, Washington University in St. Louis, 1997

Krishna, R. and Ellenberger, J., *AICHE J.*, 42(9), 2627-2634, 1996

Tomiyama, A., Kataoka, I., and Sakaguchi, T., *Nippon Kikai Gakkai Ronbunshu, B-hen*, 61(587), 2357-64, 1995

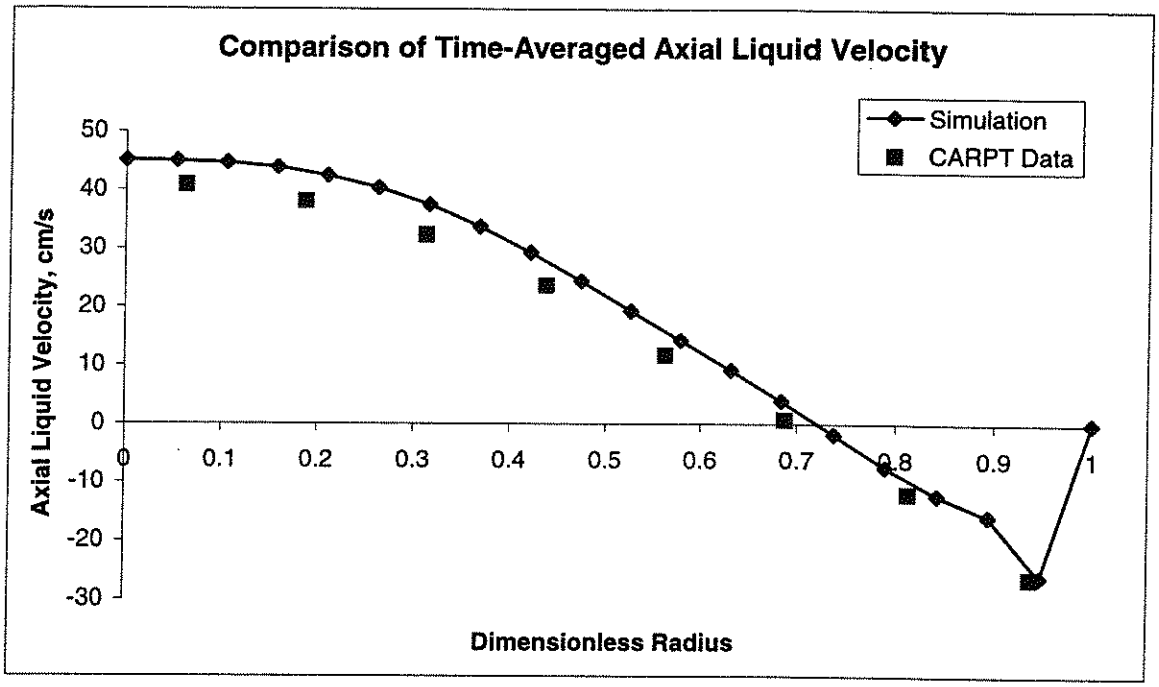

Figure 1: The time-averaged axial liquid velocity of 8-in column operated at Ug = 12 cm/s and comparison with CARPT data

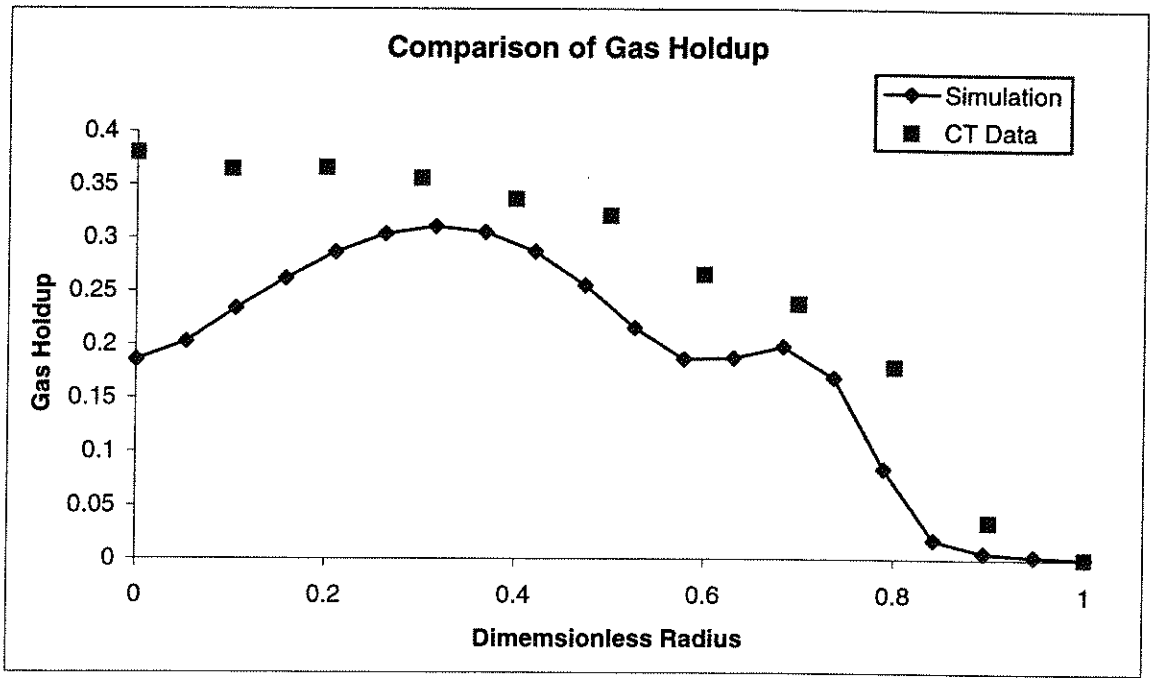

Figure 2: The time-averaged gas holdup of 8-in column operated at Ug = 12 cm/s and comparison with CT data

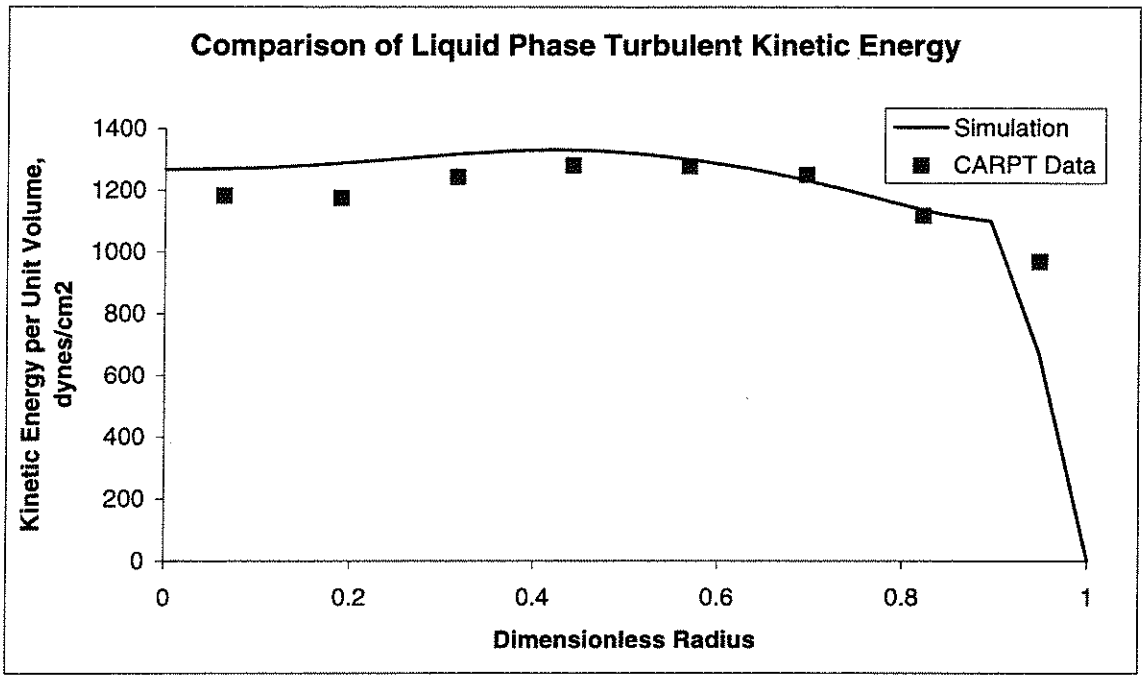

Figure 3: The time-averaged turbulent kinetic energy of 8-in column operated at Ug = 12 cm/s and comparison with CARPT data

CFD MODELING OF MULTIPHASE FLOW DISTRIBUTION IN CATALYTIC PACKED-BED REACTORS: SCALE DOWN ISSUES

A. Problem Definition

Packed-bed reactors with multiphase flow have been used in a large number of processes in refinery, fine chemicals and biochemical operations. Effective scale up of bench-scale packed-bed reactors in the development of new processes, and scale down of the commercial units in the improvement of existing processes have become predominant tasks in the research and development divisions of many companies (Sie and Krishna, 1998). The paradigms of scaling up packed-beds reactors from bench-scale to pilot and industrial units have been explored in detail in the literature (Le Nobel and Choufour, 1959; Gieman, 1988; De Wind, 1988; Sie and Krishna, 1998) and reviewed recently by Krishna and Sie (1994), Sie and Krishna (1998), Dudukovic et al (1999). The scaling down of multiphase packed beds is, in fact, even tougher since many issues such as liquid back-mixing and liquid maldistribution become more apparent when the reactor scale is reduced (Mears, 1971; Tasmatsoulis and Papayannakos, 1994). The critical question is how to effectively produce reliable bench-scale data. To answer this question fundamentally, and to come up with a new strategy for scaling down packed-beds, the studies of the following issues are required: (1) Understanding multiphase flow maldistribution in bench- and pilot-scale packed beds. (2) Assessing the effect of flow maldistribution on reactor performance in terms of conversion and selectivity; developing a method to 'correct' the bench- and pilot-scale experimental data for non-ideal flow behavior and (3) preventing flow maldistribution from happening in experimental units (e.g. using fines, van Klinken and van Dongen, 1980; Al-Dahhan and Dudukovic, 1996). In this report, we mainly focus on the first aspect, which is to understand how multiphase flow is distributed spatially and temporally in packed-bed reactors and how this affects the laboratory-scale experimental data.

B. Research Objectives

The research objectives for this study are:

1. Apply *k*-fluid model in the simulations of gas and liquid holdup distribution and their velocity field in the bench-scale trickle-bed reactors.
2. Examine the effect of periodic liquid-feed mode on the liquid holdup distribution by comparing them with the liquid distribution under steady state liquid-feed condition.

C. Research Accomplishments

The research accomplishments are discussed in the attached manuscript accepted by *3rd International Symposium in Catalysis in Multiphase Reactors*, May 28-31, Naples, Italy (2000).

1. Introduction

Packed-bed reactors with multiphase flow have been used in a large number of processes in refinery, fine chemicals and biochemical operations. Effective scale up of bench-scale packed-bed reactors in the development of new processes and scale down of the commercial units in the improvement of existing processes have become predominant tasks in the research and development divisions of many companies (Sie and Krishna, 1998). The paradigms of scaling up packed-beds reactors from bench-scale to pilot scale and industrial units have been explored in detail in the literature (Le Nobel and Choufour, 1959; Gieman, 1988; De Wind, 1988; Sie and Krishna, 1998) and reviewed recently by Krishna and Sie (1994), Sie and Krishna (1998), Dudukovic et al (1999). The scaling down of multiphase packed beds is, in fact, even tougher since many issues such as liquid back-mixing and liquid maldistribution become more apparent when the reactor scale is reduced (Mears, 1971; Tasmatsoulis and Papayannakos, 1994). The critical question is how to effectively produce reliable bench-scale data. To answer this question, and to come up with a new strategy for scaling down packed-beds, studies of the following issues are required: (1) Understanding multiphase flow maldistribution in bench- and pilot-scale packed beds. (2) Assessing the effect of flow maldistribution on reactor performance in terms of conversion and selectivity; developing a method to 'correct' the bench- and pilot-scale experimental data for non-ideal flow behavior and (3) preventing flow maldistribution from happening in experimental units (e.g. using fines, van Klinken and van Dongen, 1980; Al-Dahhan and Dudukovic, 1996). In this paper, we mainly focus on the first aspect, which is to understand how multiphase flow is distributed spatially and temporally in packed-bed reactors and how this affects the laboratory-scale experimental data.

The experimental studies of the flow pattern in packed beds have been conducted mostly for the system with 'saturated' single phase flow (e.g., gas flow or liquid upflow) using exit velocity measurements (Lerou and Froment, 1976) and few non-invasive measurements (Stephenson and Stewart, 1986; Sederman et al., 1997). Multiphase flow measurements in bench-scale packed beds have not been reported in the open literature although the recent high-resolution tomography techniques provide hopes in that direction (Lutran et al., 1989; Gladen, 1996; Chaouki et al., 1997; Reinecke et al., 1998). Therefore, numerical simulation of multiphase flow in bench scale packed beds is of significance in offering an improved understanding of such flows.

The performance of a packed bed is mainly dependent on the dynamic flow texture in the tortuous interstitial space and kinetic characteristics of the system. Dynamic multiphase flow modeling in such complex multi-dimensional space is a challenging task due to a number of issues involved. For instance, one has to find ways to deal with: (i) complicated geometry of the voidage space; (ii) various scales of flow distribution (i.e. particle scale, cell scale and bed scale); (iii) complex interactions between flowing phases and between fluids and the stationary catalyst particles. To overcome these complexities of the system, a variety of simplified phenomenological models have been developed in literature. The following approaches were suggested: (a) 'diffusion' model (see Stanek et al., 1994); (b) 'sphere-pack' model (see Zimmerman and Ng, 1986); (c) 'percolation' theory (see Crine, 1979); (d) 'porous media' method (Christensen, et al., 1986); (e) 'energy minimization' approach (Holub, 1990; Jiang et al., 1999). Most of these models dealt with gas-liquid cocurrent downflow in 2-D rectangular packed beds with relatively

large size of particles (3~6 mm) at steady state condition. The modeling of two-phase flow in a bench-scale cylindrical tube with typical particle size used in industry is simply not available. Although computational fluid dynamics (CFD) has been recently applied in case of gas flow in a single-tube fixed bed for heat transfer study (Logtenberg and Dixon, 1998), the diameters of the tube and the particles (e.g., 12 cm tube with 5 cm particles) used are completely different than those employed in the study of catalytic reactions.

In this paper, we present our recent numerical efforts on two-phase flow modeling in bench-scale cylindrical and rectangular packed beds using the CFD tool. The results are presented for operations at steady and unsteady state (e.g., periodic liquid feed), which have been previously examined in the studies of catalyst screening and reactor-performance enhancements (Khadilkar et al., 1999). The effect on the experiments of flow non-uniformity inside the packed bed are discussed. To explore the fluid dynamic mechanism for performance enhancement under periodic inflow mode, a comparison of flow distribution under steady state liquid feed and periodic liquid input in packed beds is given.

2. Flow Domain and its Description

The difficulties in modeling flow in catalytic packed beds are mainly due to the complex nature of the flow domain that is formed by passages around randomly packed particles. The structure of this interstitial space inside the packed bed is mainly determined by particle size (d_p), particle shape (ϕ), ratio of column diameter and particle diameter (D_r/d_p), and the packing method. Experimental measurement and computer simulation of porosity distribution in packed beds have been the subject of many investigations for a considerable period of time (Benenati and Brosilow, 1962; Jodrey and Tory, 1981). Although the detailed 3D porosity information can be achieved through computer simulation of random packing (Jodrey and Tory, 1981), an axisymmetric description of 2D porosity distribution, ε (r, z), can be considered a good approximation in a certain sense. The longitudinally averaged radial porosity profile, ε (r) was experimentally found to oscillate for a distance of 3 ~ 4 particle diameters from the wall, whereas the cross-sectional averaged porosity along the length of the bed, ε (z), is distributed randomly (Borkink et al., 1992). For flow simulation purpose, in axisymmetric cylindrical coordinates (r-z) one can generate a 2D pseudo-random porosity distribution constrained by the mean porosity and radial porosity profile (i.e., ε (r)). Figure 1 shows such generated porosity distribution by displaying the porosity profiles ε (r) and ε (z). The dimension of the reactor in Figure 1 is 22.5 cm in length and 2.4 cm in diameter. The spherical particles used are 1.5 mm in diameter. It is well known that for a given reactor, the radial porosity profile, ε (r) is changed with the change in particle diameter, and the axial profile, (ε (z) varies with repacking (Benenati and Brosilow, 1962), but the mean porosity retains the same value.

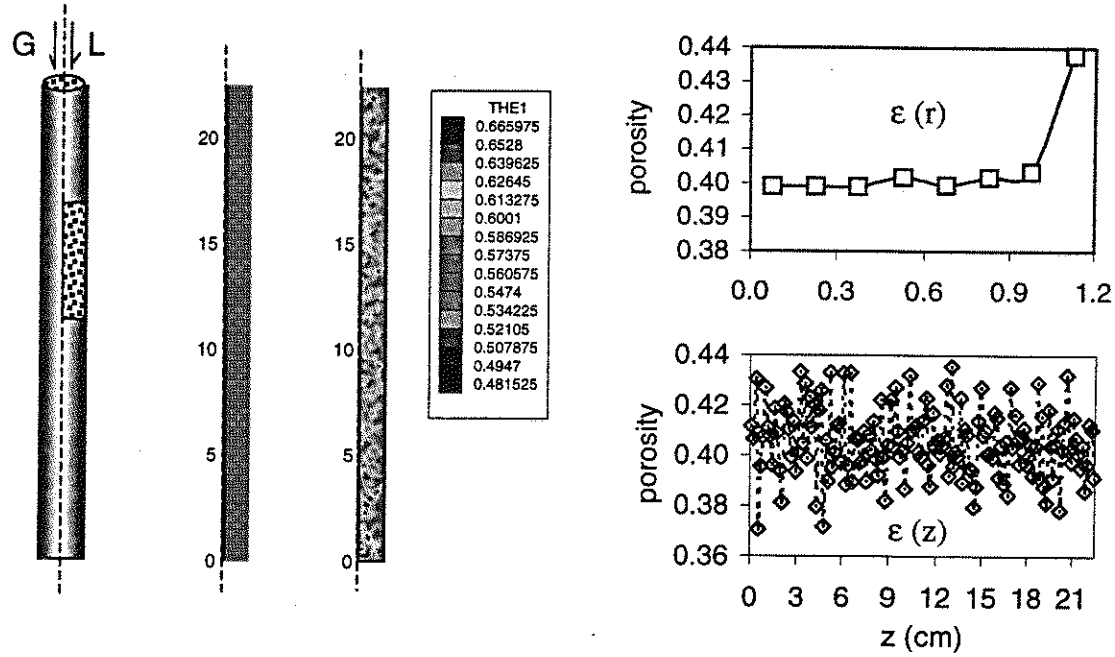

Figure1 Bench-scale cylindrical packed-bed and its porosity description (a) computer generated 2D axisymmetric solid volume fraction distribution; (b) radial porosity profile, ε (r); (c) axial porosity profile, ε (z).

We also generated a 2D porosity distribution in x-y coordinates for a bench-scale rectangular bed packed with 3 mm particles as used in our discrete cell model approach (see Jiang et al., 1999; 2000a). The inflow gas is distributed uniformly with given superficial velocity whereas inflow liquid is treated as either in steady flow or in periodic flow with uniform or non-uniform distributors.

3. Ensemble-averaged Two Fluid Model

The ensemble-averaged Eulerian/Eulerian k-fluid model implemented via CFDLIB, developed by Los Alamos National Laboratory (Kashiwa et al., 1994), is used as a transient multiphase flow simulation tool. The model has been adapted to the packed bed, and therefore, can handle gas and liquid cocurrently flowing downwards with a stationary solid phase (Kumar 1995, Khadilkar, 1998; Jiang et al, 1999). The detail descriptions of CFD modeling efforts and model applications in packed-beds are available elsewhere (Jiang et al., 2000b). Here we only provide the key flow equations and the closure laws for trickle-bed modeling as follows:

Equation of continuity:

$$\frac{\partial \rho_k}{\partial t} + \nabla \cdot \rho_k u_k = 0 \qquad (1)$$

Equation of momentum:

$$\frac{\partial \rho_k u_k}{\partial t} + \nabla \cdot \rho_k u_k u_k = F_{D(k-l)} + \rho_k g + \theta_k \nabla p - \nabla \cdot < \alpha_k \rho_0 u_k' u_k' > \qquad (2)$$

The momentum exchange term [$F_{D\ (k\text{-}l)}$] is expressed as a product of the exchange coefficient, phase volume fractions, and relative velocity of the two phases k and l as below

$$F_{D(k-l)} = \theta_k \theta_l X_{kl} (u_k - u_l) \tag{3}$$

X_{kl} is calculated by the two-phase flow Ergun equation (Holub et al., 1992) in which constant Ergun parameters are used in this study (E_1=180, E_2=1.8) and the discussion of choosing constant Ergun parameters is given elsewhere (Jiang et al., 2000a). Thus, the exchange coefficient between liquid and solid phase (L-S) and gas and solid phase (G-S) can be written as

$$X_{ks} = \left(A_{ks}\mu_k V_k + B_{ks}\rho_k V_k^2\right)\frac{1}{(1-\varepsilon)|u_k|} \tag{4a}$$

$$A_{ks} = 180\frac{(1-\varepsilon)^2}{\theta_k^3 d_p^2} \tag{4b}$$

$$B_{ks} = 1.8\frac{(1-\varepsilon)}{\theta_k^3 d_p} \tag{4c}$$

For gas-liquid drag [$X_{(G\text{-}L)}$] either no interaction is assumed for the low interaction regime or the drag coefficient of two-fluid interaction model (Attou et al., 1999) is used:

$$X_{gl} = \frac{\theta_g}{\varepsilon}\left(A_{gl}\mu_g V_r + B_{gl}\rho_k V_r^2\right)\frac{1}{(1-\varepsilon)|u_g - u_l|} \tag{5a}$$

$$A_{gl} = 180\frac{(1-\theta_g)^2}{\theta_g^3 d_p^2}\left(\frac{1-\varepsilon}{1-\theta_g}\right)^{2/3} \tag{5b}$$

$$B_{gl} = 1.8\frac{(1-\theta_g)}{\theta_g^3 d_p}\left(\frac{1-\varepsilon}{1-\theta_g}\right)^{1/3} \tag{5c}$$

$$V_r = \theta_g |u_g - u_l| \tag{5d}$$

The influence of phasic pressure differences due to the interfacial tension and the gradient of liquid volume fraction, which reflects the contribution of capillary force on liquid flow distribution, is also taken into account in pressure calculations by Equation (8). This equation was proposed by Grosser et al., (1988) and modified by Jiang et al. (1999) by introducing the particle wetting factor (f), which can be evaluated by the correlation of particle external wetting efficiency (see Al-Dahhan and Dudukovic, 1995).

$$p_L = p_G - (1-f)\frac{\theta_S E_1^{0.5}}{(1-\theta_S)d_p}\sigma_s\left[0.48 + 0.036\ln\left(\frac{1-\theta_S-\theta_L}{\theta_L}\right)\right] \tag{6}$$

The Reynolds stress term ($\nabla\cdot<\alpha_k\rho_0 u_k' u_k'>$) is negligible in simulating macroscale flow although it may be important for local scale flow modeling at high Reynolds number in packed beds (Jiang et al., 2000a).

4. Numerical Simulation Results and Discussions

To demonstrate the capability of this model, we examined both the spatial distribution and the temporal phenomena associated with liquid flow at steady state and under periodic inflow conditions. Figure 2 shows the spatial distributions of phase volume fraction, interstitial velocity and pressure at steady state inflow condition (U_{g0} = 6 cm/s and U_{l0} = 0.3 cm/s). Higher liquid holdup (THE2) occurs in higher porosity zones

(1.0-THE1) such as in the wall regions. Since local porosity value is changed by repacking the column even when using the same particles and procedure, it is clear that the point measurement of liquid-solid mass transfer coefficient $(ka)_{ls}$ using a conductivity method in repacked beds may result in a large scatter in data, which may lead to erroneous conclusions based on single point experiments. (Highfill, 1998). Local measurement with a fixed structural matrix may give some meaningful data by a statistically generated set of large number of experimental conditions (Latifi et al., 1989), which may be very time-consuming. Since the radial component of velocity is relatively much smaller than the axial component and also normally distributed around the zero value, only the axial velocity component (V_z) is shown in Figure 2 for the liquid (V_2) and the gas (V_3). Inspection of these figures indicate that the lower the porosity, the lower the liquid holdup, and the lower the liquid interstitial velocity. We do find some backflow of gas in Figure 2(e), which is similar to the experimental findings for liquid upflow inside packed beds reported by Sederman et al. (1997). The negative local gas velocity leading to local counter-current flow of gas and liquid may explain why in the high interaction regime the slit model of Holub et al (1992) needed to be modified by Al-Dahhan et al., (1998) to include a 'negative' slip between gas and liquid at the gas-liquid interface. More back mixing can be expected for gas flow in high pressure trickle-bed reactors due to the negligible gravity effect at elevated pressure. In general, pressure decreases along the bed axis (see Fig 2(f)), however, relatively lower pressure values occur at the wall region at each cross-section of the column due to higher porosity in proximity of the wall. This may cause errors in pressure measurement if one detects pressure just at the wall. Inserting multiple pressure sensors at different radial position is a way to avoid such errors, however, special care does need to be taken for the disturbance that the sensors can cause in the local flow distribution.

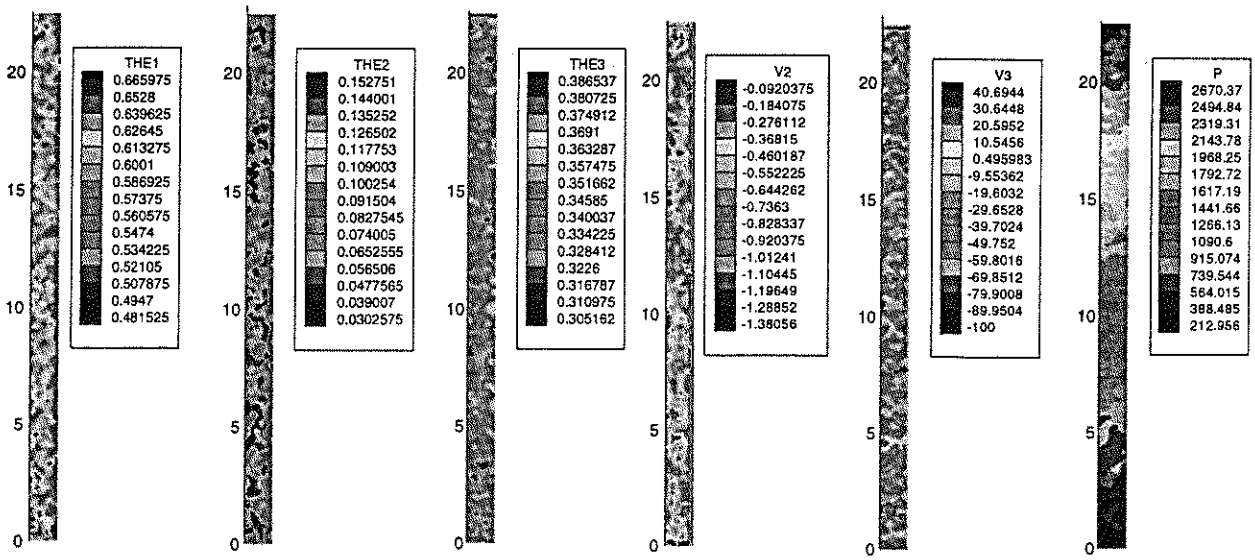

Figure 2 Contours of packed bed structure and corresponded hydrodynamic parameters: (a) solid holdup-THE1; (b) liquid holdup-THE2; (c) gas holdup-THE3; (d) axial liquid interstitial velocity-V2; (e) axial gas interstitial velocity -V3; (f) pressure at U_{g0} = 6 cm/s and U_{l0} = 0.3 m/s at steady state operation.

The temporal phenomena of liquid flow are shown in Figure 3 in a 1-inch cylindrical tube with uniform gas inflow but with a periodic liquid inflow (60s cycle time = 15s turn-on + 45s turn-off as used in reaction studies of Lange et al., 1994; Castellari & Haure, 1996; Khadilkar et al., 1999). Since the axisymmetric assumption is used in the simulation, there is no way to catch all the real time scales of the flow, but we are able to look at the time scale in the axial direction due to the dominant velocity component (V_z). It is found that the simulated liquid flow readily reaches the steady state values because the fluid cannot flow azimuthally. Once the front of the liquid stream reaches the bottom of the packed bed, the flow field is developed as shown in Figure 3. The liquid draining from the bed takes time and certain amount of liquid still stays in the bed even after another 15 seconds.

A test case with a possibility of significant liquid maldistribution was chosen for investigating the effects of induced liquid flow modulation. A 2D rectangular model bed of dimensions 29.7 cm × 7.2 cm was considered with pre-assigned porosity values to different cells (33 in the vertical (Y) direction and 8 in the horizontal (X) direction as shown in Fig 4a). Liquid flow was introduced at the two central cells at the top of the bed at mean superficial velocity of 0.1 cm/s, while gas flow was introduced in the rest of the cells at a superficial velocity of 10.0 cm/s in simulations of both steady and unsteady state operation. Steady state simulations show evidence of significant liquid maldistribution, particularly at the top and bottom of the reactor. Complete absence of liquid is seen in zones near the bottom of the reactor (Figure 4b (right)).

The liquid flow distribution observed in the steady state case was compared with transient simulations carried out with a liquid flow ON time of 15 seconds and a total cycle time of 60 seconds (45 seconds liquid OFF).

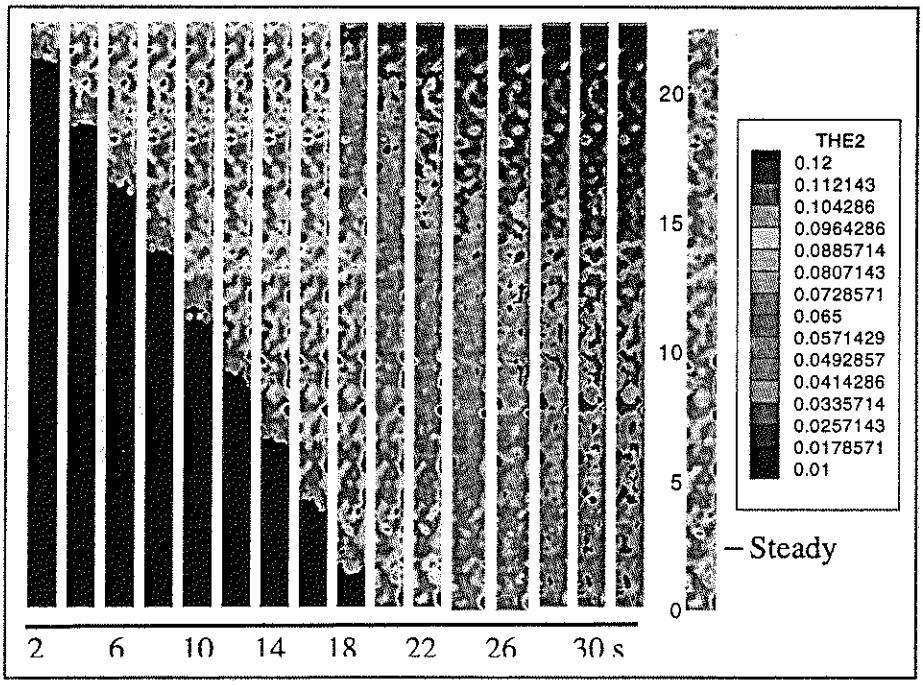

Figure 3 Liquid holdup distribution in a periodic liquid inflow modal (15s-on and 45s-off) (left) and steady sate modal (right) in 1-inch cylindrical packed bed at U_{g0} =6 cm/s and U_{l0} =0.3 cm/s.

Snapshots of liquid flow distribution were taken at several time intervals (t = 15, 25, 40 seconds from beginning of liquid ON time) to compare them with the steady state liquid holdup data obtained in the steady state case (Figures 4b, 4c, 4d). Liquid holdup variation over the reactor cross section is depicted at several axial locations at different times in a typical flow modulation cycle (Figures 5a-c). These figures clearly demonstrate that unsteady state operation ensures better uniformity in liquid distribution at all locations compared to that observed in steady state operation. This improved distribution, though not perfect, does ensure enhanced liquid supply to all locations not previously possible during steady state (in particular, the bottom zone shown in Figure 5a). This clearly shows that induced flow modulation results in better liquid spreading and even distribution of liquid over the entire cross section at each axial location at some point in time in the cycle. This also indicates that although the average liquid holdup at each location may not exceed the steady state holdup, the reactor performance may still be enhanced due to higher than steady state holdup for a sub-interval of the entire cycle. This time interval of enhanced liquid supply can allow exchange of liquid reactants and products with the stagnant liquid and with the catalyst pellets present in any particular zone. Another observation that can be made from Figure 4d is that for some time interval, all zones in the reactor become almost completely devoid of liquid, and can allow enhanced access of the gaseous reactant to externally dry catalyst during this time interval. Temperature rise and internal drying of catalyst and faster gas phase reaction may also occur in this interval, which can be quenched by the liquid in the next cycle.

The above simulation demonstrates the possibility of controlled rate enhancement due to induced flow modulation. It also facilitates our understanding and visualization of the phenomena occurring in the reactor. It confirms the reasons behind improved unsteady state performance observed experimentally and simulated in the reaction transport models (Khadilkar, 1998; Khadilkar et al., 1999; Lange et al., 1994; Castellari and Haure, 1995; Silveston, 1990). It seems that upon scale-up large reactors operated with flow modulation should perform with the same enhancement over steady state operation as seen in the scaled-down version.

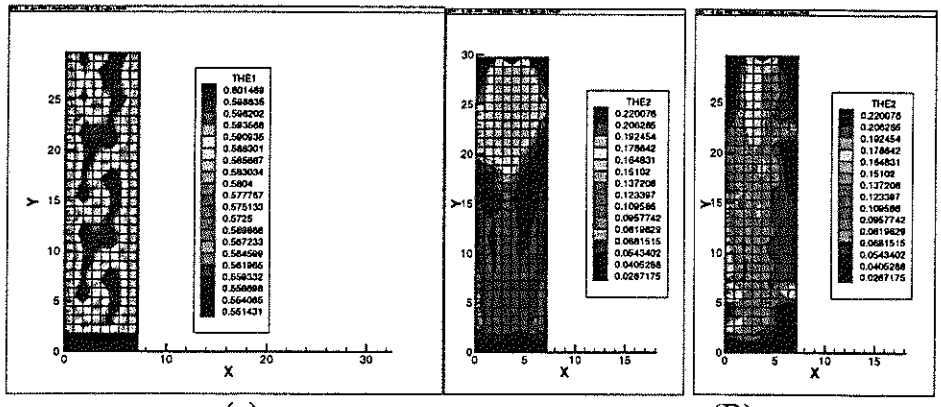

(a) (B)

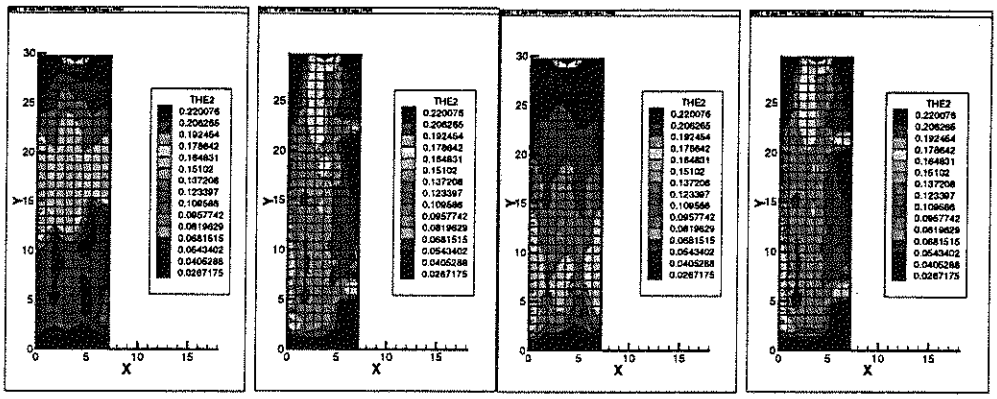

(c) (d)

Figure 4 (a) Solid holdup (THE1 = 1.0 - Bed Porosity) distribution in the model 2d rectangular bed. Snapshot of liquid holdup (THE2) contours at (b) t =15s; (c) t = 25s; (d) t = 40s from start of the liquid ON cycle (left) in comparison with steady state holdup contours (right).

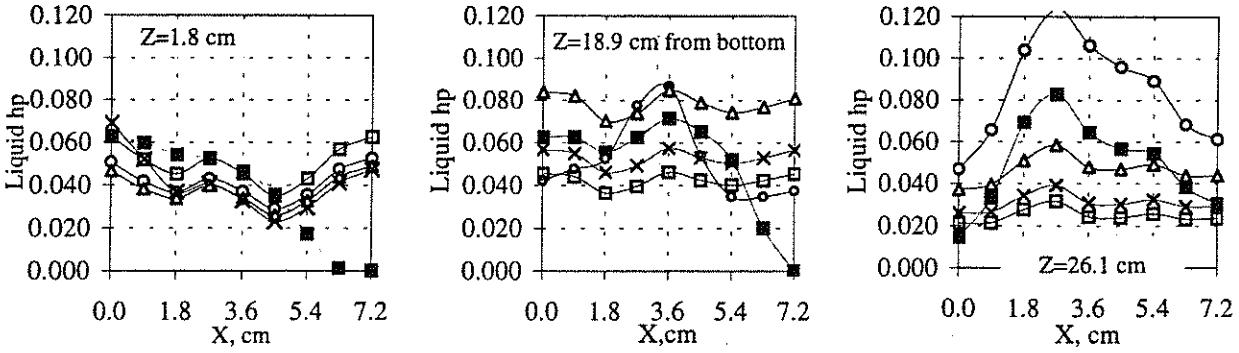

(a) (b) (c)

Figure 5 Comparison of cross sectional liquid holdup profiles at different axial locations under steady (filled squares) and unsteady state operation ((a), Z= 1.8 cm; (b), Z= 18.9 cm; (c), Z= 26.1 cm) (O-15s; Δ-25s; ×-40s; □-55s)

5. Concluding Remarks

CFD flow modeling of bench-scale packed beds provides valuable information for improving experimental protocol and data interpretation of scaled down reactors. The combination of this work with developed mixing-cell network model (Jiang et al., 1999b) allows one to evaluate the performance of packed-bed reactor more realistically, even for the system of complex reaction kinetics. Experimental validation of this work should be possible by using advanced non-invasive tomgraphic techniques such as MRI and high resolution CT.

REFERENCES

Al-Dahhan, M. H. and Dudukovic, M. P., *Chem. Engng Sci.*, 50, 2377-2389, (1995)

Al-Dahhan, M. H. and Dudukovic, M. P., *A.I.Ch.E. J.*, 42, 2594-2606 (1996)

Al-Dahhan, M. H., Khadilkar, M.R., Wu, Y. and Dudukovic, M. P., *Ind. Engng Chem. Res.* 37, 793-798 (1998)

Attou, A., Boyer, C. and Ferschneider, G., *Chem. Eng. Sci.*, 54, 785-802 (1999).

Benenati, R. F. and Brosilow, C. B., *A. I. Ch. E. J.*, 8, 359 (1962)

Borkink, J. G. H., van de Watering, C. G. and Westerterp, K. R., *Trans IChemE*, 70(A), 610-619 (1992)
Castellari, A. and Haure, P. M., *A.I.Ch.E. J.*, 41, 1593-1597 (1995)
Chaouki, J., Larachi, F. and Dudukovic, M. P., *Non-invasive monitoring of multiphase flows* (1997)
Christensen, G., McGovern, S. J. and Sundaresan, S., *A.I.Ch.E. J.*, 32, 1677-1689 (1986)
Crine, M, Marchot, P. and L'Homme, G. A., *Comp. Chen Engng* 3, 515 (1979)
Dankworth, D.C., Kevrekidis, I. G. and Sundaresan, S., *Chem. Engng Sci.*, 45, 2239 (1990)
De Wind, M., Plantenga, F. L., Heinerman, J. J. L. and Homan Free, H. W., *Appl. Catal.*, 43, 239 (1988)
Dudukovic, M. P., Larachi, F. and Mills, P. L., *Chem. Engng Sci.*, 54, 1975-1995 (1999)
Gieman, H., *Appl.Catal.*, 43, 277-286 (1988)
Gladden, L. F., *Chem.Engng Sci.*, 49, 3339-3408 (1994)
Grosser, K. A., Carbonell, R. G. and Sundaresan, S., *A.I.Ch.E. J.*, 34, 1850 (1988).
Highfill, S., M.Sc. Thesis, Washington University in St. Louis, MO, USA (1998)
Holub, R. A., Dudukovic, M. P. and Ramachandran, P.A., *Chem. Engng Sci.* 47, 2343-2348 (1992)
Holub, R. A., Ph.D. Thesis, Washington University in St. Louis, MO, USA (1990)
Jiang, Y., Khadilkar, M.R., Al-Dahhan and Dudukovic', M. P., *Chem. Engng Sci.* 54, 2109-2119 (1999a)
Jiang, Y., Al-Dahhan and Dudukovic', M. P., *AIChE Annual Meeting*, Dallas, TX (1999b).
Jiang, Y., Khadilkar, M.R., Al-Dahhan, M. H. & Dudukovic', M. P., *Chem. Engng Sci.* 55, 1829 (2000a)
Jiang, Y., Khadilkar, M.R., Al-Dahhan, M. H. & Dudukovic', M. P., CFD modeling of macro-scale flow pattern in packed beds, (*in preparation*) (2000b).
Jodrey, W. S. and Tory, E. M., *Power Technology*, 30, 111-118 (1981)
Krishna, R. and Sie, S. T., *Chem. Engng Sci.*, 49, 4029 (1994)
Kashiwa, B. A., Padial, N. T., Rauenzahn, R. M. and W. B. Vander Heyden, *ASME Symposium on Numerical Methods for Multiphase Flows*, Lake Tahoe, Nevada (1994)
Khadilkar, M. R., *Doctoral thesis*, Washington University, St. Louis, Missouri, USA (1998)
Khadilkar, R. M., Al-Dahhan, M. H. and Dudukovic, M. P., *Chem. Engng Sci.*, 54, 2585-2595 (1999)
Kumar, S. B., *CREL Annual Meeting Workshop*, Louis, MO, USA (1995).
Lange, R., Hanika, J., Strsdiotto, D., Hudgins, R. R. & Silveston, P. L, *Chem. Engng Sci.*, 49, 5615 (1994)
Latifi, M. A., Midoux, N. & Storck, A., *Chem. Engng Sci.*, 44, 2501 (1989)
Le Nobel, J. W. and Choufour, J. H., *Proc. 5th World Petroleum Congress.* Sect. III, 5th WPC Inc., New York, 233-243 (1959)
Lerou J. J. and Froment, G. F., *Chem. Engng Sci.*, 32, 853-861 (1977)
Logtenberg, S. A. and Dixon, A. G., *Chem. Engng Process.*, 37, 7-21 (1998)

Lutran, P. G., Ng, K. M. and Delikat, E. P., *Ind. Engng Chem. Res.*, 30, 951 (1991)
Mears, D. E., *Chem. Engng Sci.*, 26, 1361- 1366 (1971)
Reinecke N., Petritsch, G. Schmitz, D. and Mewes, D., *Chem. Engng Technol.*, 21, 7 (1998)
Sederman, A. J., Johns, M. L., Bramley, A. S., Alexander, P. and Gladden, L. F., *Chem. Engng Sci.*, 48, 2239-2250 (1997)
Sie, S. T. and Krishna, R., *Reviews in Chemical Engineering*, 14, 203-252 (1998)
Silveston, P. L., *in Unsteady State Processes in Catalysis*, 217-232 (1990)
Stanek, V., *Fixed Bed Operations: flow distribution and efficiency*, Ellis Horwood (1994)
Stephenson, J. L. and Stewart, W. E., *Chem. Engng Sci.*, 53, 1375 (1986)
Tasmatsoulis D. and Papayannakos, N., *Chem. Engng Sci.* 49, 523-529 (1994)
Van Klinken, J. and van Dongen, R. H. *Chem. Engng Sci., 35, 59-66* (1980)
Zimmerman, S. P. and Ng, K. M., *Chem. Engng Sci.*, 41, 861 (1986)

COMPUTATIONAL REACTION ENGINEERING

P.A. Ramachandran

Current research efforts of Professor Ramachandran are focused on (i) development of advanced numerical methods for simulation of complex problems in transport phenomena, ii) single and multiphase flow simulation and (iii) applications of mathematical modeling to chemical reaction engineering.

In the area of numerical methods, the work is focused on developing and implementing the boundary element method and the dual reciprocity method (DRM) to transport phenomena problems. It has been shown that the method is useful for a large class of transport problems. The developments in this field have been summarized in a recent book (Ramachandran, 1994). The advantages of the method are primarily due to easy mesh generation and extreme accuracy for linear and mildly non-linear problems. These advantages make the method an ideal candidate for moving boundary problems, inverse problems and problems with deformable geometry such as dynamics of single and multiple bubbles. In view of these diverse applications, we are examining the mathematical properties and convergence criterion of DRM and also developing several new concepts (such as p- and r-adaptations) to improve the accuracy of the method.

Several key publications have resulted in the course of this work. A comprehensive model to analyze the diffusion-reaction processes for a multiple set of linear kinetics has been developed and will be useful in reactor design of complex mixtures.

In the area of multiphase flow, the current focus is to solve flow problems in simulated geometries from first principles. Such studies are necessary to develop proper constitutive models for two phase flow. For example, the periodically constricted tube has been used to represent single phase flow through packed beds. Using flow simulations in complex geometries, it is possible to obtain insights into a number of transport processes in a packed bed such as axial dispersion, solid-liquid mass transfer, etc. Hence, research efforts in this direction will serve as a useful model for study of flow behavior in trickle-beds and packed bubble columns. The simulation of two phase flow is, however, considerably more complex than simulation of single phase flow. Prior work in this direction has been limited and the simulation has been confined to low Reynolds number in view of the computational difficulties. Hence the results have not been translated into practice. In view of the current developments in the numerical simulation and large scale computing, this area is expected to develop in a major way and make significant impact into reactor design. Work in this area using boundary integral methods is in progress in our laboratory and will provide a basis for flow and mass transfer modeling in simulated complex geometries. New formulations are likely to have advantages in transient flow simulations. Our efforts in this area will provide valuable insight in the design of trickle bed reactors. On a related theme, flow behavior around single and multiple bubbles is being investigated. It is expected that practical information useful to bubble column modeling will emerge as an outcome of this study. The prediction of drag forces, coalescence frequency, improved correlations for mass transfer, etc., would be the major contributions from this work. Thus, this work

complements the efforts in our laboratory on use of advanced experimental techniques for flow characterization such as CARPT and CT.

On the application side, it is proposed to investigate detailed simulation of various industrial processes such as hydrocracking, catalytic distillation, processes of interest in the manufacture of fine chemicals, etc., with active collaboration and participation from industry. Considerable work has already been done in this area and benefits to industry will be significant. One recent applied project under ARPA support is the modeling of thermo-oxidative stabilization of polyacrylonitrie (PAN) based carbon fiber. Carbon fibers are being increasingly used for structural applications. The manufacturing of carbon fibers consists of several steps. The first step is the reaction of PAN fiber with oxygen to form a stabilized product which can then be carbonized. A theoretical model is being proposed to predict and monitor the fundamental transport phenomena and chemical reactions within the complex stabilization process. This model utilizes some of my earlier work on single pore models for gas-solid non-catalytic reactions. The model considers the heterogeneous nature of the tow and is in conformity with experimental observation that a product layer develops around the core of the "PAN". Utilizing this physical picture, the model predicts the reacted core radius, oxygen concentration and temperature as a function of thickness within tow and at various positions in the oven. The model will be tested with experimental data available with Zoltek Corporation. The model for the second step of the carbon fiber production viz., carbonization is also being worked out. The ultimate goal of the modeling effort is the optimization of the process and development of strategies to reduce the cost of production.

The support of CREL participants is important to a successful completion of the above goals. It may also be noted that many of the above projects are neither fundamental nor purely applied but fall somewhere in the middle ground. Hence industrial support is perhaps the most effective source here in contrast to purely scientific agencies such as NSF. Two modes of support are sought (i) additional contribution from each participating company earmarked for computational reaction engineering and (ii) contract research in areas of interest to companies. The contribution of $5000 from each participating company would in itself provide a significant research base to complete the above activities. The benefits to the company is sustained support for scholarly research (as indicated by prior published work and citations thereof, monographs and books which are currently used by industrial practitioners) and increased understanding of complex problems in reaction engineering via advanced computer simulation. Further, additional support on a contract basis for individual projects will prove to be very cost effective for some of the company's activities. Such contracts will accelerate the progress of the projects and will give the company a significant edge over the competitors.

REFERENCES

1. P.A. Ramachandran, "*Boundary Element Methods in Transport Phenomena*", Computational Mechanics Publishers and Elsevier, Southampton, England, 1994.

2. S.R. Karur and P.A. Ramachandran, *Effectiveness Factor for Partially Wetted Catalysts*", Poster-paper 214-a4, AIChE Annual Meeting, St. Louis (1993).

3. S.R. Karur and P.A. Ramachandran, "*Dual Reciprocity BEM for Non-linear Diffusion-Reaction Problems in Porous Catalyst Particles*", AIChE Annual Meeting, Session 18-d, St. Louis (1993).

1. S.R. Karur and P.A. Ramachandran, "*Boundary Element Methods in Biomedical Engineering*", *Poster-paper, Biological and Biomedical Engineering Workshop,* Washington University (1994).

OSCULATORY INTERPOLATION IN THE METHOD OF FUNDAMENTAL SOLUTIONS FOR NON-LINEAR POISSON PROBLEMS

A. Problem Definition

The Poisson equation, $\nabla^2 u = f(x,u)$, where 'x' is the position vector and 'u' the dependent variable, is encountered in a variety of modeling situations in heat, momentum and mass transfer among others. Other examples of Poisson type of equations in computational physics include the Liouville equation, Chandrasekhar-Wares equation, Emden equation in astrophysics, geometry of conformal metrics, etc. The use of conventional numerical methods to solve such problems, viz., finite differences or finite elements, involve discretizing the entire domain of interest. For non-regular geometries, the process of element or grid generation and the associated 'book-keeping' of the nodes can prove cumbersome and expensive in the user time and the CPU time, especially for three-dimensional problems. Hence, in the last decade, there has been considerable interest to develop mesh-free methods to solve the nonlinear Poisson equation. *The Method of Fundamental Solutions (MFS)* belongs to the general class of boundary collocation methods [5] and in this procedure, the solution is represented as a set of layer potentials emanating from points located outside the solution domain. It is an eficient method for solving the Laplace equation and we have extended the method for efficient solution of nonlinear Poisson equations.

B. Research Objectives

The method of fundamental solution (also known as the Trefftz method or the singularity method) is an efficient numerical method for the solution of Laplace equation in R^n. In recent years, the method has also been applied for the solution of Poisson equations by finding the particular solution to the nonhomogeneous terms. In general, approximate particular solutions are constructed using the interpolation of the non-homogeneous terms by the radial basis functions. The method has been validated in recent papers.This manuscript presents an improvement of the solution procedure for such problems. The improvement is achieved by using radial basis functions called osculatory radial basis functions. Such functions make use of the normal gradient at boundary to obtain improved interpolation. The efficacy of the method is demonstrated for some prototypical non-linear Poisson problems and for multiple Poisson equations. The solution of these equations enables one to efficiently solve reaction diffusion problem in catalyst pellets in trickle bed reactors and can be used for the purpose of catalyst tailoring. The advantage of the method is that being grid free complex geometries can solved using the same effort as any regular shape. We illustrate this aspect using the trilobe which is a commonly used catalyst shape in the chemical industry.

C. Research accomplishments

The research accomplishments are discussed in the attached manuscript.

I. INTRODUCTION

The Poisson equation, $\nabla^2 u = f(x,u)$, where 'x' is the position vector and 'u' the dependent variable, is encountered in a variety of modeling situations in heat, momentum and mass transfer among others. Other examples of Poisson type of equations in computational physics include the Liouville equation, Chandrasekhar-Wares equation, Emden equation in astrophysics, geometry of conformal metrics, etc. The use of conventional numerical methods to solve such problems, viz., finite differences or finite elements, involve discretizing the entire domain of interest. For non-regular geometries, the process of element or grid generation and the associated 'book-keeping' of the nodes can prove cumbersome and expensive in the user time and the CPU time, especially for three-dimensional problems. Hence, in the last decade, there has been considerable interest to develop mesh-free methods to solve the nonlinear Poisson equation. Most common among these mesh free methods, is the dual reciprocity boundary element method [1-4]. Here, problem is decomposed into the solution of the Laplace equation by finding approximate particular solutions to the non-homogeneous terms. The Laplace equation in turn can be solved by a boundary-only discretization. This reduces the dimensionality of the problem by one but the method requires the evaluation of the singular integrals along the boundary. These singular integrations are easy to perform for 2-dimensional problems but can be computationally expensive for 3-dimensional case. As an alternative, one can adopt a solution procedure called the *Method of Fundamental Solutions (MFS)* to solve the Laplace part of the problem. The MFS belongs to the general class of boundary collocation methods [5] and in this procedure, the solution is represented as a set of layer potentials emanating from points located outside the solution domain. By doing so, one avoids the problem of evaluation of the singular integrals needed in the boundary element method and the dual reciprocity methods. Some pertinent prior references on the MFS method are summarized in the following paragraph.

The *Method of Fundamental Solutions* has been extensively applied for the solution of the linear partial differential equations. Some key references include the Laplace equation [6], the biharmonic equations [7], elasticity [8], fluid mechanics[9] and the linear diffusion reaction equations [10]. The method was applied to linear Poisson equation by combining this with the particular solution method [11]. More recently, the method has been extended to solve a non-linear Poisson problem (the thermal explosion problem) by Chen **[12] using the approximate particular Solutions and a simple Picard iteration to handle the iterations needed for the non-linear terms. The solution scheme for non-linear problems was improved by Balakrishnan and Ramachandran [13] who introduced the concept of a 'Matrix of Particular Solutions.' Improved iterations with the direct Newton-Raphson method could be done by this approach and the applicability of the method to a large class of nonlinear Poisson problems was demonstrated [13]. These studies [12,13] used the interpolation using the radial basis functions (RBF) for the representation of the Poisson terms and for the evaluation of the particular solution. The RBF uses only the function values at chosen points in the domain called as the knots or the centers. The information on the normal gradient at the boundary is available or needs to computed in most cases as the part of the solution for these classes of problems. The RBF approximation can be improved by using the normal gradients. This concept was introduced by Ramachandran and Karur [14] in the context of the dual reciprocity boundary element method and the basis functions which also fit the boundary values of the normal gradients were referred to as the osculatory radial basis functions (ORBF). The concept can be viewed as an extension of the familiar spline fitting commonly used in one dimensional data fitting. The ORBFs provide additional degrees of freedom, thereby permitting a more accurate interpolation with fewer number of interior knots. The purpose of the present paper is demonstrate the ORBF interpolation in the context of the MFS for non-linear Poisson problems and document the improvements in the solution as a result

of using this approach.. The layout of the paper is as follows. In Section II, a brief synopsis of the method of fundamental solution for nonlinear Poisson problems is presented in order to provide the necessary background. In Section III, we present the concept of osculatory interpolation and its implementation in the method of fundamental solution. Results for nonlinear Poisson problems with uniform and mixed boundary conditions are presented in Section IV and the concluding Section V, summarizes the key findings.

II. THE PARTICULAR SOLUTION METHOD

Consider the Poisson equation, to be solved over a domain Ω in R^2 or R^3 with enclosing boundary Γ,

$$\nabla^2 u = f(x, y, z, u) \text{ in } \Omega \tag{1}$$

with the following mixed boundary conditions imposed over the boundary Γ,

Dirichlet:

$$u = \bar{u} \text{ over } \Gamma_1 \tag{2a}$$

Neumann:

$$\frac{\partial u}{\partial n} = p = \bar{p} \quad \text{over} \quad \Gamma_2 \tag{2b}$$

where $\Gamma_1 + \Gamma_2 = \Gamma$ and the 'bar' denotes prescribed values.

Also, the more general case of Robin boundary conditions can also be considered with,

$$\frac{\partial u}{\partial n} + h\, u = -\, h\, u_o \quad \text{over } \Gamma_2 \tag{2c}$$

where 'h' is the heat/mass transfer coefficient and u_0 is the prescribed value of u of the surroundings. This boundary condition needs only minor modifications to the solution scheme.

In the method of particular solution, the solution is expressed as the sum of the homogenous problem with a set of modified boundary conditions and the particular solution which satisfies no particular set of boundary conditions, i.e.,

$$u = v + w \tag{3}$$

where, the function v satisfies the Laplace equation:

$$\nabla^2 v = 0 \text{ in } \Omega \tag{4}$$

and the function w is a particular solution defined as the solution to:

$$\nabla^2 w = f \ in \ \Omega \tag{5}$$

Thus the problem is solved as two separate parts as indicated by Eq. (3).

The solution to the homogeneous part 'v' can be obtained by the method of fundamental solutions. Here 'v' is expressed as,

$$v = \sum_{i=1}^{nb} a_i G_i \tag{6}$$

where 'G_i' is the fundamental solution to the Laplace equation, with the pole or source located at a point 'i' which is outside the domain under consideration. The coefficients a_i are found by boundary collocation, i.e. making Eq. (6) satisfy the boundary condition (on the variable v) at nb number of boundary points. The form for G_i is shown in Table 1 for two and three dimensional cases.

Table 1: The form of the fundamental solution and the particular solutions needed for the solution

2-D Case
Fundamental solutions $$G_i = -\ln r_i$$ where r_i = Euclidean distance from the pole 'i' Also $G_o = 1$ and hence the less number of source point is $nb - 1$ **Particular solutions for multiquadric** $$\psi_k \text{ or } n_k = -\frac{c^3 \log\{c\phi_k + c^2\}}{3} + \frac{\{(r_k^2 + 4c^2)\phi_k\}}{9} \text{ with } C = C_1 \text{ or } C$$
3-D Case
Fundamental solutions $$G_i = r_i^{-1}$$ **Particular solutions for multiquadric** $$\psi_k \text{ or } n_k = -\left(\frac{5c^2}{24} + \frac{r_k^2}{12}\right)\phi_k + \frac{c^4\,[\ln(r_k + \phi_k) - \ln(c)]}{8r_k} \text{ with } c = c_1 \text{ or } c_2$$

In order to evaluate the particular solution, the forcing function 'f' is approximated over Ω using radial basis functions, ϕ_k , for example, linear RBFs, thin plate spline (TPS) or multiquadrics (MQ) or RRFs compact with supports (CSRBF). Thus,

$$f = \sum_{k=1}^{nt} \phi_k \alpha_k \tag{7}$$

where α_k are a set of expansion coefficients obtained by collocating at a total of nt nodes in accordance to the following equation:

$$f_j = \sum_{k=1}^{nt} \phi_{jk} \alpha_k \quad j = 1,2,..., nt \tag{8}$$

where ϕ_{jk} is the function ϕ_k evaluated at any point j.

Eq (8) can be expressed in vector-matrix form:

$$\vec{f} = \tilde{\Phi}\vec{\alpha} \text{ or } \vec{\alpha} = \tilde{\Phi}^{-1}\vec{f} \tag{9}$$

The particular solution, 'w' which satisfies equation (5), is obtained from the particular solutions to each of the ϕ_k functions, and can be expressed as,

$$w = \sum_{k=1}^{nt} \psi_k \alpha_k \tag{10}$$

where ψ_k is given by:

$$\nabla^2 \psi_k = \phi_k \tag{11}$$

The explicit form of ψ_k can be evaluated for each type of RBF ϕ_k and the form for multiquadric (MQ) are given in Table 1 for both 2- and 3-D cases. The MQ function is defined as,

$$\nabla^2 \psi_k = \phi_k = \sqrt{c^2 + r_k^2} \tag{12}$$

where 'c' is known as the shift parameter.
Now since the solution $u = v + w$, for computational efficiency, the two parts of the solution can be combined and the composite solution can be expressed as:

$$u = \sum_{i=1}^{nb} a_i G_i + \sum_{k=1}^{nt} \psi_k \alpha_k \tag{13}$$

Using the inverse transformation in equation (9) and collocating at all the points one can rewrite this equation in vector form a as,

$$\vec{u} = \tilde{G}\vec{a} + \tilde{\Psi}\tilde{\Phi}^{-1}\vec{f} \tag{14}$$

or

$$\vec{u} = \tilde{G}\vec{a} + \tilde{\beta}\,\vec{f} \tag{15}$$

where $\beta = \tilde{\psi}\,\phi^{-1}\beta$ is called the Matrix of Particular Solutions. Eq (15) is then the compact representation of the solution.

For a Dirichlet problem one chooses '*nb*' collocation points on the boundary Γ and *nt-nb* interior points and *ne-1* source points outside the boundary. The equations for each u_k are assembled and the unknowns which are 'a_i' s and the concentration at the interior points are obtained using a Newton Raphson scheme. The details of the method can be obtained in [13]. We now proceed to the discussion of osculatory interpolation and its implementation in the above formulation.

III. OSCULATORY INTERPOLATION FOR PARTICULAR SOLUTIONS

Ramachandran and Karur (1998) introduced the concept of osculatory interpolation using radial basis function. Here the interpolation of the function '*f*' is carried out using not only the nodal values of the dependent variable but also the normal gradient at the boundaries. This requires '*nb*' additional degrees of freedom for providing the slope conditions at the '*nb*' boundary points. The interpolating equations for the forcing function '*f*' is now written as,

$$f = \sum_{k=1}^{nt} \phi_k \alpha_k + \sum_{k=1}^{nb} \varphi_k \delta_k \tag{16}$$

where the additional set of interpolating functions, φ_k which are linearly independent of ϕ_k, are introduced and δ_k are the corresponding additional interpolating coefficients. In this study the functions ϕ_k and φ_k are both chosen as multiquadrics $(c^2+r^2)^{1/2}$ with two different shift parameters. This maintains the linear independence between the two functions. Alternative choices are possible, for example ϕ_k as linear RBFs and ψ_k as TPS etc. but these are not analyzed in the computational studies presented here.

To evaluate the interpolating coefficients, one imposes the following conditions,

1. At all the interpolating nodes (boundary and interior), we set $f = f_i$, the nodal value of the forcing function, i.e.,

$$f_i = \sum_{k=1}^{nt} \phi_{ik} \alpha_k + \sum_{k=1}^{nb} \varphi_{ik} \delta_k \quad (\text{i} = 1,2,..\text{nt}) \tag{17}$$

2. At the 'nb' boundary points, the osculation conditions are imposed, i.e.,

$$\left.\frac{\partial f}{\partial n}\right|_i = \sum_{k=1}^{nt}\left(\frac{\partial \phi_k}{\partial n}\right)_i \alpha_k + \sum_{k=1}^{ne}\left(\frac{\partial \varphi_k}{\partial n}\right)_i \delta_k \quad (\text{i} = 1,2,\ldots\text{nb}) \tag{18}$$

The equations can be setup in matrix form as shown in equation (11) below and the coefficients α_k and δ_k are given by equation (12).

$$\begin{pmatrix} \vec{f} \\ \vec{f}' \end{pmatrix} = \begin{pmatrix} \tilde{\phi} & \tilde{\varphi} \\ \tilde{\phi}' & \tilde{\varphi}' \end{pmatrix} \begin{pmatrix} \vec{\alpha} \\ \vec{\delta} \end{pmatrix} \tag{19}$$

$$\begin{pmatrix} \vec{\alpha} \\ \vec{\delta} \end{pmatrix} = \begin{pmatrix} \tilde{\phi} & \tilde{\varphi} \\ \tilde{\phi}' & \tilde{\varphi}' \end{pmatrix}^{-1} \begin{pmatrix} \vec{f} \\ \vec{f}' \end{pmatrix} \tag{20}$$

This gives us the requisite coefficients for the interpolation scheme. We now proceed in a manner similar to Section II. The homogenous solution is evaluated as before. To evaluate the particular solution, one now defines two sets of particular solutions ψ, η satisfying

$$\nabla^2 \psi_k = \phi_k \tag{21}$$

$$\nabla^2 \eta_k = \varphi_k \tag{22}$$

The expressions for ψ, η with multiquadrics are given in Table 1. The solution to the problem 'u' is now given by,

$$u = \sum_{i=1}^{nb} a_i G_i + \sum_{k=1}^{nt} \psi_k \alpha_k + \sum_{k=1}^{nb} \eta_k \delta_k \tag{23}$$

and the normal gradient 'p' is given by,

$$p = u' = \sum_{i=1}^{nb} a_i \frac{\partial G_i}{\partial n} + \sum_{k=1}^{nt} \frac{\partial \psi_k}{\partial n} \alpha_k + \sum_{k=1}^{nb} \frac{\partial \eta_k}{\partial n} \delta_k \tag{24}$$

Substituting for α_k and δ_k from equation (20) we get the required collocation equations,

$$\begin{pmatrix} \vec{u} \\ \vec{b} \end{pmatrix} = \begin{bmatrix} \tilde{G} \\ \tilde{G}' \end{bmatrix} \vec{a} + \begin{bmatrix} \tilde{\psi} & \tilde{\eta} \\ \tilde{\psi}' & \tilde{\eta}' \end{bmatrix} \begin{pmatrix} \tilde{\phi} & \tilde{\varphi} \\ \tilde{\phi}' & \tilde{\varphi}' \end{pmatrix}^{-1} \begin{pmatrix} \vec{f} \\ \vec{f'} \end{pmatrix} \tag{25}$$

Equation (25) is now the representation of the solution when using the ORBF for constructing the particular solution.

For any given problem, the equations for the *'nt'* nodal values of *'u'* and *'nb'* normal gradients at the boundary are assembled and solved for the unknown coefficients a_i and the unspecified boundary values of *'u'* and fluxes and in addition the *(nt-nb)* interior values of *'u'*. The test cases and results for a few prototypical problems are discussed in the next section.

IV. TEST CASES AND RESULTS

In this section we demonstrate the efficacy of the solution procedure discussed in the earlier sections for some typical problems. We first consider a nonlinear diffusion reaction equation in a circular geometry. The governing equation is chosen as:

$$\nabla^2 u = \phi^2 u^n \ in \ \Omega \tag{26}$$

where, ϕ is the Thiele modulus which is the ratio of kinetic to transport resistances in the domain. The larger the Thiele modulus, the steeper the profiles of the dependent variable and the for very large Thiele moduli, a boundary layer of $O(1/\phi)$ is present. In such cases, traditional methods, such as finite elements require a fine discretization of the region near the boundary layer for increased accuracy. Here we demonstrate that a coarse mesh can provide reasonably accurate results when osculatory interpolation is used. Both uniform and non-uniform boundary conditions are considered.

The geometry was a circle of radius 1.0 and the 8 boundary nodes and 17 interior nodes were used for the discretization. The location of the nodes and the source points is shown in Figure 1. The shift parameters for MQ are fixed as $c_1 = 0.8$ and $c_2 = 1.0$ for the functions ϕ_k and ψ_k, respectively.

Case 1: Dirichlet Conditions

We first consider a first order reaction ($n = 1$) with Dirichlet boundary conditions for which case analytical solutions are available, viz.,

$$u = \frac{I_0(\phi r)}{I_0(\phi)} \ in \ \Omega \tag{27}$$

$$\frac{\partial u}{\partial n} = \frac{\phi I_1(\phi r)}{I_0(\phi)} \ on \ \Gamma \tag{28}$$

The comparison of the solutions are shown in Table 2 along with those without osculatory interpolation using MQ. As one can see the gradient values using osculatory interpolation are much more accurate than with traditional RBF interpolation. Even for Thiele moduli as high as 10, and the first interior point well outside the boundary layer, (O(0.5)), the fluxes are calculated with 2%. The concentration values are shown in Table 3 and compared with analytical solution. The concentration values for ϕ=10 are not representative since the nodes should be shifted closer to r = 1 here. But it is remarkable that the normal gradients are still predicted accurately.

Table 2: Normal gradient values for $n = 1$ for a first order reaction

Thiele modulus	Normal MQ	% relative error	ORBF solution	% relative error	Analytical
5	4.949	10.78	4.458	0.2	4.467
10	13.451	41.8	9.087	4.2	9.486

Table 3: Concentration profiles for a first order reaction ($n = 1$) for Case 1.

Location, r	Concentrations $\phi = 5$		Concentrations $\phi = 10$	
	ORBF	Analytical	ORBF	Analytical
0.5	0.1247	0.1208	0.045	0.0097
0.25	0.0537	0.0525	-0.003	0.0012
0.0	0.0377	0.0367	2.9E-03	3.55E-04

Table 4: Concentration profiles for a second order reaction ($n = 2$) for $\phi = 5$: Effect of MQ shape parameter: Dirichlet Condition

Location	BEMID Solution	ORBF1 $c_1 = 0.4, c_2 = 0.2$	ORBF2 $c_1 = 0.8, c_2 = 1.0$
0.9	0.7189	0.7081	0.7182
0.7	0.4372	0.4274	0.4366
0.0	0.2196	0.2153	0.2187
Gradient	3.6568	3.8259	3.6623

The case of second order reaction ($n = 2$) is considered next and the results are presented in Table 4. Here 16 boundary nodes and 65 interior nodes are used as shown in Figure 2. All the subsequent results have the same discretization. The finer discretization level was used to demonstrate the accuracy which can be obtained using osculatory MFS. Here the solution is compared with the numerical solution by a 1-D code BEMID (Ramachandran, 1993) which is considered to be sufficiently accurate for comparison purposes. The error in normal gradients here is 4% but by adjusting the shift parameters the error dropts to 0.8%. The concentration values match within the third decimal place for this choice of shift parameter and are not very sensitive to the shift parameters within a certain range. Optimization of the shift parameter is not considered here but it may be noted that this is an area of active research in the field of RBF and more developments can be expected in the future.

Case 2: Dirichlet Conditions: Complex Rate Models

Here we tested the programs for various non-linear rate forms which are some prototypical problems in physics and engineering. Results for the following three cases are presented in Table 4.

Case 1: Liouville equation.

$$f = \frac{\lambda^2}{8} \exp(-u) \tag{29}$$

which is encountered in many physical situations. Here λ^2 was set as 40 for numerical studies.

Case 2: Thermal explosion problem:

$$f = \exp(u - 1) \tag{30}$$

This represents a situation with an exponentially increasing thermal source in an confined space and the solution to this problem is needed for a safe design of combustion and other exothermic processes.

Case 3: Substrate inhibition kinetics:

$$f(u) = \phi^2 u / (1 + \alpha u + \beta u^2) \tag{31}$$

This problem is a representation of enzyme catalyzed biochemical reaction. The parameters chosen were $\phi^2 = 1040, \alpha = 50$ and $\beta = 1000$ and the problem has multiple steady states here. The results shown in Table 4 reproduced one of the steady states accurately. Bifurcation studies using this method in combination with programs such as 'AUTO' [15] can be done to check if all the steady states are predicted by this numerical scheme. We have not performed such studies and the more detailed bifurcation analysis are outside the theme of this paper.

Table 5: Solutions for exponential and substrate inhibited rate forms; Dirichlet conditions; c_1= 0.8, c_2=1.0

Rate form → Locations	Liouville equation f = 5 exp(-u)	Thermal explosion f = -exp(u-1)	Substrate inhibition f = 1040u/(1+50u+1000u^2)
u at r = 0.9	0.8589	1.0568	0.9438
u at r = 0.7	0.5964	1.1559	0.8445
u at r = 0.0	0.1127	1.3176	0.6796
p at r = 1.0	1.4332	-0.5900	0.5821

Case 3: Mixed Boundary Conditions

The advantage of a grid free method is fully realized for problems with mixed boundary conditions and nonregular geometries. This case demonstrates the efficacy of the method for a nonlinear forcing function, viz., a second order reaction with Dirichlet and Neumann boundary conditions imposed over various parts of the perimeter. Here is a unit circle considered with Dirichlet conditions (u=1) are imposed over the first and third quadrants and Neumann conditions (q=0) are imposed over the rest of the perimeter. It is to be noted that at the junction of the Dirichlet and Neumann boundaries, the flux is undefined and increases rapidly and is singular at

the junction. Representative profiles of 'u' for a Thiele modulus of 5.0 are shown for an partially wetted infinite cylinder (Table 6). The profiles qualitatively agree with those expected.

Table 6: Results of mixed (D-N) boundary condition

Boundary Values	$n = 1$	$n = 2$
p at $\theta = 0$	5.4699	4.8450
p at $\theta = \pi/8$	4.5224	3.9075
C at $\theta = 5\pi/8$	0.1693	0.3623
C at $\theta = 3\pi/4$	0.0233	0.2105
C at origin	0.0198	0.1770

Case 4: Multiple differential equations

To illustrate the efficacy of the procedure for a system of non-linear equations, we consider the hypothetical reaction scheme,

$$A \underset{k_2}{\overset{k_1}{\Leftrightarrow}} B \underset{k_4}{\overset{k_3}{\Leftrightarrow}} C$$

where the reversible reactions between A & B are assumed to be second order and the reaction from B to C is assumed to be first order.The governing equations for the independent species A & B system are given by,

$$\nabla^2 u_1 = k_1 u_1^2 - k_1 u_2^2 \tag{32}$$

$$\nabla^2 u_2 = k_3 u_2 + k_2 u_2^2 - k_1 u_1^2 - k_4 u_3 \tag{33}$$

$$\nabla^2 u_3 = k_4 u_3 - k_3 u_2 \tag{34}$$

The values of the constants for a typical simulation were, $k_1 = 5.0$, $k_2 = 1.0$, $k_3 = 5.0$. The concentration profiles of each species for a partially wetted infinite cylinder are shown in Figure 6. The solution procedure adopted was to solve the individual diffusion reaction equations separately. An initial guess for u_2 is used to start of the solution of the equation for A, and the values of u_1, u_2 , u_3 are updated with each iteration till convergence is obtained (change in sum of the squared error ~ $1e\text{-}9$).

Table 7: Results of for multiple reactions - mixed (D-N) boundary conditions as in Case 3

Boundary Values	*A*	*B*	*C*
p at $\theta = 0$	1.5645	-0.2398	-1.3248
p at $\theta = \pi/8$	1.1123	-0.2337	-0.8786
C at *(0,0)*	0.5743	1.0034	1.4223

More efficient convergence schemes can be used but our objective here was to see how the particular solution method works for multiple reactions. This has not been done in any of the earlier studies. The results indicated that the method is efficient for multiple differential equaitons of the Poisson type also. The particular solution for each individual reactions are dependent on each other but this coupling appears to produce no numerical problems.

Case 5: Nonregular geometries

In this case, we demonstrate the efficacy of the method for solving nonlinear problems in nonregular domains. We consider the example of a trilobe, shown in Figure 7. Here a third of the trilobe is discretized using the symmetry of the domain, and the Dirichlet-Neumann boundary conditions are applied over the boundary. The two cases we consider are

(i) Dirichlet - concentration of 1.0 all over the perimeter,

(ii) Dirichlet-Neumann - concentration of 1.0 over some part of the perimeter and no flux over the remainder of the perimeter.

The concentration profiles for each case with a value of ϕ=5.0 are shown in Figures 9&10, which agree qualitatively with those expected.

This study represents a case where the geometry is complex and has a 360^0 re-entrant corner. The results show that the procedure works well for this case thus indicating the generality of the method.

V. CONCLUSIONS AND SUMMARY

In this paper, we present an extension of the a grid free solution technique called the Method of Fundamental Solutions, for solving nonlinear Poisson problems. The solution method presented here uses a set of nodes in the interior in order to interpolate the function values. It may be noted that this interpolation is needed only for the purpose of obtaining an approximate particular solution. Thus there is no need to approximate any differential operators (second derivatives here) in the interior and hence a source of error associated with the finite difference and finite elements is eliminated. Further, the nodes can be distributed in any order in the interior and no special book-keeping or tracking of inter-element continuity is needed. This is another advantage of the method. Once the particular solution is obtained, the problem is reduced to a boundary collocation problem. This problem is solved by choosing a set of boundary collocation nodes and a corresponding set of source nodes which are placed outside the domain of solution. The set of collocation equations are then written for all the function values at the internal and boundary nodes as well as for the normal gradients at the boundary collocation points. These normal gradient values are also included in the interpolation of the function which is then referred

to as the osculatory interpolation. The osculation is similar to a spline fitting and permits the function to take the correct slope at each of the boundary collocation points. This increases the accuracy of the solution. The accuracy has been demonstrated for a number of test problems The test problems include systems with a complex geometry and a case of mixed boundary conditions.. Further, the method has been applied for the first time for the solution a system of differential equations and the results are impressive. For the solution of systems with larger complex domain, the method can be used in conjunction with the domain decomposition. The domain decomposition will be very effective here since many of the matrix coefficients (associated with, for example, the matrix of a particular solution) can be used in various subdomains. Further, although the results presented in this paper are for 2-dimensional problems, the method is directly applicable to 3-d or even higher dimensions. The only changes are in the expressions for the fundamental solution and the form of the particular solution as indicated in Table 1. Thus the computer programs for implementing the method is independent of the dimensionality of the problem which is a unique feature of this method.

References:

1. P.W. Partridge, C.A. Brebbia and L.C. Wrobel, *'The Dual Reciprocity Boundary Element Method'*, Computational Mechanics Publications, 1992.
2. P.A. Ramachandran, *'Boundary Element Methods in Transport Phenomena'*, Computational Mechanics Publications, Boston, 1993.
3. Karur and Ramachandran, *'Radial Basis Function Approximation in the Dual Reciprocity Method'*,Mathematical and Computer Modeling, 20, 7, 59-70, 1994.
4. S. Ahmad, and P.K. Banerjee, *'Free Vibration Analysis by BEM particular integrals'*, Journal of Engineering Mechanics, 112, 682-695.
5. I.Herrera, 'Trefftz Method' in Topics in the Boundary Element Method, edited by C.A. Brebbia (Springer-Verlag, New York, 1984).
6. G.Fairweather, A.Karageorghis, *'The method of fundamental solutions for elliptic boundary value problems'* , Advances in Computational Mathematics, 9,69-95, 1998.
7. A.Karageorghis and G.Fairweather, *'The simple layer potential method of fundamental solutions for certain biharmonic problems'*, International Journal of Numerical Methods in Fluids, 9, 1221-32,1989.
8. W.G.Jin, Y.K.Cheung, and O.C.Zienkewicz, *'Application of the Trefftz Method in plane elasticity problems'*, International Journal for Numerical Methods in Engineering, 30, 1147, 1990.
9. L.C. Nitsche and H. Brenner, *'Hydrodynamics of particulate motion in sinusoidal pores via a singularity method'*, AIChE Journal, 36(9), 1403-1419, 1990.
10. C.S.Chen, Y.F.Rashed, and M.A.Golberg, *'A mesh free method for linear diffusion equations'*, Numerical Heat Transfer,
11. M.A. Golberg, and C.S. Chen, *'Discrete Projection Methods for Integral Equations'*, Computational Mechanics Publications, Southampton, 1996.
12. C.S.Chen, *'The method of fundamental solutions for non-linear thermal explosions'*, Commmunications in Numerical Methods in Engineering, 11,675, 1995.
13. K.Balakrishnan, and P.A. Ramachandran, *'A Particular Solution Trefftz Method for Non-linear Poisson Problems in Heat and Mass Transfer'*, Journal of Computational Physics, 150, 239-267, 1999.
14. P.A. Ramachandran, and S.R. Karur, *'Multidimensional interpolation using osculatory radial basis functions'*, Computers and Mathematics with Applications, 35,11,63-73,1998.

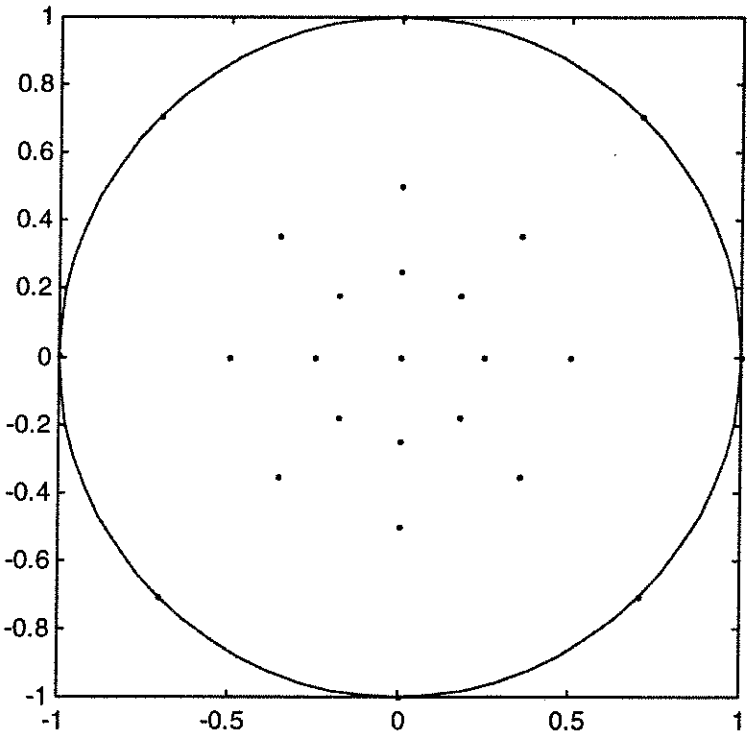

Figure 1: Coarse node placement for the circle

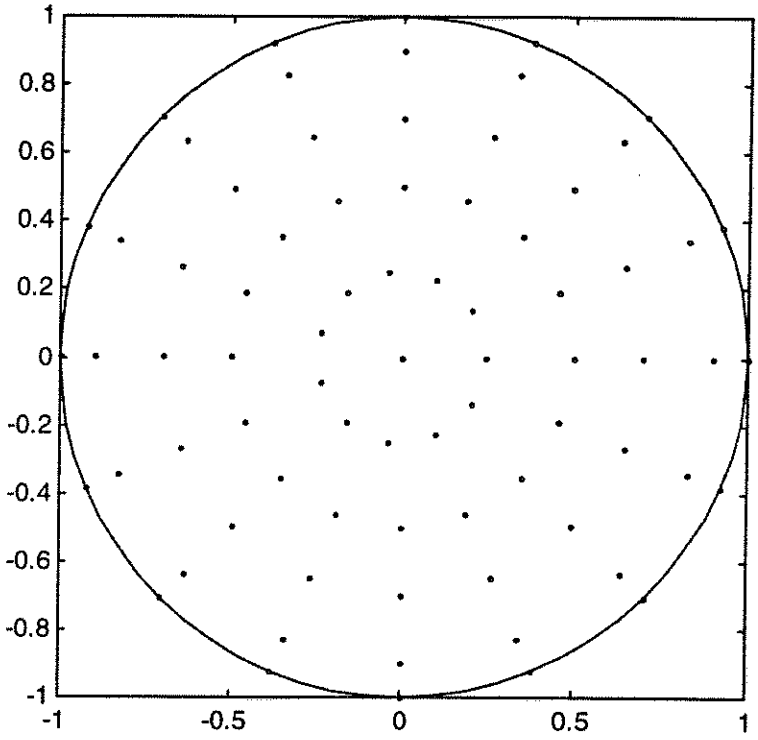

Figure 2: Fine node placement for the circle

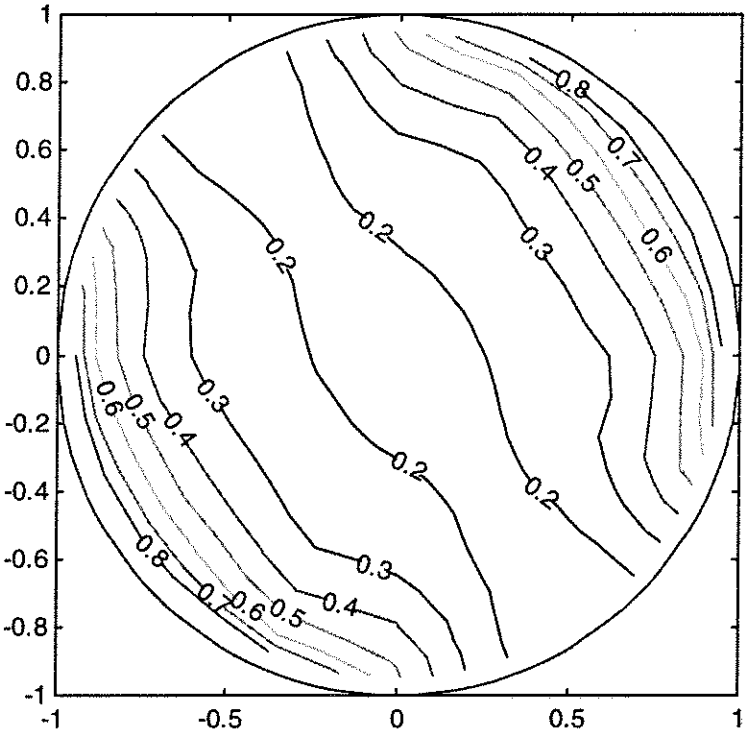

Figure 3: Concentration profiles for a second order reaction $f = 25c^2$ with mixed boundary conditions (Case 3)

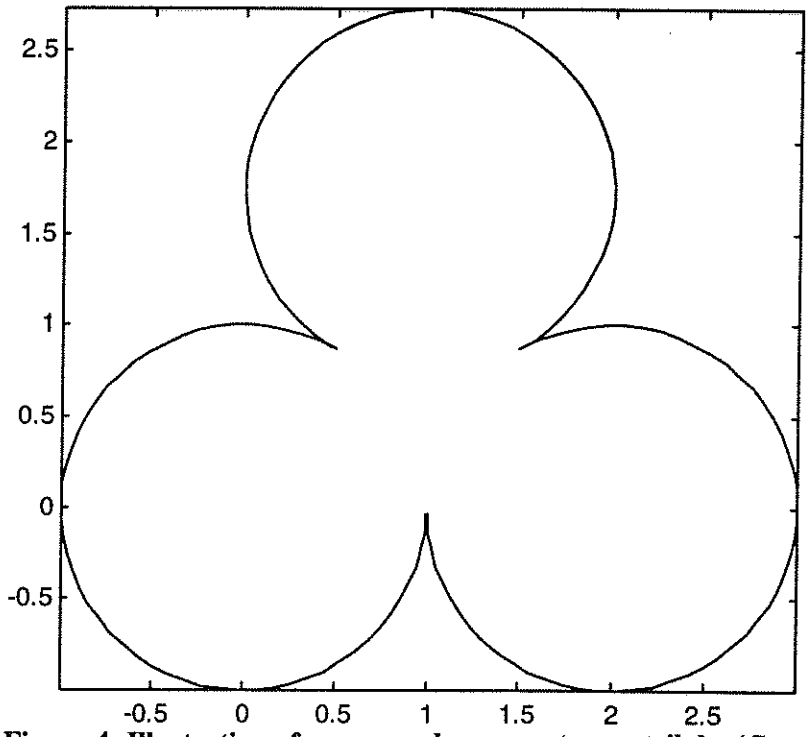

Figure 4: Illustration of a nonregular geometry - a trilobe (Case 5)

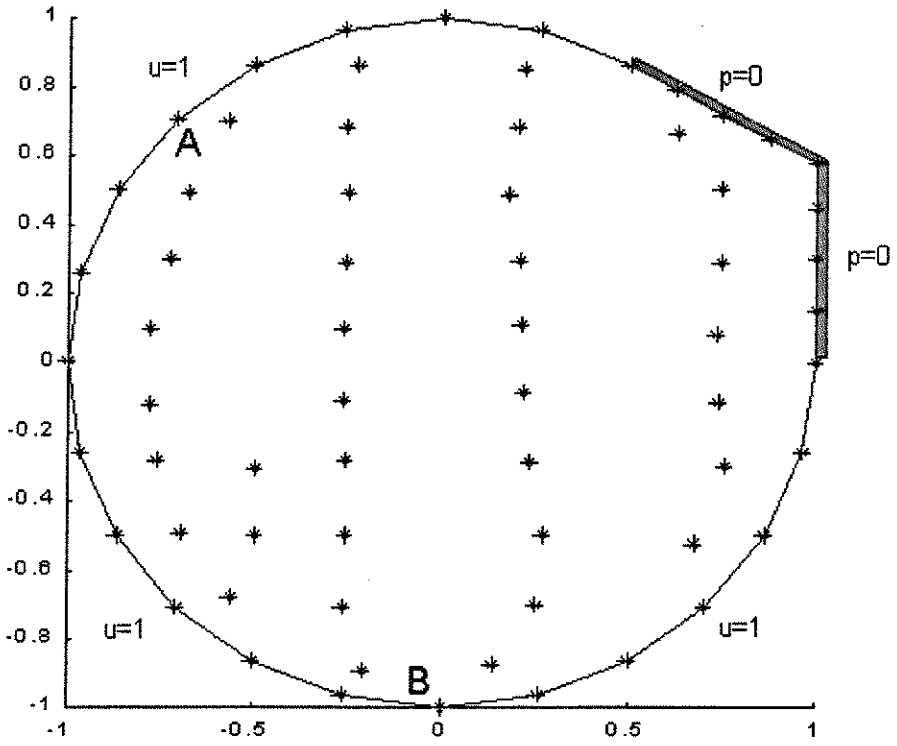

Figure 5: Node placement and boundary conditions on a cusp of the trilobe for the case when Dirichlet boundary conditions are imposed all over the surface of the trilobe

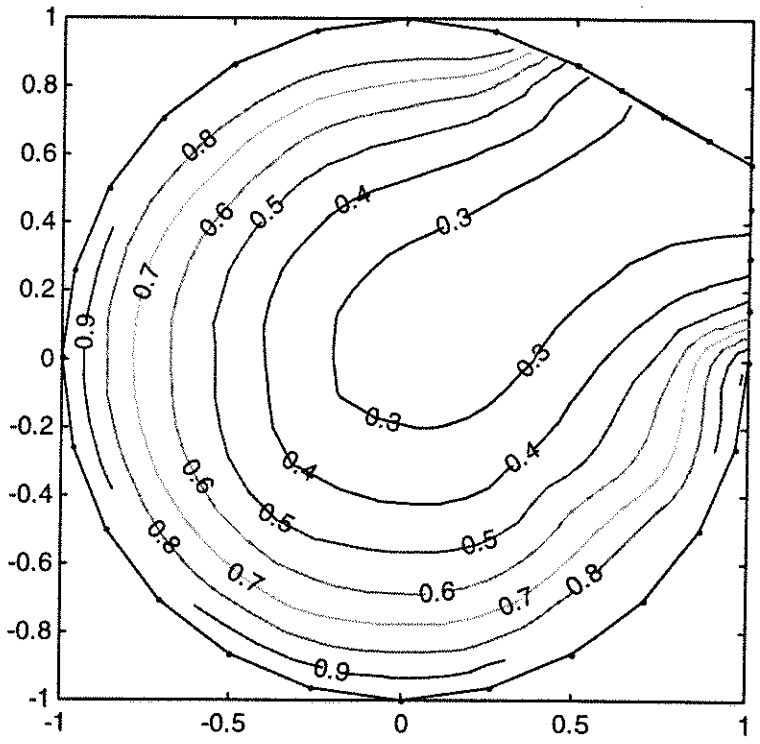

Figure 6: Concentration profiles for a trilobe with Dirichlet boundary conditions (one cusp shown) for a second order reaction ($f = 9c^2$)

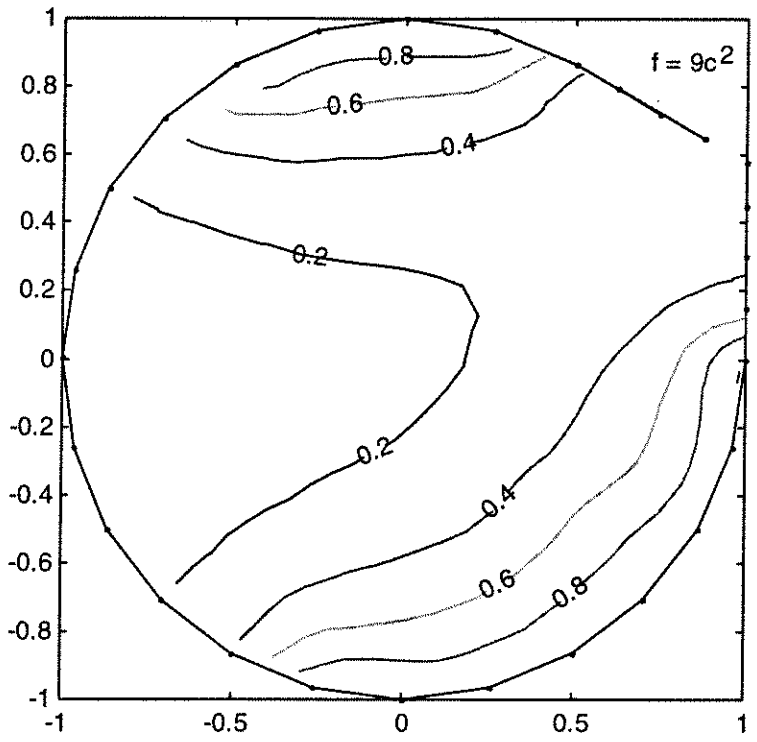

Figure 7: Concentration profiles for a trilobe with mixed boundary conditions (one cusp shown) for a second order reaction ($f = 9c^2$)

AREA I: MULTIPHASE REACTORS AND SYSTEMS

C. *NOVEL REACTORS AND TECHNOLOGIES FOR ENVIRONMENTALLY BENIGN PROCESSING*

We have always considered innovation in reactor configuration or mode of operation as an important area for further growth of multiphase reactor methodology and technology.

Our past CREL reports addressed a number of potentially novel reactors and contactors such as:

- Catalytic Strip Monolith reactor where the concentration boundary layer is periodically tripped with discontinuities in active catalyst surface.

- Novel Carrier and Reactor for Mammalian Cell Culture which utilized effective mild convection effects in porous matrices to provide for successful growth of attachment dependent cultures.

- Microencapsulation on Rotating Disks by which a variety of products can be encapsulated.

Recently, we have focused our attention increasingly on environmentally benign processing biochemical technology and devices and modes of operation that can help in achieving it.

We have completed a study of rotating packed beds during Fall of 1992. The first data and correlation for liquid holdup as a function of liquid flow rate and rotational speed is now available. Our manuscript, based on our findings, has been published in the AIChE Journal. This paper and Andjelko Basic′ thesis on rotating packed beds is available to sponsors upon request. Currently our rotating packed bed (RPB) project is dormant as we could not build up the enthusiasm among potential sponsors for looking at the RPB as a reactor for producing concentrated sulfuric acid from dilute streams with SO_2 or for its utilization in fast gas-liquid reactions to maximize intermediate formation. Now interest is building up for assessing its potential in pollution abatement processes. During the period of June 1, 1998 to May 31, 1999, Dr. J. Zhu worked on pressure drop measurements and its profile on rotating packed beds and examined various potential application areas. Financial support in this area is needed from our sponsors to explore those potential applications and performing fundamental studies to quantify the RPB performance.

Low temperature – low (moderate) pressure catalytic oxidation of industrial waste waters remains an attractive idea but is at present in a dormant stage. We plan to reactivate it if we can generate EPRI or industrial interest for it. We have conducted a study about minimizing the bromate compounds formation in the ozonation process of water impurities (this project is partially funded by EPRI).

Our study of fly ash ammonia interactions, pertinent to the problem of selective catalytic NOx, reduction via ammonia injection has been completed in the form of J.R. Turner's thesis and produced interesting, previously unknown results about this important and complex system. Recently, Dr. Turner obtained a grant to further study this important subject.

We have conducted a study on environmentally benign processing in the area of photochlorination of toluene. Our task is to analyze the effects of micro and macro mixing on the yield, and study the operation of current bubble column reactors followed by the conceptual design of an alternative reactor system, such as reactive catalytic distillation. The results of the experimental investigation and the dynamic simulation of the process are reported in detail in Z. Xu's thesis.

The projects in the above area that we briefly summarize here are:

C. *NOVEL REACTORS AND TECHNOLOGIES FOR ENVIRONMENTALLY BENIGN PROCESSING*

C1. Air Quality Engineering. **(J. Turner)**

C2. Kinetic Parameter Estimation for a Refined Scheme for Biomass Pyrolysis Differentiating Organic and Inorganic Gases. **(G. Bhatia)**

C3. Rotating Packed Beds. **(M.P. Dudukovic)**

C4. Dynamic Simulation of a Tray Column for Multicomponent Reactive Distillation Using a Rate-Based Model. **(J. Lee)**

C5. CARPT Applied to the Analysis of Photobioreactors. **(A. Kemoun, J. Fernandez)**

AIR QUALITY ENGINEERING

Jay Turner

Professor Jay Turner - a CREL alumnus - has recently introduced a new research focus area at Washington University which addresses the interface between reaction engineering, air quality, and public policy. The objective is to apply classical reaction engineering fundamentals to air quality issues with particular attention given to the relevant policy implications. Research entails a balance of theory, applied modeling, and experimental studies. Several projects in the design/development phase are described in the following paragraphs.

REACTION ENGINEERING ANALYSIS OF PARTICULATE MATTER (PM) AND VOLATILE ORGANIC COMPOUND (VOC) EMISSIONS FROM BATCH CHARCOAL KILNS. Recognizing the current limitations to a RACT-based approach for controlling emissions from charcoal kilns, we have been assessing the opportunities to achieve emission reductions through pollution prevention strategies. This project addresses charcoal kiln operation and emissions from a reaction engineering perspective. A model is being developed for the basic operation of a kiln, with key parameters obtained from laboratory-scale experiments as needed. The model will subsequently be used to identify a set of operating heuristics to reduce PM and VOC emissions yet maintain product quality and production rates. Charcoal kilns are rather interesting to model because they are batch reactors which feature both combustion and pyrolysis in the same vessel.

TECHNICAL AND POLICY ANALYSIS OF MOTOR VEHICLE PARTICULATE EMISSIONS. Current particulate matter NAAQS apply to particles smaller than ten micrometers. Several areas violate this standard and are struggling to meet the applicable State Implementation Plan requirements and transportation conformity requirements. Re-entrained road dust from motor vehicles is a significant contributor to particulate matter burdens in many nonattainment areas located in the western United States. Like most fugitive sources, road dust emissions are very difficult to quantify and control methods are few. Despite our poor understanding of this process, state and local agencies are required to invest significant resources to develop and enforce road dust control strategies yet often fall short of the emission reductions needed to comply with the above programs. Such failures can lead to the withholding of millions of dollars in Federal highway funds.

We have assessed the state-of-knowledge regarding this emission source. The current emission factor equations are perhaps adequate for assessing control measure effectiveness (indeed, this was their intended application) but are inadequate for the detailed quantitative calculations required for State Implementation Plan development and conformity analysis. We are conducting field studies to determine fugitive road dust emission factors in a more systematic and comprehensive manner than currently available. Various classes of roadways are being sample, with source apportionment techniques used to distinguish background PM, non-fugitive motor vehicle PM (e.g.,

exhaust), and resuspended road dust. A significant effort is being made to elucidate emission factors for the particulate matter fine fraction (PM-2.5), which will likely be regulated in the future pending the current review of the NAAQS standards for particulate matter.

In addition, the Air Quality Laboratory has recently received a seed grant from the Oak Ridge Associated Universities (ORAU) to develop an analytical method for quantifying tire wear emissions from roadways. Such emissions can yield latex particles to which hypersensitive allergenic responses have been attributed. However, very little is known about the emission rate and size distribution of tire wear particles.
on conformity determinations.

PROJECTS REQUIRING CREL FUNDING. Dr. Turner would be delighted to entertain research projects of interest to CREL sponsors. Potential area of interest include reaction engineering aspects of stationary source emission control, fugitive emissions characterization and control, and policy issues concerning air quality. CREL participants are encouraged to contact us if they are interested in pursuing a particular project.

KINETIC PARAMETER ESTIMATION FOR A REFINED SCHEME FOR BIOMASS PYROLYSIS DIFFERENTIATING ORGANIC AND INORGANIC GASES

See the attached report for:

A. Problem Definition
B. Research Objectives
C. Research Accomplishments

KINETIC PARAMETER ESTIMATION FOR A REFINED SCHEME FOR BIOMASS PYROLYSIS DIFFERENTIATING ORGANIC AND INORGANIC GASES

Garima Bhatia and Jay R. Turner*

Air Quality Laboratory, Department of Chemical Engineering,

Washington University, St. Louis, MO 63130, USA

Abstract

An improved reaction scheme for biomas pyrolysis has been proposed. The final objective of this research initiative is to generate suitable models for environmental impact assessment of batch charcoal kilns. This communication focuses on utilizing existing data to extract the parameters of a lumped kinetic scheme, which can subsequently be coupled with a particle scale transport model of wood pyrolysis in kilns. The proposed kinetic scheme lumps the products of wood pyrolysis into char (solid residue), char (liquid residue), organic gases and inorganic gases. This kind of lumping is suitable for environmental impact analysis. The kinetic parameters are estimated for the pyrolysis of two typical lignocellulosic materials: milled wood lignin and sweet gum hardwood. The parameters obtained from rigorous regression analysis are subsequently used to predict the trends in independent experiments with different samples.

Keywords: Biomass, wood, lignin, pyrolysis, pyrolysis gases, kinetic parameters.

---

* Corresponding author.

Introduction

Biomass pyrolysis is a process of considerable economic importance. A wide variety of commercially interesting products are obtained through different pyrolytic treatments of biomass. For example, rapid or flash pyrolysis[1, 2] of biomass provides a route to convert lignocellulosic materials into high heating value gases, heavy organic liquid products rich in olefins, and high-molecular weight paraffins useful as fuels and chemical feedstocks. On the other hand, slow pyrolysis of biomass is the process that is popularly used for industrial production of charcoal[3].

The pyrolysis of biomass materials such as wood, cellulose and lignin has been studied extensively over the last three decades, owing to the industrial relevance of the process and also due to secondary interest in fire research[4]. Kinetic investigations of biomass pyrolysis have been conducted for cellulose[5, 6], lignin[7, 8] and different kinds of wood[9-13]. The subject has also been reviewed widely, with excellent reviews available on the state of knowledge of hemicellulose decomposition kinetics[14] and cellulose pyrolysis[15]. On the theoretical side, a detailed review of the kinetic modeling and numerical simulation studies of biomass pyrolysis[16] has been published. Concern over emissions from industrial-scale or traditional charcoal production units[17-19] is also likely to lead to some research on pollution prevention issues related to wood pyrolysis in the foreseeable future.

Biomass pyrolysis is a complex process yielding hundreds of products, and the unfeasibility of studying each reaction individually has led to the use of lumped kinetic models. Typically, these lumping schemes classify the products into three groups: char, gas and tar. Char is the carbon-rich solid residue, gas is the volatile fraction containing low molecular weight products, and tar is the volatile fraction that forms a liquid at room temperature. The experimental studies conducted in the field vary in complexity from measurements of overall weight loss, to quantification of the 'lumped' species described above, to characterization of the entire spectrum of gaseous and liquid products from pyrolysis.

Typical experimental studies have been conducted to measure the overall weight loss and obtain global decomposition kinetics employing DTA and TGA techniques[20-21]. Researchers such as Thurner and Mann[9] and Agrawal[22] have measured the volatile

fractions in addition to the weight loss, in order to estimate the kinetic parameters for production of char, gas and tar by the three parallel reaction model[23]. This model has been widely used in the literature, and a schematic description is shown in Figure 1. Some researchers[5, 7, 10] have further resolved the various volatile species evolved during pyrolysis, such as CO, CO_2, CH_4 and other gases, and have obtained kinetic parameters for each individual reaction.

The three-reaction model has been found to be a simple yet adequate representation of pyrolysis kinetics for most applications, which do not warrant such a level of detail as modeling each individual reaction. However, it provides no insight into the type of gaseous products that are evolved during pyrolysis since it treats all inorganic and organic gases as a single lump. Hence the model would fall short if a theoretical study of pollution prevention from biomass pyrolysis is desired, where it is imperative to track the generation of hydrocarbon-rich gaseous components as compared to inorganic gases like CO_2 and CO.

In the present paper we propose an extension of the three reaction kinetic scheme for pyrolysis by differentiating the gaseous fraction into inorganic and organic gases, designated as 'Gas_1' and 'Gas_2' respectively. Figure 2 shows a schematic of the proposed model. The rationale behind this thought is that the production of inorganic gases such as CO and CO_2 during pyrolysis shows a correlation which has been reported by many researchers[8, 11, 13]. A similar trend is seen for organic gases, at least among the low molecular weight paraffins[8]. Hence, the mechanisms for production of the individual species within these lumps can be assumed to be similar, which would provide a justification for treating them as two distinct groups instead of a common 'Gas' lump. Such a differentiation would help to quantify the proportions of inorganic and organic gases that are evolved under different reaction conditions of biomass pyrolysis, and could be incorporated into a full-blown particle scale model that accounts for the important physical processes and variation of properties with conversion. This would contribute to the development of a scientific foundation for exploring pollution prevention strategies in the industry by providing a tool to researchers to improve the level of detail in the existing kinetic framework without adding the unnecessary complexity of modeling each individual reaction.

The objective of this study is to investigate the feasibility of introducing this refined kinetic scheme of differentiating the inorganic from the organic gases. The kinetic parameters for these fractions will be obtained using the experimental data from published literature in the field, and these parameters will be evaluated by testing the predictions against independently conducted experimental studies from other sources. The details of the experimental studies chosen from the literature are given in the next section.

Experimental studies

The kinetic parametersreported in this work have been obtained using data published in the open literature[7, 10]. The substrates for which the parameters for the proposed kinetic scheme will be evaluated are lignin and wood. The following criteria were considered while choosing the experimental studies to be used in the analysis: (1) measurement of individual gaseous species – both organic and inorganic – evolved during pyrolysis; (2) measurement of weight loss and liquid product yield due to pyrolysis; (3) experiments conducted at different recorded temperatures and (4) reasonable closure to the mass balance. Based on these criteria, the studies conducted by Peters and co-workers at M.I.T. on fast pyrolysis experiments using milled wood lignin[7] and sweet gum hardwood[10], were chosen for this analysis. These researchers measured weight loss, liquid product yield, and a wide range of gaseous pyrolysis products, including CO, CO_2, CH_4, etc at different pyrolysis temperatures. The mass balance was closed within 10%, which is considered satisfactory for such experiments.

The measurements reported by Nunn et al.[7, 10] were performed in a captive sample electrical screen heater reactor, and the gaseous products were collected and measured with a gas chromatograph fitted with a thermal conductivity detector. The heater reactor was set up to conduct non-isothermal experiments at heating rates of 1000 K/s to pre-selected peak temperatures between 600 and 1400 K, with subsequent cooling of the sample at an average rate of 200 K/s. The high heating rate and small sample mass ensured that heat and mass transfer limitations were minimized, and the experimental data could be assumed to truly reflect the intrinsic kinetics of the pyrolysis process. The final solid residue remaining and the recoverable liquid product (tar) collected during the

entire duration of the experiment were also quantified via gravimetric analysis. Thus, in addition to the overall weight loss, the yields of liquid product and ten different gaseous species over the entire course of the experiment are reported for different peak temperatures. However, no temporal data for these quantities is reported. More details of the experimental setup and sample preparation technique have been reported by Hajaligol et al.[5]

For the purposes of the current analysis, the different gaseous species reported by Nunn et al.[7, 10] are lumped into either of the 'Gas_1' (inorganic) or 'Gas_2' (organic) fractions and the final yields of these fractions calculated by summation. This data is represented in Figure 3A for milled wood lignin[7] and in Figure 3B for sweet gum hardwood[10].

The kinetic parameters obtained by fitting the data were independently checked by comparing the predicted yields against other experimental studies available in the literature. The parameters for sweet gum hardwood were checked against experimental data available for other hardwoods such as maple wood sawdust[11], holm-oak wood[12] and fir wood chips[13]; while the parameters for milled wood lignin were checked against the experimental data for Klason lignin[8]. These studies were chosen from the vast body of available literature based on their broad similarity to the reference studies of Nunn et al.[7, 10] in terms of heating rate (fast pyrolysis), substrate used (wood or lignin) and measurement of gaseous species (inorganic and organic). They do, however, have variations in the temperature ranges, reactor type and the individual gaseous species measured during pyrolysis. Details of the experimental efforts which have provided the data for this analysis are listed in Table I.

Theory

Kinetic modeling. With the components lumped together as shown schematically in Figure 2, the formation rate of each lumped component, assuming first order reactions, is given by:

$$\frac{dV_w}{dt} = -(k_1 + k_2 + k_3 + k_4)V_w = -kV_w \qquad (1)$$

$$\frac{dV_{g_1}}{dt} = k_1 V_w \qquad (2)$$

$$\frac{dV_{g_2}}{dt} = k_2 V_w \tag{3}$$

$$\frac{dV_T}{dt} = k_3 V_w \tag{4}$$

$$\frac{dV_C}{dt} = k_4 V_w \tag{5}$$

These relations are expressed in terms of mass of the lumped component normalized to the initial mass of pyrolyzable wood, and the parameters k_i (units of 1/sec) are assumed to follow an Arrhenius temperature dependence. This model – applied to the three-reaction scheme of Figure 1 – has been widely used in experimental as well as modeling studies of the pyrolysis of lignocellulosic materials. It has been applied to isothermal experiments[9] to obtain kinetic parameter estimates for the pyrolysis reactions, and used in modeling studies[16, 24] which couple the kinetics with the heat and mass transfer. In this study, we obtain the kinetic parameters for the four-reaction model of Figure 2, using the equations (1) through (5) above.

An alternative model used in many experimental studies[5, 7, 10] is the single-reaction, first-order decomposition model for the yields of individual pyrolysis products. In this model it is assumed that the sample decomposes directly to each reaction product i by a single independent reaction pathway and that the rate of formation of a product i with yield V_i (based on initial weight of sample) at time t is given by the expression:

$$\frac{dV_i}{dt} = \left(V_i^* - V_i\right) A_i \exp\left(-\frac{E_i}{RT}\right) \tag{6}$$

Here, A_i and E_i are respectively the pre-exponential factor and activation energy for component i, and V_i^* is the ultimate yield of product i at high temperature and long residence times. This model has a history of successful utilization for condensed phase substances, and has been used in calculations of pulverized coal ignition and flame stabilization[25]. It is useful in engineering calculations and convenient to apply since the kinetic parameters for any particular product can be obtained directly by fitting the experimentally measured values of yield for that product. Many researchers, including the experimental studies[7, 10] on which this work is based, have used it in their analysis.

They obtain the best-fit values of the parameters A_i, E_i and V_i^* by non-linear least-squares regression applied to the equation:

$$\ln\left[\frac{V_i^* - \tilde{V}_i}{V_i^*}\right] = -\int_0^{t_f} A_i e^{-\left(\frac{E_i}{RT(t)}\right)} dt \tag{7}$$

where $\tilde{V}_i$ is the predicted yield of product *i*.

When this model is applied to data obtained in isothermal experiments, the equation (6) for each species reduces back to the equations (1) through (5) by applying a simple mass balance on the products, and the ultimate yield of product *i* at a fixed temperature is given by:

$$V_i^* = \frac{k_i}{k_1 + k_2 + k_3 + k_4} \tag{8}$$

However, when the data is non-isothermal, a major constraint of the model is the requirement of one single constant V_i^* over all temperatures. Clearly, this is not the case in practice since the ultimate yield of various pyrolysis products have been experimentally observed[8, 12] to have a strong dependence on temperature. Hence, for the non-isothermal case, the parameters A_i, E_i and V_i^* obtained from this model have no physical significance and are simply fitting parameters for the data! However, due to ease of applicability as well as the fact that most experimental studies are conducted under near-isothermal conditions, this model has been widely used. In this study, some comparisons between the predictions of the two models are also presented.

Parameter Estimation. The kinetic parameters for the four reactions of Figure 2 are estimated using non-linear least squares regression analysis. The estimated mass of wood/lignin sample remaining at the end of the pyrolysis run of time t_f is given by:

$$\tilde{V}_w = V_{w0} \exp\left[-A\int_0^{t_f} e^{-\left(\frac{E}{RT(t)}\right)} dt\right] \tag{9}$$

where V_{w0} is the initial mass of sample, and A and E are respectively the pre-exponential factor and activation energy of the global decomposition reaction represented by equation (1).

To predict the mass of each lumped component as given in equations (2) to (5), we need the mass of unreacted sample remaining as a function of time. However, this is an unknown quantity for which there is no data available, since the experiments have measured only the total weight loss over the *entire* pyrolysis run. Further, in most experimental studies, only the total solid residue (biomass remaining + char formed) can be measured, and it is impossible to distinguish the unreacted biomass from the char product, or quantify it accurately. To overcome this difficulty, the predicted value $\tilde{V}_w$, obtained from the estimated global parameters A and E, is used. The mass of char, 'Gas_1', 'Gas_2' and tar are then given by:

$$\tilde{V}_i = V_{w0} A_i \int_0^{t_f} e^{-\left(\frac{E_i}{RT(t)}\right)} \exp\left[-A \int_0^t e^{-\left(\frac{E}{RT(\tau)}\right)} d\tau\right] dt \tag{10}$$

The function minimized is the sum of the squares of differences between the experimental and predicted values, and is given by:

$$\chi^2 = \sum_{j=1}^{n} \left[\left(V_{wtloss,j} - \tilde{V}_{wtloss,j} \right)^2 + \left(V_{gas_1,j} - \tilde{V}_{gas_1,j} \right)^2 + \left(V_{gas_2,j} - \tilde{V}_{gas_2,j} \right)^2 + \left(V_{tar,j} - \tilde{V}_{tar,j} \right)^2 \right] \tag{11}$$

where the weight loss is given by

$$\tilde{V}_{wtloss} = 1 - \left(\tilde{V}_w + \tilde{V}_c \right) \tag{12}$$

All ten parameters are obtained simultaneously by applying a Levenberg-Marquardt method for non-linear least-squares regression[26] to this problem. This method is robust and very widely used in non-linear least-squares routines. It uses the method of steepest descent far from the minimum, switching to an inverse-Hessian[27] method as the minimum is approached. The routine used also generates a 'covariance matrix' which comes out of the χ^2 minimization, and which is related to the confidence interval for the estimate.

A check on consistency is then applied, by calculating the sum of the individual rate constants $\sum_{i=1}^{4} k_i$ and comparing it to the global rate constant k obtained in the regression (equation (9)).

Results

Pyrolysis of lignin. As an initial check for the non-linear regression routine, the kinetic parameters for the individual species as given by equation (6) were calculated, and compared with the values reported by Nunn et al.[7] Table II shows the comparison for a few species, and the calculated parameters are seen to be very close to the reported values, with marginally lower standard errors than those reported in the paper. This establishes the correctness of the routines and provides confidence for further analysis using the proposed kinetic scheme.

Subsequently, the kinetic parameters for the pyrolysis of milled wood lignin were estimated using the kinetic model of equations (1) to (5) and the nonlinear regression technique described in the previous section. The predicted yields were compared against the experimental values at different peak temperatures. Figure 4A through D shows the comparison for weight loss, and the weight fraction of evolved species 'Gas_1', 'Gas_2' and tar, as a function of peak temperature. The weight loss profile is captured with a standard error of 3.2 weight %, defined by the equation:

$$S.E. = \left[\sum_{j=1}^{n} \left(V_{i,j} - \bar{V}_{i,j} \right)^2 \Big/ (n-m) \right]^{1/2} \tag{13}$$

where m is the number of estimated parameters, in this case equal to 2. The low values of weight loss at low peak temperatures indicate poor conversion of lignin to gaseous as well as solid products possibly due to the short pyrolysis time in these runs. The 'Gas_1' and 'Gas_2' profiles are predicted with standard errors of 2.7 % and 0.8 % respectively. The model predicts a steeper profile than the experimental data, and the agreement is relatively poor at the low and high peak temperatures. However, when the model represented by equation (6) is used to obtain the kinetic parameter for the 'Gas_1' lump, the prediction has a standard error of only 1.17 % and captures the low and high peak temperature behavior with fidelity (Figure 5).

The predicted tar profile, as shown in Figure 4D, goes through a maximum around 900 K, before reaching an asymptotic value. This is consistent with the trend shown by the experimental data shown on the figure.It is noteworthy that each data point represents the total yield of product over the duration of a *non-isothermal* experimental

run, during the sample may or may not have achieved full conversion. Thus, there are two possible hypotheses for the experimentally observed drop in tar yield at high temperatures. The trend may be simply due to the secondary decomposition of tar at higher peak temperatures.[7] Alternatively, the *ultimate* tar yield actually decreases with increasing temperature, and the low values at the low peak temperatures only represent incomplete conversion. The appearance of the maximum in the predicted curve is due to the second effect since the kinetic model does not include secondary reactions.

The alternative "single-reaction" model described by equation (6), however, cannot capture the maximum in the tar yield (Figure 6), even though the fitted model has a marginally lower standard error compared to Figure 5D. This is a limitation inherent in the model itself, since it can be seen from equation (6) that a trend of decreasing yield with temperature cannot be captured. Such a trend could exist only if the activation energy were negative (which is unrealistic in this case since all the reactions are endothermic), or the ultimate yield V_i^* were a function of temperature (in this case, V_i^* is a constant). However, with the tar yield given by equation (4), the temperature dependence of the ultimate yield is governed by the *difference* of the activation energies of the tar formation reaction and the global decomposition reaction (equation (8)). The kinetic parameter estimates for lignin given in Table III confirm this observation.

The predicted yields were then compared with the data for Klason lignin published in the literature[8] and the comparison is shown in Figure 7A, B for all four pyrolysis products. The theoretical predictions are for the final yields at different pyrolysis temperatures,under isothermal conditions. The experiments were conducted in a Pyroprobe 1000, which has heating times of the order of milli-seconds[8]. Thus, the experimental conditions can also be assumed to be approximately isothermal. The qualitative trends as well as the quantitative agreement for 'Gas_1' and char are captured well, with an over-prediction in the 'Gas_1' yield and an under-prediction of the char yield. The experimental data for organic gases ('Gas_2') shows a slight increase in ultimate yield at higher temperatures; however the prediction is insensitive, or shows a small decreasing trend. Experimental data for the tar yield goes through a maximum around 900 K. However, the first-order reaction model but the model fails to capture this. The experimental data for this case definitely seems to indicate an effect of secondary tar

cracking at high temperatures, which would reinforce the decreasing trend of tar yield. On the whole, the predictions seem acceptable given that the two sets of data were obtained on completely different experimental setups. An interesting point to be noted is that the alternative kinetic model of equation (6) would fail in this case since it assumes the ultimate yields of all species to be constant at all temperatures.

Wood pyrolysis. The kinetic parameters for the pyrolysis of sweet gum hardwood were estimated from the experimental data of Nunn et al.[10] The predictions for the yield of lumped species at different peak temperatures are compared against the experimental values in Figure 9A through D. The weight loss prediction has a standard error of 8.5%, while the 'Gas_1' and 'Gas_2' profiles are predicted with standard errors of 3.3% and 0.7% respectively. Again in this case, as for the milled wood lignin, the agreement between the theoretical and experimental values for 'Gas_1' and 'Gas_2' is poor for the low and high peak temperature runs. The maximum in the tar profile is captured in this case as well, and the prediction has a standard error of 7%. The estimated kinetic parameters for all the lumped species are listed in Table III. The values indicate that for milled wood lignin as well as sweet gum hardwood, the char yield shows a decreasing trend with increasing temperatures, since the activation energy of the char formation reaction is less than that of the global decomposition, in both the cases. This is consistent with the well-known trend that pyrolysis at lower temperatures is favorable for maximizing the production of charcoal from wood[28].

The estimated kinetic parameters for sweet gum hardwood were tested by comparing the predictions against a number of experimental studies of different kinds of wood. The comparison with the pyrolysis data of Scott et al.[11] for Eastern red maple sawdust is shown in Figure 9A, B. In this case, the qualitative trends for both inorganic and organic gases are predicted correctly, with yields increasing for higher temperatures. The experimental data in this case was obtained in two different kinds of reactors – a fluidized bed reactor which was operated upto 600°C and an ultrapyrolysis system operated between 600-800°C. The substrate was passed through the reactor, which had been pre-heated to a fixed temperature. Due to the high heating rate and the small residence time of the substrate in the reaction system, the runs were considered

isothermal. The predictions are also for the isothermal case, and quantitatively, the 'Gas_2' profile agrees very well with experiment, while the 'Gas_1' profile has a lower slope than obtained experimentally. For the char and tar profiles, as shown in Figure 9B, the trends of decreasing yield with increase in temperature are captured correctly. Again, for this case, the tar maximum is not captured. The char prediction shows very poor agreement with the experimental values for low temperatures, but improves significantly in the high temperature region of the curve.

We now attempt to predict the experimental data of Figueiredo et al.[12] for holm-oak wood. Figure 10 shows the predicted versus the experimental total gaseous yield. In this case, all the major individual species were not measured experimentally and hence only the total gas yields are compared. Again, the trend is qualitatively correct, with the agreement improving significantly for high temperatures.

In Figure 11, the comparison is shown for fir wood chips data reported by Di Blasi et al.[13] The profile for inorganic gases (Gas_2) shows excellent agreement with the experimental data, but the prediction for 'Gas_1' is quite poor. In this case, the estimated parameters under-predict the data at low temperatures and over-predict the high temperature data. This may be in part due to the fact that in this study, the yield of CO_2, which is the major component of the inorganic gas fraction ('Gas_1') was found to reach an asymptotic value above 800 K[13]. This trend has not been reported in other similar studies[10, 11] of wood pyrolysis, where the CO_2 yields increases monotonically at least till 1000 K.

Finally, as an independent check on the consistency of the estimated kinetic parameter values, the rate constants for the different reactions are plotted against the temperature, as shown in Figure 12A, B for milled wood lignin and sweet gum hardwood, respectively. The rate constants k_1, k_2, k_3 and k_4 are represented by the curves for char, 'Gas_1', 'Gas_2' and tar, respectively. The 'global' curve represents the global decomposition rate constant, k, while 'wood' represents the summation of the four individual decomposition constants:

$$\sum_{i=1}^{4} k_i = k_1 + k_2 + k_3 + k_4 \qquad (14)$$

For consistency, the summation should be the same as the global parameter, k, obtained in the first step of the least-squares regression, following equation (9). From Figure 12A and B, the two curves are seen to almost coincide, for both substrates, thus satisfying the consistency check. At high temperatures above 1300 K, the discrepancy starts increasing, especially for sweet gum hardwood, for which it becomes significant at 1500 K.

It may be noted, however, that for each individual pyrolysis reaction, it is possible that other sets of quite different rate parameters can also be derived which reproduce the measured data within the limits of experimental uncertainty, due to the compensatory effect of increasing the activation energy and pre-exponential factor. This is illustrated in Table IV, which shows the covariance matrix of the estimated kinetic parameters, i.e. five sets of pre-exponential factors and activation energies. The values given in Table IV represent the standard uncertainties in each parameter if the other parameters are held fixed at the values which minimize the χ^2 function given in equation (11). This is identical to the 68% confidence interval for that particular parameter[26]. Comparing the values in Tables III and IV, we find that the uncertainties in the pre-exponential factors are, in many cases, of the same order of magnitude as the actual value, while the activation energies have uncertainties about an order of magnitude lower than the parameter value.

Conclusions

In this work, the products yield data was fitted to a physically realistic model for biomass pyrolysis. The kinetic parameter values and the corresponding uncertainties were calculated using a non-linear least-squares regression routine. This is a generalized framework that can be subsequently used for kinetic parameter estimation from a set of isothermal or non-isothermal data of product yields. Studies previously published in the literature often make assumptions about the nature of the product profile, which may not necessarily be valid under all conditions. For example, the kinetic model represented by equation (6) and widely used in the literature[7, 10], assumes that the ultimate yield of any given product is a constant, irrespective of pyrolysis temperature. Similarly, the kinetic parameter estimation detailed by Thurner and Mann[9] makes an assumption that the

activation energy of the char formation reaction (reaction 3 in Figure 1) is the same as the activation energy of the weight loss reaction (reactions 1+2 in Figure 1), which leads to a constant weight loss at complete conversion, regardless of temperature. These are arbitrary assumptions and for the systems such as charcoal kilns on which controlled experiments cannot be easily performed, it is virtually impossible to verify them. The advantage of the method used in this work, is that no assumptions need to be made *a priori* about the ultimate yield of any product. In fact the kinetic parameters of the char formation reaction are calculated just from the weight loss data, without having any information about the fraction of char product present in the solid residue.

The fits of the estimated parameter values for the 'Gas_1'/'Gas_2' formation reactions with the experimental data from the original studies[7, 10] are good. The predictions are also reasonably good when compared against the measured values of inorganic and organic gas yields reported for a number of different studies by other researchers using similar substrates as those for which the parameters were derived. Work is currently under way by the authors to incorporate this information in a detailed particle scale model to describe the heat and mass transfer phenomena, coupled with kinetics, which take place in a biomass slab undergoing simultaneous pyrolysis and combustion. Subsequently, the particle scale model would be used in a reactor model simulator for a charcoal kiln. Such a tool would be invaluable in assessing the environmental impact of operation of these kilns and in optimization of the process.

The agreement between the predicted and measured values of 'Gas_1' and 'Gas_2' is encouraging and supports the argument for expanding the prevalent three-reaction scheme to make the distinction between the organic and inorganic gas lumps. The advantage of this extension is threefold. First, in experiments which are set up to measure individual gaseous species, valuable information is lost by grouping species into lumps. The alternative – modeling individual reactions – may be unnecessary and intractable. The proposed kinetic scheme enables the researcher to preserve some additional information in the lumps, namely the distinction between organic and inorganic gases, without introducing additional complexity. Second, it provides the ability to conduct a theoretical environmental impact study on emissions from pyrolytic processes. Finally, the kinetic scheme makes it possible to envisage a model that would incorporate the

kinetics of both pyrolysis and combustion of biomass, as detailed above. The future direction of this research would be to develop a sufficiently detailed model to identify an optimal set of conditions for pyrolysis and combustion which would minimize the emissions from such processes.

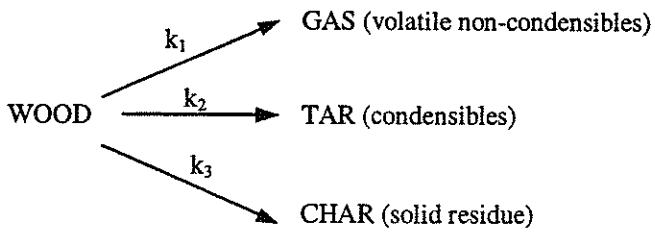

Figure 1. Three reaction model for wood pyrolysis[23].

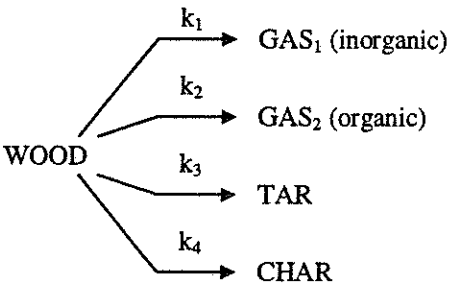

Figure 2. Proposed primary pyrolysis scheme for wood decomposition.

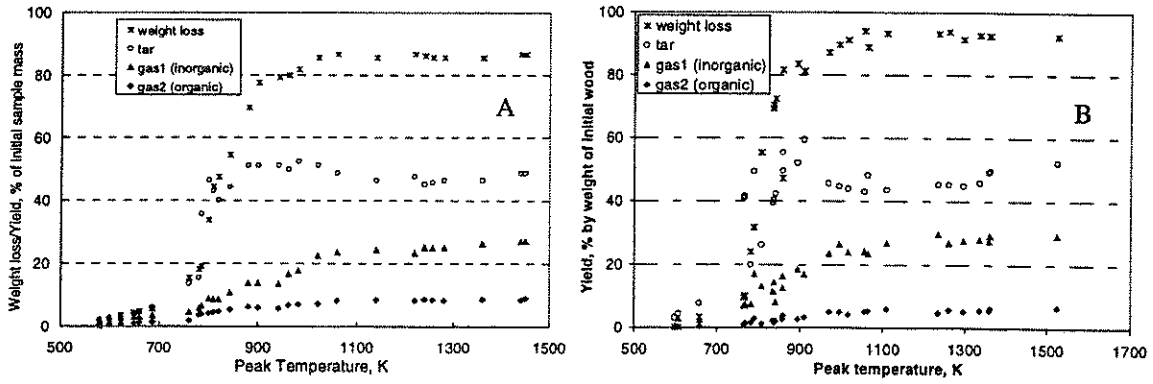

Figure 3. Experimental data for weight loss and lumped species gas_1, gas_2 and tar, as a function of peak temperature for (A) Milled wood lignin pyrolysis[7]. (B) Sweet gum hardwood pyrolysis[10].

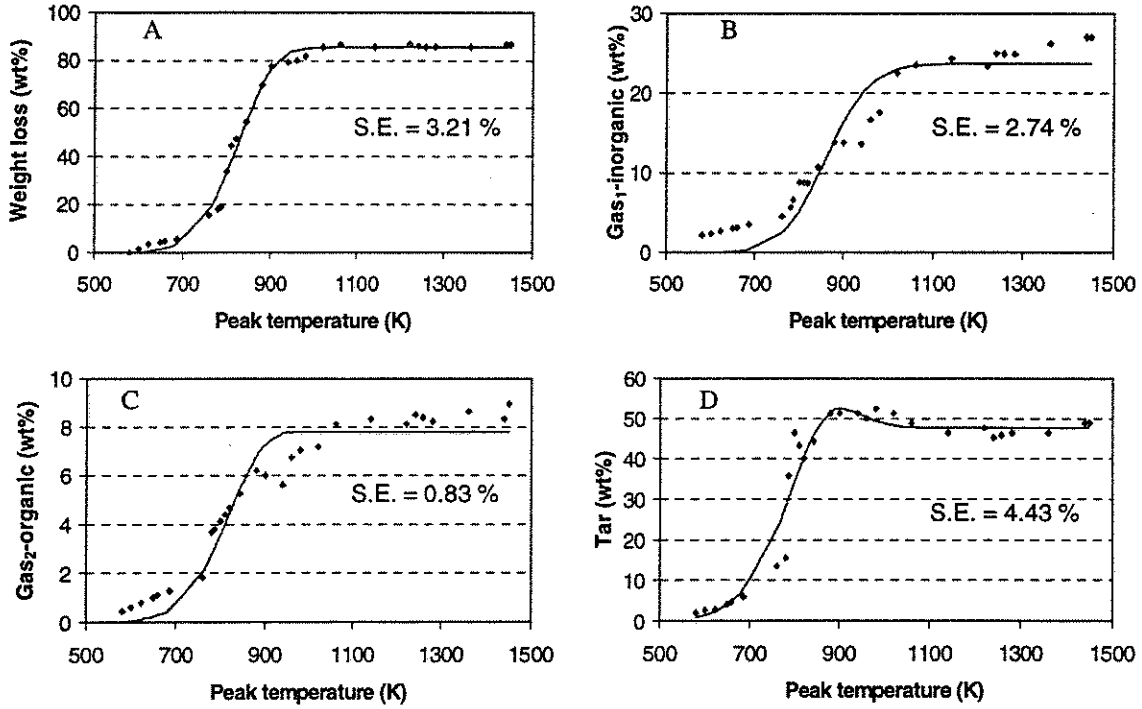

Figure 4. Comparison of experimental data with predicted yields. (A) Weight loss. (B) Gas_1 (inorganics). (C) Gas_2 (organics). (D) Tar. [Data for milled wood lignin[7]].

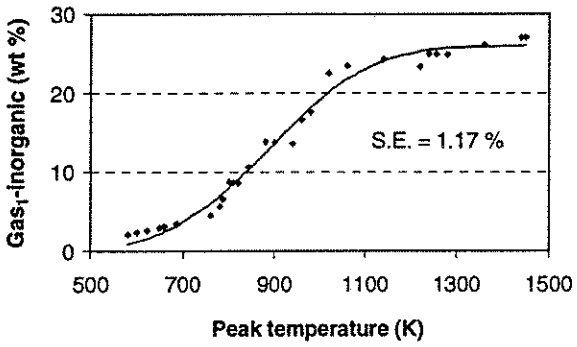

Figure 5. Comparison of experimental with predicted yields of inorganic gases using the kinetic model represented by equation (6). [Data for milled wood lignin[7]].

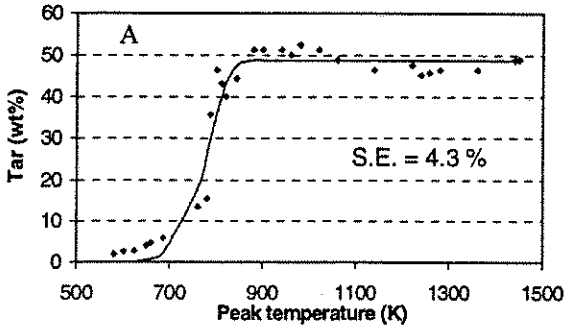

Figure 6. Comparison of experimental with predicted yields of tar using the kinetic model represented by equation (6). [Data for milled wood lignin[7]].

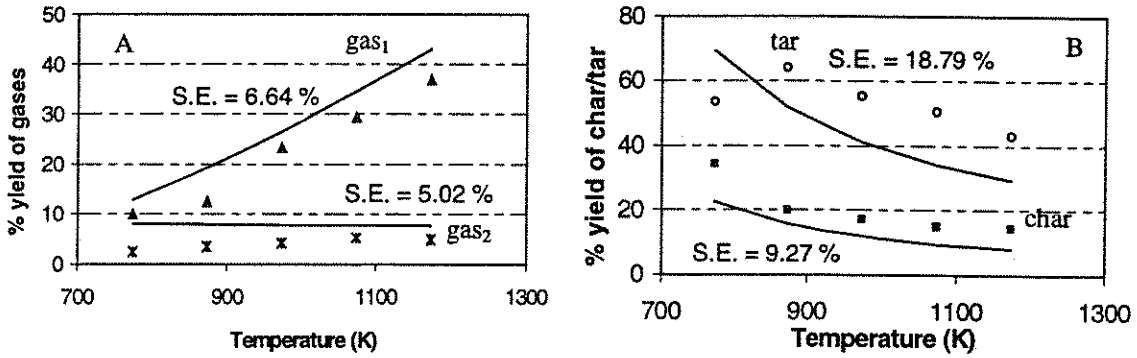

Figure 7. Comparison of experimental data with predicted yields. (A) Gas_1 (inorganics) and Gas_2 (organics). (B) Tar and Char. [Data for Klason lignin[8]].

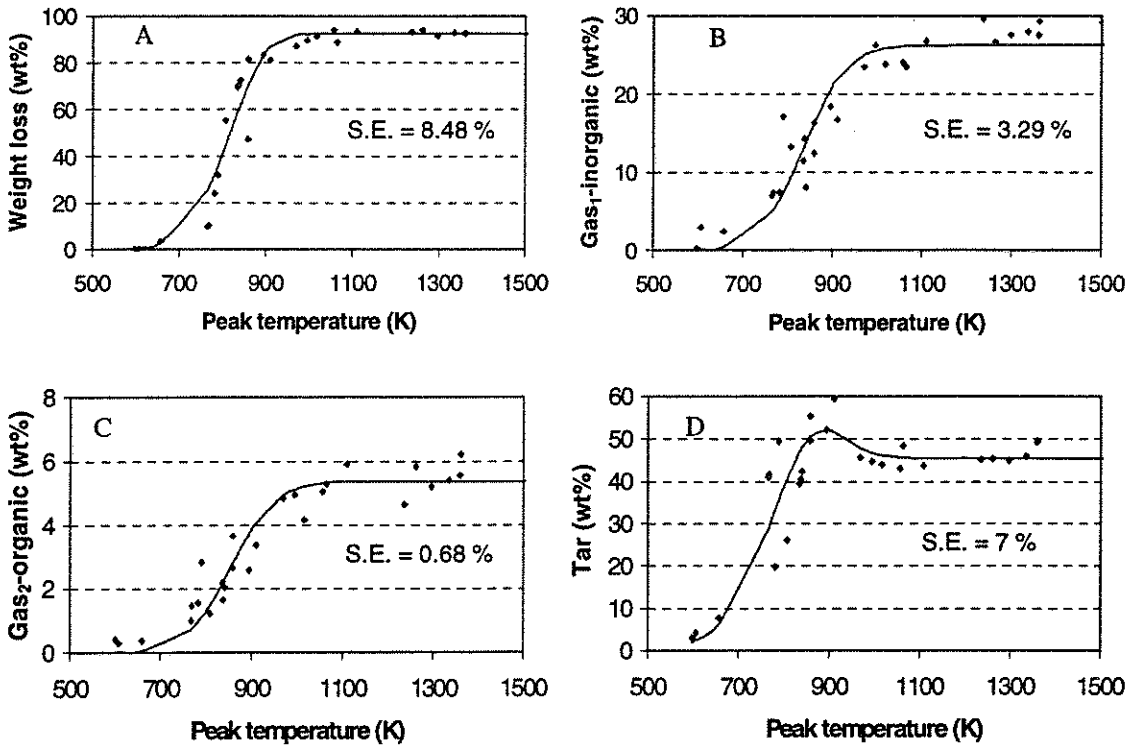

Figure 8. Comparison of experimental data with predicted yields. (A) Weight loss. (B) Gas_1 (inorganics). (C) Gas_2 (organics). (D) Tar. [Data for sweet gum hardwood[10]].

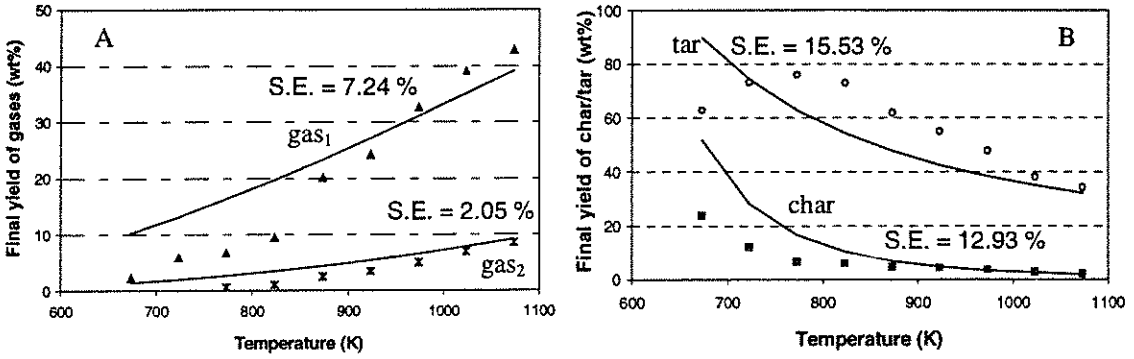

Figure 9. Comparison of experimental data with predicted yields. (A) Gas_1 (inorganics) and Gas_2 (organic). (B) Char and tar. [Data for maple wood sawdust[11]].

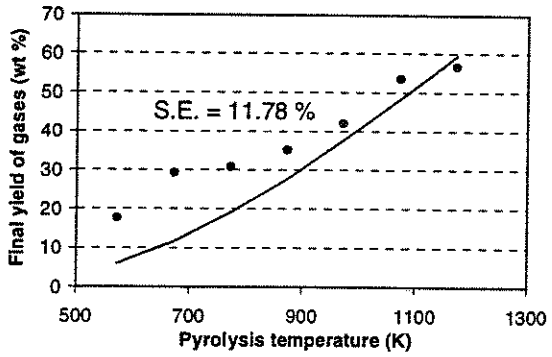

Figure 10. Comparison of experimental data with predicted yield of total gases. [Data for holm-oak wood[12]].

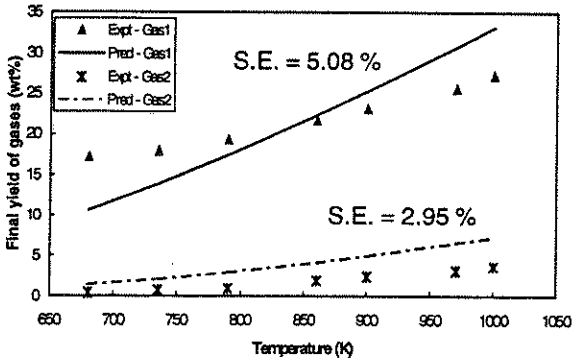

Figure 11. Comparison of experimental data with predicted yields of gases. [Data for wood chips[13]].

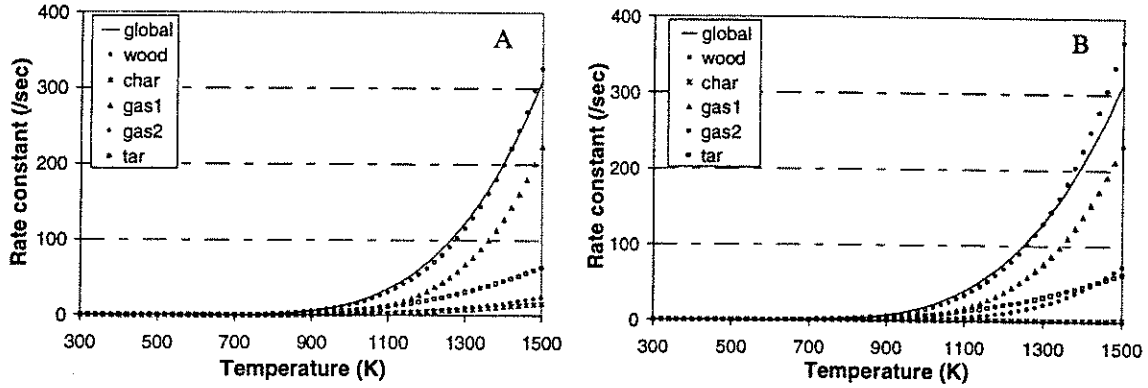

Figure 12. Rate constants for different reactions over the range of pyrolysis temperatures. (A) Milled wood lignin[7]. (B) Sweet gum hardwood[10].

Table I. Details of various studies on pyrolysis of lignocellulosic materials.

		Substrate	Reactor	Heating rate	Temp. range	Measurements
Data used for estimation	Nunn et al. (1985b)	Milled wood lignin (100 mg flakes ≤ 100 μm thick).	Electrical screen heater.	1000 K/s heating, to different peak temperatures.	600 – 1400 K.	Final weight loss, yields of gaseous species and tar.
	Nunn et al. (1985a)	Sweet gum hardwood (100 mg powder of size 45-88μm).	Electrical screen heater.	1000 K/s heating, to different peak temperatures.	600 – 1600 K.	Final weight loss, yields of gaseous species and tar.
Data used for validation	Caballero et al. (1993)	Klason lignin	Pyroprobe 1000 CDS	20 s holding time at different nominal temperatures.	800 – 1200 K.	Final char, tar, gaseous species yields.
	Figueiredo et al. (1989)	Holm-oak wood (8 mg powder of size 0.62-1 mm).	SS reactor with furnace.	60 min runs at different fixed temperatures.	600 – 1200 K.	Final yields of solid, liquids and total gas.
	Di Blasi et al. (1999)	Fir wood chips (size 1-3 mm) in a packed bed.	IR heater and quartz reactor	Not measured. Temperature assumed constant.	650 – 1050 K.	Final yields of solid, liquids, gaseous species.
	Scott et al. (1988)	Eastern red maple sawdust	Ultra pyrolysis/ fluidized bed	Instantaneous, short residence time. Isothermal runs	673 – 1073 K.	Final yields of char, liquids, gaseous species

Table II. Parameters for milled wood lignin pyrolysis based on the kinetic model of equation (6).

	Kinetic parameters (reported by Nunn et al., 1985b)				Kinetic parameters (calculated in this study)			
	log A_i (/s)	E_i (kcal/gmol)	V* (wt%)	S.E.[a] (wt%)	log A_i (/s)	E_i (kcal/gmol)	V* (wt%)	S.E.[a] (wt%)
wt. loss	5.53	19.60	84.35	5.76	5.68	20.22	84.89	3.30
total gases	2.17	9.60	36.54	1.85	1.60	6.88	34.50	1.38
CO	3.66	16.00	18.24	1.00	3.24	13.66	17.85	0.91
CH4	4.16	17.80	3.07	0.18	3.54	14.74	3.07	0.17

[a] Standard error of estimate, defined as $\left[\sum_{j=1}^{n}\left(V_j - \tilde{V}_j\right)^2 \Big/ (n-3)\right]^{1/2}$

Table III. Kinetic parameters estimated for milled wood lignin and sweet gum hardwood.

	Milled wood lignin (Nunn et al., 1985b)		Sweet gum hardwood (Nunn et al., 1985a)	
	A (/s)	E (J/gmol)	A (/s)	E (J/gmol)
Global	1.26×10^5	7.49×10^4	9.36×10^4	7.11×10^4
wood → c	1.31×10^3	5.52×10^4	7.03	2.16×10^4
wood → g1	5.66×10^5	9.78×10^4	3.48×10^5	9.12×10^4
wood → g2	8.85×10^3	7.41×10^4	2.14×10^5	9.97×10^4
wood → t	6.93×10^3	5.86×10^4	5.41×10^3	5.57×10^4

Table IV. Covariance matrix for estimated kinetic parameters.

	Milled wood lignin (Nunn et al., 1985b)		Sweet gum hardwood (Nunn et al., 1985a)	
	σ_A (/s)	σ_E (J/gmol)	σ_A (/s)	σ_E (J/gmol)
Global	3.51×10^4	1.94×10^3	2.02×10^4	1.41×10^3
wood → c	9.94×10^2	5.57×10^3	1.91	1.63×10^3
wood → g1	2.31×10^5	2.84×10^3	1.12×10^5	2.23×10^3
wood → g2	4.87×10^3	3.94×10^3	2.09×10^5	7.52×10^3
wood → t	1.37×10^3	1.22×10^3	9.6×10^2	1.12×10^3

ROTATING PACKED BEDS

A. PROBLEM DEFINITION

A rotating packed-bed for countercurrent gas-liquid contacting in a porous medium is a device in which centrifugal force is employed as an adjustable drive for flow of liquid over the porous packing while gas flow is driven by the pressure difference. The rotating packed bed (RPB) can be viewed as a centrifugal analog of conventional packed beds with, however, much higher mass transfer rates. Introduced by ICI as the HIGEE concept for distillation it was exclusively studied in CREL.

We are convinced that this device can be quite useful as a three phase reactor in enhancing the yield of intermediates in very fast gas-liquid solid catalyzed reactions, in producing a concentrated liquid product via steady state gas-liquid solid catalyzed operation and in accomplishing difficult devolitilization of reaction byproducts. The search for a suitable applied problem is on.

B. RESEARCH OBJECTIVES

Our current objective is to identify a process where the use of RPB would have the potential to dramatically improve the yield and to confirm this prediction by experimental studies. More general conclusions for a whole class of processes would then be drawn.

C. RESEARCH ACCOMPLISHMENTS

Over the years two major accomplishments have resulted from fundamental studies of RPB's in CREL:

i) We have confirmed the improvement in volumetric mass transfer coefficients in RPB's compared to gravity flow columns and have developed a correlation as a function of appropriate dimensionless groups.

ii) We have collected the first and only data for liquid holdup in RPB's and developed a correlation for its prediction. It was also shown that even in a PBR liquid may form rivulets in the direction of flow and that liquid structure in the bed is not isotropic.

Both of these accomplishments have been summarized in previous CREL annual reports which are available upon request.

D. FUTURE WORK

We are looking for a sponsor for one of the following activities:

i) Demonstrate the capabilities of the RPB to increase the yield of an intermediate in solid catalyzed gas-liquid reactions by orders of magnitude. Use proprietary process chemistry.

ii) Demonstrate the capabilities of RPB to generate, in unsteady state operation, concentrated sulfuric acid from dilute $S0_2$ streams.

iii) Demonstrate the capability of an RPB to remove particulates from a dust laden gas stream.

E. REFERENCES

1. A. Basic, "Liquid Holdup and Hydrodynamics of Rotating Packed Beds", D.Sc. Thesis, Washington University, St. Louis, December, 1992.
2. S. Munjal, "Fluid Flow and Mass Transfer in Rotating Packed Beds with Countercurrent Gas-Liquid Flow", D.Sc. Thesis, Washington University, St. Louis, December, 1986.

Dynamic simulation of a tray column for multi-component reactive distillation using a rate-based model

A. Problem Definition

Dynamic simulation plays an important role in process safety assessments and provides an improved understanding of startup and shutdown procedures. There exist extensive literatures on distillation dynamics with emphasis on process control and tray hydraulics. Many of these studies are in good agreement with experimental measurements in ordinary distillation columns. However, the situation becomes much more complicated when chemical reactions take place in these distillation columns.

It is well established that a distillation column can be used advantageously as a reactor for systems in which chemical reactions occur at temperatures and pressures suitable for distillation of components of the reactive mixture. The main advantages of this combined unit operation which is called reactive or catalytic (in presence of heterogeneous catalysts) distillation are as follow: reactant conversion can be increased by overcoming chemical equilibrium limitations through the removal of reaction products; heat duty can be reduced by utilizing the heat of reaction; and limitations of azeotropic mixture can be overcome by reaction.

Due to these practical merits of reactive distillation, extensive studies dealing with the steady state simulation and its experimental verification have been conducted over the past few decades. The examples treated in the literature are hydrolysis of acetic anhydride, esterification of acetic acid with methanol (Agreda et al., 1990) and ethanol (Alejski and Duprat, 1996), transesterification of butyl acetate with ethanol (Davis and Jeffreys, 1973), synthesis of propylene oxide from propylene chlorohydrins (Carra et al., 1979a), synthesis of epichlorohydrine from chlorohydrins (Carra et al., 1979b), synthesis of ethylene glycol from ethylene oxide (Ciric and Gu, 1994), and Nylon-6,6 production (Grosser et al., 1987). All of these are based on homogeneous reaction systems. The combination of reaction and distillation over a solid catalyst bed has also been investigated. Typical examples of such a heterogeneous reaction system are MTBE production (Smith, 1984; Sundmacher and Hoffmann, 1994, 1996; Mohl et al., 1997), cumene production (Shoemaker and Jones, 1987), and aromatic alkylation. In simulation studies physical equilibrium models are mainly used for homogeneous reaction systems as opposed to the rate-based (or non-equilibrium) models. The physical equilibrium models, which assume physical equilibrium between the vapor and the liquid phase, stem from non-reactive distillation. However, this assumption may not be reasonable for a system in which strong transport resistance and/or rapid reaction is present. Furthermore, the prediction of tray efficiencies or HETPs, which corrects the departure from equilibrium in an actual column, is extremely difficult and unreliable in case of multi-component separation with chemical reaction. Therefore, the rate-based model, which is more realistic, is the preferred method for reactive distillation columns.

We at CREL have developed a steady-state simulation code for reactive distillation tray columns, which uses the rate-based model and the Homotopy-

Continuation method to guarantee a converged solution (Lee and Dudukovic, 1998). The results showed that the rate-based model is to be preferred for the simulation of a tray column for reactive distillation because of the higher accuracy compared to the equilibrium model. As a next step, dynamic simulation should be done in order to investigate the transient column behavior and the effect of operation conditions on column dynamics. Some papers regarding dynamic simulation of reactive distillation have been published so far (Bisowarno et al., 2000; Scenna et al., 2000; Alejski and Duprat, 1996; Sneesby et al., 1997). In these papers, however, hastily simplified models of the column were applied (physical equilibrium models, material balance equation only, theoretical trays, and constant molar holdup). Therefore, a fully rate-based dynamic model which does not require the concepts of tray efficiency or HETP and which considers varying liquid holdup in the column, should be developed.

B. Research Objectives

The primary objectives of this study is to develop a fully rate-based dynamic model for reactive distillation which includes tray hydraulic correlations for varying liquid holdup on a tray as well as an algorithm for solving the coupled Differential and Algebraic Equations (DAEs), and to predict transient behavior of a reactive distillation column during the startup operation. The verification of the dynamic simulation results is achieved by comparing the long-time behavior (after 20 hours) of the column in the dynamic state with the steady-state results. To solve the resulting DAEs, either implicit methods (such as implicit two-point method) or backward differentiation formulas (such as Gear method) and the homotopy-continuation method are applied in addition to resolving the inconsistency problem. As a test, a homogeneous liquid phase reversible reaction of ethyl acetate production is studied. The effects of operating conditions (feed composition, reflux ratio, heat duties, etc.) on the column dynamics are investigated.

C. Research Accomplishments

C1. Mathematical Model

The rate-based dynamic model for a non-reactive distillation column developed by Kooijman and Taylor (1995), is adopted for the rate-based model for reactive distillation by including the chemical reaction terms and tray hydraulic correlations. The assumptions used in this study are summarized in Table 1. The process of simultaneous mass and heat transfer through the interface is modeled by means of rate equations and transfer coefficients (Krishna and Standart, 1979).

The condenser and reboiler are each considered as an equilibrium tray. Table 2 summarizes the resulting set of equations for the fully rate-based dynamic model and tray hydraulics. The rate-based model is based on the generalized Maxwell-Stefan equations for multi-component transport in a film. According to the theory of Krishna and Standart (1979), the mass transfer coefficients for multi-component systems can be calculated directly from the binary mass transfer coefficients of components. Table 3 shows

corresponding equipment parameters, which are necessary for the estimation of mass transfer coefficients.

Table 1. Assumptions used in rate-based model development

• System reaches mechanical equilibrium.
• The interface between the liquid and vapor phases is assumed to be uniform in each tray.
• The vapor and liquid bulks on each side of the interface are perfectly mixed.
• There is no accumulation of mass and heat at the interface.
• Heat of mixing can be neglected.
• The condenser and reboiler are considered as an equilibrium tray.
• The molar amounts of vapor in the condenser and reboiler are assumed to be negligible because of relatively large volume of the liquid phase
• Reactions are assumed to take place in the liquid bulk only.

C2. Solution Method for the DAEs

In chemical process models, discontinuities naturally arise because of the planned process operations (such as switching a valve) or inherent sudden changes in the process (such as phase change, flow reversals, or piecewise defined model equations). Usually, these discontinuities are modeled by a step function, which results in a discontinuity in the DAEs. To resolve the inconsistency problem, a forcing function, $\Phi = -2*t^3+3*t^2$ where t is time, is used for the first second. To solve the DAEs simultaneously, the implicit Euler method with the extrapolating method and the homotopy-continuation method are employed.

C3. Dynamic simulation results

For the purpose of predicting the transient behavior of a reactive distillation tray column during the startup operation, a series of simulations were made.

Figure 1 shows the transient response of the column after the feed composition was switched to have an equimolar ratio of two reactants (acetic acid and ethanol) during the first one second. The total molar feed rate was fixed as were the pressure, reflux ratio, and bottoms flow rate. Before switching the feed, the whole column was mainly filled with ethanol in which negligible chemical reaction took place. As soon as the feed composition was switched, which means as the reaction condition became more favorable, the reaction rate and the liquid bulk temperature on the feed tray increased quickly, and subsequently the required heat duties, inter-tray liquid and vapor flow rates, and the clear liquid height varied rapidly. The heat produced by reaction was propagated to the stripping section of the column by means of the inter-tray liquid flow, which caused the increase in the temperatures of the stripping section. About 4 minutes after the

Table 2. Mathematical model for the non-equilibrium trays

Material balance for component i on the j th tray

(Vapor phase) $$0 = V_{j+1}\frac{M_{ij+1}^V}{\sum M_{ij+1}^V} - (1+S_j^V)V_j\frac{M_{ij}^V}{\sum M_{ij}^V} + F_j^V z_{ij}^V - N_{ij} + r_{ij}^V - \frac{d\,M_{ij}^V}{dt} \quad (1)$$

(Liquid phase) $$0 = L_{j-1}\frac{M_{ij-1}^L}{\sum M_{ij-1}^L} - (1+S_j^L)L_j\frac{M_{ij}^L}{\sum M_{ij}^L} + F_j^L z_{ij}^L + N_{ij} + r_{ij}^L - \frac{d\,M_{ij}^L}{dt} \quad (2)$$

Heat balance on the jth tray

Vapor phase: $$0 = V_{j+1}\frac{E_{j+1}^V}{\sum M_{ij+1}^V} - (1+S_j^V)V_j\frac{E_j^V}{\sum M_{ij}^V} + F_j^V H_j^{VF} - h_j^V a_j(T_j^V - T_j^I) - \sum N_{ij}\tilde{H}_{ij}^V - Q_j^V - \frac{d\,E_j^V}{dt} \quad (3)$$

Liquid phase: $$0 = L_{j-1}\frac{E_{j-1}^L}{\sum M_{ij-1}^L} - (1+S_j^V)L_j\frac{E_j^L}{\sum M_{ij}^L} + F_j^L H_j^{LF} + h_j^L a_j(T_j^I - T_j^L) + \sum N_{ij}\tilde{H}_{ij}^L - Q_j^V - \frac{d\,E_j^L}{dt} \quad (4)$$

$$R(K+2C+3+i) = L_{j-1}(x_{ij-1}^L - x_{ij}^L) + F_j^L(z_{ij}^L - x_{ij}^L) + (N_{ij} - N_{ij}x_{ij}^L) + (r_{ij}^L - r_{ij}^L x_{ij}^L) - M_j^L S(K+2C+3+i)$$

Transfer equations at the interface

Vapor phase:

$$0 = N_{ij} - C_t^V \Delta V^V \sum_{k=1}^{c-1} k_{ik}^V a_j\left(\frac{M_{kj}^V}{\sum M_{ij}^V} - y_{kj}^I\right) - \frac{M_{ij}^V}{\sum M_{ij}^V}\sum_{k=1}^{c} N_{kj}, \qquad i = 1,2,\ldots,c-1 \quad \text{where } \left[k_{ik}^V\right]a = \left[B_{ik}^V\right]^{-1}a \quad (6)$$

Liquid phase:

$$0 = N_{ij} - C_t^L \Delta V^L \sum_{k=1}^{c-1} k_{ik}^L a_j\left(x_{kj}^I - \frac{M_{kj}^L}{\sum M_{ij}^L}\right) - \frac{M_{ij}^I}{\sum M_{ij}^L}\sum_{k=1}^{c} N_{kj}, \qquad i = 1,2,\ldots,c-1, \ \left[k_{ik}^L\right]a = \left[B_{ik}^L\right]^{-1}a\left[\Gamma_{ik}^L\right] \quad (7)$$

Within the interface:

$$0 = h_j^V a_j(T_j^V - T_j^I) - h_j^L a_j(T_j^I - T_j^L) + \sum_{k=1}^{c} N_{kj}(\tilde{H}_{kj}^V - \tilde{H}_{kj}^L) \quad (8)$$

Phase equilibrium equation at the interface

$$0 = K_{ij}^I x_{ij}^I - y_{ij}^I \quad (9)$$

Constraints of each phase

$$0 = \sum M_{ij}^V - \Delta V_j^V \rho_{j,av}^V / M_{wj,av}^V \quad (10) \qquad 0 = \sum M_{ij}^L - \Delta V_j^L \rho_{j,av}^L / M_{wj,av}^L \quad (11)$$

$$0 = E_j^V - \sum_{i=1}^{c} M_{ij}^V \tilde{H}_{ij}^V(T_j^V) \quad (12) \qquad 0 = E_j^L - \sum_{i=1}^{c} M_{ij}^L \tilde{H}_{ij}^L(T_j^L) \quad (13)$$

Liquid volume in a sieve tray

Liquid volume in a tray = f (liquid flow rate, vapor flow rate)

$\Delta V^L = A \cdot h_{cl}$ = (area) · (clear liquid height) (14)

$h_{cl} = (1-\varepsilon)(h_w + h_{ow})$ where ε is vapor fraction,

h_w = weir height (known), and h_{ow} = height of the liquid over the weir

$$h_{ow} = \frac{0.49}{C_d^{0.67}}\left(\frac{Q_L}{(1-\varepsilon)W}\right)^{0.67} + \frac{125(u_s - u_b)^2 \rho_{av}^V}{g(\rho_{av}^L - \rho_{av}^V)\varepsilon^2}$$ (Stichlmair and Mersmann,1978)

where Q_L is volumetric liquid flow rate [m^3/s], u_s is gas superficial velocity [m/s], and $u_b = 1.55\left(\frac{\sigma(\rho_{av}^L - \rho_{av}^V)g}{(\rho_{av}^L)^2}\right)^{0.25}\left(\frac{\rho_{av}^V}{\rho_{av}^L}\right)^{0.0417}$ is bubble velocity [m/s]

Vapor volume in a tray = Total physical volume of a tray – Liquid volume in a tray

$$\Delta V^V = V^{total} - \Delta V^L \quad (15)$$

Table 3. Specifications and tray sizing parameters

1. Reaction: $CH_3COOH + C_2H_5OH \leftrightarrow CH_3COOC_2H_5 + H_2O$
1 2 3(desired) 4

$r_3 = EXP(-7150/T)\ [\ 4.85E4\ C_1C_2\ -\ 1.23E4\ C_3C_4\ ]$ (mol/liter.sec)

2. Column:

number of trays	: 15 (condenser, 11 trays, reboiler)
number of components	: 4
feed location	: 7 th tray from the condenser
column diameter	: 0.600 m
weir length	: 0.457 m
exit weir height	: 0.050 m
liquid flow path length	: 0.374 m
active tray bubbling area	: 0.200 m^2
tray spacing	: 0.340 m
top pressure	: 1.0 x 10^5 Pa
reaction zone	: 1st to 15 th tray in the liquid bulk phase
volumetric liquid holdup	: 3 liter on each tray

3. Condenser:
equilibrium tray (tray number 1: drum; tray number 2: chiller)

reflux ratio	: 10
liquid flow rate to 3nd tray	: L_1 (known) = 2.080 mol/s
volumetric liquid holdup	: 4 liter for the drum and 4 liter for the chiller

4. Reboiler:
equilibrium tray (tray number 14: drum; tray number 15: boiler)

bottom liquid flow rate	: L_N(known) = 0.868 mol/s
volumetric liquid holdup	: 4 liter for the drum and 4 liter for the boiler

5. Feed:
total liquid flow rate = 1.076 mol/s
composition ; $x_1 = 0.0200, x_2 = 0.9800, x_3 = 0.0000, x_4 = 0.0000$ (at $t < t1$)
$x_1 = 0.4962, x_2 = 0.4808, x_3 = 0.0000, x_4 = 0.0229$ (at $t = t1$)

6. Nonideality:

liquid phase	: modified Margules equation (Suzuki et al., 1971)
vapor phase	: Ideal gas law

7. Binary diffusion coefficients:

liquid phase	: Wesselingh and Krishna(1990)
vapor phase	: Fuller, Ensley and Giddings(1969)
8. Binary mass transfer coefficients	: AIChE method(1958) and Bennet et al.(1983)
9. Heat transfer coefficients	: Chilton-Colburn analogy

switch in feed, the liquid bulk temperature of the feed tray showed a maximum. After passing through a maximum, the temperature decreased and reached a steady state, but the liquid and vapor flow rates, as well as the required heat duties, exhibited another maximum at around 1 hour (Figure 1 - (c), (d), and (e)).

To understand the cause of second maximum, another series of simulations were executed by changing the order of magnitude of the kinetic constants. Figure 1(d) and (e) shows that the height of each maximum increases with the increase in the reaction rate. The heat produced by reaction, which builds up on the feed tray from the starting time, plays a role of an extra heat source in the middle of the column, which causes the required heat duty of the reboiler to decrease until the produced heat decreases, and this causes the decrease in the liquid and vapor flow rates. As the produced heat by reaction decreases, however, the required heat duty of the reboiler must be increased to keep the reflux ratio constant, which causes subsequent increase in the vapor flow rate. As the vapor flow rate increases with the reboiler heat duty, the condenser heat duty has to increase to liquefy the increased vapor flow, which causes the increase in the internal liquid flow rates. But when the internal liquid flow rates increased sufficiently, the condenser heat duty must be decreased to keep the bottoms flow rate constant, and this causes another decrease in the liquid and vapor flow rates. By this consecutive multiple feedbacks of the condenser and reboiler, the internal flow rates finally reach a steady state. Based on the above reasoning, it can be argued that the appearance of the second maximum during the startup operation is due to the exothermic reaction in a reactive distillation tray column.

As shown in Figure 1, reaction rate is the main factor that determines the dynamic behavior of the reactive distillation column. Even if the steady-state values of the liquid and vapor flow rates are in an operable region in case of high reaction rate, the liquid and vapor flow rates may go beyond the boundary of the desirable operating region during the startup operation. This means that higher reaction rate is not always good for achieving a higher product yield because higher reaction rate may cause an unfavorable operating situation (e.g., entrainment or flooding) inside the column during the transient operation. This also implies that the results from steady-state simulations do not always guarantee the operability or controllability of the reactive distillation column.

The mass transfer rate of each component also varied rapidly with time when the feed composition was changed. The mass transfer rate of the ethyl acetate from the liquid to vapor phase was the fastest at the top of the column, but that of the acetic acid from the vapor to liquid phase was the highest at the bottom of the column. This is due to the fact that the ethyl acetate is produced in the liquid phase and is a light component, but the acetic acid is a heavy reactant. Figure 1-(f) also displays typical values of the back-calculated Mursphree tray efficiency. As shown, the individual tray efficiencies vary drastically with time, which implies that the equilibrium model could not be appropriate for dynamic simulation when chemical reaction takes place in the column.

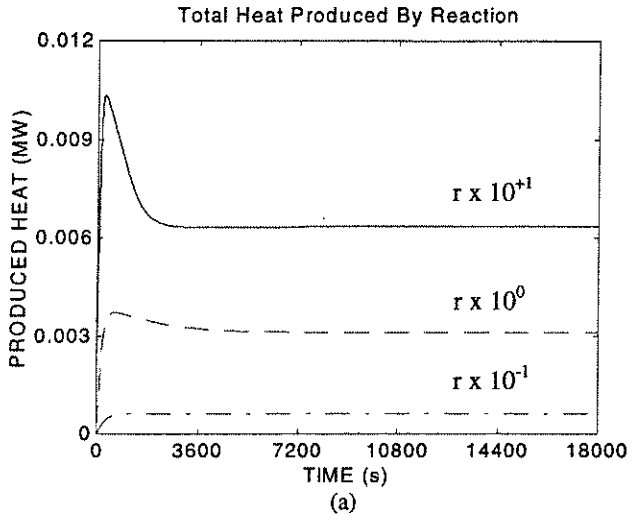
Total Heat Produced By Reaction
PRODUCED HEAT (MW)
0.012
0.009
0.006
0.003
0
r x 10^+1
r x 10^0
r x 10^-1
0
3600
7200
10800
14400
18000
TIME (s)
(a)

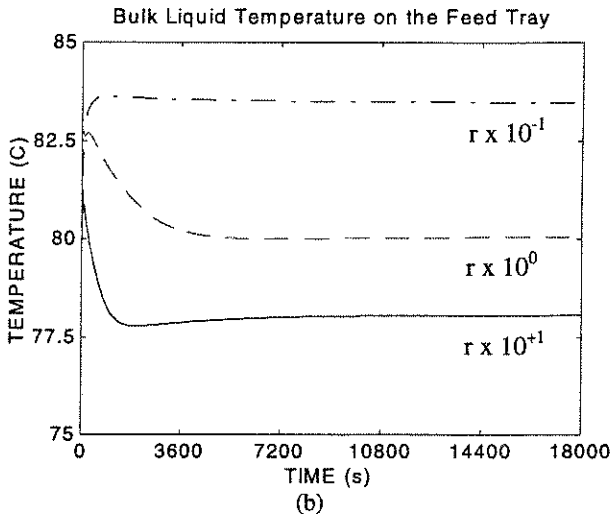
Bulk Liquid Temperature on the Feed Tray
TEMPERATURE (C)
85
82.5
80
77.5
75
r x 10^-1
r x 10^0
r x 10^+1
0
3600
7200
10800
14400
18000
TIME (s)
(b)

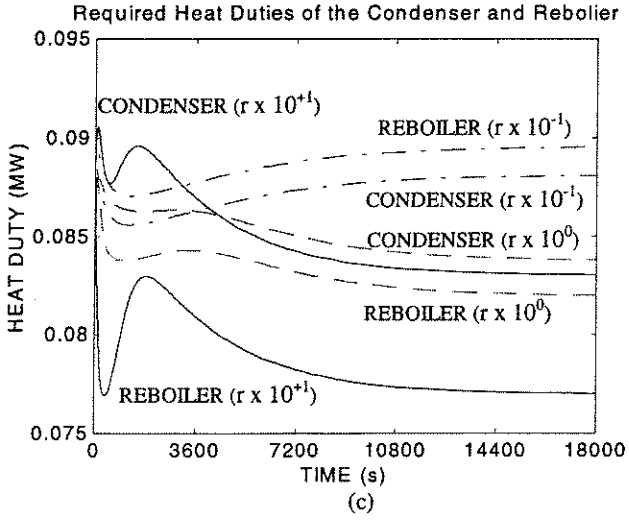
Required Heat Duties of the Condenser and Rebolier
HEAT DUTY (MW)
0.095
0.09
0.085
0.08
0.075
CONDENSER (r x 10^+1)
REBOILER (r x 10^-1)
CONDENSER (r x 10^-1)
CONDENSER (r x 10^0)
REBOILER (r x 10^0)
REBOILER (r x 10^+1)
0
3600
7200
10800
14400
18000
TIME (s)
(c)

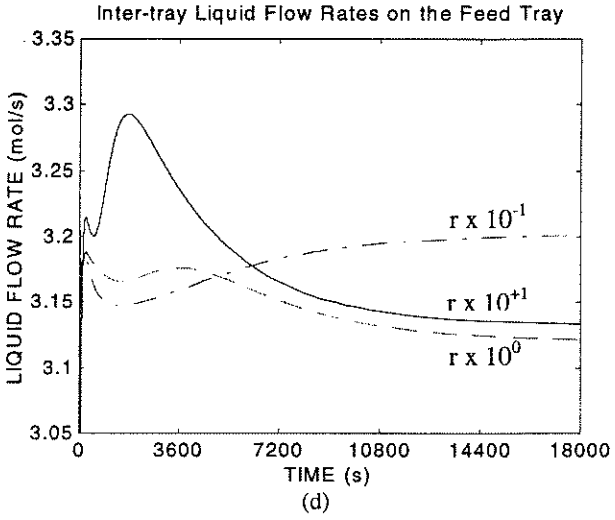
Inter-tray Liquid Flow Rates on the Feed Tray
LIQUID FLOW RATE (mol/s)
3.35
3.3
3.25
3.2
3.15
3.1
3.05
r x 10^-1
r x 10^+1
r x 10^0
0
3600
7200
10800
14400
18000
TIME (s)
(d)

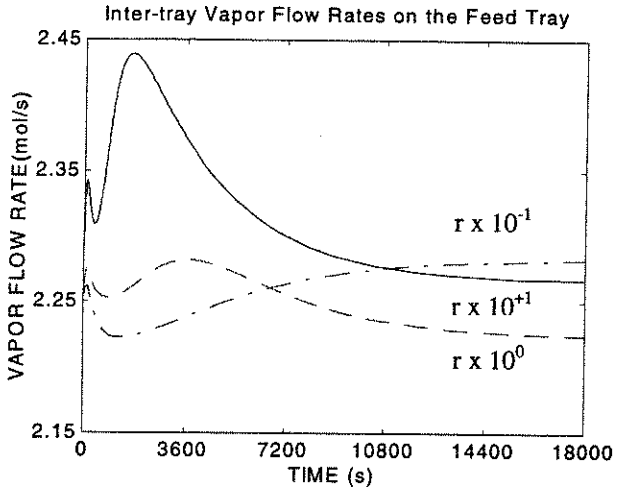

(e)

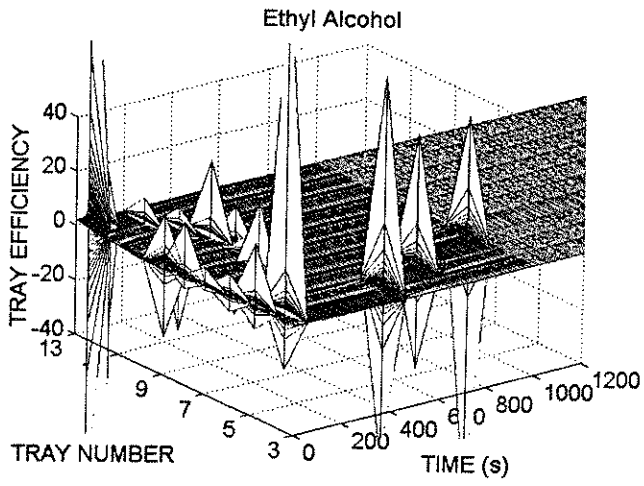

(f)

Figure 1. Transient response of each variable in the reactive distillation tray column to the change in the feed composition from (acetic acid: 0.02; ethanol: 0.98) to (acetic acid: 0.49; ethanol: 0.48; water: 0.03); the term r x 10^{-1} and r x 10^{+1} denote 10 times slower and faster reaction rate specified in the previous paper (Lee and Dudukovic, 1998) respectively.

D. Future work

The developed rate-based dynamic model for reactive distillation tray column will also be applied to other reaction systems (e.g., ethylene glycol production system). Furthermore, the fully rate-based model for a catalytic distillation column will also be developed on the basis of the model for reactive distillation. For this purpose, a combined approach of modeling and experiments will be used. In the modeling work, a fully rate-based model for catalytic distillation, which reflects the coupling of the kinetics and transport phenomena, will be implemented. To evaluate the parameters needed for the rate-based model, a series of experiments will be done on model contactors as well as on pilot scale reactors, for chosen systems of commercial interest (such as The hydrogenation of benzene to cyclohexane). The objective of this workis to develop a simulation and design tool for catalytic (reactive) distillation process, which can fulfill fast and effective screening of potential applications, feasibility study, checking of operability and controllability of the process by dynamic simulation and optimization of the process.

E. Nomenclature

a_j effective interfacial area of the j th tray (m^2/tray)

C total number of components

C_t total concentration in the bulk phase (mol/l)

E_j^L total energy of the liquid bulk on the j th tray (J)

E_j^V total energy of the vapor bulk on the j th tray (J)

F_j^L total liquid feed rate on the j th tray (mol/s)

F_j^V total vapor feed rate on the j th tray (mol/s)

H_j molar enthalpy of the bulk phase (J/mol)

$\tilde{H}_{kj}^L$ partial molar enthalpy of component i in the liquid(J/mol)

H_j^{LF} molar enthalpy of liquid feed (J/mol)

h_j heat transfer coefficient (J/m^{2}sK)

$\tilde{H}_{kj}^V$ partial molar enthalpy of component i in the vapor(J/mol)

H_j^{VF} molar enthalpy of vapor feed (J/mol)

k_{ik}^V matrix element of multicomponent mass transfer coefficients at the vapor side of the vapor-liquid interface (mol/m^{2}s)

k_{ik}^L matrix element of multicomponent mass transfer coefficients at the liquid side of the vapor-liquid interface (mol/m^{2}s)

K_{ij}^I equilibrium ratio at the interface

L_j total liquid flow rate from the j th tray (mol/s)

L_F volumetric liquid flow rate per unit weir length (m^2/s)

M_{ij}^L molar holdup of component i in the liquid phase (mol)

M_{ij}^V molar holdup of component i in the vapor phase (mol)

$M_{wj,av}$ average molecular weight on the j th tray (g/mol)

N_{ij} mass transfer rate for component i from the vapor to the liquid phase (mol/s)

N total number of trays including the condenser and the reboiler

Q_j heat duty on the j th tray (W)

r_{ij}^L formation rate of component i due to the liquid phase reaction (mol/s)

S_j^L ratio of withdrawal to liquid flow rate of inter-tray

S_j^V ratio of withdrawal to vapor flow rate of inter-tray

T_j^I temperature at the interface (K)

T_j^L temperature of bulk liquid phase (K)

T_j^V temperature of bulk vapor phase (K)

V_j total vapor flow rate from the j th tray (mol/s)

ΔV total volume of the bulk phase (l)

x_{kj}^I mole fraction of component k at the liquid side of the interface

x_{kj}^L mole fraction of component k in the bulk liquid

y_{kj}^I mole fraction of component k at the vapor side of the interface

y_{kj}^V mole fraction of component k in the bulk vapor

z_{ij} mole fraction of component i in the feed

ρ_t^V molar vapor density (mol/m^3)

Γ_{ik}^L partial derivative of activity coefficient with liquid mole fraction

F. References

1. Agreda, V. H., Partin, L. R., and Heise, W. H., "High-purity methyl acetate via reactive distillation," *Chem. Eng. Prog.*, **86**, 40 (1990)

2. Alejski, K., "Computation of the reacting distillation column using a liquid mixing model on the plates," *Computers. Chem. Engng.*, **15**, 313 (1991)

3. Alejski, K. and Duprat, F., "Dynamic simulation of the multicomponent reactive distillation," *Chem. Eng. Sci.*, **51**, 4237 (1996)

4. Bisowarno, B. H. and Tade, M. O., "Dynamic Simulation of startup in Ethyl tert-Butyl Ether reactive Distillation with Input Multiplicity", *Ind. Eng. Chem. Res.*, **39**, 1950 (2000)

5. Carra, S., Morbidelli, M., Santacesaria, E., and Buzzi, G., "Synthesis of propylene oxide from propylene chlorohydrines II. Modeling of the distillation with chemical reaction unit," *Chem. Eng. Sci.*, **34**, 1133 (1979a)

6. Carra, S., Santacesaria, E., Morbidelli, M., Schwarz, P., and Divo, C., "Synthesis of epichlorohydrin by elimination of hydrogen chloride from chlorohydrines. 2. Simulation of the reaction unit," *Ind. Engng. Chem. Process Des. Dev.*, **18**, 428 (1979b)

7. Ciric, A. R. and Gu, D., "Synthesis of nonequilibrium reactive distillation processes via mixed integer nonlinear programming," *AIChE J.*, **40**, 1479 (1994)

8. Davis, B. and Jeffreys, G. V., "The continuous trans-esterification of ethyl alcohol and butyl acetate in a sieve plate column. Part 3. Trans-esterification in a six plate sieve tray column," *Trans. Inst Chem. Engrs.*, **51**, 275 (1973)

9. Grosser, J. H., Doherty, F. M., and Malone M. F., "Modeling of reactive distillation systems," *Ind. Engng. Chem. Res.*, **26**, 983 (1987)

10. Higler, A., Taylor, R., and Krishna, R., "Nonequilibrium modeling of reactive distillation: Multiple steady satates in MTBE synthesis," *Chem. Eng., Sci.*, **54**, 1389 (1999)

11. Kooijman, H. A. and Taylor, R., "A nonequilibrium model for dynamic simulation of tray distillation columns," *AIChE J.*, **41**, 1852 (1995)

12. Krishna, R. and Standart, G. L., "Mass and energy transfer in multicomponent systems," *Chem. Eng. Commun.*, **3**, 201 (1979)

13. Lee, J.-H. and Dudukovic, M., "A comparison of the equilibrium and nonequilibrium models for a multi-component reactive distillation column", *Computers. Chem. Engng.*, **23**, 159 (1998)

14. Majer, C., Marquardt, W., and Gilles, E. D., "Reinitialization of DAE's after discontinuities," *Computers Chem. Engng.*, **19**, S507 (1995)

15. Mohl, K. D., Kienle, A., and Gilles, E. D., "Nonlinear dynamics of reactive distillation process for the production of fuel ethers," *Computers Chem. Engng.*, **21**, S989 (1997)

16. Reuter, E., Wozny, G., and Jeromin, L., "Modeling of multicomponent batch distillation processes with chemical reaction and their control systems," *Computers Chem. Engng.*, **13**, 499 (1989)

17. Scenna, N. J., Ruiz, C.A., Benz, S. J., "Dynamic Simulation for the Startup Operation of Reactive Distillation Columns", *Lat. Am. Appl. Res.*, **30**, 9 (2000)

18. Shoemaker, D. and Jones, E. M., "Cumene by catalytic distillation," *Hydrocarbon Process.*, **57**, June (1987)

19. Smith, L. A., "Catalytic distillation structure," *US Patent No. 4,443,559* (1984)

20. Sneesby, M.G., Tade, M.O., Datta, R., and Smith, T.N., "ETBE synthesis via reactive distillation. 2. Dynamic Simulation and control aspects," *Ind. Eng., Chem., Res.*, **36**, 1870 (1997)

21. Stichlmair, J. and Mersmann, A., "Dimensioning plate columns for absorption and rectification," *Int. Chem. Eng.*, **18**, 223 (1978)

22. Sundmacher, K., Uhde, G., and Hoffmann, U., "Multiple reactions in catalytic processes for the production of the fuel oxygenates MTBE and TAME: Analysis by rigorous model and experimental validation," *Chem. Eng. Sci.*, **54**, 2839 (1999)

23. Suzuki, I., Yagi, H., Komatsu, H., and Hirata, M., "Calculation of multicomponent distillation accompanied by a chemical reaction", *J. Chem. Eng. Japan*, **4**, 26 (1971)

24. Taylor, R. and Krishna R., in *Multicomponent Mass Transfer*, John Wiley, New York, 1993

25. Wesselingh, J. A. and Krishna, R., *Mass Transfer*, Ellis Horwood, Chichester, England, 1990

CARPT APPLIED TO THE ANALYSIS OF PHOTOBIOREACTORS

A. Problem Definition

The capacity of microalgae for synthesizing complex organic molecules using simple cheap inorganic compounds, such as water or carbon dioxide, is an attractive possibility for the industrial manufacturing of several products. Particular attention has attracted the possibility of producing high value products such as fine chemicals and drugs from microalgae and cyanobacteria. In spite of this interest, the development of microalga-based productive processes is meagre due to the relative high investment, high operation costs and low productivity of the culture systems now available for the phototrophic growth of microalgae. The most interesting products and processes are derived from or based on the so-called "sensitive" strains, that can not be grown in open systems due to their susceptibility are to contamination by other strains or bacteria and their sensitivity to environmental conditions. Those strains most usually only can use light as their energy source and must be grown in closed culture systems (photobioreactors, PBR). Currently, the design of photobioreactors requires extensive, costly and labor-intensive empirical development effort and the yield of processes based on phototrophic microorganisms is well below the theoretical optimum.

Rational PBR design request quantitative knowledge in the topics described next. As in any other fermentor, the productivity of a photobioreactor is the product of biomass concentration (Cb) by specific growth rate (μ), so the use of high density cultures is a must in particular with microalgae, that are slow-growing microorganisms specially compared to bacteria and yeast. This situation arises a design challenge because dense cultures are optically thick and light penetration is impeded, causing a low growth rate and thus lowering the productivity. These are two counteracting factors that have to be balanced for an optimal performance. The classical solution given to this problem is the use of short light path devices. This involves the use of small diameter tubes and result in photobioreactors with a high per liter productivity at the cost of giving a small volume and therefore a high cost per liter installed. Another drawback of this solution is that the high irradiance dose received in the end by the cultures causes a low yield of the light used and, frequently, impairs growth rate due to photoinhibition.

A different approach is to take into account the long known fact that photosynthetic growth can be sustained by a discontinuous support of light (intermittent light), as long as the intermittence parameters are kept within certain limits. This is proved in the works of many authors, like Kok (1953) Philip and Myers (1954), Terry (1986), or the more recent interesting results published by Nedbal et al. (1996). The situation in a long-light-path high-density photobioreactor resembles growth under intermittent light, with the difference that in dense cultures irradiance variations are continuous instead of discrete and is caused by the movement of the fluid dragging the microbes among zones in different illumination. Currently there is little knowledge on how light patterns inside dense photobioreactors are and therefore it is not possible to determine how design

changes can influence, modify or be used to control and optimize the light regime and get an optimum growth rate in high density cultures.

B. Research Objectives

The temporal light pattern cells are exposed to inside a photobioreactor is the consequence of fluid movement within zones of different illumination level (irradiance field). Therefore, the determination of these patterns request knowledge about:

- Irradiance field: a function of the device shape and size, external illumination, biomass concentration and its optical properties.
- Fluid movement: hydrodynamics

A lot has been done to study the irradiance field in microalgal cultures (Acien Fernandez et al., 1997, Molina Grima et al. 1997, Molina Grima et al., 1999) so that problem can be reasonably solved for most kind of PBRs to obtain the irradiance field, which is a description of the irradiance I in each space position (x,y,z) inside the PBR. This is noted as I(x,y,z) and can be obtained as a function or as a computer program. On the contrary, little is known about the movement of fluid elements inside PBRs in operating conditions. The necessary basic information is a temporal evolution of the position of a representative fluid element or, better, a particle that can represent a cell. This is described by data of position of such an element vs time, x(t), y(t), z(t). If the irradiance gradient is also known it is straightforward to obtain the irradiance time pattern as $I(x(t),y(t),z(t))=I(t)$. In this work the suitability of Computer Assisted Radioactive Particle Tracking (CARPT) to study and describe fluid movement in PBR is tested.

The research focuses on three bubble column type PBRs widely used for microalgal culture. The systems are a simple bubble column, and two other systems with internal recirculation: a split cylinder and a draught tube. All three are shown in figure 1.

The experiments were carried out in a range of operating conditions (superficial gas velocity) used in microalgal cultures. The objectives of the work were the following:

- To obtain a description of the fluid movement in each device and operating condition using Computer Automated Radioactive Particle Tracking (CARPT) for a significant period of time (20h).
- To calculate irradiance fields corresponding to different biomass concentrations in the range of microalgal cultures.
- To obtain the corresponding time irradiance pattern for each of the systems and operating conditions proposed.

- Qualitative analysis of the influence of type of system and operating conditions on the time irradiance pattern; ie: dark periods length, cycling frequency and exposure regularity.

C. Research Accomplishments

Computer Assisted Radioactive Particle Tracking (CARPT) have been used to investigate the flow in a three different devices that are usually used as photobioreactors for growing microalgae. The devices are two internal recirculation bubble columns in a split cylinder and a draught tube configuration. Available data of a plain bubble column is also analyzed. The devices are described in figure 1.

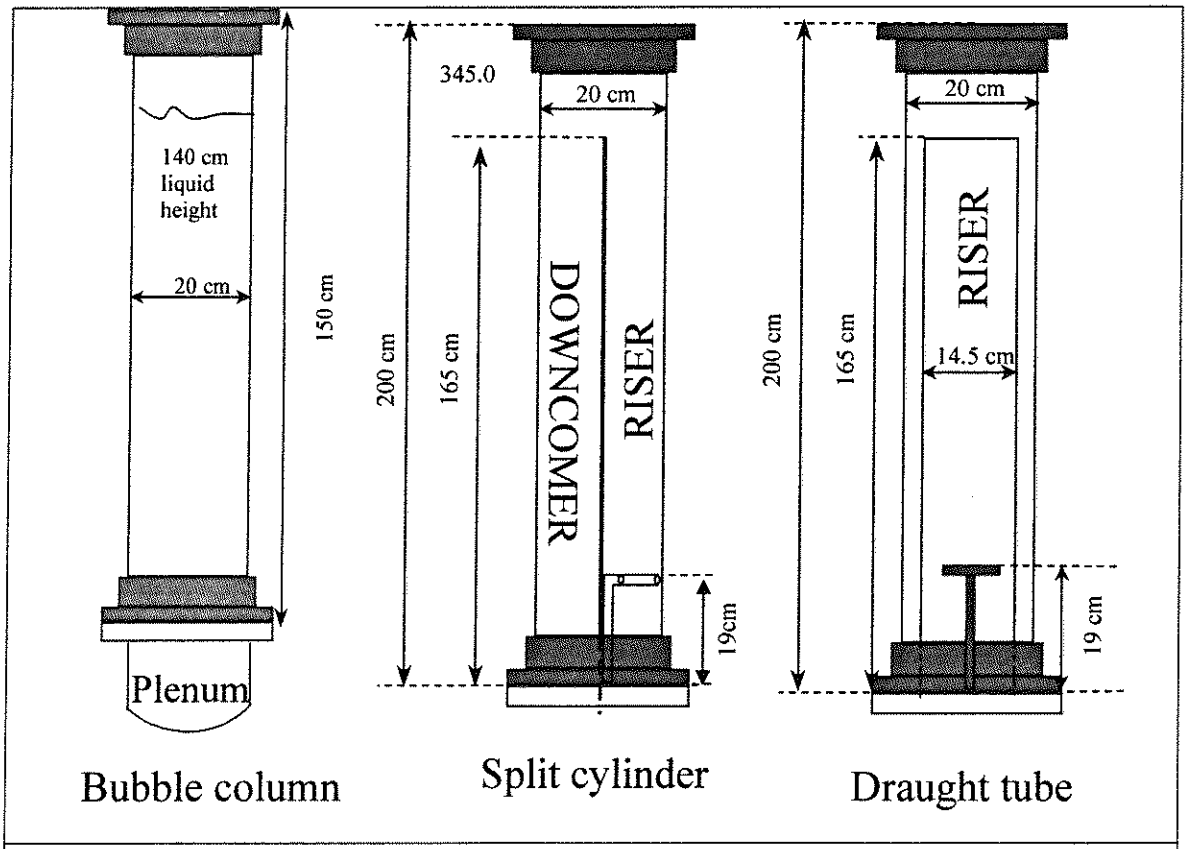

Figure 1: The three kind of PBR studied with CARPT.

Air bubbling is the method used to promote mixing and removal of photosynthetic O_2. Aeration rate is also studied because it is an operating condition of major importance in the hydrodynamic regime that establishes inside the photobioreactors. High aeration rates give rise to high mixing and thus to rapidly fluid movement while low one lead to slower dynamics.

The aeration rates studied were 1 and 5 cm/s (expressed as surfacial gas velocity), which correspond to the extreme conditions of aeration photobioreactors should be operated. rates 1 cm/s may cause cultures to settle down and flake and provide too little

oxygen removal. On the other hand, aeration rates greater than 5 cm/s may cause hydrodynamic stress in many algal strains.

CARPT setup is used to determine the liquid velocities in the devices studied and at the two selected aeration rates. Devanathan (1991) described the detail of the software and hardware. In this study, a radioactive Scandium-46 particle (1.59 mg in weight and 2.89 g/cm^3 in density with total strength of 491 μCi) emitting γ rays of constant energy at 0.89 and 1.12 MeV embedded into a polypropylene particle with a diameter of 2.38 mm is used. In order to match the density of the liquid phase, an air void is created inside the polypropylene particle so that the composite density (Scandium-polypropylene-air) is equal to the density of the liquid phase being tracked (tap water). With the particle density the same as that of the liquid, the radioactive tracer particle is neutrally buoyant, and is able to mimic successfully the dynamic behavior of the moving liquid phase. The intersection of the gamma rays emitted by the tracer particles is continuously monitored by an array of 28 NaI (Tl) scintillation detectors (5 cm in diameter), which are strategically located around the column. In order to determine the exact position of the tracer particle at each instant time, calibrations are performed for each detector, providing a relationship between the distance from the detector to the particle and the intensity counts received by the detector. Using this calibration information and the intensities of radiation received by the detectors at each sampling period (50 Hz), an inverse-mapping algorithm calculates the instantaneous position of the particle. The instantaneous velocity can then be obtained by time differentiation. Ensemble averaged velocities and other turbulence quantities can be calculated for all column locations upon running the experiment for many hours in order to get good statistics.

The model by Acien Fernandez et al. (1997) is used to determine the irradiance field used to work out the irradiance pattern I(t) experienced by the tracer. Several conditions of optical thickness are tested. Optical thickness, which is the result of multiplying the extinction coefficient Ka (m^2/g) by the biomass concentration Cb (g/m^{-3}), determines the difficulty of light penetration inside the culture. Thick cultures give rise to strong irradiance gradients while thin cultures tend to have a homogeneous field. Different conditions of optical thickness are analyzed by considering a constant Ka of 0.05 m^2/g and different biomass concentrations ranging from 100 to 10000 g/m^3 thus sweeping a range of 5 to 500 m^{-1} optical thickness.

C1. CARPT results: position data

Position data were obtained from CARPT experiments as described above for the split cylinder and the draught tube type reactors operating at 1 and 5 cm/s surfacial gas velocity. Available data of a bubble column reactor with an aeration of 5 cm/s are also presented and included in the irradiance pattern analysis. The result of CARPT experiments, position of the tracer particle described vs. time (x(t),y(t),z(t)) are shown in Figure 2.

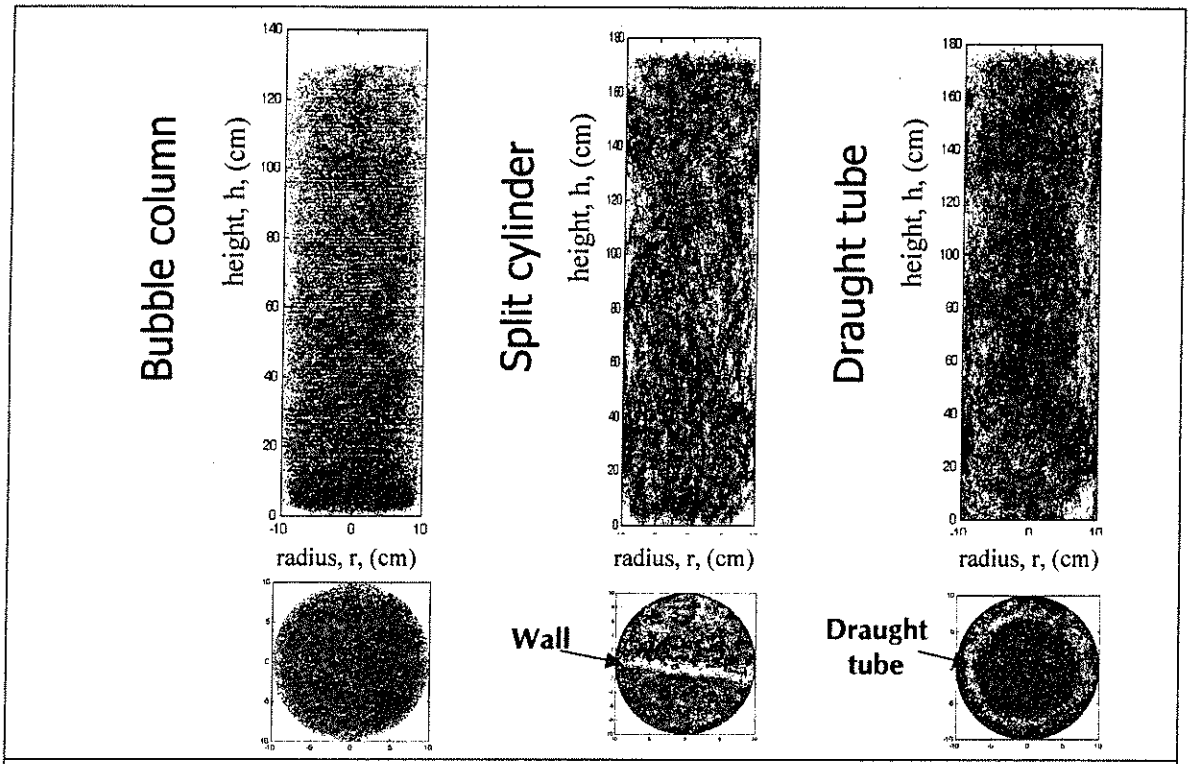

Figure 2: Position data in each of the experimental devices tested.

Data The position data obtained can be use to compute characteristic of the flow. In summary, the main characteristics among the different reactors are most disordered flow in the bubble column, showing the most frequent radial variations. Still there exists a certain structure in the axial flow, showing a rise zone towards the center of the column while the down going fluid moves close to the wall. With regard to the other two devices, both show a more ordered flow pattern caused to the splitting devices placed inside. There can be found two characteristic zones: a riser, with a higher turbulence and greater gas holdup and a downcomer. The draught tube type shows the most ordered flow pattern because the draught tube limits both the axial and radial movements.

In the present work the purpose of obtaining position data is to use it to obtain the irradiance pattern of the tracer particle.

C2. Irradiance pattern: Influence of the biomass concentration

To obtain the time irradiance pattern it is necessary the irradiance field inside the PBR. The schematic procedure for this calculation is shown in Figure 3.

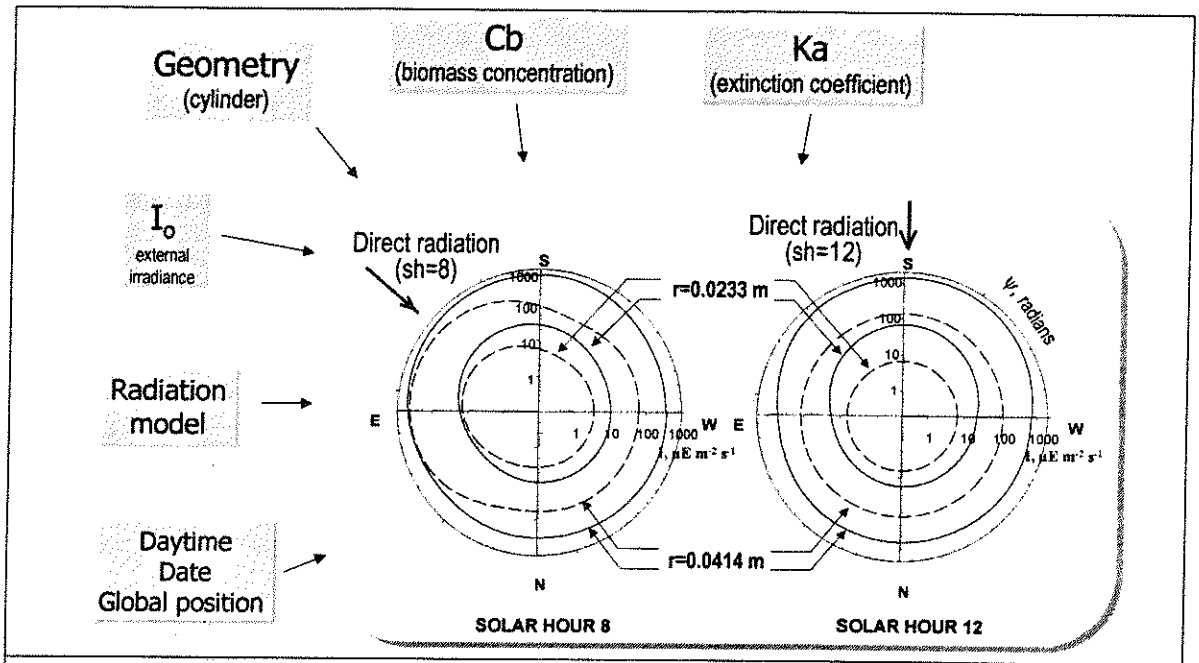

Figure 3: schematic calculation procedure in a vertical photobioreactor taking into account the possible environmental variables in external cultures.

For the sake of simplicity the calculation of the irradiance field I(x,y,z) is simplified to an homogeneous external irradiance (Io) of 1000 $\mu E\ m^{-2}\ s^{-1}$ which gives radial symmetry. Nevertheless the model by Molina Grima et al allows the calculation of I(x,y,z) in any different condition of the variables shown in Figure 3.

The coupling of the position data obtained in the CARPT experiments and the irradiance field yields the temporal irradiance patter which in influenced by reactor geometry, aeration rate and biomass concentration (or rather optical thickness). Reactor geometry and aeration rate influence the flow pattern while the irradiance field is determined by the biomass concentration and also by reactor geometry. The results obtained at 5 cm/s for different biomass concentrations are plotted in figure 4.

The most significant result is that microalgal cells when grown in a PBR of the type analyzed here receive light in a variable manner, even for a quite low biomass concentration as Cd=400 $g\ m^{-3}$, which has never been taken into account for PBR design probably due to the lack of quantitative knowledge in this field this far. This effect is more intense in the simulation at 1000 $g\ m^{-3}$, the differences now observed varying up to five times (from 100 to more than 500 $\mu E\ m^{-2}\ s^{-1}$). On the other hand, in the simulation carried out at a more realistic biomass concentration, 5000 $g\ m^{-3}$, the irradiance pattern changes substantially becoming an alternation of dark/light periods. As figure 4 shows, the delivery of light energy for photosynthesis becomes very irregular and might impair the photosynthetic yield of the system.

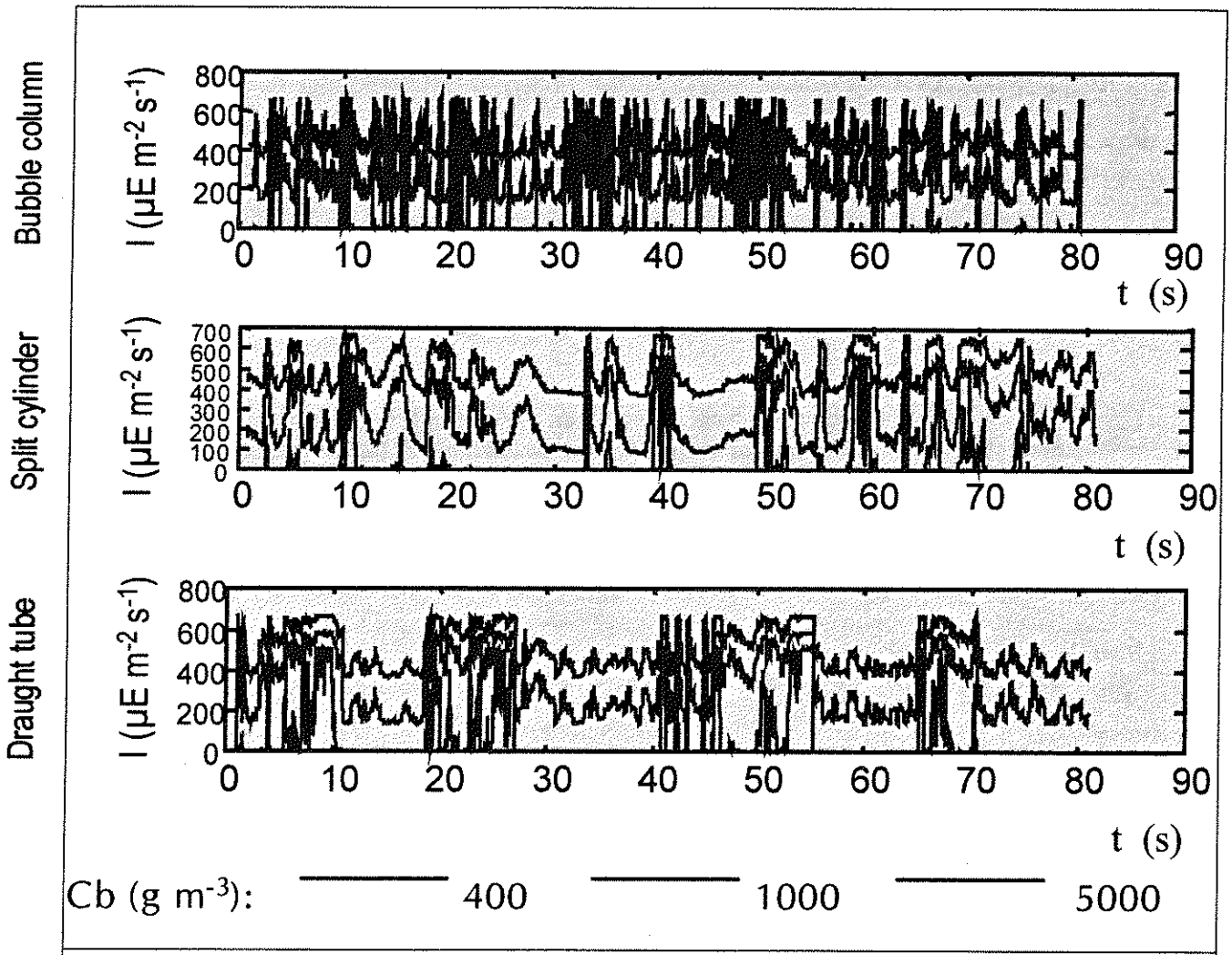

Figure 4: Irradiance pattern obtained for the three devices considered at an aeration rate 5 cm/s and for three different biomass concentrations.

As shown in figure 4, in all the three devices, the light supply becomes a neat light/dark cycling for Cb=5000 g m^{-3} with short periods of exposition to high irradiances as the cells approach the illuminated wall followed by longer dark periods caused by the residence in inner dark zones.

The most relevant matter to be highlighted from figure 4 is that CARPT experiments together with a suitable irradiance distribution model allow to quantify the magnitude of the changes in irradiance, frequencies and duration of dark periods and the influence of PBR type and configuration as well as the influence of operating conditions such as biomass concentration. It can also be mentioned that the same CARPT experiment allow to reproduce the situation taking place in external PBR, the only modification needed being the use of a more complete irradiance distribution model which is already available.

C3. Irradiance pattern: Influence of the system geometry

The plots in figure 4 also show the influence of the system geometry in the irradiance time pattern. The tracer in the bubble column experiences the most disordered pattern of exposure due to the flow pattern taking place in this kind of device. The rapid changes from light to dark are the result of the absence of internal elements that restrain the flow that allow more frequent radial movements. While rapid irradiance changes are an advantage, the drawback of this system is that the lack of order flow does not guarantee that all the cells receive frequent exposure.

The split cylinder presents a more ordered flow, with radial movements still unrestrained. It is because the radial symmetry of the irradiance distribution chosen that the irradiance patter in this device resemble the obtained in the bubble column. The only difference is that in the split cylinder the turbulence is higher in the riser and lower in the downcomer causing more rapid irradiance change and shorter dark periods in the former than in the latter, though this is difficult to appreciate in the corresponding plot.

With regard to the draught tube, the difference with the other devices are obvious, being the only one that causes an ordered irradiance pattern and consistent light/dark exposition. The characteristic exposition pattern of this device is very fast alternation of light and darkness followed by a longer dark period. The main advantage is that guarantees periodic exposure of all the population although the long dark period might be a drawback. It can be highlighted that the duration of this dark period can be adjusted by changing the relative section of the inner tube.

C4. Irradiance pattern: Influence of the aeration rate

In the devices investigated in this study depend on the bubbling of gas to provide both metabolite removal (oxygen) and agitation which is indispensable specially in optically dense cultures. Still, a too intense mixing can stress and damage the microalgal cells, so the aeration rate is usually constrained to the range of 1 to 5 cm/s (expressed as surfacial gas velocity) in the type of devices tested. The irradiance pattern at this at this two extreme conditions of Ug is displayed in figure 5 for a high biomass concentration (cb=5000 g m^{-3})

The basic results are that higher aeration promotes better mixing and faster radial and axial movements that show up as shorter dark periods and more frequent exposures. With regard to the split cylinder, in both cases the turbulence is more intense in the riser and lower in the downcomer at the two operating conditions. This is difficult to see in the plot but can be appreciated as trends of more frequent light/dark cycling when the tracer is in the riser.

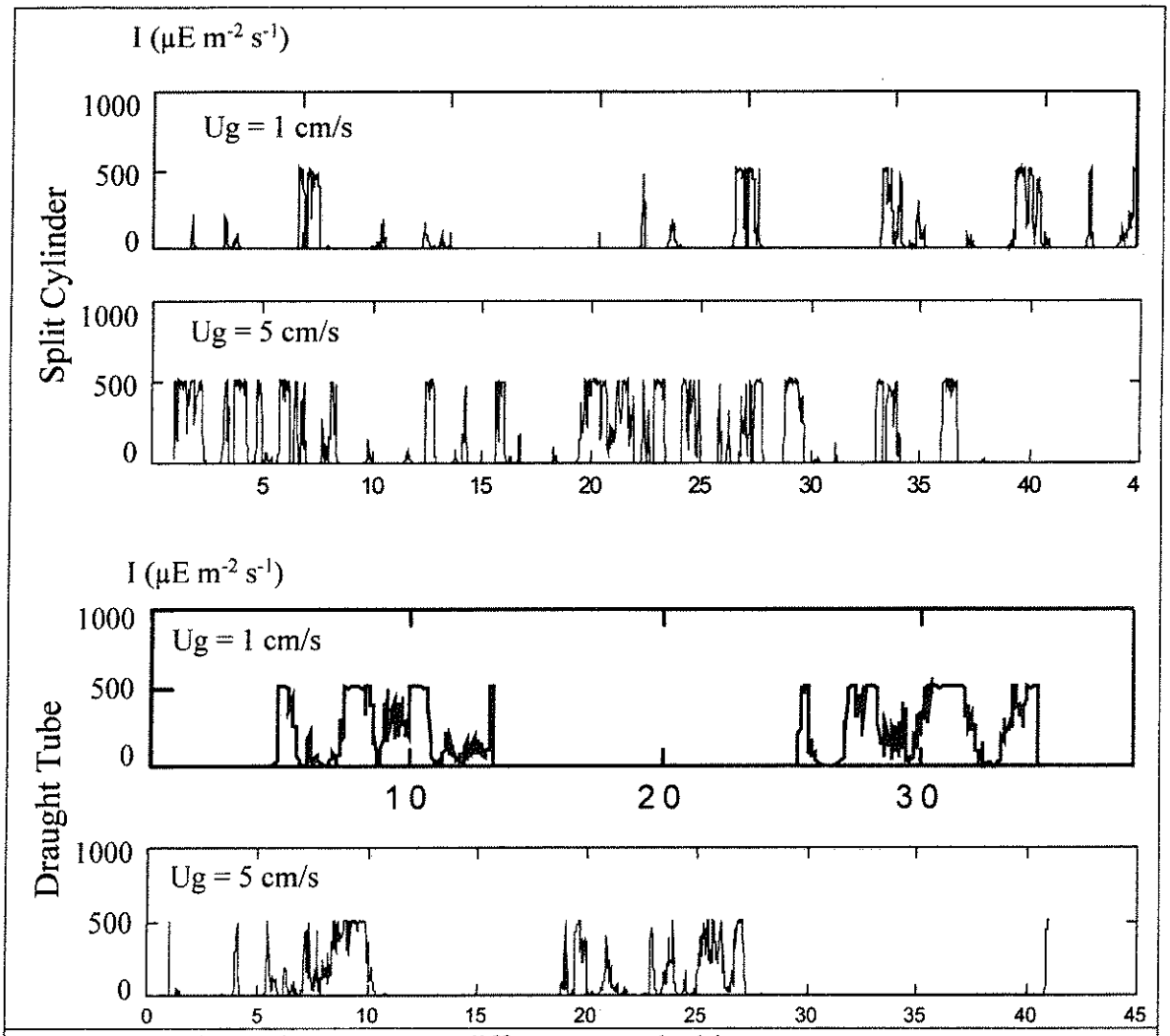

Figure 5: Irradiance time pattern at different gas velocities.

Similar results can be appreciated for the draught tube PBR, but in this case the most evident feature is that the global circulation of the fluid accelerates, increasing the frequency of the exposition. This operating variable can therefore be used to control the exposition pattern and if used together with the inner tube rate, which is, on the other hand, a design parameter allow a wide range of variation that can will used to optimize the irradiance pattern in this type of PBRs.

D. Future Work

The aim of the present work is only to show how CARPT technique can be applied to the analysis of PBRs, in which the hydrodynamics of the system used and the optical properties of the broth are interacting to cause a very heterogeneous delivery of energy to the growing microalgal cells.

Nevertheless the heterogeneity of the light supply is not necessarily a drawback, because, as has been repeatedly shown by many workers, an heterogeneous supply of light can support full growth as long as some restrictions on the average light supplied and duration of dark periods are accomplished.

To the best of our knowledge there is not this far a way of analyzing this parameters in photobioreactors. The only data available has been obtained from laboratory setups using optically thin cultures and artificial light cycling, while nothing has been done to show explicitly the existence and characteristics of these light/dark cycles taking place in industry size devices.

The future work will aim to explain how these light-dark cycles influence growth and to obtain quantitative data on the design restrictions to comply with in order to attain a maximum growth in photobioreactors regardless of the inevitable heterogeneity of the light supply.

E. References

Acien Fernandez, F. G., García Camacho, F, Sánchez Perez, J. A., Fernández Sevilla J. M., Molina Grima, E. "A model for light distribution and average irradiance incide outdoor tubular photobioreactor for the microalgal mass culture. Biotechnology and Bioengineering, 1997.

Devanathan, N., "Investigation of Liquid Hydrodyamics in Bubble Columns via Computer Automated Radioactive Particle Tracking" D. Sc. Thesis, Washington University, St. Louis, Missouri, USA, 1991.

Kok, B., "Experiments on photosynthesis by Chlorella in flashing light" in: Burlew B. (Ed.) "Algal Cultures from Laboratory to Pilot Plant" Carnegie Institution of Wahington Publication 600, Washington D. C. 63-158, 1953.

Molina Grima, E., Garcia Camacho, F., Sanchez Perez, J. A., Acien Fernandez F. G., Fernandez Sevilla, J.M. "Evaluation of photosynthetic efficiency in microalgal cultures using averaged irradiance" Enzyme and Microbial Technology, 21(5), 375-381, 1997.

Molina Grima, E., Contreras Gomez, A., Fernandez Sevilla, J. M., Acien Fernández, J. M., Garcia Camacho, F. "Use of concentric-tube airlift photobioreactors for microalgal outdoor mass cultures" Enzyme and Microbial Technology, 24, 164-172, 1999.

Nedval, L., Tichy, V. Xiong, F., Grobbelaar, J.U. "Microscopic green algae and cyanobacteria in high-frequency intermittent light" Journal of Applied Phycology, 8, 325-333, 1993.

Phillphs, J. N., Myers, J. "Growth rate of Chlorella in flashing light" Plant Physiol., 29, 152-161, 1954

Terry K. L. "Photosynthesis in Modulated Light: Quantitative Dependence of photosynthetic Enhancement on Flashing Rate" Biotechnology and Bioengineering, 28, 988-995, 1986.

AREA II: PREPARATION OF NEW MATERIALS

Faculty: M.P. Dudukovic′
B. Joseph
J.L. Kardos (MRL)
P.A. Ramachandran

Graduate Students: R. Smith

Our research consists of expanding the reaction engineering methodology to describe the transport-kinetic interactions involved in manufacturing of new materials. Both modeling, based on fundamentals, and experimental work are pursued. Our goal is to facilitate the transfer of bench scale science to manufacturing and to improve the manufacturing processes. We have utilized this approach in the past in four areas:

i) preparation of semiconductor grade silicon,
ii) autoclave process for curing of high performance composites,
iii) microencapsulation and production of biomaterials,
iv) preparation of long carbon fibers.

Our research in the semiconductor silicon area has been dormant during the past few years (except for proprietary contract studies which cannot be reported here) but we may want to revitalize some new environmental aspects of it. A new project was initiated in 1996/1997 to quantify the effect of sonification on the reactivity, effectiveness and specificity of aqueous etching and in cleaning chemistries commonly used in the electronic materials industry. Unfortunately, the graduate student involved, Rebecca Smith, departed for personal reasons without completing her work.

We continue to improve our models for devolatilization and resin flow during cure of long carbon fiber composites and we have extended their use to an increased number of polyimide systems with remarkable success. Using independently determined kinetic and mass transfer data, our model has the capability of relating operating procedure and composite quality, and is a useful tool in manufacturing. This success represents a good example of the virtues of team work involving specialists in composites (**J.L. Kardos**), reaction engineering (**M.P. Dudukovic′**) and control and optimization (**B. Joseph**). Work has been completed on modeling the manufacturing of carbon fibers and their carbonization in collaboration with the **Materials Research Laboratory** (MRL). This work is a joint effort of Professors **Kardos, Ramachandran** and **Joseph**.

Our microencapsulation project was completed a couple of years ago and will not be reported on here. Electrophoretic purification of pancreatic islets of Langerhan has also been completed and provides a good quantification of the achievable degree of purification. This project was executed in the **Biological Transport Laboratory** (BTL) with input from CREL. The project of developing a new model and material for release system has been completed. This project also is executed in the BTL with input from CREL.

A brief report is included on the following project:

II-1. Semiconductor Grade Silicon: CREL know-how is reviewed. (**M.P. Dudukovic′** and **P.A. Ramachandran)**

SEMICONDUCTOR GRADE SILICON

A. Problem Definition

Many aspects of manufacture of semiconductor grade silicon can benefit by utilizing the reaction engineering methodology. Some of these are listed below through past accomplishments and suggested future work.

B. Research Objectives

No specific objectives are set at present other than the overall goal to continue contributing via reaction engineering to improved and cleaner processes for silicon manufacture.

C. Research Accomplishments

CREL contributed over the years to solution of the following problems in Si manufacture:

1. Polysilicon crystal growth in Siemens decomposers by silicon deposition via hydrogen reduction of chlorosilanes was modeled. Optimal operational window for industrial practice was identified.
2. Polysilicon crystal growth via silane pyrolysis was modeled. The model provided guidance for design and optimal operation of Komatsu decomposers.
3. Aerosol (free space reactor) for silicon production via silane pyrolysis was modeled. The model indicated that excessive staging would be needed to reach particle size of the order of 20 μm.
4. Fluidized bed for silicon production via silane pyrolysis was modeled. Model was used to identify operating and design conditions that minimized the formation of dust (fines) and maximized CVD growth.
5. A complete heat transfer model was developed for the Czochralski crystal puller. The model related the production rate and crystal quality to operating and design variables.
6. Improved model based CZ puller control was developed. Simultaneous crystal diameter and interface shape control was achieved. Innovative idea of jet cooling was introduced. Two NASA certificates of recognition were received for the work in this area.
7. A novel etcher for large wafers was developed and implemented in industry (contract work).
8. The analysis of IPA wafer drying has been completed and suggestions for improvement of particle removal made (contract work).

D. Future Work

A new project is started to quantify the effect of sonification on the reactivity, effectiveness and specificity of aqueous etching and cleaning chemistries commonly used in the electronic materials industry. However, we are seeking opportunities to continue the work on the following topics:

A. Improved model based control of CZ pullers.
B. Novel acid etcher design.
C. Environmental control and contaminant elimination in various process steps of Si-manufacture.

E. References

1. "Reactor Models for CVD of Silicon", *Proc. Flat Plate Solar Arrat Workshop on the Science of Silicon Material Preparation*, JPL Publication 83-13, 199-226 (1983).
2. "Interface Shape in Czochralski Grown Crystals: Effect of Conduction and Radiation", R.K. Srivastava, P.A. Ramachandran, and M. P. Dudukovic′, *J. Crystal Growth*, 73, 487-504 (1985).
3. "Radiation View Factors in Czochralski Crystal Growth Apparatus for Short Crystals", R.K. Srivastava, P.A. Ramachandran and M.P. Dudukovic′, *J. Crystal Growth*, 79, 281-291 (1986).
4. "Czochralski Growth of Crystals: Simple Models for Growth Rate and Interface Shape", R.K. Srivastava, P.A. Ramachandran and M.P. Dudukovic′, *J. Electrochem. Soc.: Solid-State and Technology*, 133(5), 1009-1015 (1986).
5. "Simulation of Jet Cooling Effects on Czochralski Crystal Growth", R.K. Srivastava, P.A. Ramachandran and M.P. Dudukovic′, *J. Crystal Growth*, 76, 395-407 (1986).
6. "Aerosol Reactor Design: Effect of Reactor Type and Process Parameters on Product Aerosol Characterization", S.E. Pratsinis, T.T. Kodas, M.P. Dudukovic′, and S.K. Friedlander, *I&EC Process Design & Develop.*, 25, 634-642 (1986).
7. "The Effect of Aerosol Reactor Residence Time Distribution on Product Aerosol Characteristics", S.E. Pratsinis, T.T. Kodas, M.P. Dudukovic′ and S.K. Friedlander, *Chem. Eng. Science* 41(4), 693-702 (1986).
8. "Transport-Kinetic Effects in Manufacture of Polycrystalline Silicon", Y.B. Yang, D.Sc. Thesis, Washington University, St. Louis, MO, December, 1988.
9. "Modeling of Czochralski Crystal Growth", P.A. Ramachandran and M.P. Dudukovic′, *Final Technical Report, EPRI Contract RP-8001-1*, (1990).

AREA III: PROCESS MONITORING AND CONTROL

Faculty: Dr. B. Joseph

Projects in the following areas are in progress:

1. Accurate Estimation of Residence Time Distribution from tracer Studies
2. Detection of Faults in Process Sensors
3. Improved Control of Quality in Batch Manufacturing Operations
4. Use of Wavelet Transforms in Sensor Finger Printing
5. Reduced Order Models for On-line Monitoring and Control with Application to high value added processes.

Each project is summarized below.

1. Accurate Estimation of Residence Time Distribution from Tracer Studies

The objective of this project is to develop efficient methods to recover accurate residence time distributions from noise corrupted measurements. We have developed a polynomial based smoothing algorithm that is able to adaptively filter out the noise in the measurement.

Studies using both simulated and experimental data indicate that this method is capable of recovering accurate distributions even in the presence of substantial noise. Comparison studies show the method is superior to currently used techniques.

A software package incorporating these concepts is available. If interested please contact Dr. Joseph at joseph@wuche.wustl.edu.

2. Detection of Faults in Sensors

A common problem faced by industry is that the sensors often go out of calibration thus leading to false information about the operation of a process. This research focuses on developing techniques to monitor the health of a sensor so that each sensor can provide not only the current measurement but also a measure of the confidence associated with that measurement.

The idea that we are pursuing is to monitor the sensor status by analyzing the underlying noise dynamics. Noise is separated from the signal using a frequency decomposition. High frequency variations are generally caused by noise from a variety of sources such as electromagnetic interference, thermal imbalances, instrument induced noise and process induced noise. By isolating and categorizing this noise, we are able to monitor changes in the sensor such as sensor calibration, sensor response characteristics, and breakdown of sensor capability due to physical damage or impairments.

This methodology will be useful in applications where the sensor data plays a crucial role either in monitoring the process or controlling the process.

3. Improving Quality Control of Batch Processes

Quality control is an important issue for the US manufacturing industry. The US has the technological lead in the science and technology of advanced. A major problem in the manufacturing of these materials is the high cost associated with the processing steps. Processes are often not well understood, so the manufacturing is often based on trial and error which is expensive, inefficient, time consuming and inflexible. The problem is often compounded by the lack of adequate sensors to monitor the process on-line so that operators have to depend heavily on secondary indicators.

Improved quality control is achieved not only by proper monitoring techniques now being implemented under the auspices of Statistical Process Control/Statistical Quality Control (SPC/SQC) techniques, but also on the ability to take proper actions to compensate and correct the process. The latter usually requires considerable knowledge about the process (how the measurements interact, what information is contained in a measurement, what the effect of a process variable has on quality, etc.). Thus there is a need for highly trained expert operators to maintain the product quality.

Intelligent processing promises an alternative to conventional manufacturing methodology. The idea is to incorporate processing knowledge (in the form of mathematical models and past processing experience) in the feedback control loop. The rapid development of fast and versatile computers, combined with the recent advances in artificial intelligence provide a significant opportunity for improving material manufacturing technologies. To take advantage of this opportunity we must combine advances in a variety of disciplines including improved understanding of the manufacturing steps, advances in sensors and instrumentation, advances in process control theory and artificial intelligence.

The overall objective of this research is to develop, implement and test novel concepts for improved control of materials manufacturing processes. We have selected the autoclave process as an example because it is an industrially important manufacturing method and susceptible to large part rejection rate. We have also accumulated some experience working on the models for the curing process. Due to the high cost associated with the parts built using this process and their strategic importance in defense, there has been considerable interest on the part of industry in automation of this batch manufacturing operation.

The autoclave curing process will merely serve as a test vehicle for the ideas and concepts developed here. The objective is to build a methodology applicable over a broad spectrum of processes characterized by high manufacturing costs, large labor costs, and quality control problems. Thus we shall keep the methodology as general as possible.

4. Wavelet Transforms in Sensor Fingerprinting

Wavelet transforms is a tool for time/frequency decomposition of signals. In this project we are using wavelet transforms to

(i) characterize (fingerprint) sensors used in monitoring complex phenomena
(ii) identify and remove noise from data used in process monitoring and process modeling
(iii) Analyze historical data to discover trends and events hidden in the time series

Applications being considered include corrosion monitoring using electrochemical noise sensors, monitoring of granulation using force and torque sensors mounted on blades, and analysis of air pollution trends using yearly weather related data. Due to their versatile nature, wavelets are proving to be a powerful tool in all these applications.

5. Reduced Order Models for On-line Monitoring and Control

Fundamental models can often get very complex and compute intensive. In such situations it is desirable to develop reduced order models that are suitable for use with on-line monitoring and control algorithms.

The objective of this research is to develop methods of building reduced order models by combining a simplified set of the original model equations with data generated off-line from rigorous first principles models in combination with data collected from actual process tests. This is a powerful way to combine the advantage of fast data driven models with the accuracy of detailed fundamental models.

We are currently testing this concept by applying it to model and control and injected pultrusion process for manufacturing polymeric composites. Other possible applications include monitoring and control of polymerization reactors and systems where end product quality is easy to measure on-line.

RECENT PUBLICATIONS IN JOURNALS

1. Voorakaranam,S., J.L. Kardos and B. Joseph, " Modeling and Control of an Injection Pultrusion Process", Paper accepted by Journal of Composite Materials, Aug, 1998.

2. Voorakaranam, S. and B. Joseph, " Model Predictive Inferential Control with Application to Composites Manufacturing Process.", Paper submitted to Ind. And Eng. Chem. Res., July 1998.

3. Voorakaranam,S., J.L. Kardos and B. Joseph, " The Use of Process Models to Control and Optimize Pultrusion-Type Processes", SAMPE Journal,Vol 35, No 3, 1999.

4. Ying, Chao-Ming and Babu Joseph, " Performance and Stability Analysis of LP-MPC and QP_MPC Cascade Control Systems", Submitted to AIChE Journal, Jul, 1998.

5. Thomas, M.M, B. Joseph and J.L.Kardos, " Batch Process Quality Control Applied to Curing of Composite Materials", AIChE Journal, 43, 10, pp. 2535-2545, 1997.

6. Ying, Chao-Ming and Babu Joseph, "Sensor Fault Detection Using Noise Analysis," Submitted to Industrial & Engineering Chemistry Research, 1999.

7. Ying, Chao-Ming and Babu Joseph, "System Identification of Chemical Processes in Frequency Domain using Polynomial Model," Submitted to AIChE Journal, 1999.

8. Ying, Chao-Ming and Babu Joseph, "Linear System Identification using Polynomial Models," Submitted to Industrial & Engineering Chemistry Research, 1999.

PRESENTATIONS

1. Ying, Chao-Ming and B. Joseph, " System Identificatio Using Orthogonal Polynomial Approximations", Invited Paper for American Control Conference, Philadelphia, June, 1998.

2. Ying, Chao-Ming, Srikanth Voorakaranam, and Babu Joseph, "Analysis and Performance of the Two-stage Cascade LP-MPC Scheme," American Control Conference, Philadelphia, PA, 1998

3. Ying, Chao-Ming and Babu Joseph, "System Identification in Frequency Domain using Polynomial Models," AIChE Annual Meeting, Miami Beach, Florida, 1998.

4. Ying, Chao-Ming and Babu Joseph, "Sensor Self-Validation using Power Spectrum Density Analysis," AIChE Annual Meeting, Miami Beach, Florida, 1998.

5. Voorakaranam,S., S.Potaraju, B.Joseph and J.L.Kardos "Intelligent Control of Polymer Composites Manufacturing," *Proceedings of the NSF Design and Manufacturing Grantees Conference*, Monterrey, Mexico, January 1998

6. Potaraju,S. and B.Joseph, "Reduced Order Models for Nonlinear Output Estimation", presented at *Annual AIChE Meeting*, Miami, November, 1998

7. Potaraju S., B.,Khomami, J.L.,Kardos and B. Joseph, "A Flexible Approach to Modeling and Simulation of Fiber Reinforced Polymer Processing using Object Oriented Techniques", presented at *Annual AIChE Meeting*, Miami, November, 1998

8. Potaraju,S., and B.Joseph , "Application of Reduced Order Process Models for Nonlinear Inferential Control," *Proceedings of the* 1999 *American Control Conference,* San Diego, June 1999.

9. Voorakaranam,S., S.Potaraju, B.Joseph and J.L.Kardos "Model Based Monitoring and Control of Quality in Polymeric Composites Manufacturing," *Proceedings of the NSF Design and Manufacturing Grantees Conference*, San Diego, California, January 1999.

CREL PUBLICATIONS AND PRESENTATIONS (1990-2000)

A. RECENT PAPERS AND CHAPTERS

1. "Application of the Boundary Element Method to Nonlinear Diffusion with Reaction Problems", P.A. Ramachandran, Int. J. Num. Methods Eng., 29, 1021-1031 (1990).

2. "Autoclave Processing of Long-Fiber Thermoplastic Composites", M.P. Dudukovic′, J.L. Kardos, I.S. Yoon and Y.B. Yang, Chem. Eng. Science, 45, 2519-2526 (1990).

3. "Boundary Element Based Solution Procedure for Nonlinear Boundary Value Problems", P.A. Ramachandran, Computers and Math., 19, 63-76 (1990).

4. "Boundary Integral Solution for Axial-Dispersion with Reaction Problems", P.A. Ramachandran, Chem. Eng. J., 45, 49-54 (1990).

5. "Comparison of Axial Dispersion and Mixing-Cell Models for Detailed Design and Simulation of Fischer-Tropsch Synthesis in Slurry Bubble Column Reactors", J.R. Turner and P. L. Mills, Chem. Eng. Sci., 45(8), 2317-2324 (1990).

6. "Consider Application Requirements when Selecting Between Analog and Digital Filters", B. Joseph, Personal Engineering and Instrumentation News, 7, 2, 89-92 (1990).

7. "Detection of Flow Maldistribution in Packed Beds via Tracers", P.J. Hanratty and M.P. Dudukovic′, AIChE J., 36(1), 127-131 (1990).

8. "Diffusion-Reaction Problems Revisited via a New Boundary Element Discretization", P.A. Ramachandran, Chem. Eng. Sci., 45, 3525 (1990).

9. "Digital Implementation of PID Loops on PC's Require Special Considerations", B. Joseph, Personal Engineering and Instrumentation News, 7, 4, 72-77 (1990).

10. "Expert Systems in Process Control", B. Joseph, Control, Vol. III, 8, 58-61 (1990).

11. "Flow Mapping in Bubble Columns Using CARPT", N. Devanathan, D. Moslemian and M.P. Dudukovic′, Chem. Eng. Science, 45, 2285-2291 (1990).

12. "Knowledge Based Control of Autoclave Curing of Composites", B. Joseph and H.T. Wu., SAMPE J., 26, 6, 39-54 (1990).

13. "Measurement Selection and Detection of Measurement Bias in the Context of Model Based Control and Optimization, B. Joseph and K. Kage, Ind. and Eng. Chem. Sci., Vol. 47, No. 4, pp 917-928 (1990).

14. "Modeling of Czochralski Crystal Growth". Ramachandran, P. A. and M. P. Dudukovic. Final Technical Report, EPRI Contract RP-8001-1, (1990).

15. "Modeling of Particle Deposition in Clean Room Environments: Current Status", J.R. Turner, in Particles in Liquids and Gases: Detection, Characterization and Control, vol. 2, ed. K.L. Mittal, Plenum Press, New York (1990).

16. "Modeling the Effect of Operating Parameters on Oxygen Content in Czochralski Growth of Silicon", P.A. Ramachandran, M.P. Dudukovic´and D. Dorsey, J. Electrochem. Soc., 137, 3229-3237 (1990).

17. "Science-Based Guidelines for the Autoclave Process for Composites Manufacturing", R. S. Dave, A. Mallow, J.L. Kardos and M.P. Dudukovic´, SAMPE J., 31-38 (1990).

18. "Solution of Moving Boundary Problems for Gas-Solid Noncatalytic Reactions by Orthogonal Collocation-Revisited", M.P. Dudukovic´ and Y.B. Yang, Chem. Eng. Science, 45, 3375-3379 (1990).

19. "Vehicle Contribution to Ambient Carbonaceous Aerosols by Scaled Thermograms", J.R. Turner and S.V. Hering, Aerosol Sci. Technol., 12(3), 620-629 (1990).

20. "A Series Solution for Mass Transfer in Laminar Flow with Surface Reaction", M.P. Dudukovic´ and A. Basic', AIChE J., 37(9), 1341-1353 (1991).

21. "Boundary Integral Element Method for Linear Diffusion-Reaction Problems with a Discontinuous Boundary Condition", P.A. Ramachandran, Chem. Eng. J., 47, 169-185 (1991).

22. "Boundary Integral Solution Method for Diffusion-Reaction Problems with Both Material and Rate Nonlinearities", P.A. Ramachandran, Computers & Mathematics, 21, 7 (1991).

23. "Multiphase Reactors: Models and Experimental Verification", M.P. Dudukovic´, N. Devanathan and R. Holub, Revue de L'Institut Francais de Petrole, 46(4), 439-465 (1991).

24. "Two-Region Computational Model for D. C. Glow Discharge Plasma", S. Pirooz, P.A. Ramachandran and B.A. Shrauner, IEEE Trans. on Plasma Science, 19, 408-418 (1991).

25. "Heat Regenerators: Design and Evaluation", Dudukovic, M.P. and P. A. Ramachandran, in Heat Transfer Design Methods (J. J. McKetta, ed.), Marcel Dekker, pp. 325-347 (1992).

26. "A Blackboard Architecture for Model Based and Knowledge Based Control", H.T. Wu and B. Joseph, Chem. Eng. Sci., Vol. 47, No. 4, pp 917-928 (1992).

27. "A Phenomenological Model of Pressure Drop, Liquid Holdup, and Flow Regime Transition in Gas-Liquid Trickle Flow", R. Holub, M.P. Dudukovic´ and P.A. Ramachandran, Chem. Eng. Sci., 47(9-11), 2343-2348 (1992).

28. "Decision Making in Chemical Engineering and Expert Systems: Application of the Analytical Hierarchy Process to Reactor Selection", P. Hanratty and B. Joseph, Comp. and Chem. Eng., Vol. 16, No. 9, pp 849-860 (1992).

29. "Detection of Flow Maldistribution in Trickle-Bed Reactors via Tracers", P. J. Hanratty and M.P. Dudukovic′, Chem. Eng. Sci., 47(12), 3003-3014 (1992).

30. "Exploratory Data Analysis Using Inductive Partitioning and Regression Trees", D. Shieh and B. Joseph, Ind. Eng. Chem. Res., 31, pp 1989-1998 (1992).

31. "Exploratory Data Analysis: A Comparison of Statistical Methods with Artificial Neural Networks", F.H. Wang, D.S. Shieh and B. Joseph, Comp. and Chem. Eng. J., Vol. 16, No. 4, pp 413-423 (1992).

32. "Formation of Goethite (α-FeOOH) Through Oxidation of a Ferrous Hydroxide Slurry", D. O'Connor, P.A. Ramachandran and M.P. Dudukovic′, I&EC Research, 31(11), 2516-2526 (1992).

33. "Heat Regenerators: Design and Evaluation", in Heat Transfer Design Methods (J.J. McKetta, ed.), Marcel Dekker, pp 325-347 (1992).

34. "Knowledge Representation and Reasoning in the Presence of Uncertainty in an Expert System for Laboratory Selection", P.J. Hanratty, P.A. Ramachandran and M.P. Dudukovic′, I&EC Research, 31(1), 228-238 (1992).

35. "Liquid Backmixing in Bubble Columns", Y.B. Yang, N. Devanathan and M. P. Dudukovic′, Chem. Eng. Sci., 47(11), 2859-2864 (1992).

36. "Multiphase Reaction Engineering for Fine Chemicals and Pharmaceuticals", P. L. Mills, P.A. Ramachandran and R. V. Chaudhari, Reviews in Chemical Engineering, 8, Nos. 1-2, 1 (1992).

37. "Numerical Solution Method for Boundary Problems Containing an Undetermined Parameter", P.A. Ramachandran, J. Computational Physics, 102, 63 (1992).

38. "Radioactive Particle Tracking Technique for Investigation of Phase Recirculation and Turbulence in Multiphase Systems", D . Moslemian, N. Devanathan and M.P. Dudukovic′, Rev. Sci. Instrum., 63(10), 4361-4372 (1992).

39. "Boundary Integral Solution Procedure to Graetz-type of Problems", P.A. Ramachandran, J. Numerical Heat Transfer, 23, 257 (1993).

40. "Bubble Column Reactors: Some Recent Developments", Dudukovic, M.P. and N. Devanathan, Chemical Reactor Technology for Environmentally Safe Reactors (H. I. DeLasa, et al.l, eds.), NATO ASI Series E: Appl. Sci. 225, 379-408 (1993).

41. "Liquid Backmixing in Bubble Columns via Computer-Automated Radioactive Particle Tracking (CARPT)", Y.B. Yang, N. Devanathan and M.P. Dudukovic′, Experiments in Fluids, 16, 1-9 (1993).

42. "Modeling of Evacuated Pulse Micro Reactors", B. S. Zou and M.P. Dudukovic′, Chem. Eng. Sci., 48(13), 2345-2355 (1993).

43. "Predictive Control of Quality in Batch Manufacturing Process Using Artificial Neural Network Models", B. Joseph and F.H. Wang-Hanratty, Ind. Eng. Chem. Res., 32, 1951-1961 (1993).

44. "Pressure Drop, Liquid Holdup and Flow Regime Transition in Trickle Flow", R.A. Holub, M.P. Dudukovic′ and P.A. Ramachandran, AIChE J., 39(2), 302-321 (1993).

45. "Ammonia/Flyash Interactions and Their Impacts on Flue Gas Treatment Technologies", J.R. Turner, S. Choné and M.P.Dudukovic′, Chem. Eng Sci., 49(24A), 4315-4325 (1994).

46. "Computational Aspects of Wavelets and Wavelet Transforms", M.P. Dudukovic′, S. Palavajjhala, B. Joseph and R.L. Motard, Chapter in Wavelet Applications in Chemical Engineering, (R.L. Motard and B. Joseph, Editors), to be published by Kluwer Academic Publishers, Boston, (1994).

47. "Effect of Scale on Liquid Recirculation in Bubble Columns", S.B. Kumar, N. Devanathan and M.P. Dudukovic′, Chem. Eng. Sci., 49, 24B, 5637 (1994).

48. "Introduction to Wavelet Transforms and Time Frequency Analysis", M.P. Dudukovic′, X.D. Dai, B. Joseph and R.L. Motard, Chapter in Wavelet Applications in Chemical Engineering, (R.L. Motard and B. Joseph, Editors), to be published by Kluwer Academic Publishers, Boston (1994).

49. "Model Based Control of Polymeric Composite Materials Processing", B. Joseph, M. Thomas and J.L. Kardos, Proceedings of the 1994 NSF Design and Manufacturing Grantees Conference, MIT, Society of Manufacturing Engineers, Dearborn, MI, pp 647-648 (1994).

50. "Modeling of Pulsed Gas Transport Effects in the TAP Reactor System", B.S. Zou, M.P. Dudukovic′ and P.L. Mills, J. Catalysis, 148(12), 683-696 (1994).

51. "Pollution Prevention: Problems and Solutions", J.R. Turner (ed. L. Theodore, R.R. Dupont and J. Reynolds, Gordon and Breach), Berkshire, UK (1994).

52. "Pressure Drop and Liquid Holdup in High Pressure Trickle-Bed Reactors", M.H. Al-Dahhan and M.P. Dudukovic′, Chem. Engg. Sci., 49, 24B, 5681- 5698 (1994).

53. "Process Signal Features Analysis", X.D. Dai, B. Joseph and R.L. Motard, Chapter in Wavelet Applications in Chemical Engineering (R.L. Motard and B. Joseph, Editors), to be published by Kluwer Academic Publishers, Boston (1994).

54. "Radial Basis Function Approximation in the Dual Reciprocity Method", S.R. Karur and P.A. Ramachandran, Mathematical and Computer Modeling, 20, 59-70 (1994).

55. "The Addivity and Stability of Carbon Signatures Obtained by Evolved Gas Analysis", J.R. Turner and S.V. Hering, Aerosol Sci. Technol., 21(4), 294- 305 (1994).

56. "The Devolatilization of Polyimide Fiber Composites: Model and Experimental Verification", I.S. Yoon, Y. Yang, M.P. Dudukovic´ and J.L. Kardos, Polymer Composites, 15(3), 184-196 (1994).

57. "Augmented Thin Plate Spline Approximation in DRM", S.R. Karur, P.A. Ramachandran, Boundary Elements Communications, 6, 55-58 (1995).

58. "Catalyst Wetting Efficiency in Trickle-Bed Reactors at High Pressure", M.H. Al-Dahhan and M.P. Dudukovic´, Chem. Eng. Sci., 50, 15, 2377 (1995).

59. "Characteristics of Metallic Iron in Y-Zeolite Catalyst Reduced by Hydrogen Atom Beams", S.K. Ihm, J.H. Lee, and D.K. Lee, Reaction Kinetics and Catalyst Letters, R 28000, Vol. 57(2) (1995).

60. "Computing and Computer Applications in Engineering Education", Muthanna H. Al-Dahhan, The Proceeding of 4th World Conference on Engineering Education, Vol. II, 1, Minneapolis/St. Paul, Minnesota Oct. 15-20 (1995).

61. "Computing in the Undergraduate Chemical Engineering Curriculum: An Integrated Approach", M.H. Al-Dahhan, Chem. Eng. Educt., 29, 3, 198, Summer (1995).

62. "Expert Systems and Artificial Intelligence", B. Joseph, Chapter in Instrument Engineers' Handbook on Process Control, Third Edition, B.G. Liptak, Editor, Chilton Book Company (1995).

63. "Infusing Environmental Education into the Undergraduate Engineering Curriculum: A Minor in Environmental Engineering Science", J.R. Turner, W. P. Darby and M.P. Dudukovic´, Proceedings of the 1995 ASEE Illinois-Indiana Section Conference (1995).

64. "Liquid Catalyst Contacting Efficiency in High Pressure Trickle-Bed Reactors with/without Fines", M.H. Al-Dahhan and M.P. Dudukovic´, Extended Abstract, The Second Italian Conference on Chemical process Engineering, Firenze, May 15-17 (1995).

65. "Orthogonal Collocation in the Non-conforming Boundary Element Method", Karur, S. R., and P. A. Ramachandran, Journal of Computational Physics, 121, 373-382 (1995).

66. "Reproducible Technique for Packing Laboratory-Scale Trickle-Bed Reactors with a Mixture of Catalyst and Fines", M.H. Al-Dahhan, Y. Wu and M.P. Dudukovic′, Ind. Eng. Chem. Res., 34, 741-747 (1995).

67. "The Quasilinear Boundary Element Method for Non-liner Poisson Type Problems", J. J. Kasab, S. R. Karur and P.A. Ramachandran, Engineering Analysis with Boundary Elements, 15, 277-282 (1995).

68. "A Bidirectional Fixed-Bed Reactor for Coupling of Exothermic and Endothermic Reactions", Kulkarni M. S., M. P. Dudukovic′, AIChE J., 42, pp 2897 (1996).

69. "A Boundary Element Procedure for Solving Linear Diffusion-Reaction Networks", S. R. Karur, and P.A. Ramachandran, AIChE Journal, 42, 383-390 (1996).

70. "A Modified Contactor for Experimental Studies of Mass Transfer and Chemical Reaction Across Liquid-Liquid Interface", Al-Dahhan, M. H. and C. E. Wicks, I&EC Res., 35, 3812-3816 (1996).

71. "A Robust Algorithm for Fixed-Bed Reactors with Steep Moving Temperature and Reaction Fronts", Kulkarni, M. S., and Dudukovic′, M.P., Chem. Eng. Sci., 51, 4, 571-585 (1996).

72. "Affordable Processing of Composite Structure for the Civilian Infrastructure", J. Kardos, B. Khomami, P.A. Ramachandran, B. Yang, and R. Shepard, Proceedings of the 5th World Congress of Chemical Engineering, San Diego, California, July 14-18 (1996).

73. "An Analysis of a Bi-Directional Fixed-Bed Reactor Subject to Alternate Swings of Exothermic and Endothermic Reactions", M. S., Kulkarni, and M.P., Dudukovic′, AIChE J., accepted for publication (1996).

74. "Catalyst Bed Dilution for Improving Catalyst Wetting in Laboratory Trickle-Bed Reactors", Al-Dahhan, M. H. and M. P. Dudukovic′, AIChE J., 42, 9, 2594-2606 (1996).

75. "Comparison of Trickle-Bed and Upflow Reactor Performance at High Pressure: Model Predictions and Experimental Observations", M.R. Khadilkar, Y.X. Wu, M.H. Al-Dahhan, M.P. Dudukovic′, and M. Colakyan, , Chem. Eng. Sci.,. 51, 10, 2139 (1996).

76. "Comparison of Upflow and Downflow Two Phase Flow Reactors With and Without Fines: Experimental Observations", Y. Wu, M. Khadilkar, M. Al-Dahhan, M. Dudukovic′, I&EC Res., 35, 397 (1996).

77. "CREL – Chemical Reaction Engineering Laboratory – in Developing Environmental Technology – Cooperatively – by Eral R. Beaver", M. Al-Dahhan, CHEMTECH, 9, April (1996).

78. "Dynamics of Gas Phase and Solid Phase Reactions in Fixed-Bed Reactors", M. S., Kulkarni, and M.P., Dudukovic′, Chem. Eng. Sci., 51, 11, 3083-3099 (1996).

79. "Evaluation of Trickle-Bed Reactor Models for a Liquid Limited Reaction", Y.X. Wu, M.H. Al-Dahhan, M.R. Khadilkar and M.P. Dudukovic′, Chem. Eng. Sci., 51, 11, 2721 (1996).

80. "High Pressure Trickle-Bed Reactors: A State-of-the-Art Review", Larachi, F., M. H. Al-Dahhan, M. P. Dudukovic′ and A. Laurent, Proceeding of 12th International Congress of Chemical & Process Engineering, CHISA'96, August (1996).

81. "Improved Multiquadrics Approximation for Partial Differential Equations", Golberg, M. A., C. S. Chen, and S. R. Karur, Engineering Analysis with Boundary Elements, 18, 9-17 (1996).

82. "Improved Prediction of Pressure Drop and Liquid Holdup in High Pressure Trickle-Bed Reactors", Al-Dahhan, M. H., Y. Wu, M. R. Khadikar And M. P. Dudukovic′, Proceeding of the 5th World Congress on the Chemical Engineering - San Diego, Vol. I, 209 (1996).

83. "Influence of Mixing Intensity on the Mass Transfer Coefficient Across Liquid-liquid Interface", M.H. Al-Dahhan and C. E. Wicks, Chem. Eng. Communications, 145, 213 (1996).

84. "Intelligent Control of Product Quality in Composite Manufacturing", M.M. Thomas and B. Joseph, chapter in book: Processing of Continuous Fiber Reinforced Composites, Edited by R. S. Dave and A. Loos, to be published, Karl Hanser Verlag, Germany (1996).

85. "Liquid Mixing Based on Convection and Turbulent Dispersion in Bubble Columns", S. Degaleesan, , S. Roy, S.B. Kumar, and M.P. Dudukovic′, ISCRE 14, Brugge, Belgium, Chem. Eng. Sci., 52(10), 1967-1976 (1996).

86. "Liquid Mixing Based on Convection and Turbulent Dispersion in Bubble Columns", S. Degaleesan, , S. Roy, S.B. Kumar, and M.P. Dudukovic′, ISCRE 14, Brugge, Belgium, Chem. Eng. Sci., 51(10), 1967-1976 (1996).

87. "Predictive Control of Quality in Batch Polymerization Using a Hybrid Artificial Neural Network Model", A.Y.D. Tsen, S.S. Jang, D.S.H. Wong, and B. Joseph, AIChE Journal, 42, 2, 455-465 (1996).

88. "Process Identification Using Discrete Wavelet Transforms-Design of Prefilters", S. Palavajjhala, B. Joseph, and R.L. Motard, AIChE Journal, 42, 3, 777-790 (1996).

89. "The Fischer -Tropsch Synthesis in Slurry Bubble Column Reactors: Analysis of Reactor Performance Using the Axial Dispersion Model", Mills, P.L., Turner, J.R., Ramachandran, P.A. and Dudukovic, M.P., (Nigam, K.P.V. and Schumpe, A., eds.(Three Phase Sparged Reactors, Gordon and Breach Publ., Topics in Chemical Engineering, Vol. 8, Ch. 5, 339-386 (1996).

90. "Computer-Assisted Gamma and X-Ray Tomography: Application to Multiphase Flow Systems", Kumar, S.B., and Dudukovic, M.P., Noninvasive Monitoring of Multiphase Flows, Elsevier, (Chaouki, J., Larachi, F. and Dudukovic, M.P., eds.), , Chapter 2, 47-103 (1997).

91. "A Two-Compartment Convective-Diffusion Model for Slurry Bubble Column Reactors", Degaleesan, S., M. P. Dudukovic′, B. A. Toseland and B. L. Bhatt, Ind. Eng. Chem. Res. (1997).

92. "Assessment of the Effects of High Pressure Operation on the Liquid-Solid Mass Transfer Coefficient in Trickle-Bed Reactors", Al-Dahhan, M. H. , S. Highfill and M. Freidman, I&EC Res., 36, 4421-4426 (1997).

93. "Batch Chemical Process Quality Control Applied to Autoclave Curing of Composite Materials", M. M. Thomas, B. Joseph and J. L. Kardos, AIChE Journal (1997).

94. "Computer Assisted Gamma and X-Ray Tomography: Application to Multiphase Flow Systems", S. R. Kumar and M.P. Dudukovic′, Chapter 2 in Non-Invasive Monitoring of Multiphase Flows, Elsevier-Science, Eds. Chaouki, J., F. Larachi and M. P. Dudukovic′, Amsterdam (1997).

95. "Effect of Catalyst Wetting on the Performance of Trickle-Bed Reactors", Y. Wu, M. Khadilkar, M.H. Al-Dahhan and M. P. Dudukovic′, Proceeding of Second Joint U. S. /China Chemical Engineering Conference, Beijing, China, May 19-22 (1997).

96. "Experimental Characterization of Autoclave-Cured Glass-Epoxy Composite Laminates: Cure Cycle Effects Upon Thickness, Void Content and Related Phenomena", M. M. Thomas, B. Joseph and J. L. Kardos, Polymer Composites, (1997).

97. "Gas Holdup Measurements in Bubble Columns Using Computed Tomography", Kumar, S., D. Moslemian, M. P. Dudukovic′, AIChE J., Vol. 43, No. 6, pp 1414-1425 (1997).

98. "High Pressure Trickle-Bed Reactors: A Review", Al-Dahhan, M. H., F. Larachi, M. P, Dudukovic′ and A. Laurent, I&EC Res. (Special issue in honor of Professor Froment), 36, 3292-3314 (1997).

99. "Implementation of a Computer-Based Air Pollution Data Analysis Exercise in an Environmental Engineering Laboratory Course", Jay R. Turner and S. R. Falke, Processing of the ASEE Midwest Section Conference, Columbia, MO, April (1997).

100. "Intelligent Control of Product Quality in Composite Manufacturing", B. Joseph and M. M. Thomas, Chapter 9, Processing of Continuous Fiber Reinforced Composite, Edited by R. Dave and A. C. Loos, B. Joseph and M. M. Thomas, To be published, Hanser Publishers, New York (1997).

101. "Measurement Techniques for Local and Global Fluid Dynamic Quantities in Two and Three Phase Systems", Kumar, S.B., Dudukovic, M.P. and Toseland, B.A., Non Invasive Monitoring of Multiphase Flows, Elsevier, (Chaouki, J.l, Larachi, F. and Dudukovic, M.P., eds.), Chapter 1, 1-45 (1997).

102. "Non-Invasive Monitoring of Multiphase Flows", Chaouki, J., Larachi, F. and Dudukovic M. P. editors, Elsevier, (1997).

103. "Periodic Operation of Asymmetric Bidirectional Fixed-Bed Reactors: Temperature and Process Limitations", Kulkarni, M. S., M. P. Dudukovic′, Submitted to Ind. Eng. Chem. Res., May (1997).

104. "Periodic Operation of Asymmetric Bidirectional Fixed-Bed Reactors: Energy Efficiency", Kulkarni, M. S., M. P. Dudukovic, Chem. Eng. Sci. 52, pp 1777 (1997).

105. "Progress in Understanding the Fluid Dynamics of Bubble Column Reactors", M.P. Dudukovic, B.A. Toseland, B.L. Bhatt, Published in the DOE Annual Review Report, Pittsburgh, PA (1997).

106. "Radioactive Particle Tracking in Multiphase Reactors: Principles and Applications", Larachi, F., Chaouki, J., Kennedy, G. and Dudukovic, M.P., Noninvasive Monitoring of Multiphase Flows, Elsevier, (Chaouki, J., Larachi, F. and Dudukovic, M.P., eds.), , Chapter 11, 335-406 (1997).

107. "Radioactive Particle Tracking in Multiphase Reactors: Principles and Applications", Larachi, F., J. Chaouki, G. Kennedy and M. P. Dudukovic′, Chapter 11 in Non-Invasive Monitoring of Multiphase Flows, Elsevier-Science, Eds. Chaouki, J., F. Larachi and M. P. Dudukovic′, Amsterdam (1997).

108. "Tomographic and Particle Tracking Studies in a Liquid-Solid Riser", Roy, S., J. Chen, S. Kumar, M. H. Al-Dahhan and M. P. Dudukovic′, I&EC Res., 36, 4666 (1997).

109. "A Comparison of the Equilibrium and Nonequilibrium Models for a Multicomponent Reactive Distillation Column", J.H. Lee and M.P. Dudukovic, Computers and Chemical Engineering, **23**, 159-171 (1998).

110. "A Particular Solution Trefftz Method for Solving Non-Linear Poisson Problems in Heat/Mass Transfer", Balakrishnan, K., Submitted to Journal of Computational Physics (1998).

111. "Comparative Hydrodynamics Study in a Bubble Column Using Computer Automated Radioactive Particle Tracking (CARPT) / Computed Tomography (CT) and Particle Image Velocimetry (PIV)", J. Chen, A. Kemoun, M. H. Al-Dahhan, M. P. Dudukovic, D. J. Lee, L.-S. Fan, Chem. Eng. Sci., 54, 2199-2207, (1998).

112. "Gas Holdup Distribution in Large Bubble Columns Measured by Computed Tomography", Chen, J., P. Gupta, S. Degaleesan, M.H. Al-Dahhan, M.P. Dudukovic´, Accepted in Flow Measurement and Instrumentation J., 9, 91, (1998).

113. "Investigation of a Complex Reaction Network for Production of Amino-Alcohol: I. Experimental Observations in High Pressure Trickle-Bed Reactor", Khadilkar, M.R., M.H. Al-Dahhan, Y. Jiang, M.P. Dudukovic´, AICh J., 44, 4, 912-920 (1998).

114. "Investigation of a Complex Reaction Network for Production of Amino-Alcohol: II. Kinetics, Mechanism and Model Based Parameter Estimation", Khadilkar, M.R., M.H. Al-Dahhan, Y. Jiang, M.P. Dudukovic´, AICh J., 44, 4, 921-926 (1998).

115. "Motor Vehicle Emission Factor Estimation: State-of-Knowledge and Research Needs", Turner, J.R., Submitted to Proceedings of the ASCE Specialty Conference: Transportation Planning and Air Quality III, in press (1998).

116. "Motor Vehicle Traffic-Derived Particulate Matter Emissions", Turner, J.R., Submitted to Infrastructure (in press) (1998).

117. "Non-Invasive Flow Monitoring in Opaque Multiphase Reactors via CARPT and CT", Roy, S., J. Chen, S. Degaleesan, P. Gupta, M.H. Al-Dahhan, M.P. Dudukovic´, Proceeding of FDESM' 98 [FDESM98-5077], 1998 ASME Fluids Engineering Division Summer Meeting, June (1998).

118. "Particulate Matter Emissions Emanating from Limited Access Highways", Lamoree, D.P., J.R. Turner, Submitted to Journal of the Air & Waste Management Association (1998).

119. "Prediction of Pressure Drop and Liquid Holdup in High Presure Trickle Bed Reactors", Al-Dahhan, M.H., M.R. Khadilkar, Y. Wu, M.P. Dudukovic´, I&EC Res., 37, 793 (Special issue in honor of Professor Westerterp) (1998).

120. Starch", Y. Wu, Research Progress of Chemical Technology, Chemical Industry Publishing House, 424-427, 1998.

121. "Select of the Flocculent in Treating Wastewater of Starch by using Air-Floating Method", Y. Wu, Research Progress of Chemical Technology, Chemical Industry Publishing House, 424-427, (1998).

122. "Comparative Hydrodynamics Study in Bubble Column Using Computer Automated Radioactive Particle Tracking (CARPT) / Computed Tomography (CT) and Particle Image Velocimetry (PIV)", J. Chen, A. Kemoun, M.H. Al-Dahhan, M.P. Dudukovic, D.J. Lee, L.-S. Fan, Chem. Eng. Sci., 54, 2199-2207 (1999).

123. "Dynamic Simulation of Bubbly Flow in Bubble Columns",Y. Pan, M.P. Dudukovic, M. Chang, Chem. Eng. Sci., 54, 2481-2490, (1999).

124. "Fluid Dynamic Parameters in Bubble Columns with Internals", J. Chen, F. Li, S. Degaleesan, P. Gupta, M. H. Al-Dahhan, M. P. Dudukovic, B. Toseland, Chem. Eng. Sci., 54, 2187-2197, (1999).

125. "Modeling and Simulation of Semi-Batch Photo Reactive Distillation", Z. Xu, M.P. Dudukovic, Chem. Eng. Sci., 54, 10, 1397-1404, (1999).

126. "Parametric Study of Unsteady State Flow Modulation in Trickle Bed Reactors", M. R. Khadilkar, M. H. Al-Dahhan, M. P. Dudukovic, Chem. Eng. Sci., 54, 2585-2595, (1999).

127. "The Use of Process Models to Control and Optimize Pultrusion-Type Processes", Voorakaranam,S., J.L. Kardos and B. Joseph, SAMPE Journal, Vol 35, No 3, (1999).

128. "Trickle-Bed Reactor Models for Systems with a Volatile Liquid Phase", M.R. Khadilkar, P.L. Mills and M.P. Dudukovic, Chem. Eng. Sci., 54, 2421-2431, (1999).

129. "Two Phase Flow Distribution in 2D Trickle-Bed Reactors", Y. Jiang, M. R. Khadilkar, M. H. Al-Dahhan, M. P. Dudukovic, Chem. Eng. Sci., 54, 2409-2419, (1999).

130. "Numerical investigation of gas-driven flow in two-dimensional bubble columns", Y. Pan, M. Dudukovic and M. Chang, AIChE Journal, 46, 433-449, (2000).

B. BOOKS AND MAJOR REPORTS

1. "Modeling of Czochralski Crystal Growth", P.A. Ramachandran and M.P. Dudukovic, EPRI Contract RP-8001, Final Technical Report (1991).

2. "Analysis of Transport Phenomena in Thin Liquid Films", Ramachandran, P. A. and S. R. Karur, prepared for Argonne National Laboratory, Argonne, Illinois (1993).

3. "Boundary Element Methods in Transport Phenomena", P.A. Ramachandran, Computational Mechanics Publishers and Elsevier, Southampton, England (1994).

4. "Wavelet Applications in Chemical Engineering", R.L. Motard and B. Joseph, Editors, Kluwer Academic Publishers, Boston (1994).

5. "Conformity Issues and Transportation Modeling in Denver and Salt Lake City", J.R. Turner, for Federal Highway Administration, U. S. Department of Transportation, February (1995).

6. "Motor Vehicle-Related Issues Concerning the Particulate Matter National Ambient Air Quality Standards: An Issue Paper", J.R. Turner, for Federal Highway Administration, U. S. Department of Transportation, February (1995).

7. "Measurement Techniques for Local and Global Fluid Dynamic quantities in Two and Three Phase Systems", Kumar, S., M. P. Dudukovic´, B. A. Toseland, Topical Report Submitted to Air Products and Chemicals for the Department of Engery Contract, DOE - FC 22-95 PC 95051, March (1996).

8. "Tracer Studies of the La Porte AFDU Reactor: Dehydration of Isobutanol to Isobutylene", Chen, J., S. Degaleesan, M. P. Dudukovic´, B. L. Bhatt and B. A. Toseland, Topical Report Submitted to Air Products and Chemicals for the Department of Engery Contract, DOE - FC 22-95 PC 95051, November (1996).

9. "Non-Invasive Monitoring of Multiphase Flows", Eds. Chaouki, J., F. Larachi and M.P. Dudukovic´, Elsevier-Science, Amsterdam (1997).

C. PRESENTATIONS

1. "Autoclave Processing of Long-Fiber Thermoplastic Composites", M.P. Dudukovic, J. L. Kardos, I. S. Yoon and Y. B. Yang, ISCRE 11, Toronto, July, (1990).

2. "Flow Mapping in Bubble Columns Using CARPT", N. Devanathan, D. Moslemian and M. P. Dudukovic, ISCRE 11, Toronto, July, (1990).

3. "Knowledge Based Control of Autoclave Curing of Composites", B. Joseph and H. T. Wu, AIChE Annual Meeting, Chicago, Illinois, November (1990).

4. "Liquid Circulation in Bubble Columns via the CARPT Facility", D. Moslemian, N. Devanathan and M. P. Dudukovic, ASME Winter Meeting, Dallas, Texas, November, (1990).

5. "Multiphase Reactors: Models and Experiments", M.P. Dudukovic, N. Devanathan and R. Holub, Institute Francais du Petrole, Lyon, France, October, (1990).

6. "Quantification of Eddy Dispersion in Bubble Columns via CARPT", N. Devanathan, D. Moslemian and M. P. Dudukovic, AIChE Annual Meeting, Chicago, Illinois, November, (1990).

7. "Bubble Columns: Some Recent Developments", M.P. Dudukovic and N. Devanathan, NATO ASI on Environmentally Benign Processes and Reactors, University of Western Ontario, London, Ontario, Canada (August 1991).

8. "Knowledge Acquisition and Knowledge Representation in an Expert System for Control of a Batch Process", B. Joseph, AIChE Spring Meeting, Houston, Texas, April (1991).

9. "Knowledge Acquisition from Routine Data for Quality Control", B. Joseph, National University, Chung-Li, Taiwan, July (1991).

10. "Knowledge Representation and Reasoning in the Presence of Uncertainty in an Expert System for Laboratory Reactor Selection", P. J. Hanratty, B. Joseph and M.P. Dudukovic, AIChE Annual Meeting, San Francisco, Paper No. 92b, November (1991).

11. "Pressure Drop, Holdup and Liquid Distribution in Trickle-Bed Reactors", R. Holub, M.P. Dudukovic′ and P.A. Ramachandran, AIChE Spring Meeting, Houston, Texas, April (1991).

12. "A Phenomenological Model of Pressure Drop, Liquid Holdup, and Flow Regime Transition in Gas-Liquid Trickle Flow", R. A. Holub, M. P. Dudukovic and P. A. Ramachandran. ISCRE 12, Torino, Italy. Paper A24, June (1992).

13. "Ammonia/Flyash Interactions and Their Impact on Flue Gas Treatment Technologies", J. R. Turner and M. P. Dudukovic, AIChE Annual Meeting, Miami Beach, Paper 230n November (1992).

14. "An Expert System for the Selection of Batch Reactors", B. Joseph, Feng-Chia University, Taichung, Taiwan, July (1992).

15. "An Expert System for the Selection of Laboratory-Scale Reactors", B. Joseph, China Oil Co., Chia-Yi, Taiwan, July (1992).

16. "Batch Process Control Using Neural Networks", B. Joseph, Chiyoda Corp., Yokohama, Japan, July (1992).

17. "Batch Process Control Using Neural Networks", B. Joseph, National Taiwan University, Taipei, Taiwan, July (1992).

18. "Batch Process Control Using Neural Networks", B. Joseph, National Tsing- Hua University, Hsin-Chu, Taiwan, July, (1992).

19. "Batch Process` Control Using Neural Networks", B. Joseph, Cheng-Kong Univ., Tainan, Taiwan, July (1992).

20. "Comparison of Models for Evaluation of Catalyst Particle External Wetting in Trickle-Bed Reactors from Dynamic Tracer Response Measurements", P. L. Mills, B. S. Zou and M. P. Dudukovic, AIChE Annual Meeting, Miami Beach. Paper 55c, November (1992).

21. "Liquid Backmixing in Bubble Columns", Y. B. Yang, N. Devanathan and M. P. Dudukovic, ISCRE 12, Torino, Italy, Paper H7, June (1992).

22. "Liquid Backmixing in Bubble Columns", Y. B. Yang, N. Devanathan and M. P. Dudukovic, AIChE Annual Meeting, Miami Beach. Paper 55e, November (1992).

23. "Motion of a Sphere in a Thin Liquid Film on a Rotating Disc", J. Zhou, M. P. Dudukovic and R. E. Sparks, AIChE Annual Meeting, Miami Beach. Paper 77c, November (1992).

24. "Quantification of the Evacuated Pulse Micro Reactor", B. S. Zou and M. P. Dudukovic, AIChE Annual Meeting, Miami Beach. Paper 53b, November (1992).

25. "A Modified Contactor for Experimental Studies of Mass Transfer and Kinetics Across Liquid-liquid Interface", M.H. Al-Dahhan, Y.X. Wu and M.P. Dudukovic′, paper 213a7, AIChE Annual Meeting, St. Louis, MO, November 7-15 (1993).

26. "A Reproducible Procedure to Pack Laboratory Scale Trickle-Bed Reactors with Fines", M.H. Al-Dahhan, Y.X. Wu and M.P. Dudukovic′, paper 213a8, AIChE Annual Meeting, St. Louis, MO, November 7-15 (1993).

27. "Dual Reciprocity BEM for Non-linear Diffusion-Reactor Problems in Porous Catalyst Particles", S. R. Karur and P.A. Ramachandran, AIChE Annual Meeting, Session 18-d, St. Louis (1993).

28. "Effect of High Pressure Operation on External Liquid-Solid Contacting Efficiency in Trickle-bed Reactors", M. H. Al-Dahhan, M. P. Dudukovic′ and P. A. Ramachandran, , paper 30k, AIChE Annual Meeting, St. Louis, MO, November 7-15 (1993).

29. "Effectiveness Factor for Partially Wetted Catalysts", S. R. Karur and P.A. Ramachandran, Poster-paper 214-a4, AIChE Annual Meeting, St. Louis (1993).

30. "Influence of Mixing Rate (Phase Turbulence) on the Mass Transfer Coefficient Across a Liquid-Liquid Interface", paper 45b, AIChE Annual Meeting, St. Louis, MO, November 7-15 (1993).

31. "Liquid Backmixing in Bubble Columns Using Computer Aided Radioactive Particle Tracking", Y. B. Yang, B. S. Zou and M. P. Dudukovic, AIChE Annual Meeting, St. Louis. Paper 70g, November (1993).

32. "Ammonia/Flyash Interactions and Their Impacts on Flue Gas Treatment Technologies", J.R. Turner, S. Choné and M.P. Dudukovic, ISCRE 13, Baltimore, MD (August 1994).

33. "Boundary Element Method for a Network of Linear Reactions", at the AIChE Annual Meeting, Session 238-b, San Francisco, November (1994).

34. "Boundary Element Methods for Diffusion-Reaction Problems", Proceedings of the 14th IMACS World Congress, 1, 411-414, Atlanta, Georgia (1994).

35. "Boundary Element Methods in Biomedical Engineering", S. R. Karur and P. A. Ramachandran, Poster-paper, Biological and Biomedical Engineering Workshop, Washington University (1994).

36. "Comparison of Trickle-Bed and Upflow Reactors (Packed Bubble Columns) at High Pressure Operation", A. Choné, Y. Wu, M. Khadilkar, M. Al-Dahhan and M. P. Dudukovic′, paper 76k, AIChE Annual Meeting, San Francisco, CA, November 13-18 (1994).

37. "Effect of Scale on Liquid Recirculation and Mixing in Bubble Columns", N. Devanathan, M.P. Dudukovic and D. Moslemian, at the 13th International Society of Chemical Reaction Engineering (ISCRE) Conferece , Baltimore, MD (September 1994).

38. "Influence of Fines on Liquid-Solid Contacting Efficiency, Liquid Holdup and Pressure Drop in Laboratory Trickle-Bed Reactors at Elevated Pressusre", M.H. Al-Dahhan, M.P. Dudukovic and P.A. Ramachandran, paper 52g, AIChE Spring National Meeting, Atlanta, Georgia (April 17-21, 1994).

39. "Numerical Simulation and Experimental Verification of the Two Phase Flow in Bubble Columns", S. Kumar, B. Kashiwa, W.B. Vanderheyden, M.P. Dudukovic and N. Devanathan, presented at AIChE Annual Meeting in San Francisco (Nov., 1994).

40. "Predictive Control of Quality in Batch Polymerization Using Artificial Neural Network Models", M.P. Dudukovic′, A.Y.D. Tsen, S. S. Jang, D.S.H. Wong, Proceedings of the Fifth International Symposium on Process Systems Engineering (PSE '94), Kyongju, Korea, June (1994)

41. "Pressure Drop and Liquid Holdup in High Pressure Trickle-Bed Reactors", M.H. Al-Dahhan and M.P. Dudukovic, paper PH1, 13th International Symposium on Chemical Reaction Engineering, Baltimore, MD (September 25-28, 1994).

42. "Process Identification Using Discrete Wavelet Transforms", M.P. Dudukovic′, S. Palavajjhala and R.L. Motard, ADCHEM, 94, Proceedings of the IFAC Symposium on Advanced Control of Chemical Processes, Kyoto, Japan, May (1994).

43. "Sensor Data Analysis Using Wavelets", B. Joseph, X. D. Dai and R. L. Motard, Paper No. 234b, presented at AIChE Annual Meeting, San Francisco, Nov. (1994).

44. "Shrinking Horizon Model Predictive Control for Off and On-line Control of Autoclave Cured Composite Laminate Materials", B. Joseph, M. M. Thomas and J.L. Kardos, Nondestructive Evaluation Applied to Process Control of Composite Fabrication Conference, St. Louis, MO, Oct. (1994)

45. "A Lagrangian Method for Improving the Measurements of Computer Automated Radioactive Particle Tracking (CARPT) System", Kumar, B. S., and Dudukovic′, M.P., Presented at AIChE Annual Meeting in the Session on Experiments in Mixing, Miami Beach, Florida, November 12-13 (1995).

46. "A Langrangian Method for Improving the Measurements of Computer Automated Radioactive Particle Tracking (CARPT) System", B.S. Kumar and M.P. Dudukovic, Presented in the "Experiments in Mixing" Session of the 1995 Annual AIChE Meeting, Miami Beach, FL, November 12-17, (1995).

47. "A New Robust Algorithm for the Study of Gas Phase Incineration of Hydrocarbons by Forced Flow Reversal in a Regenerative Bed", Kulkarni, M. S., and Dudukovic´, M.P., Paper 60f, Summer AIChE Meeting, Boston, July 31 (1995).

48. "A Study of Dynamics of Gas Phase and Solid Phase Reactions in Asymmetric Fixed-Bed Reactors", Kulkarni, M. S., and Dudukovic´, M.P., Paper 79e, AIChE Meeting, Miami, Nov. 13 (1995).

49. "An Adaptive Algorithm for Process Involving Fast Reactions in Packed-Bed Reactors Subject to Forced Flow Reversal", Kulkarni, M. S., and Dudukovic´, M.P., Paper 171g, AIChE Meeting, Miami, Nov. 14 (1995).

50. "An Integrated Approach to Computing and Computer Applications in the Undergraduate Chemical Engineering Curriculum", Al-Dahhan, M., Paper 245d, AIChE Annual Meeting, Miami Beach, Florida, November 12-17 (1995).

51. "Carbon Fibers for Affordable Polymeric Composites", R. Shepard and J. Kardos, Paper 163a, AIChE Annual Meeting, Miami Beach, Florida, November 12-17 (1995).

52. "Computation of Flow Fields in Multiphase Flow Systems", B.S Kumar., W.B. Vanderheyden, N. Devanathan, M.P. Dudukovic and B.A. Kashiwa, Presented at the 15th Biannual Conference on Industrial Mixing Banff, Alberta, Canada, June 15-25 (1995).

53. "Computation of Flow Fields in Multiphase Systems", W.B. Vanderheyden, W.B. Vanderheyden, N. Devanathan and M.P. Dudukovic, accepted for presentation at 15th Biannual Conference on Industrial Mixing at Alberta, Canada (June 1995).

54. "Computing and Computer Applications in Engineering Education", Al-Dahhan, M., the Fourth World Conference on Engineering Education, St. Paul, Minnesota, October 15-20 (1995).

55. "Design of Nonlinear Adaptive Inferential Controller", H. Vedam and B. Joseph, Paper no. 180f, Presented at AIChE Annual Meeting, Miami (1995).

56. "Effect of Fines on the Performance of Downflow (trickle-bed) and Upflow (packed bubble column) Reactors", Y. Wu, M. Khadilkar, M. Al-Dahhan and M.P. Dudukovic, The Catalyst Society 14th North American Meeting, Snowbird, Utah (June 11-16, 1995).

57. "Effect of Fines on the Performance of Trickle Bed and Upflow Reactors", Khadilkar, M., Wu, Y., Al-Dahhan, M., and Dudukovic´, M.P., Paper 66e, AIChE Annual Meeting, Miami Beach, Florida, November 12-17 (1995).

58. "Effect of Moisture Uptake on the Polymerization and Devolatization of AFR700 Polyimide Composites", J.L. Vasat, J.L. Kardos and M.P. Dudukovic, 27th International SAMPE Technical Conference, October 9-12, (1995).

59. "Evaluation of Trickle Bed Reactor Models by Using Chemical Reactions", Y. Wu, M. Khadilkar, M. Al-Dahhan and M. P. Dudukovic′, 12th Midwest Chinese American Science Technology Conference", St. Louis, MO, June 11-12 (1995).

60. "Experimental Quantifications of Turbulence in Bubble Columns", Degaleesan, S. and Dudukovic′, M. P., AIChE Annual Meeting, Miami Beach, November (1995).

61. "Fingerprinting Electrochemical Noise using Wavelet Analysis", X. D. Dai, R. L. Motard, and B. Joseph, paper no. 185a, Presented at AIChE Annual Meeting, Miami (1995).

62. "Flow Patterns in a Slurry Bubble Column Reactor Under Reaction Conditions", B.A. Toseland, D.M. Brown, B.S. Zou and M.P. Dudukovic, The 2nd International Conference on Gas-Liquid-Solid Reactor Engineering, Cambridge, United Kingdom (March 27-29, 1995).

63. "Infusing Environmental Education into the Undergraduate Engineering Curriculum; A Minor in Environmental Engineering Science", J.R. Turner, W.P. Darby and M.P. Dudukovic, ASEE Illinois-Indiana Section Conference, West Lafayette, IN (March 1995).

64. "Liquid Catalyst Contacting Efficiency in High Pressure Trickle-Bed Reactors with/without Fines", M.H. Al-Dahhan and M.P. Dudukovic, The 2nd Italian Conference on Chemical Process Engineering, Firenze, 15-17, May (1995).

65. "Liquid-Solid External Contacting in Trickle-bed Reactors Operated at High Pressure", M. H. Al-Dahhan and M. P. Dudukovic′, The 2nd International Conference on Gas-Liquid-Solid Reactor Engineering, Cambridge, United Kingdom, March 27-29 (1995).

66. "Measurement of Turbulent Dispersion Coefficients in Bubble Columns using CARPT", S. Degaleesan and M.P. Dudukovic, Presented at MIXING V, Bannf, Canada, (1995).

67. "Multiphase Reactors Technology in Waste Minimization and Pollution Reduction", M.H. Al-Dahhan and M.P. Dudukovic, Emerging Technologies in Hazardous Waste Management VII, Atlanta, Georgia, September 17-20, (1995).

68. "Predictive Control of Quality in Batch Polymerization Using a Hybrid Artificial Neural Network Model", B. Joseph, A.Y.D. Tsen, S. S. Jang and D. S. H. Wong, Paper accepted by AIChE Journal, April (1995).

69. "Predictive Control of Quality in Composite Manufacturing Using Artificial Neural Network Models", M. M. Thomas and B. Joseph, Paper presented at Workshop on Neural Networks, Taipei, Taiwan, June (1995).

70. "Process Identification Using Discrete Wavelet Transforms-Design of Pre- Filters", B. Joseph, S. Palavajjhala and R.L. Motard, Paper accepted by AIChE Journal, April (1995).

71. "Shrinking Horizon Model Predictive Control for the Autoclave Curing of Composite Laminate Materials and Other Batch Processes", B. Joseph, M. M. Thomas and J.L. Kardos, Proceedings of the 1995 NSF Design and Manufacturing Grantees Conference, pp 495-497, Society of Manufacturing Engineers, Dearborn, MI (1995).

72. "The Application of Signal Analysis to Localized Corrosion", N. Nissing, X. D. Dai, R. L. Motard, and B. Joseph, Paper no. 240e, Presented at AIChE Annual Meeting, Miami (1995).

73. "Trickle-Bed Reactors: Scale-Up Issues", M.H. Al-Dahhan and M.P. Dudukovic, AIChE Annual Meeting, Miami Beach, Florida, November 12-17, (1995).

74. "Use of Discontinuous Elements in BEM for Diffusion Problems", S. Karur and P. Ramachandran, Paper 171f, AIChE Annual Meeting, Miami Beach, Florida, November 12-17 (1995).

75. "Void Fraction Measurements in Bubble Columns Using Computed Tomography", Kumar, B. S., Moslemian, D., and Dudukovic´, M. P., Presented at the ASME Forum on Measurement Techniques in Multiphase Flows, San Francisco, California Nov. 12-17 (1995).

76. "1-D Phenomenological Model for Churn-Turbulent Bubble Columns Based on Experiments", P. Gupta, M. Al-Dahhan, M. P. Dudukovic, Computational Fluid Dynamics (CFD) in Chemical Reaction Engineering Conference, Engineering Foundation Conference, San Diego, October, 13-18, (1996).

77. "A Two Dimensional Model for Liquid Mixing in Bubble Columns", S. Degaleesan, M.P. Dudukovic, B.A. Toseland and B.L. Bhatt, AIChE Annual Meeting, Chicago, November (1996).

78. "Adaptive Inferential Control of Quality in Injected Resin Transfer Molding Process", S. Voorakaranam and B. Joseph, AIChE Annual Meeting, Chicago (1996).

79. "Affordable Processing of Composite Structure for the Civilian Infrastructure", J. Kardos, B. Khomami, P.A. Ramachandran, B. Yang, and R. Shepard, Paper 73a, 5th World Congress of Chemical Engineering, San Diego, California, July 14-18 (1996).

80. "Application of Multiquadrics for the Solution of Heat and Mass Transfer Problems", Ramachandran, P. A. and S. R. Karur, AIChE Annual Meeting , Chicago (1996).

81. "Comparison of Trickle-Bed and Upflow Reactor Performance at High Pressure: Model Predictions and Experimental Observations", M, Khadilkar, Y. Wu, M.H. Al-Dahhan, M.P. Dudukovic, ISCRE 14, Belgium, 5-8 May, (1996).

82. "Dynamic Optimization of Batch Distillation", Karur, S. R. C. J. Hagedorn, V. G. Kalthod, M. J. Davidson and G. Joglekar, AIChE Spring Meeting, New Orleans, March (1996).

83. "Evaluation of a trickle bed reactor model using liquid limited chemical reaction", Y. Wu, M. Khadilkar, M. Al-Dahhan, M.P. Dudukovic, ISCRE 14, Belgium, 5-8 May, (1996).

84. "Experimental Results in the Flow in Liquid-Solid Risers", S. Roy, J. Chen, S. Kumar, M. Al-Dahhan, M. P. Dudukovic, Computational Fluid Dynamics (CFD) in Chemical Reaction Engineering Conference, Engineering Foundation Conference, San Diego, October, 13-18, (1996)

85. "High Pressure Trickle-Bed Reactors: A State-of-the-Art Review", F. Larachi, M. H. Al-Dahhan, M. P. Dudukovic, A. Laurent, 12th International Congress of Chemical & Process Engineering, CHISA'96, August, (1996).

86. "Implication of Proposed Changes to the Ozone and Particulate Matter National Ambient Air Quality Standards", Joy R. Turner, National Meeting of the Society of Environmental Journalist, St. Louis, MO, October (1996).

87. "Improved Prediction of Pressure Drop and Liquid Holdup in High Pressure Trickle-Bed Reactors", M. H. Al-Dahhan, Y. Wu, M. Khadilkar, M. P. Dudukovic, Paper 3L, 5th World Congress of Chemical Engineering, San Diego, July 14-18, (1996).

88. "Liquid Mixing Based on Convection and Turbulent Dispersion in Bubble Columns", S. Degaleesan, S. Roy, B.S. Kumar, and M.P. Dudukovic, Presented at ISCRE 14, Brugge, Blegium, April (1996).

89. "Liquid Phase Mixing in Liquid-Solid Circulating Reactor", S. Roy, J. Chen, S. Kumar, M. Al-Dahhan, M. P. Dudukovic, Paper 107d, AIChE Annual Meeting, Chicago, Illinois, November 10-15, (1996).

90. "Non-Invasive Experimental Methods for Measurements in Multiphase Flow", Kumar, S., Presented at the Engineering Foundation Conference on Computational Fluid Dynamics in Reaction Engineering, october 13-18 (1996).

91. "Ozone/Particulate Matter/Regional Haze Standards Integrated Implementation Issues", Jay R. Turner, Invited Panelist Presentation, EPA Public Meeting on Ozone and Particulate Matter National Ambient Air Quality Standards, St. Louis, MO, August (1996).

92. "Progress in Understanding the Fluid Dynamics of Bubble Column Reactors", Degaleesan, S., Kumar, S.B., Dudukovic´, M.P., Toseland, B.A., and Bhatt, B.L., The First Joint Power and Fuels System Contractors Conference, Pittsburgh, July (1996).

93. "Scale-Up, Design and Performance of Trickle-Bed Reactors", R. Heck, M. H. A-Dahhan, M. P. Dudukovic, paper 163b, AIChE Annual Meeting, Chicago, Illinois, November 10-15, (1996).

94. "Solids Mixing in an Ebullated Bed", Sunun Limtrakul", S. Kumar, and M. P. Dudukovic′, Presented at the AIChE Annual Meeting, Chicago, Session 59, Paper 59c, November 12 (1996).

95. "Use of Radial Basis Functions in the Dual Reciprocity Method for Non-linear Diffusion Reaction Problems", Ramachandran, P. A. and S. R. Karur, AIChE Annual Meeting , Chicago, November (1996).

96. "A Particular Solution Trefftz Method for Poisson Problems", Balakrishnan, K., AIChE Annual Meeting, Los Angeles, CA (1997).

97. "A Reaction Engineering Approach to Pollution Prevention for Batch Charcoal Kilns: Particle Scale Modeling", Turner, J.R., with G. Bhatia, American Institute of Chemical Engineers, 1997 Annual Meeting, Los Angeles, CA, November (1997).

98. "An Adiabatic Fixed Bed Reactor Model for a Multicomponent and Multiphase Reaction System", Duyen T. Nguyen, Paul H. Merz, Kris Parimi and P. A. Ramachandran, Chemical Reactor engineering for Sustainable Processes and Products, Chemical Reaction Engineering VI, Engineering Foundation Conference, Banff, Canada, June 8-13 (1997).

99. "Building a Pollution Prevention Toolbox for the Batch Charcoal Kiln Industry: Modeling the Slow Pyrolysis of Wood", Bhatia, G., J. Turner, Presented at the Second Annual Mid-America Environmental Engineering Conference, University of Missouri, Columbia, MO, September (1997).

100. "Column Scale Effects on Gas Holdup and Flow Pattern Bubble Columns", J. Chen, P. Gupta, F. Li, S. Degaleesan, S. Roy, M.H. Al-Dahhan, M.P. Dudukovic and B. Toseland, Paper 217d, AIChE Annual Meeting, Los Angeles, California, November 16-21 (1997).

101. "Effect of Catalyst Wetting on the Performance of Trickle-Bed Reactors", Y. Wu, M. Khadilkar, M. H. Al-Dahhan, M. P. Dudukovic, Second Joint U.S./China Chemical Engineering Conference, Beijing, China, May 19-22, (1997).

102. "Experimental Evaluation of the MiniVol Portable Sampler for Fine Particulate Matter Ambient Monitoring", Turner, J.R., with J.S. Hill, American Institute of Chemical Engineers, 1997 Annual Meeting (National Student Poster Session), Los Angeles, CA, November (1997).

103. "Flow Pattern Studies in Liquid-Solid Riser Reactor", S. Roy, J. Chen, S. Kumar, M. H. Al-Dahhan, M. P. Dudukovic, Chemical Reactor Engineering for Sustainable Processes and Products, Chemical Reaction Engineering VI, Engineering Foundation Conference, Banff, Canada, June 8-13, (1997).

104. "Fluid Dynamics in Churn-Turbulent Bubble Columns: Measurements and Modeling", M.P. Dudukovic, S. Degaleesan, P. Gupta, and S.B. Kumar, presented at the ASME Fluids Engineering Division Summer Meeting, Vancouver, Canada (1997).

105. "Gas Holdup in Bubble Columns Measured by Computer Tomography", J. Chen, P. Gupta, M. H. Al-Dahhan, S. B. Kumar, M. P. Dudukovic, Frontiers in Industrial Process Tomography - II, Delft, The Netherlands (1997).

106. "Implementation of a Computer-Based Air Pollution Data Analysis Exercise in an Environmental Engineering Laboratory Course", Turner, J.R. and S. R. Falke, ASEE Midwest Section Conference, Columbia, MO, April (1997).

107. "Infusing Environmental Education into the Chemical Engineering Curriculum: A Minor in Environmental Engineering Science", Turner, J.R. and M. P. Dudukovic′, ASEE National Conference, Milwaukee, WI, June (1997).

108. "Investigation of a Complex Reaction Network in a High Pressure Trickle Bed Reactor", Khadilkar, M., Y. Jiang, M.H. Al-Dahhan, M.P. Dudukovic′, Paper 252a, AIChE Annual Meeting, Los Angeles, California, November 16-21 (1997).

109. "Motor Vehicle Particulate Matter Emissions Estimation: State-of-Knowledge and Research Needs", Turner, J.R., ASCE Specialty Conference: Transportation Planning and Air Quality III, Lake Tahoe, CA, August (1997).

110. "Novel Techniques for Slurry Bubble Column Hydrodynamics", M. P. Dudukovic, M. H. Al-Dahhan, P. Gupta, Y. Yang, S. Degaleesan, L. S. Fan, P. Jiang, J. Reese, D. L. Lee, R. F. Mudde, M. Chang, University Coal Research Program, Department of Energy, Pittsburgh, Pennsylvania, The Annual Review Meeting, June 3-4, (1997).

111. "Prediction of Two Phase Flow Distribution in 2D Trickle Bed Reactors", Jiang, Y., M. Khadilkar, M.H. Al-Dahhan, M.P. Dudukovic′, Paper 276a, AIChE Annual Meeting, Los Angeles, California, November 16-21 (1997).

112. "Recent Advances in High Pressure Trickle-Bed Reactors", M. H. Al-Dahhan, F. Larachi (Laval University), M. P. Dudukovic, Chemical Reactor Engineering for Sustainable Processes and Products, Chemical Reaction Engineering VI, Engineering Foundation Conference, Banff, Canada, June 8-13, (1997).

113. "Simulation of Unsteady State Operation in Trickle Bed Reactors", Khadilkar, M., M.H. A-l-Dahhan, M.P. Dudukovic′, Paper 254e, AIChE Annual Meeting, Los Angeles, California, November 16-21 (1997).

114. "Simulation of Unsteady State Operation in Trickle-Bed Reactors", M. R. Khadilkar, M. H. Al-Dahhan, M. P. Dudukovic, Chemical Reactor Engineering for Sustainable Processes and Products, Chemical Reaction Engineering VI, Engineering Foundation Conference, Banff, Canada, June 8-13, (1997).

115. "Study of Trickle-Bed Reactor Performance Under Periodic Operation", M. P. Dudukovic, M. H. Al-Dahhan, M. Khadilkar, Y. Wu, Second Joint U.S./China Chemical Engineering Conference, Beijing, China, May 19-22, (1997).

116. "Tracer Data Analysis with Axial Dispersion Model for Two Pilot Plant Slurry Reactors", J. Chen, S. Degaleesan, M.H. Al-Dahhan, M.P. Dudukovic and B. Toseland, Paper 150d, AIChE Annual Meeting, Los Angeles, California, November 16-21 (1997).

117. "Trickle-Bed Reactors at High Pressure: A State-of-the-Art-Review", Larachi, F., M.H. Al-Dahhan, M.P. Dudukovic', Paper, 484, Session 48, 47th Canadian Chemical Engineering Conference, October 5-8, Edmonton, Alberta, Canada (1997).

118. "A Comparison of the Equilibrium and Rate-based Models for a Multicomponent Reactive Distillation Tray Column", J.H. Lee and M.P. Dudukovic, Paper No. 131f, The 1998 AIChE Annual Meeting, Miami Beach, FL, Nov. 15-20 (1998).

119. "A Flexible Approach to Modeling and Simulation of Fiber Reinforced Polymer Processing using Object Oriented Techniques", Potaraju S., B.,Khomami, J.L.,Kardos and B. Joseph, presented at Annual AIChE Meeting, Miami, November, (1998).

120. "A Look Inside EPA's Motor Vehicle Particulate Matter Emission Factor Model (PART5)", Turner, J.R., Air & Waste Management Association Specialty Conference on Fine Particulate Matter, Long Beach, CA, January 28-30 (1998).

121. "Analysis and Performance of the Two-stage Cascade LP-MPC Scheme," Ying, Chao-Ming, Srikanth Voorakaranam, and Babu Joseph, American Control Conference, Philadelphia, PA, (1998).

122. "Comparative Hydrodynamics Study in a Bubble Column Using Computer Automated Radioactive Particle Tracking (CARPT) / Computed Tomography (CT) and Particle Image Velocimetry (PIV)", J. Chen, A. Kemoun, M. H. Al-Dahhan, M. P. Dudukovic, D. J. lee, L.-S. Fan, ISCRE15, Newport Beach, California, September 13-16, (1998).

123. "Dynamic Simulation of Bubble Flow in Bubble Columns", Y. Pan, M.P. Dudukovic, and M. Chang, presented on the 15th International Symposium on Chemical Reaction Engineering (ISCRE 15), Newport Beach, CA, September 13-16, (1998).

124. "Experimental Investigation of Flow in a Liquid-Solid riser", S. Roy, A. Kemoun, M.H. Al-Dahhan, M.P. Dudukovic, Paper 165g, AIChE Annual Meeting, Miami Beach, Florida, November 15-20, (1998).

125. "Experimental Investigation of Liquid Flow Distribution in Trickle-Bed Reactors Under Steady State and Periodic Operation", Y. Jiang, J. Mettes, M. Khadilkar,

M.H. Al-Dahhan, paper 181-1b; won the 2nd place in National Student paper competition – section of Engineering Sciences and Fundamental, AIChE Annual Meeting, Miami Beach, Florida, November 15-20, (1998).

126. "Fluid Dynamic Parameters in Bubble Columns with Internals", J. Chen, F. Li, S. Degaleesan, P. Gupta, M. H. Al-Dahhan, M. P. Dudukovic, B. Toseland, ISCRE15, Newport Beach, California, September 13-16, (1998).

127. "Intelligent Control of Polymer Composites Manufacturing," Voorakaranam,S., S.Potaraju, B.Joseph and J.L.Kardos, Proceedings of the NSF Design and Manufacturing Grantees Conference, Monterrey, Mexico, January (1998).

128. "Liquid Flow Maldistribution and Reaction Performance in Trickle-bed Reactors", Y. Jiang, M.H. Al-Dahhan, M.P. Dudukovic, Paper 304e, AIChE Annual Meeting, Miami Beach, Florida, November 15-20, (1998).

129. "Liquid Flow Maldistribution and Reaction Performance in Trickle-bed Reactors", Y. Jiang, M.H. Al-Dahhan, M.P. Dudukovic, Paper 318bi, AIChE Annual Meeting, Miami Beach, Florida, November 15-20, (1998).

130. "Liquid Holdup Measurement Techniques in High Pressure Laboratory Trickle-Bed Reactors", W. Highfill, M.H. Al-Dahhan, Paper 318bk, AIChE Annual Meeting, Miami Beach, Florida, November 15-20, (1998).

131. "Liquid Turbulence and Backmixing in Large Diameter Bubble Columns with Internals", J. Chen, F. Li, M.H. Al-Dahhan, M.P. Dudukovic, B. Toseland, Paper 242i, AIChE Annual Meeting, Miami Beach, Florida, November 15-20, (1998).

132. "Liquid-Solid Mass Transfer Coefficient in High Pressure Trickle Bed Reactors", W. Highfill, M.H. Al-Dahhan, Paper 318bj, AIChE Annual Meeting, Miami Beach, Florida, November 15-20, (1998).

133. "Numerical Simulation of Two-Phase Flow and Tracer Experiment in Bubble Column Reactors", Y. Pan, M.P. Dudukovic and M. Chang, AIChE Annual Meeting, Miami Beach, FL, November 15-20, (1998).

134. "Parametric Analysis of One Dimensional Modeling of Gas-Liquid Flow in Bubble Column", S. Saberi, H.H. Al-Dahhan, M.P. Dudukovic, B. Toseland, Paper 242k, AIChE Annual Meeting, Miami Beach, Florida, November 15-20, (1998).

135. "Parametric Study of Unsteady State Flow Modulation in Trickle Bed Reactors", M. R. Khadilkar, M. H. Al-Dahhan, M. P. Dudukovic', ISCRE15, Newport Beach, California, September 13-16, (1998).

136. "Reduced Order Models for Nonlinear Output Estimation", Potaraju, S. and B .Joseph, presented at Annual AIChE Meeting, Miami, November, (1998).

137. "Scale-Up in Reaction Engineering" – Invited Lecture - M.H. Al-Dahhan, M.P. Dudukovic, Paper 307a, AIChE Annual Meeting, Miami Beach, Florida, November 15-20, (1998).

138. "Sensor Self-Validation using Power Spectrum Density Analysis" ,Ying, Chao-Ming and Babu Joseph, AIChE Annual Meeting, Miami Beach, Florida, (1998).

139. "System Identification Using Orthogonal Polynomial Approximations", Ying, Chao-Ming and B. Joseph, Invited Paper for American Control Conference, Philadelphia, June, (1998).

140. "System Identification in Frequency Domain using Polynomial Models," Ying, Chao-Ming and Babu Joseph, AIChE Annual Meeting, Miami Beach, Florida, (1998).

141. "Two Phase Flow Distribution in 2D Trickle-Bed Reactors", Y. Jiang, M. R. Khadilkar, M. H. Al-Dahhan, M. P. Dudukovic', ISCRE15, Newport Beach, California, September 13-16, (1998).

142. "Unsteady State Flow Modulation in Trickle Bed Reactors: Experiments and Model Predictions", M. R. Khadilkar, M.H. Al-Dahhan, M.P. Dudukovic, Paper 318bh, AIChE Annual Meeting, Miami Beach, Florida, November 15-20, (1998).

143. "Model-Based Monitoring and Control of Quality in Polymeric Composites Manufacturing", S. Voorakaranam, S. Potaraju, B. Joseph, and J.L. Kardos, Proceedings of the NSF Design and Manufacturing Grantees Conference, San Diego, California, January (1999).

144. "Characterization of Single Phase flows in a Stirred tank using Computer Automated Radioactive Particle Tracking (CARPT)", A.R. Rammohan, A. Kemoun, M.H. Al-Dahhan, and M.P. Dudukovic, Presented at Mixing XVII, Banff, Alberta, Canada, August 15-20th, (1999).

145. "Motion of Neutrally Buoyant Particles in Sitrred Vessels, CARPT Experiments and CFD Simulations", V.V. Ranade, A.R. Rammohan, A. Kemoun, M.H. Al-Dahhan, M.H., and M.P. Dudukovic, Presented at Mixing XVII, Banff, Alberta, Canada, August 15-20th, (1999).

146. "Motion of Neutrally Buoyant Particles in Sitrred Vessels, CARPT Experiments and CFD Simulations", V.V. Ranade, A.R. Rammohan, A. Kemoun, M.H. Al-Dahhan, M.H., and M.P. Dudukovic, Presented at A.I.Ch.E Annual Meeting, Dallas, Texas, U.S.A October 31st –November 5th, (1999).

147. "Characterization of Single Phase flows in a Stirred tank using Computer Automated Radioactive Particle Tracking (CARPT)", A. Kemoun, A.R. Rammohan, M.H. Al-Dahhan, M.H., and M.P. Dudukovic, Presented at A.I.Ch.E Annual Meeting, Dallas, Texas, U.S.A , October 31st –November 5th (1999).

148. "Investigation of Liquid Mixing in Churn-Turbulent Bubble Columns Using Conductivity Probes", P. Gupta, B.C. Ong, M. H. Al-Dahhan, M.P. Dudukovic, Oral Presentation, North American Mixing Forum-Mixing XVII, Banff, Alberta, Canada, (1999).

149. "Modeling of Reactive Distillation", M.P. Dudukovic, CCR Meeting on Multifunctional Reactors, Marco's Island, FL, June 13-15 (1999).

150. "Modern Approach to Reaction Engineering", M.P. Dudukovic, General Electric Plastics, Mount Vernon, IN, June 25 (1999.

151. "Slurry Bubble Column Hydrodynamics", M.P. Dudukovic, DOE Fossil Energy Clean Fuels Meeting, Cincinnati, OH, September 22 (1999).

152. "Scale-up in Reaction Engineering", M.P. Dudukovic, Air Products, Allentown, PA, October 6 (1999).

153. "Trickle-Bed Reactors", M.P. Dudukovic, DuPont, Beaumont, TX, November 8 (1999).

154. "Tracer Methods", M.P. Dudukovic, International Atomic Energy Commission, Vienna, Austria, November 22 (1999).

155. "Opaque Multiphase Reactors: Experimentation, Modeling and Troubleshooting", M.P. Dudukovic, Institute Francais du Petrole (IFP) Scientific Meeting, December 8-9 (1999).

156. "CARPT Studies of Bubble Columns", M.P. Dudukovic, 3rd IMUST Conference, Santa Barbara, CA, March 13-15 (2000)

157. "CARPT Studies of Gas-Solid Risers", M.P. Dudukovic, MFDRC Meeting, Sandia, Albuquerque, NM, April 12-14 (2000).

158. "Reaction Engineering, The Environment: Pollution Prevention and Sustainable Development", M.P. Dudukovic, National Science Foundation, Washington, DC, April 17 (2000).

159. "Distributor Effects on Gas Holdup Profiles in Bubble Columns", M.P. Dudukovic, Sandia National Laboratory, Albuquerque, NM, May 9 (2000).

160. "Bubble Column Hydrodynamics", M.P. Dudukovic, Air Products, Allentown, PA, May 24 (2000).

161. "CFD Modeling of Multiphase Flow Distribution in Catalytic Packed Bed Reactors: Scale-Down Issues", M.P. Dudukovic, 3rd International Symposium on Catalysis in Multiphase Reactors (CAMURE 3), Naples, Italy, May 29-31 (2000).

162. "A Parallel Approach to Catalyst and Reactor Selection for a Fine Chemicals Process", M.P. Dudukovic, 3rd International Symposium on Catalysis in Multiphase Reactors (CAMURE 3), Naples, Italy, May 29-31 (2000).

163. "Computer Automated Radioactive Particle Tracking (CARPT) Applied to Microalgal Photobioreactors", M. H. Al-Dahhan, A. Kemoun, J. M. Fernández Sevilla, E. Molina Grima, and F. García Camacho, *219th American Chemical Society (ACS)*, National Meeting, San Francisco, California, March 26-30, (2000).

D. SHORT COURSES OFFERED BY CREL

1. "Reaction Engineering for Multiphase Catalyzed Systems"

   P. L. Mills, M.P. Dudukovic´ and P.A. Ramachandran 3-day short course offered through the AIChE Continuing Education Program

Annual AIChE Meeting	-	Chicago, November 1990 Spring AIChE Meeting
	-	Houston, April 1991
Summer AIChE Meeting	-	Pittsburgh, August 1991
Annual AIChE Meeting	-	Miami Beach, November 1992
Spring AIChE Meeting	-	Houston, April 1993
Annual AIChE Meeting	-	St. Louis, November 1993
Summer AIChE Meeting	-	Boston, August 1995

2. "Data Acquisition and Control Using Microcomputers"

   B. Joseph

   3-day short course offered through the AIChE Continuing Education Program

Summer AIChE Meeting	-	San Diego, August 1990
Annual AIChE Meeting	-	Chicago, November 1990
Spring AIChE Meeting	-	Houston, April 1991
Regional AIChE Meeting	-	Orlando, May 1991
Fall AIChE Meeting	-	Los Angeles, November 1991
Spring AIChE Meeting	-	Boston, May 1992
Summer AIChE Meeting	-	Philadelphia, August 1992
Spring AIChE Meeting	-	Houston, April 1993
Fall AIChE Meeting	-	St. Louis, November 1993

3. "Computational Fluid Dynamics of Reactive Turbulent Flows", Rodney Fox, Kansas State University, a five day course offered at CREL, WU, St. Louis (May 1996).

4. "Multiphase Reacctors", P.L. Mills, DuPont, a five day course offered at CREL, WU, St. Louis (August 1997).

E. RECENT D.Sc. THESES

1. P. Hanratty, "Expert System Application in Chemical Engineering", December 1991.
2. V. Kalthod, "Novel Carrier and Reactor for Culture of Attachment Dependent Mammalian Cells", December 1991.
3. S. Pirooz, "Two Region Computational Modeling of DC Plasma Processes", December 1991.
4. D. Shieh, "Automated Knowledge Acquisition from Routine Data for Process and Quality Control", May 1992.
5. J. Zhou, "Microencapsulation of Particles on Rotating Discs", May 1992.
6. B.S. Zou, "Modeling the System for Temporal Analysis of Products (TAP)", May 1992.
7. A. Basic', "Liquid Holdup and Hydrodynamics of Rotating Packed Beds", December 1992.
8. H. Erk, "Phase Change Heat Regenerators: Modeling and Experimental Studies", December 1992.
9. M. Al-Dahhan, "Effects of High Pressure and Fines on the Hydrodynamics of Trickle-Bed Reactors", December 1993.
10. J.R. Turner, "Studies in Reaction Engineering of Nitrogen Oxides Abatement: I: Ammonia/Flyash Interactions and Their Impact on Flue Gas Treatment Technologies. II. Gas-Solid Catalytic Monolith Reactor Design", December 1993.
11. J. Vasat, "Experimental Verification of the Devolatilization Model for AFR700 Polyimide Composites", December 1993.
12. S. Kumar, "Computer Tomographic Measurements of Void Fraction and Modeling of the Flow in Bubble Columns", December 1994.
13. S. Palavajjhala, "Studies in Model Predictive Control with Application of Wavelet Transform", December 1994.
14. H. Vedam (M.S.), "Design a Controller Structure for Injected Resin Transfer Molding (IRTM) Process", May 1995.
15. P. Mathias, "Zero-Order Release from a Brittle Matrix Due to Osmotically-Induced Surface Erosion", December 1995.

16. M. Thomas, "Quality Control of Batch Chemical Processes with Application to Autoclave Curing of Composite Laminate Materials", December 1995.

17. S. Karur, "Boundary Element and Dual Reciprocity Methods in Reaction Engineering", May 1996.

18. R. Shepard, "Carbon Fibers for Affordable Polymeric Composites", May 1996.

19. S. Limtrakul, "Hydrodynamics of Liquid Fluidized Beds and Gas-Liquid Fluidized Beds", August, 1996.

21. K. Kumar, "Evaluation of Metal Peroxides for Bioremediation", September, 1996.

22. M. Kulkarni, "Dynamics of Asymmetric Fixed-Bed Reactors: Coupling of Exothermic and Endothermic Reactions", December, 1996.

23. Q. Wang, Gas/Liquid Phase with Reaction in Churn-Turbulent Bubble Column", August, 1996.

24. B. Sannaes at The Trondheim Institute of Technology of the University of Norway Trondheim, Norway, June, 1997.

25. S. Degaleesan, "Fluid Dynamic Measurements and Modeling of Liquid Mixing in Bubble Columns", August, 1997.

26. M.R. Khadilkar, "Performance Studies of Trickle Bed Reactors", December, 1998.

27. Z. Xu, "Highly Selective Chlorination of Toluene to Benzyl Chloride", December, 1998.

28. S.W. Highfill, "Liquid-Solid Mass Transfer Coefficient in High Pressure Trickle-Bed Reactor", December, 1998.

29. M. Roveda, "Brominated Disinfection By-Product Formation During Ozonation of Bromide-Containing Waters", December 1998.

APPENDIX A

ADDRESSES OF CREL ADVISORY BOARD MEMBERS

INDIVIDUALS

Dr. Walter Knox
Consultant
2118 Babler Ridge Lane
Glencoe, MO 63038
314-458-0950

Mr. Jean Cropley
114 Quarter Horse Drive
Scott Depot, WV 25560
jcrop2@aol.cm

AIR PRODUCTS AND CHEMICALS

Dr. Bernard Toseland
Air Products & Chemicals, Inc.
PO Box 25780
Lehigh Valley, PA 18007
610-481-8907 (phone) or 8917 / 610-481-4566 (fax)
toselaba@apci.com

BAYER

Dr. Knudsen Werner
Bayer AG
ZT-TE4, GEB E41
Germany
49-214-30-6113 (phone) / 49-214-30-31141 (fax)

CHEVRON

Dr. Kris Parimi
Chevron Research & Technology Company
100 Chevron Way
Richmond, CA 94802
510-242-4761 (phone) / 510-242-1599 (fax)
kpar@chevron.com

CONOCO

Dr. Doug S. Jack
Conono Inc.
1000 South Pine
PO Box 1267
Ponca City, OK 74602-1267
Doug.s.jack@conoco.com

Dr. Harold A. Wright
Conono Inc.
1000 South Pine
PO Box 1267
Ponca City, OK 74602-1267

DUPONT

Dr. P.L. Mills
DuPont Central Research & Development
Corporate Catalysis Center, Bldg. E304-A204
DuPont Experimental Station
Wilmington, DE 19880-0304
millspl@esvax.dupont.com

Dr. Tiby M. Leib
DuPont Engineering
1007 Market Street/N6404
Wilmington, DE 19898
302-774-5152 (phone) / 302-774-2457
tiberiu.m.leib@usa.dupont.com

EASTMAN CHEMICALS

Dr. David Hitch
Eastman Chemical Company
Research Laboratories, Bldg. 152-A
Kingsport, TN 37662
615-229-5398
dmhitch@eastman.com

ELF AQUITAINE

Dr. Jean Rene Bernard
Elf Aquitaine
CRTES BP 22
69360 Solaize, France
33-47-8026112 (phone) / 33-47-8026093 (fax)
jean-rene.bernard@eaf.elf1.fr

ELF ATOCHEM

Dr. Steven M. Galaton
Elf Atochem North America, Inc.
900 First Avenue, PO Box 61536
King of Prussia, PA 19406-0936

EXXON

Dr. Ronald D. Garton
Exxon Chemical Company
PO Box 241, 4999 Scenic Highway
Baton Rouge, LA 70821-0241

Dr. Min Chang
Exxon Research and Engineering Company
Chemical Engineering Technology
PO Box 101, 180 Park Ave, Florham Park, NJ 07932
973-765-6109 (phone) / 973-765-1189 (fax)
mchang@fpe.erenj.com

ICI KATALCO

Dr. John Middleton
ICI Katalco Technology
PO Box 8, the Heath, Runcorn
Cheshire WA7 4QD
United Kingdom
john_middleton@ici.com

Dr. Hugh Stitt
ICI Katalco
PO Box 1- Belasis Avenue
Billingham, Cleveland TS 23 1I B, United Kingdom
16-42-522704 (phone) / 16-42-522606 (fax)
hugh_stitt@ici.com

INSTITUT FRANCAIS DU PETROLE (IFP)

Dr. Christopher Boyer
IFP
CEDI "Rene Navarre", BP 3
69390 Vernaison, France
334-7802-2020 (phone) 334-7802-2015 (fax)
christophe.boyer@ifp.fr

INTEVEP

Dr. Carlos Gustavo Dassori
Intevep S.A.
LTQ-1048, PO Box 8537
Miami, FL 33102-8537
58-32-307925 (phone) / 58-32-306943 (fax)
rppcgd1-int@intevep.pdv.com

MEMC

Dr. Henry Erk
MEMC Electronic Materials, Inc.
501 Pearl Drive (City of O'Fallon), PO Box 8
St. Peters, MO 63376
314-279-5837 (phone) / 314-279-5157 (fax)
herk@memc.com

MITSUBISHI

Dr. Glen H. Ko
Mitsubishi Chemical
One Kendall Square, Suite 2200
Cambridge, MA 02139
ghk@world.std.com

Dr. Takeshi Ishikawa
Mitsubishi Chemical Corporation
Mizushima Plant
3-10, Ushiodori
Karashiki, Okayama 712, Japan
ishi@seigi2.mt.m-kagaku.co.jp

MOBIL

Dr. Fred J. Krambeck
Mobil Technology Company
MRCTEC
PO Box 480
Paulsboro, NJ 08066-0480
frederick_j_krambeck@email.mobil.com

MONSANTO

Dr. Ronald H. Kahney
Monsanto Company
The Agricultural Group
800 N. Lindbergh Blvd.
St. Louis, MO 63167

Dr. Erik D. Sall
Monsanto Company
800 N. Lindbergh Blvd., Mail Zone Q3F
St. Louis, MO 63167
314-694-4348 (phone) / 314-694-3479 (fax)
erik.d.sall@monsanto.com

PRAXAIR

Dr. Joshua B. Sweeney
Praxair Inc.
765 Old Saw Mill River Road
Tarrytown, NY 10591
914-345-6448 (phone) / 914-345-6405 (fax)
josh_sweeney@praxair.com

Dr. William R. Williams
Praxair Inc.
765 Old Saw Mill River Road
Tarrytown, NY 10591
914-345-6413 (phone) / 914-345-6405 (fax)
bill_williams@praxair.com

SASOL TECH. LTD.

Dr. Ben Jager
Sasol Technology
R&D Division
PO Box 1, Sasolburg 9570
South Africa
27-16-708-2826 (fax)

SHELL

Dr. P.A. Nelson
Shell Engineering RD&T
Westhollow Technology Center, PO Box 1380
Houston, TX 77251
281-544-8159 (phone) / 281-544-8427 (fax)
panelson@shellus.com

Dr. Lionel Paul
Shell Research, Reaction Engineering Group
PO Box 38000
1030 BN Amsterdam, The Netherlands
31-20-6303893 (phone)
lionel.j.paul@opc.shell.com

STATOIL

Dr. Dag Schanke
Statoil, Refining and Petrochemicals, R&D Centre
Arkitekt Ebbells veg 10, Rotvoll
N-7005 Trondheim, Norway
47-73-584524 (office) / 47-73-967237 (home)
dsc@statoil.com

Dr. Arne Grislingas
Statoil, Refining & Petrochemicals, R&D Centre
Arkitekt Ebbells veg. 10, Rotvoll
N-7000 Trondheim, Norway
47-73-585879 (phone) / 47-73-584345 (fax)
argri@statoil.no

UNION CARBIDE

Dr. Manuk Colakyan
Union Carbide Corporation
3200-3300 Kanawha Turnpike
Building 2000/Rm 4127, PO Box 8361
South Charleston, WV 25303
304-747-4580 (phone) / 304-747-5999 (fax)
colakymc@ucarb.com

UOP

Dr. Anil Oroskar
UOP
25 East Algonquin Road
Des Plaines, IL 60016-5017

APPENDIX B

PREVIOUS CREL RESEARCH ACTIVITIES AND ACHIEVEMENTS

PREVIOUS CREL RESEARCH ACTIVITIES AND ACHIEVEMENTS

The following is a summary of the previous CREL achievements. These are either available in previous CREL reports, published manuscripts and Doctoral and Masters Theses:

1998-1999

I. MULTIPHASE REACTORS AND SYSTEMS

- Our unique facility for computer assisted radioactive particle tracking (CARPT) has been further improved. The developed Monte Carlo based simulation programs have been verified for accurate and efficient CARPT calibration **(Y. Yang, P. Gupta, A. Kemoun).** Work is in progress to improve the CARPT calibration in stainless steel high pressure bubble column. Wavelet filtering has been applied to CARPT data (S. Degaleesan, Y. Pan). Previously, satisfactory comparison was obtained between CARPT and particle image velocimetry (PIV), heat pulse anemometry (HPA), laser doppler anemometry (LDA) and hot wire anemometry (HWA).

- Our unique computed tomography (CT) facility has been utilized to quantify the density profile in various cross sections of our test bubble columns, fluidized beds and liquid-solid risers of various diameters and to investigate the effect of spargers in bubble column. **(N. Rados, B. Ong, A. Kemoun, Y. Wu)**

- The CARPT/CT facility was also used to complete a number of proprietary contract studies in various opaque multiphase systems.

- The implementation of CARPT/CT in high pressure bubble/slurry bubble column is in progress. This facility will be used to investigate the effect of high pressure and gas velocity on the hydrodynamics of bubble/slurry bubble columns in an attempt to advance the methodology of scale-up and design of these reactors. **(A. Kemoun)**

- A new high-pressure 6" bubble/slurry bubble column facility has been developed which is equipped with ports for probes (e.g., optical and conductivity probes and differential pressure transducers, etc.) and 6 windows along the column. The experimental investigations that will be conducted on this facility and the obtained findings will complement the information obtained by CARPT/CT **(N. Rados, A. Kemoun)**

- For the first time, CARPT has been implemented in a single-phase stirred tank reactor to characterize its mixing and flow pattern. The verification of CARPT results via its comparison with the published results has been conducted. These attempts represent the first steps in using CARPT to characterize the mixing in multiphase stirred tank reactors with opaque

systems where the other advanced diagnostics techniques cannot be used. **(A. Rammohan, A. Kemoun)**

- CREL has obtained from DuPont a complete setup of a 6 inch in diameter and about 26 feet tall gas-solid riser. The setup will be installed on a bay area during this summer (June – September 1999). The project is sponsored by Sandia National Laboratory and Chevron as a part of the Multiphase Fluid Dynamics Research Consortium Program (MFDRC). Advanced and portable CARPT system will be developed for gas-solid riser and for other multiphase flow applications.

- A phenomenological two-phase cross-flow model with recycle which accounts for interphase mass transfer and bubble coalescence and breakage has been extended to describe gas phase mixing. The model will be further improved by accounting for the variation in gas holdup along the reactor due to reaction. **(P. Gupta)**

- Monte Carlo based simulation programs have been developed and verified experimentally in a small tank to accurately and efficiently generate the 3D position-counts calibration maps for CARPT calibration. This results in 3-4 orders of magnitude reduction in time and effort required to calibrate CARPT. The work is in progress to verify the simulation experimentally in high pressure bubble column. **(P. Gupta, Y. Yang, A. Kemoun)**

- A new algorithm has been developed to filter the conductivity measurements for liquid tracer data obtained by conductivity probe in gas-liquid turbulent flows. The conductivity measurements are used to characterize the mixing in churn turbulent flow regime via tracer experiments. **(P. Gupta)**

- Hydrodynamics study (e.g. overall gas holdup and pressure drop) on trayed bubble column has been performed. **(J. Alvare, M. Muether, J. Mettes)**

- The work for the high pressure slurry bubble column consortium has been initiated. **(N. Rados, B. Ong, J. Weng, Y. Wu, A. Kemoun)**

- The statistical method of moments is used with the help of CFD to characterize the flow and the bed structure distribution in trickle bed reactors. **(Y. Jiang)**

- Mixing-cell Network models that uses CFD information for design and scale-up of trickle bed reactor has been developed. **(Y. Jiang)**

- Computational Fluid Dynamics (CFD) for bubble columns, slurry bubble columns, liquid-solid riser and trickle-bed reactors using CFDLIB and Fluent codes has received significant attention and work is in progress. The simulation results are compared with CARPT, CT and PIV measurements for verification and for closure improving schemes. **(Y. Pan, S. Roy, Y. Jiang)**

- The Boundary Element Method is used for different problems related to chemical reaction engineering. **(K. Balakrishnan)**

- A numerical scheme has been developed to calculate the effectiveness factor of partially wetted catalyst with irregular shapes. **(K. Balakrishnan)**
- Dynamic of catalyst pellets under periodic operation of trickle bed reactors is accounted for to improve selectivity and performance of trickle bed reactor operated under periodic operation. **(K. Balakrishnan)**
- A theoretical and experimental investigation of wood pyrolysis and combustion in batch charcoal kilns have been performed in the Air Quality Lab. **(G. Bhatia)**
- Our unique findings regarding liquid holdup dependence in rotating packed beds (RPB) on operating conditions have resulted in the only available correlation. **(A. Basic´ and M.P. Dudukovic´).** Currently we are exploring the potential of using RPBs in clean processing and pollution abatement. **(J. Zhu, Y. Wu)**
- Work is initiated to extend the developed rate based model for the design of the trayed reactive distillation column to packed bed reactive distillation. **(J. Lee)**

1997-1998

I. MULTIPHASE REACTORS AND SYSTEMS

- Fluid dynamic parameters (time averaged velocity profiles, turbulence parameters, and gas holdup distribution) were investigated via CARPT/CT in an 18 inch (44.0 cm) bubble column with/without internals using air-water and air-drakeoil systems. **(J. Chen, L. Fan)**
- A comparison between the data obtained by CARPT/CT in 4 inch diameter column was compared with those obtained by Particle Image Velocimetry (PIV) at similar operating conditions. **(J. Chen, A. Kemoun)**
- The simple recycle with cross flow model (RCFM) for gas phase mixing was used to simulate gas tracer runs at LaPorte AFDU, Texas. **(F. Li)**
- A new algorithm was developed to filter the conductivity measurements for liquid tracer data obtained by conductivity probe in gas-liquid turbulent flows. **(P. Gupta)**
- Slurry bubble column data obtained by CARPT was processed for time average liquid velocity profile and turbulent parameters. A study that investigates the effects of reactor pressure on these parameters was initiated. **(N. Rados)**
- A high pressure and high gas capacity bubble/slurry bubble columns facility was developed to investigate the effect of pressure and high gas flow rates on the hydrodynamics of bubble/slurry bubble columns. **(A. Kemoun, P. Gupta)**

- Effects of solid-to-liquid fluxes on the hydrodynamics of a liquid-solid riser were investigated using CARPT/CT. **(S. Roy, A. Kemoun)**

- Utilizing CARPT/CT facility to study the mixing in a stirred tank was proposed and outlines. **(A. Rammohan, A. Kemoun)**

- The hydrodynamics and gas-liquid mass transfer in external-arm airlift reactors were investigated. **(G. Feneyrou)**

- Gas flow distribution in a packed bed was evaluated by a model based on energy minimization and CFDLIB. A comparison between these two approaches were performed. **(Y. Jiang, M. Khadilkar)**

- Flow distribution in a 2D trickle bed reactor was simulated based on the concept that the flow follows the path of least resistance. PC based imaging technique was used to visualize the flow and to verify the simulation results. A comparison between this model and CFDLIB is presented. **(Y. Jiang, M. Khadilkar)**

- A novel interconnected cell trickle-bed reactor model to simulate the effect of flow maldistribution on the reactor performance was developed. **(Y. Jiang)**

- A parametric study of unsteady state flow modulation in trickle bed reactors was performed. **(M. Khadilkar)**

- Trickle-bed reactor models for systems with a volatile liquid phase was developed. **(M. Khadilkar)**

- A general model for determination of contacting efficiency in trickle-bed reactor was developed. **(K. Balakrishnan)**

- Effects of reactor pressure and gas flow rate on the liquid-solid mass transfer coefficient in trickle-bed reactor using the electrochemical and dissolution methods were investigated. **(S. Highfill)**

- Computational Fluid Dynamics (CFD) for bubble columns, slurry bubble columns and trickle-bed reactors using CFDLIB codes received significant attention. **(S. Saberi, Y. Pan, S. Roy, M. Khadilkar)**

- The Boundary Element Method was used for modeling of reactions in catalytic islands. **(K. Balakrishnan)**

- A novel, robust, implicit, finite difference based algorithm was fully developed and tested for simulation of transient, steep, moving fronts. The algorithm was used for studies of periodic operation of asymmetric bi-directional fixed-bed reactors. **(M. Kulkarni)**

- A rigorous particle scale modeling of wood pyrolysis for the formation of charcoal was presented. **(G. Bhatia)**

- Exploring the potential of using RPBs in clean processing and pollution abatement was initiated. **(J. Zhu)**

- The development of a rate based model for the design of reactive distillation column was discussed. **(J. Lee)**

- Dynamic simulation of photochlorination of toluene to benzylchloride at higher selectivity using a reactive distillation was presented. **(Z. Xu)**

II. PREPARATION OF NEW MATERIALS

- A new project started to quantify the effect of sonification on the fluid boundary layers at the flat solid surface (wafer) and to determine the magnitude of mass transfer intensification to and from the surface. **(R. Smith)**.

III. PROCESS MONITORING AND CONTROL

Following are the recent activities supervised by Professor Joseph.

- The use of power spectrum density analysis in detecting faults in sensors was outlined. **(C.-M. Ying)**

- A new method based on polynomial modes was developed to obtain the age density function from tracer data. **(C-M. Ying)**

1996-1997

I. MULTIPHASE REACTORS AND SYSTEMS

- Liquid mixing in bubble columns and the axial dispersion model were studied via Taylor type analysis to develop an effective one dimensional axial dispersion coefficient in terms of convective recirculation and turbulent eddy diffusion. **(S. Degaleesan).**

- A fundamentally based two dimensional liquid mixing model for bubble columns was developed and solved using CARPT/CT data as an input parameter. **(S. Degaleesan).**

- A strategy for scale-up of bubble columns mixing parameters was proposed. **(S. Degaleesan).**

- A phenomenological two phase cross flow model with recycle which accounts for interphase mass transfer and bubble coalescence and breakage was extended for the gas phase. (**P. Gupta).**

- Monte Carlo based simulation programs were developed to accurately and efficiently generate the 3D position counts calibration maps for CARPT calibration. This resulted in 3-4 orders of magnitude reduction in time and effort required to calibrate CARPT. **(Y. Yang, P. Gupta).**

- Optical probes (both one and 4 points) were developed to measure bubble size distribution and rise velocities in slurry bubble columns. **(R. Mudde, P. Gupta).**

- A model for cyclohexane in gas-liquid reactors was proposed. **(C.-M. Ying).**

- Theoretical and experimental work was completed for studies of slurry motion in bubble columns in a project that led to a D.Sc. degree at the University of Trondheim. **(B. Sannaes).**

- The hydrodynamics of liquid and gas-liquid fluidized beds were studied and the effect of various design parameters were demonstrated. **(S. Limtrakul).**

- Tomographic and particle tracking studies in a liquid-solid riser were performed. **(S. Roy).**

- Solid holdup distribution in the liquid-solid riser was evaluated using CARPT data. **(F. Li).**

- Utilizing CARPT/CT facility to study the mixing in a stirred tank was proposed and outlined. **(A. Kemoun).**

- Prediction of gas flow distribution in packed beds with internals structure nonuniformities was presented. **(Y. Jiang, M. Khadilkar).**

- Flow distribution in a 2D trickle bed reactor was studied using developed simulation based on the concept of the flow follows the path of least resistance. PC based images technique was used to visualize the flow and to verify the simulation results. **(Y. Jiang, M. Khadilkar).**

- Phenomenological model that simulates the performance of trickle-be reactor under induced pulsing was developed. **(M. Khadilkar).**

- Experimental investigation of liquid flow distribution in a trickle-bed reactor operated under steady state and with induced pulsing were performed. **(J. Huettman, J. Mattes, Y. Jiang, M. Khadilkar).**

- Assessment of the effect of pressure on the liquid-solid mass transfer coefficient in trickle bed reactors was presented. **(M. Friedman, S. Highfill).**

- A study of the effect of pressure on the liquid-solid mass transfer coefficient in trickle-bed reactors was performed. **(S. Highfill).**

- Computational Fluid Dynamics (CFD) for bubble columns, slurry bubble columns and trickle-bed reactors using CFDLIB codes was received significant attention. **(S. Roy).**

- A novel, robust, implicit, finite difference based algorithm was fully developed and tested for simulation of transient, steep, moving fronts. The algorithm was used for studies of periodic operation of asymmetric bi-directional fixed-bed reactors. **(M. Kulkarni).**

- Polynomial methods for nonideal tracer response of identification in trickle-bed reactors were presented. **(C.-M. Ying).**

- The development of a rate based model for the design of reactive distillation column were discussed. **(J. Lee).**

- Photochlorination of toluene to benzyl chloride with higher selectivity using a reactive distillation was presented. **(Z. Xu).**

- Minimizing the formation of bromate compounds during ozonation of water impurities in water treatment process was investigated. **(M. Roveda).**

- Studies of the oxygen release rate of encapsulated metal peroxides for bioremediation were in progress. **(K. Kumar).**

II. PREPARATION OF NEW MATERIALS

- A new project was initiated to quantify the effect of sonification on the fluid boundary layers at the flat solid surface (wafer) and to determine the magnitude of mass transfer intensification to and from the surface. Successful completion of this work would allow to quantify such effect on the reactivity, effectiveness and specificity of aqueous etching and cleaning chemistries commonly used in the electronics materials industry (**R. Smith**).

III. PROCESS MONITORING AND CONTROL

- A study to develop a mathematical model and a control system that maximize production rates and can achieve good composite qualities was presented. **(S. Voorakaranam).**

- A study to design an adaptive inferential temperature control for a reaction calorimeter was completed. **(E. Causevic).**

1995-1996

I. MULTIPHASE REACTORS AND SYSTEMS

- Our unique facility for computer assisted radioactive particle tracking (CARPT) was further perfected and an improved operational manual was written. The

CARPT facility was used to complete a number of proprietary contract studies **(Y. Yang, S. Kumar, S. Degaleesan, S. Limtrakul and P. Gupta)**.

- Our unique computer tomography (CT) facility was utilized on dynamic systems (**S. Kumar**). It was demonstrated that our CT scanner can accurately quantify the density profile in various cross sections of our test bubble columns, fluidized beds and liquid-solid risers of various diameters. Also the effect of scale on liquid recirculation in bubble column was investigated using both CARPT/CT **(S. Limtrakul, S. Roy, S. Kumar)**.

- Evaluation of experimental methods for the hydrodynamics of industrial scale reactors was addressed. (**S. Kumar**)

- Numerical simulation of the flow in bubble column using CFDLIB developed at the Los Alamos National Laboratory was initiated. (**S. Kumar**)

- The error in CARPT determined fluctuating velocities was significantly reduced by implementing a wavelet based filtering system for processing of raw data. (**S. Degaleesan**)

- Equipment modifications were completed and utilized for studying the motion of large solids in three phase fluidized beds via CARPT. The hydrodynamics of liquid and gas/liquid fluidized beds were studied and the effect of various design parameters were demonstrated. (**S. Limtrakul**)

- Theoretical and experimental work was initiated for studies of slurry motion in bubble columns. (**B. Sannaes**)

- A framework was prepared and experiments were planned for studies of the fluid dynamics and flow patterns in liquid-solid risers. (**S. Roy**)

- A new phenomenological two-phase cross flow model with recycle and interphase mass transfer for bubble column was developed. (**Q. Wang, P. Gupta**)

- Liquid mixing in bubble/slurry bubble columns was described via a phenomenological model. (**S. Degaleesan**)

- An analysis of flow patterns via tracer experiments performed on an industrial scale slurry bubble column under reaction conditions (La Porte reactor) was presented. (**S. Degaleesan, J. Chen**)

- High pressure trickle-bed reactor facility was modified. A control loop was added to control the liquid level in the gas/liquid separator. The unit is now equipped with the equipment needed for periodic operation. High pressure

reactor of 5 cm diameter and 1 m long with a uniform liquid/gas distributor was constructed. **(M. Khadilkar, S. Highfill, Y. Jiang)**

- Prediction of flow distribution in trickle-bed reactors under steady state operation based on energy minimization was studied and presented. **(Y. Jiang)**

- Pressure drop and liquid holdup predictions in high pressure trickle-bed reactor were improved by accounting for the liquid-gas interaction. **(Y. W., M. Khadilkar)**

- The intrinsic kinetics of hydrogenation of α-methyl styrene at high pressure operation was studied and appropriate models were proposed. This reaction is utilized as a test reaction in trickle-bed and packed bubble column reactors. **(Y. Jiang, Y. Wu, M. Khadilkar)**

- A rigorous model to predict the performance of trickle-bed reactors under periodic operation (induced pulsing) were developed. Experimental studies of trickle-bed reactor (low to high pressure) under periodic operation were planned. **(M. Khadilkar)**

- Evaluation of the effects of high pressure operation on the liquid-solid mass transfer coefficient in trickle-bed reactors was presented. **(M. Friedman, S. Highfill)**

- A study of liquid-solid mass transfer coefficient in trickle-bed reactors under high pressure operation using simultaneously electrochemical and bed dissolution methods was initiated. **(S. Highfill)**

- The power of the boundary element method (BEM) and the dual reciprocity approach was illustrated by solving the diffusion reaction equation in partially externally wetted particles. An optimal interpolating function for the dual reciprocity method was discussed. **(S. Karur)**

- Theoretical and experimental investigations of particle removal from gaseous stream by rotofilter were discussed. **(K. Ng)**

- A rate based model for the design of reactive distillation column was developed. **(J. Lee)**

- Photochlorination of toluene to benzyl chloride at higher selectivity using a reactive distillation was presented. **(Z. Xu)**

- Minimizing the formation of bromate compounds during ozonation of water impurities in water treatment process was investigated. **(M. Roveda)**

- Studies of the oxygen release rate of encapsulated metal peroxides for bioremediation was performed. **(K. Kumar)**

II. PREPARATION OF NEW MATERIALS

- A new project was initiated to quantify the effect of sonification on the fluid boundary layers at the flat solid surface (wafer) and to determine the magnitude of mass transfer intensification to and from the surface. Successful completion of this work would allow to quantify such effect on the reactivity, effectiveness and specificity of aqueous etching and cleaning chemistries commonly used in the electronics materials industry (**R. Smith**).

- A new material and a mathematical model for zero-order release from a brittle matrix due to osmotically-induced surface erosion were developed. (**P. Mathias, BTL**)

- A modeling framework was developed for quantification and optimization of the process for long carbon fiber manufacture. (**R. Shepard, MRL**)

III. PROCESS MONITORING AND CONTROL

A new activity was initiated by Professor B. Joseph in developing an advanced control system for reaction calorimetry.

1994-1995

I. MULTIPHASE REACTORS AND SYSTEMS

- Our unique facility for single radioactive tracking (CARPT) was further improved (**B.S. Zou**) and an improved operational manual was written (**J.M. Mercier**). The CARPT facility was used to complete a number of proprietary contract studies.

- Our unique computer tomography (CT) facility was tested on dynamic systems (**S. Kumar**). It was demonstrated that our CT scanner can accurately quantify the density profile in various cross sections of our test bubble columns of various diameters. Also the effect of scale on liquid recirculation in bubble column was investigated using both CARPT/CT.

- The error in CARPT determined fluctuating velocities was significantly reduced by implementing a wavelet based filtering system for processing of raw data (**S. Degaleesan**).

- Equipment modifications were completed for studying the motion of large solids in three phase fluidized beds via CARPT. The hydrodynamics of liquid and gas/liquid fluidized beds were studied and the effect of various design parameters were demonstrated (**S. Limtrakul**).

- A theoretical framework was prepared and experiments planned for studies of slurry particles motion in bubble columns (**B. Sannaes**).
- A review of the hydrodynamics of liquid-solid circulating fluidized bed was presented (**S. Roy**).
- A new phenomenological two-phase cross flow model with recycle and interphase mass transfer for bubble column was outlined (**Q. Wang**).
- An analysis of flow patterns via tracer experiments performed on an industrial scale bubble column under reaction conditions was presented (**B.S. Zou**).
- The intrinsic kinetics of hydrogenation of α-methyl styrene at high pressure operation was studied and appropriate models were proposed. This reaction was utilized as a test reaction in trickle-bed and packed bubble column reactors (**Y. Wu and M. Khadilkar**).
- Performance comparison of downflow and upflow laboratory reactors under gas and liquid limited conditions was investigated and a criteria for the limiting reactant (gas or liquid) was presented (**M. Khadilkar and Y. Wu**).
- Investigation of the effect of fines on the performance of laboratory trickle-bed (downflow) and packed bubble column (upflow) reactors using both gas-limited and liquid-limited reaction was performed. This study demonstrated that a diluted bed with fines packed according to the CREL's procedure, is to be preferred over an upflow reactor for kinetic or scale-up studies (**M. Khadilkar and Y. Wu**).
- The validity of a plug flow with partially wetted particles model in describing the trickle-bed performance was demonstrated using the decomposition of hydrogen peroxide as a test liquid limited reaction (**Y. Wu and M. Khadilkar**).
- Improved prediction of pressure drop and liquid holdup in high pressure trickle-bed reactors was investigated (**Y. Wu and M. Khadilkar**).
- A study of trickle bed reactor (low to high pressure) periodic operation and a comprehensive phenomenological model to predict the performance of trickle-bed reactors under induced pulsing was initiated (**M. Khadilkar**).
- Various hydrodynamic models for multiphase reactors was tested using the available Los Alamos CFDLIB algorithms (**S. Kumar and M. Khadilkar**).
- The power of the boundary element method (BEM) and the dual reciprocity approach was illustrated by solving the catalyst effectiveness problem for a number of nonlinear kinetic expressions. A new boundary element algorithm to solve a network of linear reaction in catalyst particles was discussed (**S. Karur**).

- A novel, robust, implicit, finite difference based algorithm was fully developed and tested for simulation of transient, steep, moving fronts (**M. Kulkarni**). The algorithm was used for studies of unsteady state processes in packed beds.

- The theoretical and experimental investigations of particles removal from gaseous stream by Rotofilter were investigated (**K. Ng**).

- The fully based model for the design of reactive distillation column was under development (**J. Lee**).

- Photochlorination of toluene to benzyl chloride at higher selectivity using a reactive distillation was under investigation (**Z. Xu**).

- A review of heterogeneous photocatalytic destruction of organic pollutants in water was performed (**P. Gupta**).

- Minimizing the formation of bromate compounds during ozonation of water impurities in water treatment process was investigated (**M. Roveda**).

- Studies of the oxygen release rate of encapsulated metal peroxides for bioremediation were under investigation (**K. Kumar**).

II. PREPARATION OF NEW MATERIALS

- A project on manufacture of carbon fibers in collaboration with our Materials Research Laboratory (MRL) and a project on developing a new material and phenomenological model for release system in collaboration with our Biological Transport Laboratory (BTL) were added.

- A model for resin devolitilization during processing of thermoplastic composites was extended to more systems for the autoclave process for high performance long-fiber composites and new sensors were implemented (**J. Vasat**).

- A new material and a mathematical model for zero-order release from a brittle matrix due to osmotically-induced surface erosion were developed (**P. Mathias**).

- A modeling framework was developed for quantification and optimization of the process for long carbon fiber manufacture (**R. Shepard**).

III. PROCESS MONITORING AND CONTROL

- Our goal is to investigate the potential of various process monitoring techniques in a number of applications and develop the most promising ones into useful engineering tools. The main activities in this area were:

- Representation of dynamic responses using wavelets and application in implementation of Dynamic Matrix Control (**S. Palavajjhala**). This approach offers a more compact time and frequency representation of various process signals and allows for computerization of optimization and control schemes.

- On line model based quality control utilizing secondary measurements (**M. Thomas**) was developed and implemented on the autoclave process for curing of composites.

- Design of a controller structure for the injected resin transfer molding (IRTM) process (**H. Vedam**).

1993 – 1994

I. MULTIPHASE REACTORS AND SYSTEMS

- Equipment modifications were under implementation for studying the motion of large solids in three phase fluidized beds via CARPT (**S. Limtrakul**).

- A theoretical framework prepared and experiments were outlined for studies of slurry particles motion in bubble columns (**B. Sannaes**).

- A thorough analysis of tracer runs performed on an industrial scale bubble column was outlined (**B.S. Zou**).

- The effect of high pressure and addition of fines on pressure drop, liquid holdup and liquid-solid contacting in trickle beds was quantified (**M. Al-Dahhan**). New correlations and an improved understanding have resulted from this study which is fully reported in M. Al-Dahhan's thesis.

- A reproducible procedure to pack small laboratory reactors for two phase flow studies has been tested repeatedly and a final recommendation developed (**Y. Wu** and **M. Al-Dahhan**). This procedure is essential for successful representation of commercial trickle-beds via small laboratory reactors.

- Comparison of downflow and upflow laboratory packed beds for solid catalyzed gas-liquid reactions was completed at high pressure operation (**A. Choné**). While the effect of all variables can be explained phenomenologically, models were developed for a quantitative comparison with data (**M. Khadilkar, M. Al-Dahhan**).

- Decomposition of hydrogen peroxide on a new catalyst was quantified as a good liquid limiting reaction for studies of trickle beds (**Y. Wu**).

- Various hydrodynamic models for trickle beds were tested using the available Sandia-Los Alamos CFDLIB algorithms. (**M. Khadilkar**).

- The power of the boundary element method (BEM) and the dual reciprocity approach was illustrated by solving the catalyst effectiveness problem for a number of nonlinear kinetic expressions (**S. Karur**).

- A robust, implicit, finite difference based algorithm, was developed and tested for simulation of transient, steep, moving fronts (**M. Kulkarni**). The algorithm was used for studies of unsteady state processes in packed beds.

- A comprehensive study of ammonia-flyash interaction in selective catalytic reduction (SCR) of NO_x with ammonia in power plants was completed (**J.R. Turner's** thesis). This has resulted in important ramifications for use of ammonia as a flyash conditioning agent.

- Photochlorination of toluene in a reactive distillation column was initiated as a new project to illustrate the potential of reaction engineering in improving the yield of desired intermediates (**Z. Xu**).

- The theory of the reverse flow process for sulfuric acid manufacture, VOC and No_x abatement and their commercialization have gained **Dr. Y. Sh. Matros** international recognition. At CREL during 1993/94 he pursued some other aspects of unsteady-state catalytic processing with application in various areas.

II. PREPARATION OF NEW MATERIALS

- A modeling framework was developed for quantification and optimization of the process for long carbon fiber manufacture (**R. Shepard**).

III. PROCESS MONITORING AND CONTROL

- Representation of dynamic responses using wavelets and application in implementation of Dynamic Matrix Control (**R. Srinivas**). This approach offers a more compact time and frequency representation of various process signals and allows for computerization of optimization and control schemes.

- On line model based quality control utilizing secondary measurements (**M. Thomas**) was under development to be implemented on the autoclave process for curing of composites.